BEILSTEIN JOURNAL OF ORGANIC CHEMISTRY

Macrocyclic and supramolecular chemistry

Edited by Mei-Xiang Wang and Hai-Bo Yang

Imprint

Beilstein Journal of Organic Chemistry
www.bjoc.org
ISSN 1860-5397
Email: journals-support@beilstein-institut.de

The *Beilstein Journal of Organic Chemistry* is published by the Beilstein-Institut zur Förderung der Chemischen Wissenschaften.

Beilstein-Institut zur Förderung der Chemischen Wissenschaften
Trakehner Straße 7–9
60487 Frankfurt am Main
Germany
www.beilstein-institut.de

BEILSTEIN JOURNAL OF ORGANIC CHEMISTRY

A conformationally adaptive macrocycle: conformational complexity and host–guest chemistry of zorb[4]arene

Liu-Pan Yang[1,2], Song-Bo Lu[2,3], Arto Valkonen[4], Fangfang Pan[5], Kari Rissanen[4] and Wei Jiang*[2]

Full Research Paper

Open Access

Address:
[1]Academy of Advanced Interdisciplinary Studies, Southern University of Science and Technology, Xueyuan Blvd 1088, Shenzhen, 518055, China, [2]Department of Chemistry, Southern University of Science and Technology, Xueyuan Blvd 1088, Shenzhen, 518055, China, [3]School of Chemistry and Chemical Engineering, Harbin Institute of Technology, Harbin, 150001, China, [4]University of Jyvaskyla, Department of Chemistry and Nanoscience Center, P. O. Box 35, FI-40014, Jyvaskyla, Finland and [5]College of Chemistry, Central China Normal University, Wuhan, 430079, China

Email:
Wei Jiang* - jiangw@sustc.edu.cn

* Corresponding author

Keywords:
conformations; host–guest chemistry; macrocycles; supramolecular chemistry; zorb[4]arene

Beilstein J. Org. Chem. **2018,** *14,* 1570–1577.
doi:10.3762/bjoc.14.134

Received: 20 April 2018
Accepted: 13 June 2018
Published: 27 June 2018

This article is part of the thematic issue "Macrocyclic and supramolecular chemistry".

Guest Editor: M.-X. Wang

Abstract

Large amplitude conformational change is one of the features of biomolecular recognition and is also the basis for allosteric effects and signal transduction in functional biological systems. However, synthetic receptors with controllable conformational changes are rare. In this article, we present a thorough study on the host–guest chemistry of a conformationally adaptive macrocycle, namely per-*O*-ethoxyzorb[4]arene (**ZB4**). Similar to per-*O*-ethoxyoxatub[4]arene, **ZB4** is capable of accommodating a wide range of organic cations. However, **ZB4** does not show large amplitude conformational responses to the electronic substituents on the guests. Instead of a linear free-energy relationship, **ZB4** follows a parabolic free-energy relationship. This is explained by invoking the influence of secondary C–H···O hydrogen bonds on the primary cation···π interactions based on the information obtained from four representative crystal structures. In addition, heat capacity changes (ΔC_p) and enthalpy–entropy compensation phenomena both indicate that solvent reorganization is also involved during the binding. This research further deepens our understanding on the binding behavior of **ZB4** and lays the basis for the construction of stimuli-responsive materials with **ZB4** as a major component.

Introduction

Macrocyclic receptors are the principal workhorses used in supramolecular chemistry [1]. A myriad of synthetic macrocycles have sprouted during the past decade, greatly enriching the arsenal of supramolecular chemists [2-11]. The majority of artificial macrocycles are featured with rigid backbones as it is widely accepted that preorganization [12] is crucial for mini-

mizing the entropy cost in molecular recognition. In contrast, bioreceptors often possess flexible backbone structures and even undergo large amplitude conformational changes upon binding substrates [13,14]. This conformational adaptivity is the basis of the allosteric effects [15,16] and signal transduction [17] observed with bioreceptors. However, similar conformationally adaptive synthetic macrocyclic receptors are relatively rare in the literature [18-23].

During the last five years, we have developed two classes of macrocyclic receptors with biomimetic structures [24]: *endo*-functionalized molecular tubes [25-30] and conformationally adaptive macrocycles [31-37]. Among the conformationally adaptive macrocycles two types were reported: oxatub[*n*]arenes [31-36] and zorb[*n*]arenes [37]. These macrocycles possess multiple conformers due to the naphthalene flipping in analogy with the phenyl-ring flipping seen in the more common calixarenes. The conformers so formed undergo quick interconversion and each one has a slightly different cavity. Thus, these conformers consist of a complex conformational network. We have carefully looked into the properties of oxatub[*n*]arenes and found that the macrocycles have many unique properties. For example, oxatub[4]arene has a wide guest scope and can bind almost all of the common organic cations [32]. It also shows conformational responses to solvent change [33] and remote electronic substituents on the guests [34]. In addition, different alkyl side chains on oxatub[4]arenes lead to different macroscopic self-assembly behaviors [36]. Zorb[4]arene was first synthesized, reported and so named by the Georghiou group in 2005. The derivatives per-*O*-methoxy- and per-*O*-ethoxyzorb[4]arene were shown to be effective tetramethylammonium ion receptors [38]. The per-*O*-*n*-butoxyzorb[4]arene (**ZB4**, Scheme 1a) was only recently further studied by us with respect to its rich conformational properties and the consequence on macroscopic self-assembly [37]. In the present research, we report the binding behavior of **ZB4** to a much wider guest scope. We found that the guest-binding ability and conformational adaptivity of **ZB4** are quite different from that of per-*O*-*n*-butoxyoxatub[4]arene (**TA4**).

Results and Discussion

Conformational adaptability enables oxatub[4]arenes to host a wide range of organic cations [32]. **ZB4** is also a conformationally adaptive macrocycle. We wondered whether **ZB4** has a wide guest binding scope. It was reported that quaternary ammonium-based organic cations ($\mathbf{1}^+$–$\mathbf{3}^+$) can be hosted by zorb[4]arenes [37,38]. Quaternary ammonium cations $\mathbf{4}^+$ and $\mathbf{5}^+$ and other types of organic cations hosted by **TA4** ($\mathbf{6}^+$–$\mathbf{10}^+$)

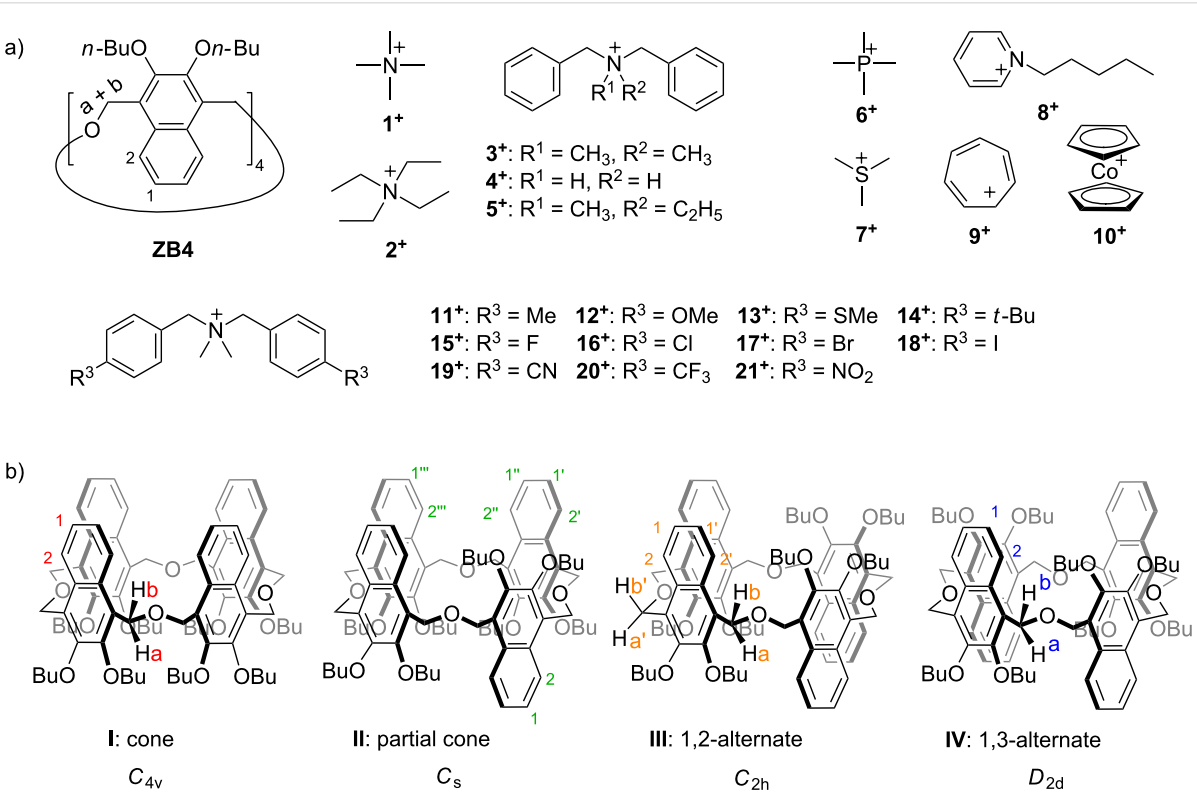

Scheme 1: (a) Chemical structures of **ZB4** and the guests involved in this research. The counterions are PF_6^-. (b) The four representative conformers of **ZB4** resulting from naphthalene flipping. Numberings on the structures are used to assign NMR signals.

were tested with **ZB4**. Most of these guests can indeed be complexed. But there are some exceptions. Changing the core quaternary ammonium structure of $\mathbf{3}^+$ completely shuts down the binding, because no obvious complexation-induced shifts were detected in the 1:1 mixture of **ZB4** with $\mathbf{4}^+$ or $\mathbf{5}^+$ (Figures S1 and S2 in Supporting Information File 1). This indicates the importance of the core quaternary ammonium ions in the host–guest complexation. All other guests can be encapsulated in the cavity of **ZB4**, and significant chemical shifts on both the guests and **ZB4** were observed in the NMR spectra (Figures S3–S7 in Supporting Information File 1). The ESI mass spectra of equimolar mixtures of guests $\mathbf{9}^+$ and $\mathbf{10}^+$ and **ZB4** were obtained (Figures S9 and S10 in Supporting Information File 1) and the predominant peaks were assigned to 1:1 complexes after losing PF_6^-.

NMR titrations and isothermal titration microcalorimetry (ITC) were then performed to obtain the association constants. For small guests such as $\mathbf{1}^+$, $\mathbf{2}^+$, $\mathbf{6}^+$–$\mathbf{9}^+$, NMR titration experiments with **ZB4** have been performed due to the fast equilibrium of the free and **ZB4**-complexed guests on the NMR time scale. All titration curves agreed well with a 1:1 stoichiometry (Figures S11–S14 in Supporting Information File 1). In case of guests $\mathbf{3}^+$ and $\mathbf{10}^+$, the binding heats were high enough to be measured. Thus the binding parameters were determined by ITC titrations (Figure S15 in Supporting Information File 1) and the results are shown in Table 1. Generally, **ZB4** shows weaker binding affinities to these guests than **TA4** does with the same counterions. For example, **ZB4** and cation $\mathbf{3}^+$, with a binding constant of 5.4×10^4 M^{-1}, was the best guest among the studied ones. However, the corresponding association constant with **TA4** has been 1.7×10^5 M^{-1}. Similar differences were also observed for cations $\mathbf{9}^+$ and $\mathbf{10}^+$, their binding affinities with **ZB4** were lower by 1–2 orders of magnitude than those with **TA4**. However, the small guests, such as $\mathbf{2}^+$ and $\mathbf{6}^+$–$\mathbf{8}^+$ share rather similar binding affinities to both **ZB4** and **TA4**.

The X-ray crystal structure of free **ZB4** shows it to exist as a self-inclusion conformation in the solid state (Figure 1a). This conformation is different from the ones containing different lower-rim alkyl groups reported earlier [37,38]. Crystals were obtained by slow evaporation of the compounds' CH_3CN solutions and the different conformations in the solid state may result from the packing of the different lower-rim alkyl groups. For the conformers with cavities (Scheme 1b), three out of the four have been predominantly selected by three different guests.

Table 1: Association constants (M^{-1}) and other thermodynamic parameters as determined by ^1H NMR titrations (400 MHz, CD_2Cl_2/CD_3CN 1:1, 298 K) or by ITC titrations in a 1:1 mixture of 1,2-dichloroethane and MeCN at 298 K.

guests[a]	K_a (M^{-1})		guests[a]	K_a (M^{-1})
$\mathbf{1}^+$[b]	4700 ± 600		$\mathbf{7}^+$	349 ± 29
$\mathbf{2}^+$[b]	590 ± 30		$\mathbf{8}^+$	468 ± 31
$\mathbf{6}^+$	524 ± 48		$\mathbf{9}^+$	1300 ± 100
guests[c]	K_a (M^{-1})	ΔG (kJ·mol^{-1})	ΔH (kJ·mol^{-1})	$-T\Delta S$ (kJ·mol^{-1})
$\mathbf{3}^+$[b]	$(5.4 \pm 1.2) \times 10^4$	−27.0 ± 0.8	−31.6	4.6
$\mathbf{10}^+$	$(4.3 \pm 1.0) \times 10^4$	−26.5 ± 0.7	−18.1	−8.4

[a]The association constants were determined by NMR titrations; [b]the binding parameters of these guests have been reported (see ref. [37]); [c]the association constants were determined by ITC titrations.

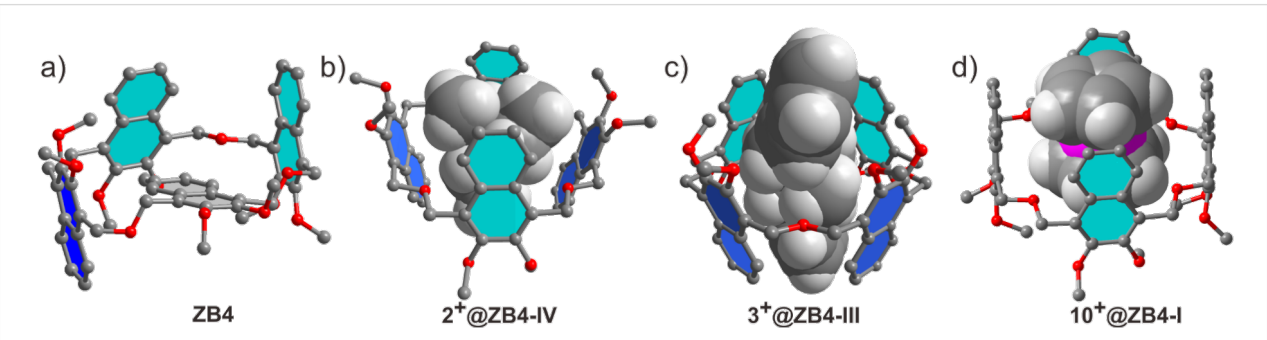

Figure 1: X-ray single crystal structure of **ZB4** and the host–guest complexes. a) **ZB4**, b) **2**$^+$**@ZB4-IV,** c) **3**$^+$**@ZB4-IV,** d) **10**$^+$**@ZB4-I**. Hydrogen atoms of the host are removed and butyl groups are shortened to methyl groups for viewing clarity. The X-ray single crystal structures of **2**$^+$**@ZB4-IV** (b) and **3**$^+$**@ZB4-III** (c) have been reported previously (see [37]).

For example, guests $\mathbf{2}^+$ and $\mathbf{3}^+$ induced conformers **IV** and **III**, respectively, to achieve optimal binding [37]. This has been unambiguously confirmed by X-ray single crystallography (Figure 1b and 1c). Guest $\mathbf{10}^+$ is a strong binder and its induction on the conformations of **ZB4** was further analyzed. The guest exchange in solution of $\mathbf{10}^+$@**ZB4** is fast/intermediate on the NMR timescale, as witnessed by broadening of all signals in the spectrum at 25 °C (Figure S7b in Supporting Information File 1). Thus, a ^{1}H NMR experiment at −20 °C was performed to slow down the guest exchange. Indeed, the protons a and b are clearly separated, suggesting that the guest exchange is now slow on the NMR timescale (Figure S7c in Supporting Information File 1). Only two signals for the aromatic protons of the host are observed, suggesting that **ZB4** predominantly exists as either conformer **I** or **IV** in the complex $\mathbf{10}^+$@**ZB4**. However, it has been not clear which one **ZB4** adopts. Fortunately, a single crystal suitable for X-ray diffraction could be obtained by slow evaporation of the solution of $\mathbf{10}^+$ and **ZB4** in a mixture of CH_2Cl_2 and CH_3CN. The crystal structure clearly shows that conformer **I** (Figure 1d) is the selected conformation by guest $\mathbf{10}^+$.

TA4 shows a large amplitude of conformational change in response to the remote electronic substituents on the guests [34]. We wondered whether a similar behavior would be observed for **ZB4**. Consequently, a series of guests with different substituents in the *para*-positions of guest $\mathbf{3}^+$ were employed to study the electronic substituent effect of the guests on the binding behavior of **ZB4**. As the guest exchange is slow on the NMR timescale the experiments were performed by ^{1}H NMR spectroscopy. Surprisingly, all the ^{1}H NMR spectra of the complexes (Figure S8 in Supporting Information File 1) shared similar peak patterns as $\mathbf{3}^+$@**ZB4**, suggesting conformer **III** (C_{2h} symmetry) [37] to be the most favored conformation for all complexes. Obviously the conformational network of **ZB4** shows no response to the electronic substituents on the guests. This is quite different from **TA4**.

In addition, there has been a linear free energy relationship between electronic properties of substituents present in the guests and their binding affinities with **TA4**, indicating that the binding affinities are affected by substituents through a field/inductive effect [34]. However, this is again quite different for **ZB4**. The association constants of **ZB4** to these guests were determined by ITC titrations (Figures S15–S26 in Supporting Information File 1), and the data are shown in Table 2. The logarithm of the corresponding association constants of $\mathbf{11}^+$–$\mathbf{21}^+$ over $\mathbf{3}^+$ were parabolic as the function of Hammett parameter (σ_p) [39] (Figure 2). For substituents $C(Me)_3$, OMe, Me, SMe, F, Cl, Br, and I, the binding affinities increase with increasing σ_p. However, the binding affinities decrease with further increasing σ_p (CF_3, NO_2, and CN). The guest with iodo substituent ($\mathbf{18}^+$) is the best, with an association constant of

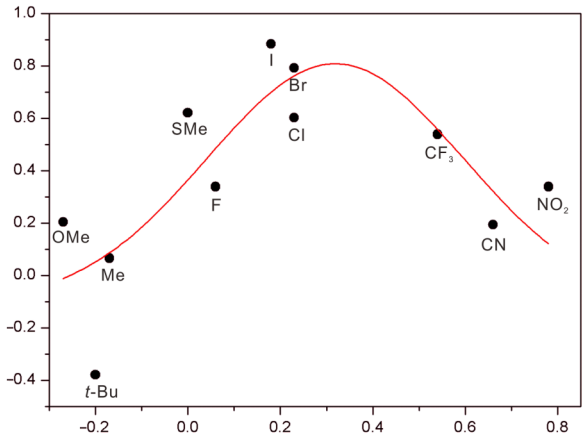

Figure 2: Parabolic free-energy relationship between $\log(K_R/K_H)$ and Hammett parameter σ_p. K_R: guests $\mathbf{11}^+$–$\mathbf{21}^+$; K_H: guest $\mathbf{3}^+$.

Table 2: Association constants (M^{-1}) and other thermodynamic parameters of **ZB4** with guests $\mathbf{11}^+$–$\mathbf{21}^+$ as determined by ITC titrations in a 1:1 mixture of 1,2-dichloroethane and MeCN at 298 K.

guests	R^3	K_a	ΔG (kJ·mol^{-1})	ΔH (kJ·mol^{-1})	$-T\Delta S$ (kJ·mol^{-1})
$\mathbf{11}^+$	CH_3	(6.4 ± 0.5) × 10^4	−27.4 ± 0.5	−37.0	9.6
$\mathbf{12}^+$	OMe	(8.8 ± 1.1) × 10^4	−28.2 ± 0.7	−38.1	9.8
$\mathbf{13}^+$	SMe	(2.3 ± 0.2) × 10^5	−30.6 ± 0.7	−50.1	19.5
$\mathbf{14}^+$	*t*-Bu	(2.3 ± 0.6) × 10^4	−24.9 ± 0.5	−40.7	15.8
$\mathbf{15}^+$	F	(1.2 ± 0.1) × 10^5	−29.0 ± 0.7	−35.6	6.6
$\mathbf{16}^+$	Cl	(2.2 ± 0.3) × 10^5	−30.6 ± 0.8	−37.3	6.7
$\mathbf{17}^+$	Br	(3.4 ± 0.2) × 10^5	−31.5 ± 0.8	−39.0	7.5
$\mathbf{18}^+$	I	(4.9 ± 0.7) × 10^5	−32.5 ± 0.9	−40.0	7.5
$\mathbf{19}^+$	CN	(8.6 ± 1.5) × 10^4	−28.2 ± 0.7	−32.4	4.2
$\mathbf{20}^+$	CF_3	(1.9 ± 0.2) × 10^5	−30.1 ± 0.9	−37.4	7.3
$\mathbf{21}^+$	NO_2	(1.2 ± 0.1) × 10^5	−30.4 ± 0.5	−32.6	3.2

4.9×10^5 M^{-1} at 25 °C. It is interesting to note that although the substituents of guests **12**$^+$ and **19**$^+$ are quite different in view of their electronic properties, they share very similar binding affinities.

What is the underlying reason for the response of binding affinities to the electronic substituent effect on the guests? Luckily, single crystals of complexes **14**$^+$**@ZB4-III**, **16**$^+$**@ZB4-III**, **18**$^+$**@ZB4-III**, and **21**$^+$**@ZB4-III** suitable for X-ray single crystallography, were obtained and their crystal structures are shown in Figure 3. The substituents of these four guests located at three representative positions in Figure 2. Therefore, a closer look at their crystal structures may provide an explanation for their surprising binding behaviors. Multiple non-covalent interactions, including C–H···O hydrogen bonds, cation···π, C–H···π and π···π interactions, are involved in all the cases. Undoubtedly, cation···π interactions between the core quaternary ammonium ions of the guests and the four naphthalene rings of the host should still be the major driving force as mentioned above. However, it was noticed that the distances between diagonal linker oxygen atoms in the backbone of the host are slightly different for the four complexes. These interactions may be tuned by the size of the host cavity. As shown in Figure 3 (bottom), the vertical and horizontal distances between the diagonal oxygen atoms are different for all the four complexes. This distance is presumably tuned through the C–H···O hydrogen bonds between the CH_2–O–CH_2 oxygen atoms and the aromatic protons of the guests. The acidities of aromatic protons on the guests are, however, influenced by the substituents. Indeed, the electron-withdrawing nitro group and the electron-donating *tert*-butyl group both result in shorter C–H···O hydrogen bonds than the chloro and iodo groups do. The cavity sizes of **ZB4** in complexes **16**$^+$**@ZB4-III** and **18**$^+$**@ZB4-III** may be better suited than those of **14**$^+$**@ZB4-III** and **21**$^+$**@ZB4-III** to host the quaternary ammonium and maximize all the non-covalent interactions. Any deviation from these cavity sizes weakens the binding. That is, the secondary C–H···O hydrogen bonds can be tuned through the substituents to leverage the primary cation···π interactions and thus the final binding affinities. This may explain the parabolic distribution of binding affinities over the Hammett parameters (σ_p) of the substituents as shown in Figure 2. The conformational adaptivity or flexibility allows **ZB4** to adapt according to the need of the guests. Simultaneously, the guest may also conformationally adapt to better interact with **ZB4**. As shown in Figure 4, the crystal structure of **18**$^+$ in **18**$^+$**@ZB4-III** is slightly different in shape from free cation **18**$^+$.

In addition, thermodynamic parameters at different temperatures for the complex between **ZB4** and **18**$^+$ were determined by ITC experiments (Figure S27 in Supporting Information File 1).

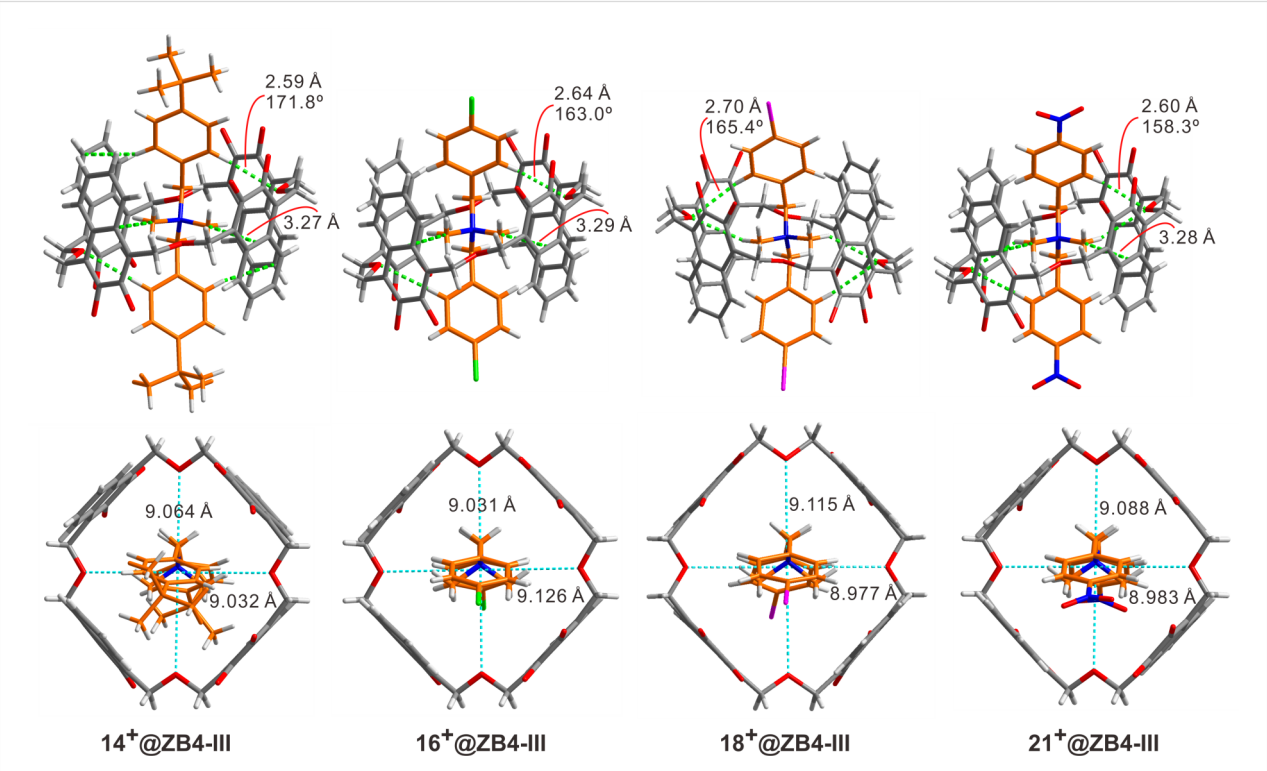

Figure 3: X-ray single crystal structures of **14**$^+$**@ZB4-III**, **16**$^+$**@ZB4-III**, **18**$^+$**@ZB4-III** and **21**$^+$**@ZB4-III**. Butyl groups of the host are removed for viewing clarity.

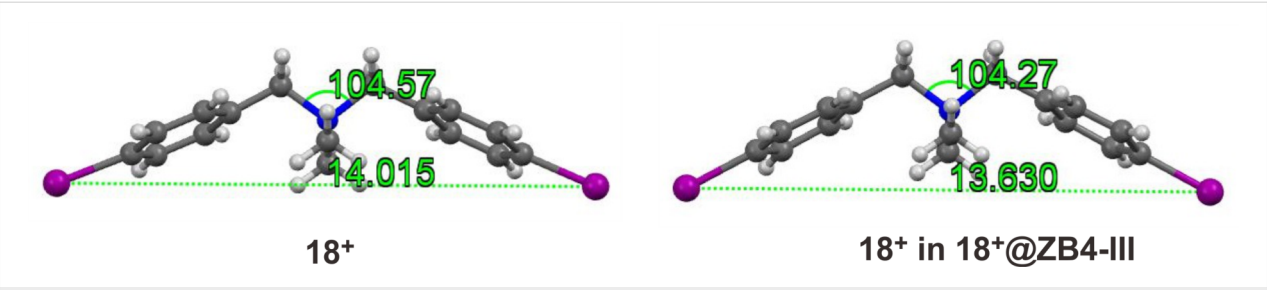

Figure 4: X-ray single crystal structures of **18⁺@ZB4-III** and **18⁺** in **18⁺@ZB4-III**.

The data are compiled in Table 3. The heat capacity change (ΔC_p) for the formation of **18⁺@ZB4** is −0.13 kJ mol^{-1} K^{-1} as determined from the slope of the linear fitting in plots of ΔH versus temperature from 283 to 313 K (Figure 5). The release of solvent molecules upon complex formation may account for the negative heat capacity change and similar heat capacity changes were also reported for the fullerenes recognition [40]. Meanwhile, the changes of ΔG for the formation of **18⁺@ZB4** complex over the temperature range 283–313 K is very small (0.31 kJ mol^{-1}), while the changes in ΔH and $-T\Delta S$ are much larger (ca. 4–4.3 kJ mol^{-1}). The changes in ΔH and $-T\Delta S$ are opposite in signs and perfectly compensate each other. The enthalpy–entropy compensation phenomenon may be explained by invoking a solvent reorganization during the formation of **18⁺@ZB4** complex, which is common for reactions taking place in aqueous solution [41].

Conclusion

In summary, we systematically studied the guest binding scope, electronic substituent effects and thermodynamic origin on the molecular recognition of **ZB4** using NMR, ITC titration and X-ray crystallography. Similar to **TA4**, **ZB4** is able to host a

Table 3: Thermodynamic parameters for the complex between **18⁺** and **ZB4** as determined by ITC in a 1:1 mixture of 1,2-dichloroethane and MeCN at different temperatures.

T (K)	K_a (M^{-1})	ΔG (kJ·mol^{-1})	ΔH (kJ·mol^{-1})	$-T\Delta S$ (kJ·mol^{-1})
283	8.4 × 10^5	−32.09	−38.59	6.50
293	5.2 × 10^5	−32.04	−39.96	7.92
298	4.2 × 10^5	−32.10	−40.72	8.62
303	3.3 × 10^5	−32.01	−41.19	9.18
308	2.6 × 10^5	−31.88	−42.08	10.2
313	2.0 × 10^5	−31.78	−42.58	10.8

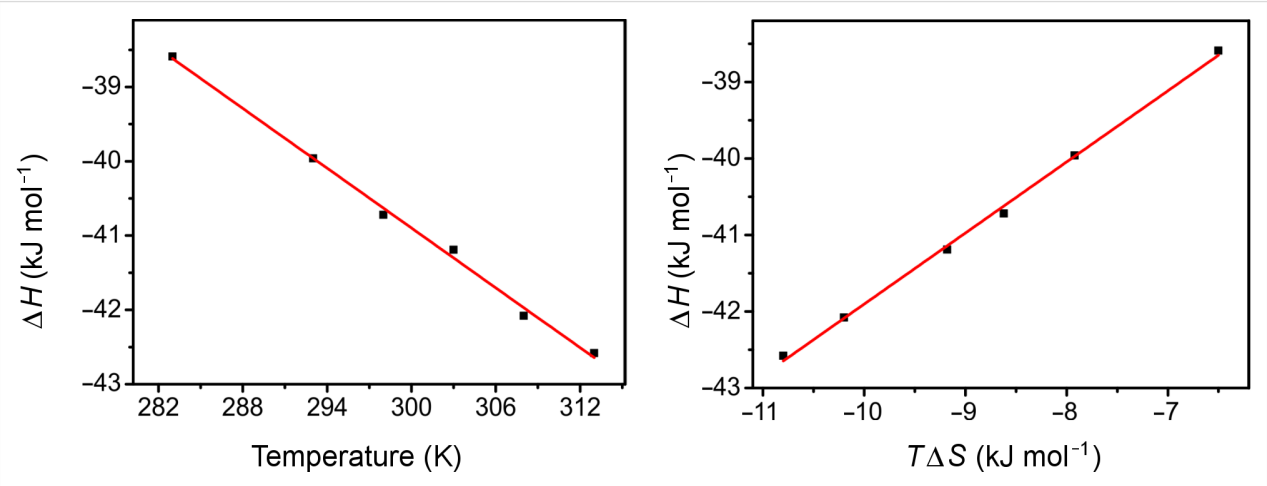

Figure 5: Linear relationships of ΔH with temperature (left, slope = −0.13, R^2 = 0.9956) and $T\Delta S$ (right, slope = 0.93, R^2 = 0.9976).

wide range of organic cations. However, in contrast to **TA4**, **ZB4** shows no large amplitude of conformational response to the electronic nature of substituents on the guests, and its binding affinities follow a parabolic rather than a linear free energy relationship. A closer look at four representative crystal structures suggested that the parabolic free energy relationship may be caused through influencing the major interactions in the host–guest complexes by tuning the weak C–H···O hydrogen bonds. Heat capacity changes and enthalpy–entropy compensation indicate that solvent reorganization is also involved during the host–guest binding. Generally, **ZB4** is quite different from **TA4**, and further enriches the arsenal of conformationally adaptive macrocycles. With these model systems, we may further understand the importance of conformational adaptivity in biomolecular recognition and even design stimuli-responsive materials by harnessing this large amplitude of conformational changes.

Supporting Information

Supporting Information File 1

Experimental procedures, NMR spectra, mass spectra, determination of association constants and X-ray single crystal data.
[https://www.beilstein-journals.org/bjoc/content/supplementary/1860-5397-14-134-S1.pdf]

Acknowledgements

This research was financially supported by the National Natural Science foundation of China (WJ: Nos. 21572097 and 21772083), Thousand Young Talents Program (WJ), and SZSTI (WJ: Nos. JCYJ20160226192118056, JCYJ20170307105848463, and KQJSCX20170728162528382). Academy of Finland (AV: project no. 314343) is also acknowledged for funding. We thank SUSTech-MCPC for the support with instruments.

ORCID® iDs

Arto Valkonen - https://orcid.org/0000-0003-2806-3807
Kari Rissanen - https://orcid.org/0000-0002-7282-8419

References

1. Schrader, T.; Hamilton, A. D. *Functional Synthetic Receptors;* Wiley-VCH: Weinheim, Germany, 2005. doi:10.1002/352760572X
2. Rambo, B. M.; Gong, H.-Y.; Oh, M.; Sessler, J. L. *Acc. Chem. Res.* **2012,** *45,* 1390–1401. doi:10.1021/ar300076b
3. Lee, S.; Chen, C.-H.; Flood, A. H. *Nat. Chem.* **2013,** *5,* 704–710. doi:10.1038/nchem.1668
4. Ogoshi, T.; Yamagishi, T.-a.; Nakamoto, Y. *Chem. Rev.* **2016,** *116,* 7937–8002. doi:10.1021/acs.chemrev.5b00765
5. Chen, H.; Fan, J.; Hu, X.; Ma, J.; Wang, S.; Li, J.; Yu, Y.; Jia, X.; Li, C. *Chem. Sci.* **2015,** *6,* 197–202. doi:10.1039/C4SC02422B
6. Liu, H.-B.; Zhang, Q.; Wang, M.-X. *Angew. Chem., Int. Ed.* **2018,** *57,* 6536–6540. doi:10.1002/anie.201802650
7. Zhang, G.-W.; Li, P.-F.; Meng, Z.; Wang, H.-X.; Han, Y.; Chen, C.-F. *Angew. Chem., Int. Ed.* **2016,** *55,* 5304–5308. doi:10.1002/anie.201600911
8. Svec, J.; Necas, M.; Sindelar, V. *Angew. Chem., Int. Ed.* **2010,** *49,* 2378–2381. doi:10.1002/anie.201000420
9. Gao, B.; Tan, L.-L.; Song, N.; Li, K.; Yang, Y.-W. *Chem. Commun.* **2016,** *52,* 5804–5807. doi:10.1039/C6CC01892K
10. Zhu, H.; Shi, B.; Chen, K.; Wei, P.; Xia, D.; Mondal, J. H.; Huang, F. *Org. Lett.* **2016,** *18,* 5054–5057. doi:10.1021/acs.orglett.6b02500
11. Jiang, B.; Wang, W.; Zhang, Y.; Lu, Y.; Zhang, C.-W.; Yin, G.-Q.; Zhao, X.-L.; Xu, L.; Tan, H.; Li, X.; Jin, G.-X.; Yang, H.-B. *Angew. Chem., Int. Ed.* **2017,** *56,* 14438–14442. doi:10.1002/anie.201707209
12. Cram, D. J. *Angew. Chem., Int. Ed. Engl.* **1986,** *25,* 1039–1057. doi:10.1002/anie.198610393
13. Koshland, D. E., Jr. *Nat. Med.* **1998,** *4,* 1112–1114. doi:10.1038/2605
14. Tama, F.; Sanejouand, Y.-H. *Protein Eng.* **2001,** *14,* 1–6. doi:10.1093/protein/14.1.1
15. Kremer, C.; Lützen, A. *Chem. – Eur. J.* **2013,** *19,* 6162–6196. doi:10.1002/chem.201203814
16. Yuan, Y.; Tam, M. F.; Simplaceanu, V.; Ho, C. *Chem. Rev.* **2015,** *115,* 1702–1724. doi:10.1021/cr500495x
17. Changeux, J.-P.; Edelstein, S. J. *Science* **2005,** *308,* 1424–1428. doi:10.1126/science.1108595
18. Ikeda, A.; Shinkai, S. *Chem. Rev.* **1997,** *97,* 1713–1734. doi:10.1021/cr960385x
19. Wang, M.-X. *Acc. Chem. Res.* **2012,** *45,* 182–195. doi:10.1021/ar200108c
20. Kim, D. S.; Sessler, J. L. *Chem. Soc. Rev.* **2015,** *44,* 532–546. doi:10.1039/C4CS00157E
21. Talotta, C.; Gaeta, C.; Qi, Z.; Schalley, C. A.; Neri, P. *Angew. Chem., Int. Ed.* **2013,** *52,* 7437–7441. doi:10.1002/anie.201301570
22. Talotta, C.; Gaeta, C.; De Rosa, M.; Ascenso, J. R.; Marcos, P. M.; Neri, P. *Eur. J. Org. Chem.* **2016,** 158–167. doi:10.1002/ejoc.201501319
23. Galan, A.; Escudero-Adán, E. C.; Frontera, A., II; Ballester, P. *J. Org. Chem.* **2014,** *79,* 5545–5557. doi:10.1021/jo5007224
24. Yang, L.-P.; Liu, W.-E.; Jiang, W. *Tetrahedron Lett.* **2016,** *57,* 3978–3985. doi:10.1016/j.tetlet.2016.07.077
25. Huang, G.; He, Z.; Cai, C.-X.; Pan, F.; Yang, D.; Rissanen, K.; Jiang, W. *Chem. Commun.* **2015,** *51,* 15490–15493. doi:10.1039/C5CC06768E
26. Huang, G.; Valkonen, A.; Rissanen, K.; Jiang, W. *Chem. Commun.* **2016,** *52,* 9078–9081. doi:10.1039/C6CC00349D
27. Huang, G.-B.; Wang, S.-H.; Ke, H.; Yang, L.-P.; Jiang, W. *J. Am. Chem. Soc.* **2016,** *138,* 14550–14553. doi:10.1021/jacs.6b09472
28. Wang, L.-L.; Chen, Z.; Liu, W.-E.; Ke, H.; Wang, S.-H.; Jiang, W. *J. Am. Chem. Soc.* **2017,** *139,* 8436–8439. doi:10.1021/jacs.7b05021
29. Huang, G.-B.; Liu, W.-E.; Valkonen, A.; Yao, H.; Rissanen, K.; Jiang, W. *Chin. Chem. Lett.* **2018,** *29,* 91–94. doi:10.1016/j.cclet.2017.07.005
30. Ma, Y.-L.; Ke, H.; Valkonen, A.; Rissanen, K.; Jiang, W. *Angew. Chem., Int. Ed.* **2018,** *57,* 709–713. doi:10.1002/anie.201711077

31. Jia, F.; He, Z.; Yang, L.-P.; Pan, Z.-S.; Yi, M.; Jiang, R.-W.; Jiang, W. *Chem. Sci.* **2015,** *6,* 6731–6738. doi:10.1039/C5SC03251B
32. Jia, F.; Wang, H.-Y.; Li, D.-H.; Yang, L.-P.; Jiang, W. *Chem. Commun.* **2016,** *52,* 5666–5669. doi:10.1039/C6CC01052K
33. Yang, L.-P.; Liu, H.; Lu, S.-B.; Jia, F.; Jiang, W. *Org. Lett.* **2017,** *19,* 1212–1215. doi:10.1021/acs.orglett.7b00181
34. Jia, F.; Yang, L.-P.; Li, D.-H.; Jiang, W. *J. Org. Chem.* **2017,** *82,* 10444–10449. doi:10.1021/acs.joc.7b01914
35. Jia, F.; Li, D.-H.; Yang, T.-L.; Yang, L.-P.; Dang, L.; Jiang, W. *Chem. Commun.* **2017,** *53,* 336–339. doi:10.1039/C6CC09038A
36. Yang, L.-P.; Jia, F.; Pan, F.; Pan, Z.-S.; Rissanen, K.; Jiang, W. *Chem. Commun.* **2017,** *53,* 12572–12575. doi:10.1039/C7CC07630D
37. Yang, L.-P.; Jia, F.; Zhou, Q.-H.; Pan, F.; Sun, J.-N.; Rissanen, K.; Chung, L. W.; Jiang, W. *Chem. – Eur. J.* **2017,** *23,* 1516–1520. doi:10.1002/chem.201605701
38. Tran, A. H.; Miller, D. O.; Georghiou, P. E. *J. Org. Chem.* **2005,** *70,* 1115–1121. doi:10.1021/jo0484427
39. Hansch, C.; Leo, A.; Taft, R. W. *Chem. Rev.* **1991,** *91,* 165–195. doi:10.1021/cr00002a004
40. Le, V. H.; Yanney, M.; McGuire, M.; Sygula, A.; Lewis, E. A. *J. Phys. Chem. B* **2014,** *118,* 11956–11964. doi:10.1021/jp5087152
41. Adriaenssens, L.; Gil-Ramírez, G.; Frontera, A.; Quiñonero, D.; Escudero-Adán, E. C.; Ballester, P. *J. Am. Chem. Soc.* **2014,** *136,* 3208–3218. doi:10.1021/ja412098v

License and Terms

BEILSTEIN JOURNAL OF ORGANIC CHEMISTRY

Synthesis of diamido-bridged bis-pillar[5]arenes and tris-pillar[5]arenes for construction of unique [1]rotaxanes and bis-[1]rotaxanes

Ying Han, Li-Ming Xu, Cui-Yun Nie, Shuo Jiang, Jing Sun and Chao-Guo Yan*

Full Research Paper

Open Access

Address:
College of Chemistry & Chemical Engineering, Yangzhou University, Yangzhou 225002, P. R. China

Email:
Chao-Guo Yan* - cgyan@yzu.edu.cn

* Corresponding author

Keywords:
bis-[1]rotaxane; mechanically interlocked molecule; pillar[5]arene; [1]rotaxane; self-assembly

Beilstein J. Org. Chem. **2018,** *14,* 1660–1667.
doi:10.3762/bjoc.14.142

Received: 17 April 2018
Accepted: 20 June 2018
Published: 04 July 2018

This article is part of the thematic issue "Macrocyclic and supramolecular chemistry".

Guest Editor: M.-X. Wang

Abstract

The pillar[5]arene mono- and di(oxyalkoxy)benzoic acids were successfully prepared in high yields by sequential alkylation of ω-bromoalkoxy-substituted pillar[5]arenes with methyl or ethyl *p*-hydroxybenzoate followed by a hydrolytic reaction under basic conditions. Under catalysis of HOBt/EDCl, the amidation reaction of pillar[5]arene mono(oxybutoxy)benzoic acid with monoamido-functionalized pillar[5]arenes afforded diamido-bridged bis-pillar[5]arenes. ^{1}H NMR and 2D NOESY spectra clearly indicated that [1]rotaxanes were formed by insertion of longer diaminoalkylene unit into the cavity of one pillar[5]arene with another pillar[5]arene acting as a stopper. The similar catalysed amidation reaction of pillar[5]arene di(oxybutoxy)benzoic acid with monoamido-functionalized pillar[5]arenes resulted in the diamido-bridged tris-pillar[5]arenes, which successfully form the unique bis-[1]rotaxanes bearing longer than diaminopropylene diamido bridges.

Introduction

The construction and dynamic motion of the mechanically interlocked molecules (MIMs) have attracted significant research interests due to their intrinsic self-assembled nature and potential applications in various aspects [1-4]. Pseudo[1]rotaxane and [1]rotaxane are one of particular supramolecular assembly system and are considered as an important building block in the construction of diverse MIMs [5-10]. [1]Rotaxane has a macrocyclic wheel component connected with a self-locked chain axle, and a bulky stopper at the terminal axle to prevent dissociation of the subcomponents. In recent years, many effects have been devoted to the construction and functionalization of pseudo[1]rotaxanes and [1]rotaxanes [11-20]. For this purpose, the well-known macrocycles such as crown ether [21-23], cyclodextrin [24-26], calixarene [27-29] and pillararene have

been successfully employed as the wheel subcomponent. Pillararenes are new star macrocyclic compounds with aromatic rings *para*-bridged by methylene units and have unique tubular shape rather than cone [30-32]. In recent years, an explosive development on the construction of various supramolecular devices and diverse responsive materials has been reported by using diverse functionalized pillararenes [33-35]. Due to easily preparation and suitable cavity, functionalized pillar[5]arenes were widely used as wheel component for constructing of the various interlocked molecules [36-42]. In the past few years, many elegant works on the construction of pseudo[1]rotaxanes and [1]rotaxanes have been developed on the basis of various mono-functionalized pillar[5]arenes [43-57]. Recently, we have successfully constructed a couple of pseudo[1]rotaxane and [1]rotaxane both in solution and in solid state developed by using mono-functionalized pillar[5]arene Schiff base, urea and pyridylimine derivatives [58-63]. In continuation of our effort on the development on the construction of [1]rotaxanes via various mono-functionalized pillar[5]arene derivatives, herein we wish to report the convenient synthesis of diamido-bridged bis-pillar[5]arenes and tris-pillar[5]arenes as well as formation of unique [1]rotaxanes and bis-[1]rotaxanes.

Results and Discussion

The synthetic route for the pillar[5]arene mono(oxyalkoxy)benzoic acids was illustrated in Scheme 1. Firstly, the alkylation of mono(bromoalkoxy)pillar[5]arene **1a**–**c** (n = 4, 5, 6) [64] with methyl or ethyl *p*-hydroxybenzoate was carried out in the refluxed medium of $KI/K_2CO_3/CH_3CN$ for one day. The pillar[5]arene mono(oxyalkoxy)benzoates **2a**–**f** were successfully prepared in high yields. Then, basic hydrolysis of pillar[5]arene mono(oxyalkoxy)benzoates **2a**–**f** in ethanol in the presence of potassium hydroxide afforded the desired pillar[5]arene mono(oxyalkoxy)benzoic acids **3a**–**c**. The structures of the prepared pillar[5]arenes **2a**–**f** and **3a**–**c** were fully characterized by the spectroscopic methods. The single crystal structures of the pillar[5]arenes **2a** (Figure 1), **2c**, **2d**, **2e** (Supporting Information File 1, Figure S1–S3) and **2f** (Figure 2) were successfully determined by X-ray diffraction. The same structural feature was obtained in the five single crystals. That is, the longer chain of methyl (ethyl) oxyalkoxybenzoate not only does not inserted in the cavity of the pillar[5]arene to form the pseudo[1]rotaxane, but also does not thread to the cavity of the neighbouring pillar[5]arene to form the supramolecular polymer. This result is consistent to the Cao's previously reported results in the series of pillar[5]arenes bearing aliphatic esters [49], in that they found the chain of methyl oxybutyrate did not threaded into the cavity of pillar[5]arene.

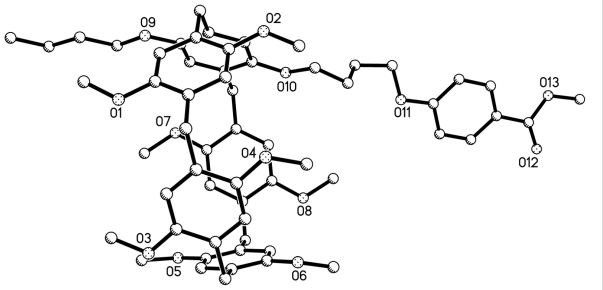

Figure 1: single crystal structure of pillar[5]arene **2a**.

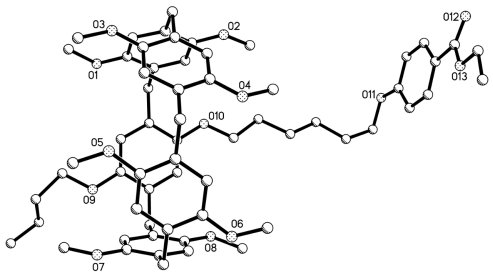

Figure 2: Single crystal structure of pillar[5]arene **2f**.

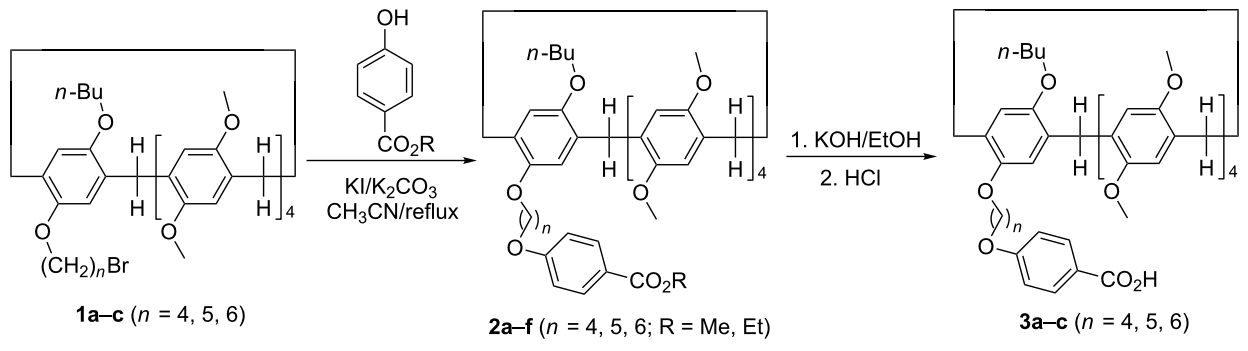

Scheme 1: Synthesis of pillar[5]arene mono(oxyalkoxy)benzoic acids **3a**–**c**.

The above synthetic pillar[5]arene mono(oxyalkoxy)benzoic acids have a longer chain functionalized group and a large macrocycle, which enabled them to be a good candidate as an efficient terminal stopper for the construction of rotaxanes. Therefore, the amidation reaction of pillar[5]arene mono(oxybutoxy)benzoic acid **3a** with our previously reported amido-functionalized pillar[5]arenes **4a**–**d** (*n* = 2, 3, 4, 6) [58] was carried out in chloroform under the combined catalysis of 1-hydroxybenzotrizole (HOBt) and 1-(3-dimethylaminopropyl)-3-ethylcarbodiimide hydrochloride (EDCl). The reaction proceeded smoothly to give diamido-bridged bis-pillar[5]arenes **5a**–**d** (*n* = 2, 3, 4, 6) in moderate yields (Scheme 2). It has been reported that the chain of *N*-(ω-aminoalkyl)oxyacetamide inserted in the cavity of pillar[5]arene in the amido-functionalized pillar[5]arene **4a**–**d** (*n* = 2, 3, 4, 6) to form pseudo[1]rotaxanes both in solution and in solid state [58]. The diamido-bridged bis-pillar[5]arenes **5a**–**d** might form the expected [1]rotaxanes. ^{1}H NMR spectrum of the bis-pillar[5]arenes **5a** clearly showed that there is no any signals at very high magnetic field (δ < 0), which indicated that the diaminoethylene chain does not inserted in the cavity of pillar[5]arene to form the expected [1]rotaxane. Therefore, the two moieties of pillar[5]arenes are just connected by the diaminoethylene chain from the outside in diamido-bridged bis-pillar[5]arenes **5a**. However, a couple of characteristic signals at very high magnetic field can be seen in the ^{1}H NMR spectra of the bis-pillar[5]arenes **5b**–**d**. There is a broad singlet at −1.82 ppm in **5b**, a mixed peak at −1.88 to −2.14 ppm in **5c** and several peaks in the range of 0.07 to −2.07 ppm in **5d**. This result clearly displayed that the unique [1]rotaxane structures were actually formed by threading the longer diaminoalkylene bridge in the cavity of one molecular pillar[5]arene, while another pillar[5]arene as the bigger stopper. Additionally, 2D NOESY spectra of the compound **5d** provided more strong evidence for the formation of [1]rotaxane (Figure 3). The NOE correlations were clearly observed between Ha, Hb, Hc, Hd, and He protons of the bridging hexylene chain with the proton Hf in the core of pillar[5]arene. The proton Hb of the bridging hexylene chain also correlated with protons of the aromatic protons Hg and Hf.

According to similar reaction procedure for the synthesis of pillar[5]arene mono(oxyalkoxy)benzoic acids **3a**–**c**, pillar[5]arene di(oxybutoxy)benzoic acid **8** was prepared in moderate yield from sequential alkylation and basic hydrolysis reaction (Scheme 3). The single crystal structure of the

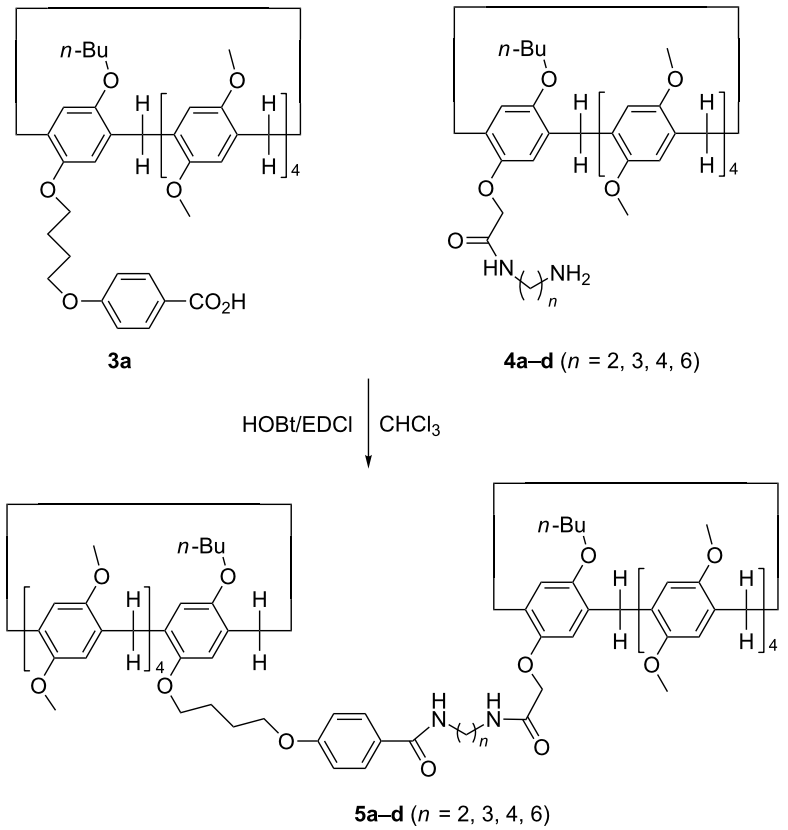

Scheme 2: Synthesis of diamido-bridged bis-pillar[5]arenes **5a**–**d**.

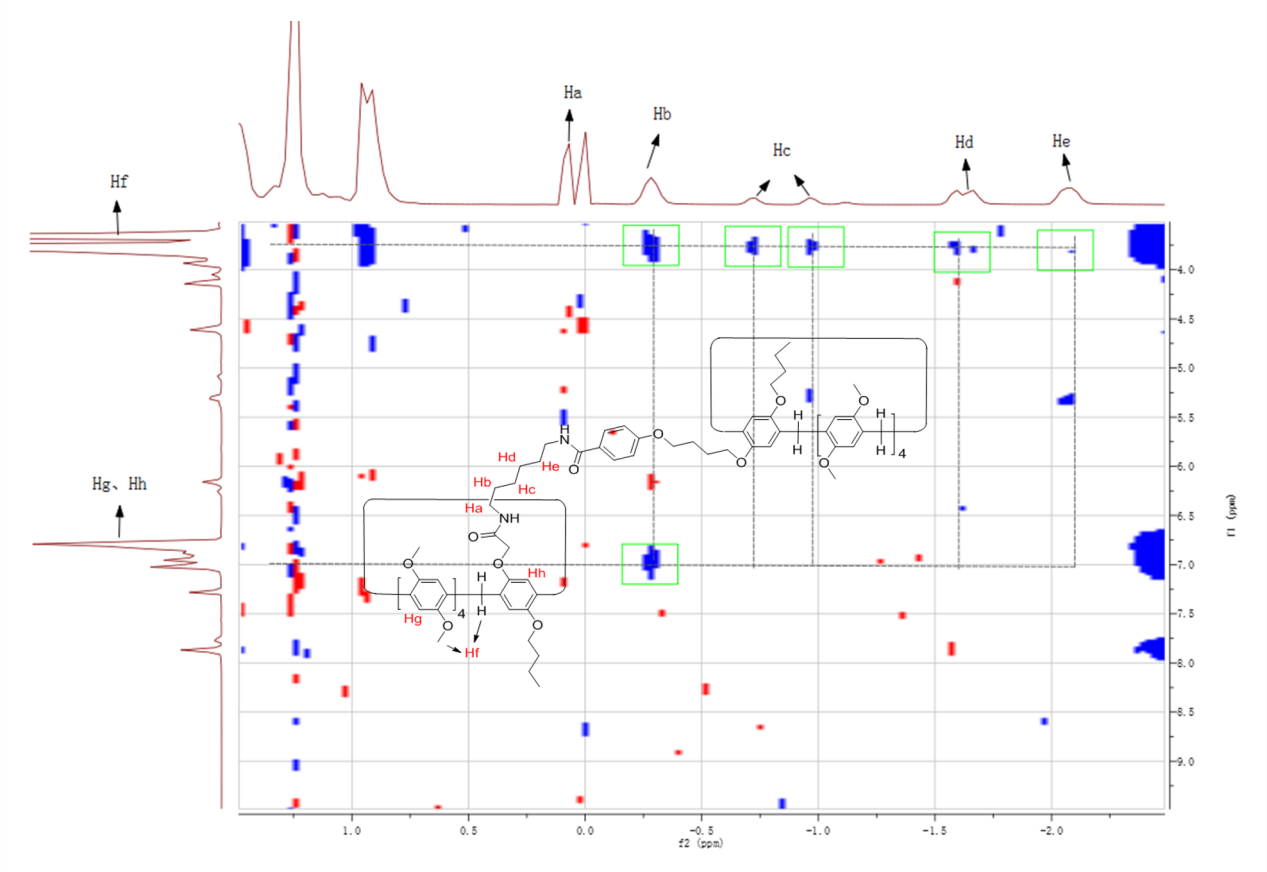

Figure 3: The 2D NOSEY spectrum of bis-pillar[5]arene **5d**.

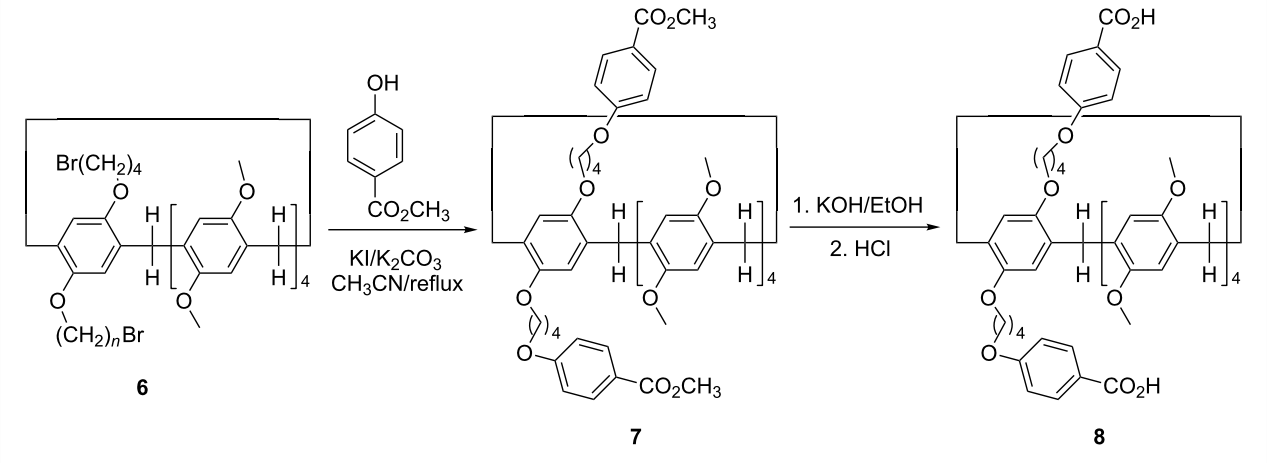

Scheme 3: Synthesis of pillar[5]arene di(oxyalkoxy)benzoic acid **8**.

pillar[5]arene di(oxybutoxy)benzoate **7** showed that the two chains of methyl oxybutoxybenzoate did not insert in the cavity of pillar[5]arene (Figure 4) as that of the above mentioned pillar[5]arene mono(oxybutoxy)benzoates **2a**–**f**. The two chains straight stretched to the opposite direction of central pillar[5]arene. It might be attribute to the electron-rich effect of the methyl oxybutoxybenzoate unit, which kept it away from the electron-rich cavity of pillar[5]arene.

Under the combined catalysis of HOBT and EDCl, the amide reaction of pillar[5]arene di(oxybutoxy)benzoic acid **8a** with two molecular amido-functionalized pillar[5]arenes **4a**–**d** in

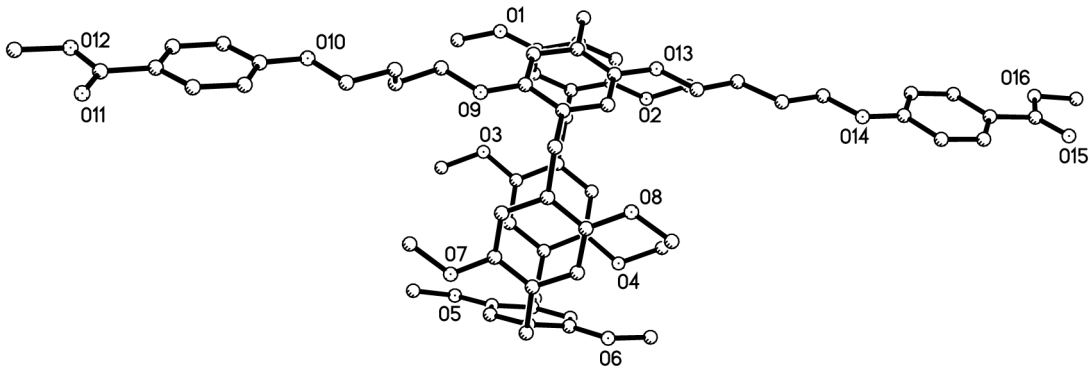

Figure 4: Single crystal structure of pillar[5]arene **7**.

chloroform afforded tris-pillar[5]arenes **9a**–**d** in moderate yields (Scheme 4). The structures of the synthetic tris-pillar[5]arenes **9a**–**d** were fully characterized by IR, HRMS, ^{1}H and ^{13}C NMR spectra. The ^{1}H NMR spectra provided stronger evidence for the formation of fascinating bis-[1]rotaxanes. Because there are no peaks with negative chemical shift in the ^{1}H NMR spectra of the tris-pillar[5]arene **9a**, it can be concluded that the three pillar[5]arenes are connected from the outsides by two diamidoethylene-bridges. There is one broad peak at −1.80 ppm in tris-pillar[5]arene **9b**, a mixed peak at −2.00 ppm in tris-pillar[5]arene **9c**, and five broad peaks at −0.29 ppm, −0.74 ppm, −0.97 ppm, −1.62 ppm and −2.08 ppm in tris-pillar[5]arene **9d**. Therefore, ^{1}H NMR spectra of **9b**–**d** indicated that the diaminoalkylene chain ambiguously inserted in the

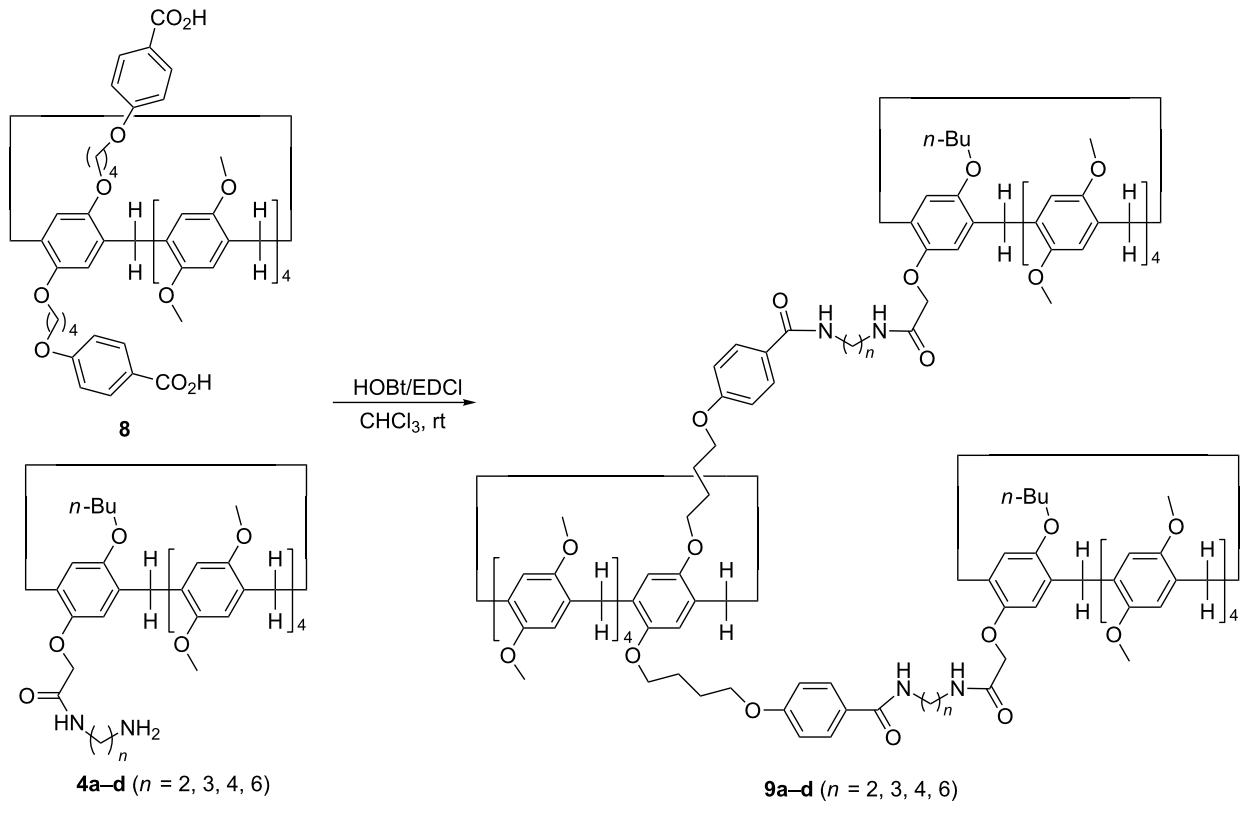

Scheme 4: Synthesis of diamido-bridged tris-pillar[5]arenes **9a**–**d**.

cavity of the pillar[5]arene. In other words, the fascinating bis-[1]rotaxane structures were formed in the tris-pillar[5]arenes **9b**–**d**. Here, the lengths of bridging chains played the critical role in the selflocked behaviour of pillar[5]arene-based [1]rotaxanes.

In order to confirm the formation of the bis-[1]rotaxanes, 2D NOESY spectra of the compounds **9a**–**d** were recorded. The 2D NOESY spectrum of compound **9d** was showed in Figure 5. There it can be seen that the NOE correlations were clearly observed between Ha, Hb, Hc, Hd, Hf, Hg, Hh protons of the bridging diaminohexylene chain and the protons Hi, Hj in the core of pillar[5]arene. Additionally, some correlations exists between protons Ha, He, Hd and Hh and active amino (N–H) group. These NOE correlations clearly indicated the two bridged diaminohexylene chain threading into the cavity of the two pillar[5]arenes to form the bis-[1]rotaxane. The similar correlations were also observed in the NOESY spectra of the tris-pillar[5]arene **9b** and **9c** (see Supporting Information File 1, Figures S5 and S6). However, there is no such correlation in the 2D NOESY spectrum of the compound **9a** (see Supporting Information File 1, Figure S4), which confirmed that the diamidoethylene bridge did not insert to the cavity of the pillar[5]arene to form [1]rotaxanes. Thus, the 2D NOESY spectra provided stronger evidence for the formation of novel bis-[1]rotaxanes for the tris-pillar[5]arenes **9c**–**d** bearing longer than diaminopropylene diamido-bridges.

Conclusion

In summary, we have conveniently prepared several pillar[5]arene mono- and di(oxyalkoxy)benzoic acids and found that the chain of alkyl oxyalkoxybenzoate did not inserted to the cavity of pillar[5]arene. More importantly, a series of diamido-bridged bis-pillar[5]arenes and tris-pillar[5]arenes were efficiently synthesized by catalyzed amidation reaction of pillar[5]arene mono- and di(oxybutoxy)benzoic acids with monoamide-functionalized pillar[5]arenes. On the basis of ^{1}H NMR and 2D NOESY spectra, we successfully concluded that the chains longer than diaminopropylene threaded into the one or two cavities of the pillar[5]arenes to form the unique [1]rotaxane and bis-[1]rotaxanes. This work not only provided a fundamental self-assembly of the mechanically interlocked molecules, but also developed the potential applications of pillar[5]arene in supramolecular chemistry. The design and construction of diverse mechanically interlocked molecules are underway in our laboratory.

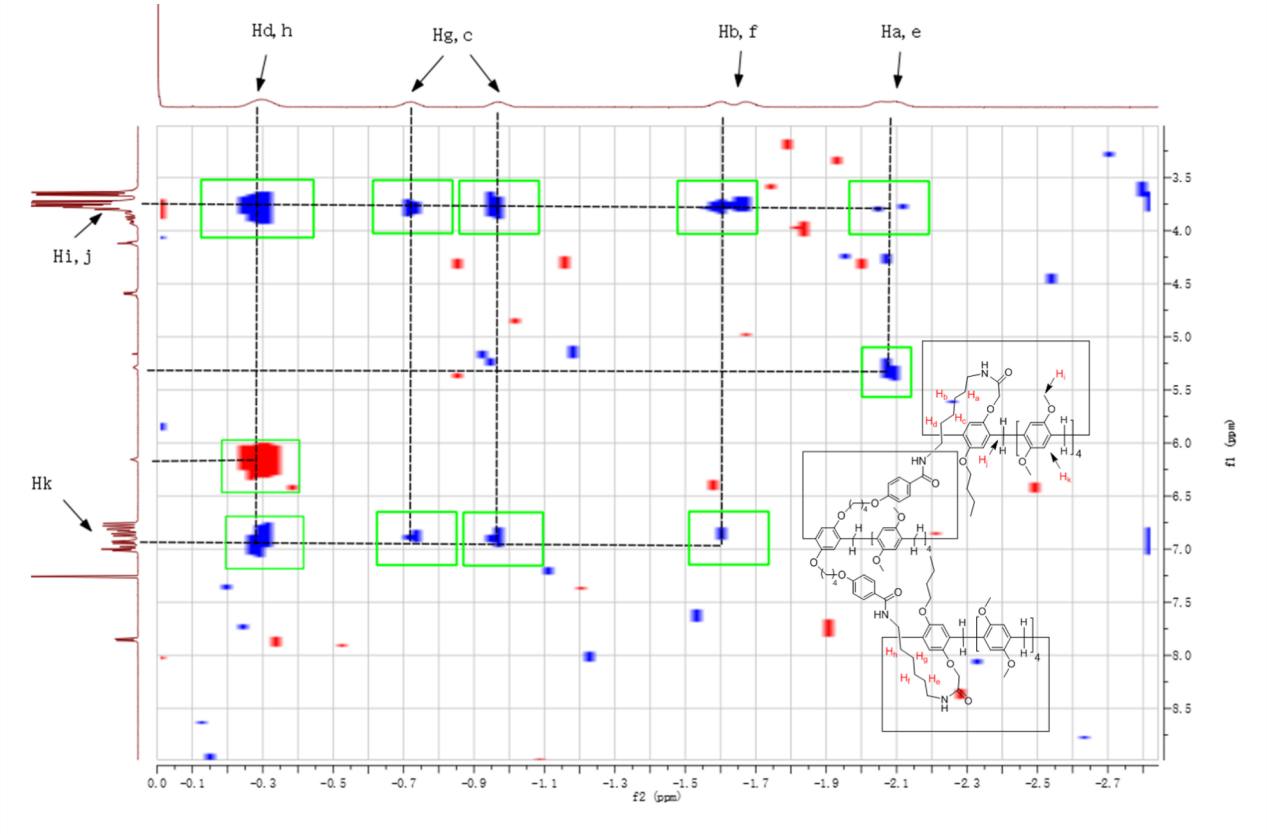

Figure 5: The 2D NOSEY spectra of tris-pillar[5]arene **9d**.

Supporting Information

Experimental procedures, analytical data, and copies of the ^{1}H and ^{13}C NMR spectra, HRMS spectra for all new products. Single crystal data for **2a** (CCDC: 1837205), **2c** (CCDC: 1837206), **2d** (CCDC: 1837207), **2e** (CCDC: 1837208), **2f** (CCDC: 1837209) and **7** (CCDC: 1846692) have been deposited at the Cambridge Crystallographic Data Centre.

Supporting Information File 1

Experimental and analytical data.
[https://www.beilstein-journals.org/bjoc/content/supplementary/1860-5397-14-142-S1.pdf]

Acknowledgements

We are grateful to the financial support by the National Natural Science Foundation of China (Grant No. 2137219) and the Priority Academic Program Development of Jiangsu Higher Education Institutions.

References

1. Wenz, G.; Han, B. H.; Müller, A. *Chem. Rev.* **2006,** *106,* 782–817. doi:10.1021/cr970027+
2. Erbas-Cakmak, S.; Leigh, D. A.; McTernan, C. T.; Nussbaumer, A. L. *Chem. Rev.* **2015,** *115,* 10081–10206. doi:10.1021/acs.chemrev.5b00146
3. Fahrenbach, A. C.; Bruns, C. J.; Li, H.; Trabolsi, A.; Coskun, A.; Stoddart, J. F. *Acc. Chem. Res.* **2014,** *47,* 482–493. doi:10.1021/ar400161z
4. Bruns, C. J.; Stoddart, J. F. *Acc. Chem. Res.* **2014,** *47,* 2186–2199. doi:10.1021/ar500138u
5. Langton, M. J.; Beer, P. D. *Acc. Chem. Res.* **2014,** *47,* 1935–1949. doi:10.1021/ar500012a
6. Zhang, M.; Yan, X.; Huang, F.; Niu, Z.; Gibson, H. W. *Acc. Chem. Res.* **2014,** *47,* 1995–2005. doi:10.1021/ar500046r
7. Qu, D.-H.; Wang, Q.-C.; Zhang, Q.-W.; Ma, X.; Tian, H. *Chem. Rev.* **2015,** *115,* 7543–7588. doi:10.1021/cr5006342
8. Xue, M.; Yang, Y.; Chi, X.; Yan, X.; Huang, F. *Chem. Rev.* **2015,** *115,* 7398–7501. doi:10.1021/cr5005869
9. Ogoshi, T.; Yamagishi, T.-a.; Nakamoto, Y. *Chem. Rev.* **2016,** *116,* 7937–8002. doi:10.1021/acs.chemrev.5b00765
10. Wang, Y.; Ping, G.; Li, C. *Chem. Commun.* **2016,** *52,* 9858–9872. doi:10.1039/C6CC03999E
11. Ma, X.; Tian, H. *Chem. Soc. Rev.* **2010,** *39,* 70–80. doi:10.1039/B901710K
12. Lewis, J. E. M.; Galli, M.; Goldup, S. M. *Chem. Commun.* **2017,** *53,* 298–312. doi:10.1039/C6CC07377H
13. Roberts, D. A.; Pilgrim, B. S.; Nitschke, J. R. *Chem. Soc. Rev.* **2018,** *47,* 626–644. doi:10.1039/C6CS00907G
14. Han, X.; Liu, G.; Liu, S. H.; Yin, J. *Org. Biomol. Chem.* **2016,** *14,* 10331–10351. doi:10.1039/C6OB01581F
15. Lewis, J. E. M.; Beer, P. D.; Loeb, S. J.; Goldup, S. M. *Chem. Soc. Rev.* **2017,** *46,* 2577–2591. doi:10.1039/C7CS00199A
16. Li, S.-H.; Zhang, H.-Y.; Xu, X.; Liu, Y. *Nat. Commun.* **2015,** *6,* No. 7590. doi:10.1038/ncomms8590
17. Chi, X.; Yu, G.; Shao, L.; Chen, J.; Huang, F. *J. Am. Chem. Soc.* **2016,** *138,* 3168–3174. doi:10.1021/jacs.5b13173
18. Eichstaedt, K.; Jaramillo-Garcia, J.; Leigh, D. A.; Marcos, V.; Pisano, S.; Singleton, T. A. *J. Am. Chem. Soc.* **2017,** *139,* 9376–9381. doi:10.1021/jacs.7b04955
19. De Bo, G.; Dolphijn, G.; McTernan, C. T.; Leigh, D. A. *J. Am. Chem. Soc.* **2017,** *139,* 8455–8457. doi:10.1021/jacs.7b05640
20. Wang, Y.; Sun, J.; Liu, Z.; Nassar, M. S.; Botros, Y. Y.; Stoddart, J. F. *Chem. Sci.* **2017,** *8,* 2562–2568. doi:10.1039/C6SC05035B
21. Hiratani, K.; Kaneyama, M.; Nagawa, Y.; Koyama, E.; Kanesato, M. *J. Am. Chem. Soc.* **2004,** *126,* 13568–13569. doi:10.1021/ja046929r
22. Ogawa, T.; Nakazono, K.; Aoki, D.; Uchida, S.; Takata, T. *ACS Macro Lett.* **2015,** *4,* 343–347. doi:10.1021/acsmacrolett.5b00067
23. Ogawa, T.; Usuki, N.; Nakazono, K.; Koyama, Y.; Takata, T. *Chem. Commun.* **2015,** *51,* 5606–5609. doi:10.1039/C4CC08982K
24. Xue, Z.; Mayer, M. F. *J. Am. Chem. Soc.* **2010,** *132,* 3274–3276. doi:10.1021/ja9077655
25. Waelés, P.; Clavel, C.; Fournel-Marotte, K.; Coutrot, F. *Chem. Sci.* **2015,** *6,* 4828–4836. doi:10.1039/C5SC01722J
26. Schröder, H. V.; Wollschläger, J. M.; Schalley, C. A. *Chem. Commun.* **2017,** *53,* 9218–9221. doi:10.1039/C7CC05259F
27. Li, H.; Zhang, H.; Zhang, Q.; Zhang, Q.-W.; Qu, D.-H. *Org. Lett.* **2012,** *14,* 5900–5903. doi:10.1021/ol302826g
28. Li, H.; Zhang, J.-N.; Zhou, W.; Zhang, H.; Zhang, Q.; Qu, D.-H.; Tian, H. *Org. Lett.* **2013,** *15,* 3070–3073. doi:10.1021/ol401251u
29. Li, H.; Li, X.; Agren, H.; Qu, D.-H. *Org. Lett.* **2014,** *16,* 4940–4943. doi:10.1021/ol502466x
30. Ma, X.; Qu, D.; Ji, F.; Wang, Q.; Zhu, L.; Xu, Y.; Tian, H. *Chem. Commun.* **2007,** 1409–1411. doi:10.1039/b615900a
31. Ma, X.; Wang, Q.; Tian, H. *Tetrahedron Lett.* **2007,** *48,* 7112–7116. doi:10.1016/j.tetlet.2007.07.209
32. Yamauchi, K.; Miyawaki, A.; Takashima, Y.; Yamaguchi, H.; Harada, A. *Org. Lett.* **2010,** *12,* 1284–1286. doi:10.1021/ol1001736
33. Ogoshi, T.; Kanai, S.; Fujinami, S.; Yamagishi, T.-a.; Nakamoto, Y. *J. Am. Chem. Soc.* **2008,** *130,* 5022–5023. doi:10.1021/ja711260m
34. Cao, D.; Kou, Y.; Liang, J.; Chen, Z.; Wang, L.; Meier, H. *Angew. Chem., Int. Ed.* **2009,** *48,* 9721–9723. doi:10.1002/anie.200904765
35. Liu, Z.; Nalluri, S. K. M.; Stoddart, J. F. *Chem. Soc. Rev.* **2017,** *46,* 2459–2478. doi:10.1039/C7CS00185A
36. Zhang, H.; Strutt, N. L.; Stoll, R. S.; Li, H.; Zhu, Z.; Stoddart, J. F. *Chem. Commun.* **2011,** *47,* 11420–11422. doi:10.1039/c1cc14934b
37. Zhang, H.; Liu, Z.; Xin, F.; Hao, A. *Chin. J. Org. Chem.* **2012,** *32,* 219–229. doi:10.6023/cjoc1107141
38. Zhang, H.; Zhao, Y. *Chem. – Eur. J.* **2013,** *19,* 16862–16879. doi:10.1002/chem.201301635
39. Zhang, H.; Ma, X.; Nguyen, K. T.; Zhao, Y. *ACS Nano* **2013,** *7,* 7853–7863. doi:10.1021/nn402777x
40. Zhang, H.; Ma, X.; Guo, J.; Nguyen, K. T.; Zhang, Q.; Wang, X.-J.; Yan, H.; Zhu, L.; Zhao, Y. *RSC Adv.* **2013,** *3,* 368–371. doi:10.1039/C2RA22123C
41. Zhang, H.; Nguyen, K. T.; Ma, X.; Yan, H.; Guo, J.; Zhu, L.; Zhao, Y. *Org. Biomol. Chem.* **2013,** *11,* 2070–2074. doi:10.1039/c2ob27340c
42. Zhang, H.; Ma, X.; Nguyen, K. T.; Zeng, Y.; Tai, S.; Zhao, Y. *ChemPlusChem* **2014,** *79,* 462–469. doi:10.1002/cplu.201300408
43. Chen, H.; Fan, J.; Hu, X.; Ma, J.; Wang, S.; Li, J.; Yu, Y.; Jia, X.; Li, C. *Chem. Sci.* **2015,** *6,* 197–202. doi:10.1039/C4SC02422B

44. Ma, J.; Meng, Q.; Hu, X.; Li, B.; Ma, S.; Hu, B.; Li, J.; Jia, X.; Li, C. *Org. Lett.* **2016,** *18,* 5740–5743. doi:10.1021/acs.orglett.6b03005
45. Sun, Y.; Fu, W.; Chen, C.; Wang, J.; Yao, Y. *Chem. Commun.* **2017,** *53,* 3725–3728. doi:10.1039/C7CC00291B
46. Li, B.; Meng, Z.; Li, Q.; Huang, X.; Kang, Z.; Dong, H.; Chen, J.; Sun, J.; Dong, Y.; Li, J.; Jia, X.; Sessler, J. L.; Meng, Q.; Li, C. *Chem. Sci.* **2017,** *8,* 4458–4464. doi:10.1039/C7SC01438D
47. Ping, G.; Wang, Y.; Shen, L.; Wang, Y.; Hu, X.; Chen, J.; Hu, B.; Cui, L.; Meng, Q.; Li, C. *Chem. Commun.* **2017,** *53,* 7381–7384. doi:10.1039/C7CC02799K
48. Ogoshi, T.; Demachi, K.; Kitajima, K.; Yamagishi, T.-a. *Chem. Commun.* **2011,** *47,* 7164–7166. doi:10.1039/c1cc12333e
49. Chen, Y.; Cao, D.; Wang, L.; He, M.; Zhou, L.; Schollmeyer, D.; Meier, H. *Chem. – Eur. J.* **2013,** *19,* 7064–7070. doi:10.1002/chem.201204628
50. Xia, B.; Xue, M. *Chem. Commun.* **2014,** *50,* 1021–1023. doi:10.1039/C3CC48014C
51. Ni, M.; Hu, X.-Y.; Jiang, J.; Wang, L. *Chem. Commun.* **2014,** *50,* 1317–1319. doi:10.1039/C3CC47823H
52. Guan, Y.; Liu, P.; Deng, C.; Ni, M.; Xiong, S.; Lin, C.; Hu, X.-Y.; Ma, J.; Wang, L. *Org. Biomol. Chem.* **2014,** *12,* 1079–1089. doi:10.1039/c3ob42044b
53. Wu, X.; Ni, M.; Xia, W.; Hu, X.-Y.; Wang, L. *Org. Chem. Front.* **2015,** *2,* 1013–1017. doi:10.1039/C5QO00159E
54. Wu, X.; Gao, L.; Sun, J.; Hu, X.-Y.; Wang, L. *Chin. Chem. Lett.* **2016,** *27,* 1655–1660. doi:10.1016/j.cclet.2016.05.004
55. Sun, C.-L.; Xu, J.-F.; Chen, Y.-Z.; Niu, L.-Y.; Wu, L.-Z.; Tung, C.-H.; Yang, Q.-Z. *Chin. Chem. Lett.* **2015,** *26,* 843–846. doi:10.1016/j.cclet.2015.05.030
56. Du, X.-S.; Wang, C.-Y.; Jia, Q.; Deng, R.; Tian, H.-S.; Zhang, H.-Y.; Meguellati, K.; Yang, Y.-W. *Chem. Commun.* **2017,** *53,* 5326–5329. doi:10.1039/C7CC02364B
57. Cheng, M.; Wang, Q.; Cao, Y.; Pan, Y.; Yang, Z.; Jiang, J.; Wang, L. *Tetrahedron Lett.* **2016,** *57,* 4133–4137. doi:10.1016/j.tetlet.2016.07.038
58. Han, Y.; Huo, G.-F.; Sun, J.; Xie, J.; Yan, C.-G.; Zhao, Y.; Wu, X.; Lin, C.; Wang, L. *Sci. Rep.* **2016,** *6,* No. 28748. doi:10.1038/srep28748
59. Huo, G.-F.; Han, Y.; Sun, J.; Yan, C.-G. *J. Inclusion Phenom. Macrocyclic Chem.* **2016,** *86,* 231–240. doi:10.1007/s10847-016-0652-x
60. Han, Y.; Huo, G.-F.; Sun, J.; Yan, C.-G.; Lu, Y.; Lin, C.; Wang, L. *Supramol. Chem.* **2017,** *29,* 547–552. doi:10.1080/10610278.2017.1287367
61. Jiang, S.; Han, Y.; Sun, J.; Yan, C.-G. *Tetrahedron* **2017,** *73,* 5107–5114. doi:10.1016/j.tet.2017.07.001
62. Jiang, S.; Han, Y.; Zhao, L.-L.; Sun, J.; Yan, C.-G. *Supramol. Chem.* **2018,** *30,* 642–647. doi:10.1080/10610278.2018.1427238
63. Jiang, S.; Han, Y.; Cheng, M.; Sun, J.; Yan, C.-G.; Jiang, J.; Wang, L. *New J. Chem.* **2018,** *42,* 7603–7606. doi:10.1039/c7nj05192a
64. Yin, C.-B.; Han, Y.; Huo, G.-F.; Sun, J.; Yan, C.-G. *Chin. Chem. Lett.* **2017,** *28,* 431–436. doi:10.1016/j.cclet.2016.09.008

License and Terms

BEILSTEIN JOURNAL OF ORGANIC CHEMISTRY

Host–guest complexes of conformationally flexible *C*-hexyl-2-bromoresorcinarene and aromatic *N*-oxides: solid-state, solution and computational studies

Rakesh Puttreddy[1], Ngong Kodiah Beyeh[2,3], S. Maryamdokht Taimoory[3], Daniel Meister[3], John F. Trant[*3] and Kari Rissanen[*1]

Full Research Paper

Open Access

Address:
[1]University of Jyvaskyla, Department of Chemistry, P. O. Box 35, 40014 Jyväskylä, Finland, [2]Department of Chemistry, Oakland University, 146 Library Drive, Rochester, Michigan 48309-4479, USA and [3]Department of Chemistry and Biochemistry, University of Windsor, 401 Sunset Avenue, Windsor, N9B 3P4, Canada

Email:
John F. Trant[*] - j.trant@uwindsor.ca;
Kari Rissanen[*] - kari.t.rissanen@jyu.fi

* Corresponding author

Keywords:
aromatic *N*-oxides; C–H···π Interactions; ditopic receptors; *endo*/*exo* complexation; host–guest chemistry; resorcinarenes

Beilstein J. Org. Chem. **2018,** *14,* 1723–1733.
doi:10.3762/bjoc.14.146

Received: 17 April 2018
Accepted: 19 June 2018
Published: 10 July 2018

This article is part of the thematic issue "Macrocyclic and supramolecular chemistry".

Guest Editor: M.-X. Wang

Abstract

Host–guest complexes of *C*-hexyl-2-bromoresorcinarene (BrC6) with twelve potential aromatic *N*-oxide guests were studied using single crystal X-ray diffraction analysis and ^{1}H NMR spectroscopy. In the solid state, of the nine obtained X-ray crystal structures, eight were consistent with the formation of BrC6-*N*-oxide *endo* complexes. The lone exception was from the association between 4-phenylpyridine *N*-oxide and BrC6, in that case the host forms a self-inclusion complex. BrC6, as opposed to more rigid previously studied *C*-ethyl-2-bromoresorcinarene and *C*-propyl-2-bromoresorcinarene, undergoes remarkable cavity conformational changes to host different *N*-oxide guests through C–H···$\pi_{(host)}$ interactions. In solution phase $CD_3OD/CDCl_3$ (1:1 v/v), all twelve *N*-oxide guests form *endo* complexes according to ^{1}H NMR; however, in more polar CD_3OD/DMSO-d_6 (9:1 v/v), only three *N*-oxides with electron-donating groups form solution-phase *endo* complexes with BrC6. In solid-state studies, 3-methylpyridine *N*-oxide+BrC6 crystallises with both the upper- and lower-rim BrC6 cavities occupied by *N*-oxide guests. Computational DFT-based studies support that lower-rim long hexyl chains provide the additional stability required for this ditopic behaviour. The lower-rim cavity, far from being a neutral hydrophobic environment, is a highly polarizable electrostatically positive surface, aiding in the binding of polar guests such as *N*-oxides.

Introduction

Resorcinarenes are macrocyclic compounds with a bowl-shaped cavity stabilised by circular intramolecular O···H–O hydrogen bonds (HBs) [1,2]. The combination of their confined cavity and conformational flexibility has driven the interest in these synthetic receptors [3], a subclass of calixarenes [4], for a wide range of applications in fields such as catalysis [5-9], sensors [10,11], coordination chemistry [12,13], biological systems [14] and especially for host–guest (H–G) chemistry [15]. Resorcinarenes can be modified at either the upper rim 2-position, lower rim, or both, to deliver supramolecular structures with the required structure for a given function [16-18]. We have shown that resorcinarenes are particularly suited hosts for both neutral and protonated *N*-heterocyclic compounds [19,20] and alkyl ammonium cations [21-25]. The resulting complexes have been extensively studied in both solid and solution state. The most common defined interactions involve encapsulation in the bowl-shaped upper rim (*endo* complexation) due to size complementarity between host cavity and guest shape, and are generally stabilised through multiple C–H···π interactions [26-28]. The cavity capacity to undergo induced conformational changes in response to the incorporation of various upper-rim substituents, differing lower-rim alkyl chain length, specific guests, and selective solvents, have made resorcinarenes an attractive platform for H–G applications. Through careful rational supramolecular design via self-assembly processes, our lab and others have combined simple 1:1 H–G building blocks into dimers [29-31], hexamers [32] or supramolecular chains (1D), sheets (2D), or lattice (3D) networks [15]. The detailed analysis of the molecular level interactions of these systems also has enabled our research to design constructs with specific individual molecular and electronic properties by tuning the structure of the interacting partners.

Over the past decade, the *N*-oxide family has attracted the attention of the H–G community in molecular recognition processes [33-35]. In order to tune the resorcinarene-PyNO H–G recognition events at the molecular level, a better understanding of the particular interactions is required. The *N*-oxide oxygen atoms potential to act as a HB acceptor for multiple simultaneous N–O···$(O–H)_{host}$ interactions raises the molecular complexity. These are the dominant non-covalent interactions, in both the solid and solution state, compared to *endo* cavity C–H···$\pi_{(host)}$ interactions that win in the presence of most other guests. Therefore, investigating H–G complexes relying on N–O···$(H–O)_{host}$ HBs is challenging especially in HB competitive solvents such as methanol and dimethyl sulfoxide (DMSO). In reports from our lab, we disclosed that the π-acidity of aromatic protons assist in orienting the *N*-oxide guest by C–H···π interactions, and that the HB accepting N–O group is positioned "up", extending out beyond the cavity to interact with solvent molecules. Our work, investigating the interactions of PyNO guests with various resorcinarene hosts, has investigated the impact of host cavity flexibility, guest's steric and electronic demands, and solvent effects, in both solution and the solid state [36-38]. For example, we recently studied *C*-ethyl-2-bromoresorcinarene (BrC2) [39] and *C*-propyl-2-bromoresorcinarene (BrC3) [40] to understand the effect of the electronic nature of the host cavity core and rigidity of the resorcinarene skeleton on the ability to host various PyNO guests. All of these studies have been focused on interactions between the guest and the host upper-rim cavity, either as *endo* guests or as *exo* complexes. However, in these studies, we have occasionally observed interactions between *N*-oxide hosts and the cavity formed by the lower rim alkyl chains. This cavity is well-known to provide additional binding sites for guest molecules [40,41]. Inspired, in the present study, we have investigated the H–G complexes of *C*-hexyl-2-bromoresorcinarene (BrC6) and twelve PyNO guest molecules (Figure 1). The incorporation of long chains in the lower rim creates a hydrophobic secondary lower-rim cavity. This provides the potential for the formation of simultaneous upper- and lower-rim *endo* complexes.

Results and Discussion

Solid-state X-ray crystallography

Nine X-ray crystal structures were obtained from BrC6 in combination with twelve PyNO guest molecules. Several attempts to obtain single crystals of BrC6 by itself, **1**+BrC6, **2**+BrC6 and **9**+BrC6 in methanol were unsuccessful. In the following discussions, for example, **1**+BrC6 indicates either from combination of guest **1** and BrC6 or *exo* complex while **1**@BrC6 denotes the *endo* complexation process. However, considering the host flexibility, 'Δ' (Table 1), which is the measure of difference between centroid-to-centroid distances of opposite host aromatic rings, guests **1**, **2**, and **9** should easily fit into BrC6 cavity for *endo* complexation processes. The lack of a crystal structure for these systems should consequently not imply that they do not encapsulate. The Δ values for BrC6 in H–G complexes are >1.0 Å (Table 1) and range between 1.08 Å and 2.39 Å, which are relatively high when compared to BrC2 (range, 0.08–1.06 Å) and BrC3 (range, 0.32–1.81 Å) values. In solid-state crystals, the lower-rim hexyl chains which prefer different orientations due to C–C bond flexibility cause BrC6 to crystallise as non-centrosymmetric hosts in all H–G complexes. In our previous PyNO–BrC2 complexes, more than 50% of BrC2 hosts are centrosymmetric [39]. In other words, long lower-rim hexyl chains cause the high Δ values observed for BrC6, which facilitates a remarkably flexible cavity for various guests. For the following discussions, the position of the guest inside the BrC6 cavity is represented as '*h*', defined as the measured distance from the centroid of the lower-rim host car-

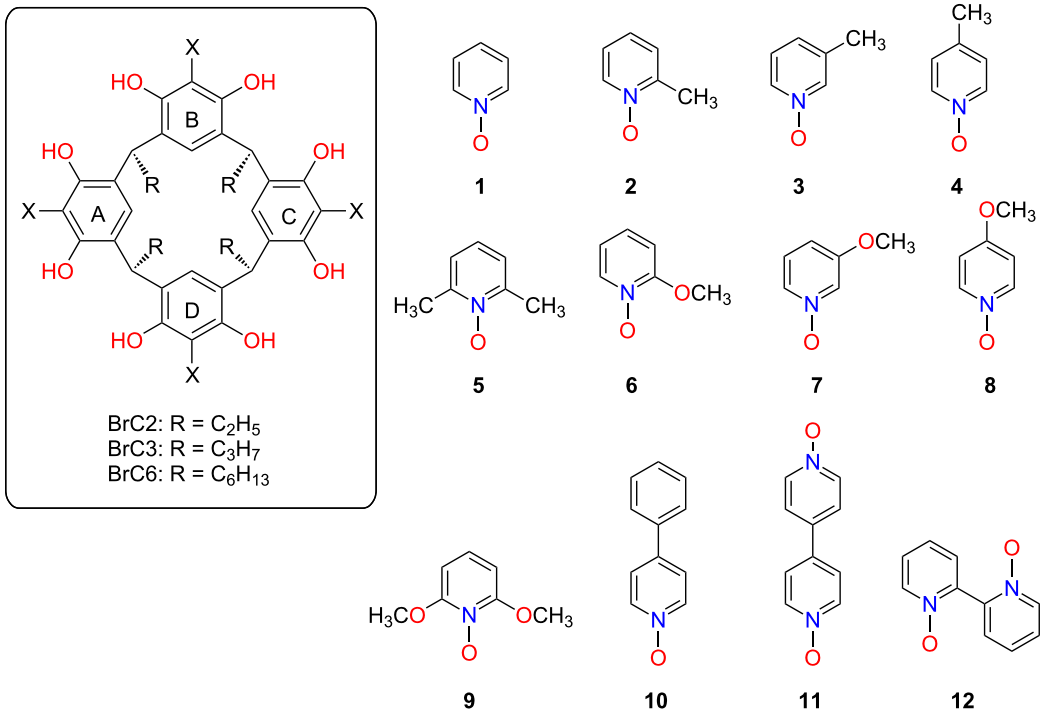

Figure 1: The chemical structures of *C*-ethyl-2-bromoresorcinarene (BrC2), *C*-propyl-2-bromoresorcinarene (BrC3) and *C*-hexyl-2-bromoresorcinarene (BrC6) as hosts and pyridine *N*-oxide (**1**), 2-methylpyridine *N*-oxide (**2**), 3-methylpyridine *N*-oxide (**3**), 4-methylpyridine *N*-oxide (**4**), 2,6-dimethylpyridine *N*-oxide (**5**), 2-methoxypyridine *N*-oxide (**6**), 3-methoxypyridine *N*-oxide (**7**), 4-methoxypyridine *N*-oxide (**8**), 2,6-dimethoxypyridine *N*-oxide (**9**), 4-phenylpyridine *N*-oxide (**10**), 4,4'-bipyridine *N,N'*-dioxide (**11**) and 2,2'-bipyridine *N,N'*-dioxide (**12**) as guests.

bon atoms to the nearest *endo* guest non-hydrogen atom. In the X-ray structure of **3**@BrC6 (Figure 2a), guest **3**, oriented parallel to the host aromatic rings (h = 3.43 Å) is positioned in one corner of the cavity with only the proton *meta*- to the N–O group interacting with a host aromatic ring. This short contact C–H···$\pi_{(host)}$ interaction is about 2.65–2.85 Å long. In **4**@BrC6 (Figure 2b), once again guest **4** is oriented parallel to the host aromatic rings (h = 3.38 Å) and the H–G recognition occurs by C–H···$\pi_{(host)}$ interaction at two sites through C2 proton (2.49–2.89 Å) and methyl group hydrogen atoms (2.93–3.0 Å). This behaviour is in contrast with H–G complex **4**@BrC2, where the BrC2 rigid cavity only allows the methyl group of **4** to insert inside the cavity forming C–H···π interactions between methyl group hydrogens and the host aromatic rings [39]. Unlike **3** and **4**, the sterically unhindered **5** sits deeper inside the cavity (Figure 2c) with h = 2.66 Å thereby forming numerous C–H···π interactions between protons *meta*- to the N–O group and host aromatic rings (2.86–3.0 Å).

Guests **6** and **7** have never been previously analysed by us in our earlier resorcinarene–PyNO H–G studies [39,40]. As shown in Figure 2, despite the BrC6 cavity's flexible nature, the position of the methoxy substituent plays a crucial role for both

Table 1: Summary of solid-state host–guest *endo*/*exo* complexations, and cavity conformation flexibility in BrC6.

Guest	*endo* /*exo*	A–C (ca., Å)	B–D (ca., Å)	Δ [(B–D) − (A–C)]	h[a] (ca., Å)
1	NA[b]	–	–	–	–
2	NA[b]	–	–	–	–
3	*endo*	6.05	7.41	1.36	3.31
4	*endo*	5.84	7.54	1.70	3.29
5[c]	*endo*	6.24	7.33	1.09	2.66
		6.23	7.34	1.11	2.62
6	*endo*	5.89	7.48	1.59	3.23
7	*endo*	5.85	7.57	1.72	3.49
8	*endo*	6.25	7.33	1.08	2.82
9	NA[a]	–	–	–	–
10	–[d]	5.76	7.60	1.84	–
11	*endo*	5.52	7.91	2.39	4.0
12[c]	*endo*	5.81	7.46	1.65	2.83
		6.04	7.43	1.39	2.77

[a]*h*: Position of the *endo* cavity guest, calculated from the centroid of the lower rim host carbons to the nearest non-hydrogen atom of the guest; [b]Crystal structure not available; [c]Asymmetric unit contains two crystallographically independent BrC6 host molecules; [d]self-inclusion complex.

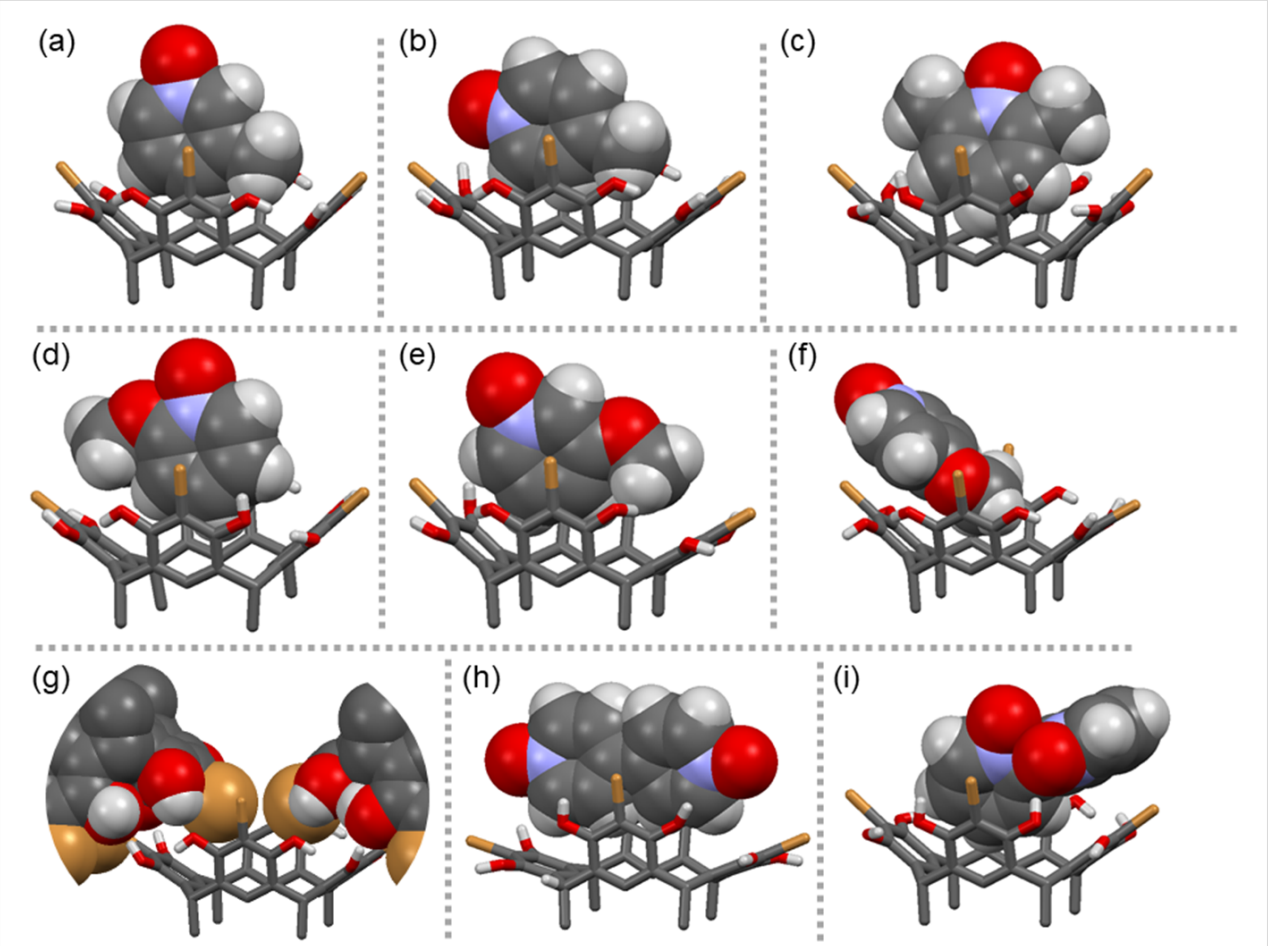

Figure 2: X-ray crystal structures of (a) **3**@BrC6, (b) **4**@BrC6, (c) **5**@BrC6, (d) **6**@BrC6, (e) **7**@BrC6, (f) **8**@BrC6, (g) BrC6 obtained from **10**+BrC6, (h) **11**@BrC6, and (i) **12**@BrC6. The *endo* cavity *N*-oxide guests are shown in CPK models, and the host in capped-stick models. The lower-rim alkyl chains and selected hydrogen atoms were omitted for viewing clarity.

guest orientation and the depth of the guest's occupation of the cavity. For example, in **6**@BrC6 (Figure 2d) and **7**@BrC6 (Figure 2e), guests **6** and **7** have h = 3.23 Å and 3.50 Å, due to their steric demands. However, in complex **8**@BrC6 (Figure 2f) the unhindered *para*-methoxy group facilitates **8** to sit deep inside the cavity at h = 2.82 Å. The guest's parallel orientation to the host aromatic rings in **6**@BrC6 is caused by either steric hindrance or unfavourable positioning. This prevents the formation of stronger C–H···π interactions; consequently, **6**@BrC6 is only stabilised by weak C–C contacts at distances of 3.31 Å. However, **7** with similar 'h' values, due to the bulky methoxy group on the core aromatic ring, is tilted towards one side with the proton *meta*- to the N–O group able to manifest C–H···π interactions with distances of 2.52 and 3.0 Å. Of all the *endo* cavity interactions, the C–H···$\pi_{(centroid)}$ has the shortest contact (2.52 Å). As shown in Figure 2f, the core aromatic ring of **8** and those of BrC6 in **8**@BrC6 are parallel to each other. As a result, the bromine of the C–Br bond and the C2-position establish short contacts of 3.52 Å. However, the prominent interactions responsible for locking the H–G complex are the C–H···π (ca. 2.92 Å) and C–H···O (ca. 2.61 and 2.71 Å) contacts between guest C3 hydrogens and the host carbon/hydroxy oxygens, respectively.

From our experience, the lack of π-acidic aromatic protons in guest **10** usually results in *exo* complexes [36,37,39]. To our surprise, **10**+BrC6 forms a self-inclusion complex of BrC6 by itself as shown in Figure 2g, the property usually preferred by resorcinarenes when solvate and guest molecules are absent inside the cavity. Note that the self-inclusion complex of BrC6 has *exo* methanol solvent hydrogen bonds to host hydroxy groups. This can possibly be explained by the longer lower-rim hexyl chains providing enough intermolecular $_{host}$(C–H)···(H–C)$_{host}$ interactions to form a stable 3D crystal lattice. On the other hand, guest **11** with two N–O groups makes the C2-protons π-acidic enough to form an *endo* complex, **11**@BrC6 (Figure 2h). The host BrC6 undergoes a remarkable conformation change elongated to one side to accommodate the

rod-shaped guest **11**. The *h* value for **11** in **11**@BrC6 is ca. 4.0 Å, which is quite high when compared to values observed for small guest molecules in BrC6 H–G complexes. However, the large Δ and *h* values are typical for rod shape guests such as **11**. Despite higher '*h*' values, guest **11** is stabilised by several C–H···π interactions between C2 protons and host aromatic rings. The distances range between 2.72 and 3.0 Å, with C–H···$\pi_{(centroid)}$ on two sides being the shortest contacts with distances of 2.49 Å and 2.67 Å. In our previous report, **11**+BrC2, due to the BrC2 rigid cavity the rod-shaped **11** form an *exo* complex [39]. In **12**@BrC6 (Figure 2i), the C–C bond rotation in guest **12** allows one aromatic ring to reside inside the cavity at *h* = 2.83 Å. The H–G molecules are positioned primarily by the π···π contacts rather than C–H···π interactions, with a short C···C contact being ca. 3.20 Å. Furthermore, since **11** is able to undergo C–C bond rotation, BrC6 tends to maintain a nearly ideal crown geometry suggesting excellent conformational complementarity between **11** and BrC6.

Comparison of ditopic H–G complexes

In **3**@BrC6, the asymmetric unit contains one host and four guest **3** molecules. Of the four guests, one resides in the upper-rim *endo* cavity, held in position by C–H···π interactions. The second sits in the lower rim between the hexyl chains and is stabilised through N–O···$(H–C)_{Ar(host)}$ and other weak non-covalent interactions. The remaining final two guests are *exo* cavity hydrogen bonded to the host's hydroxy groups. To our surprise, our previous X-ray crystal structures of **3**@BrC3 and **3**@BrC2 complexes obtained from acetone showed interactions with the putative guests (i.e., *N*-oxide and acetone molecules) by encapsulation within the upper-rim and lower-rim cavity [39,40]. Therefore, in an effort to better understand the host–guest interactions and the potentials of the secondary lower-rim binding mode, molecular mechanics (OPLS-2005) [42] calculations were performed on complexes, **3**@BrC2, **3**@BrC3 and **3**@BrC6 using Jaguar (Schrödinger) [43,44]. Consequently, the structures are modelled for both *exo* and *endo* complexes in acetone. Of note, the X-ray crystal structure of **3**@BrC6 (Figure 3e) is obtained from methanol and is presented here only for reference, while its corresponding computational model was optimised using acetone media. To ensure that we were adequately screening the host conformer space in these simulations, no constraints were enforced on either *N*-oxide or acetone molecules. The low energy structures obtained from

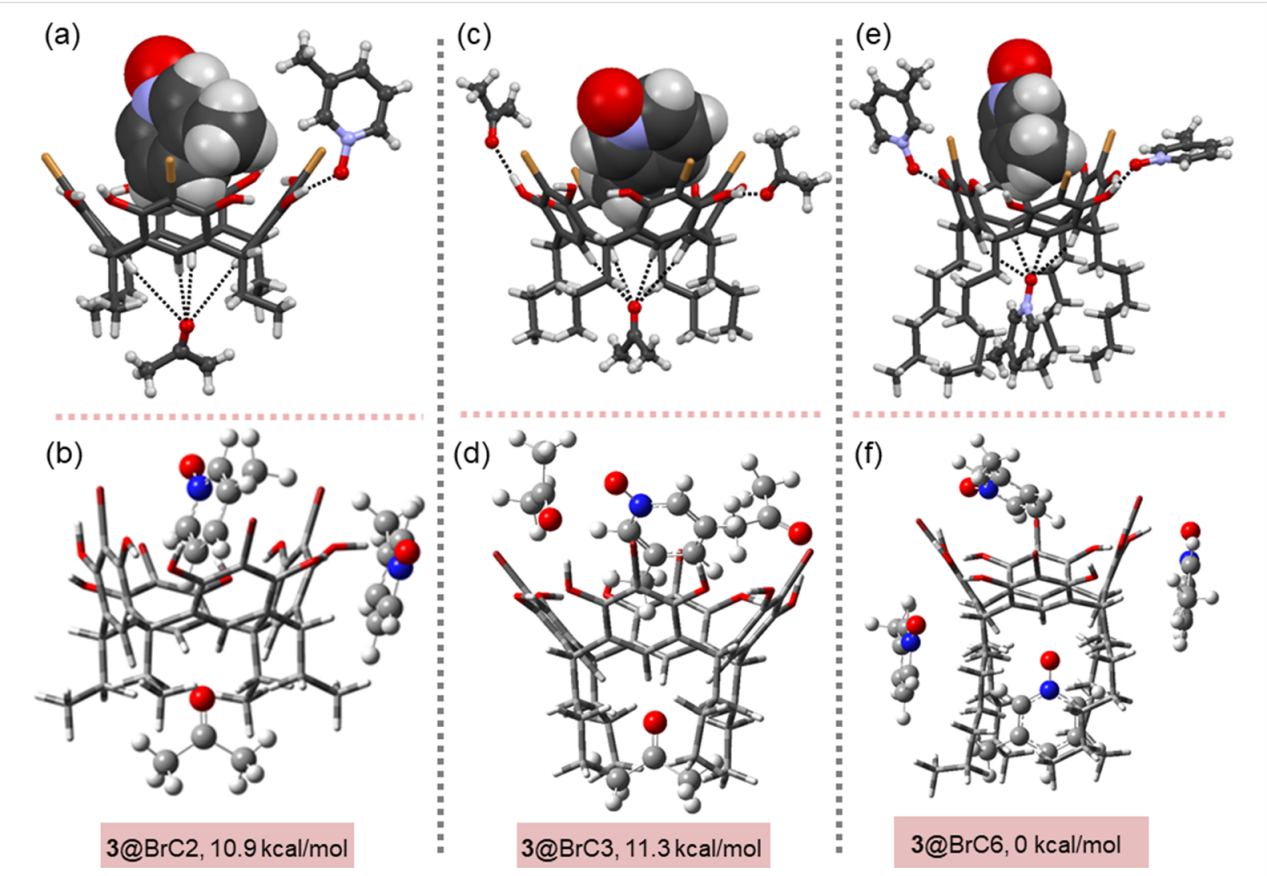

Figure 3: Comparison of X-ray crystal structures (a) **3**@BrC2, (c) **3**@BrC3, and (e) **3**@BrC6 and their DFT-based optimised geometries (b) **3**@BrC2, (d) **3**@BrC3, and (f) **3**@BrC6, respectively.

these OPLS-2005 searches were then further analysed using DFT-based techniques [45-47]. The resulting optimised geometries of the **3**@BrC2, **3**@BrC3 and **3**@BrC6 along with the M06-2X/6-31G(d,p)//ωB97X-D/6-311G(d,p) calculated relative energies of complexes with respect to the most stable complex **3**@BrC6 by following isodesmic reaction schemes (see Supporting Information File 1, Table S3) are shown in Figure 3.

In the optimised structures, the inclusion complexes of **3**@BrC6, **3**@BrC3 and **3**@BrC2 show that the N–O group of **3** in **3**@BrC6, **3**@BrC3 and **3**@BrC2 is positioned outward from the host cavity similar to solid-state X-ray crystal structures as shown in Figure 3. Further, in the lower-rim, the C=O group of acetone in **3**@BrC2 and **3**@BrC3, and N–O group of **3** in **3**@BrC6 are positioned closer to the lower-rim C–H_{Ar} forming non-classical H-bond, (C–H)$_{Ar}$···O=C/O–N, interactions. All three optimised complexes evince C–H···π interactions in both lower- and upper-rim cavities and C–H···O=C/O–N interactions at the lower-rim pocket are responsible for the ditopic behaviour of BrC2/BrC3/BrC6 and **3**. The relative energies for **3**@BrC2, **3**@BrC3 and **3**@BrC6 are 10.9, 11.3, and 0 kcal/mol, respectively, and clearly **3**@BrC6 tend to have the lowest energy and is the most stable among the three complexes. In the optimised **3**@BrC6 structure, the upper-rim *N*-oxide oxygen atom are tilted towards the hydroxy group of the host molecule to form intermolecular negative charge assisted H-bonding, C–H···O [48], interactions with a distance of 1.49 Å.

In order to gain insights into lower-rim cavity binding sites from a qualitative analysis standpoint, a molecular electrostatic potential (MEP) surface map for **3**@BrC6 was calculated. This shows that the host BrC6 lower-rim cavity is not neutral as might be expected, but instead contains a sharp positive electrostatic potential region as depicted with blue colour in Figure 4b. This provides an excellent opportunity for the negative potential regions of the *N*-oxide oxygen atom in guest **3** (red region in Figure 4a) to establish several intermolecular (C–H)$_{Ar}$···O–N H-bond interactions at the lower-rim host pocket.

In addition, we used Bader's quantum theory of atoms in molecules (QTAIM) [49] to analyse multiple non-covalent interactions (i.e., H-bonding and C–H···π) interactions in both the upper-rim *endo* cavity and the lower-rim site present in **3**@BrC6. Based on QTAIM, the presence of a bond path between the donor and the acceptor atoms containing a (3, −1) bond critical point (BCPs; highlighted as small blue circles in Figure S1, Supporting Information File 1), confirm the existence of bonds in this system. In other words, the bond critical point and bond path connecting two atoms are evidence for a real interaction rather than a simple spacial relationship. At the bond critical points, the electronic charge density [ρ(r)], and its Laplacians ($\nabla^2\rho(r)$) are important parameters to evaluate the nature and strength of interactions. Numerical values for these topological parameters related to several non-covalent interactions at both upper and lower rim of complex **3**@BrC6 are shown in Table 2 (see Supporting Information File 1, Figure S1 for the related molecular graph). Based on QTAIM analysis, the presence of several C−H···π interactions are evident from the existence of the (3, −1) bond critical point (BCPs; small red circles) between the bond path connecting the hydrogen atoms in the alkyl chain of the lower cavity in BrC6 with the *ortho, meta* and *para* carbon atoms of the *N*-oxide aromatic ring (highlighted as (C–H)$_{alkyl}$···π$_{(ortho)}$, (C–H)$_{alkyl}$···π$_{(meta)}$, (C–H)$_{alkyl}$···π$_{(para)}$). In addition, C–H···π interactions are present

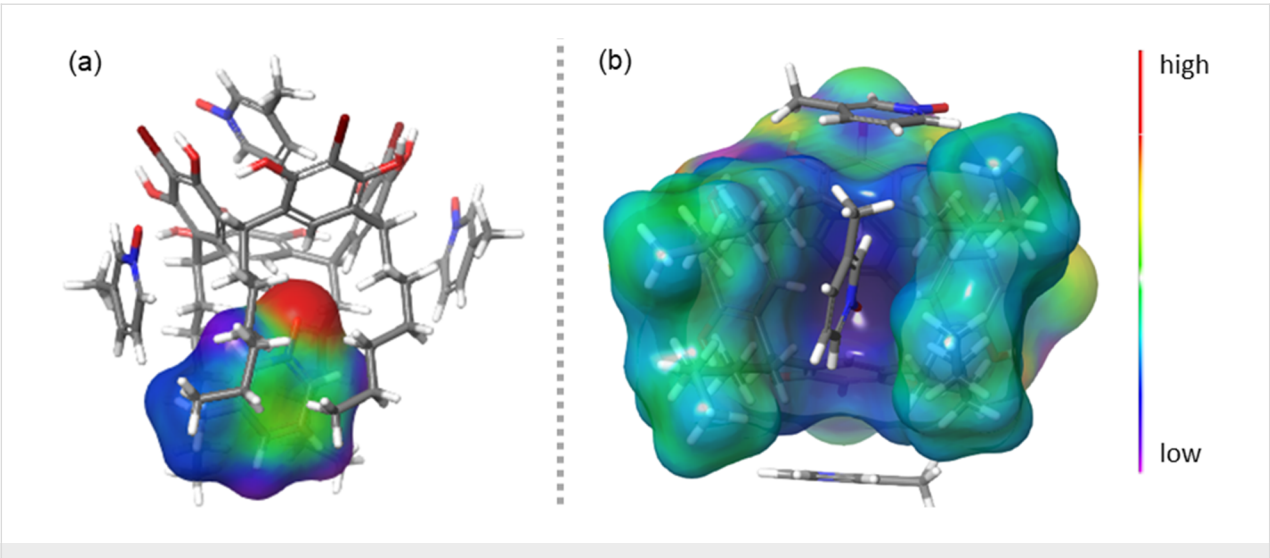

Figure 4: (a) The negative potential localised on the *N*-oxide oxygen in **3**@BrC6 and, (b) the positive charge distribution in lower-rim host cavity [+0.06 to −0.06 a.u.].

in the upper rim of the host as observed from the existence of the (3, −1) bond critical point between the bond path connecting the aromatic C−H bonds of BrC6 with *ortho, meta* and *para* carbon atoms of the *N*-oxide aromatic ring (highlighted as $(C–H)_{Ar}\cdots\pi_{(ortho)}$, $(C–H)_{Ar}\cdots\pi_{(meta)}$, $(C–H)_{Ar}\cdots\pi_{(para)}$). The ρ(r) values associated with these interactions ranged between 0.0046 to 0.0119 a.u. and the positive values of Laplacians ($\nabla^2\rho(r)$) at the BCPs were from 0.0134 to 0.0397 a.u. suggesting the existence of a weak "closed shell" [50-52] character for non-covalent interactions (such as ionic bonds, HBs, stacking type and van der Waals interactions) between **3** and BrC6 (Table 2). This is completely consistent with the observations made from the crystal structures.

Table 2: Values of the density of all electrons ρ(r) and Laplacian of electron density – $\nabla^2\rho(r)$, (Hartree) at the bond critical points (3, −1) for selected significant lower-rim non-covalent C–H···π and H-bond C–H···O–N as well as upper-rim *endo* cavity C–H···π interactions in the model system **3**@BrC6 as well as calculated energies of these bonds, $E_{(x)}$ (kcal/mol), proposed by Espinosa et al. [53,54].

Non-covalent motif	ρ(r)	$\nabla^2\rho(r)$	$E_{(x)}$[a]
Lower rim			
$(C–H)_{alkyl}\cdots\pi_{(ortho)}$	0.0074	0.0247	1.2
$(C–H)_{alkyl}\cdots\pi_{(meta)}$	0.0058	0.0180	1.2
$(C–H)_{alkyl}\cdots\pi_{(para)}$	0.0046	0.0134	0.8
$(C–H)_{alkyl}\cdots\pi_{(para)}$	0.0049	0.0156	0.8
Upper rim			
$(C–H)_{Ar}\cdots\pi_{(ortho)}$	0.0090	0.0294	1.5
$(C–H)_{Ar}\cdots\pi_{(meta)}$	0.0106	0.0332	1.9
$(C–H)_{Ar}\cdots\pi_{(para)}$	0.0099	0.0311	1.8
C–H···O–N	0.0119	0.0397	2.9
C–H···O–N	0.0104	0.0324	10.2
C–H···O–N	0.0086	0.0268	8.4
C–H···O–N	0.0113	0.0351	11.0

[a]See Supporting Information File 1 for more details and $E_{(x)}$ calculations.

^{1}H NMR host–guest solution studies

Guest binding studies of the *N*-oxide guests (**1**–**12**) by the receptor BrC6 were investigated in solution via a series of ^{1}H NMR experiments in different hydrogen bond competing solvents and solvent mixtures: acetone-d_6, methanol/chloroform ($CD_3OD/CDCl_3$) 1:1 v/v and methanol/dimethyl sulfoxide (CD_3OD/DMSO-d_6) 9:1 v/v. The above solvent mixtures were chosen due to the poor solubility of some of the guests in pure methanol. DMSO is known to be an extremely HB competitive solvent and thus prevents the clear formation of host–guest complexes [40,55], while the less competitive chloroform tends to enhance capsular assemblies [55]. Only one set of resonances from the ^{1}H NMR of the receptor BrC6 in all the solvents and solvent mixtures is observed, thus confirming a symmetrical crown conformation in solution (Figure 5). Our previous report studying the interactions between BrC3 and some *N*-oxides in acetone-d_6 revealed moderate deshielding of the hydroxy groups of the BrC3 receptor and minor deshielding of the aromatic protons of the guest when complexes were formed [40]. This confirmed that the assembly was driven by hydrogen bonding [55,56]. Taking the example of BrC6 and **3**, a similar moderate deshielding of the hydroxy groups of the BrC6 receptor and a minor deshielding of the aromatic protons of the guest signals are observed (Figure 5) confirming this assembly is also driven by hydrogen bonding. These shifts' changes are substantially increased when more electron-donating groups are present on the aromatic *N*-oxides such as with **5** (two methyl groups) and **9** (two methoxy groups, Figures S5 and S9, Supporting Information File 1). This is expected as the four electron-withdrawing bromine groups on the BrC6 receptor renders the receptor slightly electron deficient further facilitating π–π interactions. With the larger *N*-oxide guests **10**–**12**, though the shift changes of the guest are not strong enough to conclusively indicate *endo* complexation, clear changes in the hydroxy groups suggest interaction via hydrogen bonding (Figures S10–S12, Supporting Information File 1).

Due to fast H/D exchange processes on the NMR time scale at 298 K in protic solvents, the hydrogen bond interactions between host and guests were not observed. In $CD_3OD/CDCl_3$, complexation-induced chemical shift changes of the guests are observed which results from the electronic shielding effects of the core aromatic rings of the host cavity. As an example, significant up-field shift changes of up to 0.17 ppm for the *c*-proton, and smaller up-field shifts of 0.10 ppm for the *a*-proton in guest **3** were observed (Figure 5b). These shifts suggest that in solution, the N–O group of guest **3** is pointing outward from the BrC6 cavity during *endo* complexation. In the X-ray structure of **3**@BrC6, only the *c*-proton of **3** has $C–H\cdots\pi_{(host)}$ short contacts with distances ranging between ca. 2.65 Å and 2.85 Å. This supports the maximum chemical shift change of 0.17 ppm observed by ^{1}H NMR experiments for the *c*-proton in guest **3**. The ^{1}H NMR experiments for guests **1**, **2**, and **4**–**9** (Figures S2–S9, Supporting Information File 1) show similar up-field chemical shift changes for the aromatic protons of *N*-oxides suggesting guests are inside the host cavity stabilised through C–H···π interactions. Very low shift changes for **11** clearly point to a minimal interaction with the host. This is contrary to the X-ray crystal structure, **11**@BrC6, where **11** and BrC6 are locked by several C–H···π interactions, and of more prominently remarkably short $C–H\cdots\pi_{(centroid)}$ interactions (2.49 Å and 2.67 Å). Interestingly, shift changes of up to

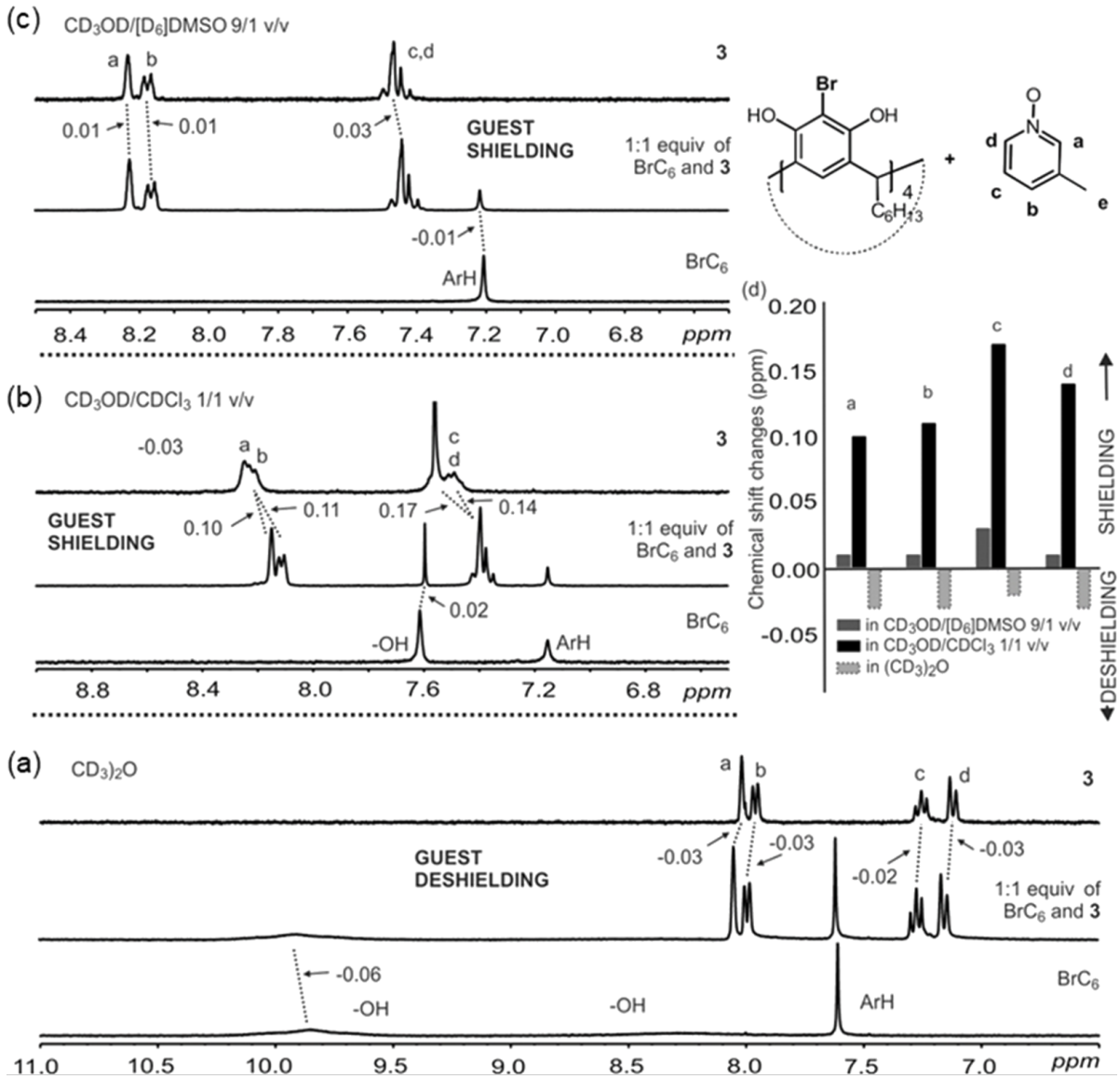

Figure 5: An expansion of the ^{1}H NMR (6.6 mM at 298 K, 500 MHz) of BrC6 complexes with **3**. Spectra are produced from BrC6, **3** and an equimolar mixture of BrC6 and **3** in: (a) $(CD_3)_2O$, (b) $CD_3OD/CDCl_3$ 1:1 v/v, and (c) CD_3OD/DMSO-d_6 9:1 v/v. Dashed lines highlight the observed shift changes of the resonances, labels are in ppm. (d) Bar chart showing the comparative shift changes of the guests in the different solvent media.

0.19 ppm for guest **12** are a clear indication for the *endo* complex. Chemical shift changes of up to 0.12 ppm for guest **10** suggest an *endo* complexation contrary to the X-ray. These observations also matches well with the presence and calculated values of energy for those interactions predicted by our computational analysis and match exactly with reported [48,53] HB interactions with medium strength as well as stacking type interactions with weak characters.

In CD_3OD/DMSO-d_6 9:1 v/v, under similar experimental conditions to $CD_3OD/CDCl_3$ 9:1 v/v, no significant chemical shift changes were observed for nine of the twelve pyridine *N*-oxides. The above results clearly show the strong influence of DMSO in interfering with the host–guest complexation between BrC6 and the aromatic *N*-oxides. However, with guests such as **5** and **9**, *endo* cavity host–guest interactions persist even in these very competitive environments (Table 3, Figures S5 and S9, Supporting Information File 1).

Conclusion

Host–guest systems formed between *C*-hexyl-2-bromoresorcinarene (BrC6) and twelve aromatic *N*-oxides have been char-

Table 3: Summary of *endo*/*exo* host–guest complexations studied in solution by ^{1}H NMR in comparison to the solid state by single crystal X-ray crystallography.

Complex	^{1}H NMR solution studies			X-ray crystal structure
	$(CD_3)_2O$	CD_3OD/$CDCl_3$ (1:1 v/v)	CD_3OD/DMSO-d_6 (9:1 v/v)	
1+BrC6	–[a]	*endo*	*exo*	NA[b]
2+BrC6	–[a]	*endo*	*exo*	NA[b]
3+BrC6	–[a]	*endo*	*exo*	*endo*
4+BrC6	–[a]	*endo*	*exo*	*endo*
5+BrC6	–[a]	*endo*	*endo*	*endo*
6+BrC6	–[a]	*endo*	*endo*	*endo*
7+BrC6	–[a]	*endo*	*exo*	*endo*
8+BrC6	–[a]	*endo*	*exo*	*endo*
9+BrC6	–[a]	*endo*	*endo*	NA[b]
10+BrC6	–[a]	*endo*	*exo*	–[c]
11+BrC6	–[a]	*endo*	*exo*	*endo*
12+BrC6	–[a]	*endo*	*exo*	*endo*

[a]H-bonds dominate the assembly in acetone and only deshielding observed; [b]Crystal structure not available; [c]Self-inclusion complex.

acterised using solid-state X-ray crystallography and ^{1}H NMR solution studies in three different hydrogen-bond-competitive solvents. In the solid state, BrC6 undergoes large cavity conformational changes to accommodate the *N*-oxide guests compared to our previously studied host systems, *C*-ethyl-2-bromoresorcinarene and *C*-propyl-2-bromoresorcinarene, thus proving BrC6 as more reliable host system for a range of *N*-oxide guests. In solution through ^{1}H NMR analyses in methanol/chloroform, significant shielding for aromatic *N*-oxide guests suggests *endo* complexation processes similar to solid state X-ray crystal structures were observed. In methanol/DMSO-d_6 chemical shift changes were observed only for three *N*-oxide guests with suitable electron-donating groups on the core aromatic ring suggesting *endo* complexation, and for other *N*-oxide guests, DMSO solvation prevents the *endo* complexation processes. In acetone-d_6, significant changes for host hydroxy groups suggest host–guest assemblies were driven by hydrogen bond interactions at the upper rim. DFT based calculations using M06-2X/6-31G(d,p)//ωB97X-D/6-311G(d) support the experimental results and show that the ditopic host–guest binding modes of 3-methylpyridine *N*-oxide+BrC6 is more favourable due to longer lower-rim hexyl chains compared to 3-methylpyridine *N*-oxide+*C*-ethyl-2-bromoresorcinarene and 3-methylpyridine *N*-oxide+*C*-propyl-2-bromoresorcinarene. The predicted low energy of 3-methylpyridine *N*-oxide+BrC6 with respect to the other complexes can be attributed to multiple intermolecular hydrogen bonding and stacking interactions at both upper and lower-rims.

Supporting Information

Supporting Information File 1

Experimental details, ^{1}H NMR solution-data, X-ray crystallography experimental details and computational data.
[https://www.beilstein-journals.org/bjoc/content/supplementary/1860-5397-14-146-S1.pdf]

Acknowledgements

The authors gratefully acknowledge financial support from the Academy of Finland (RP grant no. 298817), the University of Jyväskylä, Department of Chemistry, Oakland University, Michigan, USA and the University of Windsor, ON, Canada (Start-Up Grant no: 817074, salary support for DM). SMT and NKB were salary supported by the Ontario Centres of Excellence (OCE) and the Natural Sciences and Engineering Research Council of Canada (NSERC), grant numbers: 29240 and 519843-17. This work was made possible by the facilities of the Shared Hierarchical Academic Research Computing Network (SHARCNET: http://www.sharcnet.ca) and Compute/Calcul Canada.

ORCID® iDs

Rakesh Puttreddy - https://orcid.org/0000-0002-2221-526X
Ngong Kodiah Beyeh - https://orcid.org/0000-0003-3935-1812
S. Maryamdokht Taimoory - https://orcid.org/0000-0002-5350-227X
John F. Trant - https://orcid.org/0000-0002-4780-4968
Kari Rissanen - https://orcid.org/0000-0002-7282-8419

References

1. Sliwa, W.; Kozlowski, C. *Calixarenes and Resorcinarenes;* Wiley: Hoboken, 2009.
2. Timmerman, P.; Verboom, W.; Reinhoudt, D. N. *Tetrahedron* **1996,** *52,* 2663–2704. doi:10.1016/0040-4020(95)00984-1
3. Schneider, H.-J.; Schneider, U. *J. Inclusion Phenom. Mol. Recognit. Chem.* **1994,** *19,* 67–83. doi:10.1007/BF00708975
4. Vicens, J.; Böhmer, V., Eds. *Calixarenes: A Versatile Class of Macrocyclic Compounds;* Topics in Inclusion Science, Vol. 3; Springer: Dordrecht, The Netherlands, 1991. doi:10.1007/978-94-009-2013-2
5. Rebilly, J.-N.; Reinaud, O. *Supramol. Chem.* **2014,** *26,* 454–479. doi:10.1080/10610278.2013.877137
6. McIldowie, M. J.; Mocerino, M.; Ogden, M. I. *Supramol. Chem.* **2010,** *22,* 13–39. doi:10.1080/10610270902980663
7. Catti, L.; Pöthig, A.; Tiefenbacher, K. *Adv. Synth. Catal.* **2017,** *359,* 1331–1338. doi:10.1002/adsc.201601363
8. Bräuer, T. M.; Zhang, Q.; Tiefenbacher, K. *Angew. Chem., Int. Ed.* **2016,** *55,* 7698–7701. doi:10.1002/anie.201602382
9. Zhang, Q.; Catti, L.; Kaila, V. R. I.; Tiefenbacher, K. *Chem. Sci.* **2017,** *8,* 1653–1657. doi:10.1039/C6SC04565K

10. Mirsky, V. M.; Yatsimirsky, A. *Artificial Receptors for Chemical Sensors;* Wiley-VCH Verlag GmbH & Co, 2010. doi:10.1002/9783527632480
11. Kumar, S.; Chawla, S.; Zou, M. C. *J. Inclusion Phenom. Macrocyclic Chem.* **2017,** *88,* 129–158. doi:10.1007/s10847-017-0728-2
12. Gramage-Doria, R.; Armspach, D.; Matt, D. *Coord. Chem. Rev.* **2013,** *257,* 776–816. doi:10.1016/j.ccr.2012.10.006
13. Wieser, C.; Dieleman, C. B.; Matt, D. *Coord. Chem. Rev.* **1997,** *165,* 93–161. doi:10.1016/S0010-8545(97)90153-3
14. Ma, X.; Zhao, Y. *Chem. Rev.* **2015,** *115,* 7794–7839. doi:10.1021/cr500392w
15. Atwood, J. L.; Gokel, G. W.; Barbour, L., Eds. *Comprehensive Supramolecular Chemistry II;* Elsevier Science: Oxford, 2017. doi:10.1016/B978-0-12-803198-8.01001-4
16. Ajami, D.; Liu, L.; Rebek, J., Jr. *Chem. Soc. Rev.* **2015,** *44,* 490–499. doi:10.1039/C4CS00065J
17. Kobayashi, K.; Yamanaka, M. *Chem. Soc. Rev.* **2015,** *44,* 449–466. doi:10.1039/C4CS00153B
18. Tulli, L.; Shahgaldian, P. Calixarenes and Resorcinarenes at Interfaces. In *Calixarenes and Beyond;* Neri, P.; Sessler, J. L.; Wang, M.-X., Eds.; Springer International Publishing: Switzerland, 2016; pp 987–1010. doi:10.1007/978-3-319-31867-7_37
19. Nissinen, M.; Wegelius, E.; Falábu, D.; Rissanen, K. *CrystEngComm* **2000,** *2,* 151–153. doi:10.1039/B006193J
20. Nissinen, M.; Rissanen, K. *Supramol. Chem.* **2003,** *15,* 581–590. doi:10.1080/1061027031000160517 9
21. Rissanen, K. *Chem. Soc. Rev.* **2017,** *46,* 2638–2648. doi:10.1039/C7CS00090A
22. Beyeh, N. K.; Valkonen, A.; Rissanen, K. *CrystEngComm* **2014,** *16,* 3758–3764. doi:10.1039/C3CE42291G
23. Beyeh, N. K.; Pan, F.; Valkonen, A.; Rissanen, K. *CrystEngComm* **2015,** *17,* 1182–1188. doi:10.1039/C4CE01927J
24. Shivanyuk, A.; Rissanen, K.; Kolehmainen, E. *Chem. Commun.* **2000,** 1107–1108. doi:10.1039/b002144j
25. Busi, S.; Saxell, H.; Fröhlich, R.; Rissanen, K. *CrystEngComm* **2008,** *10,* 1803–1809. doi:10.1039/b809503e
26. Atwood, J. L.; Szumna, A. *J. Supramol. Chem.* **2002,** *2,* 479–482. doi:10.1016/S1472-7862(03)00068-6
27. Ballester, P.; Biros, S. M. CH–π and π–π Interactions as Contributors to the Guest Binding in Reversible Inclusion and Encapsulation Complexes. In *The Importance of Pi-Interactions in Crystal Engineering;* Tiekink, E. R. T.; Zukerman-Schpector, J., Eds.; John Wiley & Sons, Ltd.: Chichester, U.K., 2012; pp 79–107. doi:10.1002/9781119945888.ch3
28. Adriaenssens, L.; Ballester, P. *Chem. Soc. Rev.* **2013,** *42,* 3261–3277. doi:10.1039/c2cs35461f
29. Beyeh, N. K.; Rissanen, K. *Isr. J. Chem.* **2011,** *51,* 769–780. doi:10.1002/ijch.201100049
30. Shivanyuk, A.; Rebek, J. *J. Am. Chem. Soc.* **2003,** *125,* 3432–3433. doi:10.1021/ja027982n
31. Dalgarno, S. J.; Power, N. P.; Atwood, J. L. *Coord. Chem. Rev.* **2008,** *252,* 825–841. doi:10.1016/j.ccr.2007.10.010
32. Beyeh, N. K.; Kogej, M.; Åhman, A.; Rissanen, K.; Schalley, C. A. *Angew. Chem., Int. Ed.* **2006,** *45,* 5214–5218. doi:10.1002/anie.200600687
33. Verdejo, B.; Gil-Ramírez, G.; Ballester, P. *J. Am. Chem. Soc.* **2009,** *131,* 3178–3179. doi:10.1021/ja900151u
34. Aragay, G.; Hernández, D.; Verdejo, B.; Escudero-Adán, E. C.; Martínez, M.; Ballester, P. *Molecules* **2015,** *20,* 16672–16686. doi:10.3390/molecules200916672
35. Galán, A.; Escudero-Adán, E. C.; Frontera, A.; Ballester, P. *J. Org. Chem.* **2014,** *79,* 5545–5557. doi:10.1021/jo5007224
36. Puttreddy, R.; Beyeh, N. K.; Ras, R. H. A.; Rissanen, K. *ChemistryOpen* **2017,** *6,* 417–423. doi:10.1002/open.201700026
37. Puttreddy, R.; Beyeh, N. K.; Rissanen, K. *CrystEngComm* **2016,** *18,* 793–799. doi:10.1039/C5CE02354H
38. Beyeh, N. K.; Puttreddy, R.; Rissanen, K. *RSC Adv.* **2015,** *5,* 30222–30226. doi:10.1039/C5RA03667D
39. Puttreddy, R.; Beyeh, N. K.; Ras, R. H. A.; Trant, J. F.; Rissanen, K. *CrystEngComm* **2017,** *19,* 4312–4320. doi:10.1039/C7CE00975E
40. Puttreddy, R.; Beyeh, N. K.; Jurček, P.; Turunen, L.; Trant, J. F.; Ras, R. H. A.; Rissanen, K. *Supramol. Chem.* **2018,** *30,* 445–454. doi:10.1080/10610278.2017.1414217
41. Jie, K.; Zhou, Y.; Yao, Y.; Huang, F. *Chem. Soc. Rev.* **2015,** *44,* 3568–3587. doi:10.1039/C4CS00390J
42. Banks, J. L.; Beard, H. S.; Cao, Y.; Cho, A. E.; Damm, W.; Farid, R.; Felts, A. K.; Halgren, T. A.; Mainz, D. T.; Maple, J. R.; Murphy, R.; Philipp, D. M.; Repasky, M. P.; Zhang, L. Y.; Berne, B. J.; Friesner, R. A.; Gallicchio, E.; Levy, R. M. *J. Comput. Chem.* **2005,** *26,* 1752–1780. doi:10.1002/jcc.20292
43. *MacroModel,* Schrödinger Release 2017-2; Schrödinger, LLC: New York, NY, 2017.
44. Bochevarov, A. D.; Harder, E.; Hughes, T. F.; Greenwood, J. R.; Braden, D. A.; Philipp, D. M.; Rinaldo, D.; Halls, M. D.; Zhang, J.; Friesner, R. A. *Int. J. Quantum Chem.* **2013,** *113,* 2110–2142. doi:10.1002/qua.24481
45. Chai, J.-D.; Head-Gordon, M. *Phys. Chem. Chem. Phys.* **2008,** *10,* 6615–6620. doi:10.1039/b810189b
46. Walker, M.; Harvey, A. J. A.; Sen, A.; Dessent, C. E. H. *J. Phys. Chem. A* **2013,** *117,* 12590–12600. doi:10.1021/jp408166m
47. Tomasi, J.; Mennucci, B.; Cancès, E. *J. Mol. Struct.: THEOCHEM* **1999,** *464,* 211–226. doi:10.1016/S0166-1280(98)00553-3
48. Gilli, P.; Pretto, L.; Bertolasi, V.; Gilli, G. *Acc. Chem. Res.* **2009,** *42,* 33–44. doi:10.1021/ar800001k
49. Bader, R. F. W. *Atoms in Molecules, A Quantum Theory;* Oxford University Press: Oxford, 1990.
50. Kumar, P. S. V.; Raghavendra, V.; Subramanian, V. *J. Chem. Sci.* **2016,** *128,* 1527–1536. doi:10.1007/s12039-016-1172-3
51. Johnson, E. R.; Keinan, S.; Mori-Sánchez, P.; Contreras-García, J.; Cohen, A. J.; Yang, W. *J. Am. Chem. Soc.* **2010,** *132,* 6498–6506. doi:10.1021/ja100936w
52. Contreras-García, J.; Johnson, E. R.; Keinan, S.; Chaudret, R.; Piquemal, J.-P.; Beratan, D. N.; Yang, W. *J. Chem. Theory Comput.* **2011,** *7,* 625–632. doi:10.1021/ct100641a
53. Espinosa, E.; Molins, E.; Lecomte, C. *Chem. Phys. Lett.* **1998,** *285,* 170–173. doi:10.1016/S0009-2614(98)00036-0
54. Yurenko, Y. P.; Zhurakivsky, R. O.; Samijlenko, S. P.; Ghomi, M.; Hovorun, D. M. *Chem. Phys. Lett.* **2007,** *447,* 140–146. doi:10.1016/j.cplett.2007.09.008
55. Evan-Salem, T.; Baruch, I.; Avram, L.; Cohen, Y.; Palmer, L. C.; Rebek, J., Jr. *Proc. Natl. Acad. Sci. U. S. A.* **2006,** *103,* 12296–12300. doi:10.1073/pnas.0604757103
56. Rebek, J., Jr. *Acc. Chem. Res.* **1999,** *32,* 278–286. doi:10.1021/ar970201g

BEILSTEIN JOURNAL OF ORGANIC CHEMISTRY

Synthesis and photophysical studies of a multivalent photoreactive Ru^{II}-calix[4]arene complex bearing RGD-containing cyclopentapeptides

Sofia Kajouj[1], Lionel Marcelis[*1,2], Alice Mattiuzzi[3], Adrien Grassin[4], Damien Dufour[5], Pierre Van Antwerpen[5], Didier Boturyn[4], Eric Defrancq[4], Mathieu Surin[6], Julien De Winter[7], Pascal Gerbaux[7], Ivan Jabin[*3] and Cécile Moucheron[*1]

Full Research Paper

Open Access

Address:
[1]Laboratoire de Chimie Organique et Photochimie, Université libre de Bruxelles, Avenue F.D. Roosevelt 50, CP 160/08, 1050 Bruxelles, Belgium, [2]Engineering of Molecular NanoSystems, Ecole Polytechnique de Bruxelles, Université libre de Bruxelles (ULB), Avenue F.D. Roosevelt 50, CP165/64, B-1050 Brussels, Belgium, [3]Laboratoire de Chimie Organique, Université libre de Bruxelles, Avenue F.D. Roosevelt 50, CP 160/06, 1050 Bruxelles, Belgium, [4]Université Grenoble Alpes, Département de Chimie Moléculaire UMR CNRS 5250, CS 40700, 38058 Grenoble Cedex 09, France, [5]Analytical Platform of the Faculty of Pharmacy, Université libre de Bruxelles, Boulevard du Triomphe, Campus de la Plaine, CP205/05, 1050 Bruxelles, Belgium, [6]Laboratory for Chemistry of Novel Materials, Center for Innovation and Research in Materials and Polymers, University of Mons – UMONS, 20, Place du Parc, B-7000 Mons, Belgium and [7]Organic synthesis and Mass Spectrometry Laboratory, University of Mons - UMONS, Place du Parc 23, B-7000 Mons, Belgium

Email:
Lionel Marcelis[*] - lmarceli@ulb.ac.be; Ivan Jabin[*] - ijabin@ulb.ac.be; Cécile Moucheron[*] - cmouche@ulb.ac.be

* Corresponding author

Keywords:
anticancer drug; calixarene; cell targeting; RGD peptide; ruthenium complex

Beilstein J. Org. Chem. **2018,** *14,* 1758–1768.
doi:10.3762/bjoc.14.150

Received: 15 April 2018
Accepted: 21 June 2018
Published: 16 July 2018

This article is part of the thematic issue "Macrocyclic and supramolecular chemistry".

Guest Editor: M.-X. Wang

Abstract

Photoactive ruthenium-based complexes are actively studied for their biological applications as potential theragnostic agents against cancer. One major issue of these inorganic complexes is to penetrate inside cells in order to fulfil their function, either sensing the internal cell environment or exert a photocytotoxic activity. The use of lipophilic ligands allows the corresponding ruthenium complexes to passively diffuse inside cells but limits their structural and photophysical properties. Moreover, this strategy does not provide any cell selectivity. This limitation is also faced by complexes anchored on cell-penetrating peptides. In order to provide a selective cell targeting, we developed a multivalent system composed of a photoreactive ruthenium(II) complex tethered to a

calix[4]arene platform bearing multiple RGD-containing cyclopentapeptides. Extensive photophysical and photochemical characterizations of this Ru(II)–calixarene conjugate as well as the study of its photoreactivity in the presence of guanosine monophosphate have been achieved. The results show that the ruthenium complex should be able to perform efficiently its photoinduced cytotoxic activity, once incorporated into targeted cancer cells thanks to the multivalent platform.

Introduction

Long-living luminescent polyazaaromatic ruthenium(II) complexes are intensively studied in a biological context, in particular (i) for their ability to sense their environment and (ii) for their photoreactivity towards relevant biological targets [1-4]. Sensors for biological species are mostly based on complexes bearing the well-known dppz ligand (dppz = dipyrido[3,2-*a*:2',3'-*c*]phenazine) and its derivatives. J. K. Barton et al. demonstrated in 1990 that $[Ru(bpy)_2(dppz)]^{2+}$ behaves as a light-switch for DNA [5]: this complex is not luminescent in water but upon intercalation within the DNA base pairs stack, the complex luminescence is restored. Derivatives of $[Ru(bpy)_2(dppz)]^{2+}$ and complexes bearing similar aromatic planar ligands were developed to probe specific sites of DNA, such as mismatches [6-8], abasic sites [9] or G-quadruplexes [10,11]. Aside photosensors, photoreactive complexes able to damage biological targets were also developed. These complexes are mainly used to induce damages in cancerous cells upon light irradiation. Two types of photooxidative damages can be induced: (i) by photosensitization of singlet oxygen and subsequent generation of highly reactive oxygen species (ROS) (type I photosensitization) or (ii) by direct oxidative electron transfer to biological molecules such as DNA or amino acids (type II photosensitization). In particular, it was shown that Ru^{II} complexes containing at least two highly π-deficient polyazaaromatic ligands such as 1,4,5,8-tetraazaphenanthrene (TAP) [12-14] or 1,4,5,8,9,12-hexaazatriphenylene (HAT) [15] are able to oxidize the guanine base (G) of DNA or the tryptophan (Trp) amino acid residue through a photoinduced electron-transfer (PET) process [16-19]. Interestingly, the two radical species generated by this PET can recombine to form a covalent photoadduct [20-22]. When this photoadduct is formed with the guanine base, the activity of enzymes such as RNA polymerase or endonuclease is inhibited in vitro at the level of the photoadduct [23,24]. In order to target a specific DNA sequence, photoreactive Ru^{II} complexes have been anchored to specific antisense oligonucleotides to inhibit the expression of the complementary targeted genes under illumination [25,26]. This photoinduced gene-silencing strategy has been proven to be also efficient in living cells [27,28], paving the way for the use of photoactivable Ru^{II} complexes as photocontrolled anticancer therapeutic agents.

Despite their interesting photochemical properties, photoreactive Ru^{II} complexes have shown low cell-penetration efficiency, preventing their direct use in biological applications. More lipophilic ligands such as bathophenanthroline and modified dppz were developed and the internalization of the corresponding Ru^{II} complexes was demonstrated [29-32]. These complexes are however not photoreactive due to the absence of π-deficient ligands. More recently, Ru^{II} complexes bearing two modified TAP ligands with highly lipophilic moieties were reported [33]. These compounds are able to enter the cells and photoinduce caspase-dependent and reactive-oxygen-species-dependent apoptosis. Another strategy for the design of cell penetrating photoreactive Ru^{II} complexes consists of tethering the complex to a vector that allows a cellular uptake. In this context, Os^{II}, Rh^{III} and Ru^{II} complexes were anchored to cell penetrating peptides (CPP) such as polyarginine [34-37]. The tethering of a photoreactive Ru^{II} complex on the *transactivating transcriptional activator* (TAT) peptide was also reported and it was shown that the corresponding Ru^{II} conjugate could be internalized inside HeLa cells without any modification of the photochemical properties of the complex [38].

It should be noted that modifications of ligands to make the resulting complexes more lipophilic or the conjugation of a complex to a CPP do not provide any control on the way these complexes will be internalized by cells and prevent thus any targeting of malignant cells over healthy ones. The next step in the development of phototherapeutic agents based on polyazaaromatic Ru^{II} complexes is thus the specific targeting of cancerous cells. In this regard, $\alpha_v\beta_3$ integrin represents an interesting target as this membrane receptor is overexpressed in the endothelial cells of neoangiogenic vessels and in several human tumor cells [39,40]. It is well known that RGD-containing oligopeptides (RGD = Arg-Gly-Asp tripeptide pattern) bind selectively to $\alpha_v\beta_3$ integrin with a high affinity and a very high selectivity [41-43]. As multivalency enhances the binding strength of a ligand to its receptor [44-46], clustered RGD-containing compounds were developed and were shown to exhibit attractive biological properties for the imaging of tumors [47-50] and for the targeted drug delivery [51-53].

In the course of designing phototherapeutic agents that could specifically target cancerous cells, we envisaged to graft a photoreactive Ru^{II} complex on a multivalent platform decorated with multiple RGD-containing cyclopentapeptides. A calix[4]arene moiety was chosen as the multivalent platform as

this rigid macrocycle displays two distinct faces that can be selectively functionalized [54-56]. It is noteworthy that the calix[4]arene skeleton has been already exploited for the development of multivalent glyco- and peptidocalixarenes that can be recognized by cell-membrane receptors [57-59] and of calixarene derivatives able to specifically target membrane proteins involved in the angiogenesis process [60]. Furthermore, the use of calixarenes for biological applications is the subject of intensive researches. They are indeed exploited in various areas such as surface recognition, structural mimes or membrane receptor inhibition [61-63], and it was also shown that calixarenes themselves display antibacterial, antiviral, and anticancer properties [64].

Herein, we describe the synthesis of a multivalent phototherapeutic agent designed in order to specifically target membrane receptors involved in the angiogenesis process. The multivalent system is composed of a photoreactive $[Ru(TAP)_2phen]^{2+}$ complex tethered to a calix[4]arene platform bearing four c-[RGDfK] moieties [65] (Figure 1). Before studying this conjugate in vitro, it was first mandatory to check that the photochemistry of the Ru^{II} complex was not altered by the presence of the targeting platform. The photophysical properties of this Ru^{II}–calixarene conjugate were thus examined and compared to those of the reference complex $[Ru(TAP)_2phen]^{2+}$.

Results and Discussion

Synthesis of Ru^{II}-calixarene conjugate **9**

For the synthesis of the target multivalent system, the strategy relies on the anchoring i) of the photoreactive $[Ru(TAP)_2phen]^{2+}$ complex on the calix[4]arene small rim through a peptide-type coupling and ii) of the four c-[RGDfK] moieties on the opposite rim through a copper-catalyzed azide–alkyne cycloaddition (CuAAC) [66-68] (Figure 1). It was thus necessary to block the calix[4]arene skeleton in the cone conformation and to functionalize separately the two distinct rims (Scheme 1). Firstly, known calixarene **2** with an appending carboxylate arm on the small rim was synthesized from commercial *p*-*tert*-butylcalix[4]arene **1** according to a four-step sequence [69]. Note that propyl groups were chosen for the modification of the small rim because these groups are the smallest possible for blocking the oxygen-through-the-annulus rotation of the aromatic units [70]. The nitro groups of **2** were then reduced using $SnCl_2{\cdot}2H_2O$ in ethanol, affording tetra-amino compound **3** [69] in 50% yield. Diazotation followed by nucleophilic substitution with sodium azide gave the desired tetra-azido compound **4** in 56% overall yield from **3**. It is noteworthy that the introduction of the azido groups on the calix[4]arene scaffold was clearly confirmed by the presence of an intense band at 2108 cm^{-1} in the IR spectrum of **4**. Phenanthroline derivative **5** was synthesized from 5-glycinamido-1,10-phenanthroline in a two-step sequence consisting of a peptide-type coupling reaction with a Boc-protected glycine *N*-hydrosuccinimide ester followed by the deprotection of the amino group (see Supporting Information File 1) [71]. Different coupling agents (DCC/HOBt, EDC·HCl/HOBt, PyBOP) and conditions were then tested for the peptide-type coupling reaction between calix[4]arene **4** and phenanthroline derivative **5**. The use of an excess of **5** (2 equiv) in the presence of EDC·HCl and HOBt in DMF at room temperature led to the best yield and the easiest purification process. Under these optimal conditions, the desired compound **6** was isolated in a high 94% yield. Finally, the reaction between $[Ru(TAP)_2(H_2O)_2]^{2+}$ and **6** in DMF at 100 °C gave the Ru^{II}-calix[4]arene complex **7** in 95% yield after C18 reversed-phase silica gel column chromatographic purification. Complex **7** was fully characterized by 1D and

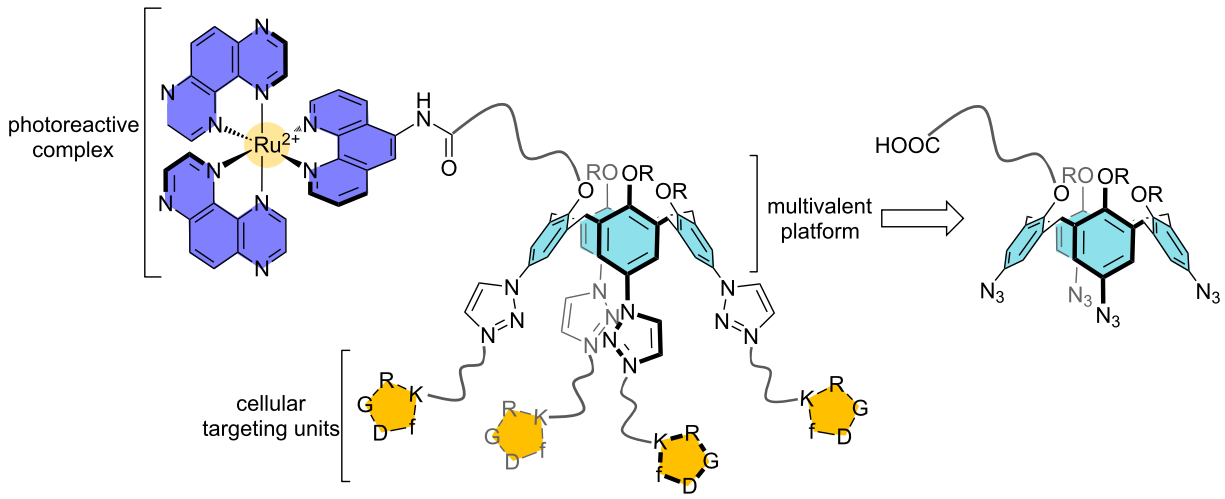

Figure 1: Targeted multivalent phototherapeutic agent and its calix[4]arene-based precursor. RGD = Arg–Gly–Asp residues, f = D-Phe residue.

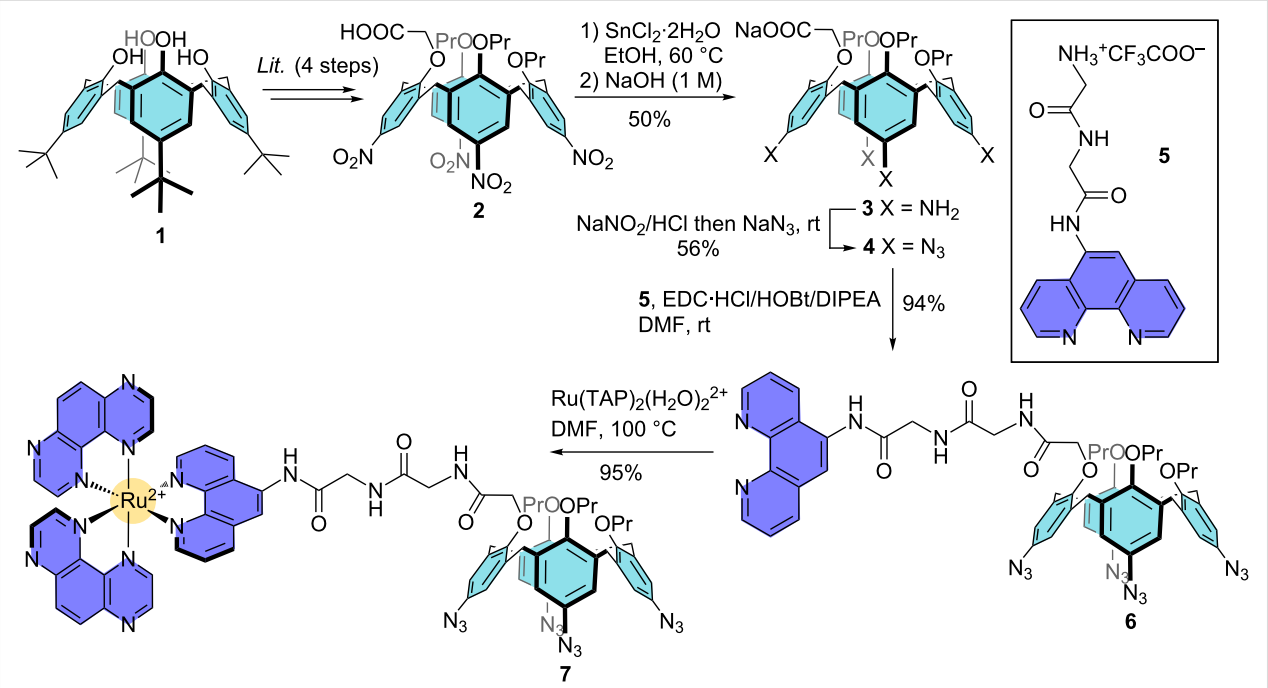

Scheme 1: Synthesis of Ru^{II}-calix[4]arene complex **7**.

2D NMR spectroscopy in CD_3CN at 600 MHz. In accordance with the presence for the chiral $Ru(TAP)_2phen$ moiety, the ^1H NMR spectrum of **7** is characteristic of a C_1 symmetrical compound as all the protons belonging to the ArH, $ArCH_2$ and OPr group are differentiated. Moreover, complex **7** was also characterized by high-resolution mass spectrometry (HRMS). The ESI mass spectrum displays two intense signals at *m*/*z* 764.736 and *m*/*z* 1642.456 that are attributed respectively to the doubly charged $\mathbf{7}^{2+}$ and singly charged $[\mathbf{7} + CF_3COO^-]^+$ by comparison between the experimental and theoretical isotope distributions (see Supporting Information File 1).

With Ru^{II}-calix[4]arene complex **7** in hands, we next moved to the introduction of the cellular targeting units on the large rim through copper-catalyzed azide–alkyne cycloaddition (CuAAC). Note that the triazole moieties that would result from such a cycloaddition are known to be stable towards hydrolysis and protease, which allows their use in a biological environment [72]. For the CuAAC, the use of Cu^I-generated in situ from a mixture of $CuSO_4{\cdot}5H_2O$ and sodium ascorbate is often reported in the field of calixarene chemistry [66,73-78]. Unfortunately, this methodology led to poor yields and a lack of reproducibility in the case of calixarene **7** and c-[RGDfK]-alkyne **8**, even when a microwave heating was used. We then evaluated the use of copper nanoparticles (CuNPs), as these nanomaterials are known to catalyze efficiently a wide range of organic reactions and notably the azide–alkyne cycloaddition [79]. Calixarene **7** was reacted with a slight excess (5 equiv) of cyclopeptide **8** in the presence of CuNPs and the mixture was heated by microwave (100 W) at 50 °C for 1 hour. The use of CuNPs greatly facilitated the monitoring of the reaction and the work-up, as these nanomaterials being easily removed from the crude mixture by simple centrifugation. To our delight, $[Ru(TAP)_2phen]^{2+}$-calix[4]arene-[c-(RGDfK)]$_4$ conjugate **9** was isolated in 31% yield after purification by semi-preparative RP-HPLC (Scheme 2). The successful synthesis and purification of conjugate **9** was also confirmed by HRMS. Indeed, the ESI mass spectrum features several peaks corresponding to characteristic ions of different charge states at *m*/*z* 1421.577 (3+), 1066.434 (4+) and 853.556 (5+) that are attributed to $[\mathbf{9} + H]^{3+}$, $[\mathbf{9} + 2H]^{4+}$ and $[\mathbf{9} + 3H]^{5+}$ by comparison between the experimental and theoretical isotope distributions (see Supporting Information File 1).

Molecular modeling simulations were carried out to provide insights into the size and morphology of conjugate **9**. An optimized geometry is presented in Figure 2, as issued from a molecular dynamics (MD) simulations. The ruthenium complex and the RGD units are spatially well-separated thanks to their grafting on opposite faces of the rigid calixarene-based platform. In this conformation, the distances between the Ru atom and each of the nearest carbon atoms of RGDfK units exceed 30 Å. Along the MD simulations, we noticed that the Ru complex remained far from the cyclic pentapeptides. This is due to the fact that the linkers of each arm are smaller than the size of the calixarene platform, preventing contacts between the Ru

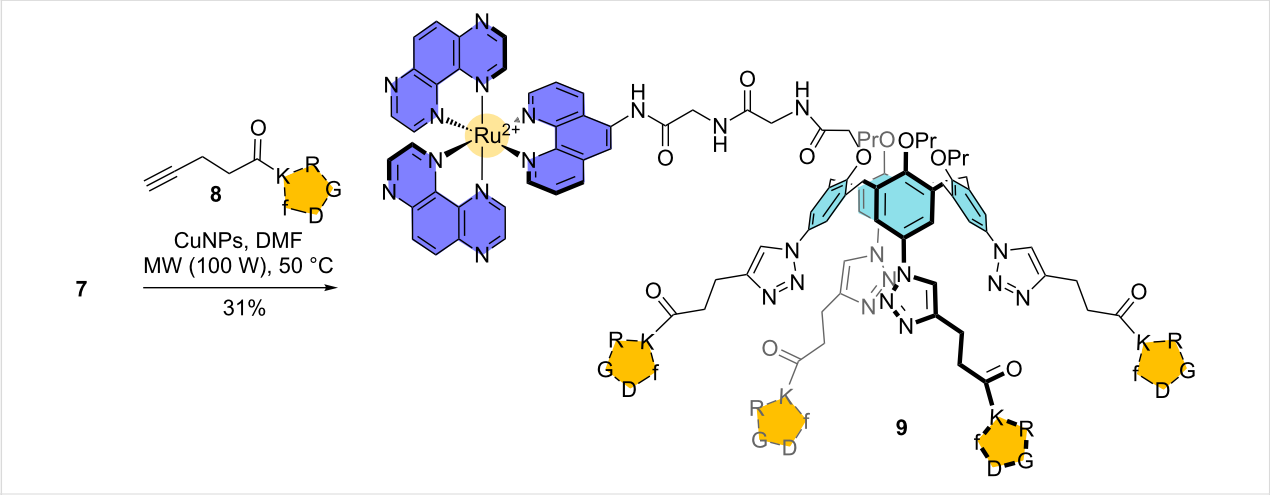

Scheme 2: Synthesis of Ru^{II}-calix[4]arene-[c-(RGDfK)]$_4$ conjugate **9**.

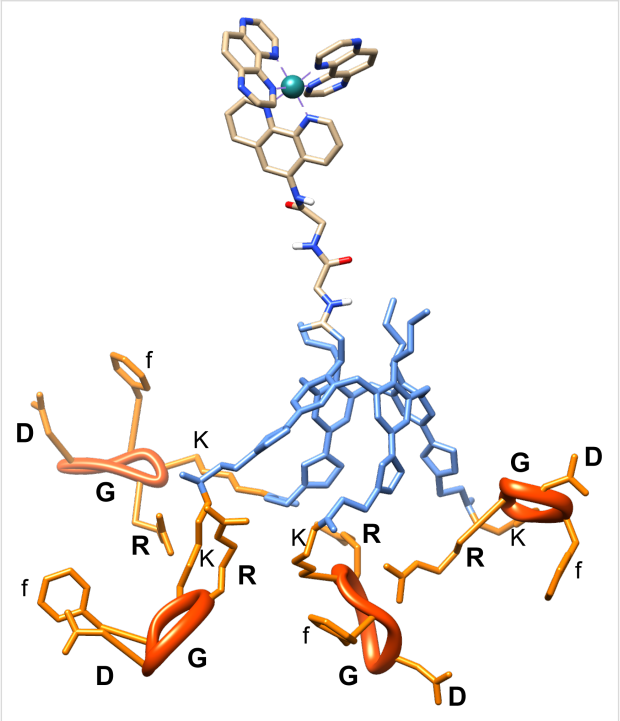

Figure 2: MD snapshot showing an optimized model of conjugate **9**. RGDfK units are depicted in orange ribbons, the calixarene is in blue and the Ru complex is colored by atom type.

complex and the RGDfK units. The global structure has an average radius of gyration R_g of 1.25 nm ± 0.1 nm. Noteworthy, the distance between the RGDfK units largely varies along the MD simulations, ranging from 10 Å to 24 Å (average at 17 Å), as estimated from the distance between equivalent carbon atoms crossing the linker and the cyclic pentapeptides. This large variation in the distance is due to the flexibility of the linkers between the calixarene platform and the RGDfK units, together with the many possibilities of H-bonding between: (i) oxygen atoms at C=O in the linker and the hydrogen atoms of (N–H) of arginine of a neighboring 'arm'; (ii) H-bonds between arginine terminal N–H and C=O of the peptide bond of phenylalanine of an adjacent cyclic pentapeptide (see Supporting Information File 1), yielding adjacent cyclic pentapeptides in close proximity for a large set of conformations.

This separation between the Ru complex and the cyclic peptides by the calixarene should be an advantage by preventing any negative effect of the RGD peptidic units on the photochemistry of the complex and, alternatively, prevents any influence of the complex on the affinity of the RGD patterns to interact with the targeted integrins. However, the possible H-bonding interactions between neighboring RGD units could be a drawback in view of the accessibility of the arginine groups to interact with the integrins.

Photophysical properties of Ru^{II}-calixarene conjugate **9**

The absorption and emission spectra of Ru-calix(RGD)$_4$ conjugate **9** (as its CF_3COO^- salt) were recorded in water at room temperature (Figure 3). These spectro-scopic data are gathered in Table 1 with the ones of the free $[Ru(TAP)_2phen]^{2+}$ complex for comparison purpose.

Conjugate **9** exhibits absorption bands at 416 and 458 nm that corresponds to dπ(Ru)–π*(phen/TAP) metal-to-ligand charge transitions (MLCT) similarly to what is observed for the untethered $[Ru(TAP)_2phen]^{2+}$ complex (MLCT bands at 412 and 464 nm). The presence of the calix[4]arene platform has thus no impact on the visible part of the spectrum. The influence of the calixarene moiety is however visible in the UV region of the spectrum (around 200 nm) where the absorption bands are more intense. This increase is due to the contribution of the peptidic

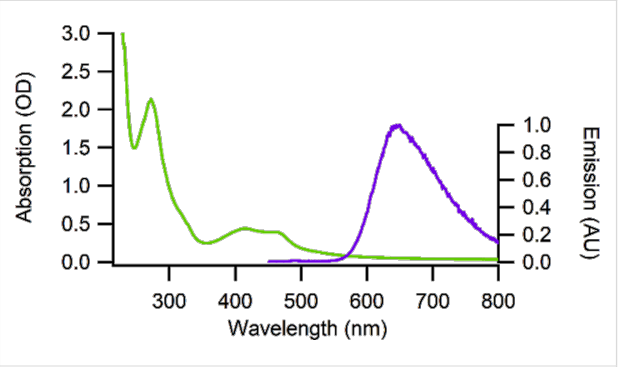

Figure 3: Absorption and emission spectra of Ru^{II}-calix[4]arene-[c-(RGDfK)]$_4$ conjugate **9** in water.

subunits of the RGD moieties and of the aromatic units of the calixarene. It should be noted that the absorption at wavelengths longer than 550 nm does not go perfectly down to zero. This phenomenon is likely due to some light scattering caused by the presence of some small aggregates in solution. It appears that conjugate **9** is not completely soluble in pure water despite the presence of the charged Ru^{II} complex and the peptidic moieties on the calix[4]arene scaffold. Fortunately, these small aggregates totally disappeared when only 5% of DMSO was added to the medium [80].

The photoluminescence emission originating from the ^{3}MLCT state is centered at 645 nm for both conjugate **9** and reference $[Ru(TAP)_2phen]^{2+}$complex. We measured the luminescence lifetime and determined the quantum yield of luminescence under air and argon atmosphere for conjugate **9** and reference $[Ru(TAP)_2phen]^{2+}$ in water with 5% DMSO in order to avoid any formation of aggregates. The data gathered in Table 1 clearly indicate that the tethering of the $[Ru(TAP)_2phen]^{2+}$ complex onto the calixarene platform does not induce any modification of the photophysical properties of the complex. In order to rule out any intramolecular quenching processes, control experiments were realized with the complex grafted onto the unmodified calixarene (conjugate **7**) in the presence of free cyclic pentapeptide units c-[RGDfK] **8** (see Supporting Information File 1). No modification of the luminescence by intermolecular quenching was observed, confirming the absence of internal quenching in the conjugate **9**.

Photoreactivity of Ru^{II}-calixarene conjugate **9**

The photoreactivity of Ru-TAP complexes is based on their ability to induce direct oxidation of guanine upon light excitation. In order to confirm that the tethering onto the calixarene platform does not impede the conjugated complex to photoreact with its biological target, we measured the evolution of the luminescence intensity and the excited state lifetime of conjugate **9** as function of the concentration of guanosine monophosphate (GMP, Figure 4).

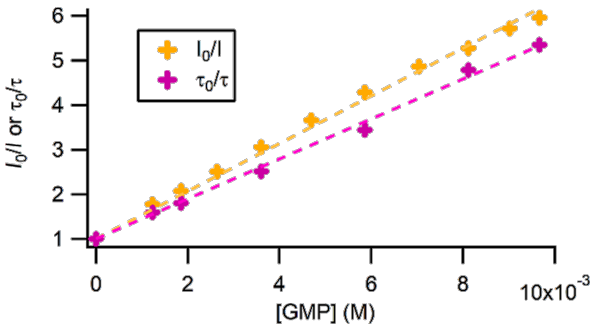

Figure 4: Luminescence intensity and excited state lifetime of conjugate **9** in the presence of GMP measured in 10 mM Tris·HCl buffer at pH 7.0.

Stern–Volmer analyses indicate that a dynamic quenching is occurring, with a quenching rate close to the diffusion limit (k_Q = 5.6 10^8 $M^{-1}s^{-1}$ in intensity and k_Q = 5.3 10^8 $M^{-1}s^{-1}$ in lifetime). This quenching of the luminescence of conjugate **9** in the presence of GMP reveals that a photoinduced electron transfer can take place between the excited complex and the guanine moiety, which could give rise to the formation of a photoadduct from the recombination of the monoreduced complex and the radical guanine generated after the photoinduced electron transfer (PET). In order to confirm the occurrence of PET, transient absorption measurements with conjugate **9** were performed in the absence and in the presence of GMP. The recorded transient absorption spectra are presented in Figure 5. In absence of GMP, the transient absorption spectrum of conjugate **9** is dominated by the luminescence, the ground state bleaching and some excited state absorption around 340 nm whereas in the presence of GMP a positive transient signal can

Table 1: Photophysical properties of conjugate **9** and $[Ru(TAP)_2phen]^{2+}$ in water.

Complex	λ^{abs} (nm)	λ^{em} (nm)	$\Phi^{Air\ a,b}$	$\Phi^{Ar\ a,b}$	$\tau_{av}^{Air\ b,c}$ (ns)	$\tau_{av}^{Ar\ b,c}$ (ns)
$[Ru(TAP)_2phen]^{2+}$	231, 272, 412, 464	645	0.029	0.055	714	891
conjugate **9**	274, 416, 458	645	0.025	0.044	901	1087

[a]Photoluminescence quantum yields are determined by comparison with $[Ru(bpy)_3]^{2+}$. Errors on Φ estimated to <20%. [b]Measurement with 5% DMSO. [c]Errors on lifetime estimated to 15%.

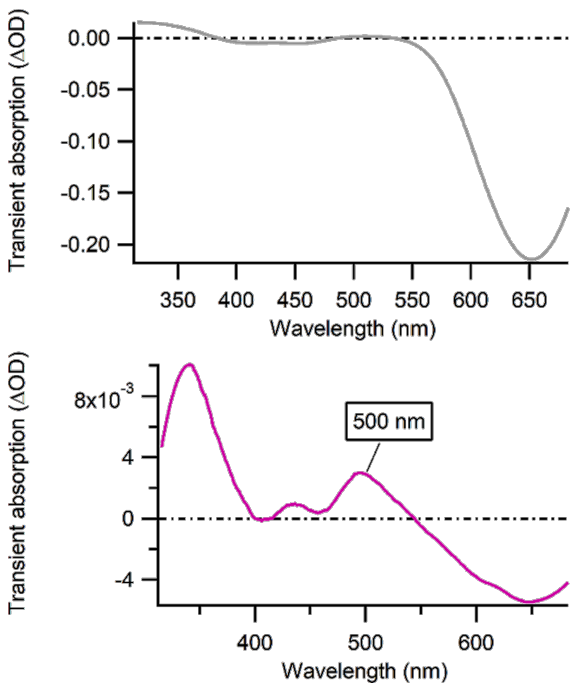

Figure 5: Transient absorption spectra of Ru^{II}-calix[4]arene-[c-(RGDfK)]$_4$ conjugate **9** (in 10 mM Tris·HCl buffer at pH 7.0) measured 500 ns after the laser pulse (gray, top) and 1 µs after the laser pulse in the presence of 10 mM GMP (purple, bottom).

be observed around 500 nm on a long time scale. This transient is specific of a monoreduced Ru^{II}-$TAP^{\bullet-}$ species [81], confirming that a PET occurs.

To verify if a photoadduct can be obtained between the complex anchored on the calixarene platform and a guanine base, a continuous irradiation of a solution containing conjugate **9** and GMP was achieved. The crude irradiation mixture was then analyzed by MALDI mass spectrometry (HRMS, Figure 6). Alongside the parent conjugate **9** ions, ionized species at higher mass-to-charge ratio (m/z = 4625.9) are detected and formally correspond to the addition of GMP minus two hydrogen atoms. The comparison between the experimental and theoretical isotope patterns confirms (inset Figure 6) that irradiation of conjugate **9** and GMP efficiently yielded the desired photoadduct.

Conclusion

The present work validates the design strategy that consists in using calix[4]arenes as addressable platforms for the elaboration of multivalent photoreactive systems that could potentially target and enter cancer cells. The selective tethering of a photoreactive Ru-TAP complex on the small rim of a calix[4]arene and the introduction of four c-[RGDfK] moieties on its large rim were efficiently achieved. In good agreement with molecular modeling simulations, it was shown that the

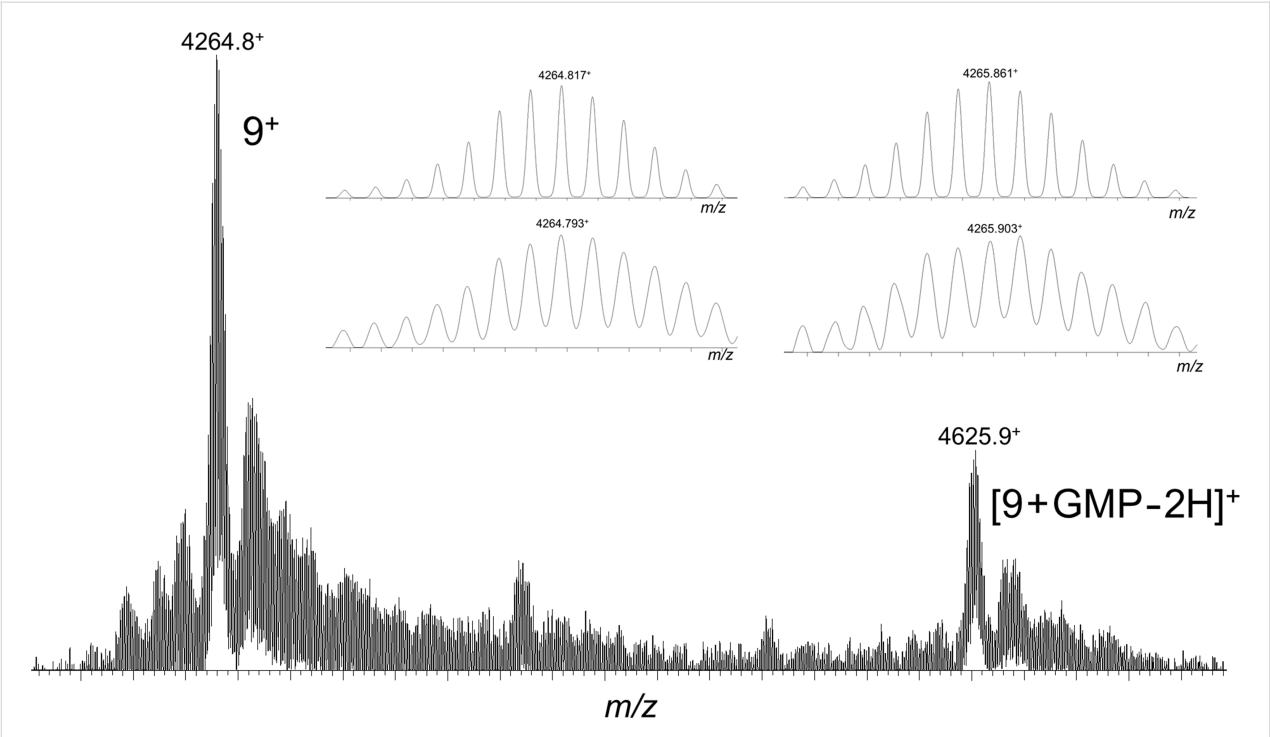

Figure 6: MALDI–MS analysis of a solution containing conjugate **9** and GMP after continuous light irradiation. In the inset, the experimental (bottom) and theoretical (top) isotope distributions are compared for both $\mathbf{9}^+$ and [**9** + GMP − 2H]$^+$ ions.

photophysical properties of the tethered complex **9** are not altered by the anchoring onto the calixarene platform and that the cyclic pentapeptide units do not interfere with the photoreactivity of the complex. Moreover, we verified that the complex is able to photoreact with its biological target, i.e., the guanine content of DNA, by demonstrating the occurrence of a photoinduced electron transfer and the formation of a covalent photoadduct between the Ru-calix(RGD)$_4$ conjugate **9** and GMP. In conclusion, the ruthenium complex should be able to perform efficiently its photoinduced cytotoxic activity, once incorporated into targeted cancer cells thanks to the multivalent platform. In cellulo studies are currently under investigation and will be reported in the near future.

Experimental

General: All the solvents and reagents for the syntheses were at least reagent grade quality and were used without further purification. Anhydrous *N*,*N*-dimethylformamide was purchased from ACROS Organics. Reactions were magnetically stirred and monitored by thin-layer chromatography using Fluka silica gel or aluminium oxide on TLC-PET foils with fluorescent indicator at 254 nm. All reactions involving ruthenium(II) were carried out in the dark. C18 reversed-phase silica gel (230−400 mesh) was used for chromatography. ^{1}H NMR spectra were recorded at ambient temperature on Bruker 300, Variant 400 and 600 MHz spectrometers and ^{13}C NMR spectra were recorded at 75, 100 or 150 MHz. Traces of residual solvents were used as internal standards for ^{1}H NMR (7.26 ppm for $CDCl_3$, 3.31 for CD_3OD, 4.79 for D_2O, 2.50 for DMSO-d_6 and 1.94 ppm for CD_3CN) and ^{13}C NMR (77.16 ppm for $CDCl_3$, 49.00 for CD_3OD, 39.52 for DMSO-d_6 and 118.26 ppm for CD_3CN) chemical shift referencing. Abbreviations: s = singlet, d = doublet, t = triplet, q = quartet, br = broad, m = massif, mult = multiplet). 2D NMR spectra (COSY, HSQC, HMBC, HSQC) were recorded to complete signal assignments. Melting points were recorded on a Stuart Scientific Analogue SMP11 or Büchi Melting Point B-545. Infrared spectra were recorded on a Bruker Alpha (ATR) spectrometer.

High-resolution mass spectra were obtained on a Waters Synapt G2-Si spectrometer (Waters, Manchester, UK) equipped with an electrospray ionization used in the positive ion mode. Source parameters were as follow: capillary voltage, 3.1 kV; sampling cone, 30 V; source Offset, 80 V; source temperature, 150 °C and desolvation temperature, 200 °C. Matrix-assisted laser desorption/ionization time-of-flight (MALDI-ToF) mass spectra were recorded using a Waters QToF Premier mass spectrometer equipped with a Nd-YAG laser of 355 nm with a maximum pulse energy of 65 μJ delivered to the sample at 50 Hz repeating rate. Time-of-flight mass analyses were performed in the reflection mode at a resolution of about 10 000. The matrix, *trans*-2-(3-(4-*tert*-butylphenyl)-2-methyl-2-propenylidene)malononitrile, was prepared as a 40 mg/mL solution in chloroform. The matrix solution (1 μL) was applied to a stainless-steel target and air-dried. The crude photoirradiation product was dissolved in acetonitrile and 1 μL aliquot of this solution was applied onto the target area (already bearing the matrix crystals) and then air-dried.

The HPLC purification process on final compound **9** was performed on a semi-preparative Infinity Agilent 1290 UHPLC system equipped with a binary pump, a thermostatically controlled injection system, a thermostatically controlled column compartment and a Diode Array detector. Waters C18 (Atlantis T3) column was used and the elution conditions are described in Supporting Information File 1.

Calix[4]arenes **2** and **3** were synthesized from commercial *p*-*tert*-butylcalix[4]arene **1** according to procedures described in the literature [69]. The experimental procedures and characterization data for calixarene derivatives **4**, **6**, **7** and **9**, phenanthroline derivative **5** and c-[RGDfK]-alkyne **8** are given in Supporting Information File 1.

The UV–vis absorption spectra were recorded on a Perkin-Elmer Lambda UV–vis spectrophotometer and the emission spectra with a Shimadzu RF-5001 PC spectrometer (detection: Hamamatsu R-928 red-sensitive photomultiplier tube, excitation source: xenon lamp 250 W). Emission quantum yields were determined by integrating the corrected emission spectra over the frequencies. $[Ru(bpy)_3]^{2+}$ in water under air was chosen as the standard luminophore (quantum yield of 0.042 under argon). The luminescence lifetimes were measured by the time-correlated single photon counting (TC-SPC) technique with the Edinburgh Instruments LifeSpecII Picosecond Fluorescence Lifetime Spectrometer equipped with a laser diode (λ = 439 nm, pulse = 100 ps). The samples were thermostatted at 20 ± 2 °C with a Haake Model NB22 temperature controller. The data were collected by a multichannel analyzer (2048 channels) with a number of counts in the first channel equal to 104. The resulting decays were deconvoluted for the instrumental response and fitted to the exponential functions using the original manufacturer software package (Edinburgh Instruments). The reduced χ^2, weighted residuals and autocorrelation function were employed to judge the quality of the fits.

For molecular modelling simulations, the initial structure of the ruthenium complex was obtained from previous DFT calculations using a previously reported methodology [82]. The geometries of the RAFTs and calixarene were built using DS BIOVIA© software and geometry-optimized using the CHARMM force-field, taking into account previous molecular

modelling simulations on cyclic peptides [83]. The structures were linked together yielding through several steps of energy minimizations, maintaining the ruthenium complex constrained in octahedral geometry by harmonic constraints. After energy minimization of the entire structure, MD simulations of 5 ns were produced in NVT ensemble at 300 K, in the generalized Born implicit solvent model. Although the MD simulation time used here is way insufficient to probe the conformational landscape of this large molecule, the conformations reported here represent relaxed geometries showing possible intermolecular contacts between the cyclic pentapeptides. The analysis and visualization of MD simulations were carried out using DS BIOVIA and Chimera [84] software.

Supporting Information

Supporting Information File 1

Supplementary information.
[https://www.beilstein-journals.org/bjoc/content/supplementary/1860-5397-14-150-S1.pdf]

Acknowledgements

S.K. thanks the Fonds pour la Formation à la Recherche dans l'Industrie et dans l'Agriculture (FRIA-FRS, Belgium) for her PhD grant. C.M. and M.S. thank the F.R.S.-FNRS ("Fonds National pour la Recherche Scientifique", Belgium) for continuing support, notably through the grants 2.4530.12, 2.4615.11, UN02715F, CDR J.0022.18, and F.4532.16. This work was also supported by the COST action CM 1202 and a "10 km de Bruxelles" grant. The mass spectrometry laboratory @ UMONS is grateful to the "Fonds National pour la Recherche Scientifique" (FNRS-Belgium) for financial support in the acquisition of the Waters QTOF premier and the Waters Synapt G2-Si mass spectrometers. D.B. and E.D. acknowledge support from the French National Research Agency (Labex program ARCANE, ANR-11-LABX-0003-01). L.M. thanks Pr. Kristin Bartik and Pr. Benjamin Elias for their continuing support. I.J. thanks the "Actions de Recherches Concertées" of the Fédération Wallonie-Bruxelles and the ULB for financial support.

ORCID® iDs

Sofia Kajouj - https://orcid.org/0000-0002-6105-1691
Lionel Marcelis - https://orcid.org/0000-0002-6324-477X
Pierre Van Antwerpen - https://orcid.org/0000-0002-4934-8863
Didier Boturyn - https://orcid.org/0000-0003-2530-0299
Eric Defrancq - https://orcid.org/0000-0002-3911-6241
Mathieu Surin - https://orcid.org/0000-0001-8950-3437
Julien De Winter - https://orcid.org/0000-0003-3429-5911
Pascal Gerbaux - https://orcid.org/0000-0001-5114-4352
Ivan Jabin - https://orcid.org/0000-0003-2493-2497
Cécile Moucheron - https://orcid.org/0000-0001-9293-0165

References

1. Kirch, M.; Lehn, J. M.; Sauvage, J.-P. *Helv. Chim. Acta* **1979,** *62,* 1345–1384. doi:10.1002/hlca.19790620449
2. Juris, A.; Balzani, V.; Barigelletti, F.; Campagna, S.; Belser, P.; von Zelewsky, A. *Coord. Chem. Rev.* **1988,** *84,* 85–277. doi:10.1016/0010-8545(88)80032-8
3. Dare-Edwards, M. P.; Goodenough, J. B.; Hamnett, A.; Seddon, K. R.; Wright, R. D. *Faraday Discuss. Chem. Soc.* **1980,** *70,* 285–298. doi:10.1039/dc9807000285
4. Puntoriero, F.; Sartorel, A.; Orlandi, M.; La Ganga, G.; Serroni, S.; Bonchio, M.; Scandola, F.; Campagna, S. *Coord. Chem. Rev.* **2011,** *255,* 2594–2601. doi:10.1016/j.ccr.2011.01.026
5. Friedman, A. E.; Chambron, J. C.; Sauvage, J. P.; Turro, N. J.; Barton, J. K. *J. Am. Chem. Soc.* **1990,** *112,* 4960–4962. doi:10.1021/ja00168a052
6. Boynton, A. N.; Marcélis, L.; Barton, J. K. *J. Am. Chem. Soc.* **2016,** *138,* 5020–5023. doi:10.1021/jacs.6b02022
7. Deraedt, Q.; Marcélis, L.; Auvray, T.; Hanan, G. S.; Loiseau, F.; Elias, B. *Eur. J. Inorg. Chem.* **2016,** *2016,* 3649–3658. doi:10.1002/ejic.201600468
8. Deraedt, Q.; Marcélis, L.; Loiseau, F.; Elias, B. *Inorg. Chem. Front.* **2017,** *4,* 91–103. doi:10.1039/C6QI00223D
9. Boynton, A. N.; Marcélis, L.; McConnell, A. J.; Barton, J. K. *Inorg. Chem.* **2017,** *56,* 8381–8389. doi:10.1021/acs.inorgchem.7b01037
10. Piraux, G.; Bar, L.; Abraham, M.; Lavergne, T.; Jamet, H.; Dejeu, J.; Marcélis, L.; Defrancq, E.; Elias, B. *Chem. – Eur. J.* **2017,** *23,* 11872–11880. doi:10.1002/chem.201702076
11. Saadallah, D.; Bellakhal, M.; Amor, S.; Lefebvre, J.-F.; Chavarot-Kerlidou, M.; Baussanne, I.; Moucheron, C.; Demeunynck, M.; Monchaud, D. *Chem. – Eur. J.* **2017,** *23,* 4967–4972. doi:10.1002/chem.201605948
12. Feeney, M. M.; Kelly, J. M.; Tossi, A. B.; Kirsch-De Mesmaeker, A.; Lecomte, J.-P. *J. Photochem. Photobiol., B* **1994,** *23,* 69–78. doi:10.1016/1011-1344(93)06985-C
13. Troian-Gautier, L.; Mugeniwabagara, E.; Fusaro, L.; Moucheron, C.; Kirsch-De Mesmaeker, A.; Luhmer, M. *Inorg. Chem.* **2016,** *56,* 1794–1803. doi:10.1021/acs.inorgchem.6b01780
14. Troian-Gautier, L.; Mugeniwabagara, E.; Fusaro, L.; Cauët, E.; Kirsch-De Mesmaeker, A.; Luhmer, M. *J. Am. Chem. Soc.* **2017,** *139,* 14909–14912. doi:10.1021/jacs.7b09513
15. Blasius, R.; Nierengarten, H.; Luhmer, M.; Constant, J.-F.; Defrancq, E.; Dumy, P.; van Dorsselaer, A.; Moucheron, C.; Kirsch-De Mesmaeker, A. *Chem. – Eur. J.* **2005,** *11,* 1507. doi:10.1002/chem.200400591
16. Marcélis, L.; Ghesquière, J.; Garnir, K.; Kirsch-De Mesmaeker, A.; Moucheron, C. *Coord. Chem. Rev.* **2012,** *256,* 1569–1582. doi:10.1016/j.ccr.2012.02.012
17. Ghesquière, J.; Le Gac, S.; Marcélis, L.; Moucheron, C.; Kirsch-De Mesmaeker, A. *Curr. Top. Med. Chem.* **2012,** *12,* 185–196. doi:10.2174/156802612799079008
18. Garnir, K.; Estalayo-Adrián, S.; Lartia, R.; De Winter, J.; Defrancq, E.; Surin, M.; Lemaur, V.; Gerbaux, P.; Moucheron, C. *Faraday Discuss.* **2015,** *185,* 267–284. doi:10.1039/C5FD00059A
19. Estalayo-Adrián, S.; Garnir, K.; Moucheron, C. *Chem. Commun.* **2018,** *54,* 322–337. doi:10.1039/C7CC06542F
20. Jacquet, L.; Davies, R. J. H.; Kirsch-De Mesmaeker, A.; Kelly, J. M. *J. Am. Chem. Soc.* **1997,** *119,* 11763–11768. doi:10.1021/ja971163z

21. Jacquet, L.; Kelly, J. M.; Kirsch-De Mesmaeker, A. *J. Chem. Soc., Chem. Commun.* **1995,** 913–914. doi:10.1039/C39950000913
22. Marcélis, L.; Rebarz, M.; Lemaur, V.; Fron, E.; De Winter, J.; Moucheron, C.; Gerbaux, P.; Beljonne, D.; Sliwa, M.; Kirsch-De Mesmaeker, A. *J. Phys. Chem. B* **2015,** *119,* 4488–4500. doi:10.1021/acs.jpcb.5b00197
23. Pauly, M.; Kayser, I.; Schmitz, M.; Dicato, M.; Del Guerzo, A.; Kolber, I.; Moucheron, C.; Kirsch-De Mesmaeker, A. *Chem. Commun.* **2002,** 1086–1087. doi:10.1039/b202905g
24. Lentzen, O.; Defrancq, E.; Constant, J. F.; Schumm, S.; García-Fresnadillo, D.; Moucheron, C.; Dumy, P.; Kirsch-De Mesmaeker, A. *J. Biol. Inorg. Chem.* **2004,** *9,* 100–108. doi:10.1007/s00775-003-0502-3
25. Marcélis, L.; Moucheron, C.; Kirsch-De Mesmaeker, A. *Philos. Trans. R. Soc., A* **2013,** 371. doi:10.1098/rsta.2012.0131
26. Marcélis, L.; Surin, M.; Lartia, R.; Moucheron, C.; Defrancq, E.; Kirsch-De Mesmaeker, A. *Eur. J. Inorg. Chem.* **2014,** *2014,* 3016–3022. doi:10.1002/ejic.201402189
27. Reschner, A.; Bontems, S.; Le Gac, S.; Lambermont, J.; Marcélis, L.; Defrancq, E.; Hubert, P.; Moucheron, C.; Kirsch-De Mesmaeker, A.; Raes, M.; Piette, J.; Delvenne, P. *Gene Ther.* **2013,** *20,* 435–443. doi:10.1038/gt.2012.54
28. Marcélis, L.; Van Overstraeten-Schlögel, N.; Lambermont, J.; Bontems, S.; Spinelli, N.; Defrancq, E.; Moucheron, C.; Kirsch-De Mesmaeker, A.; Raes, M. *ChemPlusChem* **2014,** *79,* 1597–1604. doi:10.1002/cplu.201402212
29. Puckett, C. A.; Barton, J. K. *Biochemistry* **2008,** *47,* 11711–11716. doi:10.1021/bi800856t
30. Puckett, C. A.; Barton, J. K. *J. Am. Chem. Soc.* **2007,** *129,* 46–47. doi:10.1021/ja0677564
31. Matson, M.; Svensson, F. R.; Nordén, B.; Lincoln, P. *J. Phys. Chem. B* **2011,** *115,* 1706–1711. doi:10.1021/jp109530f
32. Svensson, F. R.; Matson, M.; Li, M.; Lincoln, P. *Biophys. Chem.* **2010,** *149,* 102–106. doi:10.1016/j.bpc.2010.04.006
33. Cloonan, S. M.; Elmes, R. B. P.; Erby, M. L.; Bright, S. A.; Poynton, F. E.; Nolan, D. E.; Quinn, S. J.; Gunnlaugsson, T.; Williams, D. C. *J. Med. Chem.* **2015,** *58,* 4494–4505. doi:10.1021/acs.jmedchem.5b00451
34. Byrne, A.; Dolan, C.; Moriarty, R. D.; Martin, A.; Neugebauer, U.; Forster, R. J.; Davies, A.; Volkov, Y.; Keyes, T. E. *Dalton Trans.* **2015,** *44,* 14323–14332. doi:10.1039/C5DT01833A
35. van Rijt, S. H.; Kostrhunova, H.; Brabec, V.; Sadler, P. J. *Bioconjugate Chem.* **2011,** *22,* 218–226. doi:10.1021/bc100369p
36. Gamba, I.; Salvadó, I.; Rama, G.; Bertazzon, M.; Sánchez, M. I.; Sánchez-Pedregal, V. M.; Martínez-Costas, G.; Brissos, R. F.; Gamez, P.; Mascarenãs, J. L.; Vásquez-López, M.; Vásquez, M. E. *Chem. – Eur. J.* **2013,** *19,* 13369–13375. doi:10.1002/chem.201301629
37. Burke, C. S.; Byrne, A.; Keyes, T. E. *J. Am. Chem. Soc.* **2018,** *140,* 6945–6955. doi:10.1021/jacs.8b02711
38. Marcélis, L.; Kajouj, K.; Ghesquière, J.; Fettweis, G.; Coupienne, I.; Lartia, R.; Surin, M.; Defrancq, E.; Piette, J.; Moucheron, C.; Kirsch-De Mesmaeker, A. *Eur. J. Inorg. Chem.* **2016,** *2016,* 2902–2911. doi:10.1002/ejic.201600278
39. Max, R.; Gerritsen, R. R. C. M.; Nooijen, P. T. G. A.; Goodman, S. L.; Sutter, A.; Keilholz, U.; Ruiter, D. J.; De Waal, R. M. W. *Int. J. Cancer* **1997,** *71,* 320–324. doi:10.1002/(SICI)1097-0215(19970502)71:3<320::AID-IJC2>3.0.CO;2-#
40. Ferrara, N.; Kerbel, R. S. *Nature* **2005,** *438,* 967–974. doi:10.1038/nature04483
41. Haubner, R.; Gratias, R.; Diefenbach, B.; Goodman, S. L.; Jonczyk, A.; Kessler, H. *J. Am. Chem. Soc.* **1996,** *118,* 7461–7472. doi:10.1021/ja9603721
42. Dechantsreiter, M. A.; Planker, E.; Mathä, B.; Lohof, E.; Hölzemann, G.; Jonczyk, A.; Goodman, S. L.; Kessler, H. *J. Med. Chem.* **1999,** *42,* 3033–3040. doi:10.1021/jm970832g
43. Castel, S.; Pagan, R.; Mitjans, F.; Piulats, J.; Goodman, S.; Jonczyk, A.; Huber, F.; Vilaró, S.; Reina, M. *Lab. Invest.* **2001,** *81,* 1615–1626. doi:10.1038/labinvest.3780375
44. Mammen, M.; Choi, S.-K.; Whitesides, G. M. *Angew. Chem., Int. Ed.* **1998,** *37,* 2754–2794. doi:10.1002/(SICI)1521-3773(19981102)37:20<2754::AID-ANIE2754>3.0.CO;2-3
45. Kiessling, L. L.; Lamanna, A. C. Multivalency In Biological Systems. In *Chemical Probes in Biology;* Schneider, M. P., Ed.; Springer: Netherlands, 2003; Vol. 129, pp 345–357. doi:10.1007/978-94-007-0958-4_26
46. Gestwicki, J. E.; Cairo, C. W.; Strong, L. E.; Oetjen, K. A.; Kiessling, L. L. *J. Am. Chem. Soc.* **2002,** *124,* 14922–14933. doi:10.1021/ja027184x
47. Wu, Y.; Zhang, X.; Xiong, Z.; Cheng, Z.; Fisher, D. R.; Liu, S.; Gambhir, S. S.; Chen, X. *J. Nucl. Med.* **2005,** *46,* 1707–1718.
48. Ye, Y.; Bloch, S.; Xu, B.; Achilefu, S. *J. Med. Chem.* **2006,** *49,* 2268–2275. doi:10.1021/jm050947h
49. Shi, J.; Kim, Y.-S.; Zhai, S.; Liu, Z.; Chen, X.; Liu, S. *Bioconjugate Chem.* **2009,** *20,* 750–759. doi:10.1021/bc800455p
50. Wenk, C. H. F.; Ponce, F.; Guillermet, S.; Tenaud, C.; Boturyn, D.; Dumy, P.; Watrelot-Virieux, D.; Carozzo, C.; Josserand, V.; Coll, J.-L. *Cancer Lett.* **2013,** *334,* 188–195. doi:10.1016/j.canlet.2012.10.041
51. Temming, K.; Meyer, D. L.; Zabinski, R.; Dijkers, E. C. F.; Poelstra, K.; Molema, G.; Kok, R. J. *Bioconjugate Chem.* **2006,** *17,* 1385–1394. doi:10.1021/bc060087z
52. Foillard, S.; Sancey, L.; Coll, J.-L.; Boturyn, D.; Dumy, P. *Org. Biomol. Chem.* **2009,** *7,* 221–224. doi:10.1039/B817251J
53. Karageorgis, A.; Claron, M.; Jugé, R.; Aspord, C.; Leloup, C.; Thoreau, F.; Kurcharczak, J.; Plumas, J.; Henry, M.; Hurbin, A.; Verdié, P.; Martinez, J.; Subra, G.; Dumy, P.; Boturyn, D.; Aouacheria, A.; Coll, J.-L. *Mol. Ther.* **2017,** *25,* 534–546. doi:10.1016/j.ymthe.2016.11.002
54. Gutsche, C. D. Calixarenes: An introduction. 2nd ed.; Stoddart, J. F., Ed.; Monographs in Supramolecular Chemistry; The Royal Society of Chemistry: Cambridge, 2008. doi:10.1039/9781847558190
55. Lavendomme, R.; Zahim, S.; De Leener, G.; Inthasot, A.; Mattiuzzi, A.; Luhmer, M.; Reinaud, O.; Jabin, I. *Asian J. Org. Chem.* **2015,** *4,* 710–722. doi:10.1002/ajoc.201500178
56. Mattiuzzi, A., II; Marcélis, L.; Jabin, I.; Moucheron, C.; Kirsch-De Mesmaeker, A. *Inorg. Chem.* **2013,** *52,* 11228–11236. doi:10.1021/ic401468t
57. Casnati, A.; Sansone, F.; Ungaro, R. *Acc. Chem. Res.* **2003,** *36,* 246–254. doi:10.1021/ar0200798
58. Giuliani, M.; Morbioli, I.; Sansone, F.; Casnati, A. *Chem. Commun.* **2015,** *51,* 14140–14159. doi:10.1039/C5CC05204A
59. Sansone, F.; Casnati, A. *Chem. Soc. Rev.* **2013,** *42,* 4623–4639. doi:10.1039/c2cs35437c
60. Sun, J.; Blaskovich, M. A.; Jain, R. K.; Delarue, F.; Paris, D.; Brem, S.; Wotoczek-Obadia, M.; Lin, Q.; Coppola, D.; Choi, K.; Mullan, M.; Hamilton, A. D.; Sebti, S. M. *Cancer Res.* **2004,** *64,* 3586–3592. doi:10.1158/0008-5472.CAN-03-2673

61. Baldini, L.; Casnati, A.; Sansone, F.; Ungaro, R. *Chem. Soc. Rev.* **2007,** *36,* 254–266. doi:10.1039/B603082N
62. Sansone, F.; Baldini, L.; Casnati, A.; Ungaro, R. *New J. Chem.* **2010,** *34,* 2715–2728. doi:10.1039/c0nj00285b
63. Le Poul, N.; Le Mest, Y.; Jabin, I.; Reinaud, O. *Acc. Chem. Res.* **2015,** *48,* 2097–2106. doi:10.1021/acs.accounts.5b00152
64. Nimse, S. B.; Kim, T. *Chem. Soc. Rev.* **2013,** *42,* 366–386. doi:10.1039/C2CS35233H
65. Haubner, R.; Wester, H.-J.; Burkhart, F.; Senekowitsch-Schmidtke, R.; Weber, W.; Goodman, S. L.; Kessler, H.; Schwaiger, M. *J. Nucl. Med.* **2001,** *42,* 326–336.
66. Dondoni, A.; Marra, A. *Chem. Rev.* **2010,** *110,* 4949–4977. doi:10.1021/cr100027b
67. Rostovtsev, V. V.; Green, L. G.; Fokin, V. V.; Sharpless, K. B. *Angew. Chem., Int. Ed.* **2002,** *41,* 2596–2599. doi:10.1002/1521-3773(20020715)41:14<2596::AID-ANIE2596>3.0.CO;2-4
68. Meldal, M.; Tornøe, C. W. *Chem. Rev.* **2008,** *108,* 2952–3015. doi:10.1021/cr0783479
69. Mattiuzzi, A.; Jabin, I.; Mangeney, C.; Roux, C.; Reinaud, O.; Santos, L.; Bergamini, J.-F.; Hapiot, P.; Lagrost, C. *Nat. Commun.* **2012,** *3,* No. 1130. doi:10.1038/ncomms2121
70. Ikeda, A.; Shinkai, S. *Chem. Rev.* **1997,** *97,* 1713–1734. doi:10.1021/cr960385x
71. Deroo, S.; Defrancq, E.; Moucheron, C.; Kirsch-De Mesmaeker, A.; Dumy, P. *Tetrahedron Lett.* **2003,** *44,* 8379–8382. doi:10.1016/j.tetlet.2003.09.128
72. Kolb, H. C.; Sharpless, K. B. *Drug Discovery Today* **2003,** *8,* 1128–1137. doi:10.1016/S1359-6446(03)02933-7
73. Consoli, G. M. L.; Granata, G.; Fragassi, G.; Grossi, M.; Sallese, M.; Geraci, C. *Org. Biomol. Chem.* **2015,** *13,* 3298–3307. doi:10.1039/C4OB02333A
74. Bew, S. P.; Brimage, R. A.; L'Hermite, N.; Sharma, S. V. *Org. Lett.* **2007,** *9,* 3713–3716. doi:10.1021/ol071047t
75. Ryu, E.-H.; Zhao, Y. *Org. Lett.* **2005,** *7,* 1035–1037. doi:10.1021/ol047468h
76. Rusu, R.; Szumna, A.; Rosu, N.; Dumea, C.; Danac, R. *Tetrahedron* **2015,** *71,* 2922–2926. doi:10.1016/j.tet.2015.03.060
77. Vecchi, A.; Melai, B.; Marra, A.; Chiappe, C.; Dondoni, A. *J. Org. Chem.* **2008,** *73,* 6437–6440. doi:10.1021/jo800954z
78. Zahim, S.; Lavendomme, R.; Reinaud, O.; Luhmer, M.; Evano, G.; Jabin, I. *Org. Biomol. Chem.* **2016,** *14,* 1950–1957. doi:10.1039/C5OB02367J
79. Gawande, M. B.; Goswami, A.; Felpin, F.-X.; Asefa, T.; Huang, X.; Silva, R.; Zou, X.; Zboril, R.; Varma, R. S. *Chem. Rev.* **2016,** *116,* 3722–3811. doi:10.1021/acs.chemrev.5b00482
80. No such aggregates were detected when the conjugate **9** was used in Tris·HCl buffer for photochemical experiments.
81. Rebarz, M.; Marcélis, L.; Menand, M.; Cornut, D.; Moucheron, C.; Jabin, I.; Kirsch-De Mesmaeker, A. *Inorg. Chem.* **2014,** *53,* 2635–2644. doi:10.1021/ic403024z
82. Ghizdavu, L.; Pierard, F.; Rickling, S.; Aury, S.; Surin, M.; Beljonne, D.; Lazzaroni, R.; Murat, P.; Defrancq, E.; Moucheron, C.; Kirsch-De Mesmaeker, A. *Inorg. Chem.* **2009,** *48,* 10988–10994. doi:10.1021/ic901007w
83. Marinelli, L.; Lavecchia, A.; Gottschalk, K.-E.; Novellino, E.; Kessler, H. *J. Med. Chem.* **2003,** *46,* 4393–4404. doi:10.1021/jm020577m
84. Pettersen, E. F.; Goddard, T. D.; Huang, C. C.; Couch, G. S.; Greenblatt, D. M.; Meng, E. C.; Ferrin, T. E. *J. Comput. Chem.* **2004,** *25,* 1605–1612. doi:10.1002/jcc.20084

License and Terms

BEILSTEIN JOURNAL OF ORGANIC CHEMISTRY

Strong binding and fluorescence sensing of bisphosphonates by guanidinium-modified calix[5]arene

Jie Gao[1], Zhe Zheng[1], Lin Shi[1], Si-Qi Wu[1], Hongwei Sun[*1] and Dong-Sheng Guo[*1,2]

Full Research Paper

Open Access

Address:
[1]College of Chemistry, Key Laboratory of Advanced Energy Materials Chemistry (Ministry of Education), Nankai University, Tianjin 300071, China and [2]Collaborative Innovation Center of Chemical Science and Engineering, Nankai University, Tianjin 300071, China

Email:
Hongwei Sun[*] - sunhw@nankai.edu.cn; Dong-Sheng Guo[*] - dshguo@nankai.edu.cn

* Corresponding author

Keywords:
bisphosphonate; calixarene; fluorescence sensing; macrocyclic chemistry; indicator displacement assay

Beilstein J. Org. Chem. **2018,** *14,* 1840–1845.
doi:10.3762/bjoc.14.157

Received: 11 April 2018
Accepted: 26 June 2018
Published: 19 July 2018

This article is part of the thematic issue "Macrocyclic and supramolecular chemistry".

Guest Editor: M.-X. Wang

Abstract

Based on the indicator displacement assay (IDA) approach, we herein report the fluorescence “switch-on” sensing and quantitative detection of bisphosphonates (BPs), a class of drugs extensively used in the treatment of patients with various skeletal diseases. Guanidinium-modified calix[5]arene (GC5A) affords strong binding on the micromolar to nanomolar level towards BPs dominantly via multiple salt bridge interactions, which was evaluated by fluorescence competitive titrations. Fluorescent IDA enables the highly sensitive and label-free detection of BPs in buffer solution, and more importantly, in artificial urine. Calibration lines were therefore set up in untreated artificial urine, allowing for quantifying the concentrations of BPs in the biologically relevant low range.

Introduction

Bisphosphonates (BPs) are a kind of drugs characterized by the $-C(PO_3)_2$ group (Scheme 1a) for treating various types of bone disorders and calcium metabolic diseases [1]. They are widely used in the treatment of osteoporosis, osteitis deformans, hypercalcaemia and bone pain caused by bone metastases of malignant tumors [2,3]. In addition, BPs are increasingly considered due to their potential role in preventing and treating cancer-induced bone loss and antitumor effects [4,5]. With this regard, assays for BPs are significant for identifying the quality of pharmaceutical formulations, as well as monitoring drug plasma concentrations, analyzing drug biodistribution in bone tissue, and detecting drug excretion in urine. For example, BPs are of poor bioavailability if orally administered (generally with absorption less than 1%) and about 50% of the absorbed dose is taken up selectively by the skeleton. Therefore, tracking the concentrations of BPs in biological systems has clinical signifi-

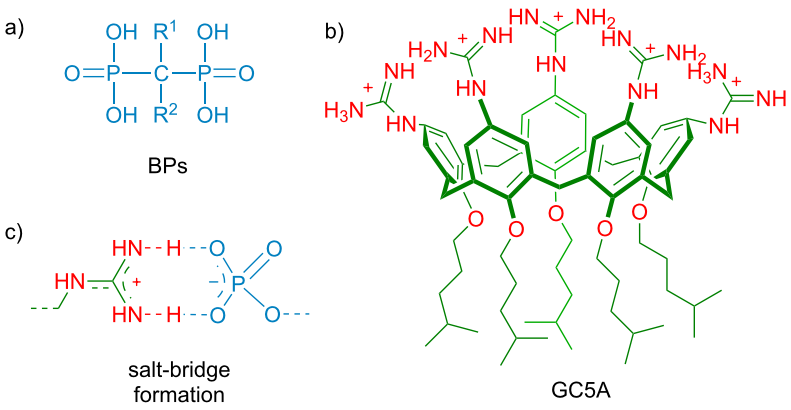

Scheme 1: The chemical structures of (a) bisphosphonates (BPs) and (b) guanidinium-modified calix[5]arene (GC5A). (c) Schematic illustration of a salt-bridge between a phosphate anion and a guanidinium cation.

cance for the doctor to record a patient's drug absorption in real time and adjust the dosage in time [6]. Numerous analytical methods, based on diverse principles, have been developed for detecting BPs in pharmaceuticals and biological materials [7,8]. Due to BPs′ high polarity, they are difficult to separate on reversed-phase columns. To make them more amenable to analysis, ion-pairing or complex-forming reagents were used to decrease the ionic character of the molecules [9]. However, this method will greatly reduce the life of the column [10]. Moreover, the absence of a chromophore in most BPs lead to the employment of derivatization by an UV–vis light-absorbing or fluorescence label for detection [11,12]. However, directly labeling BPs in biological media is difficult because many other components can reduce the efficiency of the labeling reaction. Especially in urine, it is extraordinary challenging to achieve labelling of BPs because urine generally contains a large amount of polar compounds such as phosphates, unless these are removed in advance [7]. Ion chromatography combined with conductivity detection (or other detectors) can be used to solve the problems of separation and detection of BPs, but the relatively expensive instruments often are not affordable [13]. As a result, the development of a label-free optical method for BPs detection is highly appealing in view of low cost, ease of use and high sensitivity of optical sensing modalities, but remains a challenge since BPs are considered as unlabeled analytes.

With the development of the host–guest concept in supramolecular chemistry, the indicator displacement assay (IDA), pioneered by Prof. Anslyn and co-workers, has been popularized as an alternative strategy for molecular sensing, complementary to direct sensing [14-16]. IDA refers to a signal change of an indicator upon competition between an analyte and the indicator for the binding to a receptor. The label-free method renders IDA particularly suitable for the detection of analytes lacking chromophores. The key factor in IDA is the rational design of artificial receptors that are capable of binding analytes strongly and specifically. Calixarenes are the third generation of macrocyclic receptors after crown ethers and cyclodextrins. Due to their facial modification, Prof. Böhmer demonstrated calixarenes as having “(almost) unlimited possibilities” [17]. We have focused on molecular recognition and self-assembly of water-soluble calixarene derivatives for a long time [18-24], directed by exploring biomedical applications of them [25-28]. In this work, we report a fluorescent IDA approach for detecting BPs quantitatively in not only buffer solution but also artificial urine (Scheme 2). The rationale behind the IDA approach is the strong and selective complexation of BPs by guanidinium-modified calix[5]arene (GC5A, Scheme 1b). Such label-free sensing strategy exhibits potential application in real-time monitoring concentrations of BPs in urine and pharmacokinetic studies.

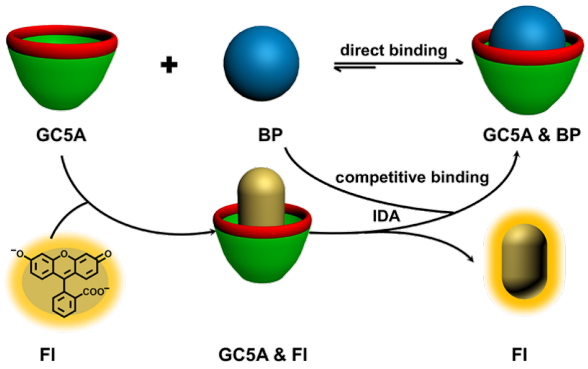

Scheme 2: Schematic illustration of the binding between BPs and GC5A and the operating IDA principle of fluorescence “switch-on” sensing of BPs by the GC5A·Fl reporter pair.

Results and Discussion

The main skeleton of BPs possesses two phosphate groups which are potential binding sites and therefore GC5A was tested as binding receptor. GC5A was prepared according to our previous procedure [26] and the guanidinium groups installed in the upper rim are expected to form multiple salt bridge interactions (charge-assisted hydrogen bonds) with the phosphate groups of BPs (Scheme 1c) [26,29].

To execute IDA, we employed fluorescein (Fl) as the reporter dye according to our previously published result [26]. Fl of high brightness is strongly encapsulated into the GC5A cavity (K_a = 5.0 × 10^6 M^{-1}), accompanied with a drastic complexation-induced fluorescence quenching (I_{free}/I_{bound} = 37). Taken together, these factors make the GC5A·Fl reporter pair an ideal combination for the projected IDA application. IDA was implemented to determine the binding affinities between GC5A and BPs via competitive fluorescence titrations. More importantly, the displacement of the reporter dye, accompanied with fluorescence recovery, offers the opportunity for fluorescence "switch-on" sensing of BPs. In general, fluorescent IDA could be operated at low μM or even nM concentrations, which is desirable with respect to sensing sensitivity.

We tested the host–guest complexation of GC5A with a total number of 9 BP drugs clinically applied (Scheme 3) by utilizing competitive fluorescence titrations. Upon gradual addition of BPs gives rise to the displacement of Fl out of the GC5A cavity, and therefore recovery of the intrinsic emission of Fl (Figure 1 and Figures S1–S8 in Supporting Information File 1). The data fitted well with the 1:1 competitive binding model, giving the K_a values as listed in Table 1. Ibandronate, alendronate and neridronate gave an around 40–100 times weaker binding than etidronate, which is probably due to the aminoalkyl-substituents present in the former compounds. However, pamidronate having an aminoethyl substituent shows comparable binding to etidronate. At present, the reason for this behavior remains unclear. Overall, the strong binding of 9 BPs with GC5A with association constants in the μM to nM range is suitable for the following sensing study.

By executing IDA based on the GC5A·Fl reporter pair, we realized the fluorescence "switch-on" sensing of BPs. We herein selected clodronate, zoledronate and etidronate to further investigate their quantitative detection. As shown in Figure 2a, increasing the concentrations of BPs resulted in a practically linear fluorescence increase. The limit of detection (LOD) for

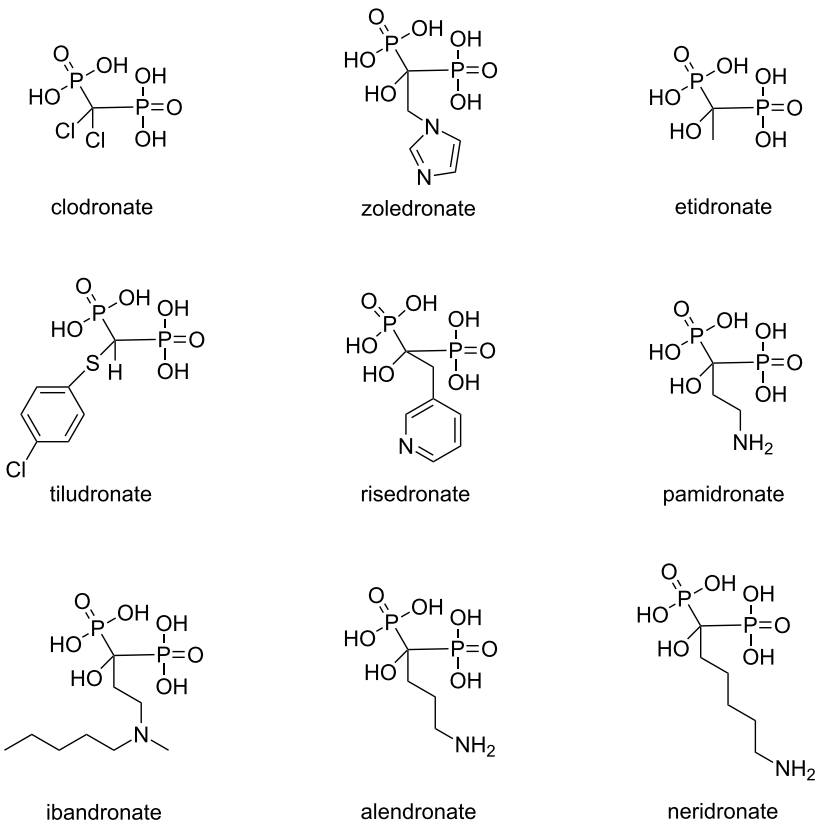

Scheme 3: The chemical structures of the selected BP drugs.

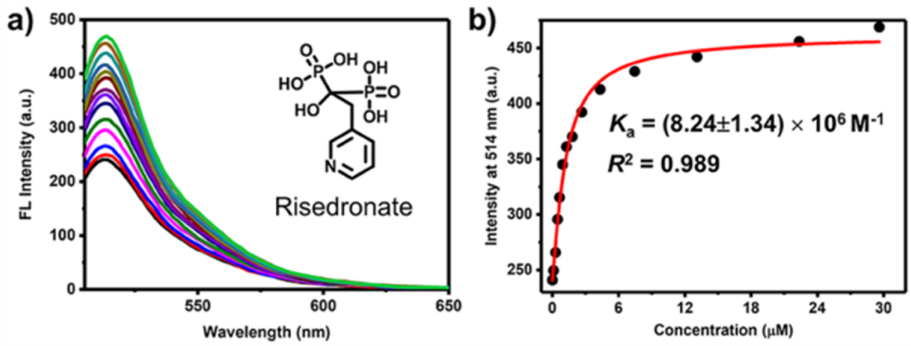

Figure 1: (a) Fluorescence competitive titration of GC5A·FI (0.9/1.0 μM) with risedronate (up to 29.6 μM) in HEPES buffer (10 mM, pH 7.4) at 25 °C, λ_{ex} = 500 nm. (b) The competitive titration curve, λ_{em} = 514 nm, and fitting data according to a 1:1 competitive binding model.

Table 1: Association constants (K_a) of BPs and GC5A determined according to the competitive titration method. All experiments were performed in HEPES buffer (10 mM, pH 7.4) at 25 °C.

BPs	K_a (M^{-1})
clodronate	(6.60 ± 0.37) × 10^7
zoledronate	(1.34 ± 0.12) × 10^7
etidronate	(1.24 ± 0.15) × 10^7
tiludronate	(8.31 ± 0.97) × 10^6
risedronate	(8.24 ± 1.34) × 10^6
pamidronate	(5.37 ± 0.71) × 10^6
ibandronate	(3.01 ± 0.65) × 10^5
alendronate	(1.80 ± 0.18) × 10^5
neridronate	(1.26 ± 0.26) × 10^5

BPs was calculated to be 4.9 nM for clodronate, 6.6 nM for zoledronate and 3.1 nM for etidronate by utilizing a 3σ/slope method [7,30,31]. These low values of LOD also demonstrate the high sensitivity of the IDA strategy based on the GC5A·Fl combination. The ultra-sensitive detection of BPs down to the low nM range benefits from not only the strong binding ability of GC5A but also the efficient fluorescence response of the GC5A·Fl reporter pair.

Compared to sensing in buffered solutions, it is more challenging to detect analytes directly in complex biological samples such as urine, blood serum or plasma, saliva, etc. The aforementioned results in HEPES buffer of high performance encouraged us to further test the IDA strategy in urine. As the urine composition is affected by individual differences, water intake, the time of urination and other factors [32], we herein

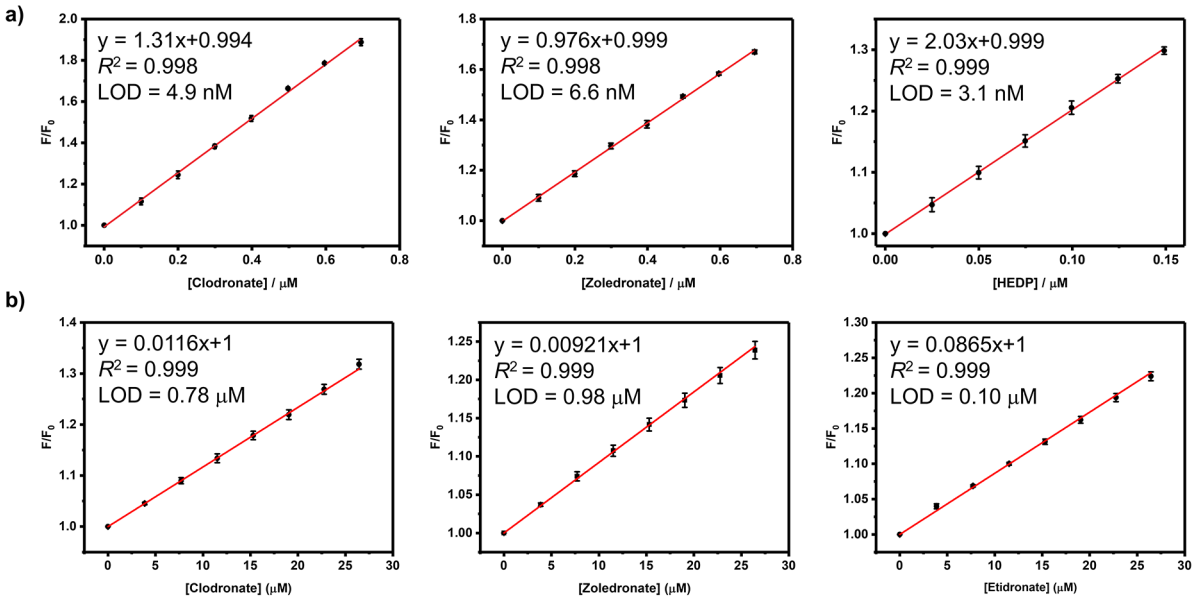

Figure 2: The set-up calibration lines of the fluorescence intensities for quantitatively determining the concentrations of clodronate, zoledronate and etidronate in (a) HEPES buffer (10 mM, pH 7.4) and (b) artificial urine at 25 °C. Error bars could not be shown if less than 0.005.

employed artificial urine as the proof-of-principle sample. Although there are numerous interfering substances in artificial urine [33], we still observed the linear increase in fluorescence of the GC5A·Fl reporter pair upon gradual addition of BPs (Figure 2b). The LOD values in artificial urine were calculated as 0.78 μM for clodronate, 0.98 μM for zoledronate, and 0.10 μM for etidronate. With respect to the requisite detection limit in urine BP concentrations typically observed in patients with bone disease after the administration of BPs [7], the present IDA strategy with such low LOD values represents a sensitive approach for detecting BPs. Based on the linear relationship of good performance (R^2: clodronate 0.999, zoledronate 0.999 and etidronate 0.999), we set up a series of calibration lines of the fluorescence output. These calibration lines of BPs are meaningful for quantitatively tracking drug excretion in urine down to the low μM range.

Conclusion

In conclusion, we have established an IDA approach based on the GC5A·Fl reporter pair for fluorescence "switch-on" sensing and quantitative detection of BPs. Thanks to the strong binding capabilities of GC5A towards BPs, we realized a highly sensitive and label-free detection of BPs through the fluorescent IDA. For accurately determining unknown concentrations of BPs down to the low μM range of tracking drug excretion, calibration lines were successfully set up in artificial urine. The present study paves a new avenue for detecting BPs in a low-cost, easily to operate, label-free and sensitive way, promising feasible application in tracking drug excretion, studying pharmacokinetic processes, and inspecting pharmaceutical quality.

Supporting Information

Supporting Information File 1

Experimental part.
[https://www.beilstein-journals.org/bjoc/content/supplementary/1860-5397-14-157-S1.pdf]

Acknowledgements

This work was supported by NSFC (21672112), the Fundamental Research Funds for the Central Universities and 111 Project (B12015), which are gratefully acknowledged.

ORCID® iDs

Dong-Sheng Guo - https://orcid.org/0000-0002-0765-5427

References

1. Russell, R. G. G. *Bone* **2011,** *49,* 2–19. doi:10.1016/j.bone.2011.04.022
2. Mouriño, V.; Boccaccini, A. R. *J. R. Soc., Interface* **2010,** *7,* 209–227. doi:10.1098/rsif.2009.0379
3. Major, P. P.; Cook, R. J.; Chen, B.-L.; Zheng, M. *Supportive Cancer Ther.* **2005,** *2,* 234–240. doi:10.3816/SCT.2005.n.017
4. Marra, M.; Salzano, G.; Leonetti, C.; Tassone, P.; Scarsella, M.; Zappavigna, S.; Calimeri, T.; Franco, R.; Liguori, G.; Cigliana, G.; Ascani, R.; La Rotonda, M. I.; Abbruzzese, A.; Tagliaferri, P.; Caraglia, M.; De Rosa, G. *Nanomedicine: NBM* **2011,** *7,* 955–964. doi:10.1016/j.nano.2011.03.004
5. Shmeeda, H.; Amitay, Y.; Tzemach, D.; Gorin, J.; Gabizon, A. *J. Controlled Release* **2013,** *167,* 265–275. doi:10.1016/j.jconrel.2013.02.003
6. Cremers, S. C. L. M.; Pillai, G.; Papapoulos, S. E. *Clin. Pharmacokinet.* **2005,** *44,* 551–570. doi:10.2165/00003088-200544060-00001
7. Lapko, V. N.; Miller, P. S.; Sheldon, C. E.; Nachi, R.; Kafonek, C. J. *Bioanalysis* **2014,** *6,* 2931–2950. doi:10.4155/bio.14.223
8. Zacharis, C. K.; Tzanavaras, P. D. *J. Pharm. Biomed. Anal.* **2008,** *48,* 483–496. doi:10.1016/j.jpba.2008.05.028
9. Matuszewski, L.; Matuszewska, A.; Mazurkiewicz, T.; Rogalski, J.; Cho, N. S.; Ohga, S. *J. Fac. Agric., Kyushu Univ. 56,* 213–216.
10. Cecchi, T. *Crit. Rev. Anal. Chem.* **2008,** *38,* 161–213. doi:10.1080/10408340802038882
11. Kline, W. F.; Matuszewski, B. K. *J. Chromatogr., Biomed. Appl.* **1992,** *583,* 183–193. doi:10.1016/0378-4347(92)80551-Z
12. Zirojevic, J.; Jovic, Z.; Djurdjevic, A.; Ciric, A.; Djurdjevic, P. *Acta Chromatogr.* **2015,** *27,* 215–237. doi:10.1556/AChrom.27.2015.2.2
13. Tsai, E. W.; Ip, D. P.; Brooks, M. A. *J. Chromatogr.* **1992,** *596,* 217–224. doi:10.1016/0021-9673(92)85010-Q
14. Hargrove, A. E.; Nieto, S.; Zhang, T.; Sessler, J. L.; Anslyn, E. V. *Chem. Rev.* **2011,** *111,* 6603–6782. doi:10.1021/cr100242s
15. Wiskur, S. L.; Ait-Haddou, H.; Lavigne, J. J.; Anslyn, E. V. *Acc. Chem. Res.* **2001,** *34,* 963–972. doi:10.1021/ar9600796
16. Nguyen, B. T.; Anslyn, E. V. *Coord. Chem. Rev.* **2006,** *250,* 3118–3127. doi:10.1016/j.ccr.2006.04.009
17. Böhmer, V. *Angew. Chem., Int. Ed. Engl.* **1995,** *34,* 713–745. doi:10.1002/anie.199507131
18. Guo, D.-S.; Wang, K.; Liu, Y. *J. Inclusion Phenom. Macrocyclic Chem.* **2008,** *62,* 1–21. doi:10.1007/s10847-008-9452-2
19. Guo, D.-S.; Uzunova, V. D.; Su, X.; Liu, Y.; Nau, W. M. *Chem. Sci.* **2011,** *2,* 1722–1734. doi:10.1039/c1sc00231g
20. Guo, D.-S.; Liu, Y. *Chem. Soc. Rev.* **2012,** *41,* 5907–5921. doi:10.1039/c2cs35075k
21. Guo, D.-S.; Yang, J.; Liu, Y. *Chem. – Eur. J.* **2013,** *19,* 8755–8759. doi:10.1002/chem.201300980
22. Guo, D.-S.; Wang, K.; Wang, Y.-X.; Liu, Y. *J. Am. Chem. Soc.* **2012,** *134,* 10244–10250. doi:10.1021/ja303280r
23. Xu, Z.; Peng, S.; Wang, Y.-Y.; Zhang, J.-K.; Lazar, A. I.; Guo, D.-S. *Adv. Mater.* **2016,** *28,* 7666–7671. doi:10.1002/adma.201601719
24. Geng, W.-C.; Liu, Y.-C.; Wang, Y.-Y.; Xu, Z.; Zheng, Z.; Yang, C.-B.; Guo, D.-S. *Chem. Commun.* **2017,** *53,* 392–395. doi:10.1039/C6CC09079F
25. Guo, D.-S.; Liu, Y. *Acc. Chem. Res.* **2014,** *47,* 1925–1934. doi:10.1021/ar500009g
26. Zheng, Z.; Geng, W.-C.; Gao, J.; Wang, Y.-Y.; Sun, H.; Guo, D.-S. *Chem. Sci.* **2018,** *9,* 2087–2091. doi:10.1039/C7SC04989G
27. Peng, S.; Barba-Bon, A.; Pan, Y.-C.; Nau, W. M.; Guo, D.-S.; Hennig, A. *Angew. Chem., Int. Ed.* **2017,** *56,* 15742–15745. doi:10.1002/anie.201707979

28. Gao, J.; Li, J.; Geng, W.-C.; Chen, F.-Y.; Duan, X.; Zheng, Z.; Ding, D.; Guo, D.-S. *J. Am. Chem. Soc.* **2018,** *140,* 4945–4953. doi:10.1021/jacs.8b02331
29. Tobey, S. L.; Anslyn, E. V. *J. Am. Chem. Soc.* **2003,** *125,* 14807–14815. doi:10.1021/ja030507k
30. Huang, G.-B.; Wang, S.-H.; Ke, H.; Yang, L.-P.; Jiang, W. *J. Am. Chem. Soc.* **2016,** *138,* 14550–14553. doi:10.1021/jacs.6b09472
31. MacDougall, D.; Crummett, W. B. *Anal. Chem.* **1980,** *52,* 2242–2249. doi:10.1021/ac50064a004
32. Bouatra, S.; Aziat, F.; Mandal, R.; Guo, A. C.; Wilson, M. R.; Knox, C.; Bjorndahl, T. C.; Krishnamurthy, R.; Saleem, F.; Liu, P.; Dame, Z. T.; Poelzer, J.; Huynh, J.; Yallou, F. S.; Psychogios, N.; Dong, E.; Bogumil, R.; Roehring, C.; Wishart, D. S. *PLoS One* **2013,** *8,* e73076. doi:10.1371/journal.pone.0073076
33. Shmaefsky, B. R. *Am. Biol. Teach.* **1990,** *52,* 170–172. doi:10.2307/4449071

License and Terms

BEILSTEIN JOURNAL OF ORGANIC CHEMISTRY

Efficient catenane synthesis by cucurbit[6]uril-mediated azide–alkyne cycloaddition

Antony Wing Hung Ng, Chi-Chung Yee, Kai Wang and Ho Yu Au-Yeung*

Full Research Paper

Open Access

Address:
Department of Chemistry, The University of Hong Kong, Pokfulam Road, Hong Kong, P. R. China

Email:
Ho Yu Au-Yeung* - hoyuay@hku.hk

* Corresponding author

Keywords:
azide–alkyne cycloaddition; catenane; click chemistry; cucurbit[6]uril; mechanical bond

Beilstein J. Org. Chem. **2018,** *14,* 1846–1853.
doi:10.3762/bjoc.14.158

Received: 12 April 2018
Accepted: 25 June 2018
Published: 20 July 2018

This article is part of the thematic issue "Macrocyclic and supramolecular chemistry".

Guest Editor: M.-X. Wang

Abstract

We report here the efficient synthesis of a series of [3]catenanes featuring the use of cucurbit[6]uril to simultaneously mediate the mechanical and covalent bond formations. By coupling the mechanical interlocking with covalent macrocyclization, formation of topological isomers is eliminated and the [3]catenanes are formed exclusively in good yields. The efficient access to these [3]catenanes and the presence of other recognition units render them promising building blocks for the construction of other high-order interlocked structures.

Introduction

Catenanes are topologically non-trivial molecules possessing mechanically interlocked macrocycles. The flexible but strong mechanical bond between the interlocked macrocycles offers a unique opportunity for exploiting catenanes as molecular machines or new materials with unusual mechanical properties [1-9]. Over the years, different templates and ring-closing reactions to form the interlocked macrocycles have been developed, but the majority of the reported catenanes is limited to the Hopf link (i.e., the simplest [2]catenane with two crossings) [9]. Synthesis of other high-order catenanes with more interlocked macrocycles and/or more crossing points remain challenging and more general synthetic strategies to catenanes are yet to be realized [10-12]. A major challenge in [*n*]catenane synthesis is the precise spatiotemporal control of the covalent formation of the macrocycles and their mechanical interlocking. Otherwise, various topological isomers such as the non-interlocked products or lower-order catenanes will form, which are detrimental to the synthesis efficiency as well as complicating the purification process [13-19].

One strategy to overcome this challenge is to couple the mechanical bond and covalent bond formation in a single step. If

the building block preorganization by reversible interactions (which will lead to mechanical interlocking) is also necessary for the covalent bond formation, the covalent trapping of the non-interlocked precursors will be suppressed and the mechanical interlocking of the macrocycles will be ensured. One example is the use of an active metal template, in which the macrocyclization is mediated by the metal ion inside the cavity of a metal-coordinating macrocycle [20]. Cucurbit[6]uril (CB[6]) has also been demonstrated to bind to ammonium-containing azides and alkynes and to mediate their cycloaddition inside the CB[6] cavity [21,22]. Yet, these strategies have been largely limited to the synthesis of rotaxane-based interlocked systems [23], probably because of the additional challenges associated with the macrocyclization in catenane synthesis. Previously, we have reported a preliminary study of a [6]catenane synthesis featuring the CB[6]-mediated azide–alkyne cycloaddition (CBAAC) using phenanthroline-based building blocks [24]. To further explore the applicability and generality of the CBAAC in the construction of mechanically interlocked molecules, we report here the efficient synthesis of a series of [3]catenanes from a combination of different azide and alkyne building blocks. These [3]catenanes were obtained in good yields (>85%) with straightforward purification procedures. The good compatibility of CBAAC with these various building blocks and the good yields of the [3]catenanes can serve as an entry point to other high-order [*n*]catenanes by introducing additional macrocycles through other non-covalent interactions.

Results and Discussion

Building block design

The bis(aminoalkyne) and bis(aminoazide) building blocks used in this study are summarized in Scheme 1. The secondary amines are designed to form ammoniums that will strongly bind to CB[6] through ion-dipole interactions under aqueous acidic conditions. Upon formation of the inclusion complex with CB[6], the azide and alkyne functionalities inside the CB[6] cavity will be placed in close proximity and their cycloaddition will be facilitated. As the cycloaddition is preceded by CB[6] binding, triazole formation will therefore ensure the interlocking of the CB[6]. A [1 + 1] macrocyclization of the diazide and dialkyne will then result in the exclusive formation of the [3]catenane with no other topological isomers.

The building blocks contain either a central hexaethylene glycol (HEG) unit or are derived from 1,5-dioxynaphthalene (DN), naphthalenediimide (NDI), 2,9-phenanthroline (Phen) or 4,4'-biphenyl (BP) cores which can engage in additional non-covalent interactions, such as metal–ligand coordination, charge transfer, π-stacking and hydrophobic interactions, for the later interlocking of additional macrocycles to give higher-order [*n*]catenanes. The new building blocks were synthesized following similar procedures as previously described [24].

Catenane synthesis by CBAAC

Synthesis of [3]catenanes

The CBAAC-mediated [3]catenane synthesis was first investigated using the dioxynaphthalene building blocks **DN-N3** and **DN-CC**. Different from the previously reported [3]catenane **Cat-0** which is derived from **DN-N3** and **Phen-CC** [24], both **DN-N3** and **DN-CC** contain the flexible ethylene glycol linkers between the terminal azide and alkyne groups, so that any other possible preorganization effects, except that of the ammonium binding to CB[6] could be eliminated to study the efficiency of CBAAC in the catenane formation. In our first trial, a 1:1:2 mixture of **DN-N3**, **DN-CC** and CB[6] in 0.2 M HCl was heated at 70 °C and the reaction mixture was analyzed by LC–MS. After heating for 1 hour, although a peak corresponding to the [1 + 1] cyclized product with *m/z* values consistent with the [3]catenane **Cat-1** could be observed, some unreacted building blocks and unidentified products were also found. Further extending the reaction time to 3, 5 or 8 hours resulted in similar chromatograms with no significant improvement of the yield of **Cat-1**. A similar observation has been reported in a CBAAC-mediated rotaxane synthesis and additional templates have been used to positively cooperate with the CB[6] binding to the ammoniums on the building blocks to improve the efficiency of CBAAC [23]. In view of the low solubility of CB[6] and the possibility of thermal-assisted azide–alkyne cycloaddition of the unbound building blocks that may lead to the incomplete cycloaddition and other side products, we decided to first assemble a pseudo[3]rotaxane CB[6] complex with either the azide or alkyne building block, before introducing the other building block to the reaction mixture. By heating a solution of **DN-N3** in the presence of two equivalents of CB[6] in 0.2 M aq HCl for 2 hours, a clear solution was formed that indicated CB[6] dissolution and formation of the inclusion complex. One equivalent of **DN-CC** was added and the mixture was further heated at 70 °C. LC–MS analysis of the reaction mixture showed that the building blocks were completely consumed after one hour of heating, and that the crude mixture contained the [3]catenane **Cat-1** as the major product with >85% yield (Scheme 2). Using **DN-CC** to first form the pseudo[3]rotaxane CB[6] complex did not affect the efficiency of CBAAC and **Cat-1** was obtained in a similar yield. These results show that the initial formation of the pseudorotaxane complex helps the CBAAC by avoiding any cycloadditions outside of the CB[6] cavity and that CBAAC can be an efficient strategy for catenane synthesis.

Cat-1 and its interlocked nature were further characterized by MS^2, ^1H and ^{13}C NMR spectroscopy. The PF_6^- salt of **Cat-1**

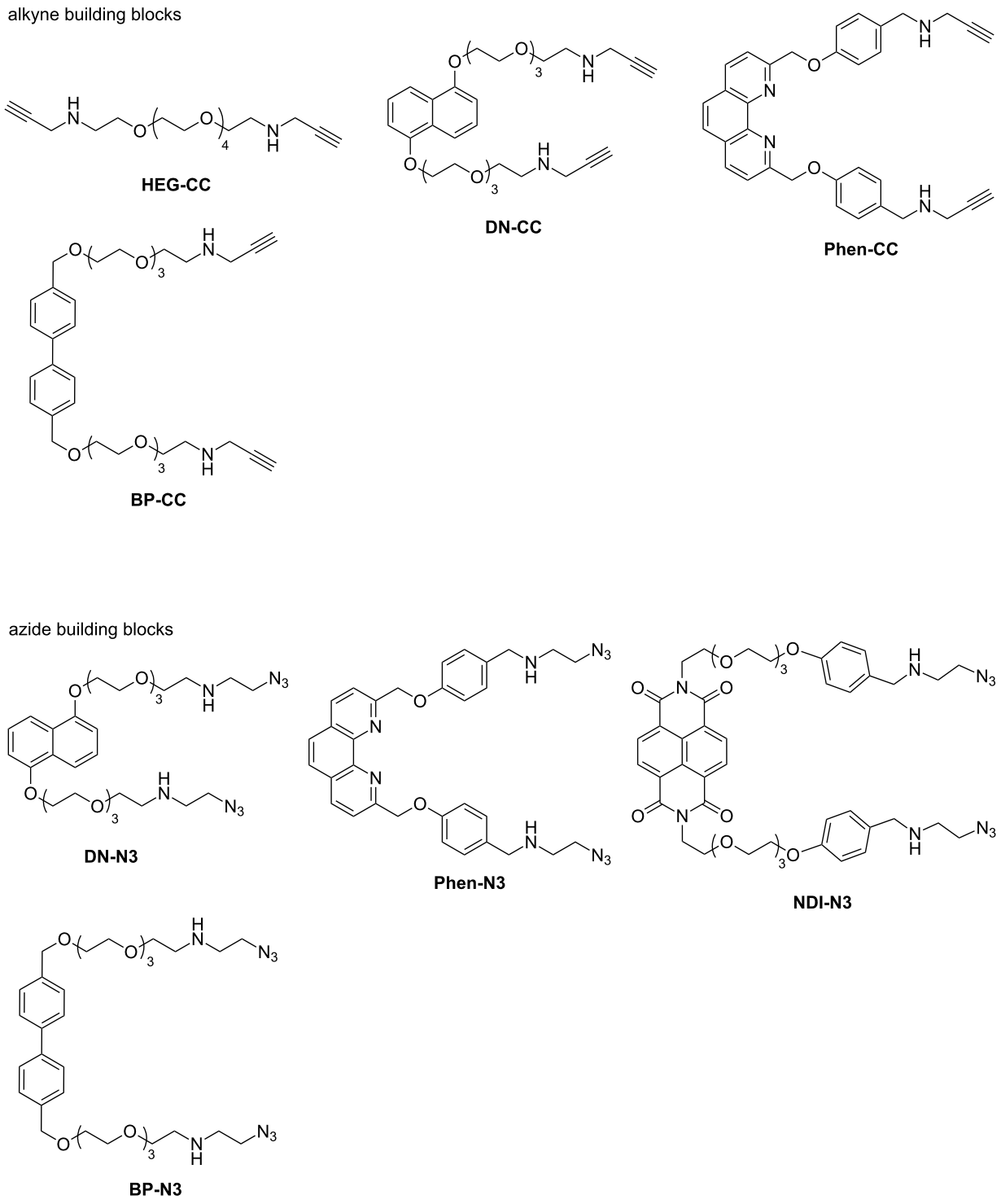

Scheme 1: Diazide and dialkyne building blocks used in this study.

was isolated in 69% yield as a white solid by precipitation with a saturated NH_4PF_6 solution and simple filtration. The ESIMS spectrum showed two peaks at *m/z* = 808.5 and 1076.3, consistent with the 3+ and 4+ ions of **Cat-1**. Similar to **Cat-0**, the MS^2 spectrum of **Cat-1** revealed CB[6]-bound fragments, showing the strong CB[6]–ammonium interactions are

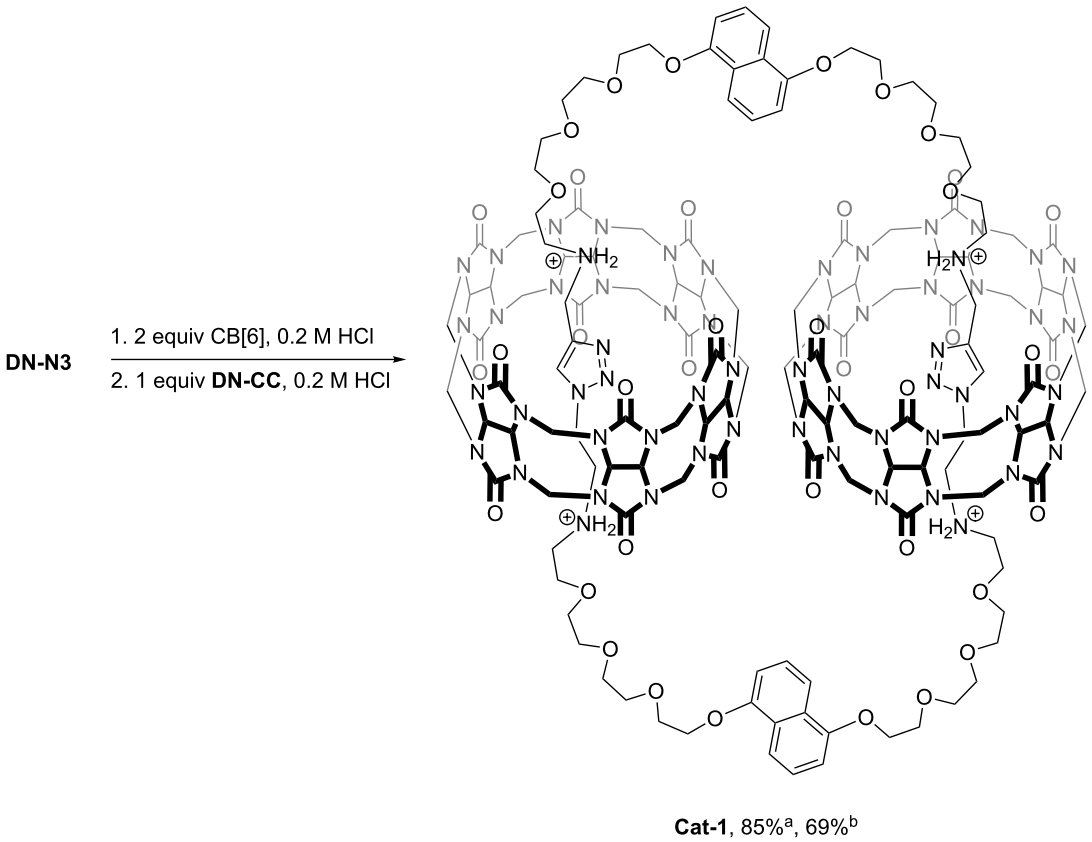

Scheme 2: Synthesis of **Cat-1** by CBAAC. [a]Assembly yield by HPLC; [b]isolated yield as PF_6^- salt.

preserved under the MS conditions. Inclusion of the triazole in the CB[6] cavity was evidenced by the upfield shifted triazole resonance from 8.5 ppm to 6.4 ppm when compared with that of free triazole in non-interlocked system [22,24,25]. NOE cross peaks between the triazole and CB[6] protons were also observed. The ^{1}H NMR spectrum of **Cat-1** showed one set of aromatic resonances, suggesting the chemical environments of two dioxynaphthalene units are highly similar and that **Cat-1** is adopting a symmetrical conformation in solution, consistent with the tight binding of the diammonium to the CB[6] and the overall flexibility of the [3]catenane structure.

With the success of CBAAC in the efficient synthesis of **Cat-1**, nine other [3]catenanes (**Cat-2**–**Cat-10**) were synthesized from different combinations of the alkyne and azide building blocks under similar conditions (Scheme 3). In all cases, LC–MS analysis of the crude reaction mixtures showed the complete consumption of the building blocks with the [3]catenane as the only major product with yields >85%. This demonstrates not only the high efficiency of CBAAC in catenane synthesis, but also the good compatibility of CBAAC with various types of building blocks. Because of the high yields of these [3]catenanes, their isolations were all straightforward. **Cat-2**–**Cat-10** were isolated either by precipitation as the PF_6^- salts or by preparative HPLC, and were fully characterized by MS, NMR and UV–vis spectroscopy. Similar to **Cat-1**, the upfield shifted triazole ^{1}H NMR resonances of **Cat-2**–**Cat-10** at ca. 6.4 ppm are consistent with the inclusion of the triazole in the CB[6] cavity [22,24,25]. The ESIMS, HRMS and MS^2 spectra are all consistent with the [3]catenanes with a similar fragmentation behavior as that of **Cat-1**. The ^{1}H NMR, ^{13}C NMR and ESIMS spectra of **Cat-2**–**Cat-10** are shown in Figure 1 and Figure 2, and in Supporting Information File 1, Figures S29–S55 and S60–S68.

With the different combinations of the additional recognition units (i.e., DN, NDI, Phen and BP) in these [3]catenanes, other macrocycles/building blocks that could favorably interact with these units could be introduced to give higher-order catenanes with multiple interlocked rings. As a preliminary study of high-order [*n*]catenane assembly using this approach, CBAAC of **BP-N3** and **DN-CC** was repeated in the presence of 10 equiva-

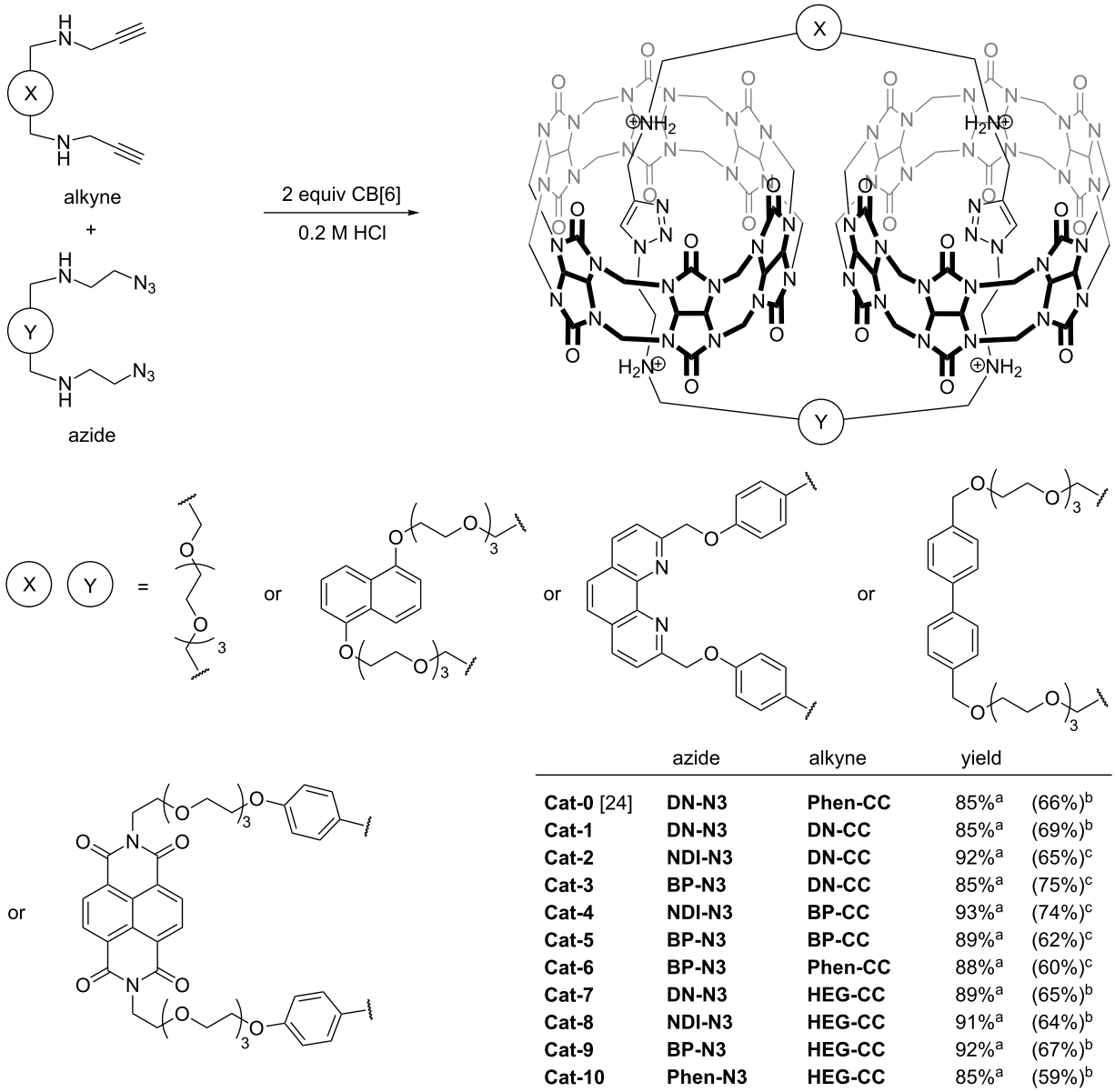

	azide	alkyne	yield	
Cat-0 [24]	**DN-N3**	**Phen-CC**	85%[a]	(66%)[b]
Cat-1	**DN-N3**	**DN-CC**	85%[a]	(69%)[b]
Cat-2	**NDI-N3**	**DN-CC**	92%[a]	(65%)[c]
Cat-3	**BP-N3**	**DN-CC**	85%[a]	(75%)[c]
Cat-4	**NDI-N3**	**BP-CC**	93%[a]	(74%)[c]
Cat-5	**BP-N3**	**BP-CC**	89%[a]	(62%)[c]
Cat-6	**BP-N3**	**Phen-CC**	88%[a]	(60%)[c]
Cat-7	**DN-N3**	**HEG-CC**	89%[a]	(65%)[b]
Cat-8	**NDI-N3**	**HEG-CC**	91%[a]	(64%)[b]
Cat-9	**BP-N3**	**HEG-CC**	92%[a]	(67%)[b]
Cat-10	**Phen-N3**	**HEG-CC**	85%[a]	(59%)[b]

Scheme 3: Synthesis of [3]catenanes by CBAAC. [a]Assembly yield by HPLC; [b]isolated yield by precipitation as PF_6^- salt; [c]isolated yield by preparative HPLC.

lents of β-cyclodextrin (β-CD), which is known to form a stable inclusion complex with the BP unit due to hydrophobic effects ($K_a \approx 7 \times 10^3$ M^{-1} in D_2O) [26] (Scheme 4). To our delight, a [4]catenane (**Cat-11**) was obtained in 60% yield along with 30% of **Cat-3**. Of note, due to a much weaker binding between the 1,5-dioxynaphthalene unit and β-CD [26,27], no [5]catenane was observed. ESIMS and MS^2 spectra of **Cat-11** are consistent with the inclusion of one β-CD (and two CB[6]). The ^1H NMR spectrum showed a slight upfield shift of the BP protons to 7.61 and 7.48 ppm when compared with that of **Cat-3** at 7.75 and 7.54 ppm. These observations are all consistent with a [4]catenane structure with the BP unit being included in the cavity of the β-CD, which is further supported by the appearance of the BP protons as two broad signals due to their slightly different chemical environment inside the β-CD (Supporting Information File 1, Figure S56). Together with our previous demonstration of the compatibility of CBAAC with Cu^+-phenanthroline coordination in a [6]catenane assembly, the successful synthesis of **Cat-11** shows the feasibility of using CBAAC with a versatile selection of building blocks and non-

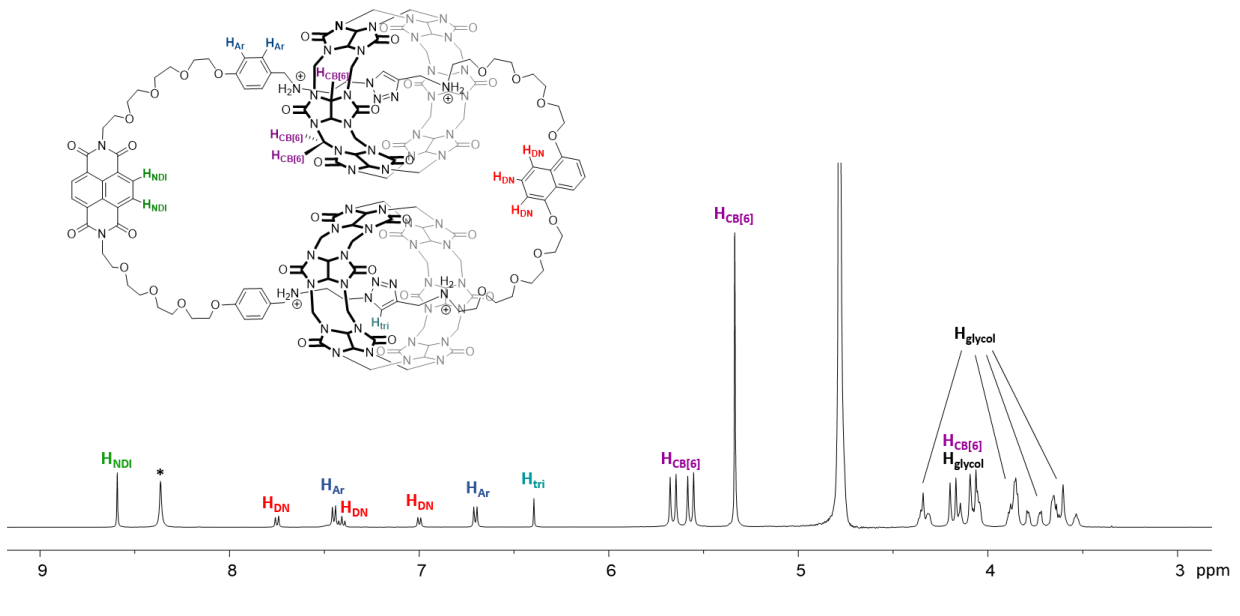

Figure 1: ^{1}H NMR (500 MHz, D_2O, 298 K) of **Cat-2**. The signal at ca. 8.3 ppm is the residual formate from preparative HPLC.

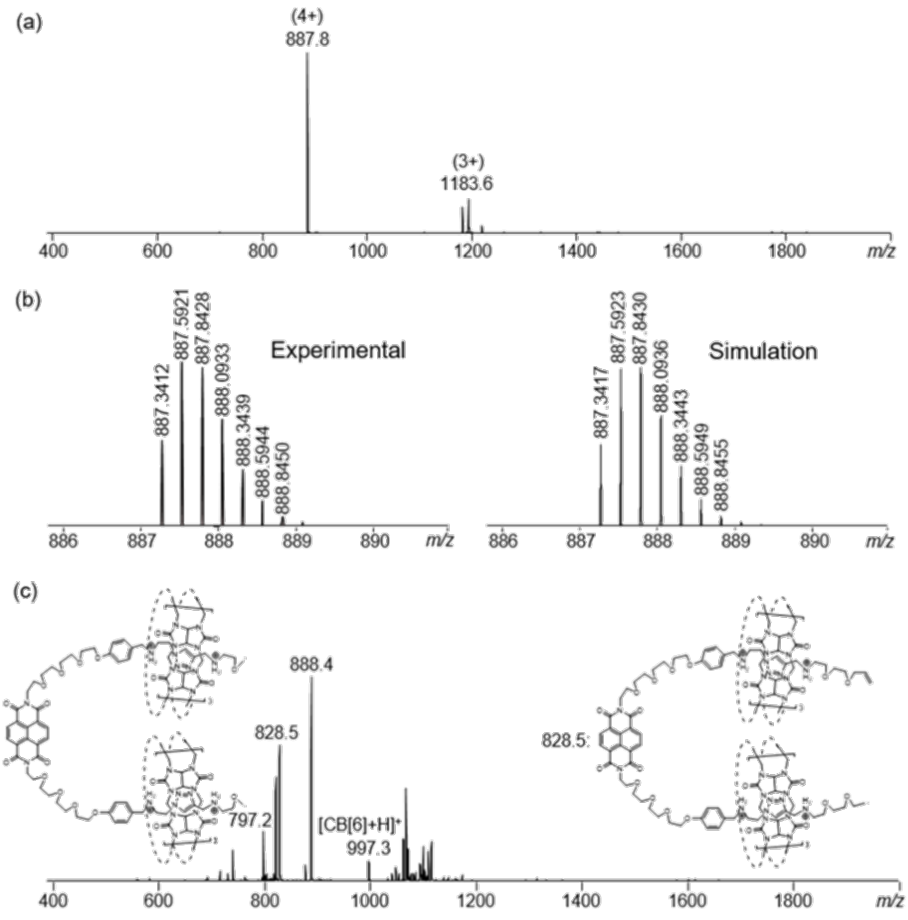

Figure 2: (a) ESIMS, (b) HRMS, and (c) MS^2 spectrum (parent ion at *m/z* = 887.8) of **Cat-2**.

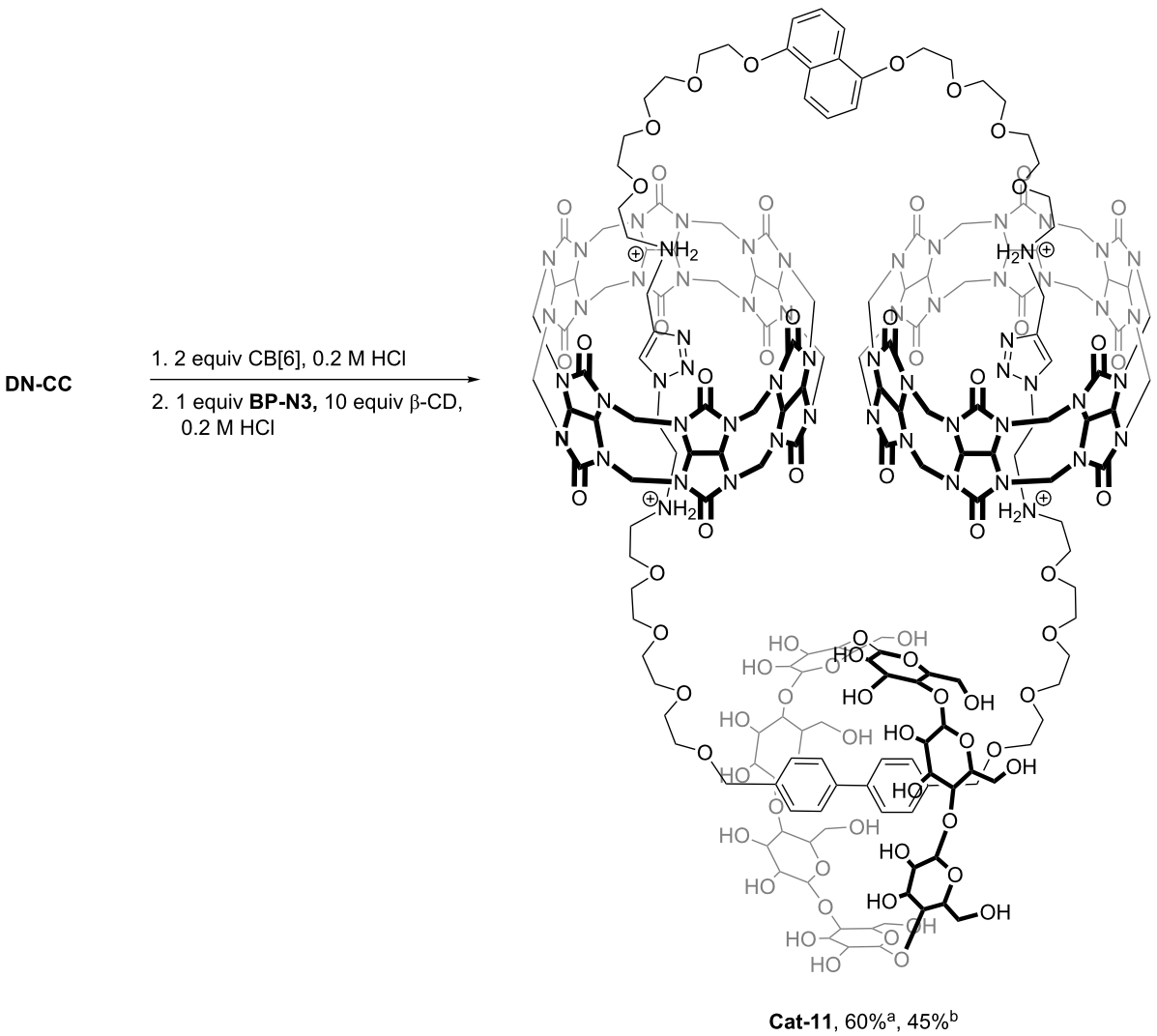

Scheme 4: Synthesis of the [4]catenane **Cat-11**. [a]Assembly yield by HPLC; [b]isolated yield by preparative HPLC.

covalent interactions to construct complex high-order [*n*]catenanes.

Conclusion

In summary, the use of CBAAC in the efficient [3]catenane syntheses is described. Ten new [3]catenanes and a [4]catenane were obtained in a simple one-pot procedure. The key feature of this strategy is that the use of CB[6] couples the mechanical interlocking with the covalent macrocycle formation, so that the catenanes were formed exclusively with no formation of other topological isomers. This CBAAC strategy is versatile and building blocks containing various recognition units can be used, therefore offering a convenient entry point to access more complex high-order catenanes with multiple interlocked macrocycles.

Supporting Information

Supporting Information File 1

Detailed experimental procedures and characterization data (MS, MS^2, ^1H and ^{13}C NMR and UV–vis spectra).
[https://www.beilstein-journals.org/bjoc/content/supplementary/1860-5397-14-158-S1.pdf]

Acknowledgements

The work described in this paper was supported by the Croucher Foundation and a grant from the Research Grants Council of the Hong Kong Special Administrative Region, China (Early Career Scheme, Project No. HKU 27300014). AWHN, CCY and KW are recipients of the Postgraduate Schol-

arship from The University of Hong Kong. We acknowledge UGC funding administered by The University of Hong Kong for support of the Electrospray Ionization Quadrupole Time-of-Flight Mass Spectrometry Facilities under support for Interdisciplinary Research in Chemical Science.

ORCID® iDs

Antony Wing Hung Ng - https://orcid.org/0000-0002-9279-9918
Ho Yu Au-Yeung - https://orcid.org/0000-0002-7216-7921

References

1. Sauvage, J.-P. *Acc. Chem. Res.* **1998,** *31,* 611–619. doi:10.1021/ar960263r
2. Nepogodiev, S. A.; Stoddart, J. F. *Chem. Soc. Rev.* **1998,** *98,* 1959–1976. doi:10.1021/cr970049w
3. Erbas-Cakmak, S.; Leigh, D. A.; McTernan, C. T.; Nussbaumer, A. L. *Chem. Rev.* **2015,** *115,* 10081–10206. doi:10.1021/acs.chemrev.5b00146
4. Evans, N. H.; Beer, P. D. *Chem. Soc. Rev.* **2014,** *43,* 4658–4683. doi:10.1039/c4cs00029c
5. Dietrich-Buchecker, C. O.; Sauvage, J. P. *Chem. Rev.* **1987,** *87,* 795–810. doi:10.1021/cr00080a007
6. Fang, L.; Olson, M. A.; Benítez, D.; Tkatchouk, E.; Goddard, W. A., III; Stoddart, J. F. *Chem. Soc. Rev.* **2010,** *39,* 17–29. doi:10.1039/B917901A
7. Beves, J. E.; Blight, B. A.; Campbell, C. J.; Leigh, D. A.; McBurney, R. T. *Angew. Chem., Int. Ed.* **2011,** *50,* 9260–9327. doi:10.1002/anie.201007963
8. Forgan, R. S.; Sauvage, J.-P.; Stoddart, J. F. *Chem. Rev.* **2011,** *111,* 5434–5464. doi:10.1021/cr200034u
9. Gil-Ramírez, G.; Leigh, D. A.; Stephens, A. J. *Angew. Chem., Int. Ed.* **2015,** *54,* 6110–6150. doi:10.1002/anie.201411619
10. Niu, Z.; Gibson, H. W. *Chem. Rev.* **2009,** *109,* 6024–6046. doi:10.1021/cr900002h
11. Raehm, L.; Hamilton, D. G.; Sanders, J. K. M. *Synlett* **2002,** 1743–1761. doi:10.1055/s-2002-34860
12. Wu, Q.; Rauscher, P. M.; Lang, X.; Wojtecki, R. J.; de Pablo, J. J.; Hore, M. J.; Rowan, S. J. *Science* **2017,** *358,* 1434–1439. doi:10.1126/science.aap7675
13. Amabilino, D. B.; Ashton, P. R.; Boyd, S. E.; Lee, J. Y.; Menzer, S.; Stoddart, J. F.; Williams, D. J. *Angew. Chem., Int. Ed. Engl.* **1997,** *36,* 2070–2072. doi:10.1002/anie.199720701
14. Bitsch, F.; Dietrich-Buchecker, C. O.; Khemiss, A. K.; Sauvage, J. P.; Van Dorsselaer, A. *J. Am. Chem. Soc.* **1991,** *113,* 4023–4025. doi:10.1021/ja00010a072
15. Li, S.; Huang, J.; Zhou, F.; Cook, T. R.; Yan, X.; Ye, Y.; Zhu, B.; Zheng, B.; Stang, P. J. *J. Am. Chem. Soc.* **2014,** *136,* 5908–5911. doi:10.1021/ja502490k
16. Langton, M. J.; Matichak, J. D.; Thompson, A. L.; Anderson, H. L. *Chem. Sci.* **2011,** *2,* 1897–1901. doi:10.1039/c1sc00358e
17. Iwamoto, H.; Tafuku, S.; Sato, Y.; Takizawa, W.; Katagiri, W.; Tayama, E.; Hasegawa, E.; Fukazawa, Y.; Haino, T. *Chem. Commun.* **2016,** *52,* 319–322. doi:10.1039/C5CC07562A
18. Black, S. P.; Stefankiewicz, A. R.; Smulders, M. M. J.; Sattler, D.; Schalley, C. A.; Nitschke, J. R.; Sanders, J. K. M. *Angew. Chem., Int. Ed.* **2013,** *52,* 5749–5752. doi:10.1002/anie.201209708
19. Au-Yeung, H. Y.; Yee, C.-C.; Ng, A. W. H.; Hu, K. *Inorg. Chem.* **2018,** *57,* 3475–3485. doi:10.1021/acs.inorgchem.7b02523
20. Crowley, J. D.; Goldup, S. M.; Lee, A.-L.; Leigh, D. A.; McBurney, R. T. *Chem. Soc. Rev.* **2009,** *38,* 1530–1541. doi:10.1039/b804243h
21. Tuncel, D.; Özsar, Ö.; Tiftik, H. B.; Salih, B. *Chem. Commun.* **2007,** 1369–1371. doi:10.1039/B616764K
22. Sinha, M. K.; Reany, O.; Yefet, M.; Botoshansky, M.; Keinan, E. *Chem. – Eur. J.* **2012,** *18,* 5589–5605. doi:10.1002/chem.201103434
23. Ke, C.; Smaldone, R. A.; Kikuchi, T.; Li, H.; Davis, A. P.; Stoddart, J. F. *Angew. Chem., Int. Ed.* **2013,** *52,* 381–387. doi:10.1002/anie.201205087
24. Wang, K.; Yee, C.-C.; Au-Yeung, H. Y. *Chem. Sci.* **2016,** *7,* 2787–2792. doi:10.1039/C5SC04774A
25. Celtek, G.; Artar, M.; Scherman, O. A.; Tuncel, D. *Chem. – Eur. J.* **2009,** *15,* 10360–10363. doi:10.1002/chem.200901504
26. Armspach, D.; Ashton, P. R.; Ballardini, R.; Balzani, V.; Godi, A.; Moore, C. P.; Prodi, L.; Spencer, N.; Stoddart, J. F.; Tolley, M. S.; Wear, T. J.; Williams, D. J. *Chem. – Eur. J.* **1995,** *1,* 33–55. doi:10.1002/chem.19950010109
27. It has been reported that the bindings of a methylated derivative of β-CD to 1,5-dioxynaphthalene derivatives were at least two order-of-magnitude weaker than that of the bindings to biphenyl guests. See reference [26] for details.

License and Terms

BEILSTEIN JOURNAL OF ORGANIC CHEMISTRY

A hemicryptophane with a triple-stranded helical structure

Augustin Long[1], Olivier Perraud[2], Erwann Jeanneau[3], Christophe Aronica[3], Jean-Pierre Dutasta[2] and Alexandre Martinez[*1]

Full Research Paper

Open Access

Address:
[1]Aix Marseille Univ, CNRS, Centrale Marseille, iSm2, Marseille, France, [2]Laboratoire de Chimie École Normale Supérieure de Lyon, CNRS, UCBL46, Allée d'Italie, F-69364 Lyon, France and [3]LMI-UMR 5615 CNRS / UCBL, Université Claude Bernard Lyon 1, 6 rue victor Grignard, 69622 Villeurbanne cedex, France

Email:
Alexandre Martinez[*] - alexandre.martinez@centrale-marseille.fr

* Corresponding author

Keywords:
CTV; hemicryptophanes; organic cages; triple helical structure

Beilstein J. Org. Chem. **2018,** *14,* 1885–1889.
doi:10.3762/bjoc.14.162

Received: 15 April 2018
Accepted: 29 June 2018
Published: 24 July 2018

This article is part of the thematic issue "Macrocyclic and supramolecular chemistry".

Guest Editor: M.-X. Wang

Abstract

A hemicryptophane cage bearing amine and amide functions in its three linkers was synthesized in five steps. The X-ray molecular structure of the cage shows a triple-stranded helical arrangement of the linkers stabilized by intramolecular hydrogen bonds between amide and amine groups. The chirality of the cyclotriveratrylene unit controls the propeller arrangement of the three aromatic rings in the opposite part of the cage. ^{1}H NMR studies suggest that this structure is retained in solution.

Introduction

Among the remarkable architectures found in biological systems, those presenting a triple helical arrangement are of particular interest. Beside its classical double strand structure formed by Watson–Crick base pairing, DNA can also organize in a triple helical fashion [1]. These three-stranded structures of DNA naturally occur and play important roles in regulating gene function and DNA metabolism. Collagen, the most abundant protein in animals, also adopts a triple helical structure: three parallel peptide chains coil about each other in a triple stranded left-handed helical structure. Its high thermal and mechanical stability results mainly from the numerous hydrogen bonds found in the triple helix framework [2]. Bioinspired structures, based on peptide backbones, have been built, allowing a better understanding of the properties of this biological system and giving rise to numerous applications ranging from artificial collagenous biomaterials to peptides for therapeutic uses [3-5].

Recently, molecular cages presenting a triple helical structure have aroused a considerable interest [6-8]: for instance, Malik et al. described the synthesis and recognition properties of an organic cage including three helicene moieties in its arms [9]. This cage presents a triple stranded helical structure with the framework fully twisted due to the arrangement of the three helicene units in a propeller fashion. Other recent examples are the triple-stranded phenylene cages presenting a helical rod-like shape synthesized by Kirsche et al. [10].

Hemicryptophanes are chiral covalent cages combining a cyclotriveratrylene (CTV, north part) unit with another C_3 sym-

metrical moiety (south part). They display recognition properties toward neurotransmitters and carbohydrates, and can act as molecular switches and supramolecular catalysts [11]. Their C_3 symmetry makes them promising candidates to build molecular cages displaying a triple helical arrangement of the linkers. Furthermore, we have previously reported that the chirality unit in the south part and the chirality of the CTV unit in the north part influence each other, suggesting that the chirality of the CTV moiety could control the helical arrangement of the linkers [12,13].

We herein report the synthesis of the hemicryptophane **1** bearing both amide and amine functions in its three likers. In solution, the ^{1}H NMR spectrum shows a C_3 symmetrical cage, which is also observed in the solid state by X-ray crystallography. Moreover, in the solid, amide and amine functional groups of different linkers interact through hydrogen bonding, leading to a triple helical arrangement of the linkers. The CTV unit is also found to strongly control the chirality of this triple helices since the CTV with a *P* (respectively *M*) configuration induces a Δ (respectively Λ) chirality of the propeller-like arrangement of the linkers.

Results and Discussion

Synthesis of cage 1

According to the synthetic pathway shown in Scheme 1, hemicryptophane host **1** was obtained in five steps [14,15]. Alkylation of vanillyl alcohol by chloroacetic acid in ethanol under reflux afforded **2** in 73% yield. The CTV triester was obtained by adding first one equivalent of HCl and then a catalytic amount of *para*-toluenesulfonic acid in methanol to compound **2**. Then, compound **3** was reacted with ethylenediamine, providing **4** in 48% yield. The reaction between 1,3,5-tris(bromomethyl)benzene and 2-hydroxybenzaldehyde provi-

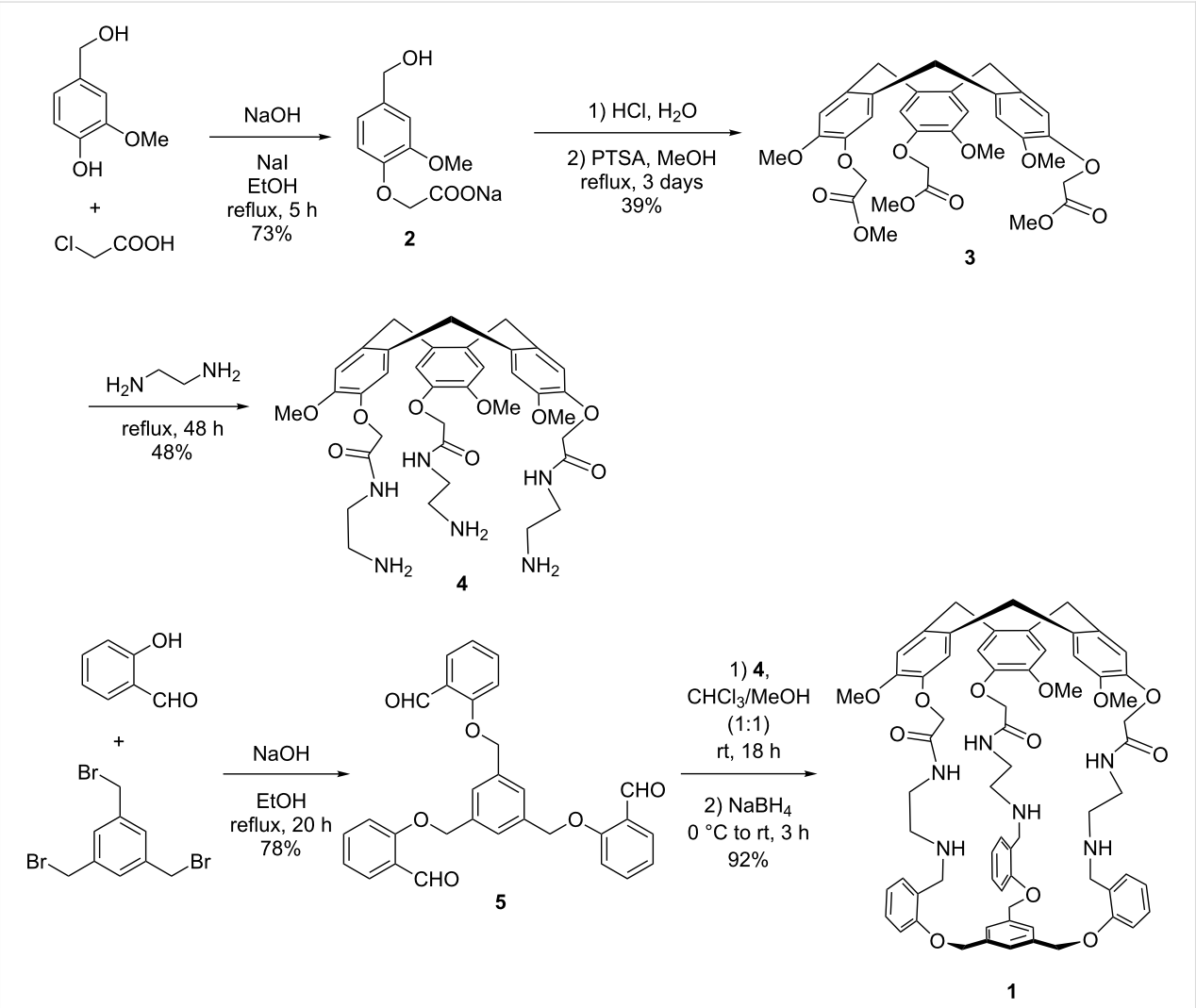

Scheme 1: Synthesis of **1**.

ded the precursor of the south unit **5** in 78% yield. Finally, a [1 + 1] macrocyclization between **4** and **5** was achieved by a reductive amination in a 1:1 $CHCl_3$/MeOH mixture. A remarkable yield of 92% was obtained for this last step. As this kind of reductive amination has been proved to be under thermodynamic control, the resulting intermediate cage bearing three imine functions is highly sable [12,13]. Hydrogen bonds between the amide group and the formed imine function could account for the high stability of this intermediate, shifting the equilibrium between the different oligomers and the cage in favor of this latter (vide infra).

^{1}H NMR of cage **1**

The ^{1}H NMR spectrum of hemicryptophane **1** in $CDCl_3$ shows that this host presents, on average, a C_3 symmetry in solution (Figure 1). The characteristic signals of the CTV unit can be observed: one signal for the OMe group at 3.94 ppm, two singlets for the aromatic protons at 6.58 and 6.75 ppm and the expected AB systems for the CH_2 bridges at 4.67 and 3.44 ppm. The aromatic protons of the benzene ring in the south part of the cage and the corresponding diastereotopic CH_2 bridges displays a singlet at 7.46 ppm and two doublets at 5.11 and 4.92 ppm, respectively. The signals of the aromatic protons of the linkers give two doublets and two triplets between 6.75 and 7.2 ppm, whereas the diastereotopic aliphatic protons exhibit expected broad multiplets between 1.50 ppm and 2.36 ppm. The Ar–CH_2–NH diastereotopic protons appear as two doublets at 3.87 and 3.49 ppm.

Structure of cage **1**

Slow evaporation of a solution of cage **1** in a 1:1 mixture of $CHCl_3$/MeOH affords crystals suitable for X-ray diffraction. In the solid, the hemicryptophane cage presents a perfect C_3 symmetry (Figure 2). Further examination of the crystal structure reveals that **1** adopts a chiral conformation where the three linkers are twisted into a triple helix with the lone pair of the amines and the amide hydrogen atoms oriented toward the cavity, while the amide oxygen atoms are oriented outwards. Intramolecular hydrogen bonding between the nitrogen of the amine function of one linker with the N–H of the amide group of another arm can account for this helical structure ($N_{amine}\cdots N_{amide}$ distances of 2.97 Å). This structure sheds light on the excellent yield achieved in the last step of the synthesis. Indeed, such intramolecular hydrogen bonding probably also

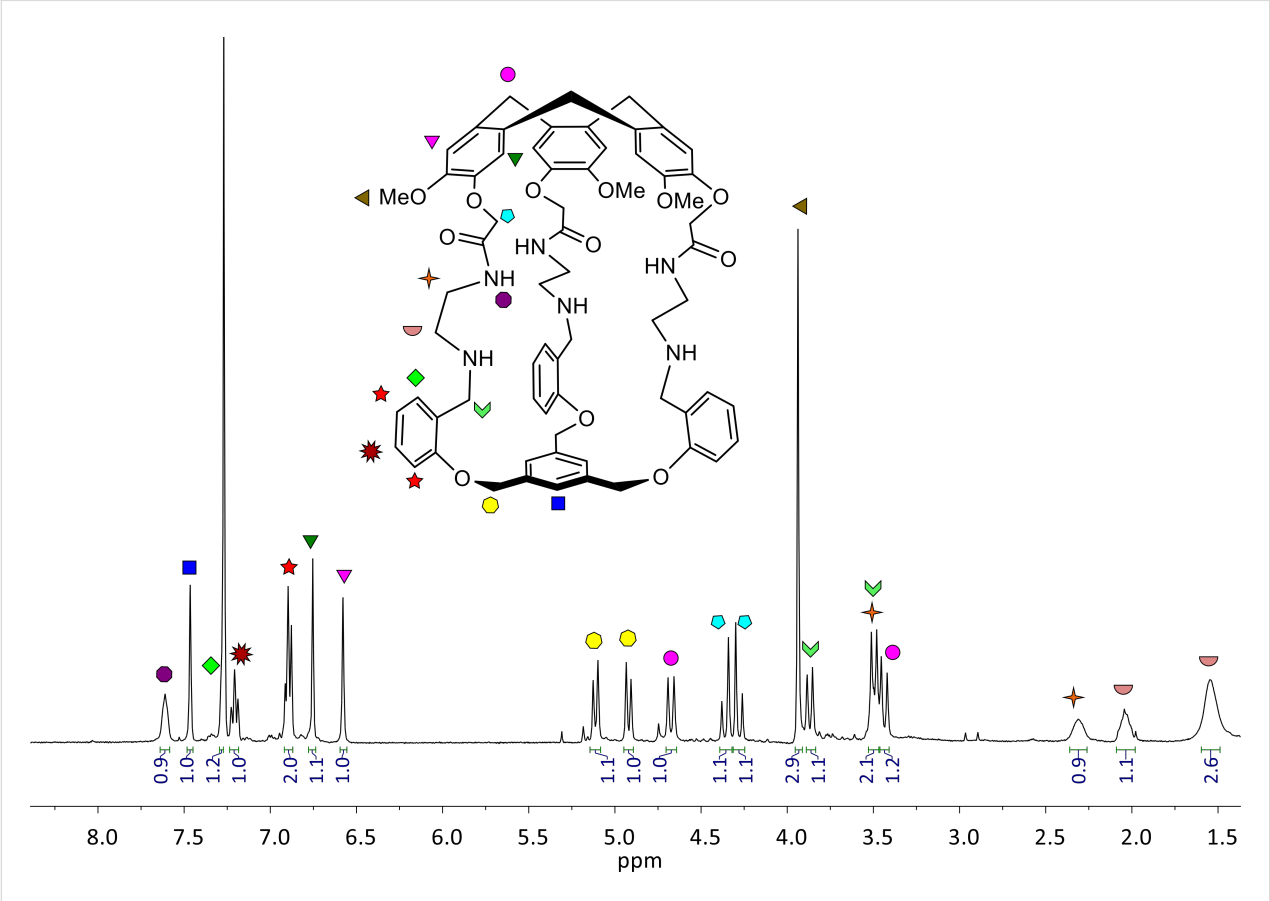

Figure 1: ^{1}H NMR spectrum of **1** (400 MHz, $CDCl_3$).

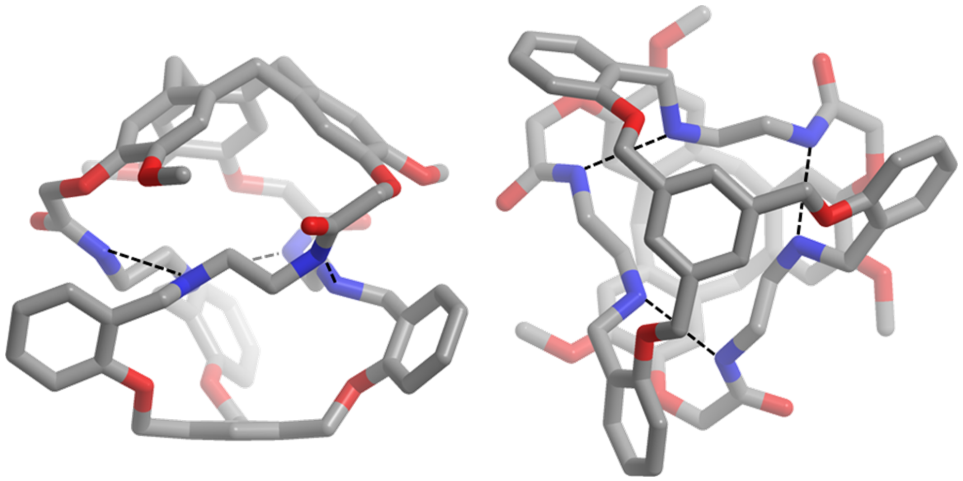

Figure 2: X-ray molecular structure of **1**. Hydrogen atoms are omitted for clarity; dashed lines represent hydrogen bonds.

occurred in the imine precursor, accounting for its high thermodynamic stability compared to oligomers that could also be formed during the reaction between **4** and **5**.

Interestingly, one can also see that the CTV with the *P* configuration (respectively *M*) imposes a Δ (respectively Λ) propeller-like arrangement of the lateral arms, with a 120° turn around the C_3 axis of the molecule (Figure 2). This also underlines how the chirality of the CTV unit propagates along the linkers to induce the propeller shape of the three aromatic rings in the south part of the hemicryptophane. This remote control of the helicity of the southern part by that of the northern CTV unit, through nine bonds, is allowed by this specific triple stranded helical structure, which induces a strong twist of the whole framework.

This helical arrangement probably also occurred in solution. Indeed, the south part of cage **1** is similar to that of cage **6** (Figure 3) and the comparison between the signals of the

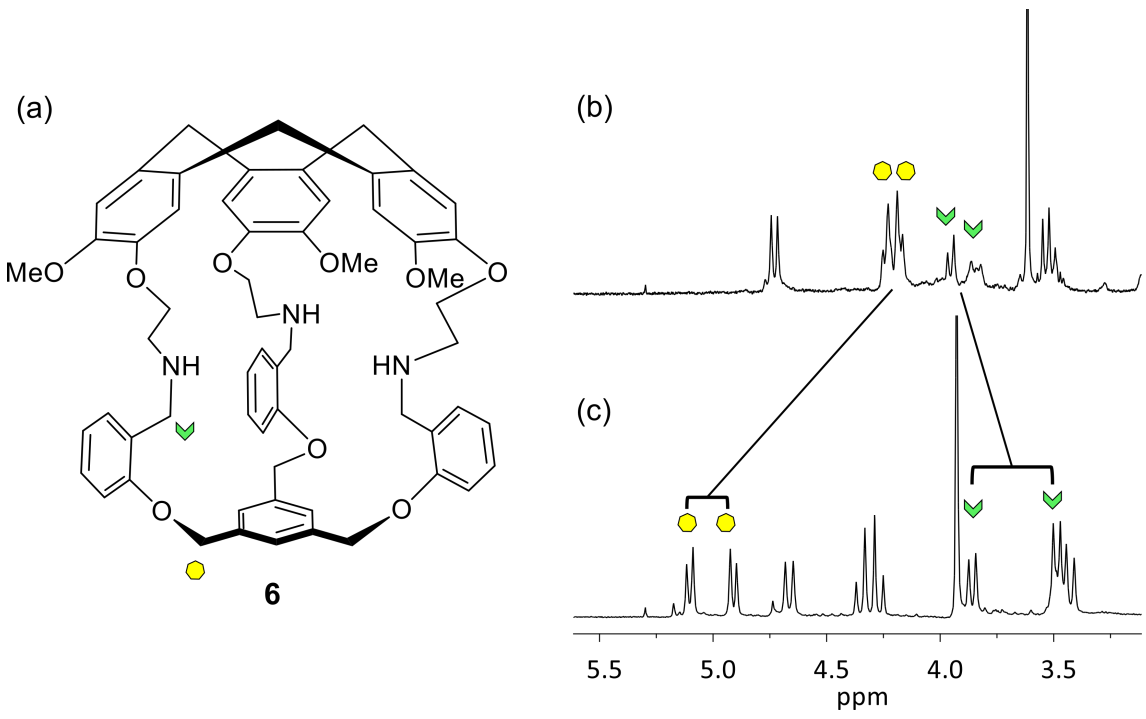

Figure 3: (a) Structure of compound **6**. (b) ^{1}H NMR of **6** ($CDCl_3$, 400 MHz). (c) ^{1}H NMR of **1** ($CDCl_3$, 400 MHz).

CH_2–NH and Ar–O–CH_2–Ar protons of cage **6** with those of cage **1** shows respectively downfield and highfield shifts of around −0.2 ppm and more than +0.8 ppm, respectively [16]. Moreover, the chemical shift differences of the two diastereotopic protons of the two AB systems are much greater for **1** than for **6** with $\Delta\delta = 0.38$ ppm for the CH_2NH and of $\Delta\delta = 0.19$ ppm for the Ar–O–CH_2–Ar of **1**, compared to 0.07 ppm and 0.05 ppm for **6**, respectively (Figure 3). This is consistent with a more rigid structure of cage **1** in solution, as suggested by the solid-state structure.

Conclusion

In summary, we have described the synthesis of a new hemicryptophane organic cage, which adopts a triple helical structure because of the propeller-like arrangement of its three linkers. The chirality of the CTV was shown to control that of the whole helical cage structure, since only *P*-Δ and *M*-Λ enantiomers were observed in solid state. NMR studies suggest that this propeller-like arrangement also occurs in solution. Further investigations are in progress in order to propagate the chirality of the CTV to even more remote opposite sites through the formation of such triple helical structures.

Supporting Information

Supporting Information File 1

Procedures for the synthesis of compounds **1**–**5**; ^{1}H, ^{13}C NMR, spectra mass spectra of compound **1** and crystallographic data.
[https://www.beilstein-journals.org/bjoc/content/supplementary/1860-5397-14-162-S1.pdf]

ORCID® iDs

Christophe Aronica - https://orcid.org/0000-0001-7098-7355
Jean-Pierre Dutasta - https://orcid.org/0000-0003-0948-6097

References

1. Jain, A.; Wang, G.; Vasquez, K. M. *Biochimie* **2008,** *90,* 1117–1130. doi:10.1016/j.biochi.2008.02.011
2. Shoulders, M. D.; Raines, R. T. *Annu. Rev. Biochem.* **2009,** *78,* 929–958. doi:10.1146/annurev.biochem.77.032207.120833
3. Hamley, I. W. *Chem. Rev.* **2017,** *117,* 14015–14041. doi:10.1021/acs.chemrev.7b00522
4. Pekkanen, A. M.; Mondschein, R. J.; Williams, C. B.; Long, T. E. *Biomacromolecules* **2017,** *18,* 2669–2687. doi:10.1021/acs.biomac.7b00671
5. Montero de Espinosa, L.; Meesorn, W.; Moatsou, D.; Weder, C. *Chem. Rev.* **2017,** *117,* 12851–12892. doi:10.1021/acs.chemrev.7b00168
6. Míguez-Lago, S.; Llamas-Saiz, A. L.; Cid, M. M.; Alonso-Gómez, J. L. *Chem. – Eur. J.* **2015,** *21,* 18085–18088. doi:10.1002/chem.201503994
7. Yamakado, R.; Mikami, K.; Takagi, K.; Azumaya, I.; Sugimoto, S.; Matsuoka, S.-i.; Suzuki, M.; Katagiri, K.; Uchiyama, M.; Muranaka, A. *Chem. – Eur. J.* **2013,** *19,* 11853–11857. doi:10.1002/chem.201301198
8. Ikeda, A.; Udzu, H.; Zhong, Z.; Shinkai, S.; Sakamoto, S.; Yamaguchi, K. *J. Am. Chem. Soc.* **2001,** *123,* 3872–3877. doi:10.1021/ja003269r
9. Malik, A. U.; Gan, F.; Shen, C.; Yu, N.; Wang, R.; Crassous, J.; Shu, M.; Qiu, H. *J. Am. Chem. Soc.* **2018,** *140,* 2769–2772. doi:10.1021/jacs.7b13512
10. Sato, H.; Bender, J. A.; Roberts, S. T.; Krische, M. J. *J. Am. Chem. Soc.* **2018,** *140,* 2455–2459. doi:10.1021/jacs.8b00131
11. Zhang, D.; Martinez, A.; Dutasta, J.-P. *Chem. Rev.* **2017,** *117,* 4900–4942. doi:10.1021/acs.chemrev.6b00847
12. Chatelet, B.; Joucla, L.; Padula, D.; Di Bari, L.; Pilet, G.; Robert, V.; Dufaud, V.; Dutasta, J.-P.; Martinez, A. *Org. Lett.* **2015,** *17,* 500–503. doi:10.1021/ol5035194
13. Gosse, I.; Robeyns, K.; Bougault, C.; Martinez, A.; Tinant, B.; Dutasta, J.-P. *Inorg. Chem.* **2016,** *55,* 1011–1013. doi:10.1021/acs.inorgchem.5b02750
14. Vériot, G.; Dutasta, J.-P.; Matouzenko, G.; Collet, A. *Tetrahedron* **1995,** *51,* 389–400. doi:10.1016/0040-4020(94)00904-9
15. Perraud, O.; Robert, V.; Gornitzka, H.; Martinez, A.; Dutasta, J.-P. *Angew. Chem., Int. Ed.* **2012,** *51,* 504–508. doi:10.1002/anie.201106934
16. Long, A.; Perraud, O.; Albalat, M.; Robert, V.; Dutasta, J.-P.; Martinez, A. *J. Org. Chem.* **2018,** *83,* 6301–6306. doi:10.1021/acs.joc.8b00276

License and Terms

BEILSTEIN JOURNAL OF ORGANIC CHEMISTRY

Asymmetric Michael addition reactions catalyzed by calix[4]thiourea cyclohexanediamine derivatives

Zheng-Yi Li[1], Hong-Xiao Tong[1], Yuan Chen[1,2], Hong-Kui Su[1], Tangxin Xiao[*1], Xiao-Qiang Sun[1] and Leyong Wang[*1,2]

Full Research Paper

Open Access

Address:
[1]Jiangsu Province Key Laboratory of Fine Petrochemical Engineering, School of Petrochemical Engineering, Changzhou University, Changzhou 213164, China and [2]Key Laboratory of Mesoscopic Chemistry of MOE, School of Chemistry and Chemical Engineering, Nanjing University, Nanjing 210023, China

Email:
Tangxin Xiao[*] - xiaotangxin@cczu.edu.cn; Leyong Wang[*] - lywang@nju.edu.cn

* Corresponding author

Keywords:
asymmetric Michael addition reaction; calix[4]arene; cyclohexanediamine; thiourea

Beilstein J. Org. Chem. **2018,** *14,* 1901–1907.
doi:10.3762/bjoc.14.164

Received: 14 April 2018
Accepted: 29 June 2018
Published: 25 July 2018

This article is part of the thematic issue "Macrocyclic and supramolecular chemistry".

Guest Editor: M.-X. Wang

Abstract

A number of upper rim-functionalized calix[4]thiourea cyclohexanediamine derivatives have been designed, synthesized and used as catalysts for enantioselective Michael addition reactions between nitroolefins and acetylacetone. The optimal catalyst **2** with a mono-thiourea group exhibited good performance in the presence of water/toluene (v/v = 1:2). Under the optimal reaction conditions, high yields of up to 99% and moderate to good enantioselectivities up to 94% ee were achieved. Detailed experiments clearly showed that the upper rim-functionalized hydrophobic calixarene scaffold played an important role in cooperation with the catalytic center to the good reactivities and enantioselectivities.

Introduction

During the past decades, asymmetric organocatalysis has played an important role as a tool for the syntheses of chiral molecules under mild conditions [1-4]. Among these reactions, the asymmetric Michael reaction is a powerful strategy to construct versatile intermediates due to its synthetic convenience and good stereoselectivity [5,6]. Accordingly, different versions of this reaction have been extensively studied. Notably, the Michael addition reaction of 1,3-dicarbonyl compounds to conjugated nitroalkenes is very important for the synthesis of chiral nitro carbonyl compounds, such as bioactive agrochemicals and drugs [7,8]. Although great progress has been made in this research field, it is still need of further effort to synthesize new efficient chiral organic catalysts for this kind of Michael reactions.

The thiourea functional group has played a critical role in organocatalysis due to its ability in forming hydrogen bonds with substrates. This may lead to activated forms of the sub-

strates allowing the corresponding reaction to occur [9-11]. For example, Jacobsen and co-workers pioneered an effective chiral thiourea catalyst which was employed in an asymmetric Strecker reaction [12,13]. In 2016, Hernández-Rodríguez and co-workers reported the preparation of bifunctional thioureas that contained either a methyl or trifluoromethyl group [14]. They discovered that the employment of chiral moieties with an α-trifluoromethyl group in thioureas show a positive effect on the selectivity and yields of the Michael reactions.

Supramolecular catalysis has drawn tremendous interest in the past few years [15-23]. In this context, calixarenes are ideal supramolecular macrocyclic scaffolds for the design of molecular receptors and organocatalysts due to their unique and tunable molecular architecture together with the ease of functionalization on the lower and upper rims [24-28]. Interestingly, their hydrophobic cavity also exhibits phase transfer catalytic function [29]. By attaching different pendants with catalytic ability to the scaffolds, this may offer us the opportunity to improve the green aspect of many reactions both in organic and aqueous medium [30]. For example, it has been reported that calixarenes linked with thiourea groups can be used to catalyze asymmetric Aldol reactions or Michael addition reactions in recent years [31-33]. Compared with the lower rim in the cone conformation of calixarenes, the functionalization of the upper rim is more challenging. Notably, it should be more valuable to exploit the cavity of upper rim-functionalized calixarenes because of the possibility of simultaneously using the hydrophobic cavity and chiral sites during a catalytic process [24,25].

Recently, we have reported a series of different functionalized organic catalysts based on calixarenes [26,34-38]. For example, we have been developed a calix[4]arene-based L-proline catalyst able to catalyze aldol reactions in aqueous solution with excellent enantioselectivity [35]. As part of our ongoing studies to develop novel types of organocatalysts for asymmetric catalysis, in this study, we aimed to synthesize novel upper rim-functionalized calix[4]thiourea cyclohexanediamine derivatives to catalyze asymmetric Michael addition reactions of acetylacetone and aromatic nitroalkenes.

Results and Discussion

Synthesis of catalysts

The chemical structures and synthetic pathways for catalysts are shown in Scheme 1 and Scheme 2, respectively. A series of upper rim-functionalized calix[4]arene-based cyclohexanediamine derivatives **1**–**3** have been prepared. Calix[4]arene derivative **5** with an amino group on the upper rim was first prepared according to a literature report [38]. Then, the amino group was converted to an isothiocyano group through reaction with phenyl chlorothionocarbonate under alkaline conditions to obtain compound **6**. Subsequently, different chiral cyclohexanediamine derivatives were reacted with calix[4]arene-based compound **6** to form the corresponding substituted thioureas. By this route the monosubstituted primary amine **1**, monosubstituted tertiary amine **2** and disubstituted tertiary amine **3**, respectively, were obtained. Of note, for the preparation of compound **1** the chiral mono-Boc-protected cyclohexanediamine was used for the coupling reaction. The protecting group was removed by treatment with CF_3COOH to afford **1**. Moreover, in order to comparatively study the role of the cavity of calix[4]arene, we also synthesized a model catalyst **4** by a similar synthetic procedure as outlined for catalyst **2**. All compounds **1**–**4** were fully characterized by NMR spectroscopy and HRMS analyses.

Optimization of reaction conditions

Generally, conjugate additions were employed for evaluating the catalytic activities of the new chiral amino-substituted

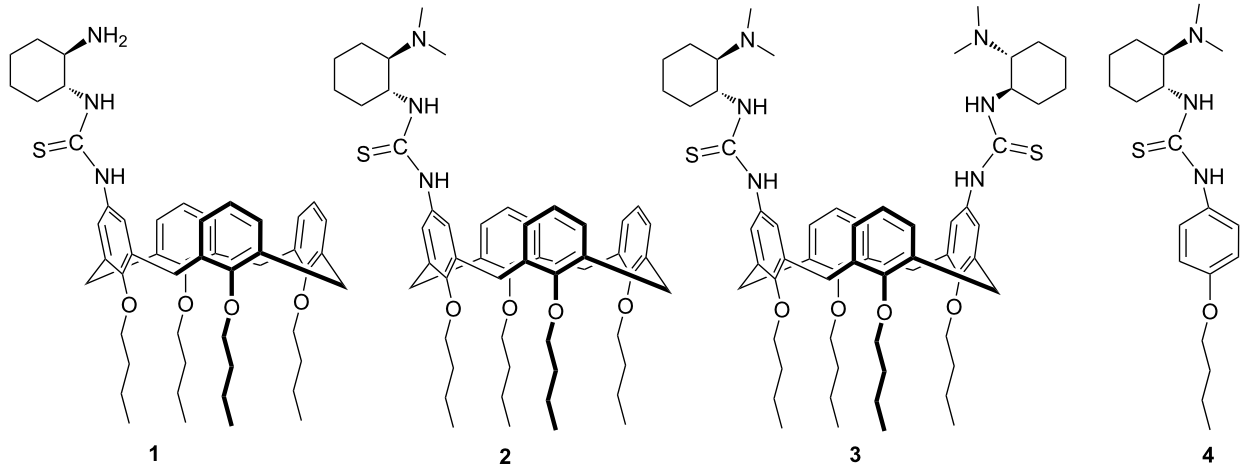

Scheme 1: Catalysts synthesized and screened in this study.

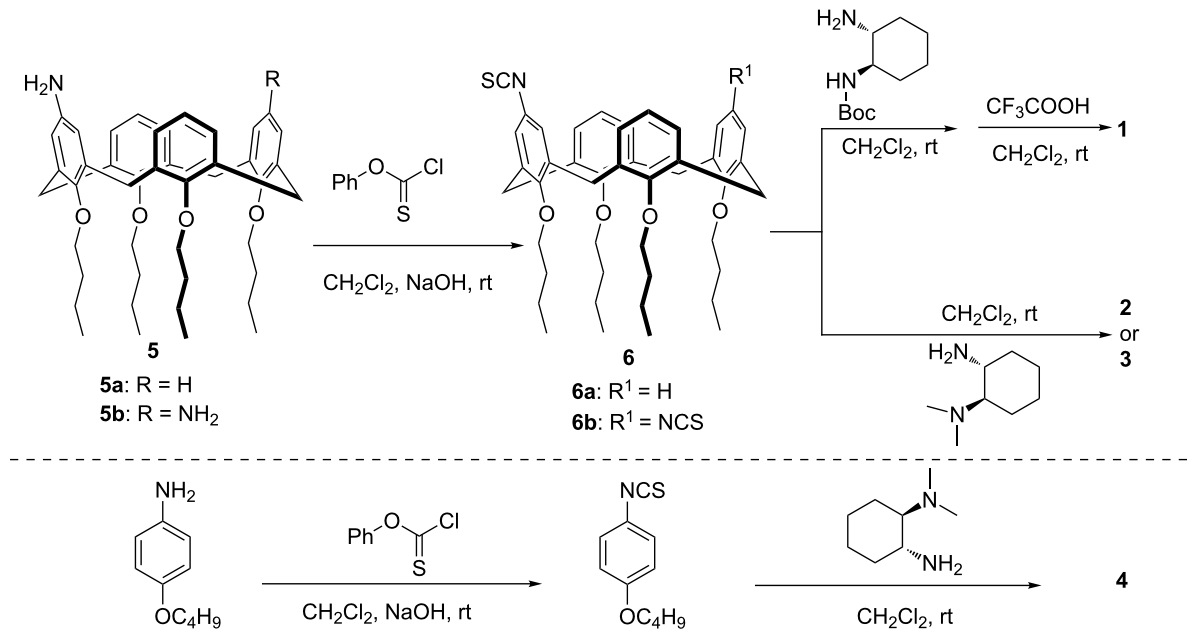

Scheme 2: Synthetic routes for organocatalysts **1**–**4**.

thioureas [33,39]. For this, the Michael addition reaction of acetylacetone (**8**) to β-nitrostyrene (**7a**) was chosen as the model reaction to evaluate the efficiency of compounds **1**–**4** as chiral organocatalysts (Table 1, entries 1–4). From Table 1, it can be seen that the yield with using the model catalyst **4** (only 75%) is significantly lower than those obtained with catalysts **1**–**3** in

Table 1: Screening of catalysts and solvents.[a]

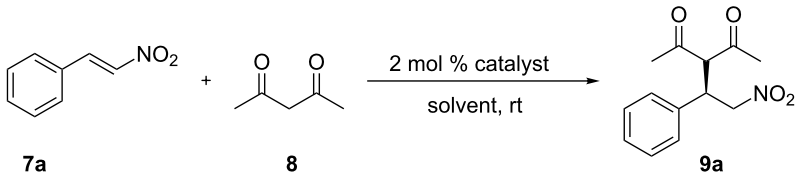

7a **8** **9a**

entry	catalyst	solvent	time (h)	yield[b] (%)	ee[c] (%)
1	**1**	H_2O	1	96	6
2	**2**	H_2O	1	99	41
3	**3**	H_2O	1	99	42
4	**4**	H_2O	6	75	28
5	**2**	toluene	48	62	90
6	**2**	CH_3CN	48	29	53
7	**2**	DMF	48	26	23
8	**2**	DMSO	48	23	23
9	**2**	1,4-dioxane	48	17	26
10	**2**	THF	48	56	77
11	**2**	CH_2Cl_2	48	37	58
12	**2**	Et_2O	48	67	68
13	**2**	*n*-hexane	48	80	50
14	**2**	neat	48	13	70

[a]Reagents and conditions: catalyst (2 mol %), nitrostyrene (0.5 mmol), and acetylacetone (1 mmol), solvent (0.5 mL), rt; [b]isolated yields; [c]determined by chiral HPLC analysis.

water (96–99%). Moreover, the reaction time using catalyst **4** was 6 h which is much longer compared to 1 h needed in case of catalysts **1**–**3**. These results showed that the catalysts comprising the calix[4]arene cavity are superior to the model catalyst in terms of catalytic reactivity. This is likely due to the formation of multiple microreactors at the water molecules' interface, with the calix[4]arene hydrophobic cavity attracting reactants and accelerating the reaction [35,40]. The primary amine-containing catalyst **1** showed poor performance compared to the corresponding tertiary-amine containing catalysts **2** and **3**. Although catalysts **2** and **3** demonstrated similar reactivities, we chose monosubstituted catalyst **2** as catalyst for further optimization according to the principle of atomic economy.

Next, the effect of solvents on the reaction catalyzed by **2** was investigated and the results are summarized in Table 1. The results revealed that both the yield and the enantioselectivity were highly dependent on the solvents. Poor yields, lower enantioselectivities and long reaction time (48 h) were observed when the reactions were performed in organic solvents or without any solvent (Table 1, entries 6–14). Interestingly, using toluene as the solvent afforded a higher enantioselectivity (90% ee) with a low yield (62%, Table 1, entry 5), while H_2O as the solvent gave higher yields (99% yield) with poor enantioselectivity (41% ee, Table 1, entry 2).

Therefore, in order to get good yield and enantioselectivity at the same time, a mixed solvent of toluene and water was chosen for the reaction (Table 2). The results showed that a good yield and enantioselectivity could be obtained when the volume ratio of toluene to water was 2:1 (Table 2, entry 5). We tried to further improve the catalytic effect by decreasing the reaction temperature and increasing the amount of acetylacetone. However, no improvements could be achieved (Table 2, entries 7 and 8). To our delight, increasing the catalyst loading of **2** from 2 mol % to 5 mol % resulted in a significant improvement in enantioselectivity (94% ee; Table 2, entry 9). However, further increasing the catalyst loading led to a slight decrease in enantioselectivity (Table 2, entry 10). Based on the above screening, the best results were obtained with 5 mol % of **2** in a mixed solvent of toluene and water (v/v = 2:1) at room temperature.

The scope of reaction substrates

With the optimal reaction conditions in hand, a set of aryl nitroolefins **7a**–**k** was then employed to explore the generality of this protocol and the results are summarized in Figure 1. All nitroolefins reacted smoothly with acetylacetone (**8**) to afford the corresponding products **9a**–**k** in high yields (90–99%) and moderate enantioselectivities for **9b**–**k** (46–76% ee). In case of **9a** an excellent enantioselectivity (94% ee) was obtained. This might be due to the fact that the nitrostyrene **7a** lacking substituents has minimal steric hindrance and tends to bind with the calixarene cavity by supramolecular host–guest interactions which could further improve the enantioselectivity. In addition, electronic effects of the substituents on the aromatic ring showed a significant influence on the reaction. The presence of a strong electron-withdrawing trifluoromethyl group afforded the product **9e** (76% ee) with higher enantioselectivity than a strong-electron donating methoxy group (**9c**, 46% ee), while products with methyl and halogen groups showed moderate enantioselectivities (59–72% ee). For the same substituent at different positions of the aromatic ring, it can be seen that in case of the electron-donating methoxy group the position of the substituent has a remarkable effect on the enantioselectivity (*meta*: 63% ee, *para*: 46% ee). However, no obvious trends could be observed in case of *ortho*- or *para*-halogenated substrates.

Table 2: Optimization of reaction conditions.[a]

entry	toluene/H_2O (v/v)	time (h)	yield[b] (%)	ee[c] (%)
1	1:1	5	99	68
2	1:2	5	99	70
3	1:3	3	99	63
4	1:5	1	99	54
5	2:1	5	99	75
6	3:1	36	63	76
7[d]	2:1	40	47	74
8[e]	2:1	7	78	63
9[f]	2:1	4	99	94
10[g]	2:1	4	99	92

[a]Reagents and conditions: catalyst **2** (2 mol %), nitrostyrene (0.5 mmol), and acetylacetone (1 mmol), toluene and water (0.48 mL), rt; [b]isolated yields; [c]determined by chiral HPLC analysis; [d]reaction performed at 0 °C; [e]2.5 mmol acetylacetone used; [f]5 mol % catalyst **2** used; [g]10 mol % catalyst **2** used.

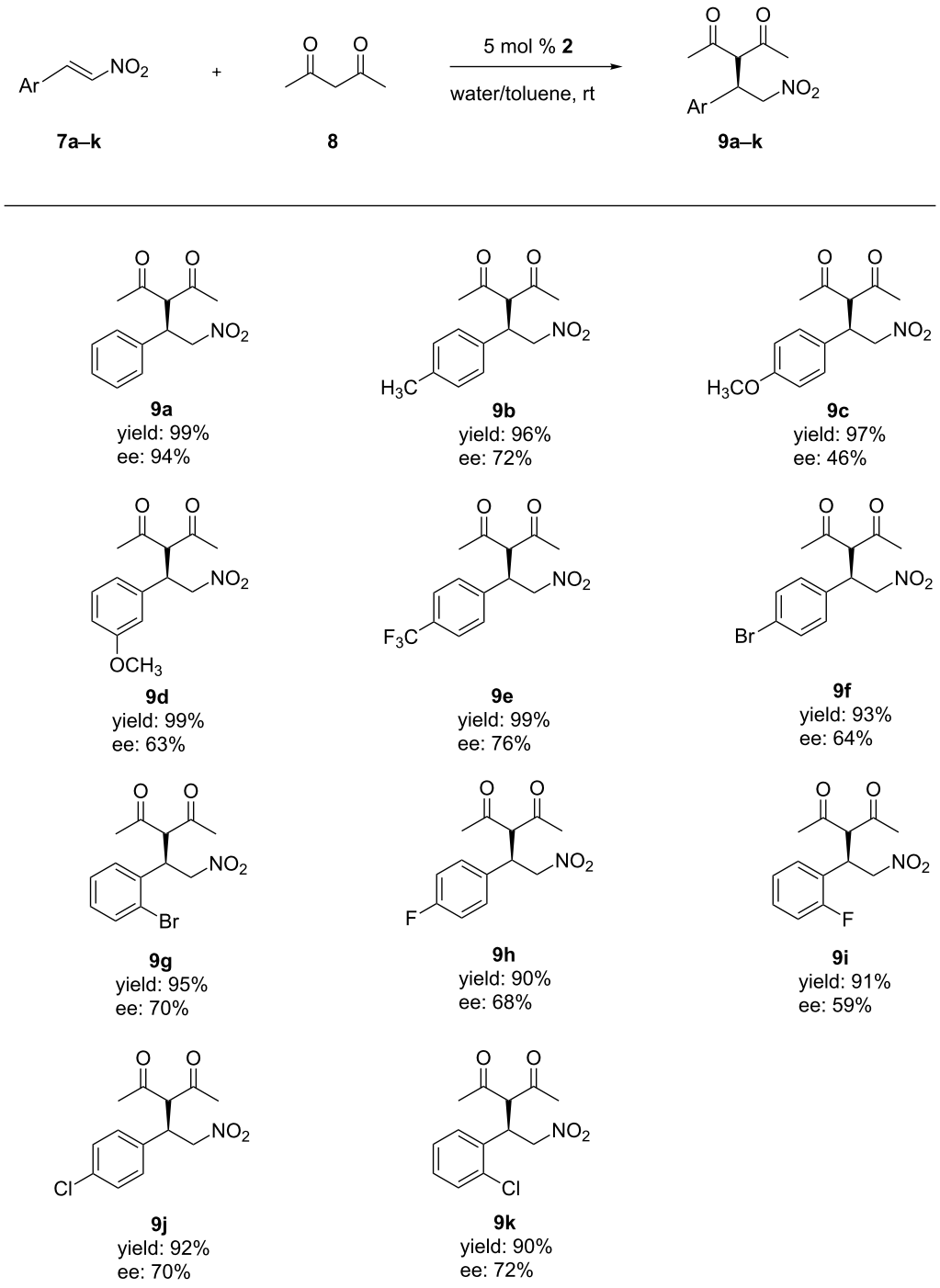

Figure 1: Asymmetric Michael addition of acetylacetone with different nitroolefins catalyzed by organocatalyst **2**. Reagents and conditions: catalyst **2** (5 mol %), nitroolefin (0.5 mmol), acetylacetone (1 mmol), toluene (0.32 mL) and water (0.16 mL), rt.

Mechanism study

There are two possibilities for the bifunctional thiourea-catalyzed asymmetric Michael addition reaction mechanism as has been summarized by Wang and co-worker [41]. In case of 1,3-dicarbonyl compounds or nitroolefins as substrates in the reaction, the question arises, which one is activated by the thiourea group through double hydrogen bonding. Based on the better enantioselectivity observed for product **9a** over **9b**–**k**, it was deduced that the binding of the nitroolefin with the calixarene cavity might be affected by the steric hindrance of the groups present on the aromatic ring. We propose the following plausible synergistic catalytic mechanism (Scheme 3). First, the two

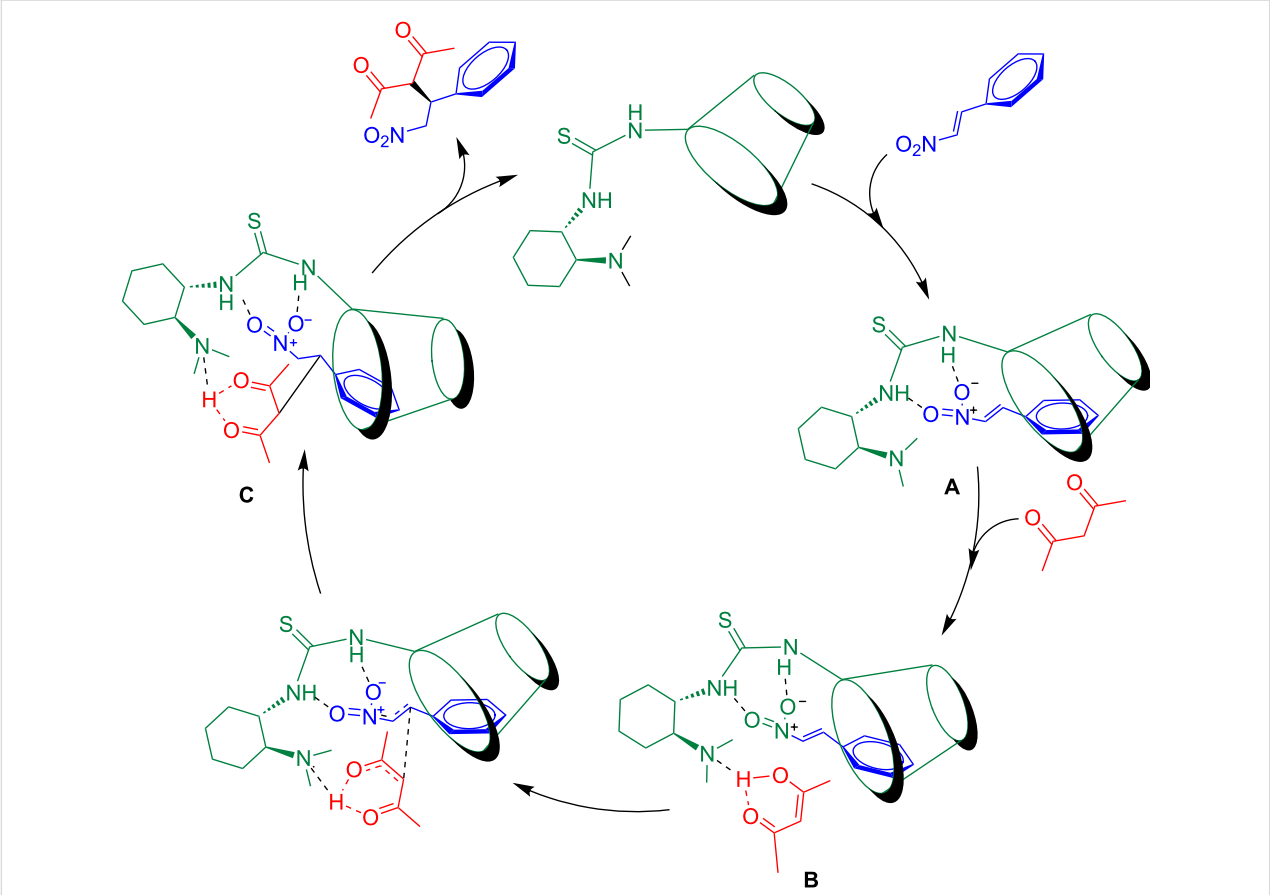

Scheme 3: Possible proposed reaction mechanism.

oxygen atoms of the nitro group in the nitrostyrene are activated through double hydrogen bonding with the thiourea group, while the benzene ring is held by a supramolecular host–guest interaction with the calixarene to form a stable transition state **A**. Then, another hydrogen bond is formed between the nitrogen atom of the tertiary amine group in **A** and acetylacetone in its enol form, leading to the formation of a ternary complex **B**. Finally, nucleophilic attack of acetylacetone on the nitrostyrene creates a new C–C bond forming binary complex **C** from which the enantioselective product is released.

Conclusion

In summary, we have synthesized a series of upper rim-functionalized calix[4]arene-based chiral cyclohexanediamine thiourea catalysts **1**–**3** and tested as organocatalysts for the enantioselective Michael reactions of nitroolefins to 1,3-dicarbonyl compounds. Under the optimal conditions, catalyst **2** smoothly catalyzed the reactions in mixed solvent of toluene and water (v/v = 2:1) at room temperature to afford the products in high yields (90–99%) and with moderate to good enantioselectivities (46–94% ee). By comparing with model catalyst **4**, the calixarene scaffold, especially its hydrophobic cavity present in catalyst **2** played an important role in controlling reaction activities and enantioselectivities.

Supporting Information

Supporting Information File 1

Experimental procedures, characterization data for all compounds and copies of NMR spectra.
[https://www.beilstein-journals.org/bjoc/content/supplementary/1860-5397-14-164-S1.pdf]

Acknowledgements

We gratefully acknowledge the financial support of the National Natural Science Foundation of China (Nos. 21572026 and 21702020), the Natural Science Foundation of Jiangsu Colleges and Universities (14KJA150002), Jiangsu Key Laboratory of Advanced Catalytic Materials and Technology (BM2012110), Advanced Catalysis and Green Manufacturing Collaborative Innovation Center (ACGM2016-06-05), and the Priority Academic Program Development of Jiangsu Higher Education Institutions.

ORCID® iDs

Zheng-Yi Li - https://orcid.org/0000-0001-9653-0687
Tangxin Xiao - https://orcid.org/0000-0002-2864-9587

References

1. Hajra, S.; Aziz, S. M.; Maji, R. *RSC Adv.* **2013,** *3,* 10185–10188. doi:10.1039/c3ra42014k
2. Vetica, F.; Chauhan, P.; Dochain, S.; Enders, D. *Chem. Soc. Rev.* **2017,** *46,* 1661–1674. doi:10.1039/C6CS00757K
3. Zhang, G.; Zhu, C.; Liu, D.; Pan, J.; Zhang, J.; Hu, D.; Song, B. *Tetrahedron* **2017,** *73,* 129–136. doi:10.1016/j.tet.2016.11.063
4. Zhong, C.; Chen, Y.; Petersen, J. L.; Akhmedov, N. G.; Shi, X. *Angew. Chem.* **2009,** *121,* 1305–1308. doi:10.1002/ange.200805558
5. Castán, A.; Badorrey, R.; Gálvez, J. A.; López-Ram-de Víu, P.; Díaz-de-Villegas, M. D. *Org. Biomol. Chem.* **2018,** *16,* 924–935. doi:10.1039/C7OB02798B
6. Uyanik, A.; Bayrakci, M.; Eymur, S.; Yilmaz, M. *Tetrahedron* **2014,** *70,* 9307–9313. doi:10.1016/j.tet.2014.10.063
7. De Simone, N. A.; Schettini, R.; Talotta, C.; Gaeta, C.; Izzo, I.; Della Sala, G.; Neri, P. *Eur. J. Org. Chem.* **2017,** 5649–5659. doi:10.1002/ejoc.201700912
8. Rapi, Z.; Démuth, B.; Keglevich, G.; Grűn, A.; Drahos, L.; Sóti, P. L.; Bakó, P. *Tetrahedron: Asymmetry* **2014,** *25,* 141–147. doi:10.1016/j.tetasy.2013.12.007
9. Andrés, J. M.; González, M.; Maestro, A.; Naharro, D.; Pedrosa, R. *Eur. J. Org. Chem.* **2017,** 2683–2691. doi:10.1002/ejoc.201601640
10. Li, X.; Deng, H.; Zhang, B.; Li, J.; Zhang, L.; Luo, S.; Cheng, J.-P. *Chem. – Eur. J.* **2010,** *16,* 450–455. doi:10.1002/chem.200902430
11. Shubina, T. E.; Freund, M.; Schenker, S.; Clark, T.; Tsogoeva, S. B. *Beilstein J. Org. Chem.* **2012,** *8,* 1485–1498. doi:10.3762/bjoc.8.168
12. Huang, H.; Jacobsen, E. N. *J. Am. Chem. Soc.* **2006,** *128,* 7170–7171. doi:10.1021/ja0620890
13. Sigman, M. S.; Jacobsen, E. N. *J. Am. Chem. Soc.* **1998,** *120,* 4901–4902. doi:10.1021/ja980139y
14. Jiménez, E. I.; Vallejo Narváez, W. E.; Román-Chavarría, C. A.; Vazquez-Chavez, J.; Rocha-Rinza, T.; Hernández-Rodríguez, M. *J. Org. Chem.* **2016,** *81,* 7419–7431. doi:10.1021/acs.joc.6b01063
15. Chate, A. V.; Bhadke, P. K.; Khande, M. A.; Sangshetti, J. N.; Gill, C. H. *Chin. Chem. Lett.* **2017,** *28,* 1577–1582. doi:10.1016/j.cclet.2017.03.007
16. Gao, J.; Ren, Z.-G.; Lang, J.-P. *Chin. Chem. Lett.* **2017,** *28,* 1087–1092. doi:10.1016/j.cclet.2016.12.035
17. Jiang, J.; Ouyang, G.; Zhang, L.; Liu, M. *Chem. – Eur. J.* **2017,** *23,* 9439–9450. doi:10.1002/chem.201700727
18. Ke, C.; Yang, C.; Mori, T.; Wada, T.; Liu, Y.; Inoue, Y. *Angew. Chem., Int. Ed.* **2009,** *48,* 6675–6677. doi:10.1002/anie.200902911
19. Thomas, C.; Gladysz, J. A. *ACS Catal.* **2014,** *4,* 1134–1138. doi:10.1021/cs500134z
20. Wang, Q.-Q.; Gonell, S.; Leenders, S. H. A. M.; Dürr, M.; Ivanović-Burmazović, I.; Reek, J. N. H. *Nat. Chem.* **2016,** *8,* 225–230. doi:10.1038/nchem.2425
21. Jin, Q. X.; Li, J.; Li, X. G.; Zhang, L.; Fang, S. M.; Liu, M. H. *Prog. Chem.* **2014,** *26,* 919–930.
22. Zhao, J.; Liu, Y. *Prog. Chem.* **2015,** *27,* 687–703.
23. Tang, Y. P.; He, Y. M.; Feng, Y.; Fan, Q. H. *Prog. Chem.* **2018,** *30,* 476–490.
24. Aktas, M.; Uyanik, A.; Eymur, S.; Yilmaz, M. *Supramol. Chem.* **2015,** *28,* 351–359. doi:10.1080/10610278.2015.1073288
25. Gutsche, C. D. *Acc. Chem. Res.* **2002,** *16,* 161–170. doi:10.1021/ar00089a003
26. Li, Z.-Y.; Chen, J.-W.; Liu, Y.; Xia, W.; Wang, L. *Curr. Org. Chem.* **2011,** *15,* 39–61. doi:10.2174/138527211793797837
27. Sahin, O.; Eymur, S.; Uyanik, A.; Akceylan, E.; Yilmaz, M. *Polycyclic Aromat. Compd.* **2018,** *38,* 168–179. doi:10.1080/10406638.2016.1176058
28. Xu, Z.-X.; Li, G.-K.; Chen, C.-F.; Huang, Z.-T. *Tetrahedron* **2008,** *64,* 8668–8675. doi:10.1016/j.tet.2008.07.001
29. Bozkurt, S.; Durmaz, M.; Yilmaz, M.; Sirit, A. *Tetrahedron: Asymmetry* **2008,** *19,* 618–623. doi:10.1016/j.tetasy.2008.02.006
30. Shimizu, S.; Shimada, N.; Sasaki, Y. *Green Chem.* **2006,** *8,* 608–614. doi:10.1039/b603962f
31. Demircan, E.; Eymur, S.; Demir, A. S. *Tetrahedron: Asymmetry* **2014,** *25,* 443–448. doi:10.1016/j.tetasy.2014.01.015
32. Durmaz, M.; Tataroglu, A.; Yilmaz, H.; Sirit, A. *Tetrahedron: Asymmetry* **2016,** *27,* 148–156. doi:10.1016/j.tetasy.2016.01.004
33. Genc, H. N.; Sirit, A. *J. Inclusion Phenom. Macrocyclic Chem.* **2018,** *90,* 39–49. doi:10.1007/s10847-017-0761-1
34. Li, Z.-Y.; Chen, J.-W.; Wang, L.; Pan, Y. *Synlett* **2009,** 2356–2360. doi:10.1055/s-0029-1217710
35. Li, Z.-Y.; Chen, Y.; Zheng, C.-Q.; Yin, Y.; Wang, L.; Sun, X.-Q. *Tetrahedron* **2017,** *73,* 78–85. doi:10.1016/j.tet.2016.11.052
36. Li, Z.-Y.; Lu, C.-X.; Huang, G.; Ma, J.-J.; Sun, H.; Wang, L.; Pan, Y. *Lett. Org. Chem.* **2010,** *7,* 461–466. doi:10.2174/157017810791824919
37. Li, Z. Y.; Xing, H. J.; Huang, G. L.; Sun, X. Q.; Jiang, J. L.; Wang, L. Y. *Sci. China: Chem.* **2011,** *54,* 1726–1734. doi:10.1007/s11426-011-4374-z
38. Li, Z.; Ma, J.; Chen, J.; Pan, Y.; Jiang, J.; Wang, L. *Chin. J. Chem.* **2009,** *27,* 2031–2036. doi:10.1002/cjoc.200990341
39. Andrés, J. M.; Losada, J.; Maestro, A.; Rodríguez-Ferrer, P.; Pedrosa, R. *J. Org. Chem.* **2017,** *82,* 8444–8454. doi:10.1021/acs.joc.7b01177
40. De Rosa, M.; La Manna, P.; Soriente, A.; Gaeta, C.; Talotta, C.; Neri, P. *RSC Adv.* **2016,** *6,* 91846–91851. doi:10.1039/C6RA19270J
41. Siau, W.-Y.; Wang, J. *Catal. Sci. Technol.* **2011,** *1,* 1298–1310. doi:10.1039/c1cy00271f

License and Terms

BEILSTEIN JOURNAL OF ORGANIC CHEMISTRY

A pyridinium/anilinium [2]catenane that operates as an acid–base driven optical switch

Sarah J. Vella and Stephen J. Loeb*

Full Research Paper

Open Access

Address:
Department of Chemistry and Biochemistry, University of Windsor, Windsor, Ontario N9B 3P4, Canada

Email:
Stephen J. Loeb* - loeb@uwindsor.ca

* Corresponding author

Keywords:
catenane; mechanically interlocked molecule; molecular switch

Beilstein J. Org. Chem. **2018,** *14,* 1908–1916.
doi:10.3762/bjoc.14.165

Received: 28 April 2018
Accepted: 05 July 2018
Published: 25 July 2018

This article is part of the thematic issue "Macrocyclic and supramolecular chemistry".

Guest Editor: M.-X. Wang

Abstract

A two-station [2]catenane containing a large macrocycle with two different recognition sites, one bis(pyridinium)ethane and one benzylanilinium, as well as a smaller **DB24C8** ring was synthesized and characterized. ^{1}H NMR spectroscopy showed that the **DB24C8** ring can shuttle between the two recognition sites depending on the protonation state of the larger macrocycle. When the aniline group is neutral, the **DB24C8** ring resides solely at the bis(pyridinium)ethane site, while addition of acid forms a charged benzylanilinium site. The **DB24C8** then shuttles between the two charged recognition sites with occupancy favoring the bis(pyridinium)ethane site by a ratio of 4:1. The unprotonated [2]catenane has a deep yellow/orange color when the **DB24C8** ring resides solely at the bis(pyridinium)ethane site and changes to colorless when the crown ether is shuttling (i.e., circumrotating) back and forth between the two recognition sites thus optically signalling the onset of the shuttling dynamics.

Introduction

[2]Rotaxane molecular shuttles [1-5] are the dynamic building blocks of a wide variety of molecular switches [6-9] and a number of sophisticated molecular machines that operate away from equilibrium [10-15]. We have previously reported [2]rotaxane molecular switches containing a single dibenzo[24]crown ether **DB24C8** wheel and two different recognition sites; benzylanilinium and 1,2-bis(pyridinium)ethane [16]. These shuttles operate as bistable switches driven by acid/base chemistry and can be optically sensed by either a change in color (yellow/colorless) for [**1F**⊂**DB24C8**]$^{2+}$ or a fluorescence change (OFF/ON) for [**1A**⊂**DB24C8**]$^{2+}$; see Figure 1.

In addition, we have also previously prepared a [3]catenane containing two dibenzo[24]crown ether **DB24C8** rings interlocked onto a much larger macrocyclic ring containing two 1,2-bis(pyridinium)ethane recognition sites linked by terphenyl spacer groups [17] (Figure 2).

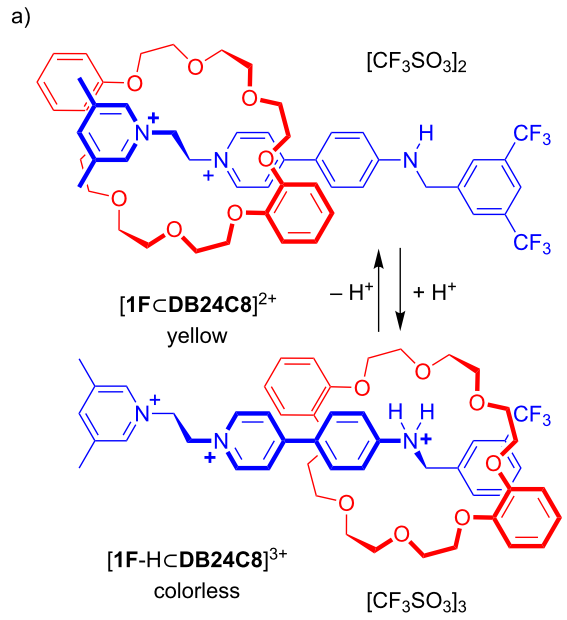

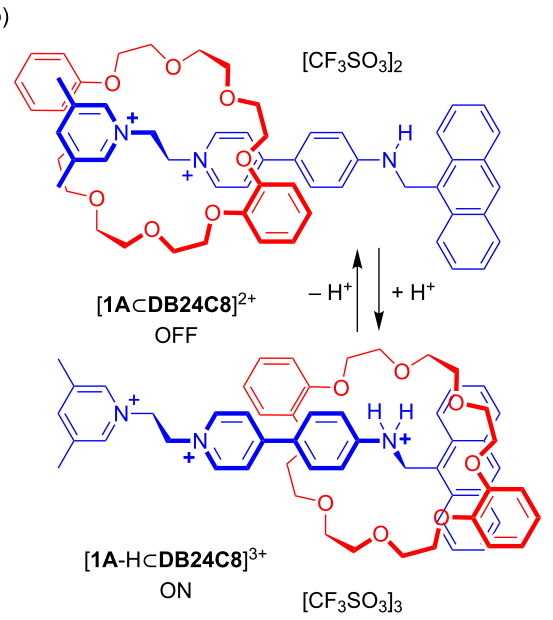

Figure 1: Two [2]rotaxane molecular shuttles with both bis(pyridinium)ethane and benzylanilinium recognition sites that can be switched by acid–base chemistry and optically sensed by a) a color change from colorless to yellow and b) a change in fluorescence from OFF to ON (CD_3CN or CD_2Cl_2). Code: F to indicate CF_3 groups; A to indicate anthracene group.

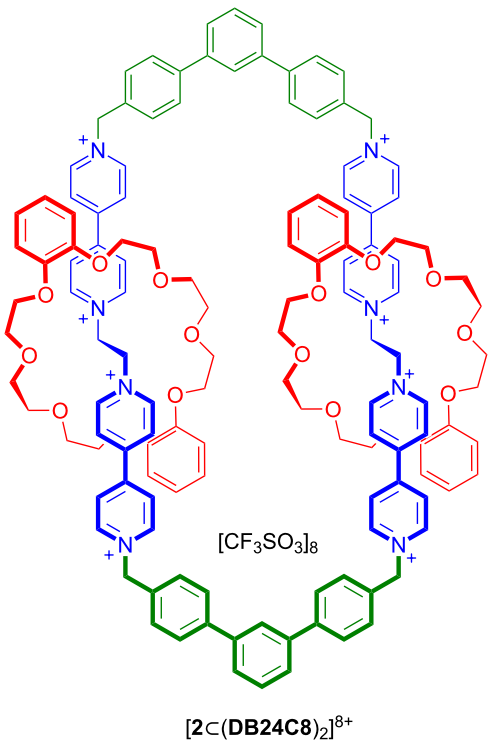

Figure 2: A [3]catenane containing two identical bis(pyridinium)ethane recognition sites on a large macrocycle and two smaller threaded **DB24C8** rings.

It was thus of interest to design and build these two different recognition sites (benzylanilinium and bis(pyridinium)ethane) into an analogous circumrotational [2]catenane molecular switch to compare to the linear [2]rotaxane molecular shuttles outlined in Figure 1. This should be possible because of the structural similarities (size and shape) between the bis(pyridinium)ethane and benzylanilinium recognition sites. Each has a two-atom chain in a low energy, *anti*-conformation linking aromatic rings and the distance between the terminal nitrogen atoms are 18.11 and 18.09 Å (MM3) for the benzylaniline and bis(dipyridinium)ethane axles **4** and $\mathbf{5}^{2+}$, respectively; see Figure 2 and Scheme 1 compound $[\mathbf{8}\subset\mathbf{DB24C8}]^{6+}$ for this comparison and concept.

Results and Discussion

Synthesis

Although the previously reported [3]catenane (Figure 2) was synthesized using a one-step, self-assembly procedure from two bis(pyridinium)ethane axles, two terphenyl spacers and two **DB24C8** crown ethers, a [2]catenane with different recognition sites requires a stepwise approach involving the incorporation of each recognition site independently. Overall, the synthesis of [2]catenane $[\mathbf{8}\subset\mathbf{DB24C8}]^{6+}$ required multiple steps and is outlined in Scheme 1. Two literature preparations were used to construct each of the known compounds, terphenyl linker **6** [18] and bis(pyridinium)ethane axle [**5**][OTf]$_2$ [19,20], while the new benzylaniline axle **4** was prepared as shown from **3** [21].

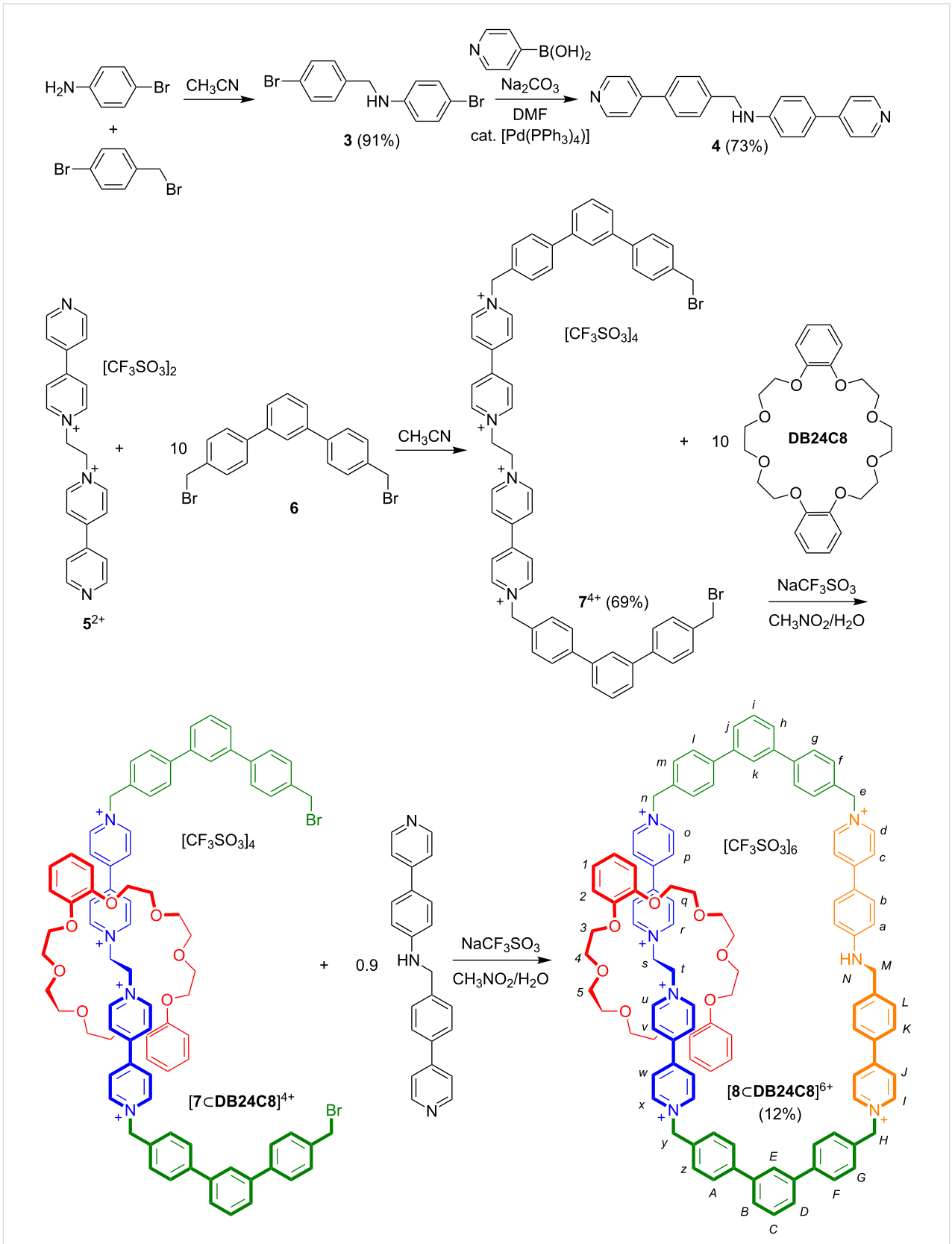

Scheme 1: Step-wise synthesis of [2]catenane [**8**⊂**DB24C8**]$^{6+}$ containing benzylanilinium and bis(pyridinium)ethane recognition sites and terphenyl spacers.

Once the precursor components were synthesized, the [2]catenane was assembled in two steps. Firstly, [**5**][OTf]$_2$ was reacted with ten equivalents of the bis(bromomethyl)terphenyl linker **6** in CH_3CN to afford [**7**][OTf]$_4$ in moderate yield. Secondly, the [2]pseudorotaxane [**7**⊂**DB24C8**]$^{4+}$ was formed using [**7**][OTf]$_4$ in the presence of **DB24C8** followed by ring closure using the benzylaniline axle **4** to yield [**8**⊂**DB24C8**][OTf]$_6$. The reaction was performed under dilute conditions with 10 equivalents of crown ether to favor ring closure and kinetic trapping of the smaller ring.

To isolate the pure [2]catenane, the reaction solvent (CH_3CN) was evaporated and the residue washed with toluene to remove excess crown ether. This was then followed by column chromatography on silica gel using a 5:3:2 mixture of CH_3OH/2 M NH_4Cl/CH_3NO_2 as the eluent. Fractions containing the product (R_f = 0.66) were combined and anion exchanged to the triflate salt to yield [2]catenane [**8**⊂**DB24C8**][OTf]$_6$.

Characterization

The ^{1}H NMR spectrum of [2]catenane [**8**⊂**DB24C8**]$^{6+}$ (298 K, CD_2Cl_2) is shown in Figure 3 and the labelling scheme for the H-atoms is given in Scheme 1. All resonances were assigned based on 2D COSY NMR spectroscopy as well as comparison to ^{1}H NMR and COSY spectra of individual components **6** and **7**$^{4+}$. Comparing the proton chemicals shifts for H-atoms *n*–*y* of [**8**⊂**DB24C8**]$^{6+}$ with those of precursor **7**$^{4+}$ shows changes in chemical shift typically associated with the close interaction of **DB24C8** with a bis(pyridinium)ethane recognition site [18]. In particular, the significant downfield shifts observed for ethylene protons *s* and *t* from 5.30 ppm in **7**$^{4+}$ to 5.56 ppm for [**8**⊂**DB24C8**]$^{6+}$ as well as *u* and *r*, the *ortho* pyridinium protons, from 9.04 ppm in **7**$^{4+}$ to 9.31 ppm for [**8**⊂**DB24C8**]$^{6+}$ are characteristic of hydrogen-bonding to the crown ether. In addition, π-stacking interactions induce upfield shifts for protons *p*, *q*, *v* and *w* from 8.48 ppm in **7**$^{4+}$ to 8.24 ppm for [**8**⊂**DB24C8**]$^{6+}$. Protons *o*, *x*, *n* and *y* do not shift appreciably because the crown ether does not extend far enough to interact with these protons. In contrast, the chemical shifts for protons *a*–*d* and *I*–*L* on the benzylaniline portion of the large ring of [**8**⊂**DB24C8**]$^{6+}$ do not shift significantly inferring that in the neutral aniline state the crown ether resides exclusively at the bis(pyridinium)ethane site of the [2]catenane. Table 1 summarizes the chemical shift differences between the [2]catenane [**8**⊂**DB24C8**]$^{6+}$ and precursor **7**$^{4+}$ which contains no crown ether.

A sample of [**8**⊂**DB24C8**]$^{6+}$ (1:1 CH_3OH/CH_3CN) was analyzed by high-resolution electrospray mass spectrometry (HRESIMS). Sufficient resolution for each of the 2+, 3+, 4+ and 5+ molecular ions allowed for exact mass measurements (<5 ppm) confirming the catenated nature of the structure. Table 2 summarizes the observed values.

Acid–base driven switching

The analysis of the ^{1}H NMR spectrum (CD_3CN, 298 K) of [**8**⊂**DB24C8**]$^{6+}$ indicates that the **DB24C8** ring resides exclusively at the bis(pyridinium)ethane recognition site. This is

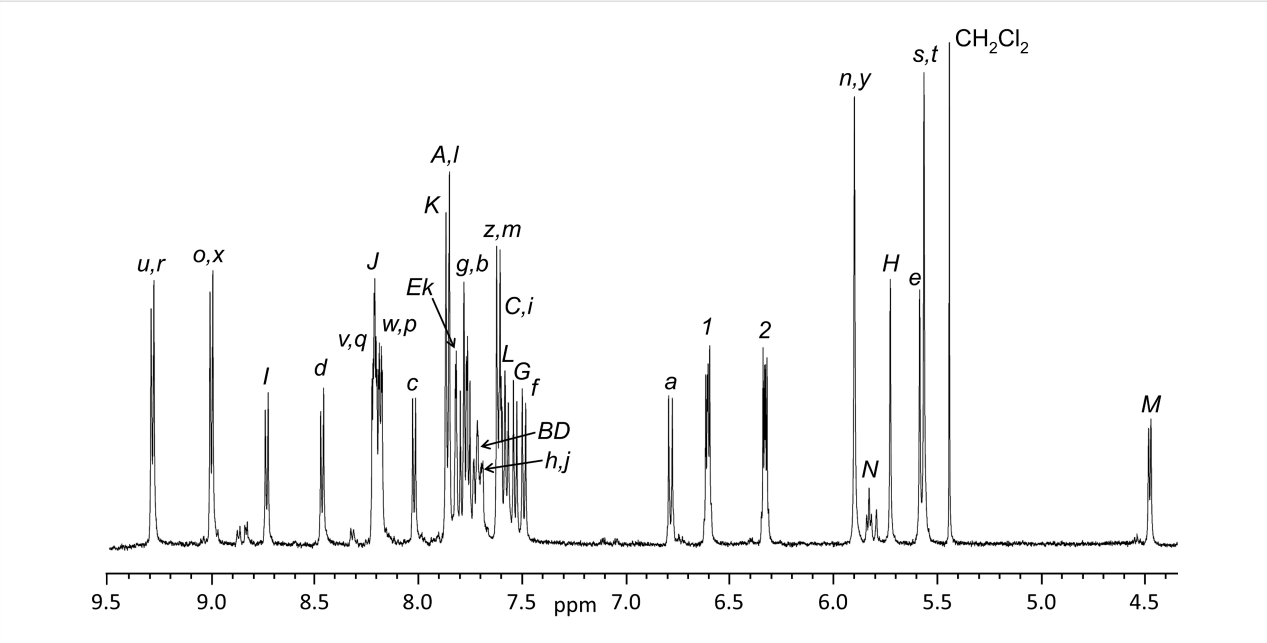

Figure 3: ^{1}H NMR spectrum of [2]catenane [**8**⊂**DB24C8**]$^{6+}$ (500 MHz, 298 K, CD_2Cl_2) showing the assigned proton chemical shifts; see Scheme 1 for labelling.

Table 1: Summary of major chemical shift differences between precursor $\mathbf{7}^{4+}$ and catenane [**8**⊂**DB24C8**]$^{6+}$.

protons[a]	$\mathbf{7}^{4+}$	[**8**⊂**DB24C8**]$^{6+}$
n, y	5.89	5.90
o, x	9.05	9.03
p, w	8.47	8.19
q, v	8.50	8.22
r, u	9.04	9.31
s, t	5.30	5.56

[a]All chemical shift values given in ppm relative to TMS in CD_3CN at 298 K.

easily understood as the neutral benzylaniline site does not allow for appreciable non-covalent interactions and cannot compete for the **DB24C8** ring with the dicationic bis(pyridinium)ethane site. However, the addition of one equivalent of triflic acid (CF_3SO_3H) to a solution of [**8**⊂**DB24C8**]$^{6+}$ results in protonation of the aniline nitrogen atom to give [8-**H**⊂DB24C8]$^{7+}$ and a second viable recognition site for the crown ether.

Figure 4 shows a partial ^{1}H NMR spectrum of protonated [**8**-H⊂**DB24C8**]$^{7+}$ in CD_3CN at 298 K. The smaller **DB24C8** ring can now reside at either of the bis(pyridinium)ethane or benzylanilinium sites and these two possible co-conformations are designated **A** and **B** in Figure 4a. The ethylene protons at the core of the bis(pyridinium)ethane motif, labelled *s* and *t* in **A** and *s'* and *t'* in **B** are clearly distinguishable and show that there is a 4:1 ratio of **A**:**B** indicating that the smaller **DB24C8** ring prefers to occupy the bis(pyridinium)ethane site over the benzylanilinium site and that shuttling between the two sites is slow on the NMR timescale under these experimental conditions. Addition of base (NEt_3) returns the system to its original state and the process can be cycled by repeated addition of acid (CF_3SO_3H) and base without significant degradation of the compound as verified by ^{1}H NMR spectroscopy.

Interestingly, these results are contrary to those observed for the [2]rotaxane molecular shuttles [**1F**⊂**DB24C8**]$^{2+}$ and [**1A**⊂**DB24C8**]$^{2+}$ shown in Figure 1. For that system, the benzylanilinium site was preferred 3:1 for [**1F**⊂**DB24C8**]$^{2+}$ and 9:1 for [**1A**⊂**DB24C8**]$^{2+}$ in CD_3CN and when CD_2Cl_2 was used the systems were completely bistable with **DB24C8** preferring to reside exclusively at the bis(pyridinium)ethane site when unprotonated and exclusively at the benzylanilinium site when protonated.

The UV–visible spectra of [**8**⊂**DB24C8**]$^{6+}$ and [**8**-H⊂**DB24C8**]$^{7+}$ are shown in Figure 5 for 2.0×10^{-5} M solutions in CH_3CN. The molar absorptivity (ε) of [**8**⊂**DB24C8**]$^{6+}$ was calculated to be 22,680 L mol^{-1} cm^{-1} with λ_{max} at 412 nm. The large absorption is due to an intramolecular charge transfer (ICT) band arising from charge transfer between the aniline nitrogen and pyridinium group of the benzylanilinium recognition site. However, this ICT band (412 nm) is eliminated by protonating the aniline nitrogen to form [**8**-H⊂**DB24C8**]$^{7+}$. Therefore, when the [2]catenane absorbs strongly showing a deep yellow/orange solution this indicates that the crown resides solely on the bis(pyridinium)ethane site for [**8**⊂**DB24C8**]$^{6+}$ but, when the [2]catenane does not absorb in the UV–visible region yielding a colorless solution this means the crown ether must be shuttling (i.e., circumrotating) back and forth between the two co-conformations, **A** and **B**, of [**8**-H⊂**DB24C8**]$^{7+}$.

Conclusion

A two-station circumrotational [2]catenane has been synthesized and its operation described. The system consists of a large macrocycle containing two different recognition sites, one bis(pyridinium)ethane and one benzylanilinium with a single smaller **DB24C8** ring that can shuttle between the two recognition sites depending on the protonation state of the larger macrocycle. When the aniline group is neutral, the **DB24C8** ring resides only at the bis(pyridinium)ethane site. However, addition of acid activates the benzylanilinium site allowing the ring to shuttle between the two, now competing, recognition sites. It was found that **DB24C8** prefers the bis(pyridinium)-ethane site over the protonated benzylanilinium site in a ratio of 4:1. This is quite different from similar [2]rotaxane molecular shuttles (Figure 1) where, once protonated, the benzylanilinium

Table 2: Summary of major HRESIMS peaks for catenane [**8**⊂**DB24C8**]$^{6+}$.

molecular ion	calculated *m*/z	experimental *m*/z	Δ (ppm)
{[**8**⊂**DB24C8**][OTf]$_4$}$^{2+}$	1116.7969	1116.7972	0.3
{[**8**⊂**DB24C8**][OTf]$_3$}$^{3+}$	694.8804	694.8835	4.5
{[**8**⊂**DB24C8**][OTf]$_2$}$^{4+}$	483.9222	483.9246	5.0
{[**8**⊂**DB24C8**][OTf]}$^{5+}$	357.3472	357.3465	2.0

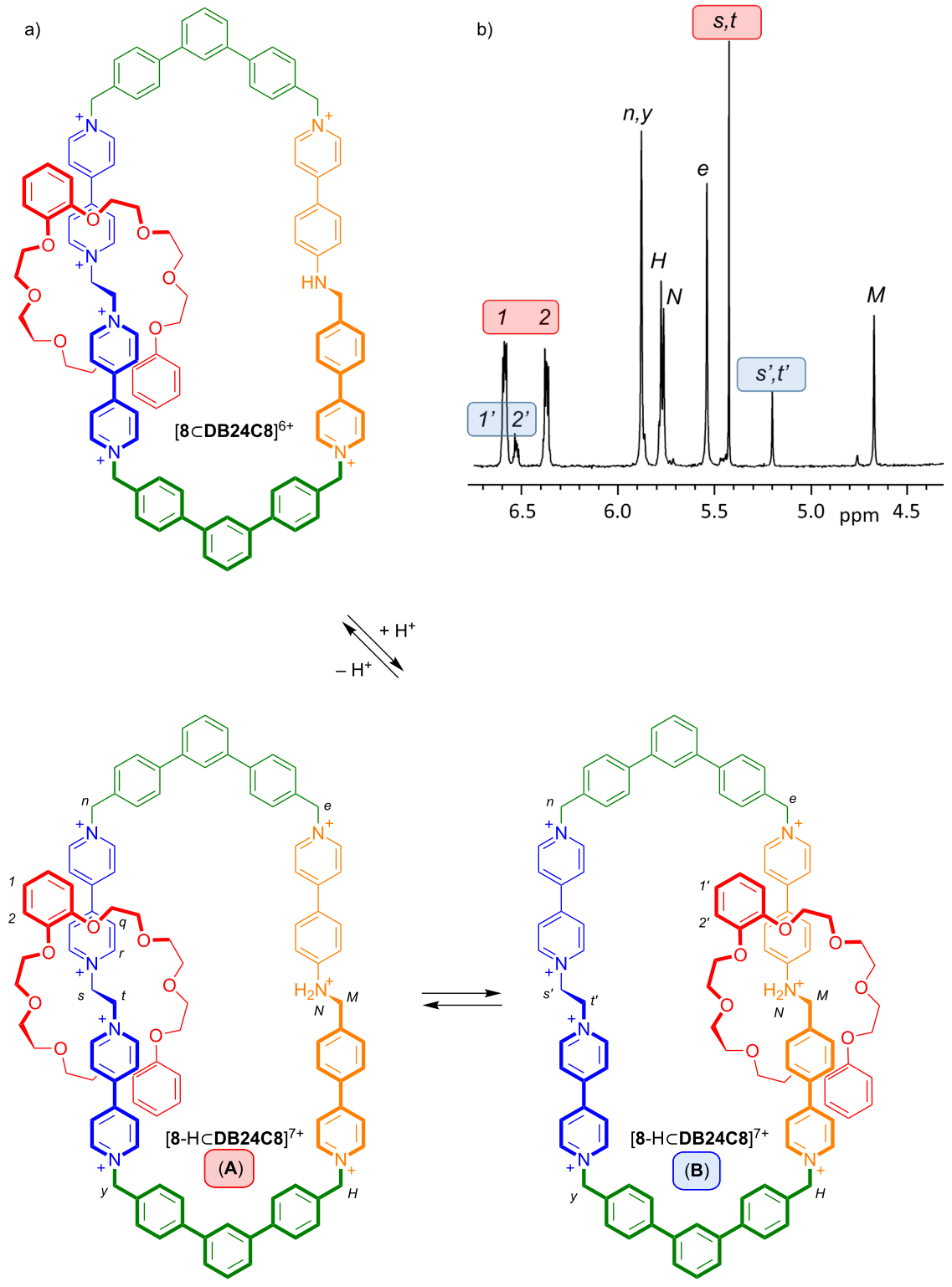

Figure 4: a) The [2]catenane [**8**⊂**DB24C8**]$^{6+}$ can be protonated to yield [**8**-H⊂**DB24C8**]$^{7+}$ in two different co-conformations **A** and **B**. b) The partial ^{1}H NMR spectrum (500 MHz, 298 K, CD_3CN) of [**8**-H⊂**DB24C8**]$^{7+}$ shows key resonances for both co-conformations **A** (red) and **B** (blue). See Scheme 1 for labelling; atoms of co-conformer **B** are labelled with a prime, e.g., *s*' versus *s*.

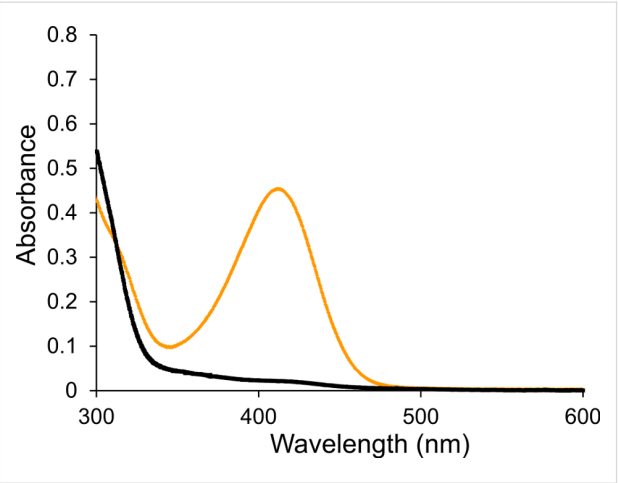

Figure 5: UV–visible spectra of [**8**⊂**DB24C8**]$^{6+}$ (orange trace) and [**8**-H⊂**DB24C8**]$^{7+}$ (black trace) in CH_3CN solution at 2.0 × 10^{-5} M and 298 K.

site was preferred (CD_3CN) and in some cases exclusively (CD_2Cl_2) generating a true ON/OFF bistable switch; unfortunately, the [2]catenane switch is insoluble in CD_2Cl_2 when protonated so a comparison could not be undertaken in this solvent. This difference in site populations between [2]rotaxane and [2]catenane is due to the presence of electron-withdrawing CF_3 groups on the [2]rotaxane which make the benzylanilinium site more favorable in this case. Since it is fairly straightforward to change the nature of the stoppering groups of a [2]rotaxane dumbbell while the cyclic nature of the large ring makes it difficult to derivatize, [2]rotaxanes are deemed easier to fine-tune from a structural perspective than [2]catenanes. Although we were able to create an optically sensitive [2]catenane molecular shuttle with the bis(pyridinium)ethane and benzylanilinium recognition motifs, we could not achieve the true ON/OFF, bistable molecular switching previously observed for analogous [2]rotaxanes.

Experimental

General comments

4-Bromobenzyl bromide, 4-bromoaniline, 4-pyridylboronic acid, 1,3-dichlorobenzene, *p*-tolylmagnesium bromide, *n*-butyllithium and *N*-bromosuccinimide were purchased from Aldrich and used as received. Benzoyl peroxide was purchased from Acros and used as received. Compounds **3** [18], [**5**][OTf]$_2$ [19,20] and **6** [21] were prepared using literature methods. Solvents were dried using an Innovative Technologies solvent purification system. Thin-layer chromatography (TLC) was performed using Teledyne Silica gel 60 F254 plates and viewed under UV light. Column chromatography was performed using Silicycle ultra-pure silica gel (230–400 mesh). The solvents were dried and distilled prior to use. NMR spectra were recorded on a Bruker Avance III console equipped with an 11.7 T magnet (e.g., 500 MHz for ^{1}H). Samples were locked to the deuterated solvent and all chemical shifts reported in ppm referenced to tetramethylsilane. Mass spectra were recorded on a Waters Xevo G2-XS instrument. Solutions with concentrations of 0.001 molar were prepared in methanol and injected for analysis at a rate of 5 µL/min using a syringe pump.

Synthesis of **4**

DMF (250 mL) and H_2O (100 mL) were added to a round bottom Schlenk flask (500 mL) and degassed with N_2 for 2 h. To this solvent mixture, **3** (1.11 g, 0.00325 mol), 4-pyridylboronic acid (1.00 g, 0.00814 mol) and Na_2CO_3 (2.07 g, 0.195 mol) were added and the solution degassed for an additional 1 h. Catalyst [$Pd(PPh_3)_4$] (0.188 g, 16.3 mmol) was added and the solution degassed for an additional 30 min. The reaction was then refluxed for 5 days and the progress of the reaction monitored using ^{1}H NMR spectroscopy. After the 5 days, the reaction was cooled to room temperature and the solvents removed by evaporation. The residue was dissolved in CH_2Cl_2 (100 mL) and washed with H_2O (3 × 50 mL). The CH_2Cl_2 layer was dried over anhydrous $MgSO_4$, filtered and concentrated. Compound **4** precipitated as a pale yellow powder which was collected by vacuum filtration. The filtrate was then evaporated under vacuum and the residue subjected to column chromatography (SiO_2, 1% MeOH/$CHCl_3$, R_f = 0.13) to yield further product. The batches of product (from precipitate and filtrate) were combined and recrystallized from acetone. Yield, 0.800 g, 73%; mp 186–188 °C; ^{1}H NMR (500 MHz, CD_3CN, 298 K) δ 8.60 (d, ^3J = 6.1 Hz, 2H), 8.48 (d, ^3J = 6.1 Hz, 2H), 7.71 (d, ^3J = 8.2 Hz, 2H), 7.59 (d, ^3J = 6.2 Hz, 2H), 7.54 (d, ^3J = 8.7 Hz, 2H), 7.51 (d, ^3J = 8.2 Hz, 2H), 7.49 (d, ^3J = 6.2 Hz, 2H), 6.73 (d, ^3J = 8.7 Hz, 2H), 5.41 (br t, 1H), 4.46 (d, ^3J = 6.2 Hz, 2H); ^{13}C NMR (125 MHz, CD_3CN, 298 K) δ 151.1, 150.3, 149.8, 147.6, 146.8, 140.5, 140.2, 129.9, 128.4, 127.9, 127.6, 120.8, 120.4, 113.1, 47.6; HRMS (ESI) *m*/*z*: [M + H]$^+$ calcd for [$C_{23}H_{20}N_3$]$^+$, 338.1657; found, 338.1650.

Synthesis of [**7**][OTf]$_4$

[**5**][OTf]$_2$ (0.400 g, 0.626 mmol) and **6** (2.61 g, 6.26 mmol) were dissolved in CH_3CN (75 mL) and stirred at room temperature for 7 days. The resulting precipitate was filtered, collected and stirred in CH_2Cl_2 for 20 min and filtered to remove excess **6**. The precipitate was then anion exchanged to the triflate salt in a two-layer CH_3NO_2/NaOTf(aq) solution. The layers were separated and the CH_3NO_2 layer washed with H_2O (3 × 5 mL) and then dried over anhydrous $MgSO_4$. The CH_3NO_2 was removed by rotary evaporation and [**7**][OTf]$_4$ isolated as a pale yellow solid. Yield 0.700 g, 69%; mp >180 °C (dec.); ^{1}H NMR (500 MHz, CD_3CN, 298 K) δ 9.05 (d, ^3J = 6.9 Hz, 4H), 9.04 (d, ^3J = 6.9 Hz, 4H), 8.50 (d, ^3J = 6.1 Hz, 4H), 8.47 (d, ^3J = 6.1 Hz, 4H), 7.91 (s, 2H), 7.86 (d, ^3J = 8.2 Hz, 4H), 7.71 (d,

^3J = 8.2 Hz, 4H), 7.68 (d, ^3J = 7.9 Hz, 2H), 7.67 (d, ^3J = 8.2 Hz, 4H), 7.62 (d, ^3J = 8.0 Hz, 4H), 7.57 (t, ^3J = 7.9, ^3J = 8.1 Hz, 2H), 7.54 (d, ^3J = 8.2 Hz, 4H), 5.89 (s, 4H), 5.30 (br s, 4H), 4.66 (s, 4H); HRMS (ESI) *m/z*: $[M - OTf]^+$ calcd, 1457.1114; found, 1457.1144.

Synthesis of [**8**⊂**DB24C8**][OTf]$_6$

[**7**][OTf]$_4$ (0.155 g, 0.0963 mmol) and **DB24C8** (0.432 g, 0.963 mmol) were dissolved in a two phase CH_3NO_2/H_2O mixture and stirred at room temperature for 30 min to allow [2]pseudorotaxane formation. Compound **4** (0.0330 g, 0.0963 mmol) was then added along with NaOTf (0.0330 g, 0.193 mmol) and the reaction stirred at room temperature for 21 days. The water layer was separated and the CH_3NO_2 evaporated. The resulting residue was washed with CH_2Cl_2 (3 × 10 mL) to remove excess **DB24C8** and subjected to column chromatography on silica gel (5:3:2 mixture of CH_3OH/NH_4Cl (2 M)/CH_3NO_2). Fractions containing the product (R_f = 0.66) were combined and the solvents evaporated. The residue was dissolved in a two layer CH_3NO_2/NaOTf(aq) solution to anion exchange to the triflate salt. The H_2O layer was removed and the CH_3NO_2 layer washed with H_2O (3 × 5 mL) to extract any remaining salts. The CH_3NO_2 layer was dried with anhydrous $MgSO_4$ and then evaporated to yield [**8**⊂**DB24C8**][OTf]$_6$ as a yellow-orange solid. Yield 0.030 g, 12%; mp >210 °C (dec.); HRMS (ESI) *m/z*: $[M - 2OTf]^{2+}$ calcd for $[C_{113}H_{103}F_{12}N_7O_{20}S_4]^{2+}$, 1116.7969, found, 1116.7972; $[M - 3OTf]^{3+}$ calcd for $[C_{112}H_{103}F_9N_7O_{17}S_3]^{3+}$, 694.8804, found, 694.8835; $[M - 4OTf]^{4+}$ calcd for $[C_{111}H_{103}F_6N_7O_{14}S_2]^{4+}$, 483.9222, found, 483.9246; $[M - 5OTf]^{5+}$ calcd for $[C_{110}H_{103}F_3N_7O_{11}S]^{5+}$, 357.3472, found, 357.3465; ^{1}H NMR (500 MHz, CD_2Cl_2, 298 K) δ 9.31 (d, $^3J_{rq}$ = 6.7 Hz, 2H, *r*), 9.31 (d, $^3J_{uv}$ = 6.7 Hz, 2H, *u*), 9.03 (d, $^3J_{op}$ = 6.8 Hz, 2H, *o*), 9.03 (d, $^3J_{xw}$ = 6.8 Hz, 2H, *x*), 8.76 (d, $^3J_{IJ}$ = 6.8 Hz, 2H, *I*), 8.49 (d, $^3J_{dc}$ = 6.9 Hz, 2H, *d*), 8.22 (d, $^3J_{qr}$ = 6.7 Hz, 2H, *q*), 8.22 (d, $^3J_{vu}$ = 6.7 Hz, 2H, *v*), 8.22 (d, $^3J_{JI}$ = 6.8 Hz, 2H, *J*), 8.19 (d, $^3J_{po}$ = 6.8 Hz, 2H, *p*), 8.19 (d, $^3J_{wx}$ = 6.8 Hz, 2H, *w*), 8.04 (d, $^3J_{cd}$ = 6.9 Hz, 2H, *c*), 7.87 (d, $^3J_{lm}$ = 8.2 Hz, 2H, *l*), 7.87 (d, $^3J_{Az}$ = 8.2 Hz, 2H, *A*), 7.87 (d, $^3J_{KL}$ = 8.2 Hz, 2H, *K*), 7.83 (s, 1H, *k*), 7.83 (s, 1H, *E*), 7.80 (d, $^3J_{gf}$ = 8.4 Hz, 2H, *g*), 7.78 (d, $^3J_{ba}$ = 8.7 Hz, 2H, *b*), 7.77 (d, $^3J_{FG}$ = 8.6 Hz, 2H, *F*), 7.74–7.70 (d, 1H, *h*), 7.74–7.70 (d, 1H, *j*), 7.74–7.70 (d, 1H, *B*), 7.74–7.70 (d, 1H, *D*), 7.64 (d, $^3J_{ml}$ = 8.2 Hz, 2H, *m*), 7.64 (d, $^3J_{zA}$ = 8.2 Hz, 2H, *z*), 7.62 (dd, 1H, *i*), 97.62 (dd, 1H, *C*), 7.58 (d, $^3J_{LK}$ = 8.2 Hz, 2H, *L*), 7.55 (d, $^3J_{GF}$ = 8.6 Hz, 2H, *G*), 7.51 (d, $^3J_{fg}$ = 8.4 Hz, 2H, *f*), 6.79 (d, $^3J_{ab}$ = 8.7 Hz, 2H, *a*), 6.62 (m, $^3J_{ortho}$ = 5.8, $^3J_{meta}$ = 3.6 Hz, 4H, *1*), 6.33 (m, $^3J_{ortho}$ = 5.8, $^3J_{meta}$ = 3.6 Hz, 4H, *2*), 5.90 (s, 2H, *n*), 5.90 (s, 2H, *y*), 5.87 (t, $^3J_{NM}$ = 5.6 Hz, 1H, *N*), 5.74 (d, 2H, *H*), 5.59 (s, 2H, *e*), 5.56 (s, 2H, *s*), 5.56 (s, 2H, *t*), 4.48 (d, $^3J_{MN}$ = 5.6 Hz, 2H, *M*), 4.04–3.99 (m, 24H, *3–5*).

Acknowledgements

The authors thank NSERC of Canada for funding; SJL for a Discovery grant and SJV for a post graduate scholarship. The authors acknowledge that the majority of this material was sourced from Vella, S. J. *New Interlocked Molecular Machines*. Ph.D. Thesis, University of Windsor, Windsor, ON, Canada, 2006.

ORCID® iDs

Stephen J. Loeb - https://orcid.org/0000-0002-8454-6443

References

1. Bruns, C. J.; Stoddart, J. F. *The Nature of the Mechanical Bond;* John Wiley & Sons: Hoboken, New Jersey, 2017.
2. Stoddart, J. F. *Angew. Chem., Int. Ed.* **2017,** *56,* 11094–11125. doi:10.1002/anie.201703216
3. Anelli, P. L.; Spencer, N.; Stoddart, J. F. *J. Am. Chem. Soc.* **1991,** *113,* 5131–5133. doi:10.1021/ja00013a096
4. Zhu, K.; Vukotic, V. N.; Loeb, S. J. *Angew. Chem., Int. Ed.* **2012,** *51,* 2168–2172. doi:10.1002/anie.201108488
5. Vukotic, V. N.; Zhu, K.; Baggi, G.; Loeb, S. J. *Angew. Chem., Int. Ed.* **2017,** *56,* 6136–6141. doi:10.1002/anie.201612549
6. Bruns, C. J.; Stoddart, J. F. *Acc. Chem. Res.* **2014,** *47,* 2186–2199. doi:10.1021/ar500138u
7. Badjić, J. D.; Balzani, V.; Credi, A.; Silvi, S.; Stoddart, J. F. *Science* **2004,** *303,* 1845–1849. doi:10.1126/science.1094791
8. Thordarson, P.; Bijsterveld, E. J. A.; Rowan, A. E.; Nolte, R. J. M. *Nature* **2003,** *424,* 915–918. doi:10.1038/nature01925
9. Xue, M.; Yang, Y.; Chi, X.; Yan, X.; Huang, F. *Chem. Rev.* **2015,** *115,* 7398–7501. doi:10.1021/cr5005869
10. Ragazzon, G.; Baroncini, M.; Silvi, S.; Venturi, M.; Credi, A. *Nat. Nanotechnol.* **2015,** *10,* 70–75. doi:10.1038/nnano.2014.260
11. Berná, J.; Leigh, D. A.; Lubomska, M.; Mendoza, S. M.; Pérez, E. M.; Rudolf, P.; Teobaldi, G.; Zerbetto, F. *Nat. Mater.* **2005,** *4,* 704–710. doi:10.1038/nmat1455
12. Collier, C. P.; Mattersteig, G.; Wong, E. W.; Luo, Y.; Beverly, K.; Sampaio, J.; Raymo, F. M.; Stoddart, J. F.; Heath, J. R. *Science* **2000,** *289,* 1172–1175. doi:10.1126/science.289.5482.1172
13. Fahrenbach, A. C.; Warren, S. C.; Incorvati, J. T.; Avestro, A.-J.; Barnes, J. C.; Stoddart, J. F.; Grzybowski, B. A. *Adv. Mater.* **2013,** *25,* 331–348. doi:10.1002/adma.201201912
14. Feringa, B. L. *Angew. Chem., Int. Ed.* **2017,** *56,* 11060–11078. doi:10.1002/anie.201702979
15. Cheng, C.; McGonigal, P. R.; Schneebeli, S. T.; Li, H.; Vermeulen, N. A.; Ke, C.; Stoddart, J. F. *Nat. Nanotechnol.* **2015,** *10,* 547–553. doi:10.1038/nnano.2015.96
16. Vella, S. J.; Tiburcio, J.; Loeb, S. J. *Chem. Commun.* **2007,** 4752–4754. doi:10.1039/b710708k
17. Hubbard, A. L.; Davidson, G. J. E.; Patel, R. H.; Wisner, J. A.; Loeb, S. J. *Chem. Commun.* **2004,** 138–139. doi:10.1039/B312449E
18. Hart, H.; Rajakumar, P. *Tetrahedron* **1995,** *51,* 1313–1336. doi:10.1016/0040-4020(94)01016-S
19. Loeb, S. J.; Tiburcio, J.; Vella, S. J.; Wisner, J. A. *Org. Biomol. Chem.* **2006,** *4,* 667–680. doi:10.1039/b514528g
20. Attalla, M. I.; McAlpine, N. S.; Summers, L. A. *Z. Naturforsch.* **1984,** *39b,* 74–78. doi:10.1515/znb-1984-0113
21. Pan, J.; Han, X.; Sun, N.; Wu, H.; Lin, D.; Tien, P.; Zhou, H.-B.; Wu, S. *RSC Adv.* **2015,** *5,* 55100–55108. doi:10.1039/C5RA07286G

BEILSTEIN JOURNAL OF ORGANIC CHEMISTRY

An amphiphilic *pseudo*[1]catenane: neutral guest-induced clouding point change

Tomoki Ogoshi*[1,2], Tomohiro Akutsu[1] and Tada-aki Yamagishi[1]

Full Research Paper

Open Access

Address:
[1]Graduate School of Natural Science and Technology, Kanazawa University, Kakuma-machi, Kanazawa 920-1192, Japan and [2]WPI Nano Life Science Institute, Kanazawa University, Kakuma-machi, Kanazawa 920-1192, Japan

Email:
Tomoki Ogoshi* - ogoshi@se.kanazawa-u.ac.jp

* Corresponding author

Keywords:
amphiphilic molecules; host–guest complexes; lower critical solution temperature; pillar[*n*]arenes; *pseudo*[1]catenane

Beilstein J. Org. Chem. **2018,** *14,* 1937–1943.
doi:10.3762/bjoc.14.167

Received: 20 April 2018
Accepted: 27 June 2018
Published: 26 July 2018

This article is part of the thematic issue "Macrocyclic and supramolecular chemistry".

Guest Editor: M.-X. Wang

Abstract

The hydrophobic/hydrophilic ratio in a molecule largely affects its assembled properties in aqueous media. In this study, we synthesized a new bicyclic compound which could dynamically change its hydrophobic/hydrophilic ratio by chemical stimulus. The bicyclic compound consisted of amphiphilic pillar[5]arene and hydrophobic alkyl chain rings, and formed a self-inclusion structure in aqueous media, which was assigned as a *pseudo*[1]catenane structure. The hydrophobic chain ring was hidden inside the pillar[5]arene cavity in the *pseudo*[1]catenane structure, thus the bicyclic compound was soluble in water at 20 °C with a clouding point at 24 °C. The *pseudo*[1]catenane was converted to the de-threaded structure upon addition of the neutral guest 1,4-dicyanobutane, which displaced the alkyl chain ring from the inside to the outside of the cavity. The hydrophobic alkyl chain ring was now exposed to the aqueous media, causing aggregation of the hydrophobic alkyl chain rings, which induced insolubilization of the bicyclic compound in aqueous media at 20 °C and a decrease in its clouding point.

Introduction

Thermo-responsive molecules exhibiting a lower critical solution temperature (LCST) are very important for applications such as controlled drug release [1], molecular separation [2], and tissue culture substrates [3]. Poly(*N*-isopropylacrylamide) (pNIPAAm) is a widely used thermo-responsive polymer, which exhibits a clouding point around 32 °C [1-4]. Recently, thermo-responsive molecules with additional functions have been developed to replace pNIPAAm [5-10]. For example, we have developed thermo-responsive macrocyclic molecules which exhibit LCST behavior regulated by host–guest chemistry [5-7]. The molecules consist of a non-ionic amphiphilic part containing tri(ethylene oxide) moieties, and a hydrophobic part consisting of a pillar[*n*]arene core (Figure 1a; **1**, $n = 5$; **2**, $n = 6$).

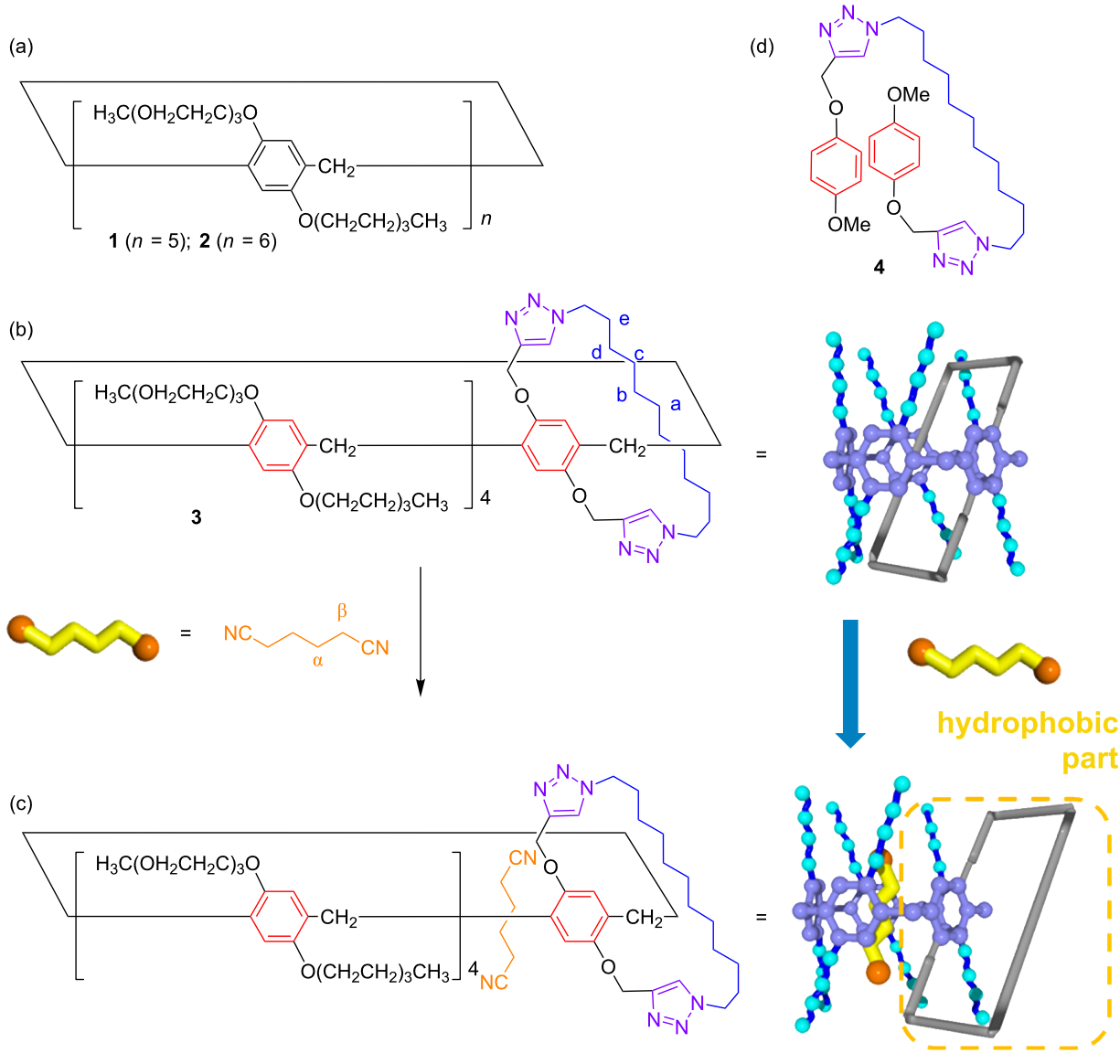

Figure 1: Chemical structures of (a) tri(ethylene oxide)-substituted pillar[*n*]arenes (**1**, *n* = 5; **2**, *n* = 6), (b) *pseudo*[1]catenane **3**, (c) de-threaded form of **3** by complexation with 1,4-dicyanobutane, and (d) model compound **4**.

Pillar[*n*]arenes, which were first reported by our group [11], were used as the macrocyclic component because of their high functionality and superior host–guest properties with neutral guests [12-16]. The amphiphilic pillar[*n*]arenes **1** and **2** exhibit clouding points at 41 and 42 °C, respectively [5,6]. The oligo(ethylene oxide) moieties are solvated with water molecules at room temperature, but de-solvation occurs upon heating, which triggers aggregation of the hydrophobic pillar[*n*]arene cores. The amphiphilic pillar[*n*]arenes can capture guest molecules with encapsulation of an ionic guest molecule resulting in a change of the hydrophobic/hydrophilic ratio, and consequently a change in the clouding point. The clouding point of **1** increased upon addition of a cationic guest as the hydrophilic ratio in the molecule increased by formation of the complex with the hydrophilic cationic guest [5]. We also demonstrated photoresponsive LCST behavior by using a photoresponsive host–guest complex system between amphiphilic pillar[6]arene **2** and a photoresponsive cationic azobenzene guest [6]. However, neutral guest molecules could not induce a clear LCST change because encapsulation of the neutral guest in the hydrophobic pillar[*n*]arene core did not significantly change the hydrophobic/hydrophilic ratio. In this study, we successfully induced an LCST change using a neutral guest and a new pillar[5]arene derivative. We synthesized a new bicyclic compound consisting of an amphiphilic pillar[5]arene and hydrophobic alkyl chain rings **3** (Figure 1b). This bicyclic com-

pound formed a self-inclusion structure in aqueous media, which was assigned as a *pseudo*[1]catenane structure. The hydrophobic alkyl chain ring was hidden in the pillar[5]arene cavity in the *pseudo*[1]catenane structure, thus **3** was soluble in water at 20 °C and exhibited a clouding point at 24 °C. However, a de-threaded structure formed upon addition of a neutral guest, 1,4-dicyanobutane. The supramolecular structural change contributed to a significant increase in the hydrophobic ratio of the molecule, which induced insolubilization of **3** in aqueous media at 20 °C and a decrease of the clouding point temperature. Neutral guest-responsive LCST changes are very rare, while there have been some examples of LCST control using ionic chemical stimuli [5,6].

Results and Discussion

Supramolecular structure and clouding point of bicyclic compound 3

The bicyclic compound **3** was prepared using a copper(I)-catalyzed alkyne–azide cycloaddition (CuAAC) ''click'' reaction (see details in the experimental section). In addition, model compound **4** was also synthesized as a reference (Figure 1d). Compound **3** is soluble in various organic and aqueous solvents as it comprises eight amphiphilic tri(ethylene oxide) chains. We investigated the supramolecular structure of **3** by ^{1}H NMR spectroscopy. In $CDCl_3$, the signals from the alkyl chain of **3** (blue peaks, a–e, Figure 2) were observed upfield compared with the ones of the model compound **4** (Figure 2a). This is due to an aromatic shielding by the pillar[5]arene cavity, indicating that **3** mainly formed a *pseudo*[1]catenane structure in $CDCl_3$. The linear alkyl chains can act as guests for pillar[5]arenes, thus the *pseudo*[1]catenane structure was stable in $CDCl_3$ [17-19]. In D_2O, as in $CDCl_3$, the proton signals from the alkyl chain ring (blue peaks, a–e) were also observed upfield (Figure 2c), indicating the formation of a *pseudo*[2]catenane structure in D_2O. The alkyl chain ring not only acts as a good guest for the pillar[5]arene, but also as a hydrophobic portion, thus the *pseudo*[2]catenane structure would be favored in D_2O.

As for pillar[5]arene **1** with 10 tri(ethylene oxide) chains, compound **3** also exhibits LCST behavior. Compound **3** is soluble in aqueous media at 20 °C, the solution becomes turbid at 40 °C, and turns back to a clear solution upon cooling. The clouding point of **3** was determined by monitoring the transmittance change (Figure 3). The clouding point of **3**, determined by monitoring the transmittance change, was 24 °C (2 mM in aqueous solution, Figure 3a, black line) which is 18 °C lower than the clouding point of **1** (42 °C, Figure 3b, black line) [5]. This is due to the fact that the benzene units carrying the hydrophobic alkyl chain ring in **3** are more hydrophobic than the tri(ethylene oxide)-substituted benzene unit in **1**, although the hydrophobic alkyl chain ring was hidden inside the cavity by formation of the *pseudo*[1]catenane structure in aqueous media.

Effect of a supramolecular structural change on the clouding point

To displace the alkyl chain ring of **3** from the inside to the outside of the cavity, a competitive guest molecule, 1,4-dicyanobutane, was added. 1,4-Dicyanobutane was chosen because it forms highly stable 1:1 host–guest complexes with pillar[5]arenes ($K > 10^4$ M^{-1}) [20]. Figure 2d shows the ^{1}H NMR spectra of **3** in the presence of 1,4-dicyanobutane. In the spectrum, additional peaks were observed upon the addition

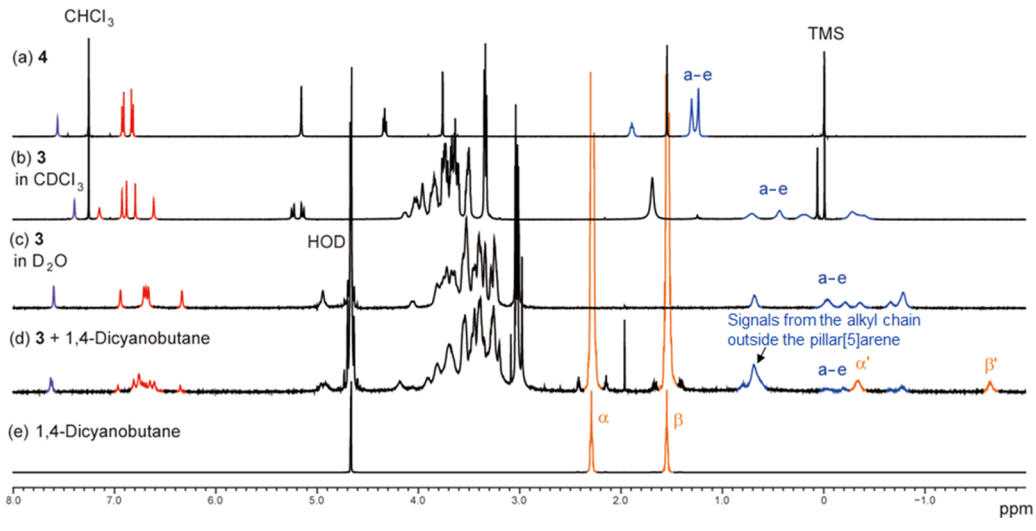

Figure 2: ^{1}H NMR spectra of (a) model compound **4** (2 mM at 25 °C in $CDCl_3$), (b) **3** (2 mM at 25 °C in $CDCl_3$), (c) **3** (2 mM at 10 °C in D_2O), (d) **3** (2 mM) and 1,4-dicyanobutane (20 mM) at 10 °C in D_2O and (e) 1,4-dicyanobutane (20 mM at 10 °C in D_2O). Resonances are labeled as shown in Figure 1.

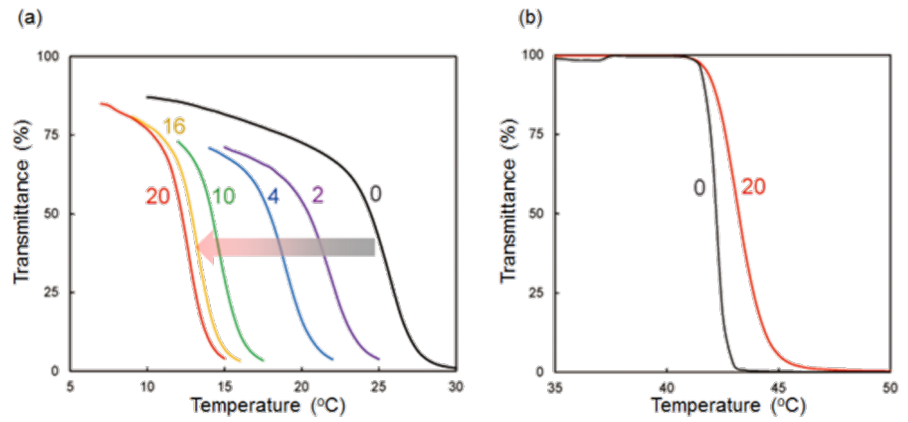

Figure 3: Temperature dependence of light transmittance at 650 nm of an aqueous solution of (a) **3** (2 mM) upon addition of 1,4-dicyanobutane (0–20 mM) and (b) **1** (2 mM) in the presence and absence of 1,4-dicyanobutane (20 mM) on heating.

of 1,4-dicyanobutane (orange peaks α' and β') in Figure 2d. For comparison Figure 2e shows the spectrum of 1,4-dycanaobutane (orange peaks α and β). Similar signals were also observed in the host–guest complexes of 1,4-dicyanobutane with other pillar[5]arenes [17,20], and were assigned as the proton signals from the methylene protons of the 1,4-dicyanobutane in the cavity of pillar[5]arene **3**. The complex formation of **3** and 1,4-dicyanobutane indicates the displacement of the alkyl chain ring from the inside to the outside of the cavity by 1,4-dicyanobutane. The association constant between the *pseudo*[1]catenane structure **3** and 1,4-dicyanobutane estimated by ^{1}H NMR at 25 °C was 13.9 M^{-1} (Supporting Information File 1, Figure S6), which is remarkably lower than the association constant between **1** and 1,4-dicyanobutane (4.6×10^4 M^{-1}, Figure S8 in Supporting Information File 1). The *pseudo*[1]catenane structure is very stable, thus the alkyl chain ring acts as a competitive guest to 1,4-dicyanobutane.

The effect of the supramolecular structural change from the *pseudo*[1]catenane to the de-threaded structure on the clouding point change was investigated next. Even at a low concentration of the competitive guest 1,4-dicyanobutane (2 mM), the clouding point clearly decreased, indicating de-threading of the hydrophobic alkyl chain extremely contributed to the change in the hydrophobic/hydrophilic ratio. With increasing concentrations of 1,4-dicyanobutane, the clouding points gradually decreased from 24 °C to 12 °C (Figure 3a). Formation of the de-threaded form by complexation between **3** and 1,4-dicyanobutane induced aggregation of the alkyl chain ring on the outside of the cavity. However, only a very minor change in the clouding point was observed upon addition of 1,4-dicyanobutane to an aqueous solution of **1** (Figure 3b, indicating that the hydrophobic/hydrophilic ratio did not change much by the host–guest complexation between **1** and 1,4-dicyanobutane because 1,4-dicyanobutane was hidden inside the hydrophilic pillar[5]arene cavity. Therefore, the supramolecular structural change of **3** induced a dramatic change in its hydrophobic/hydrophilic ratio, and consequently the clouding point change. Based on the supramolecular structural change, the neutral guest, 1,4-dicyanobutane can be used for changing the clouding point of **3**.

We then demonstrated a chemically responsive transmittance change using the supramolecular structural change. An aqueous solution containing **3** at 20 °C was clear (Figure 4a) as the clouding point of the self-inclusion structure **3** is 24 °C. Upon addition of the neutral guest 1,4-dicyanobutane, the solution changed from clear to turbid (Figure 4c) as the clouding point of the complex is 12 °C.

The details of this neutral guest-responsive LCST change are summarized in Figure 4. Compound **3** formed a *pseudo*[1]catenane structure in aqueous media (Figure 4a), with the water-insoluble hydrophobic part of the alkyl chain ring hidden inside the hydrophilic pillar[5]arene cavity, meaning that **3** was soluble in water. The clear solution of **3** became turbid upon addition of the competitive neutral guest 1,4-dicyanobutane. The competitive guest displaced the hydrophobic alkyl chain ring from the inside to the outside of the cavity (Figure 4b), causing aggregation of the hydrophobic alkyl chain ring by hydrophobic interactions (Figure 4c).

Conclusion

We have successfully prepared a new amphiphilic bicyclic compound **3**. A key feature of the molecule is that the hydrophobic part of the alkyl chain ring is hidden by formation of a *pseudo*[1]catenane structure. The movement of the alkyl chain ring from the inside to the outside of the cavity upon the addi-

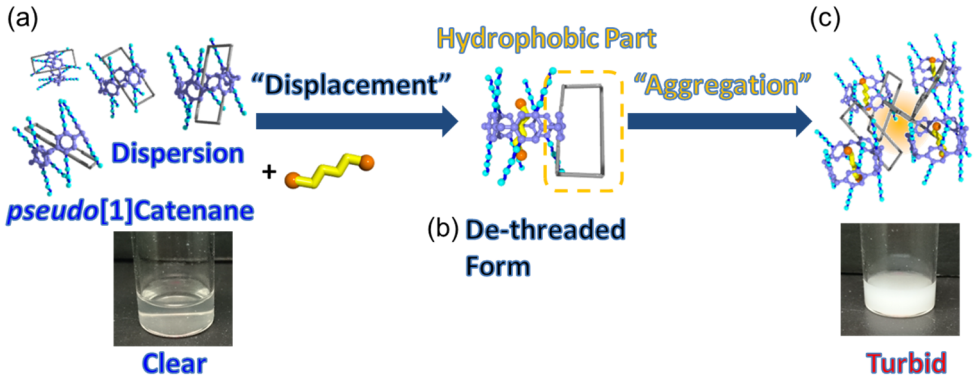

Figure 4: Photographs of (a) **3** and (c) a mixture of **3** (2 mM) and 1,4-dicyanobutane (20 mM) in aqueous media at 20 °C and schematic representation of neutral-guest responsive clouding point change using supramolecular structural change from *pseudo*[1]catenane to de-threaded form upon (b) addition of a competitive guest, 1,4-dicyanobutane.

tion of the competitive guest molecule dramatically contributed to the clouding point change. A neutral guest molecule, 1,4-dicyanobutane, was able to induce a change in the clouding point via a supramolecular structural change from a *pseudo*[1]catenane to the de-threaded form. Bicyclic structures have previously been used to induce color changes by adding guests, and are also referred to as "molecular chameleons" and "catenane-chameleons" [21,22]. However, to the best of our knowledge, the use of a dynamic supramolecular structural change of **3** to induce an LCST change is the first example in this area. Thus, this work may open the way for the design of a new generation of molecular assembly systems using supramolecular structures such as rotaxane, catenanes, polyrotaxanes and polycatenanes.

Experimental

Materials. All solvents and reagents were used as supplied. Compounds **1** and **4** were synthesized according to previous reported procedures [5,17].

Measurements. The ^{1}H NMR spectra were recorded at 500 MHz and ^{13}C NMR spectra were recorded at 125 MHz with a JEOL-ECA500 spectrometer. UV–vis absorption spectra were recorded with a JASCO V-670 using 1 cm quartz cuvettes. Cloud points were determined by transmission changes (at 650 nm) of the solutions heated at 0.1 °C/min; cloud point values were defined as the temperature at which the transmission decreases by 50% [23].

Pillar[5]arene carrying 2 alkyne groups on the same unit (5). In a similar manner as described in [24], **5** was prepared. Under a nitrogen atmosphere, pillar[5]arene carrying one hydroquinone unit **6** [7] (Scheme 1, 417 mg, 0.230 mmol) was dissolved in acetone (10 mL). K_2CO_3 (159 mg, 1.15 mmol) was added and the reaction mixture was stirred. Then, propargyl bromide (2.30 g, 2.30 mmol) was added and the reaction mixture was heated at 80 °C for 24 h. The reaction mixture was cooled to room temperature and the precipitate was removed by filtration. After the filtration, the solvents were evaporated to afford a solid. Column chromatography (silica gel; methanol/ethyl acetate 1:9) afforded **5** as a solid (298 mg, 0.161 mmol, yield: 70%). ^{1}H NMR (500 MHz, $CDCl_3$) δ 6.88, 6.84, 6.83, 6.81, 6.78 (s, 10H, phenyl), 4.53 (d, 4H, methylene), 4.00, 3.42–3.83 (m, 106H, methylene), 3.27–3.39 (m, 24H, methyl), 2.27 (t, 2H, alkyne) ppm; ^{13}C NMR (125 MHz, $CDCl_3$) δ 150.0, 149.8, 149.3, 129.1, 129.0, 128.6, 128.4, 115.6, 115.4, 115.2, 115.1, 71.9, 70.9, 70.8, 70.6, 70.4, 70.3, 68.3, 68.2, 68.1, 68.0, 59.0, 56.5, 29.7, 29.3 ppm; HRMS–ESI (*m*/*z*): $[M + Na]^+$ calcd for $C_{97}H_{146}NaO_{34}$, 1877.9593; found, 1877.9612.

Bicyclic compound 3. In a similar manner as described in [17], we synthesized bicyclic compound **3**. Tris[(1-benzyl-1*H*-1,2,3-triazol-4-yl)methyl]amine (31.8 mg, 60.0 μmol) and $[Cu(CH_3CN)_4]PF_6$ (22.3 mg, 60.0 μmol) were added to a solution containing **5** (111 mg, 60.0 μmol) and 1,12-diazidododecane (15.1 mg, 60.0 μmol) in dichloromethane (300 mL), and the mixture was stirred at 25 °C for 12 h. The resulting solution was concentrated in vacuo. Column chromatography (silica gel, ethyl acetate/methanol 1:1) afforded the bicyclic compound **3** (12.6 mg, 6.00 μmol, yield: 10%).^{1}H NMR (500 MHz, $CDCl_3$) δ 7.40 (s, 2H, triazole), 7.15 (s, 2H, phenyl), 6.93 (s, 2H, phenyl), 6.89 (s, 2H, phenyl), 6.80 (s, 2H, phenyl), 6.62 (s, 2H, phenyl), 5.21 (dd, 4H, methylene), 3.50–4.14 (m, 110H, methylene), 3.34–3.36 (m, 24H, methyl), −0.27–0.72 (br, 20H, methylene of alkyl chain) ppm; ^{13}C NMR (125 MHz, $CDCl_3$) δ 150.4, 149.8, 149.7, 149.6, 149.4 129.0, 128.6, 128.3, 124.3, 115.7, 115.0, 71.9, 70.8, 70.7, 70.6, 70.3, 68.4, 68.1, 67.8, 67.6, 59.0, 29.7, 29.0, 28.8, 28.5, 27.3, 24.5 ppm; HRMS–ESI (*m*/*z*): $[M + 2Na]^{2+}$ calcd for $C_{109}H_{170}N_6Na_2O_{34}$, 1076.5777; found, 1076.5635.

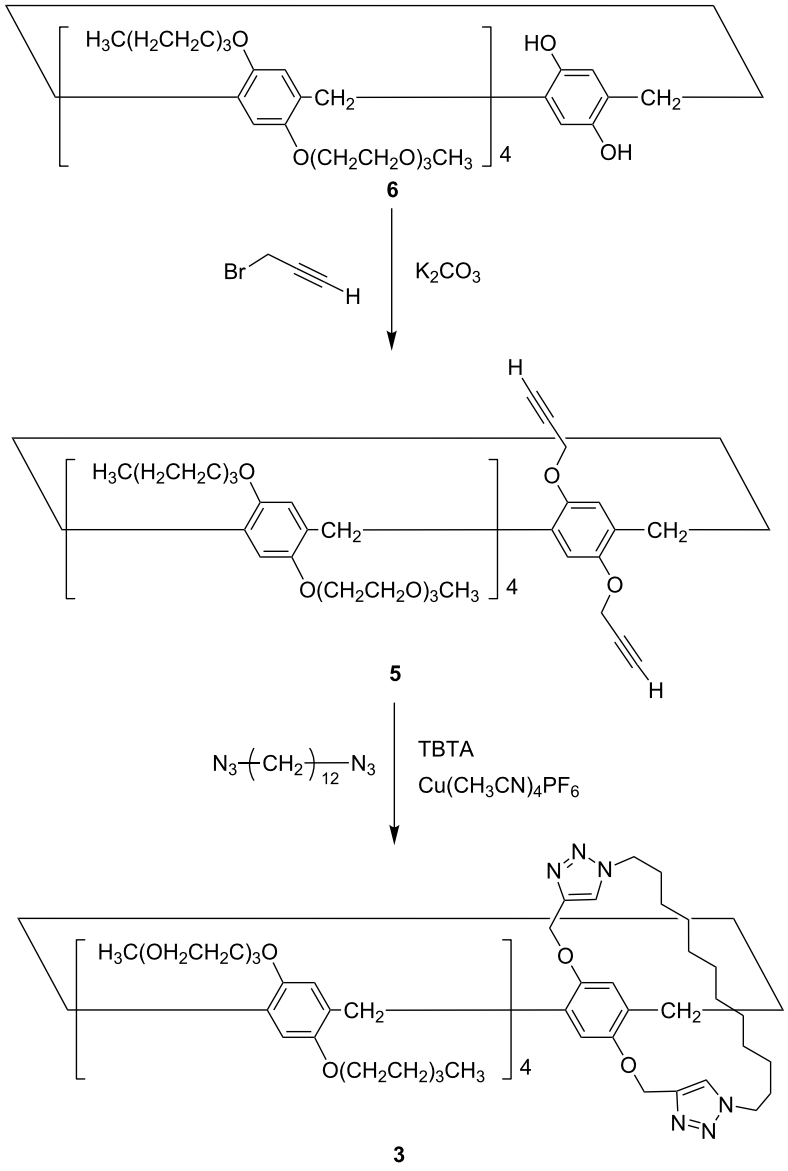

Scheme 1: Synthesis of the bicyclic compound **3**.

Determination of association constants. In a similar manner as described in [6], association constants of the host–guest complexes were determined. In the host–guest complex of 1,4-dicyanobutane with **3** in D_2O, the chemical exchange between the complexed and uncomplexed species was slow on the NMR timescale. Thus, the ^{1}H NMR spectra of mixtures of **3** with 1,4-dicyanobutane showed two sets of resonances for complexed (Figure 2d, peaks α' and β') and uncomplexed 1,4-dicyanobutane (peaks, α and β). The association constant for the host–guest complexes between 1,4-dicyanobutane and **3** at 10 °C was 24.5 M^{-1}, which was calculated from integrations of the complexed (Supporting Information File 1, Figure S5, orange peak β') and uncomplexed signals (Supporting Information File 1, Figure S5, orange peak β) of 1,4-dicyanobutane. The association constant of the complex at 25 °C extrapolated by van 't Hoff plots (Figure S6 in the Supporting Information File 1) was 13.9 M^{-1}.

In the host–guest complex of 1,4-dicyanobutane with **1** in D_2O, chemical exchange between the complexed and uncomplexed species was also slow on the NMR timescale. Thus, ^{1}H NMR spectra of mixtures of **1** with 1,4-dicyanobutane showed two sets of resonances for complexed (Figure 2d, peaks α' and β') and uncomplexed 1,4-dicyanobutane (peaks, α and β). The association constant for the host–guest complex of 1,4-dicyanobutane and **1** at 25 °C was 4.7 × 10^4 M^{-1}, which was calculated

from the integrations of the complexed (Supporting Information File 1, Figure S7, orange peak β') and uncomplexed signals (Supporting Information File, Figure S7, orange peak β) of 1,4-dicyanobutane.

Supporting Information

Supporting Information File 1

^{1}H and ^{13}C NMR spectra of **3** and **5**, variable temperature ^{1}H NMR spectra of a mixture of **3** and **5** with 1,4-dicyanobutane and van 't Hoff plots.
[https://www.beilstein-journals.org/bjoc/content/supplementary/1860-5397-14-167-S1.pdf]

Acknowledgements

T. O. gratefully appreciates the financial support from JSPS KAKENHI Grant Numbers 15H00990, 15KK0185, 16H04130, 17H05148, 18H04510, JST PRESTO (JPMJPR1313) and Kanazawa University CHOZEN Project. NanoLSI is supported by the World Premier International Research Center (WPI) Initiative, Japan.

ORCID® iDs

Tomoki Ogoshi - https://orcid.org/0000-0002-4464-0347

References

1. Pişkin, E. *Int. J. Pharm.* **2004,** *277,* 105–118. doi:10.1016/j.ijpharm.2003.06.003
2. Feil, H.; Bae, Y. H.; Feijen, J.; Kim, S. W. *J. Membr. Sci.* **1991,** *64,* 283–294. doi:10.1016/0376-7388(91)80099-R
3. Takezawa, T.; Mori, Y.; Yoshizato, K. *Bio/Technology* **1990,** *8,* 854–856. doi:10.1038/nbt0990-854
4. Aseyev, V. O.; Tenhu, H.; Winnik, F. M. Temperature Dependence of the Colloidal Stability of Neutral Amphiphilic Polymers in Water. In *Conformation-Dependent Design of Sequences in Copolymers II;* Khokhlov, A. R., Ed.; Advances in Polymer Science, Vol. 196; Springer: Berlin, Heidelberg, 2006; pp 1–85. doi:10.1007/12_052
5. Ogoshi, T.; Shiga, R.; Yamagishi, T.-a. *J. Am. Chem. Soc.* **2012,** *134,* 4577–4580. doi:10.1021/ja300989n
6. Ogoshi, T.; Kida, K.; Yamagishi, T.-a. *J. Am. Chem. Soc.* **2012,** *134,* 20146–20150. doi:10.1021/ja3091033
7. Ogoshi, T.; Akutsu, T.; Tamura, Y.; Yamagishi, T.-a. *Chem. Commun.* **2015,** *51,* 7184–7186. doi:10.1039/C5CC01630D
8. Dong, S.; Zheng, B.; Yao, Y.; Han, C.; Yuan, J.; Antonietti, M.; Huang, F. *Adv. Mater.* **2013,** *25,* 6864–6867. doi:10.1002/adma.201303652
9. Yu, G.; Zhou, J.; Chi, X. *Macromol. Rapid Commun.* **2015,** *36,* 23–30. doi:10.1002/marc.201400570
10. Chi, X.; Wang, P.; Li, Y.; Ji, X. *Tetrahedron Lett.* **2015,** *56,* 4545–4548. doi:10.1016/j.tetlet.2015.06.005
11. Ogoshi, T.; Kanai, S.; Fujinami, S.; Yamagishi, T.-a.; Nakamoto, Y. *J. Am. Chem. Soc.* **2008,** *130,* 5022–5023. doi:10.1021/ja711260m
12. Ogoshi, T.; Yamagishi, T.-a.; Nakamoto, Y. *Chem. Rev.* **2016,** *116,* 7937–8002. doi:10.1021/acs.chemrev.5b00765
13. Xue, M.; Yang, Y.; Chi, X.; Zhang, Z.; Huang, F. *Acc. Chem. Res.* **2012,** *45,* 1294–1308. doi:10.1021/ar2003418
14. Strutt, N. L.; Zhang, H.; Schneebeli, S. T.; Stoddart, J. F. *Acc. Chem. Res.* **2014,** *47,* 2631–2642. doi:10.1021/ar500177d
15. Li, C. *Chem. Commun.* **2014,** *50,* 12420–12433. doi:10.1039/C4CC03170A
16. Kakuta, T.; Yamagishi, T.; Ogoshi, T. *Chem. Commun.* **2017,** *53,* 5250–5266. doi:10.1039/C7CC01833A
17. Ogoshi, T.; Akutsu, T.; Yamafuji, D.; Aoki, T.; Yamagishi, T.-a. *Angew. Chem., Int. Ed.* **2013,** *52,* 8111–8115. doi:10.1002/anie.201302675
18. Zhang, Z.; Luo, Y.; Chen, J.; Dong, S.; Yu, Y.; Ma, Z.; Huang, F. *Angew. Chem., Int. Ed.* **2011,** *50,* 1397–1401. doi:10.1002/anie.201006693
19. Ogoshi, T.; Demachi, K.; Kitajima, K.; Yamagishi, T.-a. *Chem. Commun.* **2011,** *47,* 10290–10292. doi:10.1039/c1cc14395f
20. Shu, X.; Chen, S.; Li, J.; Chen, Z.; Weng, L.; Jia, X.; Li, C. *Chem. Commun.* **2012,** *48,* 2967–2969. doi:10.1039/c2cc00153e
21. Wolf, R.; Asakawa, M.; Ashton, P. R.; GómezLópez, M.; Hamers, C.; Menzer, S.; Parsons, I. W.; Spencer, N.; Stoddart, J. F.; Tolley, M. S.; Williams, D. J. *Angew. Chem., Int. Ed.* **1998,** *37,* 975–979. doi:10.1002/(SICI)1521-3773(19980420)37:7<975::AID-ANIE975>3.0.CO;2-L
22. Leigh, D. A.; Moody, K.; Smart, J. P.; Watson, K. J.; Slawin, A. M. Z. *Angew. Chem., Int. Ed. Engl.* **1996,** *35,* 306–310. doi:10.1002/anie.199603061
23. Munteanu, M.; Choi, S. W.; Ritter, H. *Macromolecules* **2009,** *42,* 3887–3891. doi:10.1021/ma900397m
24. Ogoshi, T.; Yamafuji, D.; Kotera, D.; Aoki, T.; Fujinami, S.; Yamagishi, T.-a. *J. Org. Chem.* **2012,** *77,* 11146–11152. doi:10.1021/jo302283n

License and Terms

BEILSTEIN JOURNAL OF ORGANIC CHEMISTRY

Synthesis and characterization of π–extended "earring" subporphyrins

Haiyan Guan, Mingbo Zhou, Bangshao Yin, Ling Xu* and Jianxin Song*

Letter

Open Access

Address:
Key Laboratory of Chemical Biology and Traditional Chinese Medicine Research (Ministry of Education of China), Key Laboratory of Application and Assemble of Organic Functional molecules, Hunan Normal University, Changsha 410081, P. R. China

Email:
Ling Xu* - xulingchem@hunnu.edu.cn; Jianxin Song* - jxsong@hunnu.edu.cn

* Corresponding author

Keywords:
aromaticity; earring subporphyrin; π-extended; supramolecular chemistry

Beilstein J. Org. Chem. **2018,** *14,* 1956–1960.
doi:10.3762/bjoc.14.170

Received: 14 April 2018
Accepted: 04 July 2018
Published: 30 July 2018

This article is part of the thematic issue "Macrocyclic and supramolecular chemistry".

Guest Editor: M.-X. Wang

Abstract

A π-extended "earring" subporphyrin **3** was synthesized from β,β′-diiodosubporphyrin and diboryltripyrrane via a Suzuki–Miyaura coupling and following oxidation. Its Pd complex **3Pd** was also synthesized and both of the compounds were fully characterized by ^{1}H NMR, MS and X-ray single crystal diffraction. The ^{1}H NMR spectra and single crystal structures revealed that aromatic ring current did not extend to the "ear" in both of the two compounds. Their UV–vis/NIR spectra were recorded and the absorption of both compounds is extended to the NIR region and that the absorption of **3Pd** is further red-shifted and more intense.

Findings

Since its first synthesis in 2006 [1,2], subporphyrin, the lowest homolog of porphyrins, has received considerable attention [3-8] due to its 14π-electron configuration and bowl-shaped structure. In addition the intense absorption in the UV–vis region [9-24] makes it a promising building block in pigments. The functionalization of subporphyrin can proceed at various sites such as the central boron atom [25-30], *meso*- [31,32] and β-position [33-35]. By using the method developed by Osuka the β,β′-diborylsubporphyrins [36] can be obtained in high yields. A subsequent Suzuki–Miyaura coupling smoothly affords various β-aryl-substituted subporphyrins [37]. Alternatively, some β-aryl/vinyl-substituted subporphyrins can be synthesized from aryl/vinyl borate and the corresponding β,β′-dihalosubporphyrins, which can be obtained by the treatment of β,β′-diborylsubporphyrins with NBS/NIS in the presence of a Cu(I) salt [36].

Recently, our group successfully prepared multiple cavities π-extended "earring" porphyrins through the aforementioned Suzuki–Miyaura coupling reaction and subsequent oxidation

[38]. In this case β,β′-dibromo/tetrabromoporphyrins and diboryltripyrrane were applied as reactants. We discovered that both the π-extended "earring" porphyrins and the corresponding Pd complexes exhibited remarkably near-infrared absorptions.

Based on our previous work, we herein designed a subporphyrin with one "earring". The different geometry and properties could be envisioned due to the bowl-shaped structure and 14π-electron configuration of subporphyrin. To construct the skeleton of the "earring" subporphyrin, we performed a Suzuki–Miyaura coupling reaction between β,β′-diiodosubporphyrin **1** [37] and diboryltripyrrane **2** [38] (Scheme 1). Monitored by TLC, we merely observed a complicated mixture without any major band during the progress of the reaction. However, several clear bands emerged after stirring the mixture overnight at ambient conditions. This observation revealed that the coupling products could be oxidized by air and thereafter the target "earring" subporphyrin **3** was obtained in an isolated yield of 15% after column chromatography.

The mass spectrum of **3** exhibits a parent-ion peak at m/z = 911.4036 (calcd for $C_{64}H_{48}BN_6$ $[M]^+$ = 911.4028), which is in agreement with its structure. The ^{1}H NMR spectrum of **3** (Figure 1) indicates it a symmetric structure. The peak appearing at 17.02 ppm is assigned to the NH since a D_2O exchange experiment lead to its disappearance. While the peak at 15.82 ppm can be assigned to the *meso*-H of the subporphyrin moiety, which is shifted to a lower field region in comparison to 8.60 ppm of 4-tolyl-(5,10-di-(4-tolyl)-subporphyrinato)boron(III) (**1a**). These two signals at 17.02 ppm and 15.82 ppm can be attributed to the antiaromatic character of the ear-containing macrocycle, which is quite similar to the analogous "earring" porphyrin [38]. Furthermore, the antiaromaticity of the ear-containing macrocycle is proved by the large positive NICS value in the hole as well as the anticlockwise ring currency (see Supporting Information File 1 for details).

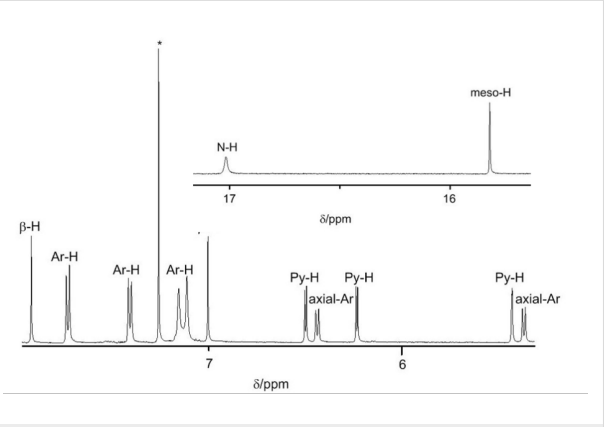

Figure 1: Partial ^{1}H NMR spectrum of **3**.

Although some characteristic peaks in the ^{1}H NMR spectrum of the "earring" subporphyrin are quite similar to those of "earring" porphyrin, there are some differences in their structures. This is mainly due to the fact that the bowl-shaped subporphyrin core differs significantly from the saddle-shaped or nearly planar porphyrin core. To elucidate the differences in their structures, we endeavored to cultivate single crystals of **3** and collected the data. The diffraction data unambiguously confirmed the designated structure (Figure 2) and revealed that all peripheral C–C bonds in the subporphyrin moiety are of similar lengths (1.383(6)–1.447(5) Å). In contrast, the C–C bond lengths in the tripyrrin moiety alternate (1.341(5)–1.472(5) Å). These data clearly indicate that the subporphyrin moiety remains its aromaticity while the tripyrrin moiety participates in an antiaromatic system as shown in Scheme 1. The cavity surrounded by the tripyrrin moiety owns a long axis of 4.229(4) Å and a short axis of 4.201(5) Å, which are almost the same. Despite of this the cavity is not circular because the three N atoms in the tripyrrin moiety and the nearest *meso*-C of the subporphyrin moiety are not ideally coplanar. This feature can be proved by the dihedral angles of two adjacent pyrrole units

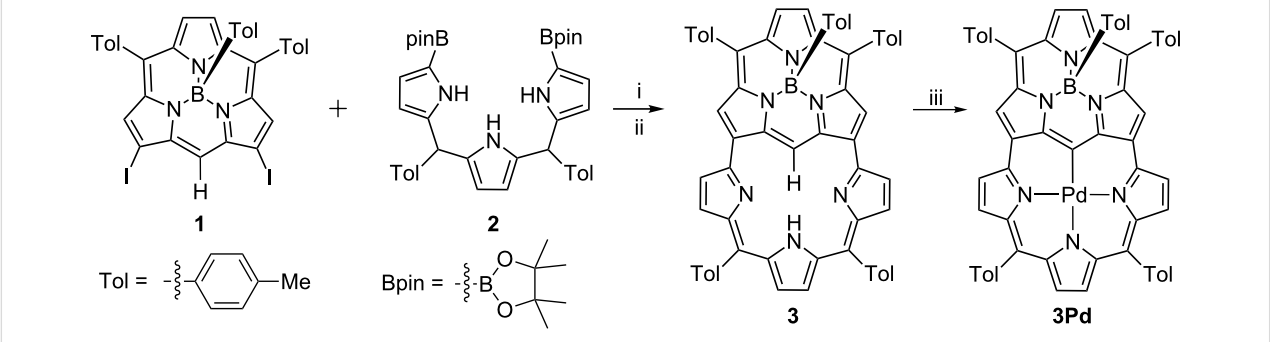

Scheme 1: Synthesis of "earring" subporphyrin and its Pd complex. Synthetic procedure: (i) Diboryltripyrrane (2.5 equiv), $Pd_2(dba)_3$ (10 mol %), SPhos (2-dicyclohexylphosphino-2',6'-dimethoxybiphenyl, 40 mol %), Cs_2CO_3 (2 equiv), CsF (2 equiv), Tol/DMF 2:1, reflux, 48 h; (ii) in air, rt, overnight; (iii) $Pd(OAc)_2$ (3 equiv), CH_2Cl_2/MeOH 5:1, rt, overnight.

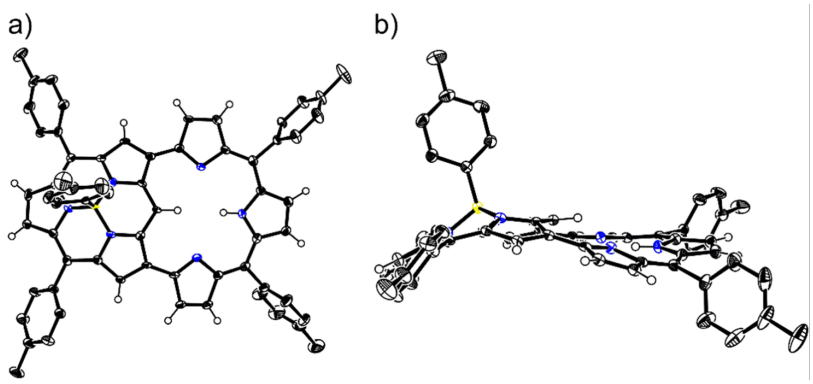

Figure 2: X-ray crystal structures of **3**: a) top view; b) side view. Thermal ellipsoids are drawn at the 50% probability level. All hydrogens on tolyl groups are omitted for clarity.

in the tripyrrin moiety, which are as large as 15.8(1)° and 16.1(1)°, respectively. We assume that the twisted structure results from the strain transmitted from the subporphyrin moiety. Furthermore, we speculate that this strain should be the origin of the much lower yield of **3** comparing to the corresponding "earring" porphyrins.

Concerning the diameter of the cavity and the strain of the skeleton, we assumed that some metal ions may insert into the hole surrounded by the tripyrrin moiety. Experimentally, **3Pd** can be formed quantitatively by simply mixing $Pd(OAc)_2$ with a CH_2Cl_2/MeOH solution of **3** at room temperature. This transformation is confirmed by MS with a parent-ion peak at m/z = 1015.24 (calcd for $C_{64}H_{46}BN_6Pd$, $[M]^+$ = 1015.29).

In the ^{1}H NMR spectrum of **3Pd** (Figure 3), no signals are detected in the very low field region. This indicates that the Pd is inserted in the cavity of **3** with the deprotonation of both N-H and *meso*-H. Meanwhile all signals belong to aromatic hydrogens shifted to a slightly higher field region after the complexation with Pd, which reveals that the insertion of the metal does not change the antiaromatic pathways in **3**.

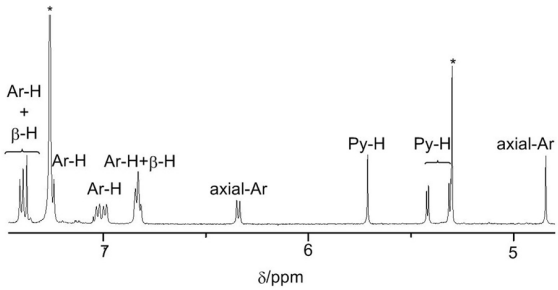

Figure 3: Partial ^{1}H NMR spectrum of **3Pd**.

Fortunately we obtained single crystals of **3Pd** from its CH_2Cl_2/$CDCl_3$/MeOH solution via vapor diffusion. All of the bond lengths were carefully measured based on the diffraction results (Figure 4). We found that despite all peripheral C–C bond

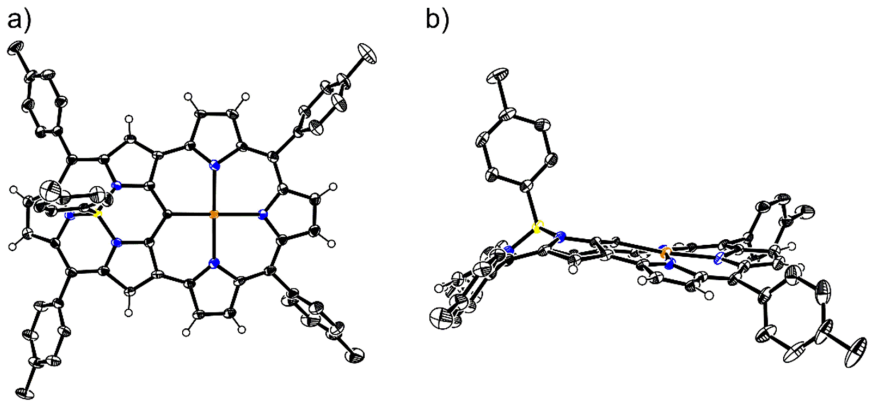

Figure 4: X-ray crystal structures of **3Pd**: a) top view; b) side view. Thermal ellipsoids are at the 30% probability level. All hydrogens on tolyl are omitted for clarity.

lengths in the tripyrrin moiety were still alternating (1.348(5)–1.441(4) Å), the differences among them were somewhat smaller compared to those of **3**. While the cavity surrounded by the tripyrrin moiety in **3Pd** has a long axis of 4.123(3) Å (N–N distance) and a short axis of 4.076(4) Å (N–C distance), both of which are shorter than that of **3**. This contraction is probably due to a slight mismatch of the radii between the Pd center and the cavity. In addition, this mismatch also leads to a further twist of the pyrrole units in the tripyrrin moiety. The dihedral angles of two adjacent pyrrole units in the tripyrrin moiety are 13.7(1)° and 18.4(1)°, respectively. The difference between the two dihedral angles is much larger than that in **3**.

The UV–vis/NIR absorption spectra of **3** and **3Pd** are shown in Figure 5. However, no fluorescence emission can be observed for **3** and **3Pd**. Both **3** and **3Pd** display broad Soret bands and Q-like bands and all bands are red-shifted compared to the corresponding bands of **1a**. In addition the absorptions of the Soret bands in **3** and **3Pd** are much weaker than in case of **1a**. For **3**, its tail of Q-like band extends to over 1000 nm. While for **3Pd**, its tail of Q-like band extends to over 1400 nm with several observable peaks. This remarkable absorption in the NIR region is comparable with that of the analogue "earring" porphyrins and reveals the π-conjugation between the subporphyrin and tripyrrin moiety.

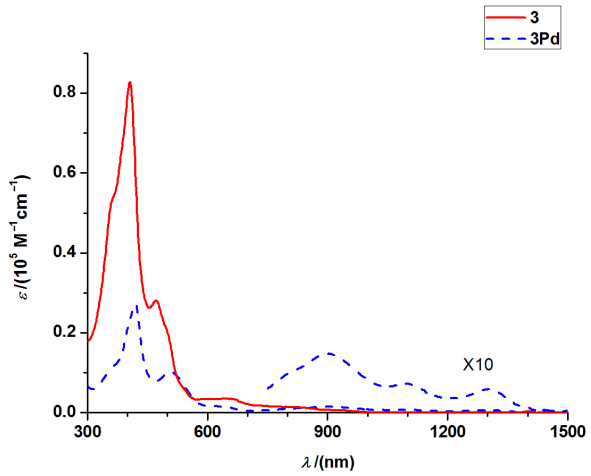

Figure 5: UV–vis/NIR spectra of **3** and **3Pd**.

Conclusion

In summary, we synthesized a π-extended "earring" subporphyrin from β,β′-diiodosubporphyrin and diboryltripyrrane via a Suzuki–Miyaura coupling and following oxidation. This "earring" subporphyrin's cavity allows for complexation of Pd atom to form the corresponding Pd complex. The ^{1}H NMR spectra of the compounds reveal that the aromatic ring current does not extend to the "ear". Both the structure of "earring" subporphyrin and that of its Pd complex were elucidated by X-ray single crystal diffraction analysis. In addition, their UV–vis/NIR spectra revealed that the absorption region is extended to the NIR region and that the absorption of the Pd complex is further red-shifted and more intense. This work extends the research of "earring" porphyrins to "earring" subporphyrins. Investigations on their photophysical properties and further functionalization are underway.

Supporting Information

Supporting Information File 1

Experimental part.
[https://www.beilstein-journals.org/bjoc/content/supplementary/1860-5397-14-170-S1.pdf]

Supporting Information File 2

Crystallographic information file of compound **3**.
[https://www.beilstein-journals.org/bjoc/content/supplementary/1860-5397-14-170-S2.cif]

Supporting Information File 3

Crystallographic information file of compound **3Pd**.
[https://www.beilstein-journals.org/bjoc/content/supplementary/1860-5397-14-170-S3.cif]

Acknowledgements

The work was supported by the National Nature Science Foundation of China (Grant Nos. 21702057, 21602058, 21772036), Scientific Research Fund of Hunan Provincial Science and Technology Department (Grant No. 2017JJ3199), Scientific Research Fund of Hunan Provincial Education Department (Grant No. 17B156). We thank Prof. Shubin Liu and Mr. Donghai Yu for their help in DFT calculations.

ORCID® iDs

Ling Xu - https://orcid.org/0000-0002-3126-5787
Jianxin Song - https://orcid.org/0000-0002-1756-5898

References

1. Inokuma, Y.; Kwon, J. H.; Ahn, T. K.; Yoo, M.-C.; Kim, D.; Osuka, A. *Angew. Chem., Int. Ed.* **2006,** *45,* 961. doi:10.1002/anie.200503426
2. Torres, T. *Angew. Chem., Int. Ed.* **2006,** *45,* 2834. doi:10.1002/anie.200504265
3. Inokuma, Y.; Osuka, A. *Dalton Trans.* **2008,** 2517. doi:10.1039/b719808f
4. Xiao, J.; Jiang, H. *Chin. J. Org. Chem.* **2009,** *29,* 1750.
5. Osuka, A.; Tsurumaki, E.; Tanaka, T. *Bull. Chem. Soc. Jpn.* **2011,** *84,* 679. doi:10.1246/bcsj.20110118

6. Claessens, C. G.; González-Rodríguez, D.; Rodríguez-Morgade, S.; Medina, A.; Torres, T. *Chem. Rev.* **2014,** *114,* 2192. doi:10.1021/cr400088w
7. Shimizu, S. *Chem. Rev.* **2017,** *117,* 2730. doi:10.1021/acs.chemrev.6b00403
8. Mack, J. *Chem. Rev.* **2017,** *117,* 3444. doi:10.1021/acs.chemrev.6b00568
9. Takeuchi, Y.; Matsuda, A.; Kobayashi, N. *J. Am. Chem. Soc.* **2007,** *129,* 8271. doi:10.1021/ja0712120
10. Kobayashi, N.; Takeuchi, Y.; Matsuda, A. *Angew. Chem., Int. Ed.* **2007,** *46,* 758. doi:10.1002/anie.200603520
11. Inokuma, Y.; Yoon, Z. S.; Kim, D.; Osuka, A. *J. Am. Chem. Soc.* **2007,** *129,* 4747. doi:10.1021/ja069324z
12. Inokuma, Y.; Easwaramoorthi, S.; Yoon, Z. S.; Kim, D.; Osuka, A. *J. Am. Chem. Soc.* **2008,** *130,* 12234. doi:10.1021/ja804846v
13. Inokuma, Y.; Easwaramoorthi, S.; Jang, S. Y.; Kim, K. S.; Kim, D.; Osuka, A. *Angew. Chem., Int. Ed.* **2008,** *47,* 4840. doi:10.1002/anie.200801192
14. Makarova, E. A.; Shimizu, S.; Matsuda, A.; Luk'yanets, E. A.; Kobayashi, N. *Chem. Commun.* **2008,** 2109. doi:10.1039/b801712c
15. Xu, T.; Lu, R.; Liu, X.; Chen, P.; Qiu, X.; Zhao, Y. *Eur. J. Org. Chem.* **2008,** 1065. doi:10.1002/ejoc.200700981
16. Liu, X.; Lu, R.; Xu, T.; Xu, D.; Zhan, Y.; Chen, P.; Qiu, X.; Zhao, Y. *Eur. J. Org. Chem.* **2009,** 53. doi:10.1002/ejoc.200800646
17. Easwaramoorthi, S.; Shin, J.-Y.; Cho, S.; Kim, P.; Inokuma, Y.; Trurumaki, E.; Osuka, A.; Kim, D. *Chem. – Eur. J.* **2009,** *15,* 12005. doi:10.1002/chem.200901671
18. Hayashi, S.-y.; Inokuma, Y.; Osuka, A. *Org. Lett.* **2010,** *12,* 4148. doi:10.1021/ol101746d
19. Hayashi, S.-y.; Inokuma, Y.; Easwaramoorthi, S.; Kim, K. S.; Kim, D.; Osuka, A. *Angew. Chem., Int. Ed.* **2010,** *49,* 321. doi:10.1002/anie.200906005
20. Remiro-Buenamañana, S.; Díaz-Moscoso, A.; Hughes, D. L.; Bochmann, M.; Tizzard, G. J.; Coles, S. J.; Cammidge, A. N. *Angew. Chem., Int. Ed.* **2015,** *54,* 7510. doi:10.1002/anie.201502662
21. Copley, G.; Hwang, D.; Kim, D.; Osuka, A. *Angew. Chem., Int. Ed.* **2016,** *55,* 10287. doi:10.1002/anie.201604432
22. Chandra, B.; Mondal, N.; Kumar, B. S.; Panda, P. K. *J. Porphyrins Phthalocyanines* **2016,** *20,* 429. doi:10.1142/S1088424616500255
23. Tsukamoto, T.; Shimada, T.; Takagi, S. *ACS Appl. Mater. Interfaces* **2016,** *8,* 7522. doi:10.1021/acsami.5b11988
24. Tsurumaki, E.; Hayashi, S.-y.; Tham, F. S.; Reed, C. A.; Osuka, A. *J. Am. Chem. Soc.* **2011,** *133,* 11956. doi:10.1021/ja2056566
25. Saga, S.; Hayashi, S.-y.; Yoshida, K.; Tsurumaki, E.; Kim, P.; Sung, Y. M.; Sung, J.; Tanaka, T.; Kim, D.; Osuka, A. *Chem. – Eur. J.* **2013,** *19,* 11158. doi:10.1002/chem.201302454
26. Zhao, S.; Liu, C.; Guo, Y.; Xiao, J.-C.; Chen, Q.-Y. *Synthesis* **2014,** *46,* 1674. doi:10.1055/s-0033-1341055
27. Tsurumaki, E.; Sung, J.; Kim, D.; Osuka, A. *J. Am. Chem. Soc.* **2015,** *137,* 1056. doi:10.1021/ja5126269
28. Tsurumaki, E.; Sung, J.; Kim, D.; Osuka, A. *Angew. Chem., Int. Ed.* **2016,** *55,* 2596. doi:10.1002/anie.201511590
29. Kotani, R.; Yoshida, K.; Tsurumaki, E.; Osuka, A. *Chem. – Eur. J.* **2016,** *22,* 3320. doi:10.1002/chem.201504719
30. Azarias, C.; Pawelek, M.; Jacquemin, D. *J. Phys. Chem. A* **2017,** *121,* 4306. doi:10.1021/acs.jpca.7b03644
31. Kitano, M.; Hayashi, S.-y.; Tanaka, T.; Yorimitsu, H.; Aratani, N.; Osuka, A. *Angew. Chem., Int. Ed.* **2012,** *51,* 5593. doi:10.1002/anie.201201853
32. Shimizu, D.; Mori, H.; Kitano, M.; Cha, W.-Y.; Oh, J.; Tanaka, T.; Kim, D.; Osuka, A. *Chem. – Eur. J.* **2014,** *20,* 16194. doi:10.1002/chem.201405110
33. Tsurumaki, E.; Inokuma, Y.; Easwaramoorthi, S.; Lim, J. M.; Kim, D.; Osuka, A. *Chem. – Eur. J.* **2009,** *15,* 237. doi:10.1002/chem.200801802
34. Tsurumaki, E.; Osuka, A. *Chem. – Asian J.* **2013,** *8,* 3042. doi:10.1002/asia.201300869
35. Yoshida, K.; Osuka, A. *Chem. – Asian J.* **2015,** *10,* 1526. doi:10.1002/asia.201500225
36. Kitano, M.; Okuda, Y.; Tsurumaki, E.; Tanaka, T.; Yorimitsu, H.; Osuka, A. *Angew. Chem., Int. Ed.* **2015,** *54,* 9275. doi:10.1002/anie.201503530
37. Kitano, M.; Tanaka, T.; Osuka, A. *Organometallics* **2017,** *36,* 2559. doi:10.1021/acs.organomet.7b00130
38. Rao, Y.; Kim, T.; Park, K. H.; Peng, F.; Liu, L.; Liu, Y.; Wen, B.; Liu, S.; Kirk, S. R.; Wu, L.; Chen, B.; Ma, M.; Zhou, M.; Yin, B.; Zhang, Y.; Kim, D.; Song, J. *Angew. Chem., Int. Ed.* **2016,** *55,* 6438. doi:10.1002/anie.201600955

License and Terms

BEILSTEIN JOURNAL OF ORGANIC CHEMISTRY

Rational design of boron-dipyrromethene (BODIPY) reporter dyes for cucurbit[7]uril

Mohammad A. Alnajjar[1], Jürgen Bartelmeß[2], Robert Hein[1], Pichandi Ashokkumar[2,3], Mohamed Nilam[1], Werner M. Nau[1], Knut Rurack[2] and Andreas Hennig[*1]

Full Research Paper

Open Access

Address:
[1]Department of Life Sciences and Chemistry, Jacobs University Bremen, Campus Ring 1, 28759 Bremen, Germany, [2]Chemical and Optical Sensing Division, Bundesanstalt für Materialforschung und -prüfung (BAM), Richard-Willstätter-Str. 11, 12489 Berlin, Germany and [3]Laboratory of Bioimaging and Pathology, UMR 7021 CNRS, Faculty of Pharmacy, University of Strasbourg, 74 Route du Rhin, F-67401 Illkirch-Graffenstaden, France

Email:
Andreas Hennig[*] - a.hennig@jacobs-university.de

* Corresponding author

Keywords:
BODIPY; cucurbituril; fluorescence; pH; photoinduced electron transfer; supramolecular chemistry

Beilstein J. Org. Chem. **2018,** *14,* 1961–1971.
doi:10.3762/bjoc.14.171

Received: 15 April 2018
Accepted: 06 July 2018
Published: 30 July 2018

This article is part of the thematic issue "Macrocyclic and supramolecular chemistry".

Guest Editor: M.-X. Wang

Abstract

We introduce herein boron-dipyrromethene (BODIPY) dyes as a new class of fluorophores for the design of reporter dyes for supramolecular host–guest complex formation with cucurbit[7]uril (CB7). The BODIPYs contain a protonatable aniline nitrogen in the *meso*-position of the BODIPY chromophore, which was functionalized with known binding motifs for CB7. The unprotonated dyes show low fluorescence due to photoinduced electron transfer (PET), whereas the protonated dyes are highly fluorescent. Encapsulation of the binding motif inside CB7 positions the aniline nitrogen at the carbonyl rim of CB7, which affects the pK_a value, and leads to a host-induced protonation and thus to a fluorescence increase. The possibility to tune binding affinities and pK_a values is demonstrated and it is shown that, in combination with the beneficial photophysical properties of BODIPYs, several new applications of host–dye reporter pairs can be implemented. This includes indicator displacement assays with favourable absorption and emission wavelengths in the visible spectral region, fluorescence correlation spectroscopy, and noncovalent surface functionalization with fluorophores.

Introduction

Cucurbit[*n*]urils (CBn, *n* = 5–8, 10, and 14) are a class of macrocyclic host molecules which are water soluble, nontoxic, and are able to bind a large variety of neutral and cationic guests in their inner cavity with high affinity [1-4]. This unique combination of properties has enabled numerous applications in the life sciences, for example, for protein binding [5,6], stabi-

lization [7], immobilisation [8], isolation [9], self-assembly [10,11], and regulation [12], or for drug solubilisation and delivery [13-15].

The combination of CBs with fluorescent dyes directly enables (bio)sensing applications through the indicator displacement principle [16,17]. Therein, the fluorescence properties of a dye are altered when encapsulated by the host, and when a competitive binder displaces the dye from the cavity, the properties of the non-encapsulated dye are regenerated. This principle has enabled, for example, real-time monitoring of enzymatic activity [18-20], the detection of membrane-transport activity [21] and membrane fusion [22], and even cellular imaging appears to be a potential future prospect [23,24].

However, most combinations of macrocyclic hosts and dyes that have so far been reported [16] are only of limited use for these currently emerging life science applications of CBs. Many of the fluorescent dyes which bind to CBs with significant fluorescence changes have a limited photostability, in particular under intense laser light illumination in confocal laser scanning microscopy [23,25], or absorb at shorter wavelengths, where biological samples show a high background from autofluorescence [26,27]. An ideal fluorescent dye would be highly photostable in biological media, have long-wavelength absorption to minimize background fluorescence from biological samples, and it would have a high fluorescence quantum yield in either bound or unbound state with a large difference in fluorescence intensity between both. In addition, a tuneable hydrophobicity to render the dye–CB complex membrane permeable or not, and a tuneable affinity for the macrocycle would be desirable.

One possibility is the utilization of monofunctionalized CBs with outer cavity-attached fluorescent dyes [22,24]. This principally allows for the modular construction of various Förster resonance energy transfer (FRET) pairs as demonstrated with a Cy3-attached CB7, or the design of self-inclusion complexes, in which an outer cavity-attached rhodamine was intramolecularly bound in the CB7 cavity. As an alternative, it has been previously suggested that host-assisted protonation of a cavity-binding functional moiety (an "anchor group") and a suitably attached protonation-sensitive fluorescent dye yields a rational and modular approach towards CB–dye pairs [25]. This strategy had been previously applied to carbazole, aminonaphthalenesulfonate and aminopyrene as fluorescent dyes [25-28].

Herein, we systematically explore the utility of boron-dipyrromethenes (BODIPYs) with an aniline substituent in the *meso*-position as fluorescent dyes in this type of anchor approach (Figure 1). BODIPYs are a class of fluorescent dyes that are particularly suitable for applications in medical imaging, and as fluorescent labels in biology, biochemistry and related fields [29,30]. They are characterized by narrow absorption and fluorescence emission bands with small Stokes shifts, high molar absorption coefficients, and high quantum yields. Their excitation and emission maxima are in the visible region, usually above 470 nm, and they show high thermal and photochemical stability under various conditions, particularly under physiological conditions. Although most BODIPYs are insensitive to pH changes, pH-activatable optical probes for cancer imaging have been reported, in which an aniline substituent in the *meso*-position of the BODIPY core led to efficient fluorescence quenching by photoinduced electron transfer (PET), whereas the protonated form was brightly fluorescent [31]. We report herein the synthesis and photophysical characterization of BODIPY derivatives with an aniline substituent in the *meso*-position to which different anchor groups have been attached, and we investigate their complexation behaviour with CB7. The goal was to explore the suitability of this approach, the possibility to fine-tune binding constants with different anchor groups and to provide BODIPYs with different absorption and emission wavelengths as well as pK_a values of the aniline substituent.

Results and Discussion

Synthesis

In this paper, various routes were explored to synthesize the desired BODIPY dyes bearing an anchor group for binding to CB7 (Scheme 1). **1** was obtained by alkylation of *p*-aminobenzaldehyde with benzyl bromide and subsequent reaction of the obtained 4-(benzylamino)benzaldehyde with 2,4-dimethylpyrrole to afford the BODIPY dye by condensation under acidic conditions (route A) [32,33]. Since all efforts to obtain **2** via route A were not successful, even using Finkelstein conditions in aprotic solvents with high boiling points with various bases [34,35], BDP-NH_2 was synthesized according to a reported literature procedure [32], and then converted into the desired BODIPY anchor dye by reductive amination with the respective aldehyde using sodium triacetoxyborohydride as a mild reducing agent (route B) [36]. **3** was also synthesized by reductive amination by reacting BDP-NH_2 with 4-[*N*-(*tert*-butyloxycarbonyl)]amino-1-butanal [37] followed by Boc deprotection with TFA. **4** was prepared by a substitution reaction from the parent *meso*-pentafluorobenzyl-BODIPY BDP-F_5 with aminomethylcyclohexane (route C), following an established synthetic approach [38]. For the preparation of the aminomethyladamantane derivative **5**, a route via a bromophenyl-BODIPY BDP-Br followed by a Buchwald–Hartwig coupling was performed. For the latter, a previously published Pd/XPhos containing catalytic system was successfully utilized (route D) [39].

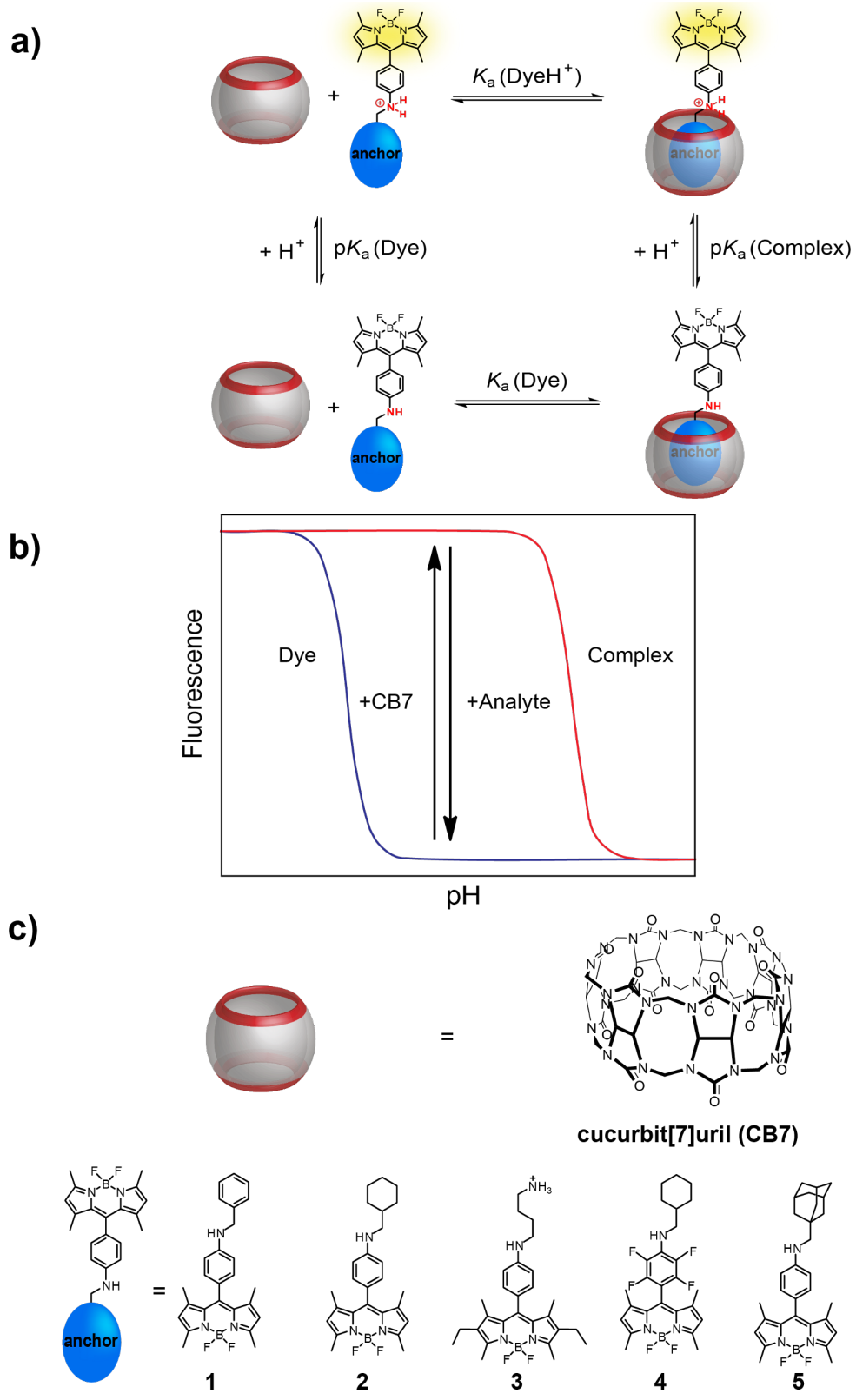

Figure 1: a) The “anchor group” approach for a rational design of CB–dye pairs involving a thermodynamic cycle of protonation and binding. b) Simulated pH titration curves of dye (blue) and CB7–dye complex (red) demonstrating the sensing principle based on the pK_a of the dye and the complex in the presence and absence of analyte. c) Structures of CB7 and BODIPY derivatives.

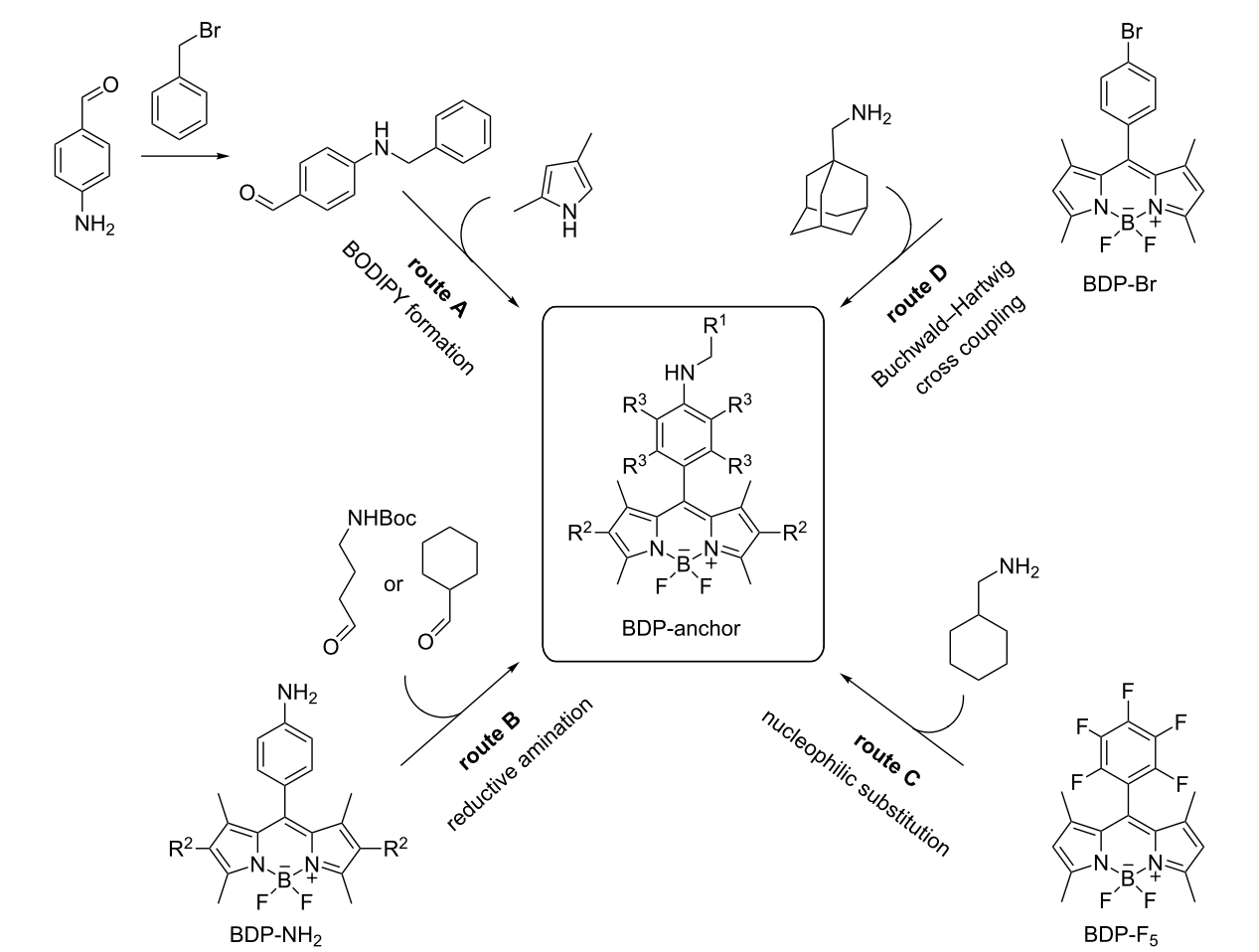

Scheme 1: Synthesis of BODIPY derivatives.

Spectroscopic characterization of dyes

To ensure that the dyes do not aggregate under the conditions used for further measurements, concentration-dependent absorption and fluorescence spectra were measured first. In neutral water containing either 5% or 30% (v/v) acetonitrile (ACN), the aniline nitrogen in the *meso*-position of all BODIPY dyes is unprotonated (see below) and with 30% ACN, a linear dependence of the fluorescence intensity on the concentration of the dyes with no significant alterations of the shape of the absorption and emission bands was observed over the whole range of concentrations used herein (up to 5 μM). In 5% ACN, however, dye aggregation was indicated by a downward curvature in the fluorescence intensity plots at dye concentrations above 60 to 120 nM. Further experiments were therefore conducted in 30% ACN.

The absorption maximum was centred at ca. 500 nm for all aniline dyes (Figure 2a and Table 1) and the emission maximum was centred at ca. 510 nm for **1** and **2**, whereas **3** showed a significantly red-shifted emission maximum at 540 nm, because we used the hexaalkylated instead of the tetraalkylated BODIPY core for this dye, trying to achieve maximum fluorescence output. The spectra of the tetrafluorinated BODIPY **4** showed an overall red shift with the absorption maximum at 510 nm and the emission maximum at 530 nm. The molar absorption coefficients of the BODIPY derivatives were around 90,000 $M^{-1}cm^{-1}$, which agrees well with related BODIPY derivatives in the literature [30,40-44].

With decreasing pH, a strong increase in fluorescence was observed for all dyes (Figure 2b), which is due to the protonation of the aniline nitrogen in the *meso*-position of the BODIPY core lowering the HOMO energy level of the aniline group. Negligible changes in absorption spectra and in the position of the emission maxima were in accordance with the anticipated PET mechanism [31,45]. Further, the change in free energy, ΔG, associated with PET was calculated using the Rehm–Weller equation [46]. Therefore, we used a reduction potential of −1.55 V for the 1,3,7,9-tetramethyl-BODIPY core acceptor of **1**, **2**, and **5** [47] and of −1.81 V for the 2,8-diethyl-1,3,7,9-tetramethyl-

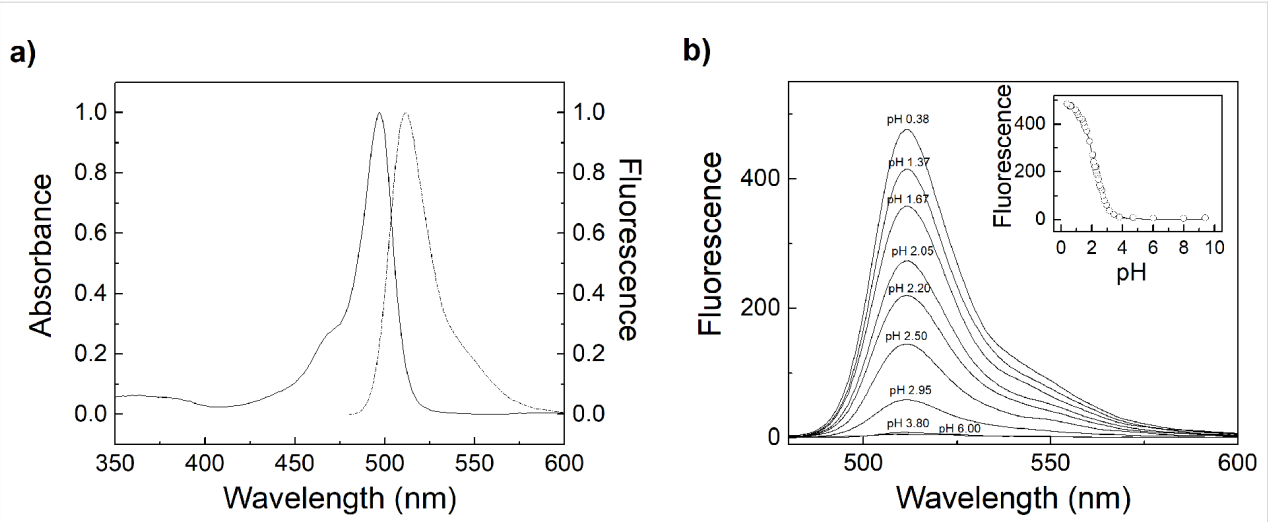

Figure 2: a) Normalized absorption (solid line) and normalized fluorescence emission spectrum (dotted line) of 0.72 µM **1** in 30% (v/v) ACN in water, pH 7.0, and b) fluorescence spectra in 30% (v/v) ACN in water with varying pH. Inset: Fluorescence pH titration measured with λ_{exc} = 470 nm and λ_{em} = 510 nm.

Table 1: Photophysical properties of the synthesized BODIPY derivatives.[a]

	1	2	3	4	5
ε [$M^{-1}cm^{-1}$]	97,000	97,000	93,000	85,300	99,000
$\lambda_{abs.max}$ [nm]	496	497	500	510	497
$\lambda_{em.max}$ [nm]	511	510	540	530	510
Φ_f (Dye) [%]	1.1	6.2	0.017	2.0	2.4
Φ_f ($DyeH^+$) [%]	54	51	0.12	41[b]	30.5
pK_a (Dye)	2.2	2.6	2.7	−0.3	3.6

[a]Measured in 30% (v/v) ACN in water except for the molar absorption coefficient ε, which was determined in neat ACN. [b]Determined from the CB7 complex at 4 mM CB7. Note that the fluorescence quantum yields of the dyes are not affected by complexation (see text for details).

BODIPY core acceptor of **3** in acetonitrile [47], an oxidation potential of +0.0625 V for the aniline donor [48,49], and the vibrational zero electronic energy was determined as 2.46 eV from absorption and emission spectra. This gave Δ*G* values of −87.6 kJ mol^{-1} for **1**, **2**, and **5** and of −62.5 kJ mol^{-1} for **3**, which clearly demonstrates that PET is energetically favourable.

Fitting of the pH titration curves revealed pK_a values in the range of 2–3 for the aniline nitrogen and a pK_a value of −0.14 for the tetrafluoroaniline nitrogen of BODIPYs (Table 1). This range agrees well with the electron-withdrawing nature of the BODIPY core and with reported pK_a values, for example, for aniline (pK_a = 4.58), 4-nitroaniline (pK_a = 1.02), 4-cyanoaniline (pK_a = 1.74), or pentafluoroaniline (pK_a = −0.30) [50,51]. At basic pH values, no spectroscopic changes were noted except for **3**, which showed a broadening and a marked decrease of the absorption band (Figure S17, Supporting Information File 1). This presumably originates from a deprotonation of the terminal alkylammonium group of the putrescine chain, which could fold back and enable an intramolecular charge transfer state of the amine lone pair with the BODIPY chromophore. In accordance with this hypothesis, a positive solvatochromism with varying contents of ACN was observed (Figure S18, Supporting Information File 1).

The fluorescence quantum yields of the unprotonated BODIPY dyes were determined in 30% (v/v) ACN in water (at pH 7.4) and of the protonated BODIPY dyes in 30% ACN in 0.1 M HCl. For both, fluorescein in 0.1 M NaOH was used as the reference (Φ_f = 0.89) [52]. These measurements revealed an increase in fluorescence by a factor of 7 to 50 upon protonation for the investigated BODIPYs, which is sufficient for the desired sensing applications (Table 1) [20,53]. Surprisingly, and despite the hexaalkylated core was used, the fluorescence quantum yields of protonated as well as unprotonated **3** were more than 100-fold lower than the quantum yields of the other derivatives. Such reduced quantum yields have been previously reported for some BODIPYs substituted with diamines in the aniline *meso*-position, and the decreased quantum yields were ascribed to the loose-bolt effect [41,54,55].

Complexation with CB7

Addition of excess CB7 to the BODIPY dyes at low pH values, in which the dyes are fully protonated, or at high pH values above the pK_a value of the BODIPY•CB7 complex (see below) had no effect on the spectroscopic properties of the dyes. For

example, the fluorescence quantum yield of **2** was identical in absence and presence of CB7 at pH 1.5. At intermediate pH values, however, the fluorescence of the dyes increased upon addition of CB7 (Figure 3). This result is in accordance with the anticipated anchor group mechanism leading to a complexation-induced protonation of the dye (Figure 1). It also suggests that the BODIPY core is not encapsulated in the macrocyclic cavity and that encapsulation of the anchor group by CB7 has no effect on the spectroscopic properties of the dyes. At intermediate pH, the protonated fraction of the dye will be strongly bound by CB7, which affects the protonation equilibrium of the dye and leads to more protonated dye being produced. The net outcome is an increase in fluorescence intensity (upward arrow in "detection window" in Figure 1b). Multiple binding titrations performed at different pH values were fully consistent with the mechanism (Figure 3b). At low pH values, the fluorescence intensity in absence of CB7 was higher and the fluorescence increase upon addition of CB7 was steeper, because more dye molecules are already protonated, whereas at higher pH values more CB7 was required to reach the final fluorescence intensity of the fully protonated dyes.

Unfortunately, the absence of any detectable changes for the fully protonated or unprotonated dyes upon addition of CB7 prevented a direct determination of the respective binding constants, K_a(DyeH$^+$) and K_a(DyeH), at low and high pH values. We therefore developed a global fitting procedure (see Supporting Information File 1), in which the binding titrations at different pH values are simultaneously analysed to provide the values for the binding constants of the protonated and unprotonated dye, K_a(DyeH$^+$) and K_a(Dye), as well as the pK_a values of the BODIPY•CB7 complex pK_a(Complex), see Table 2. The pK_a value of the uncomplexed dye, pK_a(Dye), was obtained from a simple pH titration and fixed during the global fitting procedure.

Table 2: Properties of the CB7–BODIPY host–guest complexes.[a]

	1	2	4	5
pK_a(Complex)[b]	5.0	5.3	1.5	8.2
ΔpK_a	2.8	2.7	1.8	4.6
K_a(Dye)[c] [M^{-1}]	30	5000	240	n.a.[d]
K_a(DyeH$^+$)[c] [M^{-1}]	1.9×10^4	2.6×10^6	1.5×10^4	n.a.[d]

[a]Measured in 30% (v/v) ACN/H_2O. [b]Error ±0.2 pK_a units. [c]Error in K_a ca. 20%. [d]Binding constants could not be determined due to the very slow exchange kinetics of the 5•CB7 complex, see also Figure S19 (Supporting Information File 1).

The binding affinities of the BODIPY dyes were significantly lower than the reported binding constants of the respective anchor groups in water [4]. To allow a better comparison, we determined the binding constants of the benzylammonium (Bnz) and cyclohexylmethylammonium (cyH) cations by displacement titrations (see below) in our mixture of 30% (v/v) ACN/H_2O, which gave K_a(Bnz) = 1.4×10^5 M^{-1} and K_a(cyH) = 1.5×10^7 M^{-1}. This indicated that the binding affinity is lowered 100 to 1000-fold by reducing the hydrophobic effect in presence of 30% acetonitrile as also previously noted for water/DMSO mixtures [56]. The attachment of the BODIPY chromophore to the anchor groups thus reduces the binding constant by an additional factor of 10 for the aniline *meso*-group and by a factor of 1000 for the tetrafluoroaniline group in **4**. We ascribe this to steric hindrance between the carbonyl-fringed CB7 rim and the fluorine atoms in the tetrafluoroaniline, which are slightly larger than the hydrogen atoms [57]. The data obtained with **3** could not be fitted satisfactorily,

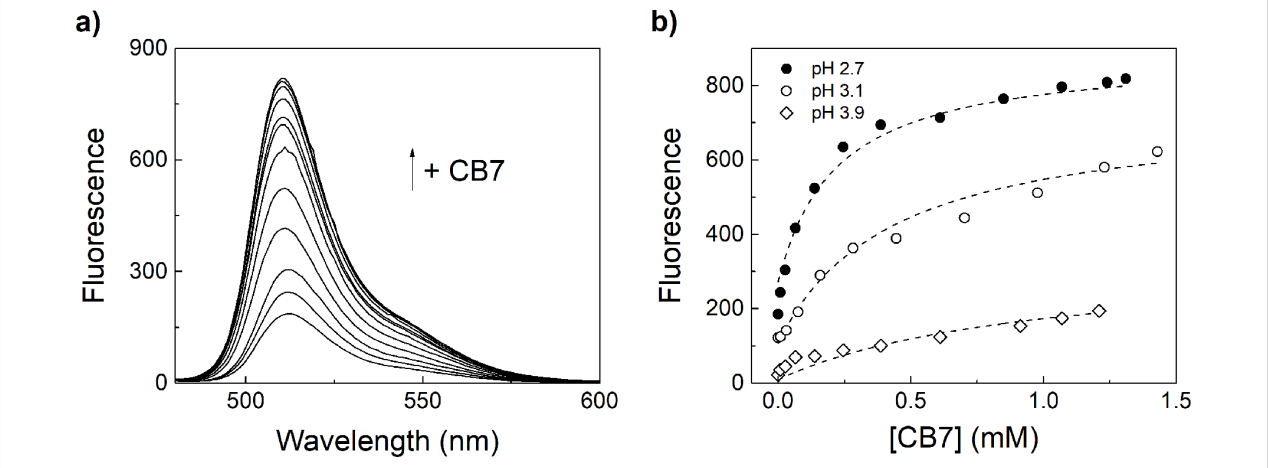

Figure 3: a) Fluorescence spectral changes (λ_{exc} = 470 nm) upon addition of CB7 to 50 nM **1** in 10 mM citrate buffer, pH 2.7, containing 30% (v/v) ACN in water, and b) respective titration plot (λ_{em} = 510 nm) at varying pH. The dashed lines were obtained by a global fitting according to the thermodynamic cycle in Figure 1 (see Supporting Information File 1 for details).

which is presumably due to the more complex photophysics of this dye (see above) and the exchange of **5** was too slow to equilibrate during the titration within reasonable time (Figure S19, Supporting Information File 1).

The pK_a values of the host–dye complex were independently determined by pH titrations in presence of excess CB7 and analysed assuming quantitative complex formation (Figure 4). Overall, the pK_a values from the direct titration and from the global fitting agreed reasonably well, and the complexation-induced pK_a shifts were in the typical range reported for CB7 host–guest complexes [58].

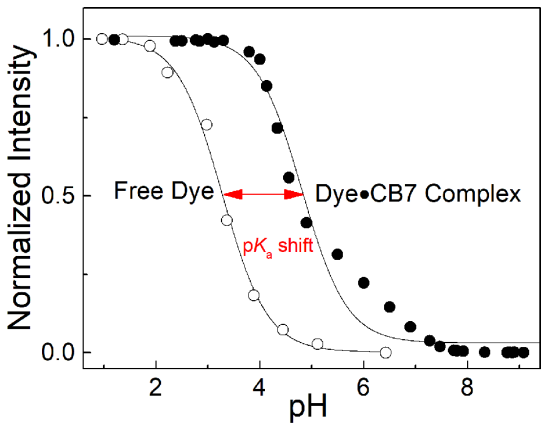

Figure 4: Fluorescence pH titration of **2** and the respective complex (in presence of 3 mM CB7) in 30% (v/v) ACN in water with varying pH. Fluorescence was measured with λ_{exc} = 470 nm and λ_{em} = 510 nm.

Application of BODIPY-CB7 complexes

The availability of BODIPY dyes, which respond towards complexation by CB7, enables a large variety of potential applications of the resulting host–dye reporter pairs. As first example, the CB7–BODIPY pairs can be applied as sensors using the indicator displacement principle [17,18,21,59]. This is demonstrated by sensing of cyclohexylmethylamine and aniline as model analytes (Figure 5). In order to determine the binding constants of the two analytes, the apparent binding constant of **2** at pH 3.1 was taken (K_{app} = 6.7 × 10^5 M^{-1}) and the displace-

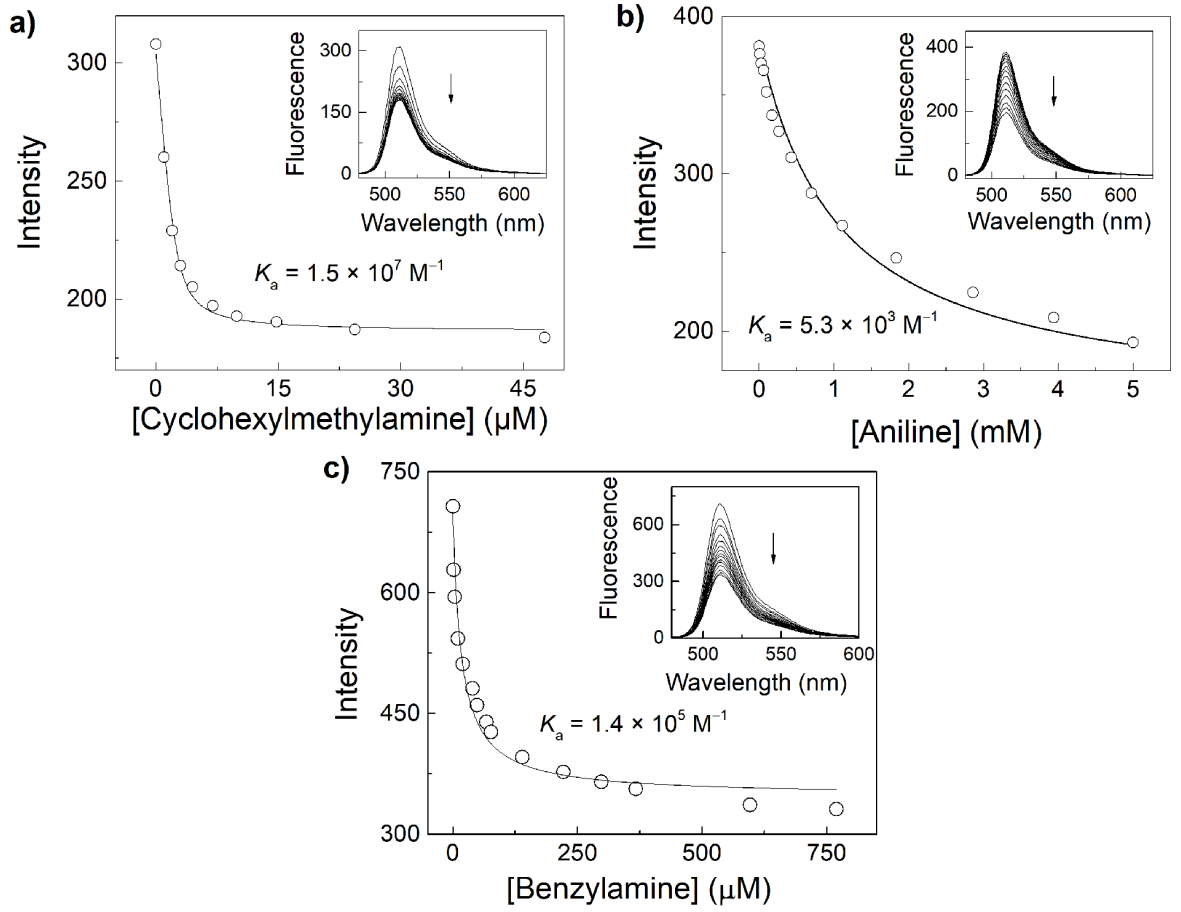

Figure 5: Fluorescence displacement titrations (λ_{ex} = 470 nm, λ_{em} = 510 nm). a) 5 μM **2** and 2.5 μM CB7 with cyclohexylmethylamine. b) 7 μM **2** and 2.5 μM CB7 with aniline. c) 0.5 μM **2** and 0.2 μM CB7 with benzylamine in 10 mM citrate buffer in 30% (v/v) ACN in water, pH 3.1.

ment titrations were analysed with a competitive titration model [18,25]. This gave binding constants of 1.5×10^7 M^{-1} for the cyclohexylmethylammonium cation, 5.3×10^3 M^{-1} for the anilinium cation and 1.4×10^5 M^{-1} for the benzylammonium cation in the 10 mM citrate buffer in 30% (v/v) ACN in water.

As another advantage over previously established supramolecular reporter dyes, the absorption maximum of the BODIPYs introduced herein matches the emission wavelength of an Ar laser, which is still the most common excitation source in fluorescence correlation spectroscopy (FCS) and fluorescence microscopy. FCS has been established to study dynamic processes in biological systems and, more recently, also in materials science, but its use in supramolecular chemistry is so far very rare [60-64]. It can be applied to investigate translational and rotational diffusion of supramolecules as well as exchange kinetics. To demonstrate the compatibility of the new BODIPY dyes with FCS, we have determined the diffusion coefficient of the **2**•CB7 complex in comparison to the free **2** dye. FCS autocorrelation curves (Figure 6) were analysed to obtain the diffusion times t_{diff} of **2** and the **2**•CB7 complex and then converted into diffusion coefficients D using the reported standard rhodamine 6G ($D = 2.80 \times 10^{-6}$ cm^2 s^{-1}) [60,65]. This gave $D = 4.87 \times 10^{-6}$ cm^2 s^{-1} for **2** and $D = 3.39 \times 10^{-6}$ cm^2 s^{-1} for the **2**•CB7 complex, which perfectly matches the range reported for other dyes and their respective CB7 complexes [60]. In accordance with inclusion of the anchor group into the CB7 cavity and thus exclusion complex formation of the BODIPY core, the photostability of the dyes was not affected by CB7 complex formation (Figure S20, Supporting Information File 1).

The compatibility of BODIPYs with common excitation sources and filter sets also enables their use in fluorescence microscopy. To demonstrate, we have used polymer microparticles with surface-bound CB7 [66] and added them to a solution containing a mixture of **5** and 1-(aminomethyl)adamantane (AMADA). The latter was added to reduce the surface group density of the dye and prevent undesired self-quenching at high surface concentrations of the fluorophore. After centrifugation and washing of the polymer particles, surface-bound **5** could be clearly visualized by fluorescence microscopy on CB7-functionalized polymer particles, whereas polymer particles lacking CB7 on the surface did not show any fluorescence (Figure 7).

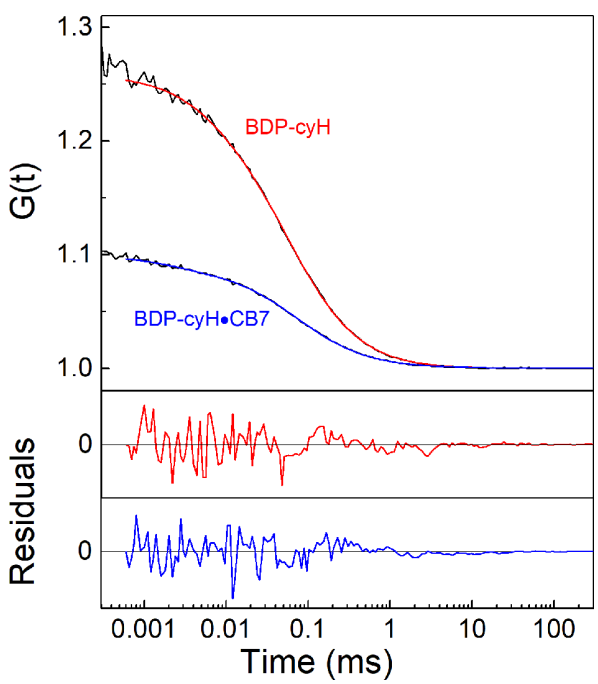

Figure 6: FCS autocorrelation curves obtained with 10 nM **2** in the absence (red fitted line) and presence (blue fitted line) of 100 μM CB7 at pH 1.5 in 30% (v/v) ACN in water. The fitted diffusion times for the free dye and the complex were 54.1 and 77.9 μs, respectively.

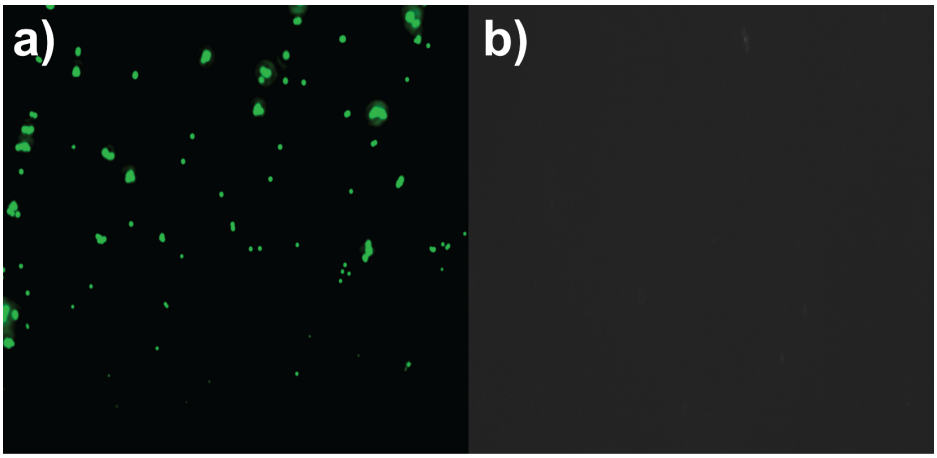

Figure 7: Fluorescence microscopy images of 1 mg/mL polymer microspheres a) with or b) without surface-bound CB7 after incubation with 10 nM **5** and 1 μM AMADA in 10 mM citrate, pH 3.3 (30% (v/v) ACN in water) and centrifugation to immobilize **5** through supramolecular host–guest binding.

This result is consistent with specific host–guest binding of **5** to CB7 on the surface, which suggests the use of **5** for straightforward surface functionalization to create nanophotonic devices as well as for multimodal surface group quantifications, e.g., using their optical properties for fluorescence and their fluorine heteroatom for X-ray photoelectron spectroscopy [67-69].

Conclusion

We have established herein BODIPYs as fluorophores in the anchor group strategy towards the design of reporter dyes for CB7. The resulting dyes have absorption and emission wavelengths which are compatible with established instrumentation in life science applications and show pronounced fluorescence changes upon host binding. The affinity of the dyes for the CB7 host was successfully adjusted by using different anchor groups and was only minimally reduced in comparison with the unmodified anchor groups. This strategy enables several applications of fluorescent host–guest complexes, for example, indicator displacement assays with absorption and emission wavelengths in the visible spectral region, fluorescence correlation spectroscopy, and noncovalent surface functionalization with fluorophores. Furthermore, the strategy is similarly applicable to pH-sensitive fluoresceins, cyanines or rhodamines, in which protonation and deprotonation of suitably positioned amino groups can also modulate their fluorescence properties. It can also be used to design dyes which reduce their fluorescence upon binding, e.g., when electron-poor groups are generated by protonation which are quenched intramolecularly by donor-excited PET [70-74].

Supporting Information

Supporting Information File 1

Experimental details and supporting figures.
[https://www.beilstein-journals.org/bjoc/content/supplementary/1860-5397-14-171-S1.pdf]

Acknowledgements

Financial support from the DFG (HE 5967/4-1 and NA 686/11-1), BAM's Focus Area Analytical Sciences (KonSens Project) and the Alexander-von-Humboldt Foundation is gratefully acknowledged. We also thank Claudius Walter, Prof. Dr. Mathias Winterhalter, and Prof. Dr. Richard Wagner for help with the FCS measurements and Ms. Shuai Zhang for providing a sample of CB7-functionalized polymer beads.

ORCID® iDs

Mohammad A. Alnajjar - https://orcid.org/0000-0002-2261-6127
Jürgen Bartelmeß - https://orcid.org/0000-0002-1977-612X
Robert Hein - https://orcid.org/0000-0001-8567-0924
Pichandi Ashokkumar - https://orcid.org/0000-0002-2505-9039
Werner M. Nau - https://orcid.org/0000-0002-7654-6232
Knut Rurack - https://orcid.org/0000-0002-5589-5548
Andreas Hennig - https://orcid.org/0000-0003-0444-5923

References

1. Assaf, K. I.; Nau, W. M. *Chem. Soc. Rev.* **2015,** *44,* 394–418. doi:10.1039/C4CS00273C
2. Lagona, J.; Mukhopadhyay, P.; Chakrabarti, S.; Isaacs, L. *Angew. Chem., Int. Ed.* **2005,** *44,* 4844–4870. doi:10.1002/anie.200460675
3. Kim, J.; Jung, I.-S.; Kim, S.-Y.; Lee, E.; Kang, J.-K.; Sakamoto, S.; Yamaguchi, K.; Kim, K. *J. Am. Chem. Soc.* **2000,** *122,* 540–541. doi:10.1021/ja993376p
4. Barrow, S. J.; Kasera, S.; Rowland, M. J.; del Barrio, J.; Scherman, O. A. *Chem. Rev.* **2015,** *115,* 12320–12406. doi:10.1021/acs.chemrev.5b00341
5. Chinai, J. M.; Taylor, A. B.; Ryno, L. M.; Hargreaves, N. D.; Morris, C. A.; Hart, P. J.; Urbach, A. R. *J. Am. Chem. Soc.* **2011,** *133,* 8810–8813. doi:10.1021/ja201581x
6. Li, W.; Bockus, A. T.; Vinciguerra, B.; Isaacs, L.; Urbach, A. R. *Chem. Commun.* **2016,** *52,* 8537–8540. doi:10.1039/C6CC03193E
7. Webber, M. J.; Appel, E. A.; Vinciguerra, B.; Cortinas, A. B.; Thapa, L. S.; Jhunjhunwala, S.; Isaacs, L.; Langer, R.; Anderson, D. G. *Proc. Natl. Acad. Sci. U. S. A.* **2016,** *113,* 14189–14194. doi:10.1073/pnas.1616639113
8. Young, J. F.; Nguyen, H. D.; Yang, L.; Huskens, J.; Jonkheijm, P.; Brunsveld, L. *ChemBioChem* **2010,** *11,* 180–183. doi:10.1002/cbic.200900599
9. Lee, D.-W.; Park, K. M.; Banerjee, M.; Ha, S. H.; Lee, T.; Suh, K.; Paul, S.; Jung, H.; Kim, J.; Selvapalam, N.; Ryu, S. H.; Kim, K. *Nat. Chem.* **2011,** *3,* 154–159. doi:10.1038/nchem.928
10. Hou, C.; Li, J.; Zhao, L.; Zhang, W.; Luo, Q.; Dong, Z.; Xu, J.; Liu, J. *Angew. Chem., Int. Ed.* **2013,** *52,* 5590–5593. doi:10.1002/anie.201300692
11. Nguyen, H. D.; Dang, D. T.; vanDongen, J. L. J.; Brunsveld, L. *Angew. Chem., Int. Ed.* **2010,** *49,* 895–898. doi:10.1002/anie.200904413
12. Dang, D. T.; Nguyen, H. D.; Merkx, M.; Brunsveld, L. *Angew. Chem., Int. Ed.* **2013,** *52,* 2915–2919. doi:10.1002/anie.201208239
13. Hettiarachchi, G.; Nguyen, D.; Wu, J.; Lucas, D.; Ma, D.; Isaacs, L.; Briken, V. *PLoS One* **2010,** *5,* e10514. doi:10.1371/journal.pone.0010514
14. Jin Jeon, Y.; Kim, S.-Y.; Ho Ko, Y.; Sakamoto, S.; Yamaguchi, K.; Kim, K. *Org. Biomol. Chem.* **2005,** *3,* 2122–2125. doi:10.1039/b504487a
15. Zhao, Y.; Buck, D. P.; Morris, D. L.; Pourgholami, M. H.; Day, A. I.; Collins, J. G. *Org. Biomol. Chem.* **2008,** *6,* 4509–4515. doi:10.1039/b813759e
16. Dsouza, R. N.; Pischel, U.; Nau, W. M. *Chem. Rev.* **2011,** *111,* 7941–7980. doi:10.1021/cr200213s
17. Nguyen, B. T.; Anslyn, E. V. *Coord. Chem. Rev.* **2006,** *250,* 3118–3127. doi:10.1016/j.ccr.2006.04.009
18. Hennig, A.; Bakirci, H.; Nau, W. M. *Nat. Methods* **2007,** *4,* 629–632. doi:10.1038/nmeth1064
19. Biedermann, F.; Hathazi, D.; Nau, W. M. *Chem. Commun.* **2015,** *51,* 4977–4980. doi:10.1039/C4CC10227D

20. Dsouza, R. N.; Hennig, A.; Nau, W. M. *Chem. – Eur. J.* **2012,** *18,* 3444–3459. doi:10.1002/chem.201103364
21. Ghale, G.; Lanctôt, A. G.; Kreissl, H. T.; Jacob, M. H.; Weingart, H.; Winterhalter, M.; Nau, W. M. *Angew. Chem., Int. Ed.* **2014,** *53,* 2762–2765. doi:10.1002/anie.201309583
22. Gong, B.; Choi, B.-K.; Kim, J.-Y.; Shetty, D.; Ko, Y. H.; Selvapalam, N.; Lee, N. K.; Kim, K. *J. Am. Chem. Soc.* **2015,** *137,* 8908–8911. doi:10.1021/jacs.5b05385
23. Norouzy, A.; Azizi, Z.; Nau, W. M. *Angew. Chem., Int. Ed.* **2015,** *54,* 792–795. doi:10.1002/anie.201407808
24. Bockus, A. T.; Smith, L. C.; Grice, A. G.; Ali, O. A.; Young, C. C.; Mobley, W.; Leek, A.; Roberts, J. L.; Vinciguerra, B.; Isaacs, L.; Urbach, A. R. *J. Am. Chem. Soc.* **2016,** *138,* 16549–16552. doi:10.1021/jacs.6b11140
25. Praetorius, A.; Bailey, D. M.; Schwarzlose, T.; Nau, W. M. *Org. Lett.* **2008,** *10,* 4089–4092. doi:10.1021/ol8016275
26. Schnurr, M.; Sloniec-Myszk, J.; Döpfert, J.; Schröder, L.; Hennig, A. *Angew. Chem., Int. Ed.* **2015,** *54,* 13444–13447. doi:10.1002/anie.201507002
27. Florea, M.; Nau, W. M. *Angew. Chem., Int. Ed.* **2011,** *50,* 9338–9342. doi:10.1002/anie.201104119
28. Lazar, A. I.; Rohacova, J.; Nau, W. M. *J. Phys. Chem. B* **2017,** *121,* 11390–11398. doi:10.1021/acs.jpcb.7b10651
29. Boens, N.; Leen, V.; Dehaen, W. *Chem. Soc. Rev.* **2012,** *41,* 1130–1172. doi:10.1039/C1CS15132K
30. Loudet, A.; Burgess, K. *Chem. Rev.* **2007,** *107,* 4891–4932. doi:10.1021/cr078381n
31. Urano, Y.; Asanuma, D.; Hama, Y.; Koyama, Y.; Barrett, T.; Kamiya, M.; Nagano, T.; Watanabe, T.; Hasegawa, A.; Choyke, P. L.; Kobayashi, H. *Nat. Med.* **2009,** *15,* 104–109. doi:10.1038/nm.1854
32. Wagner, R. W.; Lindsey, J. S. *Pure Appl. Chem.* **1996,** *68,* 1373–1380. doi:10.1351/pac199668071373
33. Neres, J.; Bonnet, P.; Edwards, P. N.; Kotian, P. L.; Buschiazzo, A.; Alzari, P. M.; Bryce, R. A.; Douglas, K. T. *Bioorg. Med. Chem.* **2007,** *15,* 2106–2119. doi:10.1016/j.bmc.2006.12.024
34. Wang, B.; Yu, F.; Li, P.; Sun, X.; Han, K. *Dyes Pigm.* **2013,** *96,* 383–390. doi:10.1016/j.dyepig.2012.09.006
35. Lu, C.; Guo, Y.; Li, J.; Yao, M.; Liao, Q.; Xie, Z.; Li, X. *Bioorg. Med. Chem. Lett.* **2012,** *22,* 7683–7687. doi:10.1016/j.bmcl.2012.09.105
36. Abdel-Magid, A. F.; Carson, K. G.; Harris, B. D.; Maryanoff, C. A.; Shah, R. D. *J. Org. Chem.* **1996,** *61,* 3849–3862. doi:10.1021/jo960057x
37. Zhao, T.; Kurpiewska, K.; Kalinowska-Tłuścik, J.; Herdtweck, E.; Dömling, A. *Chem. – Eur. J.* **2016,** *22,* 3009–3018. doi:10.1002/chem.201504520
38. Vives, G.; Giansante, C.; Bofinger, R.; Raffy, G.; Del Guerzo, A.; Kauffmann, B.; Batat, P.; Jonusauskas, G.; McClenaghan, N. D. *Chem. Commun.* **2011,** *47,* 10425–10427. doi:10.1039/c1cc13778f
39. Zhang, Y.; Fang, H.-m.; Zhang, X.-t.; Wang, S.; Xing, G.-w. *ChemistrySelect* **2016,** *1,* 1–6. doi:10.1002/slct.201500016
40. Guo, S.; Ma, L.; Zhao, J.; Küçüköz, B.; Karatay, A.; Hayvali, M.; Yaglioglu, H. G.; Elmali, A. *Chem. Sci.* **2014,** *5,* 489–500. doi:10.1039/c3sc52323c
41. Volkova, Y.; Brizet, B.; Harvey, P. D.; Denat, F.; Goze, C. *Eur. J. Org. Chem.* **2014,** 2268–2274. doi:10.1002/ejoc.201301900
42. Wu, W.; Zhao, J.; Guo, H.; Sun, J.; Ji, S.; Wang, Z. *Chem. – Eur. J.* **2012,** *18,* 1961–1968. doi:10.1002/chem.201102634
43. Awuah, S. G.; Polreis, J.; Biradar, V.; You, Y. *Org. Lett.* **2011,** *13,* 3884–3887. doi:10.1021/ol2014076
44. Hagmann, W. K. *J. Med. Chem.* **2008,** *51,* 4359–4369. doi:10.1021/jm800219f
45. Pischel, U.; Uzunova, V. D.; Remón, P.; Nau, W. M. *Chem. Commun.* **2010,** *46,* 2635–2637. doi:10.1039/b927595a
46. Rehm, D.; Weller, A. *Isr. J. Chem.* **1970,** *8,* 259–271. doi:10.1002/ijch.197000029
47. Lincoln, R.; Greene, L. E.; Krumova, K.; Ding, Z.; Cosa, G. *J. Phys. Chem. A* **2014,** *118,* 10622–10630. doi:10.1021/jp5059148
48. Suatoni, J. C.; Snyder, R. E.; Clark, R. O. *Anal. Chem.* **1961,** *33,* 1894–1897. doi:10.1021/ac50154a032
49. Winget, P.; Weber, E. J.; Cramer, C. J.; Truhlar, D. G. *Phys. Chem. Chem. Phys.* **2000,** *2,* 1231–1239. doi:10.1039/a909076b
50. Shoute, L. C. T.; Mittal, J. P.; Neta, P. *J. Phys. Chem.* **1996,** *100,* 3016–3019. doi:10.1021/jp9513374
51. Gross, K. C.; Seybold, P. G. *Int. J. Quantum Chem.* **2000,** *80,* 1107–1115. doi:10.1002/1097-461x(2000)80:4/5<1107::aid-qua60>3.0.co;2-t
52. Würth, C.; Grabolle, M.; Pauli, J.; Spieles, M.; Resch-Genger, U. *Nat. Protoc.* **2013,** *8,* 1535–1550. doi:10.1038/nprot.2013.087
53. Gotor, R.; Ashokkumar, P.; Hecht, M.; Keil, K.; Rurack, K. *Anal. Chem.* **2017,** *89,* 8437–8444. doi:10.1021/acs.analchem.7b01903
54. Mula, S.; Elliott, K.; Harriman, A.; Ziessel, R. *J. Phys. Chem. A* **2010,** *114,* 10515–10522. doi:10.1021/jp106626v
55. Turro, N. J.; Ramamurthy, V.; Scaiano, J. *Modern Molecular Photochemistry of Organic Molecules,* 1st ed.; University Science Books: Sausalito, CA, U.S.A., 2010.
56. Senler, S.; Cheng, B.; Kaifer, A. E. *Org. Lett.* **2014,** *16,* 5834–5837. doi:10.1021/ol502479k
57. Böhm, H.-J.; Banner, D.; Bendels, S.; Kansy, M.; Kuhn, B.; Müller, K.; Obst-Sander, U.; Stahl, M. *ChemBioChem* **2004,** *5,* 637–643. doi:10.1002/cbic.200301023
58. Barooah, N.; Mohanty, J.; Pal, H.; Bhasikuttan, A. C. *Proc. Natl. Acad. Sci., India, Sect. A* **2014,** *84,* 1–17. doi:10.1007/s40010-013-0101-9
59. Carvalho, C. P.; Uzunova, V. D.; Da Silva, J. P.; Nau, W. M.; Pischel, U. *Chem. Commun.* **2011,** *47,* 8793–8795. doi:10.1039/c1cc12954f
60. Mohanty, J.; Nau, W. M. *Angew. Chem.* **2005,** *117,* 3816–3820. doi:10.1002/ange.200500502
61. Al-Soufi, W.; Reija, B.; Novo, M.; Felekyan, S.; Kühnemuth, R.; Seidel, C. A. M. *J. Am. Chem. Soc.* **2005,** *127,* 8775–8784. doi:10.1021/ja0508976
62. Granadero, D.; Bordello, J.; Pérez-Alvite, M. J.; Novo, M.; Al-Soufi, W. *Int. J. Mol. Sci.* **2010,** *11,* 173–188. doi:10.3390/ijms11010173
63. Koner, A. L.; Nau, W. M. *Supramol. Chem.* **2007,** *19,* 55–66. doi:10.1080/10610270600910749
64. Cui, S.-C.; Tachikawa, T.; Fujitsuka, M.; Majima, T. *J. Phys. Chem. C* **2011,** *115,* 1824–1830. doi:10.1021/jp1110828
65. Rigler, R.; Mets, Ü.; Widengren, J.; Kask, P. *Eur. Biophys. J.* **1993,** *22,* 169–175. doi:10.1007/bf00185777
66. Zhang, S.; Domínguez, Z.; Assaf, K. I.; Nilam, M.; Thiele, T.; Schedler, U.; Nau, W. M.; Hennig, A., unpublished results.
67. Fischer, T.; Dietrich, P. M.; Unger, W. E. S.; Rurack, K. *Anal. Chem.* **2016,** *88,* 1210–1217. doi:10.1021/acs.analchem.5b03468
68. Hennig, A.; Dietrich, P. M.; Hemmann, F.; Thiele, T.; Borcherding, H.; Hoffmann, A.; Schedler, U.; Jäger, C.; Resch-Genger, U.; Unger, W. E. S. *Analyst* **2015,** *140,* 1804–1808. doi:10.1039/c4an02248c

69. Dietrich, P. M.; Hennig, A.; Holzweber, M.; Thiele, T.; Borcherding, H.; Lippitz, A.; Schedler, U.; Resch-Genger, U.; Unger, W. E. S. *J. Phys. Chem. C* **2014,** *118,* 20393–20404. doi:10.1021/jp505519g
70. Zhou, P.; Liu, J.; Yang, S.; Chen, J.; Han, K.; He, G. *Phys. Chem. Chem. Phys.* **2012,** *14,* 15191–15198. doi:10.1039/c2cp42167d
71. Kucki, M.; Fuhrmann-Lieker, T. *J. R. Soc., Interface* **2012,** *9,* 727–733. doi:10.1098/rsif.2011.0424
72. Kobayashi, T.; Urano, Y.; Kamiya, M.; Ueno, T.; Kojima, H.; Nagano, T. *J. Am. Chem. Soc.* **2007,** *129,* 6696–6697. doi:10.1021/ja070376d
73. Urano, Y.; Kamiya, M.; Kanda, K.; Ueno, T.; Hirose, K.; Nagano, T. *J. Am. Chem. Soc.* **2005,** *127,* 4888–4894. doi:10.1021/ja043919h
74. Peng, X.; Song, F.; Lu, E.; Wang, Y.; Zhou, W.; Fan, J.; Gao, Y. *J. Am. Chem. Soc.* **2005,** *127,* 4170–4171. doi:10.1021/ja043413z

License and Terms

BEILSTEIN JOURNAL OF ORGANIC CHEMISTRY

Synthesis of new *p-tert*-butylcalix[4]arene-based polyammonium triazolyl amphiphiles and their binding with nucleoside phosphates

Vladimir A. Burilov*[1], Guzaliya A. Fatikhova[1], Mariya N. Dokuchaeva[1], Ramil I. Nugmanov[1], Diana A. Mironova[1], Pavel V. Dorovatovskii[2], Victor N. Khrustalev[2,3], Svetlana E. Solovieva[1,4] and Igor S. Antipin[1,4]

Full Research Paper

Open Access

Address:
[1]Kazan Federal University, 18 Kremlevskaya st., Kazan 420008, Russian Federation, [2]National Research Center "Kurchatov Institute", 1 Ak. Kurchatov Square, Moscow 123182, Russian Federation, [3]Peoples' Friendship University of Russia (RUDN University), 6 Miklukho-Maklay Street, Moscow 117198, Russin Federation and [4]A. E. Arzubov Institute of Organic & Physical Chemistry, 8 Arzubov Street, Kazan 420088, Russian Federation

Email:
Vladimir A. Burilov* - ultrav@bk.ru

* Corresponding author

Keywords:
ADP; amphiphile; ATP; calix[4]arene; CuAAC; eosin Y probe; molecular recognition; polydiacetylene; self-assembly; triazole

Beilstein J. Org. Chem. **2018,** *14,* 1980–1993.
doi:10.3762/bjoc.14.173

Received: 14 April 2018
Accepted: 13 July 2018
Published: 31 July 2018

This article is part of the thematic issue "Macrocyclic and supramolecular chemistry".

Guest Editor: M.-X. Wang

Abstract

The synthesis of new calix[4]arenes adopting a *cone* stereoisomeric form bearing two or four azide fragments on the upper rim and water-soluble triazolyl amphiphilic receptors with two or four polyammonium headgroups via copper-catalyzed azide–alkyne cycloaddition reaction has been performed for the first time. It was found that the synthesized macrocycles form stable aggregates with hydrodynamic diameters between 150–200 nm and electrokinetic potentials about +40 to +60 mV in water solutions. Critical aggregation concentration (CAC) values were measured using a micelle method with pyrene and eosin Y as dye probes. The CAC values of tetraalkyl-substituted macrocycles **12a**,**b** (5 μM for both) are significantly lower than those for dialkyl-substituted macrocycles **10a**,**b** (790 and 160 μM, respectively). Premicellar aggregates of macrocycles **10a**,**b** and **12a**,**b** with the dye eosin Y were used for nucleotides sensing through a dye replacement procedure. It is unusual that disubstituted macrocycles **10a**,**b** bind more effectively a less charged adenosine 5'-diphosphate (ADP) than adenosine 5'-triphosphate (ATP). A simple colorimetric method based on polydiacetylene vesicles decorated with **10b** was elaborated for the naked-eye detection of ADP with a detection limit of 0.5 mM.

Introduction

During the last two decades many researcher groups have paid much attention to the synthesis of host molecules with high affinity to biologically important anions [1-5]. Among these anions, nucleotide recognition and sensing represents an especially important research area due to the great biological significance of these anions. Adenine-containing nucleotides are very important as a universal energy source and as intracellular mediators in many biological processes [6]. In the cellular metabolism, adenosine 5'-triphosphate (ATP) is hydrolyzed to adenosine 5'-monophosphate (AMP) or adenosine 5'-diphosphate (ADP) by enzymes [7]. Thus, the receptors for nucleotides must possess selectivity towards these anions. From this point of view, nucleotide receptors based on polyammonium cations are of great demand because the electrostatic interactions of such polyammonium systems and negatively charged phosphates are strong. Hydrogen bonding [8] and π-stacking interactions between the adenine groups of the nucleotide and the receptor's aromatic moieties [9] can additionally contribute to the complex stability and binding selectivity. Polyammoniums mimic the biologically important acyclic polyamines such as putrescine, spermidine, and spermine, which have strong affinities to AMP, ADP and ATP [10]. Usually polyammonium cation receptors bind the nucleotides according to their negative charge values: ATP > ADP > AMP. It is accompanied with increasing complex stability, which depends on charge–charge interactions between the receptor and the nucleotide. Only a few publications have been reported about receptors that more effectively interact with less charged nucleotides. For instance, Kuchelmeister et al. synthesized a receptor with two symmetric peptide arms decorated with guanidinium-based anion binding sites. This receptor showed a stronger binding of AMP in comparison with ADP and ATP [11]. Another polyammonium receptor synthesized by Mascaros et al. [12] showed selective recognition of ADP in the presence of ATP in water.

Undoubtedly, macrocyclic receptors have a number of advantages in the design of molecular receptors, providing preorganization of the binding sites offering multipoint interactions with a substrate for the effective complexation [13]. Calix[4]arenes and their thia analogues have many advantages over other macrocycles that are frequently used as synthetic receptors, such as cyclodextrins [14], cucurbiturils [15], and pillararenes [16]. Calixarenes are easily functionalized at both their upper and lower rims with various stereoisomers obtainable; the initial macrocycles can be synthesized in a simple manner, they are not toxic, etc. [17-22]. Amphiphilic calixarenes are particularly interesting because they can be regarded as surfactants having a host–guest recognition site [23]. So, they are able to form nanoaggregates in aqueous solutions, thus providing the concentration of the active binding sites into nanoaggregate for multivalent binding with the substrate [24]. We recently synthesized a series of cationic receptors based on the *p-tert*-butylthiacalix[4]arene platform with *1,3-alternate* conformation having polyammonium binding sites. They were shown to effectively interact with calf thymus DNA causing a 4-fold compaction of the latter [25]. Related macrocycles containing two cationic imidazolium fragments demonstrated a high affinity to ATP [26].

Herein we report the synthesis of new amphiphilic water-soluble calix[4]arene derivatives with *cone* conformation containing two or four polyammonium groups on the upper rim by using a click chemistry approach and the results of binding studies toward nucleotides in aqueous solutions.

Results and Discussion

Synthesis of polyammonium calix[4]arene derivatives

The functionalization of calix[4]arenes with azide groups paves the way to introduce a wide variety of functional groups [27] on the upper rim of the macrocycle by, e.g., the copper-catalyzed azide–alkyne cycloaddition (CuAAC) reaction [28]. An alternative way is the functionalization of calix[4]arenes by terminal alkynyl groups. However, in this case further transformations by CuAAC reactions are limited mainly due to the fact that low molecular weight organic azides, especially containing less than 3 carbon atoms are highly explosive [29]. Usually azide groups are installed in the upper rim of the macrocycle by a chloromethylation reaction and subsequent nucleophilic substitution by azide anions [30,31] forming rather flexible azidomethyl fragments. In this investigation more rigid arylazide calixarene derivatives were chosen as precursors for the synthesis of the targeted macrocycles having an enlarged cavity for the effective binding of large biomolecules (Scheme 1).

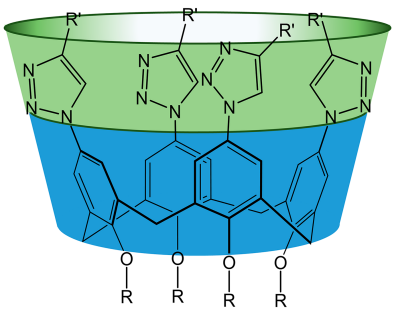

Scheme 1: The general structure of triazolylcalix[4]arene derivatives.

The targeted calixarene diazide derivative **4** and the corresponding tetraazide **8** were synthesized as outlined in Scheme 2. In the first step the complete O-alkylation of the parent *p-tert*-butylcalix[4]arene was performed to give the products **5a**,**b**. To achieve the selective distal alkylation of the macrocycle's lower rim (compounds **1a**,**b**) a microwave approach developed in our group was applied [32]. Then the di- and tetraalkylated products were nitrated according to literature procedures [33,34] affording the di or tetranitro derivatives **2a**,**b** and **6a**,**b** in good yields. The reduction of the nitro groups to the corresponding amines was successfully performed by hydrazine hydrate [35,36]. In this case, Ni on silica/alumina was used as the catalyst instead of pyrophoric Raney nickel. Finally, a diazotization procedure with subsequent azide substitution [37,38] gave calix[4]arene azide derivatives **4** and **8**. For the latter reaction a mixture of DMF/glacial acetic acid 3:1 was found to be the optimal solvent.

The structures of macrocycles **4** and **8** were established by ^{1}H and ^{13}C NMR spectroscopy as well as by IR spectroscopy and MALDI–TOF mass spectrometry. Their compositions were determined by elementary analysis. A standard set of signals typical for distal disubstituted calixarenes was found in the ^{1}H NMR spectra of **4a** and **b** (Supporting Information File 1, Figures S5 and S6): a singlet of OH protons at 8.33–8.37, two singlets of aromatic protons at 6.95–6.96 and 6.69–6.70 ppm, doublets of bridged CH_2 fragments at 4.31–4.32 and 3.31 ppm. In the case of tetraazides **8a**,**b** (Supporting Information File 1, Figures S7 and S8) the signals of the aromatic protons appear as a singlet at 6.29 ppm. The signals of the bridge meth-

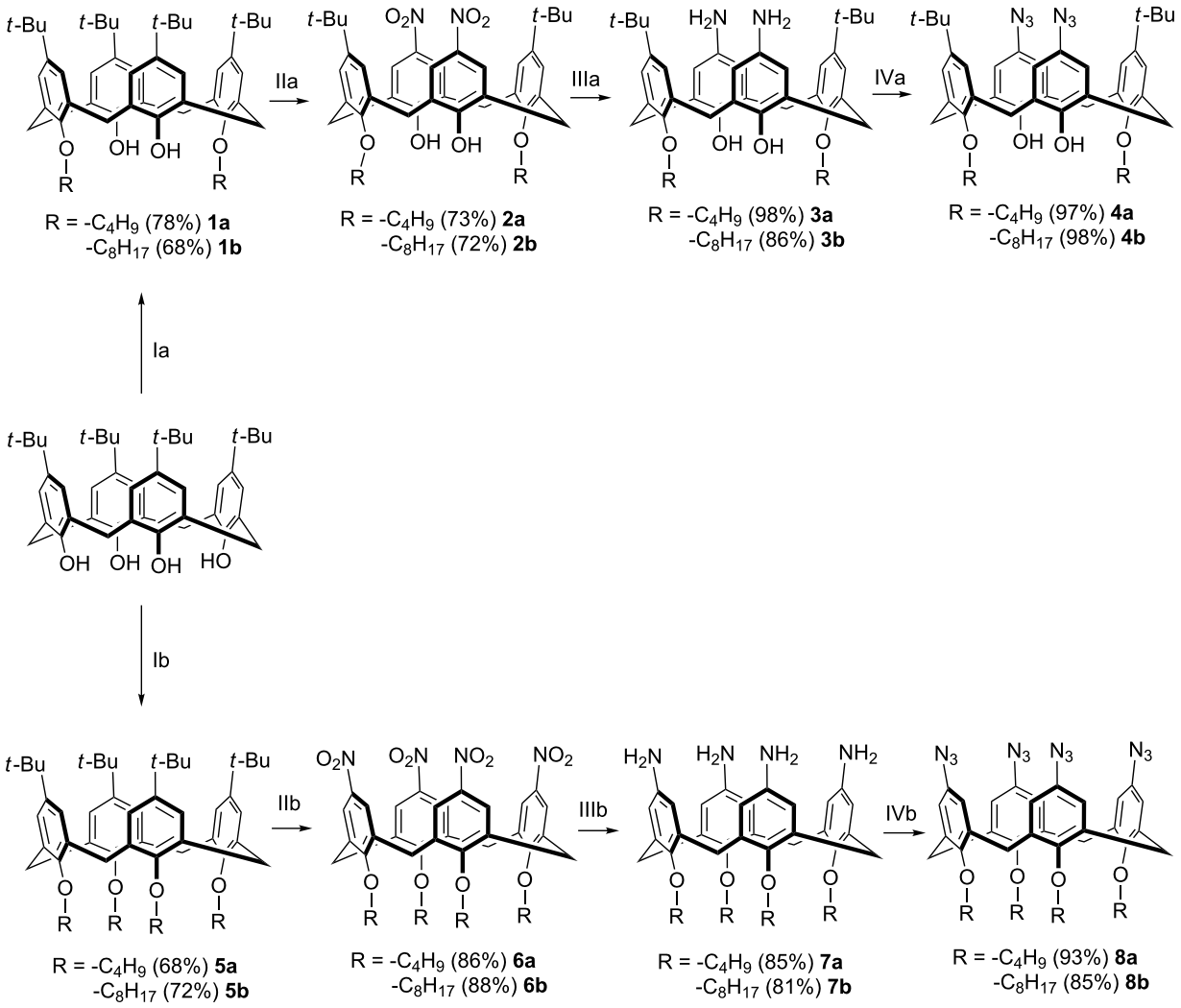

Scheme 2: Synthesis of di- (**4a**,**b**) and tetraazido (**8a**,**b**) calix[4]arene derivatives. Conditions: Ia: AlkBr, K_2CO_3, acetone, 130 °C, MW heating 400 W; IIa: HNO_3, CH_2Cl_2, 0 °C; IIIa: NH_2NH_2, Ni/silica/alumina, EtOH, reflux; IVa: $NaNO_2$, AcOH/DMF, 0 °C, NaN_3; Ib: AlkBr, NaH, DMF, rt; IIb: HNO_3 (100%), AcOH, CH_2Cl_2, 0 °C; IIIb: NH_2NH_2, Ni/silica/alumina, EtOH, reflux; IVb: $NaNO_2$, AcOH/DMF, 0 °C, NaN_3.

ylene protons appear as two doublets at 4.39–4.40 and 3.09–3.10 ppm. The presence of the azide groups was confirmed by valence asymmetric bond vibrations at 2109 cm^{-1} in the IR spectra of **4** and **8**. The MALDI mass spectra of all obtained azides gave molecular ion peaks with expulsion of two (in the case of **4**) or four (in the case of **8**) N_2 fragments due to the lability of the azide group upon laser desorption [39].

The spatial structure of the product **8a** was established by X-ray crystallography and is presented in Figure 1 including the atomic numbering scheme. The full X-ray crystallographic data are provided in Supporting Information File 1. The molecule of **8a** adopts a pinched-cone conformation as evidenced by the differences of the interatomic distances between carbon atoms C3···C17 (4.018 Å) and C10···C24 (10.051 Å). A similar conformation is adopted by calix[4]arenes containing non-bulky substituents at the upper rim [34].

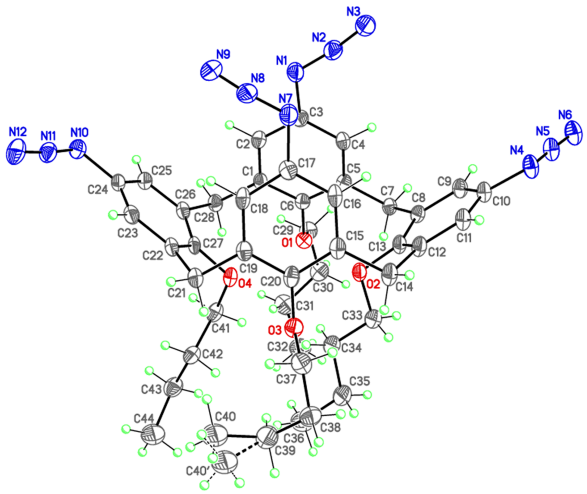

Figure 1: Molecular structure of **8a** (50% ellipsoids). The dashed line indicates the alternative position of the disordered *n*-butyl group with the minor occupancy.

Then, azido compounds **4a**,**b** and **8a**,**b** were subjected to copper-catalyzed reaction with 3-bis[2-(*tert*-butoxycarbonylamino)ethyl]propargylamine (Scheme 3). The syntheses were carried out for 4 hours at 40 °C in toluene and the target BOC-protected products **9a**,**b** and **11a**,**b** were isolated in good yields. The appearance of a new signal of triazole ring protons and a new set of signals of the methylene group protons between the

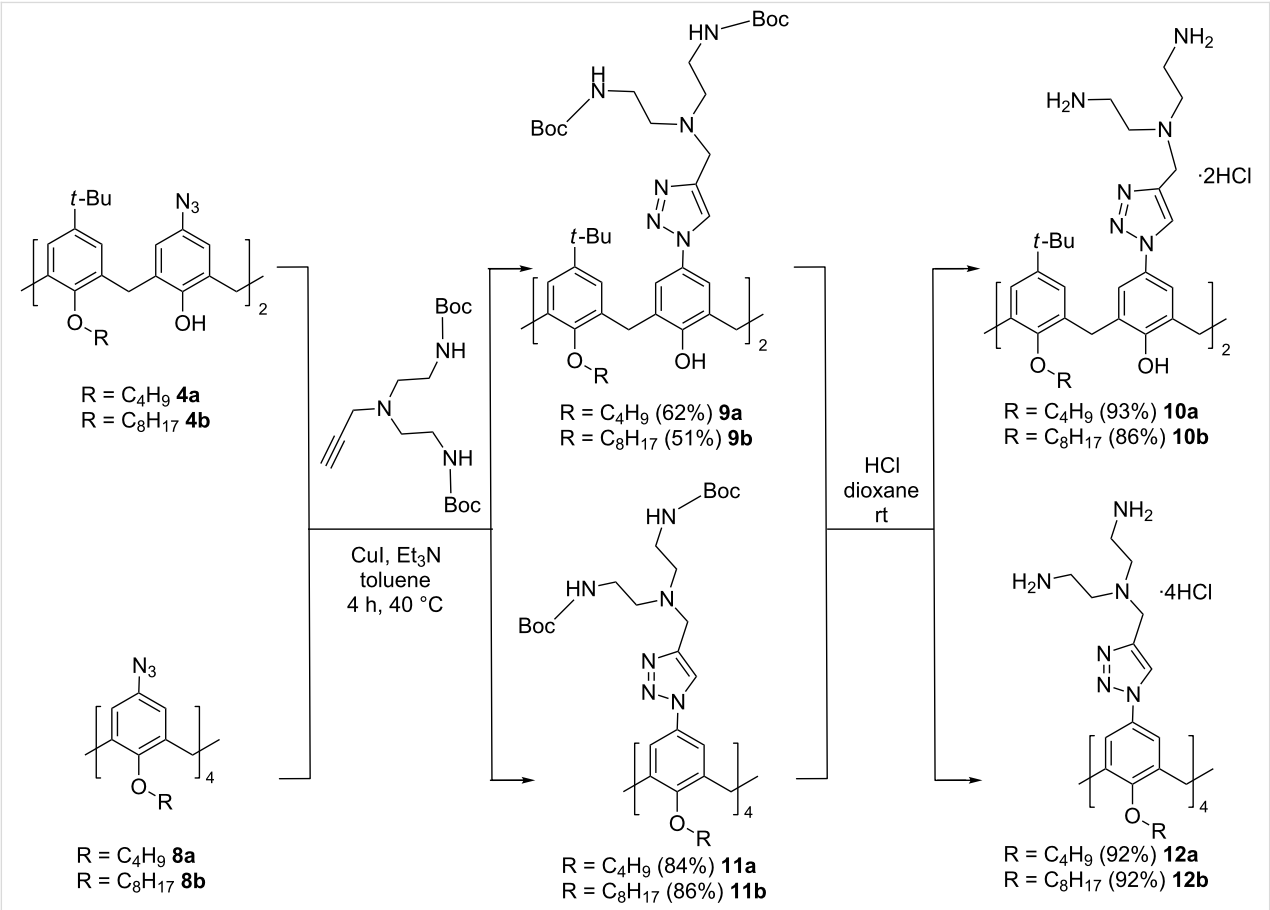

Scheme 3: Synthesis of polyammonium macrocycles **10a**,**b** and **12a**,**b**.

triazole ring and the tertiary nitrogen atom as well as the signals of the ethylene fragments and BOC groups in the ^{1}H NMR spectra fully corresponded to the proposed structures of **9** and **11** (Supporting Information File 1, Figures S9, S10, S13, and S14). The polyamines **10a**,**b** and **12a**,**b** were obtained in high yields after BOC deprotection with HCl in dioxane as water-soluble di- and tetrahydrochlorides, correspondingly.

The structures of the final products were established by 2D ^{1}H-^{1}H NOESY NMR. For example, in the case of macrocycle **10b** (Figure 2) the cross-peaks between signals of neighboring aromatic protons (δ = 7.32 and 7.92 ppm) indicate a cone stereoisomeric form of the macrocycle. Moreover, the observation of cross-peaks between hydroxy protons 4 and the methylene bridge protons 5 and 5', on the one hand, and the methylene protons 6–8 in the octyl chain (δ = 3.98, 3.18 and 2.04 ppm), on the other hand, is also in line with this conclusion. Thus, the 2D NMR data are completely consistent with the proposed structure of **10b**. It should be noted that there are unexpected interactions of *tert*-butyl protons 2 with methylene protons 6 as well as between aromatic protons 1 with hydroxy protons 4 that can be attributed to a strong aggregation of the amphiphilic molecules in the solution.

Aggregation properties of **10a**,**b** and **12a**,**b** in aqueous solutions and binding with nucleotides

All synthesized derivatives **10a**,**b** and **12a**,**b** are well soluble in water/MES buffered solutions. We used the determination of the critical aggregation concentration (CAC) to elucidate the compounds' aggregation behavior. This was performed by the dye micellization method using pyrene and eosin Y (EY) as fluorescent and spectrophotometric probes, respectively (Table 1). The nonpolar pyrene can be incorporated into hydrophobic domains of the aggregates due to hydrophobic interac-

Table 1: CAC values determined by dye (pyrene and EY) micellization method.[a]

macrocycle	CAC, μM	
	EY	pyrene
10a	6.4	790
10b	4.8	160
12a	4.5	5.0
12b	2.8	5.0

[a]Concentration (EY) = 10 μM; concentration (pyrene) = 5 μM.

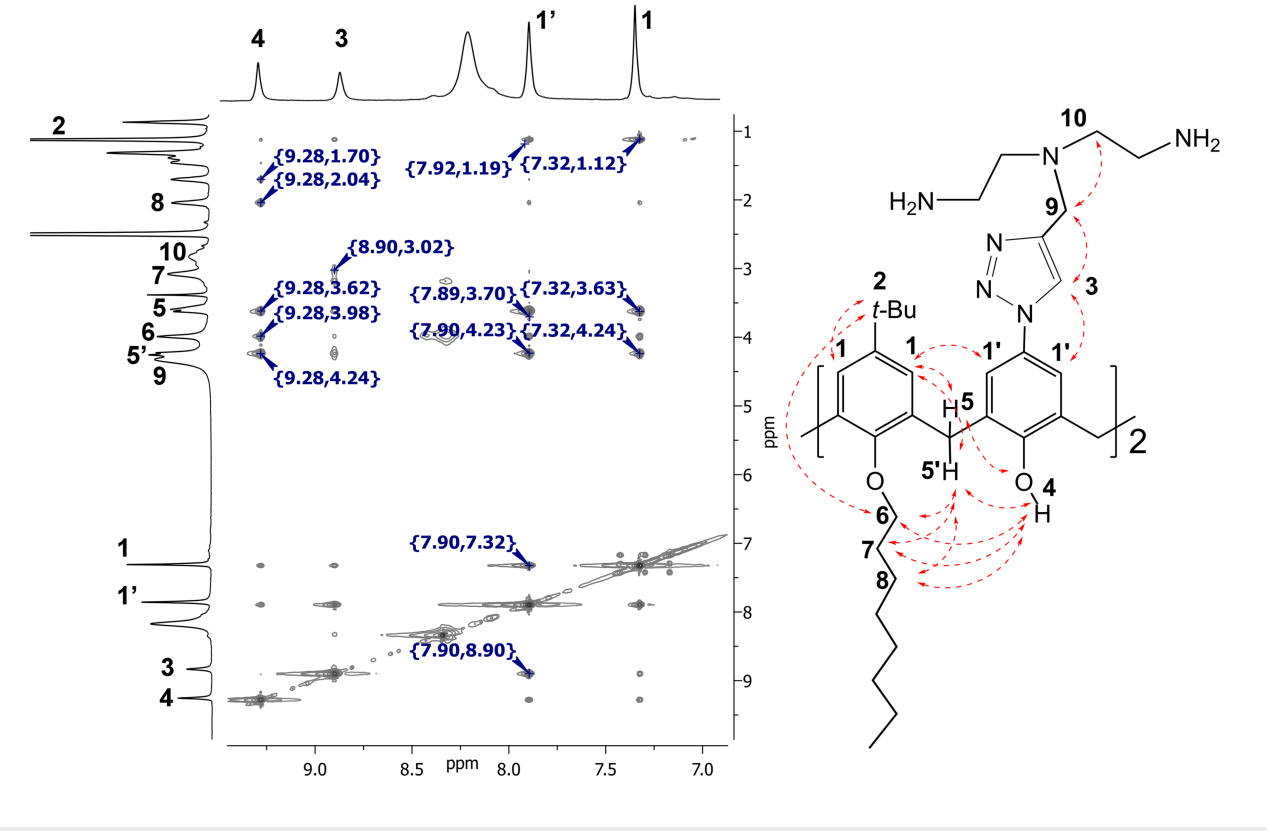

Figure 2: 2D NOESY H^1-H^1 NMR spectra of **10b** in DMSO-d_6.

tions. Pyrene insertion is measured by analyzing the ratio of the intensities of the first and third bands (373 and 384 nm, respectively) in its emission spectrum [40]. EY, an anionic xanthene dye, also can be used for CAC determination as its absorption spectrum shows a shift of the maximum absorption wavelength (λ_{max}) in the presence of micelles or vesicles [41]. The inflection point in the plot of EY λ_{max} vs surfactant concentration should be treated as the CAC of the amphiphile [42].

As can be seen from Table 1 the CAC values determined by the two methods are significantly different, especially in the case of macrocycles **10a**,**b**. These differences are assigned to the different natures of the used dyes. In the case of EY, which is a dianion at pH 7, the interaction with the dicationic calixarenes **10a**,**b** results in the formation of a non-charged complex, which can be referred to a non-ionic surfactant. Generally, non-ionic surfactants possess lower CACs than ionic ones owing to the lack of electrostatic repulsions between head groups [43]. In the case of pyrene there is no charge compensation and interactions occur exclusively with hydrophobic domains of the aggregates. Thus, using pyrene reveals the real CAC value, while with EY the CAC value corresponds to the dye–calixarene complex. In the case of **12a**,**b** the differences of CAC values determined by EY and pyrene are not significant. Obviously, in this case EY does not form a neutral dye–calixarene complex due to the increased number of ionized groups in the tetrasubstituted calixarene. However, it is worth paying attention to the extremely large difference between the CAC (pyrene) values of **10a** and **12a** as well as **10b** and **12b**. It can be caused by strong hydrophobic intermolecular interactions of **12a**,**b**, which leads to the formation of aggregates at substantially lower concentrations as compared with the less hydrophobic **10a**,**b**. A similar trend (decrease of about two orders) was observed for the CAC of gemini surfactants possessing two hydrophobic alkyl tails in comparison with ordinary ones having one alkyl tail [44].

Additionally, the aggregation properties were investigated by dynamic (DLS) and electrophoretic (ELS) light scattering methods and the obtained results are collected in Table 2. Both di- and tetrasubstituted macrocycles do form nanoparticles in aqueous solution with hydrodynamic diameters within the range of 150–200 nm. The electrokinetic potential of the aggregates corresponds to the positive charge of the calixarene headgroups and is about +40 to +60 mV which indicates the formation of stable colloids. The addition of negatively charged EY to **10a**,**b** reduces the electrokinetic potential practically up to the isoelectric point. This confirmed the abovementioned conclusion concerning the formation of a non-charged complex as a reason of low CAC values measured by EY as the probe. A similar behavior also was observed for the tetrasubstituted derivatives **12a**,**b**.

Recently, we reported receptor systems for sulfonate surfactants [45] and ATF [26], based on an EY competitive displacement from aggregates, decorated by positive charged thiacalixarene macrocycles. This approach was used for macrocycles **10a**,**b** and **12a**,**b** as well. Primarily, the fundamental regularities of dye complexation with **10a**,**b** and **12a**,**b** were studied in detail. The stoichiometry of the EY–calixarene complexes was determined by the isomolar series method at two concentrations: below and above the CAC values, measured with EY as the probe (Table 3).

At concentrations below the CAC (1 μM), the monomeric molecules of the macrocycles **10a**,**b** form with EY a discrete 1:1 host–guest complex [X^{2-}calix^{2+}], where X^{2-} and calix^{2+} represent the dye and calixarene ions, respectively. By increasing the concentration to values above the CAC complexes with 3:2 stoichiometry are observed. This indicates that the interaction of forming aggregates with EY relies on both electrostatic interactions with positively charged headgroups and hydro-

Table 2: DLS and ELS data of aggregates formed by macrocycles **10** and **12**.[a]

entry	system	*d* [nm]	PDI	ζ [mV]
1	**10a**	194 ± 3	0.385 ± 0.17	+50 ± 4
2	**10b**	153 ± 18	0.419 ± 0.06	+42 ± 13
3	**12a**	176 ± 11	0.244 ± 0.04	+43 ± 6
4	**12b**	140 ± 54	0.443 ± 0.01	+64 ± 8
5	**10a** + EY	157 ± 2	0.500 ± 0,06	+14 ± 5
6	**10b** + EY	208 ± 9	0.327 ± 0.01	+6 ± 2
7	**12a** + EY	99 ± 1	0.314 ± 0.04	+24 ± 4
8	**12b** + EY	202 ± 5	0.364 ± 0.06	+14 ± 7
9	**10b** + EY + ADP	164 ± 7	0,412 ± 0,07	−6 ± 2
10	**10b** + EY + ATP	256 ± 43	0,619 ± 0,09	−20 ± 9

[a]All measurements were done in 50 mM MES buffer at pH 6.5; concentration (calixarene) = 10 μM, concentration (EY) = 10 μM (**10a**,**b**) or 20 μM (**12a**,**b**).

Table 3: Stoichiometry of the EY–calixarene complexes.[a]

calixarene	dye/calixarene ratio[b]	dye/calixarene ratio[c]
10a	1:1	3:2
10b	1:1	3:2
12a	2:1	7:3
12b	2:1	4:1

[a]All measurements were done in 50 mM MES buffer at pH 6.5; [b]at total concentration = 1 μM; [c]at total concentration = 50 μM.

phobic interactions with hydrophobic regions of calixarene aggregates that are typical for xanthene dyes [41]. The length of the alkyl chains in **10a**,**b** does not affect the complex stoichiometry.

Compounds **12a**,**b** at concentrations below the CAC form dye–calixarene complexes of 2:1 stoichiometry [$(X^{2-})_2$calix^{4+}]. As in the previous case the aggregation (concentration above the CAC) leads to a change in stoichiometry with 7:3 for the less lipophilic compound **12a** and 4:1 for **12b**. Thus, the presence of four alkyl substituents on the calixarene platform significantly influences the solubilizing capacity of the macrocycles with respect to EY.

To create a receptor system based on the dye displacement in an amphiphilic host molecule/aggregate, an optimal concentration of the amphiphilic molecule should be precisely established. First, the greatest changes in the dye spectrum should be observed at this concentration. Second, the dye should not be fully absorbed in the hydrophobic domain of an aggregate to be easily released into solution after any changes that occur with the molecule/aggregate. In this context premicellar aggregates are good candidates to design supramolecular systems for recognition and sensing purposes.

Thereby, premicellar concentrations of calixarenes **10a**,**b** (6 and 4 μM, respectively) and **12a**,**b** (4 and 2 μM, respectively) were selected to design a receptor system based on the principle of competitive EY displacement by the guests. At these concentrations, a bathochromic shift accompanied by hypochromic effect in the EY absorption spectrum (Supporting Information File 1, Figure S1) is observed in addition to a change of the environment polarity due to the dye embedding into the hydrophobic domain of the premicellar aggregates [46]. The absorbance spectra of the ternary system calixarene/EY/guest have been recorded in aqueous buffer solutions and a series of nucleotides (AMP, ADP and ATP) as guests for the competitive EY displacement were tested.

It was found that the addition of increasing concentrations of ADP or ATP resulted in significant changes of the calixarene/EY absorption spectra and finally practically corresponded to free EY (Supporting Information File 1, Figure S2). This clearly indicates a dye release from the calixarene aggregates into the solution. For better visualization, the optical response (OR) of the calixarene/EY system was calculated according to the Equation 1:

$$\mathrm{OR} = 100*[1-((A_{\mathrm{EY}}-A_1)*(\lambda_1-\lambda_{\mathrm{EY}}))/((A_{\mathrm{EY}}-A_0)*(\lambda_0-\lambda_{\mathrm{EY}}))]\%, \quad (1)$$

where A_{EY} is the free EY absorption intensity, A_1 and A_0 are the absorption intensities of the calixarene/EY system in the presence and absence of the guest, respectively. λ_{EY} is the wavelength of EY absorption maximum, λ_1 and λ_0 are the wavelengths of the absorption maxima of calixarene/EY spectra in the presence and absence of the guest, respectively.

In contrast to ADP and ATP, AMP had no effect on the optical response that can be explained by weak interactions of the monoanionic nucleotide with the di- and tetracationic calixarenes (Figure 3). Obviously, AMP does not effectively interact with the two distally located binding sites of the calixarenes and is not able to expel the dianionic dye from the aggregates. A quite different picture is observed for ADP and ATP, which are present in the dianionic and trianionic form at pH 6.5 [12].

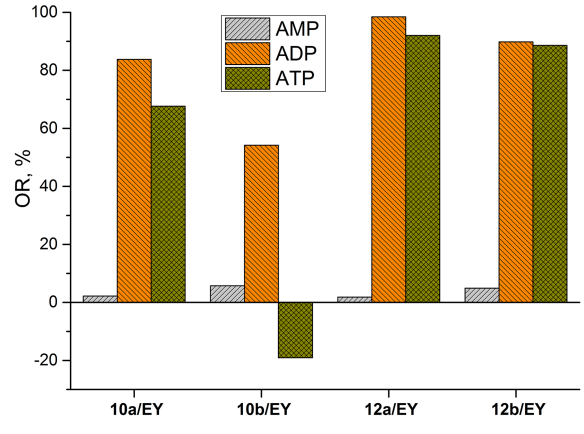

Figure 3: The optical response (OR) of the calixarene/EY systems toward adenosine phosphates. Concentration (EY) = 5 μM, concentration (**10a**) = 4 μM, concentration (**10b**) = 6 μM, concentration (**12a**) = 4 μM, concentration (**12b**) = 2 μM, concentration (adenosine phosphate) = 2 mM, concentration (MES) = 50 mM (pH 6.5).

To estimate the ATP/ADP binding selectivity with the positively charged macrocycles a quantum chemical study of the **10a**

complexes with ATP and ADP has been carried out. For calculations, the Gaussian 09 program with the DFT/B3LYP method based on the 6-311g basis set with CPCM solvation model with water as the solvent was used [47]. The energy of complex formation was calculated as a difference between free energy of calix[4]arene + ADP/ATP complex and isolated calix[4]arene and ADP/ATP dianion. The complex structures corresponding to the minimum energy as well as supramolecular binding motif of ADP and ATP are presented in Figure 4. As can be seen ADP more effectively embeds into the molecular cleft formed by two ammonium moieties due to a good host–guest geometric size and/or shape complementarity (Figure 4a and c). The three phosphate groups of ATP have a larger size and cannot realize a similar supramolecular motif in the complex. For this reason the triphosphate fragment is rotated by ≈60° around the calixarene axis relative to the diphosphate position (Figure 4b and d). This leads to a weakening of the host–guest binding and to a decrease of ATP complex energy by 1.4 kcal/mol compared to ADP. So the ADP/ATP optical responses for macrocycles **10a**, **12a**,**b** (Figure 3) can be rationalized in terms of the binding properties of the investigated nucleotides. Moreover, the presence of intramolecular hydrogen bonding (Figure 4a and b) can explain the protonation of only one nitrogen atom despite the close protonation constants of both primary amino groups in the ethylenediamine fragment (pK_2 = 9.08 and pK_3 = 9.97 for the diethylenetriamine conjugated acid [48]). Thus, stabilization of the monocationic form prevents the formation of a dicationic species.

The premicellar aggregates of the lipophilic dicationic macrocycle **10b** demonstrate a significant difference of optical response on the presence of ADP and ATP in the solution. Generally, there are two pathways of dye release upon decomplexation: (i) into the buffer solution or (ii) into the aggregate

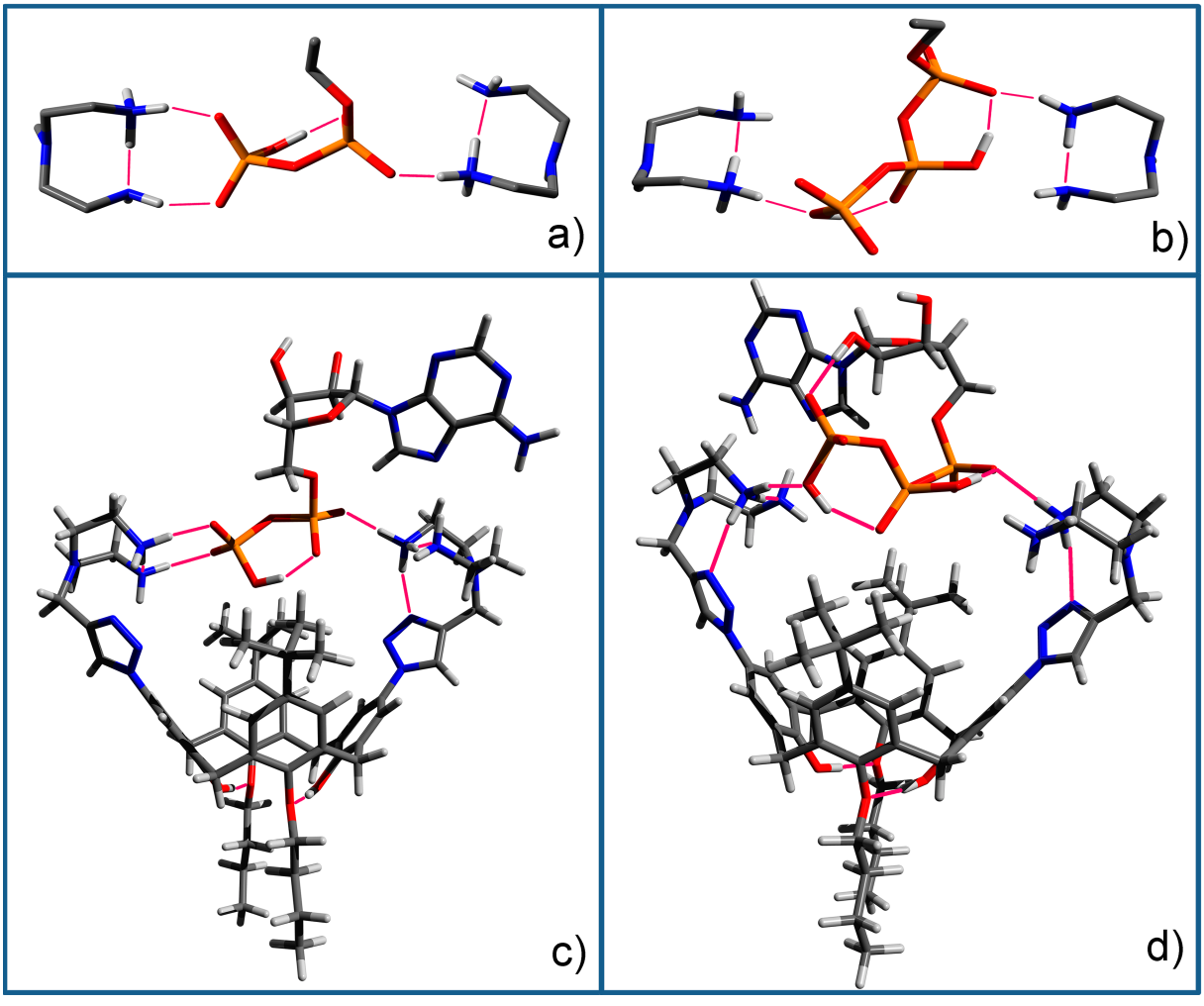

Figure 4: Supramolecular binding motif of diphosphate (a) and triphosphate (b) groups of nucleotides with the protonated diethylenetriamine substituents of the calixarene (ribose and adenine fragments are omitted for clarity) and optimized complex structure of **10a** with ADP (c) and ATP (d) according to DFT calculations.

lipophilic domain. However, predominance of each way depends on many factors, such as packaging density of aggregates and their general lipophilicity. To reveal this, absorbance spectra of the **10b**–EY system in the presence of ADP and ATP were recorded (Figure 5a and b).

The addition of small amounts of nucleotides leads to a bathochromic shift of the EY adsorption due to a deeper penetration of EY molecules into the hydrophobic domain of the aggregates and a corresponding decrease of the environment's polarity (curve 4, Figure 5a). Thus, after decomplexation the EY molecules primarily concentrate inside the aggregate. A hypsochromic shift in the EY spectra pointing to the dye's release from the aggregates into the solution (curve 6, Figure 5a) is observed at excess concentrations of the nucleotides. However, ADP and ATP cause different changes in the EY spectra. Excess ADP causes release of the dye from the aggregates and appearance of free EY absorption at 516 nm (curve 6, Figure 5a) whereas the dye remains inside the aggregates in the presence of excess ATP (Figure 5b). It is important to note that no EY relocation into the aggregate hydrophobic domain is observed for the less lipophilic calixarene **10a** (Supporting Information File 1, Figure S2a and b).

The interaction of the dicationic calixarene **10b** with ADP results in an uncharged complex, which can be referred to a non-ionic surfactant. At the same time, binding of **10b** with ATP affords a negatively charged complex (Table 2, entries 9 and 10). Obviously the formation of the uncharged complex of **10b** with ADP increases the density of the aggregates through a reduction of repulsion between headgroups [43] thus leading to a dye release from the hydrophobic domain of the aggregates into the buffer solution. Whereas the binding with ATP does not greatly affect the aggregate packing and the dye remains in the hydrophobic core of the aggregate. Therefore, a different packing of aggregates is the main reason for the observed ADP/ATP selectivity of calixarene **10b**.

Polydiacetylene–**10b** vesicles for ADP/ATP sensing

Polydiacetylenes (PDAs), alternating ene-yne conjugated molecules, induce a blue-to-red color transition by the distortion of their backbone. They can be easily prepared through photopolymerization of supramolecularly assembled diacetylenes [49]. The functionalization of a PDA matrix with appropriate receptor fragments offers the possibility to sense various analytes by naked-eye detection. Noncovalent doping of diacetylene surfactant matrix by amphiphilic receptors with subsequent photopolymerization is a commonly used approach for the design of colorimetric analytical devices [50]. Taking into account the cationic nature of the synthesized calixarene macrocycles, the amido-diacetylene lipid bearing a terminal amino group *N*-(2-aminoethyl)pentacosa-10,12-diynamide (AEPCDA) was applied for the formation of the PDA matrix (Scheme 4). The synthesis of AEPCDA was carried out from 10,12-pentacosadiynoic acid according to the literature method [51].

AEPCDA vesicles containing calixarene **10b** were produced by the well-known film hydration method. To identify an optimal calixarene–AEPCDA ratio a series of PDA vesicles containing 1, 5, 10, 50 mol % of **10b** was prepared. Polymerization of AEPCDA–calixarene vesicles was performed under UV irradiation using 254 nm light in quartz cuvettes of 1 cm path length. The absorbance peak at 674 nm, corresponding to the blue form of the polymer, reached its maximum after 15 minutes of irradiation. It was found that the calixarene **10b** itself acted as stabi-

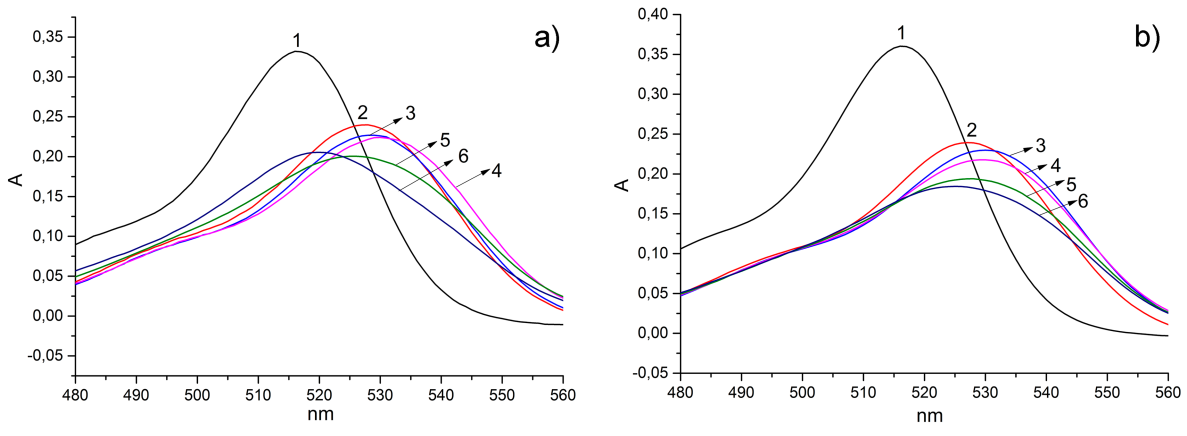

Figure 5: UV spectra of EY (1), **10b**–EY (2), and **10b**–EY in the presence of 0.005 (3), 0.05 (4), 0.5 (5) and 2 (6) mM of ADP (a) or ATP (b). Concentration (EY) = 5 μM, concentration (**10b**) = 6 μM, concentration (MES) = 50 mM (pH 6.5).

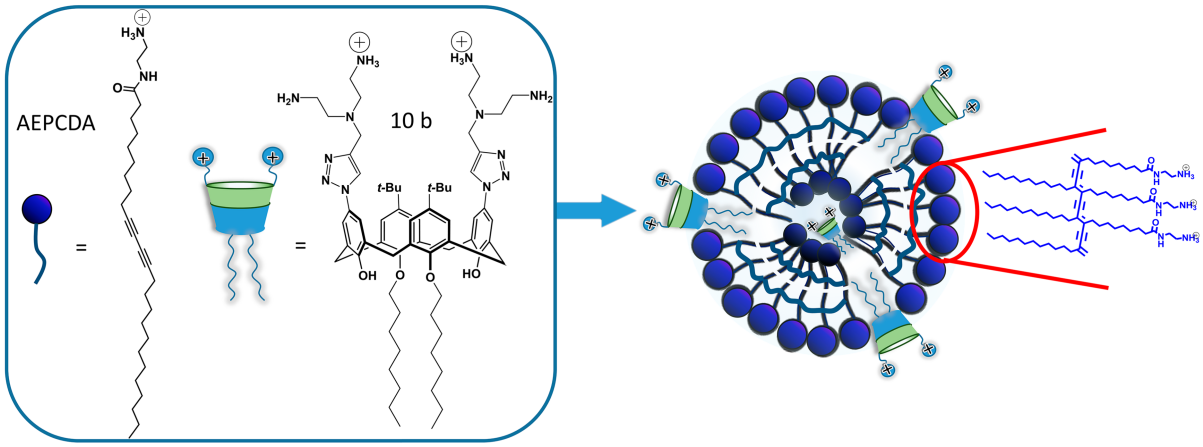

Scheme 4: Structure of AEPDA and the corresponding AEPCDA–**10b** polydiacetylene vesicle.

lizer for AEPCDA vesicles: a hyperchromic effect upon the addition of calixarene up to 50 mol % was observed (Figure 6).

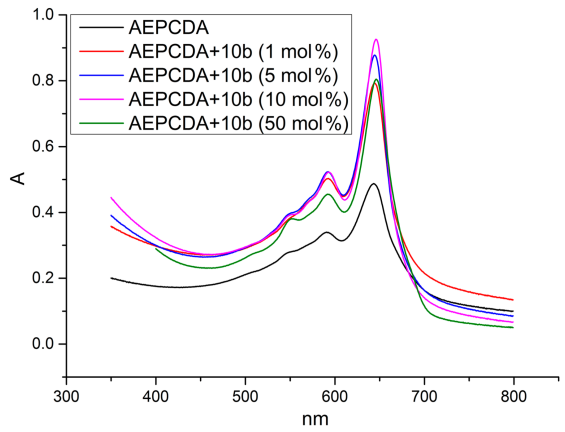

Figure 6: UV spectra of the AEPCDA polydiacetylene vesicles in the presence of different amounts of **10b**; concentration (AEPCDA) = 0.2 mM, concentration (**10b**) = 0.002–0.1 mM in 10 mM MES buffer, pH 6.5.

This means that the addition of the non-polymerizable calixarene **10b** to AEPCDA results in an increase of the diacetylene photopolymerization degree. This effect is quite unusual and can be associated with the change of the vesicles packing upon the addition of **10b** and the formation of higher organized nanostructures. DLS data confirmed this suggestion. In the presence of **10b** the size of polydiacetylene vesicles sharply decreases (Table 4 and Supporting Information File 1, Figure S3). This leads to an optimal distance between the diacetylene fragments resulting in a more effective photopolymerization.

Table 4: DLS and ELS data for AEPCDA–**10b** polydiacetylene vesicles in the presence/absence of ADP/ATP.[a]

system	*d*, nm	PDI	ζ, mV
AEPCDA	402 ± 109	0.530 ± 0.08	+45 ± 6
AEPCDA + **10b**	94 ± 1	0.175 ± 0.01	+47 ± 4

[a]All measurements were carried out in 50 mM MES buffer at pH 6.5; concentration (AEPCDA) = 0.2 mM, concentration (**10b**) = 0.1 mM, concentration (nucleotide) = 0.5 mM in 10 mM MES buffer, pH 6.5.

The obtained AEPCDA vesicles containing 50 mol % of **10b** were used for the colorimetric recognition of ADP and ATP. The values of colorimetric response (CR) of the AEPCDA–**10b** vesicles were calculated according to Equation 2 [52], which characterize the conversion to the red phase in percent:

$$CR = [PB_0 - PB_1] / PB_0 * 100\%, \quad (2)$$

where PB_1 and PB_0 is the percent of the blue form in the presence and the absence of the analyte and is defined as follows (Equation 3):

$$PB = A_{blue} / [A_{blue} + A_{red}] * 100\%, \quad (3)$$

where A_{blue} is the absorbance at 640 nm and A_{red} is the absorbance at 540 nm.

According to the obtained data (Figure 7) AEPCDA–**10b** vesicles exhibit a colorimetric response toward ADP starting at 0.25 mM of the latter, while there is no response to ATP in this concentration range. Moreover, the response toward ADP can be detected with the naked eye beginning at ADP concentrations as low as 0.5 mM.

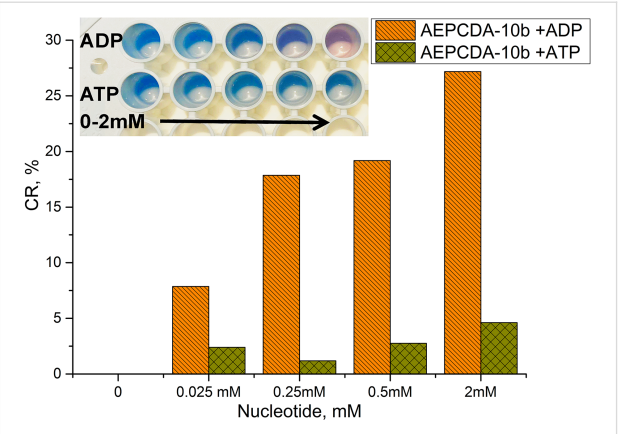

Figure 7: Photographs of a portion of a 96-well plate containing AEPCDA–**10b** polydiacetylene vesicles in the absence (first hole from left) or presence of ADP or ATP; concentration (AEPCDA) = 0.2 mM, concentration (**10b**) = 0.1 mM (a) concentration (nucleotide) = 0.025, 0.25, 0.5, 2 mM in 10 mM MES buffer, pH 6.5.

Thus, the mechanism of the colorimetric response of **10b**-decorated AEPCDA polydiacetylene vesicles upon binding to ADP can be a result of a complexation-induced distortion of the calixarene cavity provoking thus perturbation of the PDA backbone.

Conclusion

For the first time new calix[4]arenes adopting a *cone* stereoisomeric form bearing two or four azide groups directly located at the macrocycles' aromatic rings have been synthesized and used for the preparation of water-soluble triazolyl amphiphilic receptors with two or four polyammonium headgroups by CuAAC reaction with 3-bis[2-(*tert*-butoxycarbonylamino)ethyl]-propargylamine. These macrocycles form stable aggregates in aqueous solutions with average hydrodynamic diameters of 150–200 nm and electrokinetic potentials about +40 to +60 mV. CAC values measured by the dye micellization method with pyrene and eosin Y (EY) as dye probes were used to identify optimal concentration conditions for the design of supramolecular architectures for the recognition and sensing based on the principle of competitive EY displacement by adenine-containing nucleotides. The incorporation of **10b** into a polydiacetylene matrix allowed to create covalently bonded vesicles for the selective detection of ADP.

Experimental

Material and methods

All reagents were purchased from either Acros or Sigma-Aldrich and were used without further purification. Solvents were purified according to standard methods [53]. 3-Bis[2-(*tert*-butoxycarbonylamino)ethyl]propargylamine [54], **1a** (5,11,17,23-tetra-*tert*-butyl-25,27-dibutoxy-26,28-dihydroxycalix[4]arene) [32]; **2a** (5,17-di-*tert*-butyl-11,23-dinitro-25,27-dibutoxy-26,28-dihydroxycalix[4]arene) [33], **3a** (5,17-di-*tert*-butyl-11,23-diamino-25,27-dibutoxy-26,28-dihydroxycalix[4]-arene) [33], **1b** (5,11,17,23-tetra-*tert*-butyl-25,27-dioctyloxy-26,28-dihydroxycalix[4]arene) [34], **2b** (5,17-di-*tert*-butyl-11,23-dinitro-25,27-dioctyloxy-26,28-dihydroxycalix[4]arene) [34], as well as **5a** (5,11,17,23-tetra-*tert*-butyl-25,26,27,28-tetrabutoxycalix[4]arene) [36], **6a** (5,11,17,23-tetranitro-25,26,27,28-tetrabutoxycalix[4]arene) [36], **7a** (5,11,17,23-tetraamino-25,26,27,28-tetrabutoxycalix[4]arene) [35] and **5b** (5,11,17,23-tetra-*tert*-butyl-25,26,27,28-tetraoctyloxycalix[4]-arene) [35], **6b** (5,11,17,23-tetranitro-25,26,27,28-tetraoctyl-oxycalix[4]arene) [35], **7b** (5,11,17,23-tetraamino-25,26,27,28-tetraoctyloxycalix[4]arene) [36] and *N*-(2-aminoethyl)penta-cosa-10,12-diynamide [50] were prepared following literature procedures. TLC was performed on Merck UV 254 plates with Vilber Lourmat VL-6.LC UV lamp (254 nm) control. Elemental analysis of the synthesized compounds was done on a PerkinElmer PE 2400 CHNS/O Elemental Analyzer. NMR spectra were recorded on a Bruker Avance 400 Nanobay with signals from residual protons of deuterated solvents ($CDCl_3$ or DMSO-d_6) as internal standard. MALDI mass spectra were measured on an UltraFlex III TOF/TOF with PNA matrix, laser Nd:YAG, λ = 355 nm. The IR spectra were recorded on a Bruker Vector-22 spectrometer. Samples were prepared as suspension in mineral oil or as thin films, obtained from chloroform solutions dried on the surface of the KBr disc. Melting points were measured using a Stuart SMP10 apparatus.

UV–vis absorbance spectra

The UV–vis-spectra were recorded on a Lambda 35 UV/VIS spectrophotometer (Perkin Elmer Instruments) in an optical cell with 1.0 cm light pass at 298 K.

Dynamic light scattering (DLS) measurements

Dynamic light scattering (DLS) experiments and zeta-potential measurements (ELS) were carried out on a Zetasizer Nano ZS instrument (Malvern Instruments, USA) with 4 mW 633 nm He–Ne laser light source and a light scattering angle of 173°. The data were treated with DTS software (Dispersion Technology Software 5.00). The solutions were filtered through Millex HV 0.45 μM filter before the measurements to remove dust. The experiments were carried out in the disposable plastic cells DTS 0012 (Sigma-Aldrich, USA) at 298 K with at least three experiments for each system. Statistical data treatment was done using t-Student coefficient and the particle size determination error was <2%. The prepared samples were ultrasonicated for 30 min at 25 °C before measurements.

Fluorescence spectroscopy

Fluorescence experiments were performed in 1.0 cm quartz cuvettes and recorded on a Fluorolog FL-221 spectrofluo-

rimeter (HORIBA Jobin Yvon) in the range of 350 to 430 nm at excitation wavelength 335 nm with 2.5 nm slit for the pyrene. All studies were carried out in buffered aqueous solution (MES buffer, pH 6.5) at 298 K.

X-ray data

The crystal of **8a** ($C_{44}H_{52}N_{12}O_4$, M = 812.98) is monoclinic, space group $P2_1/n$, at T = 100 K: a = 15.003(3) Å, b = 19.652(4) Å, c = 15.368(3) Å, β = 104.71(3)°, V = 4382.6(16) Å^3, Z = 4, d_{calcd} = 1.232 g/cm^3, F(000) = 1728, μ = 0.172 mm^{-1}. X-ray diffraction data were collected at the 'Belok' beamline (λ = 0.96990 Å) of the National Research Center 'Kurchatov Institute' (Moscow, Russian Federation) using a Rayonix SX-165 CCD detector. A total of 720 images (33746 reflections, 8078 independent reflections, R_{int} = 0.0882) were collected with an oscillation range of 1.0° (φ scan mode, $2\theta_{max}$ = 72.0°) using two different orientations for the crystal. The semiempirical correction for absorption was applied using the *Scala* program (T_{min} = 0.950; T_{max} = 0.980) [55]. The data were indexed, integrated and scaled using the utility *iMOSFLM* implemented in the CCP4 program [56,57]. The structure was solved by intrinsic phasing modification of direct methods [58] and refined by full-matrix least squares technique on F^2 with anisotropic displacement parameters for non-hydrogen atoms. One of the four *n*-butyl groups is disordered over two sites with the occupancies of 0.6:0.4. The hydrogen atoms were placed in calculated positions and refined within riding model with fixed isotropic displacement parameters [U_{iso}(H) = 1.5U_{eq}(C) for the CH_3-groups and 1.2U_{eq}(C) for the other groups]. The final divergence factors were R_1 = 0.0949 for 5301 independent reflections with $I > 2\sigma(I)$ and wR_2 = 0.2482 for all independent reflections, S = 0.941. The calculations were carried out using the SHELXTL program [59]. Crystallographic data for **1** have been deposited with the Cambridge Crystallographic Data Center, CCDC 1831063. Copies of this information may be obtained free of charge from the Director, CCDC, 12 Union Road, Cambridge CB2 1EZ, UK (fax: +44 1223 336033; e-mail: deposit@ccdc.cam.ac.uk or http://www.ccdc.cam.ac.uk).

Vesicle preparation and polymerization procedure

In a similar manner as described before [22], concentrated dichloromethane solutions of *N*-(2-aminoethyl)pentacosa-10,12-diynamide (AEPCDA) and the appropriate amounts of calixarene were mixed together and the organic solvent was removed by expulsion with N_2 at room temperature to give a thin lipid film on the glass surface, which was dried under reduced pressure (0.01 Torr) for 2 h to remove all traces of organic solvent. Then a buffer solution (MES, 50 mM, pH 6.5) was added. The samples were then sonicated for 2 h at 60 °C. The resulting vesicle solution was filtered through a 1.2 μm filter and kept at 4 °C for 12 h. Polymerization was carried out by irradiating the solutions with 254 nm UV light (1 mW/cm^2) for 15 min under vigorous stirring in 10 mm quartz cuvettes, placed in a thermostat holder at 25 °C.

Quantum chemical calculations

Quantum chemical calculations were done in several steps: selection of optimal conformers; organization of initial complex geometry; complex optimization procedure. The conformers search procedure has been done only for calix[4]arene's triazolyl substituents due to complexity of the whole molecule. Conformers of calix[4]arene substituents and ATP/ADP were generated with cxcalc plug-in (ChemAxon, ChemAxon Jchem https://chemaxon.com/download/jchem-suite) using MMF94 force field, followed by the duplicates discard using in house tool and geometry optimization with PM7 [60] semi-empirical method implemented in the MOPAC 2016 program [61] with discard of repeated duplicates. Then unique conformers were combined with calix[4]arene core, and corresponding cations and complexes with ATP/ADP were optimized by DFT calculations. For DFT calculations Priroda 16 program [62] with build-in PBE functional on L2 basis level [63] was used. Then optimized structures were calculated using DFT calculations with CPCM model of solvation in water with Gaussian 09 program [47] with B3LYP functional on 6-311g basis level.

Supporting Information

Supporting Information File 1

Synthetic procedures, characterization data and copies of spectra.
[https://www.beilstein-journals.org/bjoc/content/supplementary/1860-5397-14-173-S1.pdf]

Acknowledgements

We thank the Russian Science Foundation for the financial support of this work (grant No. 14-13-01151).

ORCID® iDs

Vladimir A. Burilov - https://orcid.org/0000-0001-7089-3340
Guzaliya A. Fatikhova - https://orcid.org/0000-0001-5910-3547
Ramil I. Nugmanov - https://orcid.org/0000-0002-8541-9681
Diana A. Mironova - https://orcid.org/0000-0003-1943-3300
Victor N. Khrustalev - https://orcid.org/0000-0001-8806-2975
Svetlana E. Solovieva - https://orcid.org/0000-0001-7106-6777
Igor S. Antipin - https://orcid.org/0000-0002-9882-7035

References

1. Ngo, H. T.; Liu, X.; Jolliffe, K. A. *Chem. Soc. Rev.* **2012,** *41,* 4928–4965. doi:10.1039/C2CS35087D

2. García-España, E.; Díaz, P.; Llinares, J. M.; Bianchi, A. *Coord. Chem. Rev.* **2006,** *250,* 2952–2986. doi:10.1016/j.ccr.2006.05.018
3. Li, A.-F.; Wang, J.-H.; Wang, F.; Jiang, Y.-B. *Chem. Soc. Rev.* **2010,** *39,* 3729–3745. doi:10.1039/b926160p
4. Zhou, Y.; Xu, Z.; Yoon, Y. *Chem. Soc. Rev.* **2011,** *40,* 2222–2235. doi:10.1039/c0cs00169d
5. Ng, S.; Lim, H. S.; Ma, Q.; Gao, Z. *Theranostics* **2016,** *6,* 1683–1702. doi:10.7150/thno.15850
6. Liemburg-Apers, D. C.; Imamura, H.; Forkink, M.; Nooteboom, M.; Swarts, H. G.; Brock, R.; Smeitink, J. A. M.; Willems, P. H. G. M.; Koopman, W. J. H. *Pharm. Res.* **2011,** *28,* 2745–2757. doi:10.1007/s11095-011-0492-8
7. Molz, S.; Tharine, D.-C.; Decker, H.; Tasca, C. I. *Brain Res.* **2008,** *1231,* 113–120. doi:10.1016/j.brainres.2008.07.009
8. Perrault, D. M.; Chen, X.; Anslyn, E. V. *Tetrahedron* **1995,** *51,* 353–362. doi:10.1016/0040-4020(94)00901-6
9. Bazzicalupi, C.; Bencini, A.; Berni, E.; Bianchi, A.; Fornasari, P.; Giorgi, C.; Masotti, A.; Paoletti, P.; Valtancoli, B. *J. Phys. Org. Chem.* **2001,** *14,* 432–443. doi:10.1002/poc.385
10. Nakai, C.; Glinsmann, W. *Biochemistry* **1977,** *16,* 5636–5641. doi:10.1021/bi00644a039
11. Kuchelmeister, H. Y.; Schmuck, C. *Chem. – Eur. J.* **2011,** *17,* 5311–5318. doi:10.1002/chem.201003393
12. Mascaros, P. A.; Bazzicalupi, C.; Bianchi, A.; Giorgi, C.; Valero, M. D. G.; Garzón, R. L.; Salido, M. L. G.; Valtancoli, B. *Chem. Commun.* **2011,** *47,* 2814–2816. doi:10.1039/C0CC05054G
13. Sansone, F.; Baldini, L.; Casnati, A.; Ungaro, R. *New J. Chem.* **2010,** *34,* 2715–2728. doi:10.1039/c0nj00285b
14. Wenz, G.; Han, B.-H.; Müller, A. *Chem. Rev.* **2006,** *106,* 782–817. doi:10.1021/cr970027+
15. Lagona, J.; Mukhopadhyay, P.; Chakrabarti, S.; Isaacs, L. *Angew. Chem., Int. Ed.* **2005,** *44,* 4844–4870. doi:10.1002/anie.200460675
16. Yakimova, L. S.; Shurpik, D. N.; Stoikov, I. I. *Chem. Commun.* **2016,** *52,* 12462–12465. doi:10.1039/c6cc05797g
17. Antipin, I. S.; Kazakova, E. K.; Habicher, W. D.; Konovalov, A. I. *Russ. Chem. Rev.* **1998,** *67,* 905–922. doi:10.1070/RC1998v067n11ABEH000472
18. Stoikov, I. I.; Repejkov, S. A.; Antipin, I. S.; Konovalov, A. I. *Heteroat. Chem.* **2000,** *11,* 518–527. doi:10.1002/1098-1071(2000)11:7<518::AID-HC10>3.0.CO;2-#
19. Neri, P.; Sessler, J. L.; Wang, M.-X. *Calixarenes and Beyond;* Springer: Netherlands, 2016; p 1062.
20. Vavilova, A. A.; Stoikov, I. I. *Beilstein J. Org. Chem.* **2017,** *13,* 1940–1949. doi:10.3762/bjoc.13.188
21. Solovieva, S. E.; Burilov, V. A.; Antipin, I. S. *Macroheterocycles* **2017,** *10,* 134–146. doi:10.6060/mhc170512a
22. Burilov, V.; Valiyakhmetova, A.; Mironova, D.; Sultanova, E.; Evtugyn, V.; Osin, Y.; Katsyuba, S.; Burganov, T.; Solovieva, S.; Antipin, I. *New J. Chem.* **2018,** *42,* 2942–2951. doi:10.1039/c7nj04099g
23. Shinkai, S.; Mori, S.; Koreishi, H.; Tsubaki, T.; Manabe, O. *J. Am. Chem. Soc.* **1986,** *108,* 2409–2416. doi:10.1021/ja00269a045
24. Zadmard, R.; Schrader, T. *J. Am. Chem. Soc.* **2005,** *127,* 904–915. doi:10.1021/ja045785d
25. Ibragimova, R. R.; Burilov, V. A.; Aimetdinov, A. R.; Mironova, D. A.; Evtugyn, V. G.; Osin, Y. N.; Solovieva, S. E.; Antipin, I. S. *Macroheterocycles* **2016,** *9,* 433–441. doi:10.6060/mhc161180b
26. Burilov, V. A.; Mironova, D. A.; Ibragimova, R. R.; Evtugyn, V. G.; Osin, Y. N.; Solovieva, S. E.; Antipin, I. S. *Bionanosci.* **2018,** *8,* 337–343. doi:10.1007/s12668-017-0484-1
27. Song, M.; Sun, Z.; Han, C.; Tian, D.; Li, H.; Kim, J. S. *Chem. – Asian J.* **2014,** *9,* 2344–2357. doi:10.1002/asia.201400024
28. Rostovtsev, V. V.; Green, L. G.; Fokin, V. V.; Sharpless, K. B. *Angew. Chem., Int. Ed.* **2002,** *41,* 2596–2599. doi:10.1002/1521-3773(20020715)41:14<2596::AID-ANIE2596>3.0.CO;2-4
29. Smith, P. A. S. *The Chemistry of Open-chain Organic Nitrogen Compounds, Band 2, XII;* Verlag W. A. Benjamin Inc.: New York-Amsterdam, 1966; p 531.
30. Fujii, S.; Nishina, K.; Yamada, S.; Mochizuki, S.; Ohta, N.; Atsushi, T.; Sakurai, K. *Soft Matter* **2014,** *10,* 8216–8223. doi:10.1039/c4sm01355g
31. Bew, S. P.; Brimage, R. A.; L'Hermit, N.; Sharma, S. V. *Org. Lett.* **2007,** *9,* 3713–3716. doi:10.1021/ol071047t
32. Burilov, V. A.; Nugmanov, R. I.; Ibragimova, R. R.; Solovieva, S. E.; Antipin, I. S.; Konovalov, A. I. *Mendeleev Commun.* **2013,** *23,* 113–115. doi:10.1016/j.mencom.2013.03.022
33. Verboom, W.; Durie, A.; Egberink, R. J. M.; Asfari, Z.; Reinhoudt, D. N. *J. Org. Chem.* **1992,** *57,* 1313–1316. doi:10.1021/jo00030a050
34. Kenis, P. J. A.; Noordman, O. F. J.; Schönherr, H.; Kerver, E. G.; Snellink-Ruël, B. H. M.; van Hummel, G. J.; Harkema, S.; van der Vorst, C. P. J. M.; Hare, J.; Picken, S. J.; Engbersen, J. F. J.; van Hulst, N. F.; Vancso, G. J.; Reinhoudt, D. N. *Chem. – Eur. J.* **1998,** *4,* 1125–1134. doi:10.1002/(SICI)1521-3765(19980710)4:7<1225::AID-CHEM1225>3.0.CO;2-6
35. Dordea, C.; Brisach, F.; Haddaoui, J.; Arnaud-Neu, F.; Bolte, M.; Casnati, A.; Böhmer, V. *Supramol. Chem.* **2010,** *22,* 347–357. doi:10.1080/10610271003678511
36. Tomapatanaget, B.; Tuntulani, T. *Tetrahedron Lett.* **2001,** *42,* 8105–8109. doi:10.1016/S0040-4039(01)01722-1
37. Maurin, A.; Varatharajan, S.; Colasson, B.; Reinaud, O. *Org. Lett.* **2014,** *16,* 5426–5429. doi:10.1021/ol502650c
38. Buttress, J. P.; Day, D. P.; Courtney, J. M.; Lawrence, E. J.; Hughes, D. L.; Blagg, R. J.; Crossley, A.; Matthews, S. E.; Redshaw, C.; Page, P. C. B.; Wildgoose, G. G. *Langmuir* **2016,** *32,* 7806–7813. doi:10.1021/acs.langmuir.6b02222
39. Li, Y.; Hoskins, J. N.; Sreerama, S. G.; Grayson, S. M. *Macromolecules* **2010,** *43,* 6225–6228. doi:10.1021/ma100599n
40. Aguiar, J.; Carpana, P.; Molina-Bolíver, J. A.; Carnero Ruiz, C. *J. Colloid Interface Sci.* **2003,** *258,* 116–122. doi:10.1016/S0021-9797(02)00082-6
41. Hunter, R. J. *Foundations of Colloid Science;* Oxford University Press: Oxford, 1987; p 673.
42. Patist, A.; Bhagwat, S. S.; Penfield, K. W.; Aikens, P.; Shah, D. O. *J. Surfactants Deterg.* **2000,** *3,* 53–58. doi:10.1007/s11743-000-0113-4
43. Castaldi, M.; Ortona, O.; Paduano, L.; Vitagliano, V. *Langmuir* **1998,** *14,* 5994–5998. doi:10.1021/la980457a
44. Camesano, T. A.; Nagarajan, R. *Colloids Surf., A* **2000,** *167,* 165–177. doi:10.1016/S0927-7757(99)00473-2
45. Burilov, V. A.; Mironova, D. A.; Ibragimova, R. R.; Nugmanov, R. I.; Solovieva, S. E.; Antipin, I. S. *Colloids Surf., A* **2017,** *515,* 41–49. doi:10.1016/j.colsurfa.2016.12.007
46. Chakraborty, M.; Panda, A. K. *Spectrochim. Acta, Part A* **2011,** *81,* 458–465. doi:10.1016/j.saa.2011.06.038
47. *Gaussian 09,* Revision B. 01.; Gaussian, Inc.: Wallingford, CT, 2009.
48. Kurzak, B.; Kroczewska, D.; Jezierska, J. *Polyhedron* **1998,** *17,* 1831–1841. doi:10.1016/S0277-5387(97)00528-7

49. Lee, S.; Kim, J.-Y.; Chen, X.; Yoon, J. *Chem. Commun.* **2016,** *52,* 9178–9196. doi:10.1039/c6cc03584a
50. Kolusheva, S.; Zadmard, R.; Schrader, T.; Jelinek, R. *J. Am. Chem. Soc.* **2006,** *128,* 13592–13598. doi:10.1021/ja064957z
51. Thongmalai, W.; Eaidkong, T.; Ampornpun, S.; Mungkarndee, R.; Tumcharern, G.; Sukwattanasinitt, M.; Wacharasindhu, S. *J. Mater. Chem.* **2011,** *21,* 16391–16397. doi:10.1039/c1jm12795k
52. Kolusheva, S.; Kafri, R.; Katz, M.; Jelinek, R. *J. Am. Chem. Soc.* **2001,** *123,* 417–422. doi:10.1021/ja0034139
53. Armarego, W. L. F.; Chai, C. *Purification of Laboratory Chemicals;* Elsevier: New York, 2009; p 743.
54. Méndez-Ardoy, A.; Gómez-García, M.; Mellet, C. O.; Sevillano, N.; Girón, M. D.; Salto, R.; Santoyo-González, F.; Fernández, J. M. G. *Org. Biomol. Chem.* **2009,** *7,* 2681–2684. doi:10.1039/B903635K
55. Evans, P. R. *Acta Crystallogr., Sect. D* **2006,** *62,* 72–82. doi:10.1107/S0907444905036693
56. Winn, M. D.; Ballard, C. C.; Cowtan, K. D.; Dodson, E. J.; Emsley, P.; Evans, P. R.; Keegan, R. M.; Krissinel, E. B.; Leslie, A. G. W.; McCoy, A.; McNicholas, S. J.; Murshudov, G. N.; Pannu, N. S.; Potterton, E. A.; Powell, H. R.; Read, R. J.; Vagin, A.; Wilson, K. S. *Acta Crystallogr., Sect. D* **2011,** *D67,* 235–242. doi:10.1107/S0907444910045749
57. Battye, T. G. G.; Kontogiannis, L.; Johnson, O.; Powell, H. R.; Leslie, A. G. W. *Acta Crystallogr., Sect. D* **2011,** *D67,* 271–281. doi:10.1107/S0907444910048675
58. Sheldrick, G. M. *Acta Crystallogr., Sect. A* **2015,** *A71,* 3–8. doi:10.1107/S2053273314026370
59. Sheldrick, G. M. *Acta Crystallogr., Sect. C* **2015,** *C71,* 3–8. doi:10.1107/S2053229614024218
60. Stewart, J. J. P. *J. Mol. Model.* **2013,** *19,* 1–32. doi:10.1007/s00894-012-1667-x
61. *MOPAC2016;* Stewart Computational Chemistry: Colorado Springs, CO, USA, 2016.
62. Laikov, D. N.; Ustynyuk, Y. A. *Russ. Chem. Bull.* **2005,** *54,* 820–826. doi:10.1007/s11172-005-0329-x
63. Laikov, D. N. *Chem. Phys. Lett.* **2005,** *416,* 116–120. doi:10.1016/j.cplett.2005.09.046

License and Terms

BEILSTEIN JOURNAL OF ORGANIC CHEMISTRY

A self-assembled photoresponsive gel consisting of chiral nanofibers

Lei Zou*, Dan Han, Zhiyi Yuan, Dongdong Chang and Xiang Ma*

Letter

Open Access

Address:
Key Laboratory for Advanced Materials and Institute of Fine Chemicals, School of Chemistry & Molecular Engineering, East China University of Science & Technology, Shanghai 200237, China

Email:
Lei Zou* - zoulei@ecust.edu.cn; Xiang Ma* - maxiang@ecust.edu.cn

* Corresponding author

Keywords:
chirality; nanostructure; organogel; photoresponse; self-assembly

Beilstein J. Org. Chem. **2018,** *14,* 1994–2001.
doi:10.3762/bjoc.14.174

Received: 16 April 2018
Accepted: 10 July 2018
Published: 01 August 2018

This article is part of the thematic issue "Macrocyclic and supramolecular chemistry".

Guest Editor: M.-X. Wang

Abstract

A novel compound based on a glutamic acid skeleton, containing azobenzene as a photoresponsive group and ureidopyrimidinone (UPy) as a connection site, was designed and synthesized. The monomer is capable of forming an organogel in nonpolar organic solvents and different types of nanostructures in other solvents. The state of the gel and the chirality of the nanostructures could both be adjusted by subsequent light irradiation at different wavelengths. The helical nanofiber-like morphology was verified in the internal structure of the gel. The performance of this gel was investigated by a series of methods, such as UV–vis absorption spectroscopy, circular dichroism, scanning electron microscopy and rheological techniques. This work provides a new method for facile synthesis of chiro-optical gels.

Introduction

Supramolecular gels [1,2] immobilized by three-dimensional networks through self-assembly have drawn significant attention in the past decades. They are normally fabricated by means of noncovalent intermolecular interactions [3], such as π–π stacking, hydrogen bonding, van der Waals forces, hydrophobic, electrostatic, host–guest and other interactions. Interestingly, some of them can be assembled into distinctive nanostructures through gel formation [4-6].

Various functional nanostructures have shown great potential for applications in many important areas, for example, nanofabrication [5,7-10], drug delivery [11,12], and chemosensing [13,14]. Among the supramolecular gels, the low-molecular-weight gels (LMWGs) [15,16] are those that self-assemble into gels in organic solvents with molecular weights of <2000 Da. The weak noncovalent intermolecular interactions between LMWGs make them more sensitive to external conditions

[6,17-19], such as solvent, light and temperature. These characteristics meet currents demands for conveniently controlling the assembly of materials according to their size, shape, and morphology.

Chiral functional materials have aroused much attention for their potential applications. Liu and co-workers [20-31] have built a multifunctional controllable gel system, which utilized L-glutamic lipid to construct nanofibers, nanotwists, and nanotubes with the property of chirality. Azobenzene, which is structurally photosensitive, is widely chosen to construct optically controlled systems [17,30,32-35]. This moiety is also frequently employed as a building block because of its strong π–π stacking in nonpolar solvents.

Herein, a novel compound **3** containing both chiral L-glutamic lipid and azobenzene was designed and synthesized (Scheme 1). It is used as a candidate to form a new chiro-optical system [30,36-41]. Ureidopyrimidinone (UPy), as a connection site, is also introduced to make quadruple hydrogen bonding [42-44]. The structure and schematic representation of **3** are shown in Figure 1. The possible assembly process of the nanostructure is proposed as well. It is found that compound **3** is able to form a gel in nonpolar solvents. The assembled structures of **3** in different solvents were also investigated. The photoresponsiveness of the formed nanostructure was investigated concomitantly as well.

Results and Discussion

The monomolecular compound **3** can be easily synthesized in 3 steps. The compound has the necessary features for gel formation. The quadruple hydrogen bonding created by UPy moieties is quite stable in nonpolar solvents. Therefore, the molecule can easily assemble into dimers. Then, the *trans*-isomers of azobenzene can stack with each other via π–π interactions. Further, the acylamino group of the glutamic acid moiety at the center of the molecule also promotes this aggregation through hydrogen bonding interactions. Finally, the chirality of glutamic acid may be magnified along with the formation of supramolecular structure.

To investigate the potential photoresponsiveness of compound **3**, the UV–vis absorption spectrum was measured to trace photochemical and photophysical properties of the solution of compound **3** (1.0×10^{-5} M in chloroform). As shown in Figure 2, the azobenzene *trans*-isomer displayed a strong absorbance peak at 352 nm. When exposed to ultraviolet light of 365 nm, the peak at 352 nm obviously decreased and reached a photostationary state within 5 minutes. The equilibrium could be reversed by subsequent exposure to visible light (420 nm) and UV light (365 nm) irradiation, whereby the equilibrium could be reached within 6 min and 4 min, respectively. However, the fatigue durability of this compound did not meet the expected requirement; after two cycles of light irradiation, the photoresponsiveness was clearly weakened. This defect may be

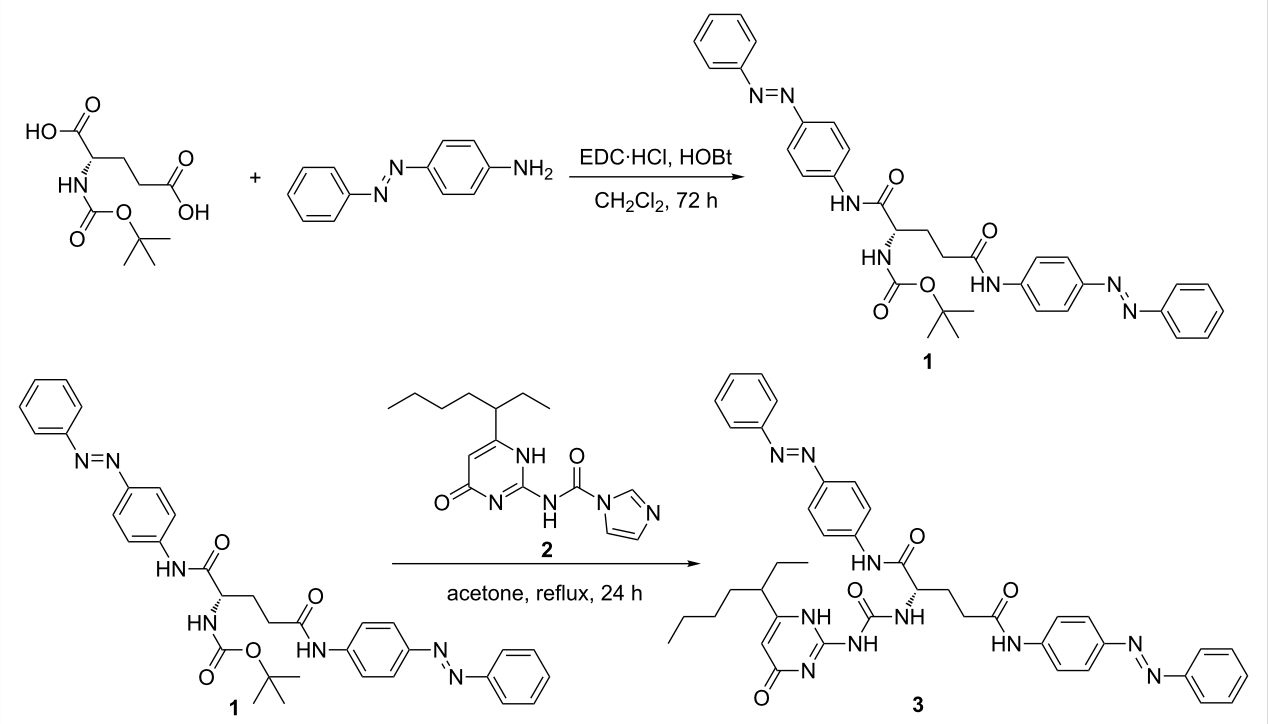

Scheme 1: The preparation of compound **3**.

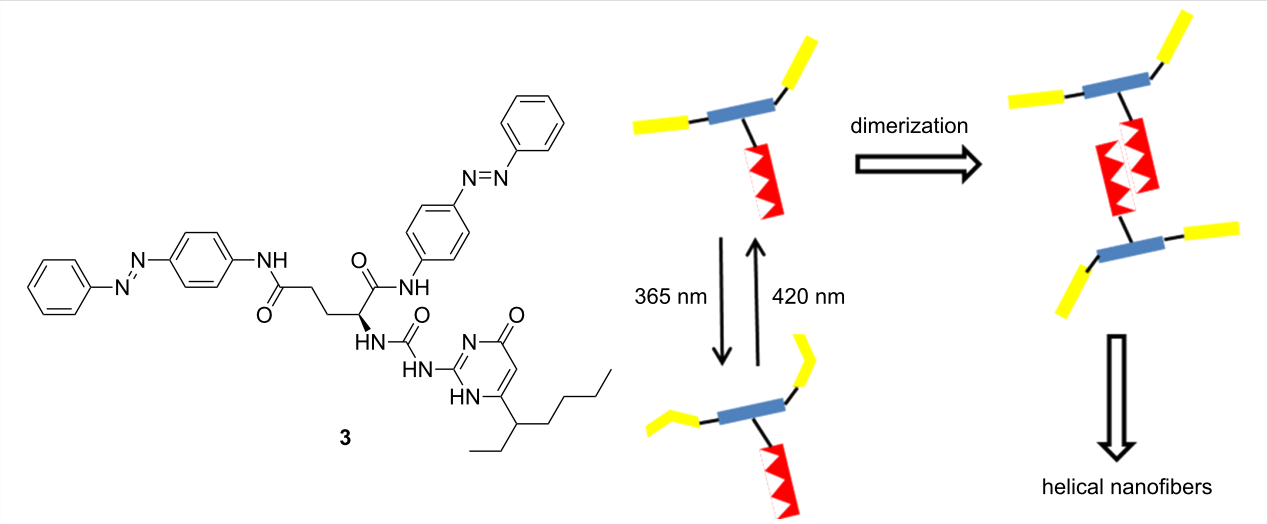

Figure 1: The chemical structure and the schematic representation of compound **3** as well as the proposed assembly process of the nanostructure.

ascribed to the rigid structure of compound **3**. These two azobenzene moieties within the molecule are close and the dimerization of the UPy moiety results in a more crowded structure.

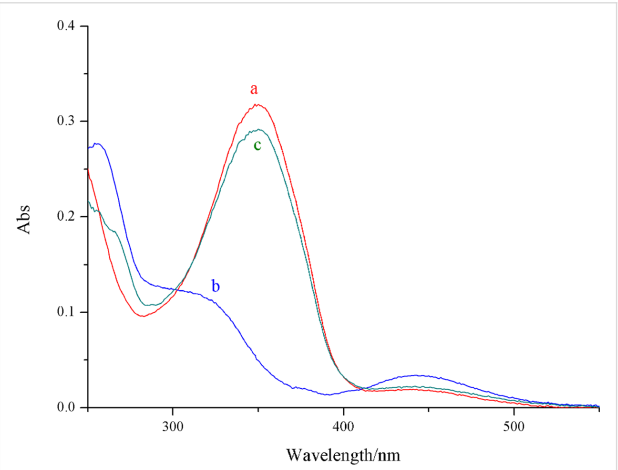

Figure 2: UV–vis absorbance spectra of a) compound **3** and b) irradiated by a light source of 365 nm and c) then treated by light of 420 nm. The concentration was 1.0×10^{-5} M in $CHCl_3$.

The circular dichroism (CD) spectrum was then measured to trace the different states of aggregation in solution of compound **3** in different solvents. Benzene, toluene, *p*-xylene, chloroform, tetrachloromethane and DMSO were chosen as solvents to prepare solutions with uniform concentration (3.0×10^{-5} M). As evidenced in the CD spectrum (Figure 3), the CD signal in a solution of DMSO and chloroform was very weak, and the CD signal in tetrachloromethane and *p*-xylene was not very strong but discernible. On the other hand, the CD signal in aromatic solvents, like benzene and toluene, was strong enough to confirm the formation of chiral structures. These results indicate that the chiral nanostructures can be only obtained in solvents with lower polarity, especially in aromatic solvents.

To study the chirality of compound **3** and its reaction to light stimulation, **3** (in CCl_4) was exposed to visible irradiation or UV light. The CD spectrum was then recorded. In Figure 3b, two obvious peaks at 300 nm and 375 nm evidence the existence of the chiral structure in the solution. This CD signal disappeared after irradiation with light at 365 nm, implying that the chiral structure in the solution had been destroyed. The obvious chiral signal reappeared when the same solution was exposed to visible light of 420 nm before reaching a stable state. However, this process was partially reversible. The compound **3** cycling test, with more than 8 cycles, caused the total disappearance of the CD signal and the process was then no longer reversible (Figure S8, Supporting Information File 1).

The morphology of compound **3** was further characterized by scanning electron microscopy (SEM, Figure 4). The samples were prepared by evaporating the solution of compound **3** on a surface of mica, and the differences in various solvents were also investigated. The sample in DMSO did not show a chiral self-assembled nanostructure owing to the destruction of quadruple hydrogen bonding and π–π stacking in DMSO. However, beautiful acicular fibers could be detected on the surface treated with a chloroform solution, and a dendritic network was observed on the sample made from benzene solution (Figure S9, Supporting Information File 1). The photoresponsiveness of compound **3** was also investigated by drying the chloroform solution of compound **3**, which was exposed to sufficient UV light (365 nm) beforehand, on the surface of mica and

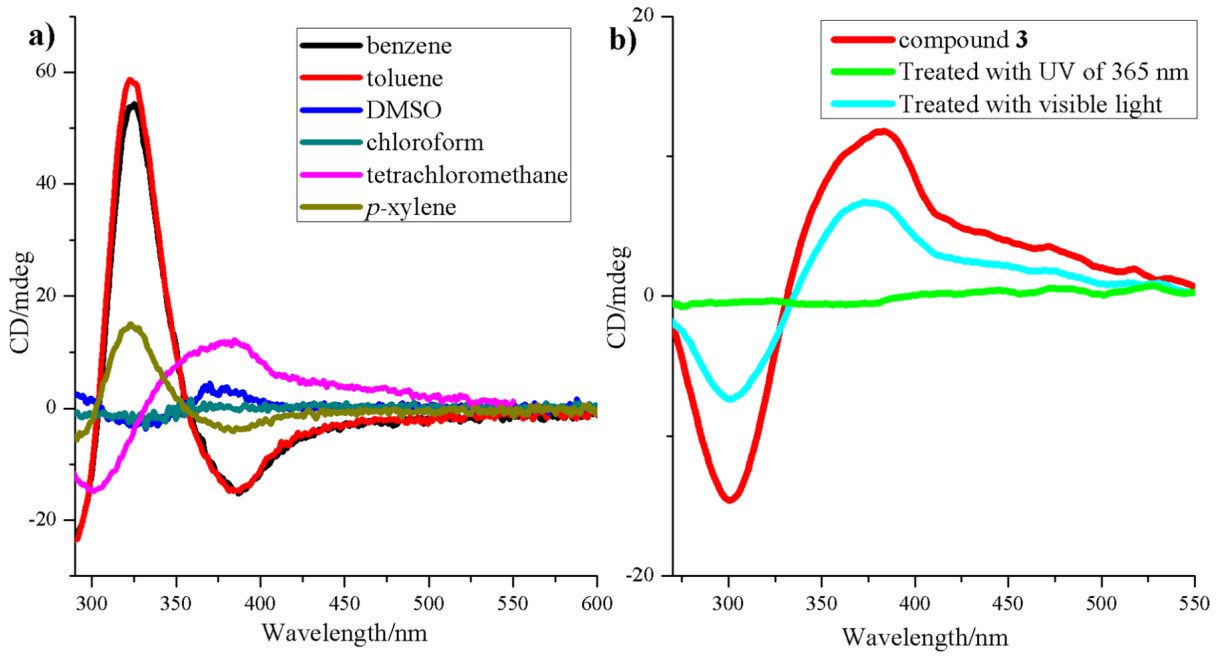

Figure 3: CD spectrum of compound **3** in solutions of a) benzene, toluene, *p*-xylene, chloroform, tetrachloromethane and DMSO with identical concentration (3.0×10^{-5} M), b) before and after being exposed to UV (λ = 365 nm) and visible (λ = 420 nm) light.

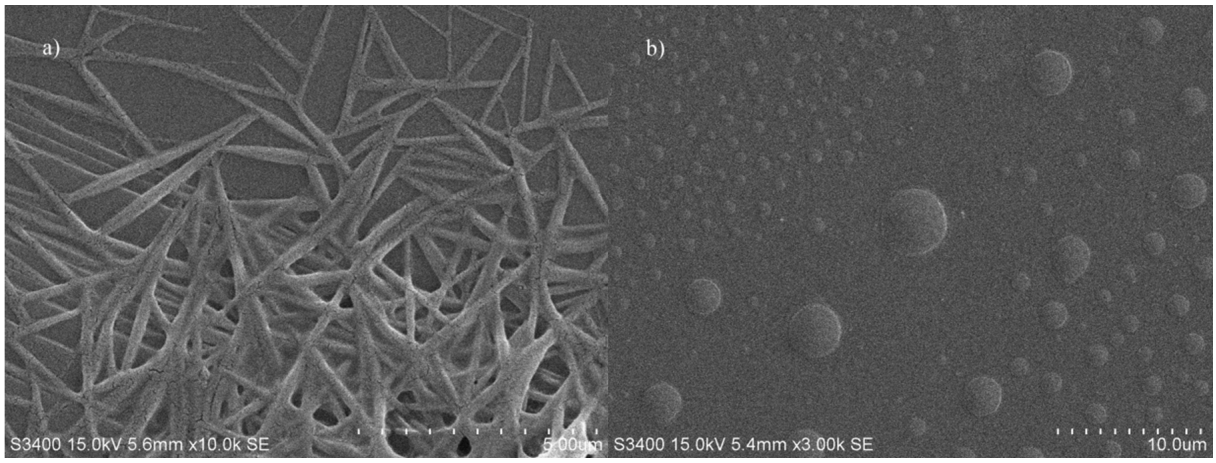

Figure 4: SEM images of the microstructure a) obtained by the self-assembled compound **3** in $CHCl_3$ on the surface of mica and then b) treated with UV light (365 nm).

detected by SEM, whereby only small discs were found as shown in Figure 4b. This implies that the UV light of 365 nm can efficiently destroy the self-assembled structure, and the nanostructures of the assembled compound **3** can be adjusted by both solvent and light.

The formation of organogels in various solvents was conducted to test the gelation ability of compound **3**. The gel was fabricated by melting compound **3** in solution by heating for about 20 min, followed by allowing the solution to rest at room temperature for 30 min. The gelation ability of compound **3** in various organic solvents was investigated by using the "stable to inversion of a test tube" method (Figure 5a). Here we arrive at the conclusion that compound **3** can only form an organogel in nonpolar aromatic solvents such as benzene and *p*-xylene. Table 1 lists the solvent parameters and the gel-forming ability of compound **3** in various organic solvents. The critical gelation concentration (CGC) is also noted. We took the gel formed in benzene as the example for the following investigations. The rheological technique (Figure 5b) was used to measure the rheo-

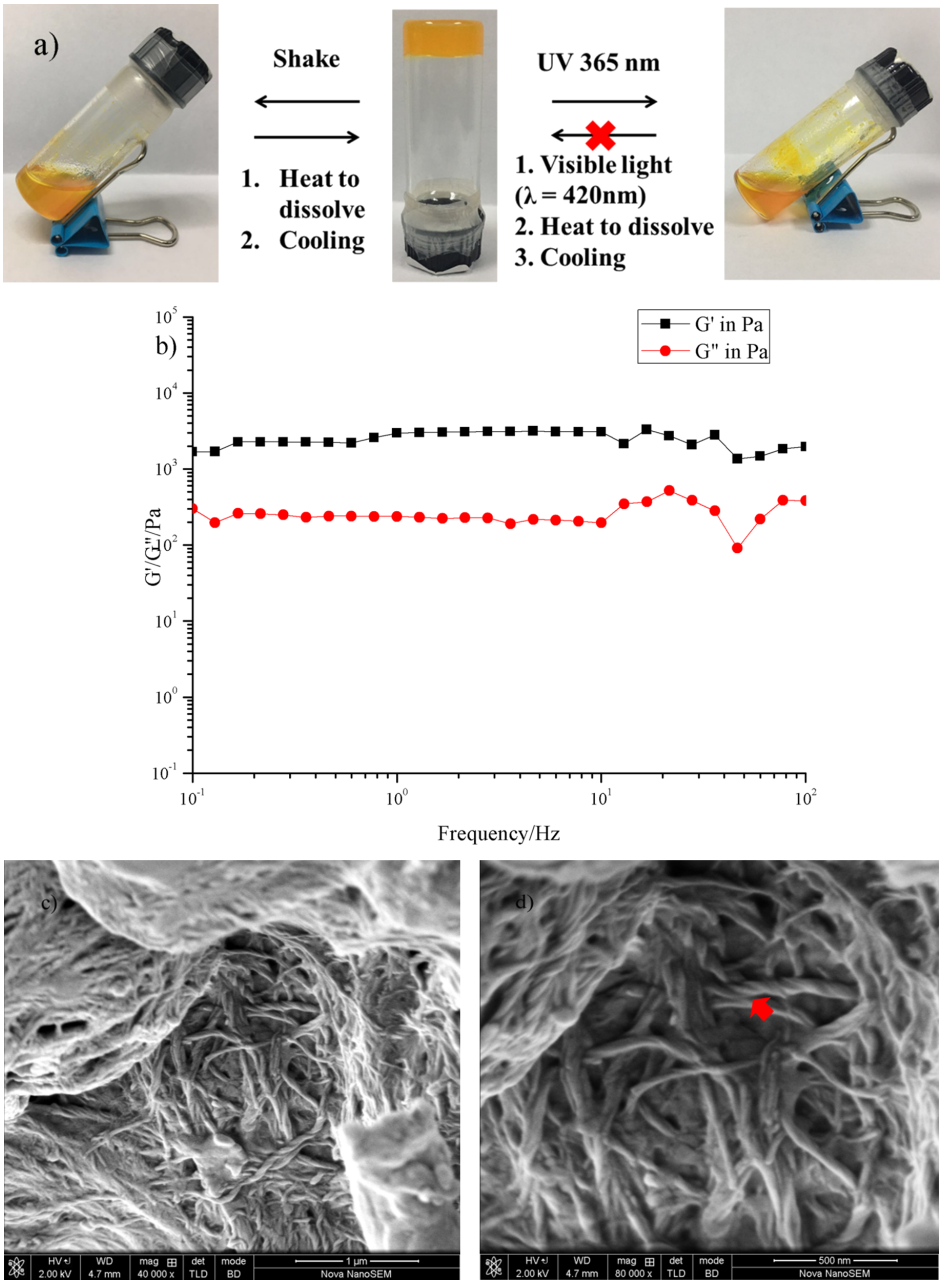

Figure 5: a) The gel-to-sol transformation of the samples via different routes. b) Dynamic frequency sweep of the gel fabricated in benzene. (c,d) FESEM images of compound **3** xerogels.

logical properties of this gel system first. The dynamic frequency spectra of the gel indicated that the elastic modulus G' was higher than the viscous modulus G" when the frequency ω was between 0.1 and 100 Hz. This showed that the system conforms to the character of the gel. However, the gel is not stable under shaking, where it is broken into a mixture of solution and small pieces. After melting these particles again then natural cooling, the gel state was once again obtained.

Field emission scanning electron microscopy (FESEM) was utilized to characterize the xerogels obtained by freeze drying. As shown in Figure 5c,d, plenty of helical nanotwists could be found in the xerogel. These fibers were intertwined together to form a 3D nanostructure. This result partially showed the gel formation pathway. Compound **3** may form dimers at the beginning, which can be detected by high-resolution mass spectrometry (Figure S7, Supporting Information File 1). Then, the dimers

Table 1: Gelation ability of compound **3** in various organic solvents.

solvent	CGC[a] [mg mL^{-1}]
hexane	P
cyclohexane	P
CCl_4	G (7.5)
benzene	G (6.5)
methylbenzene	HG
p-xylene	G (5.0)
$CHCl_3$	S
CH_2Cl_2	S
THF	S
acetone	S
acetonitrile	S
DMF	S

[a]G = gel; P = precipitation; S = solution; HG = half gel.

and single molecules **3** were able to assemble together through π–π stacking and hydrogen bonding to fabricate the nanofibers. Finally, those fibers twisted with each other to form nanotwists of wider diameter.

Finally, the gel system was irradiated with ultraviolet light or visible light to test its stimuli response. Under 365 nm light exposure, the gel melted into a turbid liquid within 20 min. However, the system could not easily be reversed due to the poor reversibility of compound **3** in benzene that was investigated previously.

Conclusion

We have synthesized a novel chiral compound containing azobenzene as the photoresponsive group and UPy as the connection site. The monomer was capable of forming chiral nanostructures and a low-molecular-weight organogel in non-polar organic solvents. The monomer also can form different types of nanostructures in different solvents, and the kind of solvent was found to be crucial for the chirality of the assembled structure. The gel-to-sol process could also be modified by shaking and UV light. The rheological behavior of the gel was investigated and found to meet the basic requirement of a gel. The inner structure of the gel was determined to be a cross-linked network made of chiral nanotwists. This work provides a novel method to build chiro-optical soft material systems.

Experimental

Synthesis of compound **1**

1-Ethyl-3-(3-dimethylaminopropyl)carbodiimide hydrochloride (EDC·HCl, 8.04 g, 0.044 mol) and 1-hydroxybenzotriazole (HOBt, 5.94 g,0.044 mol) were added to a 200 mL CH_2Cl_2 solution of Boc-L-glutamic acid (5 g, 0.02 mol) and 4-amino-azobenzene (7.8838 g, 0.04 mol), then the obtained mixture was stirred at room temperature for 72 h under an Ar atmosphere. The obtained yellow solid was isolated by filtration and washed three times with CH_2Cl_2. The crude product was recrystallized from THF/H_2O to yield compound **1** as a yellow solid (10.53 g, 87% yield). ^{1}H NMR (400 MHz, DMSO-d_6) δ 10.43 (s, 1H), 10.33 (s, 1H), 8.02–7.71 (m, 12H), 7.68–7.43 (m, 6H), 7.22 (d, J = 7.6 Hz, 1H), 4.18 (dd, J = 13.5, 7.9 Hz, 1H), 2.17–1.90 (m, 2H), 1.36 (d, J = 34.1 Hz, 9H); ^{13}C NMR (100 MHz, DMSO-d_6) δ 171.44, 170.83, 155.43, 151.99, 147.58, 147.35, 142.35, 142.05, 131.04, 130.97, 129.38, 123.64, 122.32, 122.28, 119.50, 119.17, 78.23, 54.78, 32.92, 28.17, 27.07, 25.09; HRMS m/z: $[M + H]^+$ calcd for $C_{34}H_{36}N_7O_4^+$, 606.2829; found, 606.2830.

Synthesis of compound **3**

Compound **2** was easily prepared according to a literature method [45]. Five mL of trifluoroacetic acid was dropped into a 25 mL CH_2Cl_2 solution of compound **1** (1.0 g, 1.65 mmol), then the mixture was stirred at room temperature for 2 h under an Ar atmosphere. Evaporation of the resulting red solution was performed under reduced pressure, and small amounts of CH_2Cl_2 was frequently added to the bottle until the trifluoroacetic acid was removed entirely. The resulting yellow solid was added to an acetone solution of compound **2** (1.22 g, 4.03 mmol) under an Ar atmosphere, then the mixture was heated at reflux for 24 h. The evaporation (under reduced pressure) and further purification of the resulting solution was carried out by column chromatography using CH_2Cl_2/CH_3OH (50:1, v/v) and CH_2Cl_2/CH_3OH (10:1, v/v) to afford **3** as a yellow solid (620 mg, 62.5% yield). ^{1}H NMR (400 MHz, DMSO) δ 11.29 (s, 1H), 10.67 (s, 1H), 10.34 (s, 1H), 9.68 (s, 1H), 8.30 (s, 1H), 8.01–7.68 (m, 12H), 7.68–7.43 (m, 6H), 5.77 (s, 1H), 4.64 (s, 1H), 2.22 (dd, J = 13.5, 6.0 Hz, 2H), 2.05 (dd, J = 13.6, 6.7 Hz, 1H), 1.55 (dd, J = 15.8, 10.0 Hz, 4H), 1.29–1.04 (m, 6H), 0.85–0.71 (m, 6H); ^{13}C NMR (100 MHz, DMSO) δ 170.51, 151.99, 147.79, 147.34, 142.30, 141.65, 131.11, 130.96, 129.41, 129.37, 123.57, 122.34, 122.26, 119.70, 119.17, 53.14, 29.13, 22.15, 13.86, 11.84; HRMS m/z: $[M + Na]^+$ calcd for $C_{41}H_{44}N_{10}O_4Na^+$, 763.3445; found, 763.3443.

Supporting Information

Supporting Information File 1

Additional schemes and figures, general remarks, synthesis and characterization data, including copies of ^{1}H and ^{13}C NMR spectra.

[https://www.beilstein-journals.org/bjoc/content/supplementary/1860-5397-14-174-S1.pdf]

Acknowledgements

This work was financially supported by the National Natural Science Foundation of China (Nos. 21722603, 21302056 and 21476075).

ORCID® iDs

Xiang Ma - https://orcid.org/0000-0002-8679-4491

References

1. Babu, S. S.; Praveen, V. K.; Ajayaghosh, A. *Chem. Rev.* **2014,** *114,* 1973–2129. doi:10.1021/cr400195e
2. Ma, X.; Tian, H. *Acc. Chem. Res.* **2014,** *47,* 1971–1981. doi:10.1021/ar500033n
3. Zhou, Z.; Yan, X.; Cook, T. R.; Saha, M. L.; Stang, P. J. *J. Am. Chem. Soc.* **2016,** *138,* 806–809. doi:10.1021/jacs.5b12986
4. Zhang, L.; Qin, L.; Wang, X.; Cao, H.; Liu, M. *Adv. Mater.* **2014,** *26,* 6959–6964. doi:10.1002/adma.201305422
5. Xu, C.; Xu, L.; Ma, X. *Chin. Chem. Lett.* **2018,** *29,* 970–972. doi:10.1016/j.cclet.2017.11.045
6. Ma, X.; Tian, H. *Acta Polym. Sin.* **2017,** *1,* 27–36.
7. Zhang, Q.; Qu, D.-H.; Ma, X.; Tian, H. *Chem. Commun.* **2013,** *49,* 9800–9802. doi:10.1039/c3cc46297h
8. Li, T.; Li, X.; Wang, J.; Ågren, H.; Ma, X.; Tian, H. *Adv. Opt. Mater.* **2016,** *4,* 840–847. doi:10.1002/adom.201500694
9. Wang, S.; Wang, F.; Li, C.; Li, T.; Cao, D.; Ma, X. *Sci. China: Chem.* **2018,** *61,* in press.
10. Zhang, Q.; Yao, X.; Qu, D.-H.; Ma, X. *Chem. Commun.* **2014,** *50,* 1567–1569. doi:10.1039/c3cc48491b
11. Fong, W.-K.; Hanley, T. L.; Thierry, B.; Kirby, N.; Boyd, B. J. *Langmuir* **2010,** *26,* 6136–6139. doi:10.1021/la100644s
12. Du, J. D.; Hong, L.; Tan, A.; Boyd, B. J. *J. Phys. Chem. B* **2018,** *122,* 1766–1770. doi:10.1021/acs.jpcb.7b12234
13. Salvia, M.-V.; Salassa, G.; Rastrelli, F.; Mancin, F. *J. Am. Chem. Soc.* **2015,** *137,* 11399–11406. doi:10.1021/jacs.5b06300
14. Hortalá, M. A.; Fabbrizzi, L.; Marcotte, N.; Stomeo, F.; Taglietti, A. *J. Am. Chem. Soc.* **2003,** *125,* 20–21. doi:10.1021/ja027110l
15. Wang, X.; Duan, P.; Liu, M. *Chem. – Asian J.* **2014,** *9,* 770–778. doi:10.1002/asia.201301518
16. Geng, H.; Ye, L.; Zhang, A.-y.; Li, J.; Feng, Z.-g. *Langmuir* **2016,** *32,* 4586–4594. doi:10.1021/acs.langmuir.6b01059
17. Koumura, N.; Kudo, M.; Tamaoki, N. *Langmuir* **2004,** *20,* 9897–9900. doi:10.1021/la048334f
18. Duan, P.; Li, Y.; Li, L.; Deng, J.; Liu, M. *J. Phys. Chem. B* **2011,** *115,* 3322–3329. doi:10.1021/jp110636b
19. Cai, Y.; Guo, Z.; Chen, J.; Li, W.; Zhong, L.; Gao, Y.; Jiang, L.; Chi, L.; Tian, H.; Zhu, W.-H. *J. Am. Chem. Soc.* **2016,** *138,* 2219–2224. doi:10.1021/jacs.5b11580
20. Jiang, H.; Zhang, L.; Chen, J.; Liu, M. *ACS Nano* **2017,** *11,* 12453–12460. doi:10.1021/acsnano.7b06484
21. Liu, C.; Yang, D.; Jin, Q.; Zhang, L.; Liu, M. *Adv. Mater.* **2016,** *28,* 1644–1649. doi:10.1002/adma.201504883
22. Qin, L.; Duan, P.; Xie, F.; Zhang, L.; Liu, M. *Chem. Commun.* **2013,** *49,* 10823–10825. doi:10.1039/c3cc47004k
23. Shen, Z.; Wang, T.; Liu, M. *Chem. Commun.* **2014,** *50,* 2096–2099. doi:10.1039/c3cc48350a
24. Wang, X.; Duan, P.; Liu, M. *Chem. Commun.* **2012,** *48,* 7501–7503. doi:10.1039/c2cc33246a
25. Li, Y.; Wang, T.; Liu, M. *Soft Matter* **2007,** *3,* 1312–1317. doi:10.1039/b710165a
26. Xie, F.; Qin, L.; Liu, M. *Chem. Commun.* **2016,** *52,* 930–933. doi:10.1039/c5cc08076b
27. Duan, P.; Qin, L.; Zhu, X.; Liu, M. *Chem. – Eur. J.* **2011,** *17,* 6389–6395. doi:10.1002/chem.201003049
28. Duan, P.; Liu, M. *Phys. Chem. Chem. Phys.* **2010,** *12,* 4383–4389. doi:10.1039/b923595g
29. Zhang, L.; Wang, X.; Wang, T.; Liu, M. *Small* **2015,** *11,* 1025–1038. doi:10.1002/smll.201402075
30. Cao, H.; Jiang, J.; Zhu, X.; Duan, P.; Liu, M. *Soft Matter* **2011,** *7,* 4654–4660. doi:10.1039/c1sm05219e
31. Jin, X.; Jiang, J.; Liu, M. *ACS Nano* **2016,** *10,* 11179–11186. doi:10.1021/acsnano.6b06233
32. Yang, D.; Zhang, L.; Yin, L.; Zhao, Y.; Zhang, W.; Liu, M. *Soft Matter* **2017,** *13,* 6129–6136. doi:10.1039/c7sm00935f
33. Ji, L.; Ouyang, G.; Liu, M. *Langmuir* **2017,** *33,* 12419–12426. doi:10.1021/acs.langmuir.7b02285
34. Xie, F.; Ouyang, G.; Qin, L.; Liu, M. *Chem. – Eur. J.* **2016,** *22,* 18208–18214. doi:10.1002/chem.201603998
35. Liu, Z.-X.; Feng, Y.; Yan, Z.-C.; He, Y.-M.; Liu, C.-Y.; Fan, Q.-H. *Chem. Mater.* **2012,** *24,* 3751–3757. doi:10.1021/cm302318b
36. Zhu, X.; Li, Y.; Duan, P.; Liu, M. *Chem. – Eur. J.* **2010,** *16,* 8034–8040. doi:10.1002/chem.201000595
37. Jung, S. H.; Jeon, J.; Kim, H.; Jaworski, J.; Jung, J. H. *J. Am. Chem. Soc.* **2014,** *136,* 6446–6452. doi:10.1021/ja5018199
38. Cao, H.; Yuan, Q.; Zhu, X.; Zhao, Y.-P.; Liu, M. *Langmuir* **2012,** *28,* 15410–15417. doi:10.1021/la303263g
39. Wang, Y.; Xu, J.; Wang, Y.; Chen, H. *Chem. Soc. Rev.* **2013,** *42,* 2930–2962. doi:10.1039/c2cs35332f
40. Niu, D.; Ji, L.; Ouyang, G.; Liu, M. *Chem. Commun.* **2018,** *54,* 1137–1140. doi:10.1039/c7cc09049h
41. Cao, H.; Zhu, X.; Liu, M. *Angew. Chem., Int. Ed.* **2013,** *52,* 4122–4126. doi:10.1002/anie.201300444
42. Miao, W.; Wang, S.; Liu, M. *Adv. Funct. Mater.* **2017,** *27,* 1701368. doi:10.1002/adfm.201701368
43. Wang, Q.; Cheng, M.; Jiang, J.-L.; Wang, L.-Y. *Chin. Chem. Lett.* **2017,** *28,* 793–797. doi:10.1016/j.cclet.2017.02.008
44. Li, Q.; Liu, C.; Wen, J.; Wu, Y.; Shan, Y.; Liao, J. *Chin. Chem. Lett.* **2017,** *28,* 1857–1874. doi:10.1016/j.cclet.2017.05.007
45. Keizer, H. M.; Sijbesma, R. P.; Meijer, E. W. *Eur. J. Org. Chem.* **2004,** 2553–2555. doi:10.1002/ejoc.200300752

BEILSTEIN JOURNAL OF ORGANIC CHEMISTRY

Coordination-driven self-assembly vs dynamic covalent chemistry: versatile methods for the synthesis of molecular metallarectangles

Li-Li Ma[‡1], Jia-Qin Han[‡1,2], Wei-Guo Jia[*2] and Ying-Feng Han[*1]

Full Research Paper

Open Access

Address:
[1]Key Laboratory of Synthetic and Natural Functional Molecule Chemistry, College of Chemistry and Materials Science, Northwest University, Xi'an 710127, China and [2]College of Chemistry and Materials Science, The Key Laboratory of Functional Molecular Solids, Ministry of Education, Anhui Normal University, Wuhu 241002, China

Email:
Wei-Guo Jia[*] - wgjiasy@mail.ahnu.edu.cn; Ying-Feng Han[*] - yfhan@nwu.edu.cn

* Corresponding author ‡ Equal contributors

Keywords:
coordination-driven self-assembly; dynamic covalent chemistry; half-sandwich rhodium complex; metallarectangles; one-pot reaction; supramolecular chemistry

Beilstein J. Org. Chem. **2018,** *14,* 2027–2034.
doi:10.3762/bjoc.14.178

Received: 01 June 2018
Accepted: 19 July 2018
Published: 03 August 2018

This article is part of the thematic issue "Macrocyclic and supramolecular chemistry".

Guest Editor: M.-X. Wang

Abstract

Supramolecular coordination assemblies have a range of potential applications in chemical and biological sciences. Herein, simple modular methods for the synthesis of metallarectangles are described. The desired tetranuclear metallarectangles were synthesized by using coordination-driven self-assembly of half-sandwich rhodium-based organometallic clip units and organic ligands. The reaction of such an organometallic clip with 4-formylpyridine provided a dinuclear molecular tweezer with pendant aldehyde groups, and subsequent [4 + 4] condensation reactions with diamines provides another route to the target metallarectangles in good yields. The same assemblies can also be easily isolated in one-pot procedures by mixing the organometallic clip, diamines and 4-formylpyridine.

Introduction

Over the past two decades, supramolecular structures with organometallic half-sandwich fragments have attracted much attention, including metallarectangles, metallacages and Borromean-type rings. Moreover, many of these structures have been utilized for various applications, such as catalysts, host–guest chemistry and others [1-17]. Through the use of a range of diverse functional ligands, the coordination-driven self-assembly has been proven to be a powerful tool to construct supramolecular architectures with controlled shapes and sizes [18-30]. Using this strategy, a host of exciting supramolecular

structures have been constructed by using two elaborately designed building blocks, such as dinuclear half-sandwich molecular clips and appropriate pyridyl ligands. The sizes and structures of the obtained molecular rectangles, cages or rings can be easily tuned by adjusting the length and shape of the bridging ligands and molecular clips. We and others have reported a suite of [2 + 2] tetranuclear metallarectangles, each formed using dinuclear molecular clips and pyridyl-based donor ligands [6-9,31-36]. The introduction of dynamic covalent bonds (such as imine C=N bonds), could allow the multicomponent assembly of such architectures using rather simple precursors, however, studies along these lines are rare [37]. Thus, the preparation of single and discrete supramolecular architectures via dynamic covalent bond-driven self-assembly remains challenging. Severin and co-workers have recently shown that metallamacrocycles and cages based on half-sandwich ruthenium could be obtained in one-pot reactions from simple building blocks [38,39]. This finding prompted us to investigate whether condensation reactions between amines and 4-formylpyridine can be used simultaneously with coordination bond formation to construct metallarectangle structures in one-pot reactions, thereby reducing both waste and the number of reaction steps.

In this work we successfully combine coordination-driven self-assembly and dynamic covalent chemistry through imine bond formation between amines and 4-formylpyridine to construct the desired rectangular tetrarhodium molecular rectangles.

Results and Discussion

The different approaches to the synthesis of tetranuclear molecular rectangles used in this work are shown in Scheme 1. We and others have used a two-step supramolecular design strategy for the formation of half-sandwich metal-based metallarectangles and metallacages [6-9]. Following this approach, two self-assembled metallarectangles with different bridging linkers **3a**,**b** were synthesized by utilizing the [$Cp^*_2Rh_2(\mu\text{-}\eta^2\text{-}\eta^2\text{-}C_2O_4)Cl_2$] unit as molecular clips (Scheme 1, method A).

Precursor complex **1**, which bears two labile triflato ligands was prepared in situ by chloride abstraction from [$Cp^*_2Rh_2(\mu\text{-}\eta^2\text{-}\eta^2\text{-}C_2O_4)Cl_2$] with AgOTf. Stirring a mixture of **1** and **L1** in a 1:1 molar ratio in methanol for 24 h resulted in a homogeneous, dark-red solution. The ^{1}H NMR spectrum of the obtained solution displays significant downfield shifts of the pyridyl signals, consistent with the loss of electron density upon coordination of the nitrogen atom to the metal centers (Figure 1a,b). Analysis of the reaction solution using electrospray ionization mass spectrometry (ESIMS) showed a signal at m/z = 476.1010, corresponding to a tertracation species of complex **3a**. The peak was isotopically resolved and agrees well with the theoretical isotopic distribution. In addition, the IR spectrum of the rhodium metallarectangle **3a** showed a C=N stretching band at 1618 cm^{-1}.

The same self-assembly protocol can also be used for the synthesis of metallarectangle **3b**. The combination of two labile-ligand precursor complexes **1** and two pyridyl-based ligands **L2** in a 1:1 molar ratio led to the formation of **3b** in good yield. The ^{1}H NMR spectrum of the reaction mixture revealed the formation of a single species. In the ^{1}H NMR spectrum of **3b**, only one sharp set of characteristic peaks was found. Again, significant downfield shifts of the pyridyl proton signals were observed, indicating the efficient self-assembly of the rhodium-based assembly (Figure 2a,b). Clear evidence for the formation of a discrete tetranuclear organometallic product was obtained from ESI mass spectrometry. Similar to that observed in complex **3a**, a peak at m/z = 450.0868 was observed, which is attributable to [**3b** − 4OTf]$^{4+}$, and its isotopic pattern is in good agreement with the theoretical distribution (Figure 3, right). The absorption band at 1620 cm^{-1} in the IR spectrum indicated the existence of an imine group.

The geometries of the metallarectangles **3a** and **3b** were expected to be similar, as they comprise two oxalate-bridged half-sandwich rhodium fragments linked by two Schiff-base ligands **L1** or **L2**, giving the desired tetranuclear metallarectangles. In order to test the possibility of using dynamic covalent chemistry to assemble these metallarectangles, we attempted a further method (Scheme 1, method B) to synthesize these assemblies. As shown in Scheme 1, a dinuclear molecular tweezer complex **2** bearing two pendant aldehyde groups can be formed from the labile ligand complex **1** and 4-formylpyridine, and subsequent reaction with diamines would potentially give tetranuclear metallarectangles. When equimolar amounts of either *trans*-4,4'-stilbenediamine or 1,5-diaminonaphthalene were added to methanol solutions of complex **2**, and allowed to react for 24 h at room temperature, the formation of tetranuclear [4 + 4] condensation products **3a** (Figure 1c) and **3b** (Figure 2c) was observed, respectively. Complexes **3a** and **3b** were isolated in good yields, and their structures were confirmed by ^{1}H NMR spectroscopy and ESI mass spectrometry.

After establishing that the condensation reaction of **2** with amines is an efficient method to form metallarectangles, we sought to test the possibility of forming the desired assemblies in a one-pot reaction, i.e., the combination of coordination-driven and dynamic covalent self-assembly strategies (Scheme 1, method C) [33]. When a mixture of the labile ligand complex **1**, *trans*-4,4'-stilbenediamine and 4-formylpyridine in a 1:1:1 molar ratio in methanol was allowed to react for 24 h at room temperature, the clear, quantitative formation of complex **3a** was revealed by NMR spectrometry (Figure 1e). The analo-

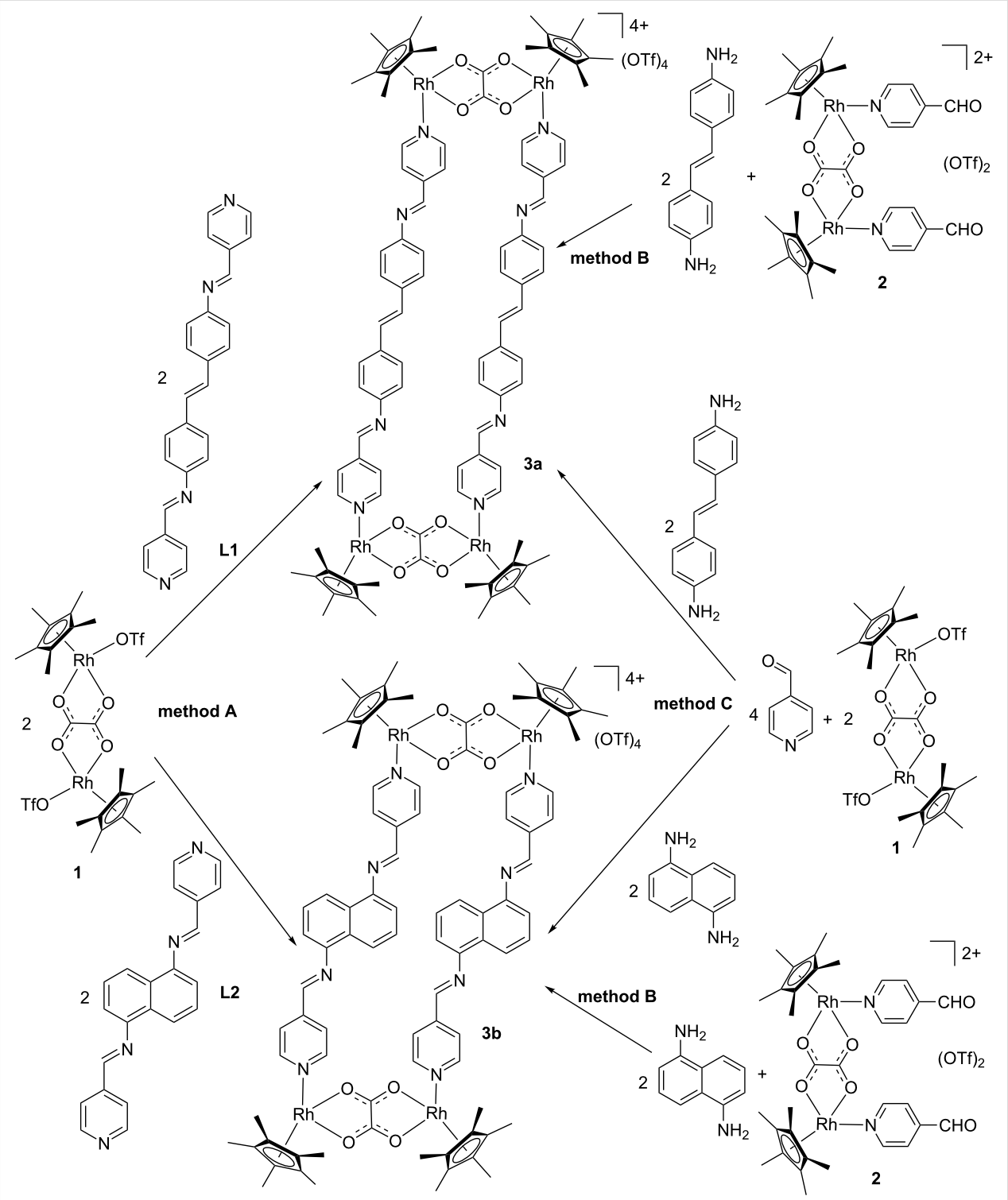

Scheme 1: Synthesis of half-sandwich rhodium metallarectangles via three different methods. Method A: coordination-driven self-assembly of organometallic clips and organic ligands; method B: [4 + 4] condensation reactions of half-sandwich rhodium-based dialdehyde complexes with diamines; method C: assembly of metallarectangles with organometallic clip, diamines and 4-formylpyridine in a one-pot procedure.

gous one-pot construction of **3b** was also successful (Figure 2e). Notably, the isolated yields of the metallarectangles are higher than the overall yields of the two-step method.

Since attempts to obtain X-ray quality single crystals of the target metallarectangles were unsuccessful, molecular simulations were performed to gain further insight into the

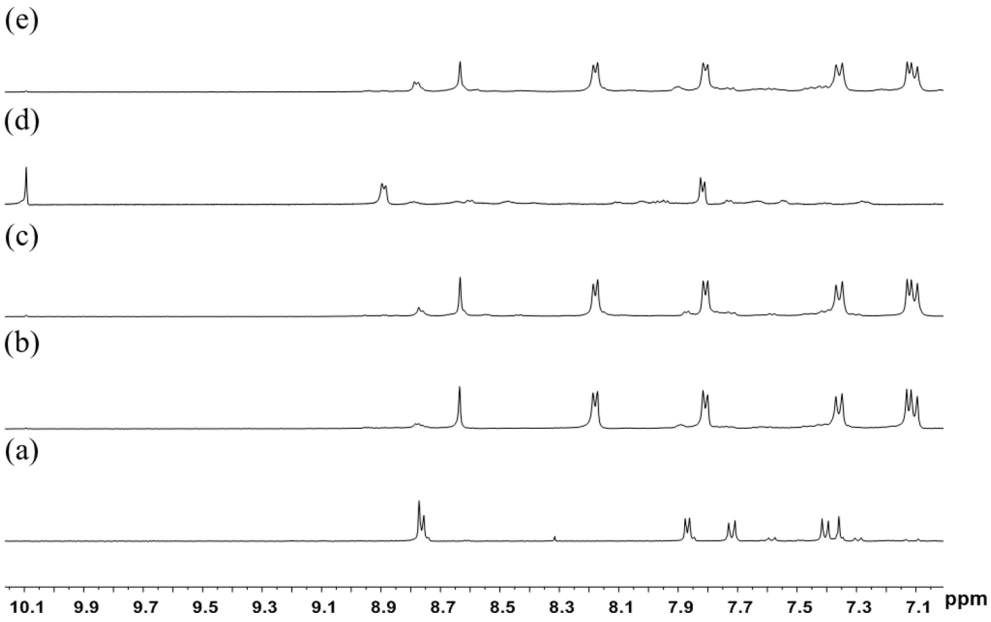

Figure 1: Partial ^{1}H NMR spectra (400 MHz, DMSO-d_6, ppm) of (a) **L1**; (b) the sample of metallarectagle **3a** obtained by coordination-driven self-assembly of organometallic clip **1** and **L1** (method A); (c) the sample of metallarectagle **3a** obtained through [4 + 4] condensation reactions of half-sandwich rhodium-based dialdehyde complex **2** with *trans*-4,4'-stilbenediamine (method B); (d) half-sandwich rhodium-based dialdehyde **2**; (e) the product of self-assembly of organometallic clip **1**, *trans*-4,4'-stilbenediamine and 4-formylpyridine in a one-pot procedure (method C).

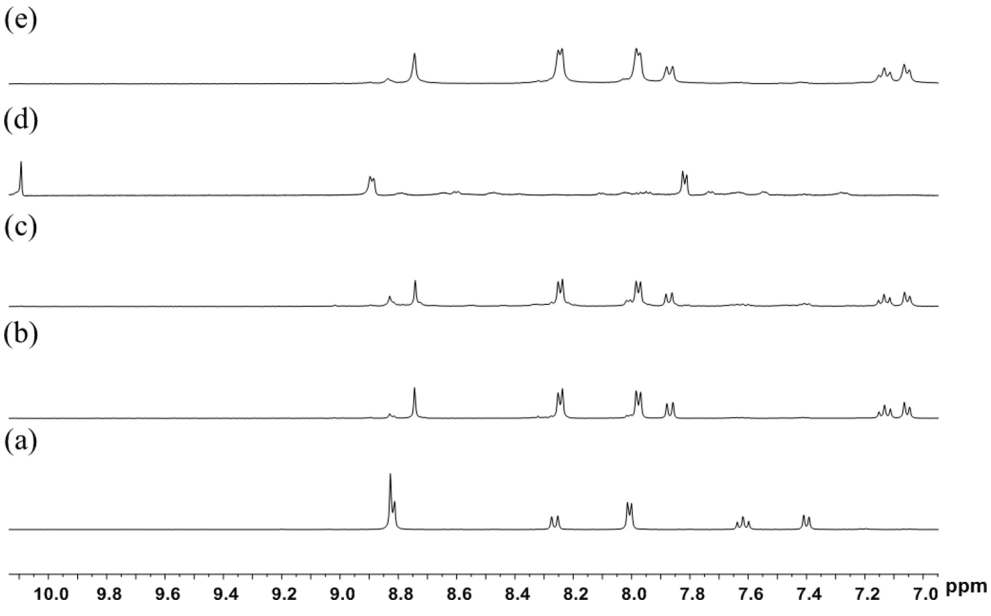

Figure 2: Partial ^{1}H NMR spectra (400 MHz, DMSO-d_6, ppm) of (a) **L2**; (b) a sample of metallarectangle **3b** obtained by coordination-driven self-assembly of organometallic clip **1** and **L2** (method A); (c) a sample of metallarectangle **3b** obtained by [4 + 4] condensation reactions of half-sandwich rhodium-based dialdehyde complex **2** with 1,5-diaminonaphthalene (method B); (d) half-sandwich rhodium-based dialdehyde **2**; (e) the product of assembly of organometallic clip **1**, 1,5-diaminonaphthalene and 4-formylpyridine in a one-pot procedure (method C).

structures of the assemblies **3a** and **3b**. The optimized structures of each assembly featured a similar rectangular metallacyclic macrocycle structure (Figure 4). The sizes of the assembled structures were estimated to be 26.3 × 5.6 Å (**3a**) and 20.1 × 5.6 Å (**3b**).

Conclusion

In summary, a modular protocol for the synthesis of metallarectangles is described. The desired tetranuclear metallarectangles can be obtained via three different approaches: 1) exploiting the coordination-driven self-assembly of half-

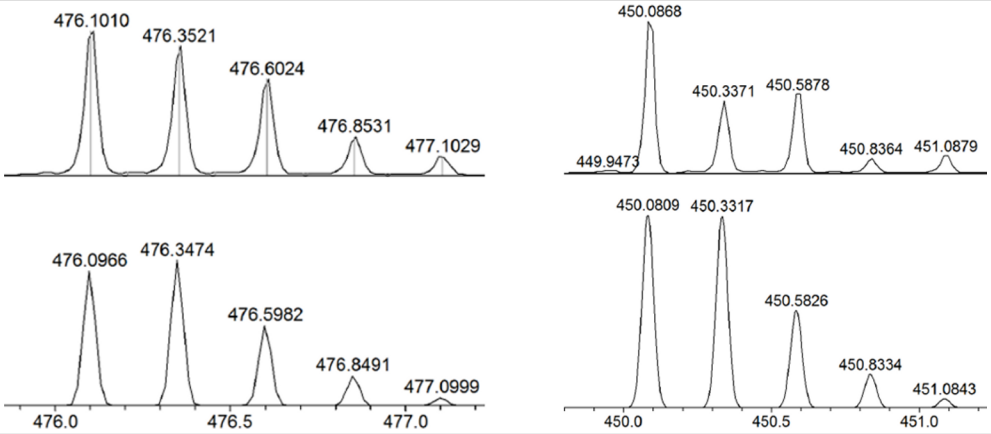

Figure 3: Calculated (bottom) and experimental (top) ESI-MS spectra of the tetracationic half-sandwich rhodium metallarectangles [**3a** – 4OTf]$^{4+}$ (left) and [**3b** – 4OTf]$^{4+}$ (right).

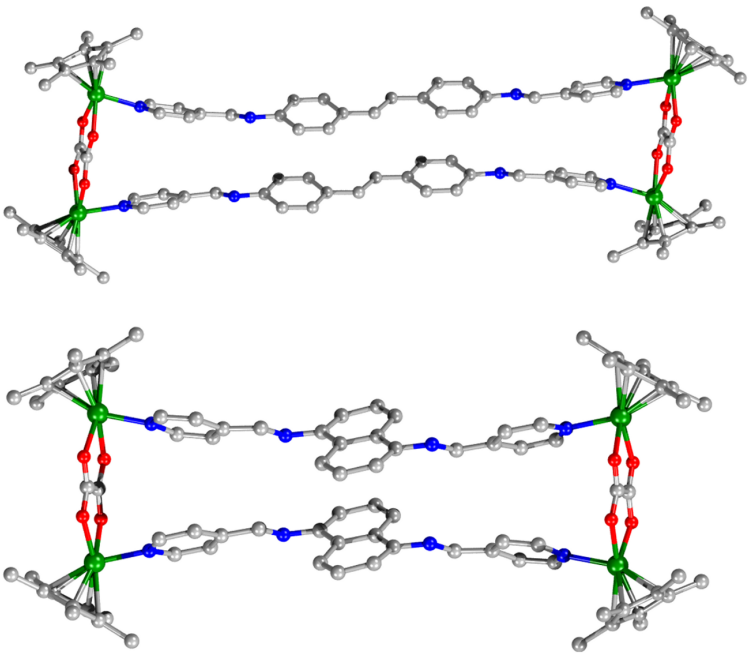

Figure 4: Optimized structures of the charged metallarectangles **3a** (top) and **3b** (bottom), optimized with the molecular mechanics force field. The graphics were produced using the Diamond software package. Colors: C, gray; O, red; N, blue; rhodium, green (hydrogen atoms have been removed for clarity).

sandwich rhodium-based organometallic clips and organic ligands, 2) [4 + 4] condensation reactions of diamines with dinuclear molecular tweezer complex bearing pendant aldehyde groups, and 3) a sample one-pot procedure involving mixing the organometallic clips, diamines and 4-formylpyridine. Our results thus present versatile and efficient approaches to the synthesis of molecular metallarectangles with intricate topologies. The methods shown here are potentially useful for the synthesis of functional molecular metallacages, and the experimental efforts in this direction are currently underway.

Experimental

Materials and methods

All manipulations were performed under an atmosphere of nitrogen using standard Schlenk techniques. Commercial grade solvents and reagents were used without further purification. $[Cp^*_2Rh_2(\mu\text{-}\eta^2\text{-}\eta^2\text{-}C_2O_4)Cl_2]$ [25], *trans*-4,4'-stilbenediamine [40] and **L2** [41] were prepared according to literature procedures. Methanol was purified by standard methods prior to use. NMR (400 MHz) spectra were obtained on a Bruker AVANCE III spectrometer. IR spectra of the solid samples (KBr tablets)

were recorded on a Bruker EQUINOX-55 (TENSOR27) IR spectrometer. Mass spectra were obtained with UltiMate3000 spectrometers.

General procedure for the synthesis of **L1** and **L2**

L1: To 4-formylpyridine (195 mg, 1.82 mmol) in dry CH_3OH (20 mL) was added *trans*-4,4'-stilbenediamine (191 mg, 0.91 mmol) at room temperature. The mixture was stirred at room temperature for 24 h and then filtered. The resulting yellow solid was washed with methanol (2 × 5 mL) and diethyl ether (2 × 5 mL) to give **L1** (318 mg, 90%). ^{1}H NMR (400 MHz, DMSO-d_6, ppm) δ 8.77 (s, 2H, -NCH-), 8.76 (d, J = 6.0 Hz, 4H), 7.87 (d, J = 6.0 Hz, 4H), 7.72 (d, J = 8.4 Hz, 4H), 7.41 (d, J = 8.4 Hz, 4H), 7.36 (s, 2H, -CH=CH-); IR (KBr, cm^{-1}): 3419 (m), 1597 (s), 1411 (m), 962 (m), 831 (s), 632 (m), 561 (s).

L2: A modified synthetic procedure adapted from literature methods [33] was used. To 4-formylpyridine (215 mg, 2.0 mmol) in dry CH_3OH (20 mL) was added 1,5-diaminonaphthalene (160 mg, 1.0 mmol) at room temperature. The mixture was stirred at room temperature for 24 h and then filtered. The resulting yellow solid was washed with diethyl ether (2 × 3 mL) and crystallized from CH_2Cl_2/hexane (1:1) to give **L2** (220 mg, 65%). ^{1}H NMR (400 MHz, DMSO-d_6, ppm) δ 8.83 (s, 2H, -NCH-), 8.82 (d, J = 6.0 Hz, 4H), 8.26 (d, J = 8.4 Hz, 2H), 8.01 (d, J = 6.0 Hz, 4H), 7.62 (t, 2H), 7.40 (d, J = 7.2 Hz, 2H); IR (KBr, cm^{-1}): 3024 (w), 1624 (s), 1597 (s), 1404 (s), 1317 (s), 1232 (s), 925 (s), 790 (s), 652 (m).

Synthesis of complex **2** $[Cp^*_2Rh_2(\mu\text{-}\eta^2\text{-}\eta^2\text{-}C_2O_4)(4\text{-}CHOPy)_2](OTf)_2$

AgOTf (36 mg, 0.14 mmol) was added to a solution of $[Cp^*_2Rh_2(\mu\text{-}\eta^2\text{-}\eta^2\text{-}C_2O_4)Cl_2]$ (45 mg, 0.07 mmol) in CH_3OH (15 mL) at room temperature and the mixture was stirred for 1 h, followed by filtration to remove insoluble materials. Then 4-formylpyridine (16 mg, 0.14 mmol) was added to the filtrate and the mixture was stirred for 24 h. The volume was reduced to 3 mL in vacuo. Upon the addition of diethyl ether, a light-yellow solid was precipitated and washed with diethyl ether (3 × 3 mL) and dried under vacuum (60 mg, 80%).^{1}H NMR (400 MHz, DMSO-d_6, ppm) δ 10.09 (s, 2H, -CHO), 8.89 (d, J = 5.0 Hz, 4H), 7.82 (d, J = 5.0 Hz, 4H), 1.55 (s, 30H, Cp*-H); HRMS–ESI (m/z): [**2** − 2OTf]$^{2+}$ calcd for $C_{34}H_{40}O_{12}N_2F_6S_2Rh_2$, 390.0571; found, 390.0541.

Synthesis of $[Cp^*_4Rh_4(\mu\text{-}\eta^2\text{-}\eta^2\text{-}C_2O_4)_2(L1)_2](OTf)_4$ (**3a**)

Method A: AgOTf (36 mg, 0.14 mmol) was added to a solution of $[Cp^*_2Rh_2(\mu\text{-}\eta^2\text{-}\eta^2\text{-}C_2O_4)Cl_2]$ (45 mg, 0.07 mmol) in CH_3OH (30 mL) at room temperature and the mixture was stirred for 1 h, followed by filtration to remove insoluble materials. Then a solution of **L1** (27 mg, 0.07 mmol) in 15 mL $CHCl_3$ was added dropwise to the filtrate. The mixture was stirred at room temperature for 24 h to give a deep red solution. The volume was reduced to 3 mL in vacuo. Upon the addition of diethyl ether, a black-red solid was precipitated and washed with $CHCl_3$ (2 × 3 mL) and dried under vacuum (61 mg, 70%). ^{1}H NMR (400 MHz, DMSO-d_6, ppm) δ 8.64 (s, 4H, -NCH-), 8.18 (d, J = 6.0 Hz, 8H), 7.81 (d, J = 6.4 Hz, 8H), 7.36 (d, J = 8.8 Hz, 8H), 7.12 (d, J = 6.0 Hz, 8H), 7.09 (s, 4H), 1.57 (s, 60H, Cp*-H). HRMS–ESI (m/z): [**3a** − 4OTf]$^{4+}$ calcd for $C_{100}H_{100}O_{20}N_8F_{12}S_4Rh_4$, 476.0966; found, 476.0986.

Method B: *trans*-4,4'-Stilbenediamine (14 mg, 0.07 mmol) was added to a solution of **2** (76 mg, 0.07 mmol) in CH_3OH (15 mL) at room temperature and the mixture was stirred for 24 h to give a deep red solution. Upon the addition of diethyl ether, a black-red solid was precipitated and washed with diethyl ether (3 × 3 mL) and dried under vacuum (63 mg, 72%). HRMS–ESI (m/z): [**3a** − 4OTf]$^{4+}$ calcd for $C_{100}H_{100}O_{20}N_8F_{12}S_4Rh_4$, 476.0966; found, 476.0963.

Method C: AgOTf (36 mg, 0.14 mmol) was added to a solution of $[Cp^*_2Rh_2(\mu\text{-}\eta^2\text{-}\eta^2\text{-}C_2O_4)Cl_2]$ (45 mg, 0.07 mmol) in CH_3OH (10 mL) at room temperature and the mixture was stirred for 1 h, followed by filtration to remove insoluble materials. Then *trans*-4,4'-stilbenediamine (15 mg, 0.07 mmol) was added to the filtrate. A solution of 4-formylpyridine (15 mg, 0.14 mmol) in 7 mL $CHCl_3$ was then added dropwise to the mixture and stirred for 24 h. The solvent was concentrated to about 3 mL. Diethyl ether was then added, and a black-red solid precipitated, which was washed with diethyl ether (3 × 3 mL) and chloroform (2 × 3 mL) and dried under vacuum (66 mg, 75%). HRMS–ESI (m/z): [**3a** − 4OTf]$^{4+}$ calcd for $C_{100}H_{100}O_{20}N_8F_{12}S_4Rh_4$, 476.0966; found, 476.1010.

Synthesis of $[Cp^*_4Rh_4(\mu\text{-}\eta^2\text{-}\eta^2\text{-}C_2O_4)_2(L2)_2](OTf)_4$ (**3b**)

Method A: AgOTf (36 mg, 0.14 mmol) was added to a solution of $[Cp^*_2Rh_2(\mu\text{-}\eta^2\text{-}\eta^2\text{-}C_2O_4)Cl_2]$ (45 mg, 0.07 mmol) in CH_3OH (15 mL) at room temperature and the mixture was stirred for 1 h, followed by filtration to remove insoluble materials. Then a solution of **L2** (24 mg, 0.07 mmol) in 7 mL $CHCl_3$ was added dropwise to the filtrate. The mixture was stirred at room temperature for 24 h and filtered. The resulting yellow solid was washed with chloroform (2 × 3 mL) and dried under vacuum (61 mg, 70%). ^{1}H NMR (400 MHz, DMSO-d_6, ppm) δ 8.74 (s, 4H, -NCH-), 8.25 (d, J = 6.0 Hz, 8H), 7.98 (d, J = 6.0 Hz, 8H), 7.87 (d, J = 8.8 Hz, 4H), 7.13 (t, 4H), 7.05 (d, J = 6.8 Hz, 4H), 1.59 (s, 60H, Cp*-H); HRMS–ESI (m/z):

[**3b** − 4OTf]$^{4+}$ calcd for $C_{92}H_{92}O_{20}N_8F_{12}S_4Rh_4$, 450.0809; found, 450.0873.

Method B: 1,5-Diaminonaphthalene (11 mg, 0.07 mmol) was added to a solution of **2** (76 mg, 0.07 mmol) in CH_3OH (20 mL) at room temperature and the mixture was stirred for 24 h to give a deep red solution. The volume was reduced to 3 mL in vacuo. Upon addition of diethyl ether, a yellow solid precipitated, which was washed with diethyl ether (3 × 5 mL) and dried under vacuum (61 mg, 73%). HRMS–ESI (*m*/*z*): [**3b** − 4OTf]$^{4+}$ calcd for $C_{92}H_{92}O_{20}N_8F_{12}S_4Rh_4$, 450.0809; found, 450.0807.

Method C: AgOTf (36 mg, 0.14 mmol) was added to a solution of [$Cp^*_2Rh_2(\mu\text{-}\eta^2\text{-}\eta^2\text{-}C_2O_4)Cl_2$] (45 mg, 0.07 mmol) in CH_3OH (15 mL) at room temperature and the mixture was stirred for 1 h, followed by filtration to remove insoluble materials. Then, 1,5-diaminonaphthalene (11 mg, 0.07mmol) was added to the filtrate. A solution of 4-formylpyridine (15 mg, 0.14 mmol) in 7 mL $CHCl_3$ was added dropwise to the mixture and stirred for 24 h. A yellow solid precipitated, which was washed with chloroform (2 × 3 mL) and dried under vacuum (60 mg, 72%). HRMS–ESI (*m*/*z*): [**3b** − 4OTf]$^{4+}$ calcd for $C_{92}H_{92}O_{20}N_8F_{12}S_4Rh_4$, 450.0809; found, 450.0868.

Acknowledgements

The authors gratefully acknowledge financial support from the NSFC (Nos. 21722105, 21102004, 21771146), the Scientific Research Foundation for the Returned Overseas Scholars of Shaanxi Province (2017001), the Shaanxi Key Laboratory of Physical-inorganic Chemistry (17JS133), the FM & EM International Joint Laboratory of Northwest University, and NSF of Anhui Province (1708085MB44).

ORCID® iDs

Wei-Guo Jia - https://orcid.org/0000-0001-7976-7543
Ying-Feng Han - https://orcid.org/0000-0002-9829-4670

References

1. Fish, R. H. *Coord. Chem. Rev.* **1999,** *185–186,* 569–584. doi:10.1016/S0010-8545(99)00011-9
2. Severin, K. *Coord. Chem. Rev.* **2003,** *245,* 3–10. doi:10.1016/S0010-8545(03)00028-6
3. Severin, K. *Chem. Commun.* **2006,** 3859–3867. doi:10.1039/b606632c
4. Boyer, J. L.; Kuhlman, M. L.; Rauchfuss, T. B. *Acc. Chem. Res.* **2007,** *40,* 233–242. doi:10.1021/ar050215j
5. Thanasekaran, P.; Lee, C.-C.; Lu, K.-L. *Acc. Chem. Res.* **2012,** *45,* 1403–1418. doi:10.1021/ar200243w
6. Cook, T. R.; Vajpayee, V.; Lee, M. H.; Stang, P. J.; Chi, K.-W. *Acc. Chem. Res.* **2013,** *46,* 2464–2474. doi:10.1021/ar400010v
7. Han, Y.-F.; Jia, W.-G.; Yu, W.-B.; Jin, G.-X. *Chem. Soc. Rev.* **2009,** *38,* 3419–3434. doi:10.1039/b901649j
8. Han, Y.-F.; Jin, G.-X. *Chem. Soc. Rev.* **2014,** *43,* 2799–2823. doi:10.1039/C3CS60343A
9. Han, Y.-F.; Jin, G.-X. *Acc. Chem. Res.* **2014,** *47,* 3571–3579. doi:10.1021/ar500335a
10. Lu, Y.; Deng, Y.-X.; Lin, Y.-J.; Han, Y.-F.; Weng, L.-H.; Li, Z.-H.; Jin, G.-X. *Chemistry* **2017,** *3,* 110–121. doi:10.1016/j.chempr.2017.06.006
11. Mirtschin, S.; Slabon-Turski, A.; Scopelliti, R.; Velders, A. H.; Severin, K. *J. Am. Chem. Soc.* **2010,** *132,* 14004–14005. doi:10.1021/ja1063789
12. Conrady, F. M.; Fröhlich, R.; Schulte to Brinke, C.; Pape, T.; Hahn, F. E. *J. Am. Chem. Soc.* **2011,** *133,* 11496–11499. doi:10.1021/ja205021p
13. Lee, H.; Elumalai, P.; Singh, N.; Kim, H.; Lee, S. U.; Chi, K.-W. *J. Am. Chem. Soc.* **2015,** *137,* 4674–4677. doi:10.1021/jacs.5b02573
14. Zhang, W.-Y.; Lin, Y.-J.; Han, Y.-F.; Jin, G.-X. *J. Am. Chem. Soc.* **2016,** *138,* 10700–10707. doi:10.1021/jacs.6b06622
15. Liu, Q.; Zhang, W.-H.; Lang, J.-P. *Coord. Chem. Rev.* **2017,** *350,* 248–274. doi:10.1016/j.ccr.2017.06.027
16. Lang, J.-P.; Xu, Q.-F.; Chen, Z.-N.; Abrahams, B. F. *J. Am. Chem. Soc.* **2003,** *125,* 12682–12683. doi:10.1021/ja036995d
17. Zhang, W.-H.; Ren, Z.-G.; Lang, J.-P. *Chem. Soc. Rev.* **2016,** *45,* 4995–5019. doi:10.1039/C6CS00096G
18. Wang, W.; Wang, Y.-X.; Yang, H.-B. *Chem. Soc. Rev.* **2016,** *45,* 2656–2693. doi:10.1039/C5CS00301F
19. Cotton, F. A.; Lin, C.; Murillo, C. A. *Acc. Chem. Res.* **2001,** *34,* 759–771. doi:10.1021/ar010062+
20. Fujita, M.; Tominaga, M.; Hori, A.; Therrien, B. *Acc. Chem. Res.* **2005,** *38,* 369–378. doi:10.1021/ar040153h
21. Caulder, D. L.; Raymond, K. N. *Acc. Chem. Res.* **1999,** *32,* 975–982. doi:10.1021/ar970224v
22. Saalfrank, R. W.; Maid, H.; Scheurer, A. *Angew. Chem., Int. Ed.* **2008,** *47,* 8794–8824. doi:10.1002/anie.200702075
23. Qiu, X.-T.; Yao, R.; Zhou, W.-F.; Liu, M.-D.; Liu, Q.; Song, Y.-L.; Young, D. J.; Zhang, W.-H.; Lang, J.-P. *Chem. Commun.* **2018,** *54,* 4168–4171. doi:10.1039/C8CC01950A
24. Zhang, W.-H.; Liu, Q.; Lang, J.-P. *Coord. Chem. Rev.* **2015,** *293–294,* 187–210. doi:10.1016/j.ccr.2014.12.010
25. Lang, J.-P.; Xu, Q.-F.; Yuan, R.-X.; Abrahams, B. F. *Angew. Chem., Int. Ed.* **2004,** *43,* 4741–4745. doi:10.1002/anie.200460076
26. Liu, D.; Lang, J.-P.; Abrahams, B. F. *J. Am. Chem. Soc.* **2011,** *133,* 11042–11045. doi:10.1021/ja203053y
27. Sun, L.-Y.; Sinha, N.; Yan, T.; Wang, Y.-S.; Tan, T. T. Y.; Yu, L.; Han, Y.-F.; Hahn, F. E. *Angew. Chem., Int. Ed.* **2018,** *57,* 5161–5165. doi:10.1002/anie.201713240
28. Cook, T. R.; Stang, P. J. *Chem. Rev.* **2015,** *115,* 7001–7045. doi:10.1021/cr5005666
29. Zhang, Y.-Y.; Gao, W.-X.; Lin, L.; Jin, G.-X. *Coord. Chem. Rev.* **2017,** *344,* 323–344. doi:10.1016/j.ccr.2016.09.010
30. Wu, G.-Y.; Chen, L.-J.; Xu, L.; Zhao, X.-L.; Yang, H.-B. *Coord. Chem. Rev.* **2018,** *369,* 39–75. doi:10.1016/j.ccr.2018.05.009
31. Zhang, H.-N.; Gao, W.-X.; Deng, Y.-X.; Lin, Y.-J.; Jin, G.-X. *Chem. Commun.* **2018,** *54,* 1559–1562. doi:10.1039/C7CC09448E
32. Han, Y.-F.; Li, H.; Jin, G.-X. *Chem. Commun.* **2010,** *46,* 6879–6890. doi:10.1039/c0cc00770f
33. Han, Y.-F.; Lin, Y.-J.; Jia, W.-G.; Jin, G.-X. *Organometallics* **2008,** *27,* 4088–4097. doi:10.1021/om800426e
34. Han, Y.-F.; Jia, W.-G.; Lin, Y.-J.; Jin, G.-X. *Organometallics* **2008,** *27,* 5002–5008. doi:10.1021/om800490s
35. Han, Y.-F.; Jia, W.-G.; Lin, Y.-J.; Jin, G.-X. *Angew. Chem., Int. Ed.* **2009,** *48,* 6234–6238. doi:10.1002/anie.200805949

36. Vajpayee, V.; Bivaud, S.; Goeb, S.; Croué, V.; Allain, M.; Popp, B. V.; Garci, A.; Therrien, B.; Sallé, M. *Organometallics* **2014,** *33,* 1651–1658. doi:10.1021/om401142j
37. Zarra, S.; Wood, D. M.; Roberts, D. A.; Nitschke, J. R. *Chem. Soc. Rev.* **2015,** *44,* 419–432. doi:10.1039/C4CS00165F
38. Granzhan, A.; Schouwey, C.; Riis-Johannessen, T.; Scopelliti, R.; Severin, K. *J. Am. Chem. Soc.* **2011,** *133,* 7106–7115. doi:10.1021/ja200580x
39. Schouwey, C.; Scopelliti, R.; Severin, K. *Chem. – Eur. J.* **2013,** *19,* 6274–6281. doi:10.1002/chem.201300098
40. Liu, X.; Liu, H.; Zhou, W.; Zheng, H.; Yin, X.; Li, Y.; Guo, Y.; Zhu, M.; Ouyang, C.; Zhu, D.; Xia, A. *Langmuir* **2010,** *26,* 3179–3185. doi:10.1021/la903838w
41. Min, D.; Cho, B.-Y.; Lee, S. W. *Inorg. Chim. Acta* **2006,** *359,* 577–584. doi:10.1016/j.ica.2005.09.041

License and Terms

BEILSTEIN JOURNAL OF ORGANIC CHEMISTRY

A switchable [2]rotaxane with two active alkenyl groups

Xiu-Li Zheng, Rong-Rong Tao, Rui-Rui Gu, Wen-Zhi Wang and Da-Hui Qu*

Full Research Paper

Open Access

Address:
Key Laboratory for Advanced Materials and Institute of Fine Chemicals, School of Chemistry and Molecular Engineering, East China University of Science and Technology, 130 Meilong Road, Shanghai, 200237, China

Email:
Da-Hui Qu* - dahui_qu@ecust.edu.cn

* Corresponding author

Keywords:
alkenyl bond; functional crown ether; stimuli-responsiveness; switchable rotaxane

Beilstein J. Org. Chem. **2018,** *14,* 2074–2081.
doi:10.3762/bjoc.14.181

Received: 16 April 2018
Accepted: 17 July 2018
Published: 08 August 2018

This article is part of the thematic issue "Macrocyclic and supramolecular chemistry".

Guest Editor: M.-X. Wang

Abstract

A novel functional [2]rotaxane containing two alkenyl bonds was designed, synthesized and characterized by ^{1}H, ^{13}C NMR spectroscopy and HRESI mass spectrometry. The introduction of alkenyl bonds endowed the [2]rotaxane a fascinating ability to react with versatile functional groups such as alkenyl and thiol functional groups. The reversible shuttling movement of the macrocycle between two different recognition sites on the molecular thread can be driven by external acid and base. This kind of rotaxane bearing functional groups provides a powerful platform for preparing stimuli-responsive polymers.

Introduction

Along with the development of supramolecular chemistry, much attention has been paid to the design and synthesis of novel and complicated mechanical interlocked molecules (MIMs) [1-7]. During the past years, a large number of different MIMs has been constructed, such as handcuff catenane [8], molecular elevators [9,10], molecular muscles [11,12], trefoil necklace [13-15], molecular walkers [16-18] and molecular pumps [19,20]. Combining the stimuli-responsive microscopic units with traditional materials to achieve morphological changes or other novel properties in smart materials is continuously receiving wide attention. Hence, in recent years, scientists have put more interests on the macroscopic changes caused by the stimuli-responsiveness of constituent units, which act as important precursors for constructing stimuli-responsive supramolecular materials [21,22].

Rotaxanes [23-31], as one of the most important MIMs, have been deeply investigated because of their excellent properties and convenient synthesis. By introducing various functional groups, such kind of MIMs has been used to construct stimuli-responsive materials, which diversified and improved the functions of traditional polymers. Up to now, the repertoire of available functional rotaxanes as building blocks for the fabrication of stimuli-responsive polymers remains limited because of the fact that the induction of active and functional groups make the preparation of rotaxanes more difficult and complicated. There-

fore, it is urgent to enrich both the family of stimuli-responsive units and the methods for constructing this kind of smart materials.

In this paper, we report the design, synthesis, characterization and shuttling motion of a [2]rotaxane **R1**, which is modified with two naked alkenyl bonds. In this [2]rotaxane, a functional dibenzo-24-crown-8 (DB24C8) macrocycle is interlocked with an flexible chain and could perform reversible shuttling between two different recognition sites under the stimuli of external acid and base. The alkenyl bonds were chosen as the functional group due to their considerable stability during the synthesis and remarkable reaction activity. The latter indicates the ability of reacting with different functional groups such as alkenyl bonds in the presence of Grubbs' catalyst and thiol groups irradiated by UV light. Besides, the shuttling movement of the DB24C8 macrocyclic ring was confirmed by ^{1}H NMR spectroscopy.

Results and Discussion

The structures of the two states of [2]rotaxane **R1** are shown in Scheme 1. In the target structure [2]rotaxane **R1**, the DB24C8 macrocycle is functionalized with an alkenyl unit on one of the benzene groups. Two distinguishable recognition sites, a dibenzylammonium (DBA) and an amide binding site, are introduced to the axle and linked with a long alkyl chain. The amide moiety could act as another combining station when the DBA site is deprotonated by external base. Besides, in the structure, one side of the chain is terminated by a bulky stopper bearing three long alkyl chains to prevent the macrocyclic moiety from slipping out the thread. Meanwhile, the long alkyl chains make it easy to form gels when the alkenyl units are reacted to generate polymers. On the other side, a naked alkenyl bond is introduced in the *para* position of the aromatic stopper. In the presence of external acid–base stimuli, the macrocyclic ring could be driven back and forth along the linear thread. Deprotonation of the DBA site by base makes the DB24C8 moiety

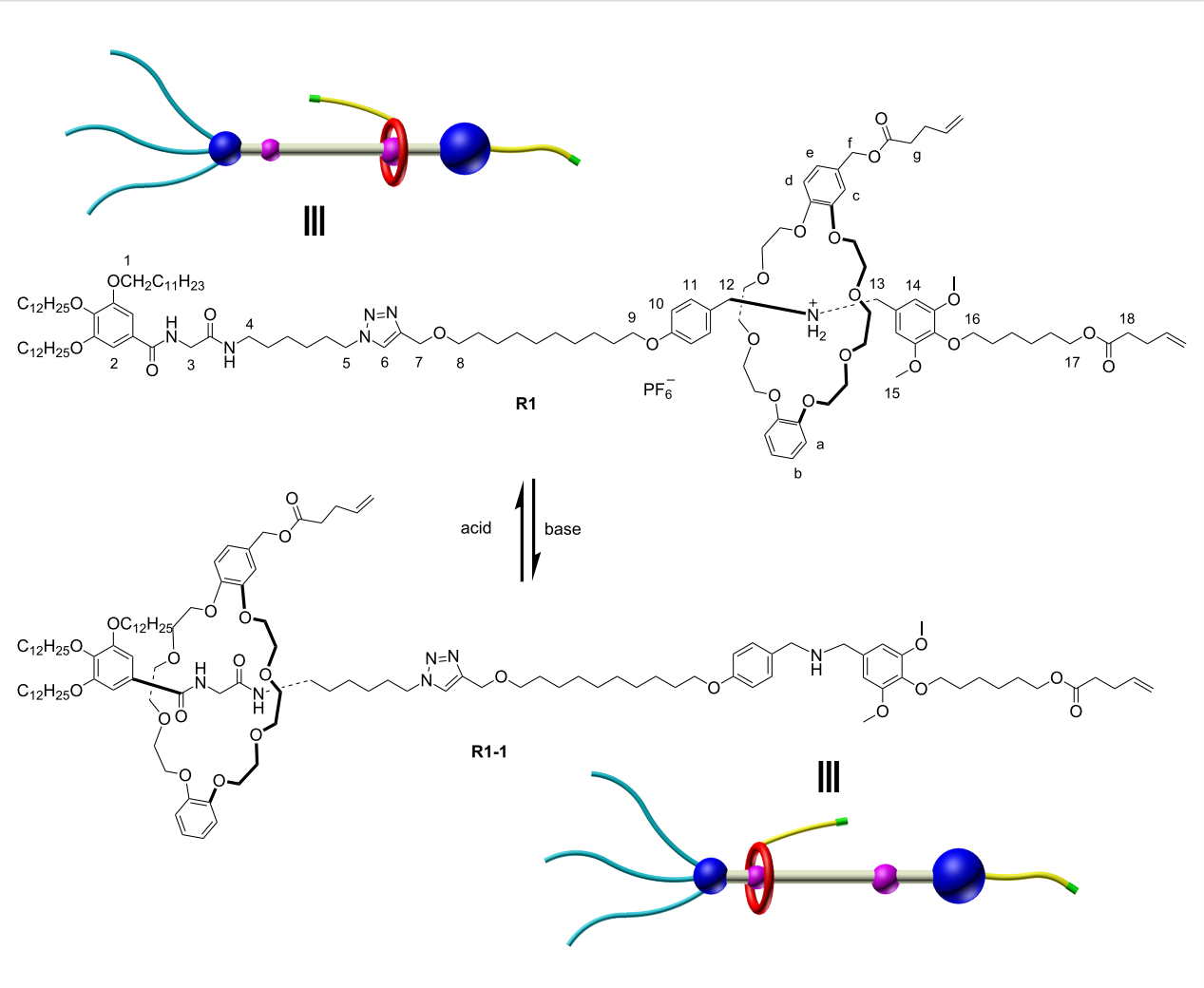

Scheme 1: Chemical structures and acid-base stimuli responsiveness of target [2]rotaxane **R1** and deprotonated [2]rotaxane **R1-1**.

slide to the amide station and the macrocycle could move back to the DBA recognition site when acid was added (Scheme 1).

The synthesis routes of the target compound [2]rotaxane **R1** are shown in Scheme 2. Compounds **1** [32], **2** [33], **6** [34], **7** [35] and functional crown ether **9** [36] were synthesized according to the previous literature. The key intermediate compound **5**, containing a prior DBA recognition station and possessing alkynyl and ethylenic groups at two terminals respectively, was prepared from aldehyde **1** and amine **2**. A "Schiff base" reaction was introduced at first and treated with $NaBH_4$, protected by di-*tert*-butyl pyrocarbonate to get compound **3**. The esterification reaction was carried out subsequently between hydroxy compound **3** and allylacetic acid to afford compound **4**, which was further reacted with CF_3COOH and followed by the anion exchange in the methyl alcohol with saturated NH_4PF_6 solution to obtain compound **5**. For another key intermediate **8**, containing an amide site for stabilizing the DB24C8 macrocycle, a 1,2,3-tris(dodecyloxy) benzene group as a stopper and an azide group which is used for the reaction with other moieties, was prepared through the amide reaction between compound **6** and 6-azidohexan-1-amine in the presence of 2-chloro-4,6-dimethoxy-1,3,5-triazine and *N*-methylmorpholine. Finally, the classical and effective "Click" reaction was used to produce the target compound [2]rotaxane **R1**. The crown ether **9** and dibenzylammonium ion ($R_2NH_2^+$) containing intermediate compound **5** were assembled in dichloromethane through host–guest interaction and capped with compound **8** under Cu(I)-catalyzed azide–alkyne cycloaddition to get the final [2]rotaxane with two distinguishable recognition sites.

The target [2]rotaxane **R1** was then characterized by ^1H NMR spectroscopy and high-resolution electrospray ionization (HRESI) mass spectrometry. The HRESI mass spectra of [2]rotaxane **R1** showed a major peak at *m*/*z* 2083.3862, corresponding to the species of **R1** losing one PF_6^- anion, i.e., $[M - PF_6^-]^+$. The ^1H NMR spectrum also fitted the **R1** structure well and reveals that the DB24C8 macrocycle **9** prefers

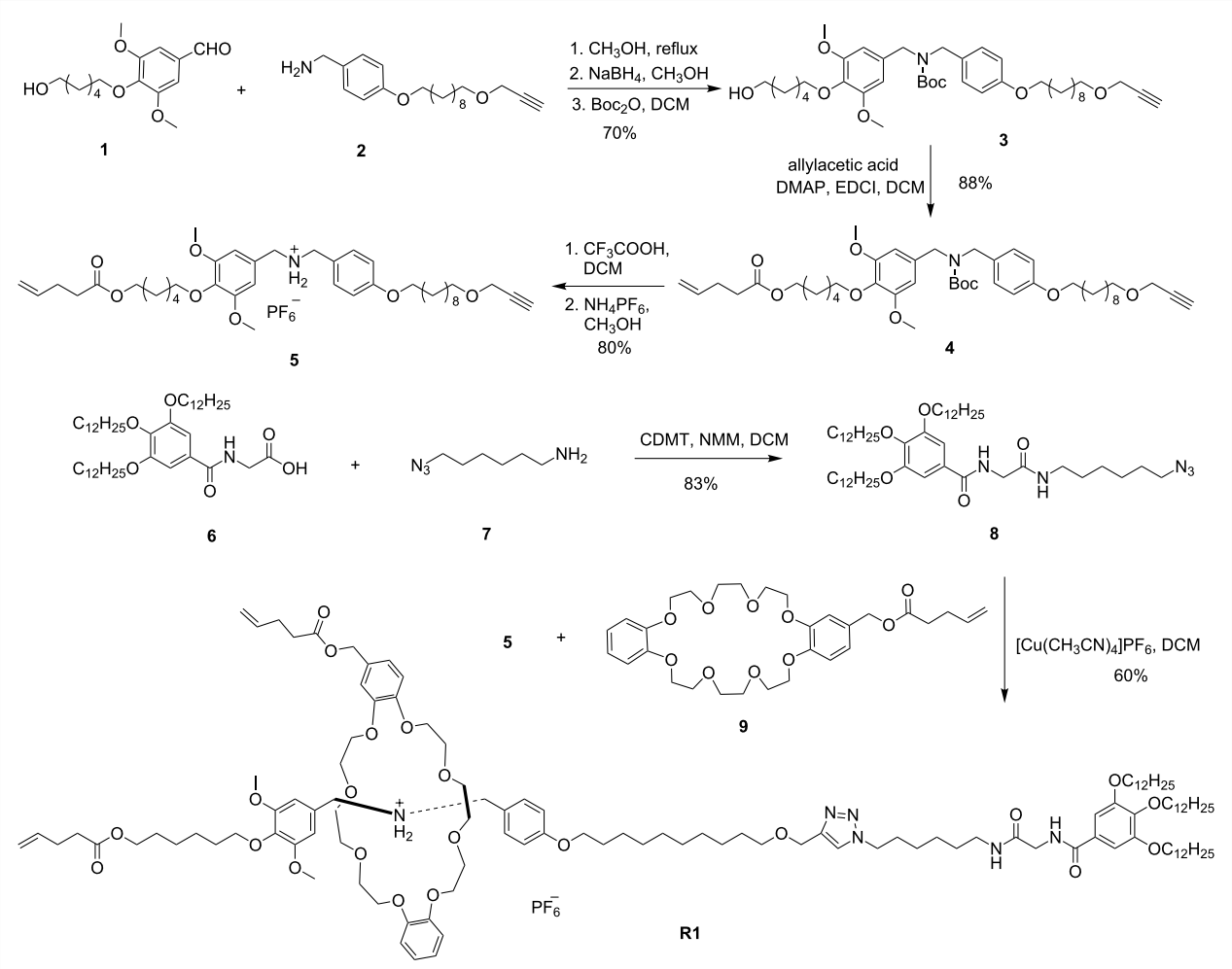

Scheme 2: Syntheses of key intermediates **5**, **8** and target [2]rotaxane **R1**.

encompassing the DBA recognition site. Comparing the ^{1}H NMR spectrum of the rotaxane product **R1** with the reactants **8** and **5** (Figure 1), the resonances of protons H5 and H7 were both shifted downfield ($\Delta\delta_{H5}$ = 1.09 ppm and $\Delta\delta_{H7}$ = 0.51 ppm) while a new peak appeared at 7.56 ppm. This new peak corresponds to H6 coming from the alkynyl–azide cycloaddition. Meanwhile, the signal of H12 and H13 split into two signals and underwent downfield shifts ($\Delta\delta_{H12}$ = 0.73 ppm and $\Delta\delta_{H13}$ = 0.87 ppm) while those of H11 and H10 moved upfield ($\Delta\delta_{H11}$ = −0.08 ppm and $\Delta\delta_{H10}$ = −0.20 ppm). Nevertheless, there were no obvious changes in protons of H3, H4 and H2, indicating that the macrocycle stayed at the DBA recognition site. These results were consistent with the previous literature report by our group [37]. All the evidences discussed above demonstrate that the axle compound successfully threaded into the macrocycle and consequently formed the target [2]rotaxane **R1**.

The reversible shuttling motion of the functional DB24C8 macrocycle between the two different recognition sites on the axle was also confirmed by the ^{1}H NMR spectroscopy. After addition of 2 equiv1,8-diazabicyclo[5.4.0]undec-7-ene (DBU) to [2]rotaxane **R1** in $CDCl_3$ to deprotonate the ammonium moiety, the DB24C8 macrocycle moved to the amide station. As shown in Figure 2, the protons H12, H13 shifted upfield ($\Delta\delta_{H12}$ = −0.99 ppm and $\Delta\delta_{H13}$ = −0.75 ppm) and incorporated into one signal peak from two while the H11 and H10 shifted slightly downfield ($\Delta\delta_{H11}$ = 0.05 ppm and $\Delta\delta_{10}$ = 0.19 ppm) due to the deprotonation of the $R_2NH_2^+$ and the migration of macrocycle. At the same time, the peaks for the protons around the amide site changed, for H4, H5, H6 with $\Delta\delta_{H4}$ = −0.26 ppm, $\Delta\delta_{H5}$ = −0.14 ppm and $\Delta\delta_{H6}$ = −0.09 ppm, respectively and H_3 with a $\Delta\delta_{H3}$ = 0.51 ppm due to the association with the DB24C8 macrocycle through hydrogen bonding. All the evidences reveal that the functionalized macrocycle migrated from the DBA recognition site to the amide station when an external base was added to the solution of rotaxane **R1**. Then, 3 equiv trifluoroacetic acid were added to reprotonate the -NH- moiety, the ^{1}H NMR spectrum restored to the initial state, showing that the macrocyclic compound **9** moved back to the DBA recognition site. Therefore, the reversible shuttling movement of DB24C8 moiety along the thread between two recognition sites driven by acid-base stimuli has been confirmed.

To further demonstrate the binding mode of the functional macrocycle with the axle, 2D ROESY NMR spectra of rotaxane

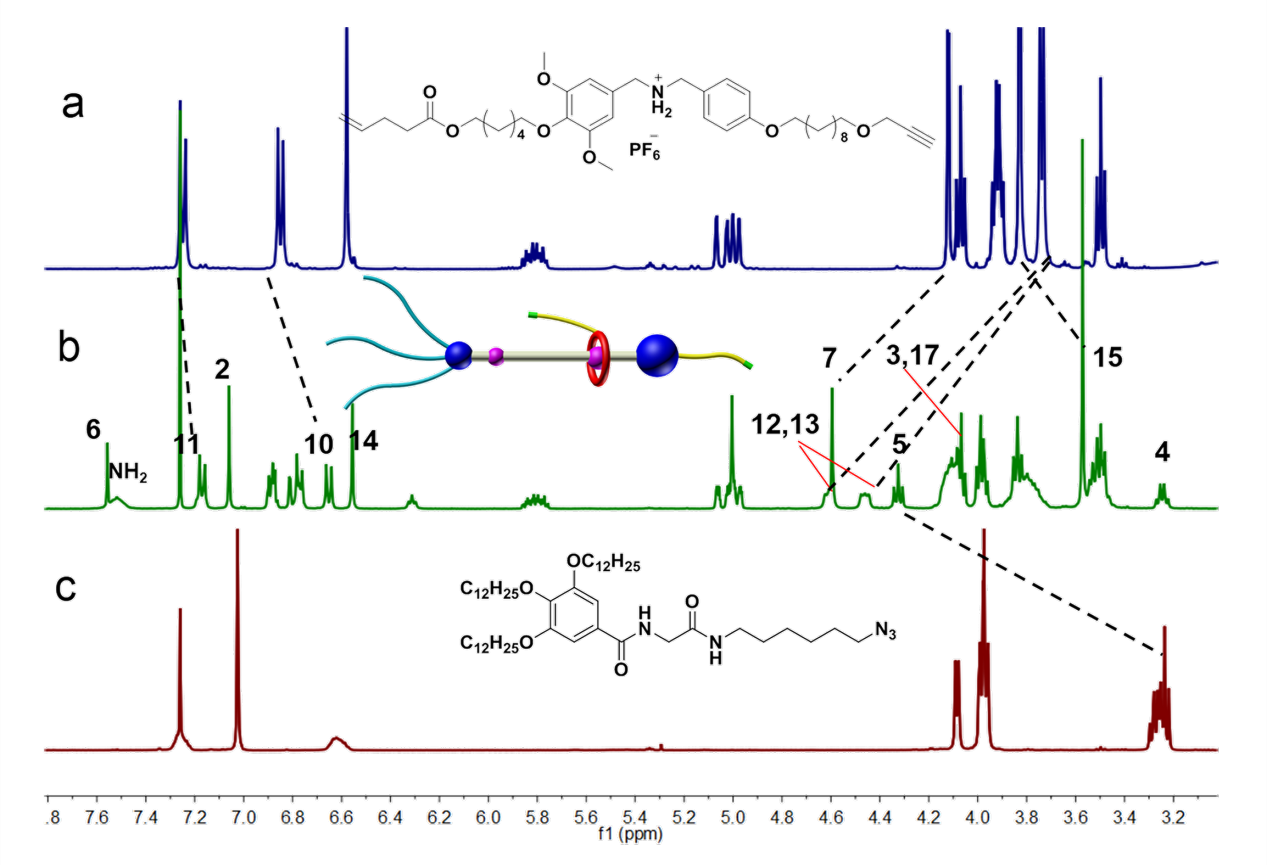

Figure 1: Partial ^{1}H NMR spectra (400 MHz, $CDCl_3$, 298 K). (a) Compound **5**, (b) target [2]rotaxane **R1**, (c) azide compound **8**.

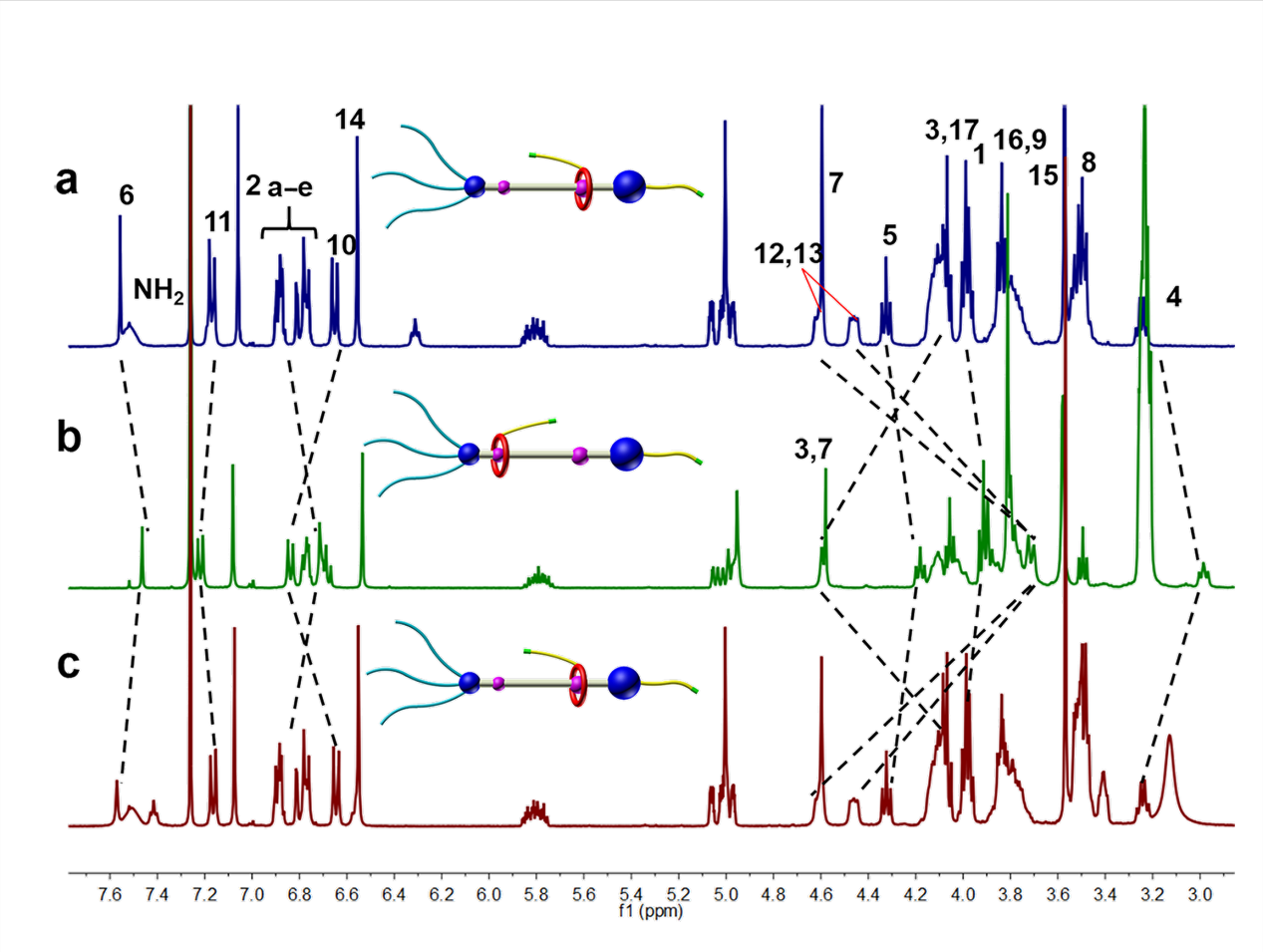

Figure 2: Partial ^{1}H NMR spectra (400 MHz, $CDCl_3$, 298 K). (a) [2]Rotaxane **R1**, (b) deprotonation by the addition of 2.0 equiv of DBU to (a), (c) reprotonation with addition of 3.0 equiv of TFA to (b).

R1 before and after the deprotonation in $CDCl_3$ were obtained. As shown in Figure 3a, the cross-peaks of phenyl protons H10 (peak A), H14 (peak B), H11 (peak C) (around the DBA recognition site) and methylene protons on the functional crown ether indicate that the DB24C8 macrocycle was located on the DBA site, corresponding to the structure of [2]rotaxane **R1**. After addition of 2 equiv DBU to the solution of **R1**, the NOE correlations between the phenyl proton H2 (peak D) near the amide

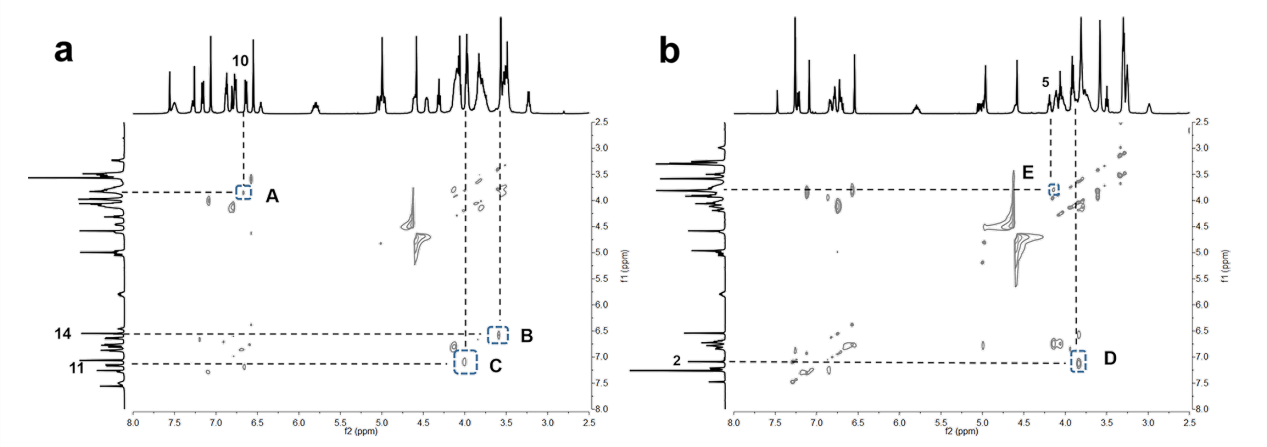

Figure 3: Partial 2D ROESY NMR spectra (500 MHz, $CDCl_3$, 298 K). (a) [2]Rotaxane **R1**, (b) deprotonation with addition of 2.0 equiv of DBU to (a).

station, H5 (peak E) on the thread and methylene proton on DB24C8 could be observed (see Figure 3b), illustrating the position of the DB24C8 ring on the amide recognition site.

Conclusion

In summary, a novel functional [2]rotaxane **R1** with two alkenyl bonds on the DB24C8 macrocycle and axle, respectively, was prepared and well characterized. The shuttling movement of the functionalized DB24C8 macrocycle between the DBA recognition site and amide moiety could be realized by stimuli of external acid-base and was investigated by ^{1}H NMR and 2D ROESY NMR spectroscopy. The naked alkenyl groups could react with other functional groups such as alkenyl and thiol groups to prepare stimuli-responsive polymers. Besides, the introduction of long alkyl chains makes the polymers easier to form gels. This kind of functional rotaxane enriches the species of building blocks to construct stimuli-responsive polymers and smart materials.

Experimental

General and materials

^{1}H NMR and ^{13}C NMR spectra were measured on a Bruker AV-400 spectrometer. The electronic spray ionization (ESI) mass spectra were tested on a LCT Premier XE mass spectrometer.

Chemicals were used as received from Acros, Aldrich, Fluka, or Merck. All solvents were reagent grade, which were dried and distilled prior to use according to standard procedures. The molecular structures were confirmed via ^{1}H NMR, ^{13}C NMR and high-resolution ESI mass spectroscopy. The synthesis of compound **1**, **2**, **6**, **7**, **9** have already been reported.

Synthesis

Compound 8: The mixture of compound **6** (5.0 g, 6.83 mmol), compound **7** (2.9 g, 20.49 mmol) and 2-chloro-4,6-dimethoxy-1,3,5-triazine (CDMT, 3.6 g, 20.49 mmol) was placed in a 250 mL round-bottom flask and dissolved by 100 mL methylene chloride. Then, *N*-methylmorpholine (NMM, 3.5 g, 34.15 mmol) was added into the solution slowly under ice bath cooling. Afterwards, the mixture was stirred at 40 °C for 12 h under an argon atmosphere. The reaction mixture was cooled to room temperature, the solution was evaporated under reduced pressure and the residue was purified via column chromatography (SiO_2, PE/EA = 3:1) to give compound **8** (4.9 g, 83%) as a white solid. ^{1}H NMR ($CDCl_3$, 400 MHz, 298 K) δ 7.30–7.23 (m, 1H), 7.02 (s, 2H), 6.67–6.65 (m, 1H), 4.28 (d, J = 5.2 Hz, 2H), 4.02–3.93 (m, 6H), 3.31–3.19 (m, 4H), 1.80–1.72 (m, 6H), 1.61–1.49 (m, 4H), 1.48–1.40 (m, 6H), 1.36–1.23 (m, 52H), 0.87 (t, J = 6.8 Hz, 9H); ^{13}C NMR ($CDCl_3$, 100 MHz, 298 K) δ 169.2, 167.8, 153.1, 141.3, 128.1, 105.6, 73.5, 69.2, 51.2, 44.1, 39.5, 31.9, 30.2, 29.70, 29.68, 29.66, 29.62, 29.56, 29.39, 29.36, 29.34, 29.31, 28.7, 26.4, 26.3, 26.07, 26.05, 22.7, 14.1; HRMS–ESI–TOF (m/z): $[M + K]^+$ calcd for $C_{51}H_{93}N_5O_5K^+$, 894.6808; found, 894.6813.

Compound 3: A mixture of **1** (3.0 g, 10.63 mmol) and **2** (4.0 g, 12.75 mmol) in methyl alcohol (100 mL) was refluxed overnight under a nitrogen atmosphere. After the reaction mixture was cooled to room temperature, $NaBH_4$ (1.6 g, 30.5 mmol) was then added to the solution in portions while colling in an ice bath. After the mixture was stirred overnight, the solvent was removed under vacuum, and the residue was extracted by dichloromethane. The organic layer was washed by brine, dried with Na_2SO_4, and then concentrated to give the free amine compound. To the solution of the amine in dry DCM (50 mL) was added di-*tert*-butyldicarbonate (3.5 g, 15.95 mmol) and the mixture was stirred for 5 h at room temperature. Then, the reaction mixture was washed with water, dried over Na_2SO_4 and evaporated in vacuo to give a crude product, which was purified by column chromatography (SiO_2, PE/EA = 2:1) to afford product **3** (4.4 g, 60%) as a yellow oil. ^{1}H NMR ($CDCl_3$, 400 MHz, 298 K) δ 7.20–7.01 (m, 2H), 6.83 (d, J = 8.4 Hz, 2H), 6.37 (d, J = 26.0 Hz, 2H), 4.29 (dd, J = 32.8 Hz, J = 18.4 Hz, 4H), 4.12 (s, 2H), 3.97–3.87 (m, 4H), 3.78 (s, 6H), 3.62 (t, J = 6.4 Hz, 2H), 3.49 (t, J = 6.4 Hz, 2H), 2.41 (s, 1H), 1.79–1.70 (m, 4H), 1.61–1.54 (m, 4H), 1.52–1.35 (m, 15H), 1.37–1.27 (m, 10H); ^{13}C NMR ($CDCl_3$, 100 MHz, 298 K) δ 171.2, 158.3, 153.2, 129.6, 129.3, 128.7, 114.3, 104.9, 104.3, 79.9, 74.0, 73.2, 70.2, 67.9, 62.7, 60.3, 57.9, 56.0, 32.6, 29.9, 29.6, 29.30, 29.27, 29.2, 28.4, 26.0, 25.9, 25.5, 25.4; HRMS–ESI–TOF (m/z): $[M + Na]^+$ calcd for $C_{40}H_{61}NO_8Na^+$, 706.4289; found, 706.4295.

Compound 4: To the mixture of compound **3** (2.0 g, 2.92 mmol) and allylacetic acid (0.88 g, 8.77 mmol) in DCM (50 mL) was added EDCI (2.24 g, 11.68 mmol) and DMAP (0.36 g, 2.92 mmol) while cooling with an ice bath. After that the mixture was stirred overnight at room temperature and then washed the mixture with brine (3 × 50 mL). The organic layer was dried over anhydrous sodium sulfate. The combined organic layer was evaporated, and the residue was purified via column chromatography (SiO_2, PE/EA = 15:1) to give compound **4** (1.97 g, 88%) as a yellow oil. ^{1}H NMR ($CDCl_3$, 400 MHz, 298 K) δ 7.21–7.03 (m, 2H), 6.84 (d, J = 8.4 Hz, 2H), 6.38 (d, J = 22.8 Hz, 2H), 5.87–5.76 (m, 1H), 5.09–4.95 (m, 2H), 4.29 (dd, J = 32.0 Hz, J = 16.4 Hz, 4H), 4.13 (d, J = 2.4 Hz, 2H), 4.08 (t, J = 6.8 Hz, 2H), 3.94 (t, J = 6.4 Hz, 4H), 3.78 (s, 6H), 3.50 (t, J = 6.8 Hz, 2H), 5.18–2.33 (m, 5H), 1.81–1.70 (m, 4H), 1.68–1.39 (m, 21H), 1.34–1.28 (m, 8H); ^{13}C NMR ($CDCl_3$, 100 MHz, 298 K) δ 173.1, 158.4, 155.9, 153.4, 136.7, 129.7, 129.3, 128.7, 115.4, 114.4, 104.9, 104.3,

80.0, 74.0, 73.1, 70.4, 70.2, 67.9, 64.4, 57.9, 56.0, 33.5, 29.9, 29.4, 29.33, 29.30, 29.2, 28.8, 28.6, 28.4; HRMS–ESI–TOF (*m*/z): $[M + Na]^+$ calcd for $C_{45}H_{67}NO_9Na^+$, 788.4708; found, 788.4732.

Compound 5: TFA (1.9 mL, 25.72 mmol) was added to a solution of the product **4** (1.97 g, 25.72 mmol) in dichloromethane (50 mL) and the mixture was stirred for 10 h at room temperature. The organic solvent was evaporated under reduced pressure to get a yellow solid, which was dissolved in MeOH (50 mL) and 20 mL saturated aqueous solution of NH_4PF_6 was added. After stirring for 5 h at room temperature, the mixture was diluted with CH_2Cl_2 (100 mL), the organic layer was separated and evaporated under reduced pressure to get the crude product, which was purified by column chromatography (SiO_2, CH_2Cl_2/MeOH = 50:1) to afford product **5** (1.67 g, 80%) as a yellow solid. ^{1}H NMR ($CDCl_3$, 400 MHz, 298 K) δ 7.26 (d, *J* = 8.8 Hz, 2H), 6.84 (d, *J* = 8.8 Hz, 2H), 6.57 (s, 2H), 5.90–5.74 (m, 1H), 5.13–4.89 (m, 2H), 4.13 (d, *J* = 2.4 Hz, 2H), 4.08 (t, *J* = 6.8 Hz, 2H), 3.97–3.88 (m, 4H), 3.84 (s, 6H), 3.74 (d, *J* = 6.0 Hz, 4H), 3.51 (t, *J* = 6.4 Hz, 2H), 2.48–2.32 (m, 5H), 1.81–1.70 (m, 4H), 1.69–1.55 (m, 4H), 1.53–1.38 (m, 6H), 1.36–1.28 (m, 10H); ^{13}C NMR ($CDCl_3$, 100 MHz, 298 K) δ 173.3, 160.3, 153.4, 136.8, 136.5, 131.4, 125.2, 121.4, 115.4, 115.0, 106.6, 79.9, 74.1, 73.1, 70.2, 68.0, 64.3, 57.9, 56.0, 51.6, 51.2, 33.4, 29.43, 29.38, 29.30, 29.28, 29.1, 28.8, 28.4, 26.0, 25.9, 25.5, 25.1; HRMS–ESI–TOF (*m*/*z*): $[M - PF_6^-]^+$ calcd for $C_{40}H_{60}NO_7^+$, 666.4364; found, 666.4361.

Compound R1: A mixture of **5** (300 mg, 0.370 mmol) and crown ether **9** (414 mg, 0.739 mmol) was dissolved in dry CH_2Cl_2 (10 mL) and stirred for 0.5 h at room temperature. Then compound **8** (475 mg, 0.555 mmol) and $[Cu(CH_3CN)_4]PF_6$ (138 mg, 0.370 mmol) were added to the solution. The mixture was stirred for two days under an argon atmosphere at room temperature. After removal of the solvent, the residue was purified via column chromatography (SiO_2, CH_2Cl_2/MeOH = 80:1) to give compound **R1** (495 mg, 60%) as a yellow solid. ^{1}H NMR ($CDCl_3$, 400 MHz, 298 K) δ 7.61–7.42 (m, 3H), 7.33 (t *J* = 4.8 Hz, 1H), 7.16 (d *J* = 8.8 Hz, 2H), 7.06 (s, 2H), 6.91–6.83 (m, 3H), 6.82–6.72 (m, 4H), 6.63 (d *J* = 8.8 Hz, 2H), 6.58–6.45 (m, 3H), 5.87–5.71 (m, 2H), 5.09–4.91 (m, 6H), 4.68–4.53 (m, 4H), 4.51–4.40 (m, 2H), 4.31 (t, *J* = 7.2 Hz, 2H), 4.13–4.04 (m, 10H), 4.00–3.93 (m, 6H), 3.85–3.70 (m, 12H), 3.56 (s, 6H), 3.53–3.46 (m, 8H), 3.23 (dd, *J* = 12.8 Hz, *J* = 6.8 Hz, 2H), 2.46–2.32 (m, 8H), 2.07–1.99 (m, 2H), 1.92–1.83 (m, 2H), 1.78–1.58 (m, 12H), 1.51–1.36 (m, 14H), 1.31–1.22 (m, 62H), 0.86 (t, *J* = 6.4 Hz, 9H); ^{13}C NMR ($CDCl_3$, 100 MHz, 298 K) δ 173.1, 172.8, 169.2, 167.5, 159.8, 153.4, 153.0, 147.3, 147.1, 145.2, 141.0, 137.4, 136.6, 136.5, 130.6, 129.4, 128.3, 127.4, 122.8, 122.5, 121.8, 121.7, 115.5, 115.4, 114.4, 112.8, 112.33, 112.26, 105.7, 105.5, 73.4, 73.2, 70.8, 70.4, 70.1, 70.0, 69.1, 68.1, 68.0, 67.9, 65.8, 64.4, 64.1, 55.9, 52.3, 52.1, 50.0, 43.8, 39.1, 33.5, 33.4, 31.9, 30.3, 29.9, 29.7, 29.64, 29.62, 29.58, 29.53, 29.36, 29.32, 29.30, 29.27, 29.1, 28.9, 28.8, 28.7, 28.5, 26.03, 26.01, 25.9, 25.8, 25.7, 25.6, 25.4, 22.6, 14.1; HRMS–ESI–TOF (*m*/*z*): $[M - PF_6^-]^+$ calcd for $C_{121}H_{193}N_6O_{22}^+$, 2083.4196; found, 2083.3862.

Supporting Information

Supporting Information File 1

^{1}H, ^{13}C NMR spectra and HRESI mass spectra of compounds **3**, **4**, **5**, **8** and [2]rotaxane **R1**.
[https://www.beilstein-journals.org/bjoc/content/supplementary/1860-5397-14-181-S1.pdf]

Acknowledgements

We thank the support of NSFC/China (21672060), the Fundamental Research Funds for the Central Universities (WJ1616011, WJ1213007, 222201717003), the Programme of Introducing Talents of Discipline to Universities (B16017).

ORCID® iDs

Da-Hui Qu - https://orcid.org/0000-0002-2039-3564

References

1. Saha, S.; Stoddart, J. F. *Chem. Soc. Rev.* **2007,** *36,* 77–92. doi:10.1039/B607187B
2. Dasgupta, S.; Wu, J.-S. *Chem. Sci.* **2012,** *3,* 425–432. doi:10.1039/C1SC00613D
3. Qu, D.-H.; Tian, H. *Chem. Sci.* **2011,** *2,* 1011–1015. doi:10.1039/c0sc00653j
4. Zhu, L.-L.; Yan, H.; Nguyen, K. T.; Tian, H.; Zhao, Y.-L. *Chem. Commun.* **2012,** *48,* 4290–4292. doi:10.1039/c2cc17114g
5. Dzyuba, E. V.; Baytekin, B.; Sattler, D.; Schalley, C. A. *Eur. J. Org. Chem.* **2012,** 1171–1178. doi:10.1002/ejoc.201101231
6. Rao, S.-J.; Zhang, Q.; Mei, J.; Ye, X.-H.; Gao, C.; Wang, Q.-C.; Qu, D.-H.; Tian, H. *Chem. Sci.* **2017,** *8,* 6777–6783. doi:10.1039/C7SC03232C
7. Gao, C.; Luan, Z.-L.; Zhang, Q.; Rao, S.-J.; Qu, D.-H.; Tian, H. *Org. Lett.* **2017,** *19,* 3931–3934. doi:10.1021/acs.orglett.7b01853
8. Hartlieb, K. J.; Blackburn, A. K.; Schneebeli, S. T.; Forgan, R. S.; Sarjeant, A. A.; Stern, C. L.; Cao, D.; Stoddart, J. F. *Chem. Sci.* **2014,** *5,* 90–100. doi:10.1039/C3SC52106K
9. Badjić, J. D.; Balzani, V.; Credi, A.; Silvi, S.; Stoddart, J. F. *Science* **2004,** *303,* 1845–1849. doi:10.1126/science.1094791
10. Badjić, J. D.; Ronconi, C. M.; Stoddart, J. F.; Balzani, V.; Silvi, S.; Credi, A. *J. Am. Chem. Soc.* **2006,** *128,* 1489–1499. doi:10.1021/ja0543954
11. Goujon, A.; Du, G.; Moulin, E.; Fuks, G.; Maaloum, M.; Buhler, E.; Giuseppone, N. *Angew. Chem., Int. Ed.* **2016,** *55,* 703–707. doi:10.1002/anie.201509813

12. Goujon, A.; Lang, T.; Mariani, G.; Moulin, E.; Fuks, G.; Raya, J.; Buhler, E.; Giuseppone, N. *J. Am. Chem. Soc.* **2017,** *139,* 14825–14828. doi:10.1021/jacs.7b06710
13. Roh, S.-G.; Park, K.-M.; Park, G.-J.; Sakamoto, S.; Yamaguchi, K.; Kim, K. *Angew. Chem., Int. Ed.* **1999,** *38,* 637–641. doi:10.1002/(SICI)1521-3773(19990301)38:5<637::AID-ANIE637>3.0.CO;2-4
14. Kim, K. *Chem. Soc. Rev.* **2002,** *31,* 96–107. doi:10.1039/a900939f
15. Chang, C.-F.; Chuang, C.-J.; Lai, C.-C.; Liu, Y.-H.; Peng, S.-M.; Chiu, S.-H. *Angew. Chem., Int. Ed.* **2012,** *51,* 10094–10098. doi:10.1002/anie.201205498
16. von Delius, M.; Geertsema, E. M.; Leigh, D. A. *Nat. Chem.* **2009,** *2,* 96–101. doi:10.1038/nchem.481
17. Lewandowski, B.; De Bo, G.; Ward, J. W.; Papmeyer, M.; Kuschel, S.; Aldegunde, M. J.; Gramlich, P. M. E.; Heckmann, D.; Goldup, S. M.; D'Souza, D. M.; Fernandes, A. E.; Leigh, D. A. *Science* **2013,** *339,* 189–193. doi:10.1126/science.1229753
18. Qu, D.-H.; Tian, H. *Chem. Sci.* **2013,** *4,* 3031–3035. doi:10.1039/c3sc51160j
19. Cheng, C.; McGonigal, P. R.; Schneebeli, S. T.; Li, H.; Vermeulen, N. A.; Ke, C.; Stoddart, J. F. *Nat. Nanotechnol.* **2015,** *10,* 547–553. doi:10.1038/nnano.2015.96
20. Meng, Z.; Xiang, J.-F.; Chen, C.-F. *J. Am. Chem. Soc.* **2016,** *138,* 5652–5658. doi:10.1021/jacs.6b01852
21. Brunsveld, L.; Folmer, B. J. B.; Meijer, E. W.; Sijbesma, R. P. *Chem. Rev.* **2001,** *101,* 4071–4098. doi:10.1021/cr990125q
22. Cao, Z.-Q.; Miao, Q.; Zhang, Q.; Li, H.; Qu, D.-H.; Tian, H. *Chem. Commun.* **2015,** *51,* 4973–4976. doi:10.1039/C4CC09976A
23. Raymo, F. M.; Stoddart, J. F. *Chem. Rev.* **1999,** *99,* 1643–1664. doi:10.1021/cr970081q
24. Balzani, V.; Credi, A.; Silvi, S.; Venturi, M. *Chem. Soc. Rev.* **2006,** *35,* 1135–1149. doi:10.1039/b517102b
25. Tian, H.; Wang, Q.-C. *Chem. Soc. Rev.* **2006,** *35,* 361–374. doi:10.1039/b512178g
26. Champin, B.; Mobian, P.; Sauvage, J.-P. *Chem. Soc. Rev.* **2007,** *36,* 358–366. doi:10.1039/B604484K
27. Crowley, J. D.; Goldup, S. M.; Lee, A.-L.; Leigh, D. A.; McBurney, R. T. *Chem. Soc. Rev.* **2009,** *38,* 1530–1541. doi:10.1039/b804243h
28. Hänni, K. D.; Leigh, D. A. *Chem. Soc. Rev.* **2010,** *39,* 1240–1251. doi:10.1039/B901974J
29. Zhu, L.-L.; Yan, H.; Wang, X.-J.; Zhao, Y.-L. *J. Org. Chem.* **2012,** *77,* 10168–10175. doi:10.1021/jo301807y
30. Cui, J.-S.; Ba, Q.-K.; Ke, H.; Valkonen, A.; Rissanen, K.; Jiang, W. *Angew. Chem., Int. Ed.* **2018,** *57,* 7809–7814. doi:10.1002/anie.201803349
31. Gao, C.; Luan, Z.-L.; Zhang, Q.; Yang, S.; Rao, S.-J.; Qu, D.-H.; Tian, H. *Org. Lett.* **2017,** *19,* 1618–1621. doi:10.1021/acs.orglett.7b00393
32. Guidry, E. N.; Li, J.; Stoddart, J. F.; Grubbs, R. H. *J. Am. Chem. Soc.* **2007,** *129,* 8944–8945. doi:10.1021/ja0725100
33. Jiang, Y.; Guo, J.-B.; Chen, C.-F. *Org. Lett.* **2010,** *12,* 4248–4251. doi:10.1021/ol101920b
34. Kawakami, H.; Toma, K. Diamide type gelling agent. Jpn. Kokai Tokkyo Koho JP2004262809A, Sept 24, 2004.
35. Li, F.-F.; Li, Y.-J.; Zhou, Z.-C.; Lv, S.-X.; Deng, Q.-R.; Xu, X.; Yin, L.-C. *ACS Appl. Mater. Interfaces* **2017,** *9,* 23586–23601. doi:10.1021/acsami.7b08534
36. Candrill, S. J.; Grubbs, R. H.; Lanari, D.; Leung, K. C.-F.; Nelson, A.; Poulin-Kerstien, K. G.; Smidt, S. P.; Stoddart, J. F.; Tirrell, D. A. *Org. Lett.* **2005,** *7,* 4213–4216. doi:10.1021/ol051599g
37. Zhang, H.; Liu, Q.; Li, J.; Qu, D.-H. *Org. Lett.* **2013,** *15,* 338–341. doi:10.1021/ol3032686

License and Terms

BEILSTEIN JOURNAL OF ORGANIC CHEMISTRY

Calix[6]arene-based atropoisomeric pseudo[2]rotaxanes

Carmine Gaeta, Carmen Talotta* and Placido Neri

Full Research Paper

Open Access

Address:
Dipartimento di Chimica e Biologia " A. Zambelli", Università di Salerno, Via Giovanni Paolo II 132, 84084 Fisciano (Salerno), Italy

Email:
Carmen Talotta* - ctalotta@unisa.it

* Corresponding author

Keywords:
atropoisomers; calixarene; conformation; pseudorotaxane; social isomerism

Beilstein J. Org. Chem. **2018,** *14,* 2112–2124.
doi:10.3762/bjoc.14.186

Received: 02 May 2018
Accepted: 26 July 2018
Published: 14 August 2018

This article is part of the thematic issue "Macrocyclic and supramolecular chemistry".

Guest Editor: M.-X. Wang

Abstract

Some examples of atropoisomeric pseudorotaxanes in which the isomerism arises by the different conformations adopted by the wheel are reported here. Upon threading hexahexyloxycalix[6]arene **1** with ammonium axles $\mathbf{2}^+$ or $\mathbf{3}^+$, bearing biphenyl or trifluoromethylbenzyl moieties, respectively, two atropoisomeric pseudorotaxanes were formed in which the calix[6]-wheel **1** adopts the *1,2,3-alternate* and *cone* conformations. The interconversion between them cannot be obtained by simple rotation around the $ArCH_2Ar$ bonds of the calixarene wheel, which is blocked by the presence of the axle inside its cavity. Therefore, it can only be obtained through a mechanism of de-threading/re-threading of the axle. In all the examined cases, the *1,2,3-alternate* and *cone* atropoisomers are, respectively, the kinetic and the thermodynamic ones.

Introduction

Mechanomolecules [1-4], such as rotaxanes and catenanes show interesting properties as nanodevices for catalysis [5-8], recognition, and sensing [9-13]. Beyond these ascertained potentialities, interpenetrated architectures show fascinating structures that still stimulate the imagination of scientists.

An amazing aspect of rotaxanes and catenanes is their ability to adopt novel forms of isomerism. More in detail, (pseudo)rotaxane or catenane architectures can show novel stereoisomeric forms as a result of the "social" [14] relationship between their components.

Recently, Goldup's group assembled a mechanically planar chiral rotaxane [15,16] (**I** and **I***, Figure 1) consisting of achiral components. The combination of a macrocycle with rotational asymmetry and a directional thread with non-equivalent ends is the cause of chirality in this example (Figure 1). Interestingly, our group showed that a chiral pseudorotaxane can be generated upon threading a tertiary ammonium axles in a directional (non-flat) calixarene-wheel (**II** and **II***, Figure 1) [17]. In this case the chirality is created by the directionality of the calixarene wheel in a *cone* conformation, which differentiates the two alkyl chains around the prochiral ammonium center.

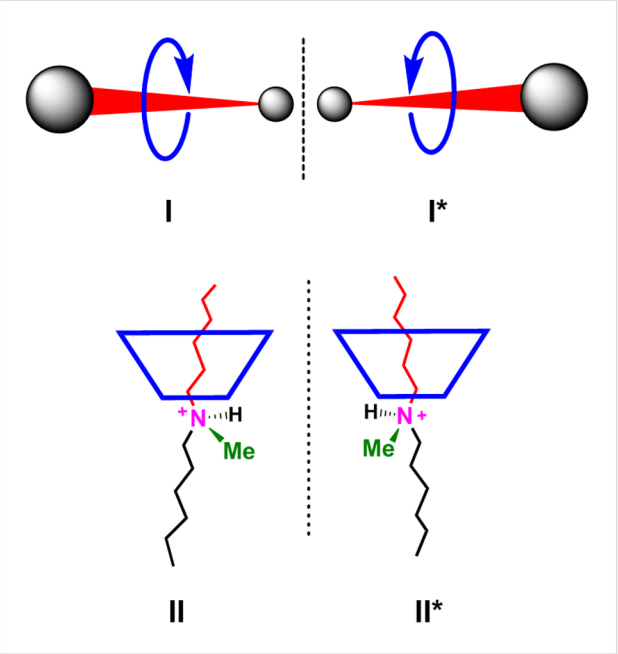

Figure 1: Cartoon representation of the chiral rotaxane of the Goldup group [15,16] (**I** and **I***) and of the chiral pseudorotaxane (**II** and **II***) reported by our group [17].

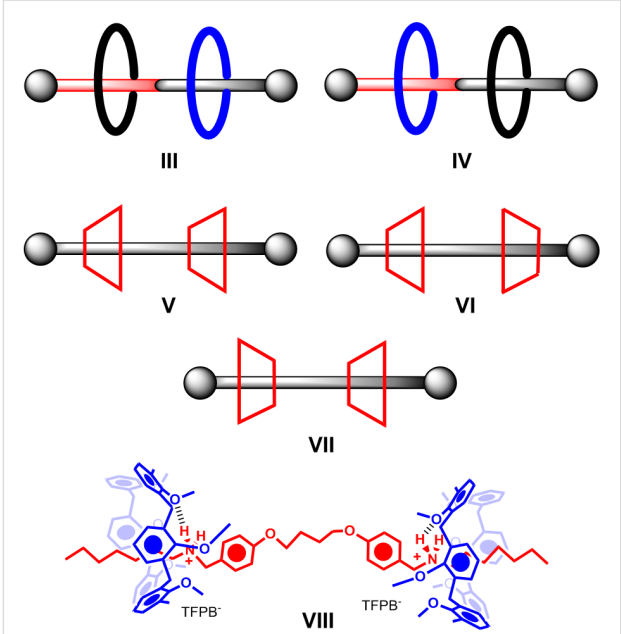

Figure 2: Cartoon representation of the rotaxane sequence isomers reported by Leigh [17] (**III** and **IV**) and of the pseudorotaxane sequential stereoisomers (**V**–**VII**) reported by our group [19-21].

In 2010, for the first time, an example of sequence isomerism was reported by Leigh's group [18], caused by two different flat wheels that can be located differently along a directional thread **III** and **IV** (Figure 2). As an evolution of this concept, we envisaged a sequence stereoisomerism if two directional non-flat wheels, such as calixarenes or cyclodextrins, are threaded along an axle to give a pseudo[3]rotaxane architecture **V**–**VII** (Figure 2), where three sequential stereoisomers can arise. We showed that this stereoisomerism can be effectively controlled when two calix[6]arene wheels are threaded along a bis(benzylalkylammonium) axle [19], where the stereoselective formation of the pseudo[3]rotaxane with *endo*-alkyl orientation **VIII** was observed [19].

Calixarene macrocycles [22] have found numerous applications in several areas of supramolecular chemistry, such as (bio)molecular recognition [23] and catalysis [24]. The widespread use of the calixarene derivatives is due to their convenient synthesis and to their chemical and conformational versatility [25]. In fact, calixarene macrocycles present a conformational isomerism that in the case of calix[6]arenes gives rise to eight discrete conformations (Figure 3) [26]: *cone, partial-cone, 1,2-alternate, 1,3-alternate, 1,4-alternate, 1,2,3-alternate, 1,2,4-alternate,* and *1,3,5-alternate*. This conformational versatility has long attracted much attention, and therefore empirical rules have been reported in order to assign the calixarene conformations [27,28]. The "^{1}H NMR Δδ" rule reported by Gutsche [29], is focused on the difference of chemical shifts between each pair of calixarene $ArCH_2Ar$ methylene protons. These can show diasterotopicity resulting in AX or AB systems. Specifically, a ^{1}H NMR methylene proton Δδ value of at least 0.7 shows that the two respective proximal aromatic rings are oriented *syn*, as in the *cone* conformation. In contrast, a Δδ value of 0.3 or less is attributable to an *anti*-orientation between the phenol rings, as in alternate conformations. The de Mendoza's "^{13}C NMR single rule" [30,31], is focused on the ^{13}C NMR chemical shift of the $ArCH_2Ar$ methylene C, which is 30–33 ppm for the *syn*-orientation of the proximal phenol rings and typically 36–39 ppm with *anti*-positioned phenol rings as in alternate conformations.

As exemplified above, the calix[6]arene macrocycle has been widely used as wheel for the assembly of pseudorotaxane architectures [32,33], where it usually adopts a *cone* conformation. The examples reported by us [33-38] (Figure 4b) and by Arduini [32,39] (Figure 4a) showed that the directionality of the calixarene wheel in the *cone* conformation plays a pivotal role in the formation of stereoisomeric directional pseudo[2]rotaxanes, rotaxanes, and catenanes. Also in this case [38], we were able to obtain a stereoselective threading of the *cone* calix[6]arene-wheel with alkylbenzylammonium axles (Figure 4b), in which the *endo*-alkyl pseudo[2]rotaxane stereoisomer was the favoured one [38].

The threading of calix[6]arene macrocycles in conformations different than the cone one has been rarely observed [17]. Interestingly, the assembling of interpenetrated structures in which

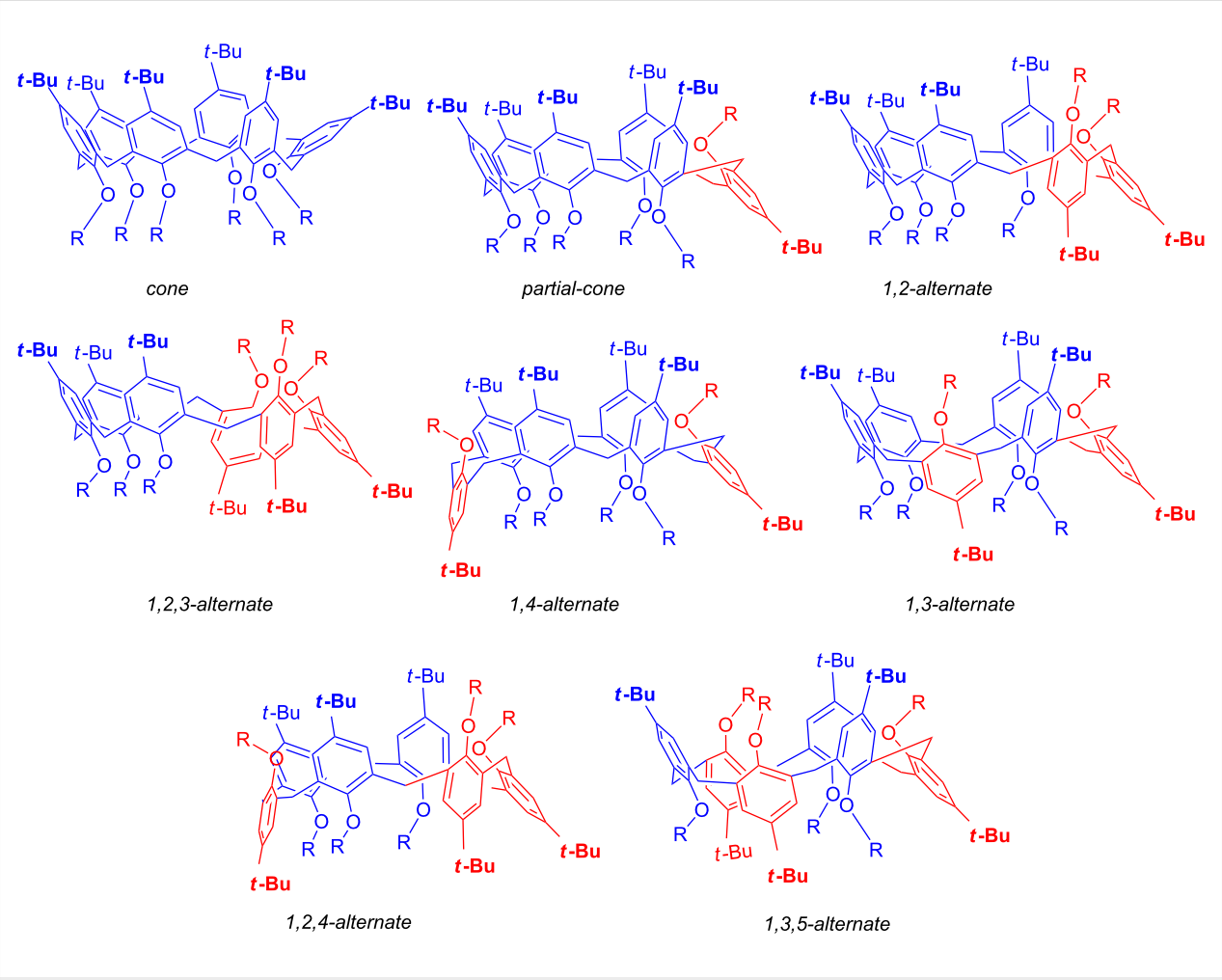

Figure 3: The possible 8 discrete conformations of a calix[6]arene macrocycle [26].

the wheel adopts different conformational isomers, could pave the way to mechanomolecules which exhibit novel isomeric forms.

Prompted by these considerations, some examples of pseudorotaxane isomers in which the isomerism arises by the different conformations adopted by the calixarene wheel are reported here.

Results and Discussion

With this goal in mind, we conducted an initial screening in order to select the ammonium axles and the calix[6]arene-wheel most suitable for our purposes. At the end of our screening, we focused our attention on hexahexyloxycalix[6]arene **1** as the wheel and bis(4-biphenylmethyl)ammonium ($\mathbf{2}^+$) and bis(4-trifluoromethylbenzyl)ammonium ($\mathbf{3}^+$, $TFPB^-$ salts) as the threads. The synthetic pathway to $\mathbf{2}^+\cdot TFPB^-$ and $\mathbf{3}^+\cdot TFPB^-$ salts is outlined in Scheme 1, while calix[6]arene **1** was obtained following a known procedure [40].

The ^1H NMR spectrum of hexahexyloxycalix[6]arene **1** in $CDCl_3$ at 298 K shows broad $ArCH_2Ar$ signals indicative of a conformational mobility of the macrocycle in which the inversion between the calix[6]arene conformations (Figure 5), occurs by means of rotation around the $ArCH_2Ar$ bonds.

By lowering the temperature, the $ArCH_2Ar$ signal decoalesced to form a single AX system (3.34/4.49 ppm) and one broad singlet (3.77 ppm). This pattern is only compatible with the presence of a *1,2,3-alternate* conformation of calix[6]arene **1** (Figure 5). This was confirmed by a 2D HSQC spectrum of **1** at 233 K which evidenced the presence of $ArCH_2Ar$ correlations between the AX system at 3.34/4.49 ppm with a carbon resonance at 29.4 ppm, related to *syn*-oriented Ar rings [29]. Diagnostic of the presence of the *1,2,3-alternate* conformation of **1** is the presence of the broad singlet at 3.71 ppm which correlates in the HSQC spectrum with a carbon resonance at 34.1 ppm [30], related to *anti*-oriented Ar rings. A close inspection of the 1D and 2D NMR spectrum of **1** in $CDCl_3$ at 233 K

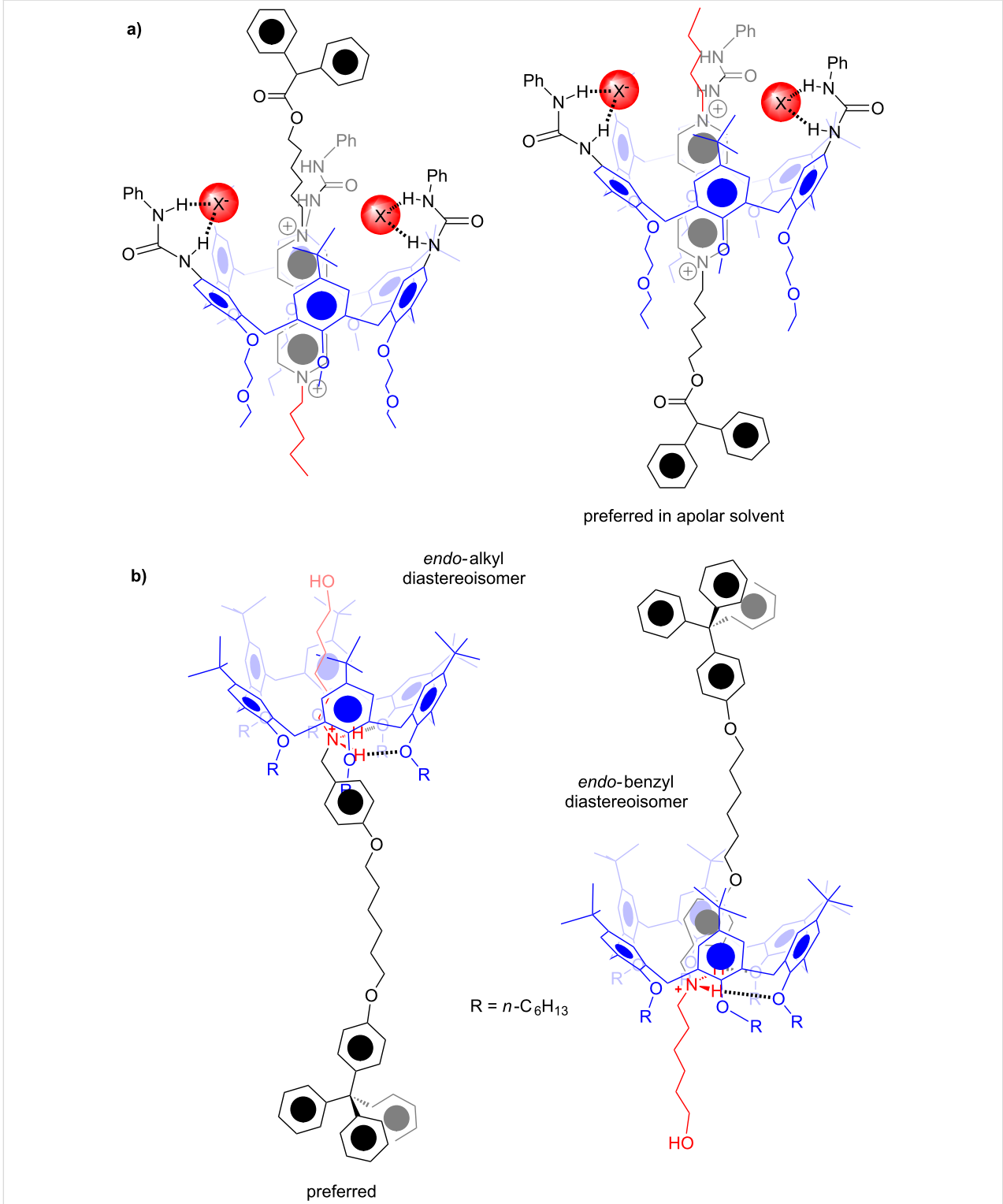

Figure 4: Diastereoisomeric pseudorotaxanes obtained by threading a directional calixarene wheel with directional axles.

clearly evidenced the presence of a less abundant conformer of **1**. The nature of this minor conformer can be inferred by the work of Reinhoudt and co-workers which showed [41] that the conformations preferentially adopted by calix[6]arene hexaethers are the *cone* and *1,2,3-alternate* ones. In accordance, 2D COSY and HSQC spectra of **1** at 233 K clarified that this minor conformer was the *cone* one through the presence of an AX system at 3.35/4.42 ppm (COSY), which correlates with a

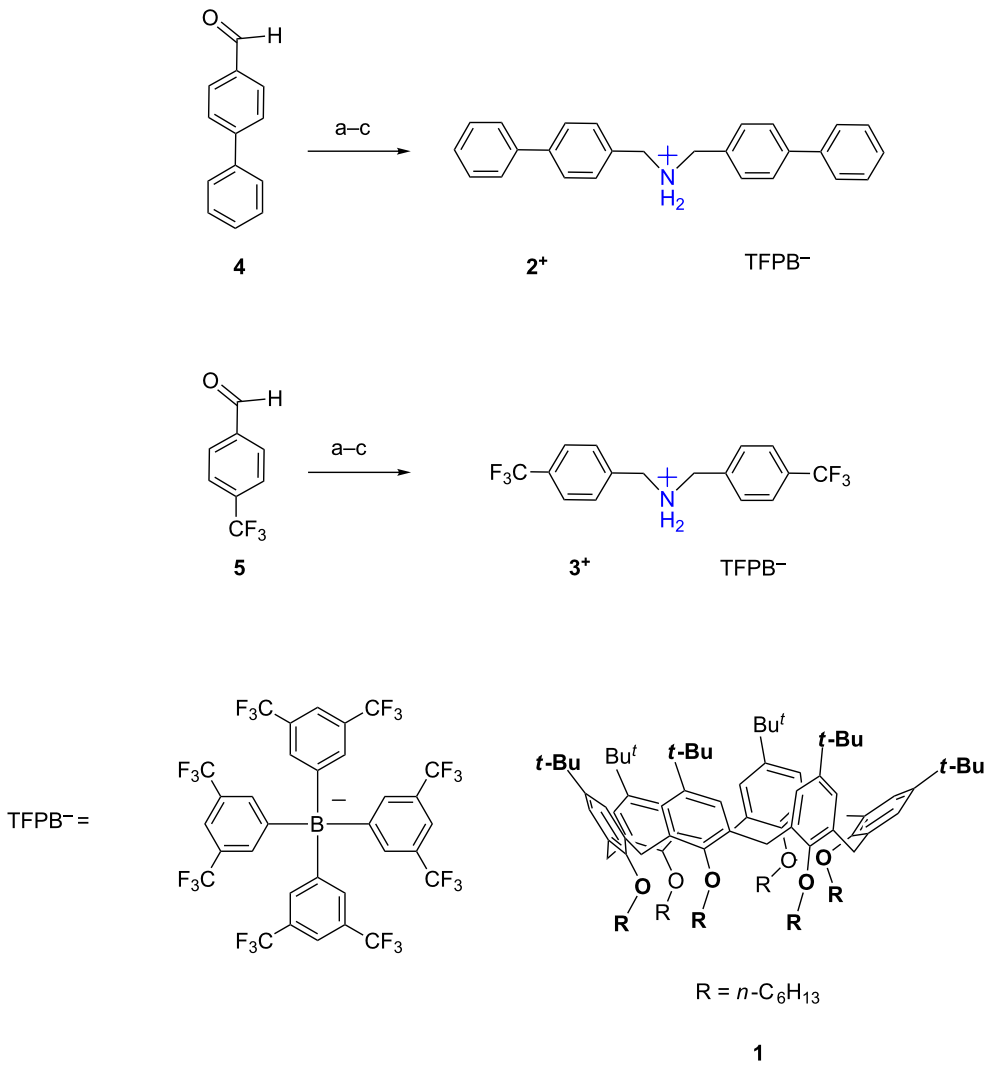

Scheme 1: Synthesis of threads $\mathbf{2}^+$ and $\mathbf{3}^+$. Reagents and conditions: a) hexamethyldisilazane, $LiClO_4$, 30 min, 60 °C; b) CH_3OH, $NaBH_4$, 2 h, 25 °C; c) TFPBNa, dry MeOH, 25 °C, 18 h.

carbon resonance at 29.1 ppm (HSQC), related to *syn*-oriented Ar rings (*cone* conformation). The coalescence temperature of the methylene protons was ascertained at 328 K in $CDCl_3$; below this temperature the conformations of **1** were frozen, while at temperatures above 328 K the conformational interconversion is fast with respect to the NMR time scale (400 MHz). From the coalescence data we calculated a barrier of 14.6 kcal/mol for this process. In summary, the VT ^{1}H NMR studies indicate that the *1,2,3-alternate* is the most stable conformation for hexahexyloxycalix[6]arene **1** in solution. This conclusion is in perfect accord with the results previously reported by Reinhoudt [41], which evidenced an increased stabilization of the *1,2,3-alternate* conformation of calix[6]arenes when the alkyl substituents at the lower rim are increased in size [41].

As expected [40], no evidence of interaction between $\mathbf{2}^+$ and **1** was detected by NMR, when $\mathbf{2}^+$ was added as its chloride salt to a $CDCl_3$ solution of **1**. However, when $\mathbf{2}^+$ was added as its $TFPB^-$ salt to a $CDCl_3$ solution of **1**, then dramatic changes were observed in the ^{1}H NMR spectrum of **1** (Figure 6).

In detail, immediately after the mixing of **1** and $\mathbf{2}^+$ we observed the sharpening of all signals and the appearance of an AX system at 5.50/6.70 ppm attributable to aromatic H-atoms of the axle $\mathbf{2}^+$ shielded inside the calixarene cavity. These changes were indicative of the formation of a pseudorotaxane $\mathbf{2}^+\subset\mathbf{1}$. With this result in hand, we turned our attention to the conformation adopted by the calix[6]arene-wheel **1** in pseudorotaxane $\mathbf{2}^+\subset\mathbf{1}$. A 2D COSY spectrum of 1:1 mixture of

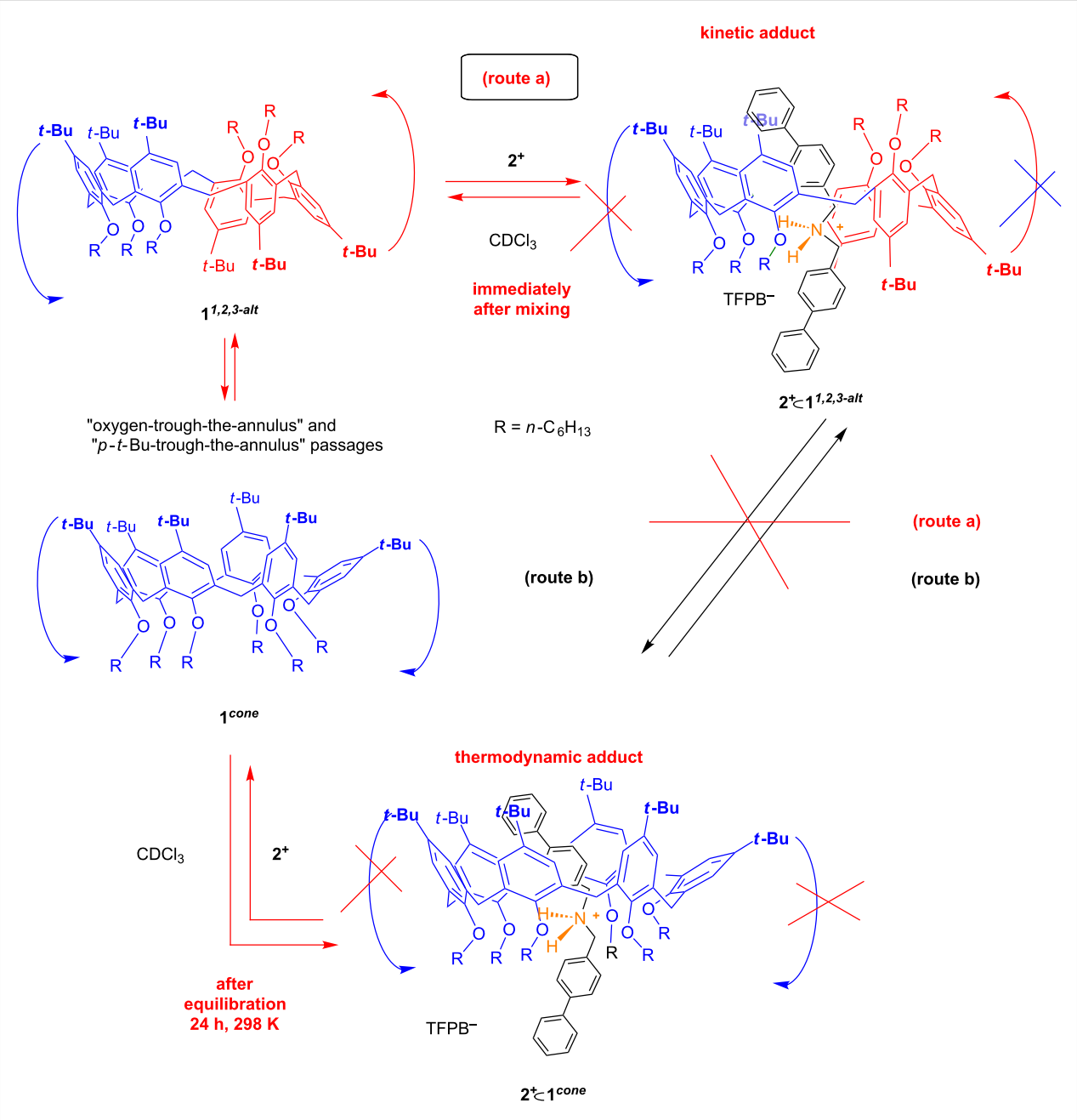

Figure 5: Possible mechanism for the formation of the two atropoisomeric pseudo[2]rotaxanes $2^+\subset\mathbf{1}^{cone}$ and $2^+\subset\mathbf{1}^{1,2,3\text{-}alt}$.

1 and 2^+, immediately after mixing in $CDCl_3$, revealed the presence of a single AX systems at 3.53/4.73, which correlates with a carbon resonance at 28.9 ppm, respectively, due to the $ArCH_2Ar$ methylene groups between *syn*-oriented Ar rings. A close inspection of the 2D HSQC spectrum revealed the presence of a cross-peak at 3.93/36.5 ppm attributable to an $ArCH_2Ar$ methylene bridge between *anti*-oriented Ar rings. These data clearly indicate that calixarene-wheel **1** adopts the *1,2,3-alternate* conformation in pseudorotaxane $2^+\subset\mathbf{1}^{1,2,3\text{-}alt}$ (Figure 5 and Figure 6).

A further inspection of the 1D and 2D (COSY-45 and HSQC) spectra of the 1:1 mixture of **1** and 2^+ in $CDCl_3$ immediately after mixing, revealed the presence of a less abundant pseudo[2]rotaxane species in which probably the calixarene wheel **1** adopts a *cone* conformation $2^+\subset\mathbf{1}^{cone}$ (Figure 5). Initially, the ratio between the two isomeric pseudorotaxane $2^+\subset\mathbf{1}^{cone}/2^+\subset\mathbf{1}^{1,2,3\text{-}alt}$ is 1/20, as calculated by integration of the corresponding ^1H NMR signals. Interestingly, after 10 h at 298 K (Figure 6), the intensity of the ^1H NMR signals of pseudorotaxane $2^+\subset\mathbf{1}^{1,2,3\text{-}alt}$ was decreased while that of

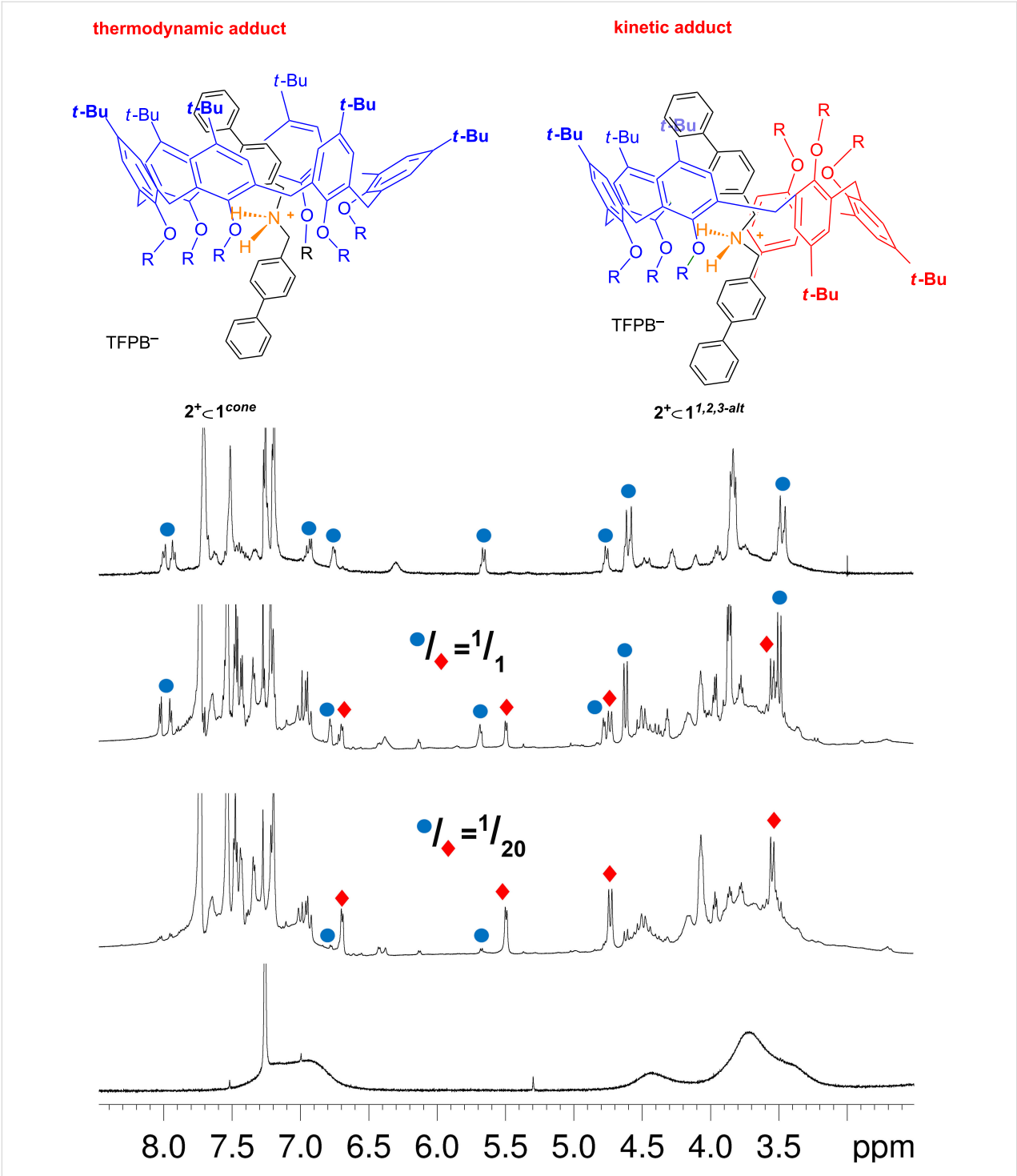

Figure 6: ^{1}H NMR spectra (600 MHz, $CDCl_3$, 298 K) of, from bottom to top: hexahexyloxycalix[6]arene **1**; a 1:1 mixture (0.003 M) of **1** and $\mathbf{2}^+\cdot\mathbf{TFPB}^-$ immediately after mixing; after 10 h; after 18 h.

$\mathbf{2}^+\subset\mathbf{1}^{cone}$ was increased. After 18 h at 298 K, the disappearance of $\mathbf{2}^+\subset\mathbf{1}^{1,2,3\text{-}alt}$ was complete and only $\mathbf{2}^+\subset\mathbf{1}^{cone}$ pseudorotaxane could be detected by 1D and 2D NMR studies (Figure 6). In fact, a 2D COSY spectrum of the 1:1 mixture of **1** and $\mathbf{2}^+$ in $CDCl_3$, after 18 h at 298 K, showed the presence of an $ArCH_2Ar$ AX system at 3.47/4.62 ppm which correlates in the HSQC spectrum with a carbon resonance at 28.4 ppm related to *syn*-oriented Ar rings. An AX system was present in the COSY spectrum at 4.78/5.68 ppm attributable to aromatic protons of the axle $\mathbf{2}^+$ shielded inside the calixarene cavity. This

shielded AX system correlates in the HSQC spectrum with aromatic carbon resonances at 129.8 and 126.8 ppm, respectively.

The ^{1}H NMR spectrum of the mixture of **1** and $\mathbf{2}^+$ in $CDCl_3$ remained unchanged after 48 h at 298 K, thus showing that the system had reached the equilibrium condition. At this point, an apparent association constant of 6.2 ± 0.3 × 10^3 M^{-1} was calculated by quantitative ^{1}H NMR analysis (tetrachloroethane as internal standard) [37] for the formation of $\mathbf{2}^+\subset\mathbf{1}^{cone}$ pseudorotaxane. In conclusion, after the initial formation of the kinetically favored pseudorotaxane $\mathbf{2}^+\subset\mathbf{1}^{1,2,3\text{-}alt}$ (Figure 5), the thermodynamic pseudorotaxane $\mathbf{2}^+\subset\mathbf{1}^{cone}$ prevails (Figure 5 and Figure 6). As demonstrated above, the *1,2,3-alternate* conformation of **1** is the most populated in solution, consequently, the threading of this conformation, besides being faster, it is also favored by its abundance in solution.

The greater thermodynamic stability of the $\mathbf{2}^+\subset\mathbf{1}^{cone}$ atropoisomer over the $\mathbf{2}^+\subset\mathbf{1}^{1,2,3\text{-}alt}$ one, was confirmed by DFT calculations at the B3LYP/6-31G(d,p) level of theory using Grimme's dispersion corrections (IOp(3/124=3)) [42]. The DFT-optimized structure of the $\mathbf{2}^+\subset\mathbf{1}^{cone}$ atropoisomeric pseudorotaxane (Figure 7, left) results stabilized by two H-bond interactions between the ammonium group and the oxygen atoms of the calixarene wheel **1**, (average N···O distance = 3.10 Å; average N–H···O angle = 157°). In addition, C–H···π interactions were detected among the methylene groups of the axle $\mathbf{2}^+$ inside the calix cavity, and the aromatic rings of **1** [42], (average C–H···$\pi^{centroid}$ distance = 3.17 Å [42]; average C–H···$\pi^{centroid}$ angle = 160° [43]).

In addition, the biphenyl portion of $\mathbf{2}^+$ hosted inside the calix cavity was involved in π···π interactions with the aromatic walls (Figures S11–S13, Supporting Information File 1) and C–H···π interactions with the *tert*-butyl groups of the calixarene wheel (Figure S13, Supporting Information File 1). Differently, in the DFT-optimized structure of $\mathbf{2}^+\subset\mathbf{1}^{1,2,3\text{-}alt}$ atropoisomer (Figure 7, right), the stabilization of the $\mathbf{2}^+\subset\mathbf{1}^{1,2,3\text{-}alt}$ atropoisomer was brought, principally by two H-bonding interactions between the ammonium group of $\mathbf{2}^+$ and the oxygen atoms of *anti*-oriented phenol rings of **1** with an average N···O distance of 3.05 Å and a narrower N–H···O angle of 167.1°. Single-point calculations at the B3LYP/6-31G(d,p) level of theory using Grimme's dispersion corrections (IOp(3/124=3)), indicated that the $\mathbf{2}^+\subset\mathbf{1}^{cone}$ atropoisomer was more stable than the $\mathbf{2}^+\subset\mathbf{1}^{1,2,3\text{-}alt}$ one by 2.4 kcal mol^{-1}. At this point, it is worthy to consider the interconversion between the two isomeric pseudorotaxane $\mathbf{2}^+\subset\mathbf{1}^{1,2,3\text{-}alt}$ and $\mathbf{2}^+\subset\mathbf{1}^{cone}$. It could take place through two possible mechanisms (Figure 5): a) de-threading of axle $\mathbf{2}^+$ from

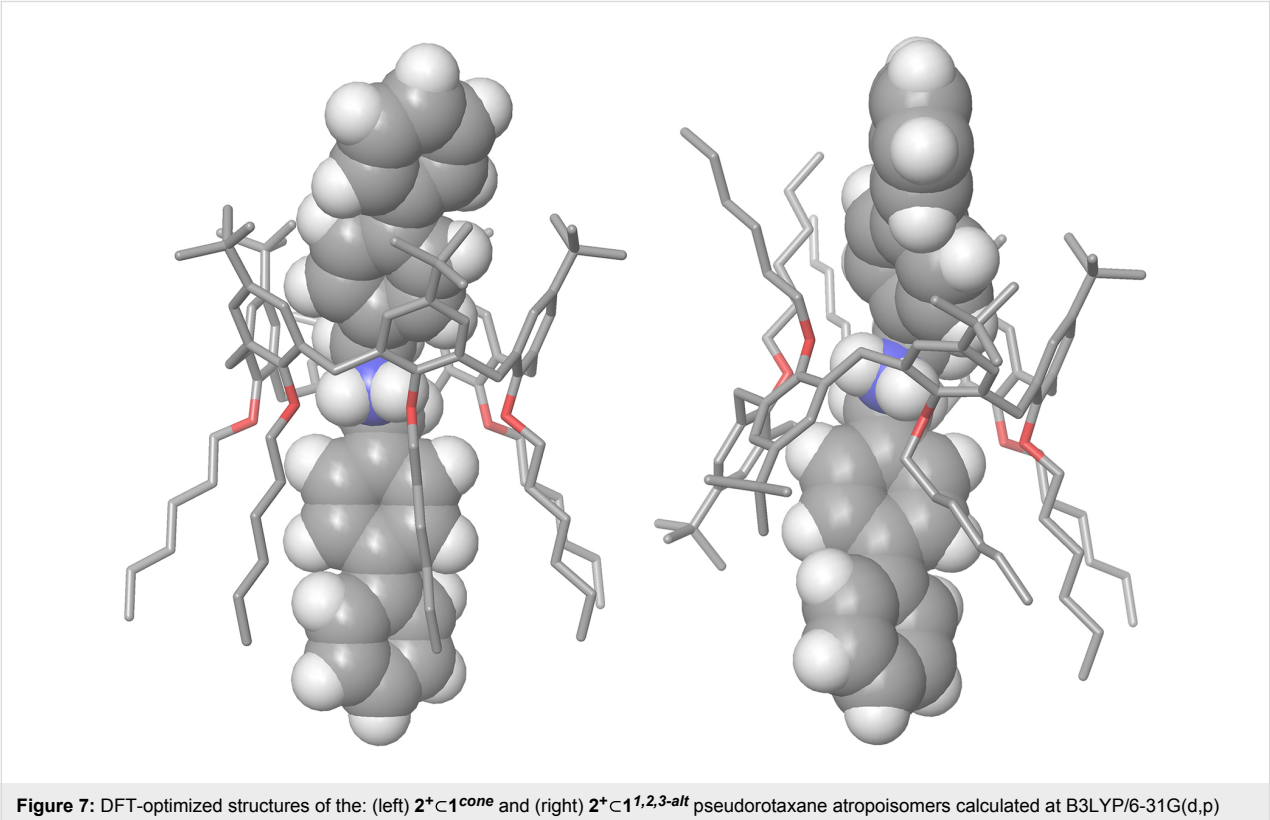

Figure 7: DFT-optimized structures of the: (left) $\mathbf{2}^+\subset\mathbf{1}^{cone}$ and (right) $\mathbf{2}^+\subset\mathbf{1}^{1,2,3\text{-}alt}$ pseudorotaxane atropoisomers calculated at B3LYP/6-31G(d,p) level of theory and using Grimme's dispersion corrections (IOp(3/124 = 3)).

$\mathbf{2}^{+}\subset\mathbf{1}^{1,2,3\text{-}alt}$ and a subsequent re-threading with **1** in a *cone* conformation; b) a direct conformational interconversion between the *1,2,3-alternate* and *cone* conformations of the calixarene wheel **1** in both $\mathbf{2}^{+}\subset\mathbf{1}$ pseudorotaxanes. Previously reported data [34] clearly showed that the mechanism "b" in Figure 5 can be ruled out because the presence of an axle inside the cavity of **1** impedes the "through-the-annulus" passage of both rims of **1**. From this consideration, we concluded that the two pseudorotaxanes $\mathbf{2}^{+}\subset\mathbf{1}^{1,2,3\text{-}alt}$ and $\mathbf{2}^{+}\subset\mathbf{1}^{cone}$ can be considered as two atropoisomeric forms. In fact, the interconversion between them cannot be obtained by simple rotation around chemical bonds of the calixarene wheel, which is blocked by the presence of the axle inside its cavity.

Previously [34] we reported a similar case in which the monostoppered alkylbenzylammonium axle $\mathbf{6}^{+}$ gives rise to two atropoisomeric pseudorotaxanes $\mathbf{6}^{+}\subset\mathbf{1}^{cone}$ and $\mathbf{6}^{+}\subset\mathbf{1}^{1,2,3\text{-}alt}$ (Figure 8). Also in this instance, the pseudorotaxanes $\mathbf{6}^{+}\subset\mathbf{1}^{1,2,3\text{-}alt}$ and $\mathbf{6}^{+}\subset\mathbf{1}^{cone}$ were observed as the kinetic and thermodynamic adduct, respectively, with an interconversion time of 12 h at 353 K. A further example regards the threading of the narrower penta-*O*-methyl-*p*-*tert*-butylcalix[5]arene **7** with pentylbenzylammonium axle $\mathbf{8}^{+}$ [35]. Two atropoisomeric pseudorotaxanes were formed, namely $\mathbf{8}^{+}\subset\mathbf{7}^{cone}$ and $\mathbf{8}^{+}\subset\mathbf{7}^{paco}$ (Figure 9), in which the calix[5]-wheel adopted a *cone* and a *partial-cone* conformation, respectively [35]. Also in this case, the atropoisomer with an "inverted" calixarene wheel $\mathbf{8}^{+}\subset\mathbf{7}^{paco}$ is the kinetic product, while the other with a calix-*cone* conformation $\mathbf{8}^{+}\subset\mathbf{7}^{cone}$ is the thermodynamic one [35].

At this point we turned our attention to the threading properties of bis(4-trifluoromethylbenzyl)ammonium axle $\mathbf{3}^{+}$. When **1** and $\mathbf{3}^{+}\cdot\mathrm{TFPB}^{-}$ were mixed in $CDCl_3$ two atropoisomeric pseudo[2]rotaxane, $\mathbf{3}^{+}\subset\mathbf{1}^{cone}$ and $\mathbf{3}^{+}\subset\mathbf{1}^{1,2,3\text{-}alt}$ (Figure 10), were formed in a 1/10 ratio, as revealed by 1D and 2D NMR studies. Also in this case, after equilibration at 298 K for 24 h, this preference was reversed in favour of the $\mathbf{3}+\subset\mathbf{1}^{cone}$ atropoisomer, with a $\mathbf{3}^{+}\subset\mathbf{1}^{cone}/\mathbf{3}^{+}\subset\mathbf{1}^{1,2,3\text{-}alt}$ ratio of 8/1. From the equilibrium mixture, an apparent association constant of $9.3 \pm 0.4 \times 10^{2}\ M^{-1}$ was calculated by quantitative ^{1}H NMR analysis (tetrachloroethane as internal standard) for the formation of $\mathbf{3}^{+}\subset\mathbf{1}^{cone}$ pseudorotaxane. In a similar way, an apparent association constant of $120 \pm 15\ M^{-1}$ was found for $\mathbf{3}^{+}\subset\mathbf{1}^{1,2,3\text{-}alt}$ pseudorotaxane.

As evidenced for axle $\mathbf{2}^{+}$, also in this case, after the initial formation of the kinetic pseudorotaxane $\mathbf{3}^{+}\subset\mathbf{1}^{1,2,3\text{-}alt}$ (Figure 10), the thermodynamic atropoisomer $\mathbf{3}^{+}\subset\mathbf{1}^{cone}$ prevails. However, differently from the $\mathbf{2}^{+}$ case where the kinetic product was no longer detectable in the final equilibrium mixture, here a size-

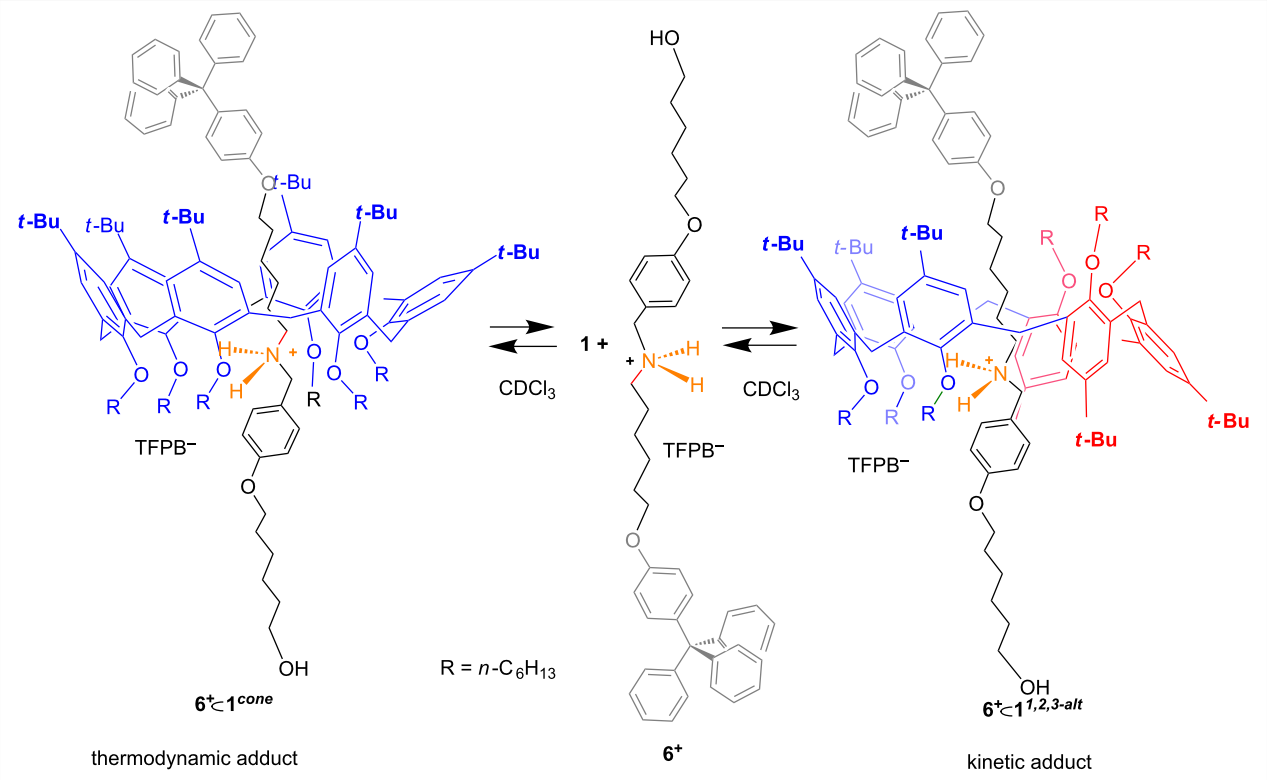

Figure 8: The two pseudorotaxane atropoisomers obtained by threading hexahexyloxycalix[6]arene **1** with monostoppered alkylbenzylammonium axle $\mathbf{6}^{+}$.

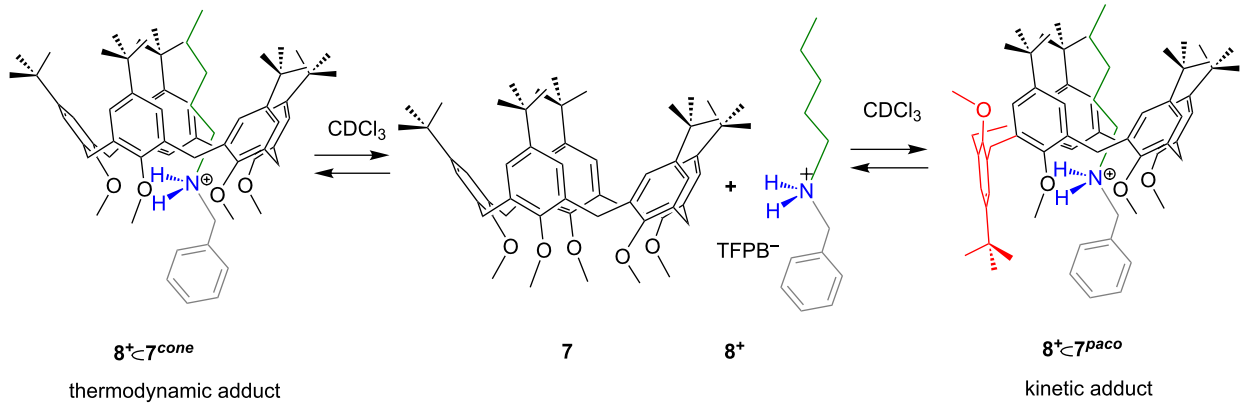

Figure 9: The two pseudorotaxane atropoisomers obtained by threading penta-*O*-methyl-*p*-*tert*-butylcalix[5]arene **7** with pentylbenzylammonium axle **8**$^+$.

able amount of the kinetic pseudorotaxane $\mathbf{3}^+\subset\mathbf{1}^{1,2,3\text{-}alt}$ can be observed at the equilibrium indicating a smaller energy difference with respect to the thermodynamic atropoisomer $\mathbf{3}^+\subset\mathbf{1}^{cone}$. This can be ascribed to a higher destabilization of the *cone* atropoisomer due to a higher number of unfavourable "fluorophobic" interactions between the CF_3 group and the *t*-Bu-Ar moieties.

Conclusion

We have here reported a study on isomeric pseudorotaxanes in which the isomerism arises by the different conformation adopted by the calix[6]arene wheel. Among the eight possible discrete conformations of the calix[6]arene macrocycle, the *cone* and *1,2,3-alternate* ones were observed in the pseudorotaxane architectures obtained by threading a hexahexyloxycalix[6]arene with axles bearing biphenyl or trifluoromethylbenzyl moieties. The interconversion between the *cone* and *1,2,3-alternate* conformations occurs, in free calix[6]arene, by means of the "oxygen-through-the-annulus" and/or "*p*-substituent-through-the-annulus" passages. The presence of the ammonium axles inside the calixarene cavity prevents these passages; consequently two atropoisomeric pseudorotaxanes were formed. We showed that the interconversion between the two atropoisomeric pseudorotaxanes can only occur through a mechanism of de-threading/re-threading of the axle. In all the examined cases, the *1,2,3-alternate* and *cone* atropoisomers are the kinetic and thermodynamic pseudorotaxane, respectively. We do believe that novel and intriguing calixarene-based mechanomolecules, with expanded properties or functions, could be obtained by an appropriate stoppering or catenation of such atropoisomeric pseudorotaxanes.

Experimental

ESI(+)–MS measurements were performed on a Micromass Bio-Q triple quadrupole mass spectrometer equipped with electrospray ion source, using a mixture of H_2O/CH_3CN (1:1) and 5% HCOOH as solvent. Flash chromatography was performed on Merck silica gel (60, 40–63 μm). All chemicals were reagent grade and were used without further purification. Anhydrous solvents were purchased from Aldrich. When necessary compounds were dried in vacuo over $CaCl_2$. Reaction temperatures were measured externally. Reactions were monitored by TLC on Merck silica gel plates (0.25 mm) and visualized by UV light, or by spraying with H_2SO_4–$Ce(SO_4)_2$ or phosphomolybdic acid. NMR spectra were recorded on a Bruker Avance-600 spectrometer [600 (^{1}H) and 150 MHz (^{13}C)], Bruker Avance-400 spectrometer [400 (^{1}H) and 100 MHz (^{13}C)], Bruker Avance-300 spectrometer [300 (^{1}H) and 75 MHz (^{13}C)], or Bruker Avance-250 spectrometer [250 (^{1}H) and 63 MHz (^{13}C)]; chemical shifts are reported relative to the residual solvent peak ($CHCl_3$: δ 7.26, $CDCl_3$: δ 77.23; CD_3OH: δ 4.87, CD_3OD: δ 49.0;). Standard pulse programs, provided by the manufacturer, were used for 2D COSY-45, 2D ROESY and 2D NOESY/EXSY experiments.

General procedure for the preparation of $\mathbf{2}^+$ and $\mathbf{3}^+\cdot TFPB^-$ salts

Derivative **4** (or **5**, 2.2 mmol) was dissolved at 60 °C in liquid $(Me_3Si)_2NH$ (0.71 g, 4.4 mmol, 0.92 mL), $LiClO_4$ (0.02 g, 2.2 mmol) was added and the reaction was kept under stirring at 60 °C until a white solid was formed (30 min). The solution was allowed to cool down at room temperature and dry MeOH (4.0 mL) was added. The mixture was kept under stirring for 2 h and then cooled at 0 °C. $NaBH_4$ (1.12 g, 11.0 mmol) was added and the mixture was kept under stirring at 0 °C for 15 min and then allowed to warm up at room temperature. After 2 hours the solvent was removed, the solid was dissolved in ethyl acetate (100 mL) and washed with an aqueous saturated solution of $NaHCO_3$ (100 mL) and H_2O (50 mL). The organic layer was dried over Na_2SO_4 and the solvent was removed under reduced

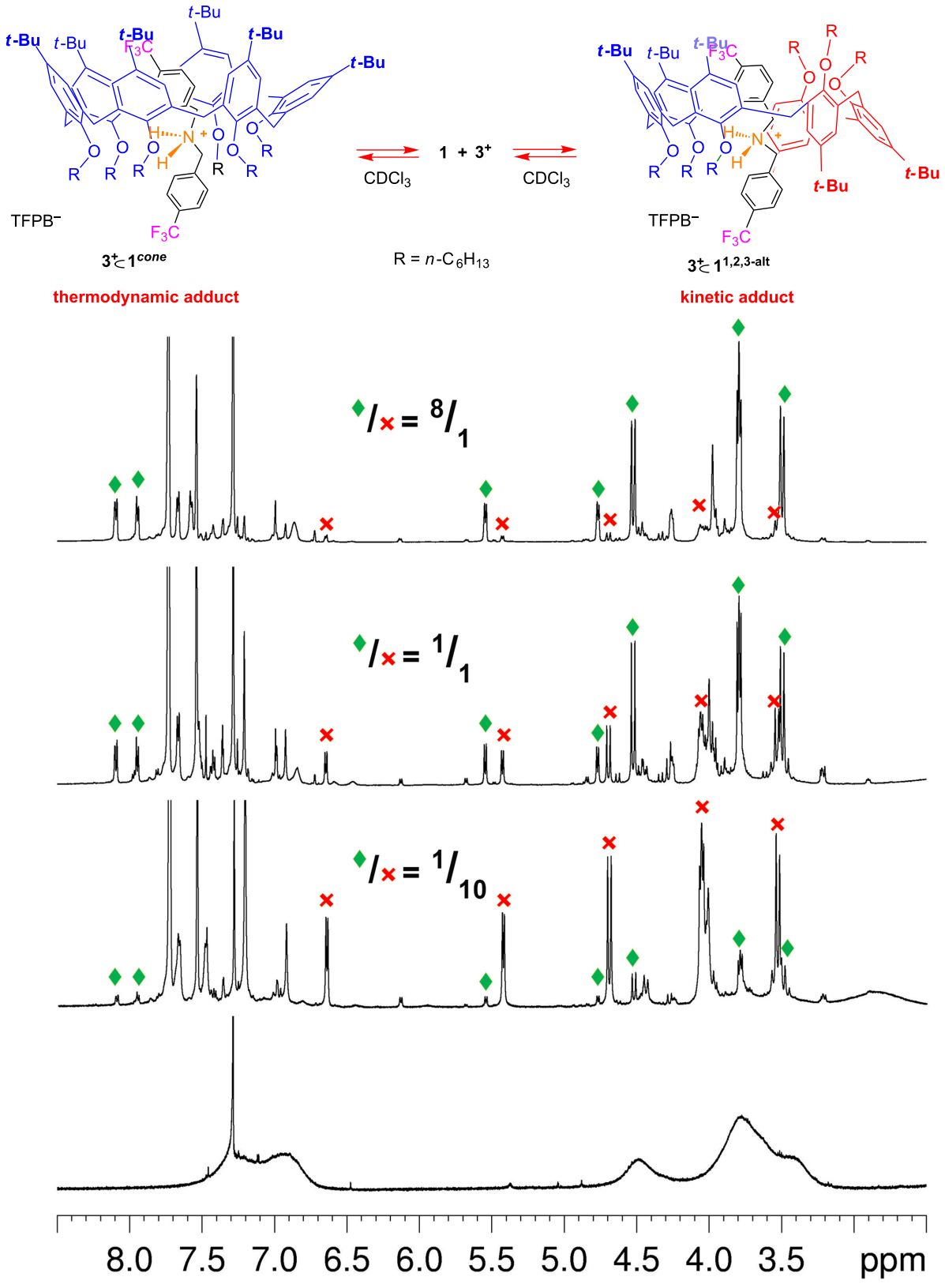

Figure 10: ^{1}H NMR spectra (600 MHz, $CDCl_3$, 298 K) of, from bottom to top: hexahexyloxycalix[6]arene **1**; a 1:1 mixture (0.003 M) of **1** and $\mathbf{3}^+\cdot TFPB^-$ immediately after mixing; after 2 h; after 18 h, mechanism for the formation of the two atropoisomeric pseudo[2]rotaxanes $\mathbf{3}^+\subset\mathbf{1}^{cone}$ and $\mathbf{3}^+\subset\mathbf{1}^{1,2,3\text{-}alt}$.

pressure, to give secondary amine derivative. Amine was used without further purification in the next step. Secondary amine derivative (1.16 mmol) was dissolved in MeOH (20 mL) at room temperature and an aqueous solution of HCl (37% w/w, 0.20 mL) was added dropwise. The mixture was kept under stirring for 30 min, until the formation of a white precipitate. The solid was collected by filtration, washed with MeOH (10 mL) and CH_3CN (10 mL) and dried under vacuum to give the ammonium chloride derivative. The chloride salt (0.68 mmol) and sodium tetrakis[3,5-bis(trifluoromethyl)phenyl]borate (0.60 g, 0.68 mmol) were dissolved in dry MeOH (15 mL). The solution was stirred for 18 h in the dark, then the solvent was removed and deionized water was added, obtaining a light brown precipitate, that was filtered off and dried under vacuum to give threads $\mathbf{2}^+$ or $\mathbf{3}^+$.

Derivative $\mathbf{2}^+$

Light brown solid, 0.73 g, 0.60 mmol, 88% yield (respect chloride salt); mp 135–138 °C; ESI(+) MS (*m*/*z*): 350.2 (M^+); ^{1}H NMR (400 MHz, CD_3OD, 298 K) δ 4.34 (s, 4H), 7.37–7.41 (overlapped, 6H), 7.61–7.67 (overlapped, 20H), 7.76 (d, J = 7.8 Hz, 4H); ^{13}C NMR (100 MHz, CD_3OD, 298 K) δ 51.7, 118.4, 118.4, 118.5, 121.7, 124.4, 127.1, 128.0, 128.8, 129.0, 130.0, 130.1, 130.2, 130.3(2), 130.5(2), 130.6, 131.2, 131.5, 135.8, 141.3, 143.9, 162.1, 162.6, 163.1, 163.6; anal. calcd for $C_{58}H_{36}BF_{24}N$: C, 57.40; H, 2.99; found: C, 57.39; H, 3.01.

Derivative $\mathbf{3}^+$

Light brown solid, 0.57 g, 0.48 mmol, 70 % yield (respect chloride salt); mp 125–128 °C; ESI(+) MS (*m*/*z*): 334.1 (M^+); ^{1}H NMR (300 MHz, CD_3OD, 298 K) δ 3.7 (s, 4H), 7.30–7.32 (overlapped, 20H); ^{13}C NMR (75 MHz, CD_3OD, 298 K) δ 52.6, 118.3, 118.5, 118.6, 122.0, 125.4, 127.3, 128.3, 128.9, 129.1, 130.0, 130.3, 130.4, 130.5(2), 130.6, 131.2, 131.6, 135.8, 141.4, 144.0, 162.2, 162.7, 163.2, 163.5; anal. calcd for $C_{48}H_{26}BF_{30}N$: C, 48.14; H, 2.19; found: C, 48.13; H, 2.17.

General procedure for the preparation of pseudorotaxane derivatives

The calixarene derivative **1** (3.0 mM) and ammonium salt $\mathbf{2}^+$ or $\mathbf{3}^+$ (3.0 mM) were dissolved in $CDCl_3$ (0.5 mL). Each solution was sonicated for 15 min at room temperature and then was transferred into a NMR tube for 1D and 2D NMR spectra acquisition.

Determination of apparent K_{ass} value for pseudorotaxanes $\mathbf{2}^+\subset\mathbf{1}^{cone}$, $\mathbf{3}^+\subset\mathbf{1}^{cone}$ and $\mathbf{3}^+\subset\mathbf{1}^{1,2,3\text{-}alt}$, by quantitative ^{1}H NMR analysis. The sample was prepared by dissolving calixarene **1** (3.0×10^{-3} M) and the ammonium TFPB salt $\mathbf{2}^+$ or $\mathbf{3}^+$ (3.0×10^{-3} M) in $CDCl_3$ (0.5 mL) containing 1.0 μL of TCHE (d = 1.596 g/mL) as an internal standard. The complex concentration [complex] was evaluated by integration of the ^{1}H NMR signal of TCHE versus the signals of the pseudorotaxane. The following equation was used to obtain the moles of the complex:

$$\frac{G_a}{G_b} = \frac{F_a}{F_b} \times \frac{N_b}{N_a} \times \frac{M_a}{M_b},$$

where G_a = grams of TCHE, G_b = grams of pseudorotaxane, F_a and F_b = areas of the signal of the TCHE and shielded aromatic protons of axle inside the calixarene cavity, N_a and N_b = numbers of nuclei that cause the signals (N_a for TCHE; N_b for pseudorotaxane) and M_a and M_b = molecular masses of TCHE (a) and pseudorotaxane (b).

Supporting Information

Supporting Information File 1

VT NMR studies of hexyloxycalix[6]arene **1**, 2D COSY and HSQC spectra of atropoisomeric pseudorotaxanes, details of DFT calculations and atomic coordinates.
[https://www.beilstein-journals.org/bjoc/content/supplementary/1860-5397-14-186-S1.pdf]

Acknowledgements

The authors acknowledge the Regione Campania (POR CAMPANIA FESR 2007/2013 O.O.2.1, CUP B46D140-02660009) for the FT-ICR mass spectrometer facilities, Farma-BioNet (CUP B25C13000230007), the Centro di Tecnologie Integrate per la Salute" (CITIS, project PONa3_00138) for the 600 MHz NMR facilities and Università di Salerno for financial support.

ORCID® iDs

Carmine Gaeta - https://orcid.org/0000-0002-2160-8977
Carmen Talotta - https://orcid.org/0000-0002-2142-6305
Placido Neri - https://orcid.org/0000-0003-4319-1727

References

1. Bruns, C. J.; Stoddart, J. F. *The Nature of the Mechanical Bond: From Molecules to Machines,* 1st ed.; John Wiley & Sons, 2017.
2. Feringa, B. L. *Angew. Chem., Int. Ed.* **2017,** *56,* 11060–11078. doi:10.1002/anie.201702979
3. Sauvage, J.-P. *Angew. Chem., Int. Ed.* **2017,** *56,* 11080–11093. doi:10.1002/anie.201702992
4. Stoddart, J. F. *Angew. Chem., Int. Ed.* **2017,** *56,* 11094–11125. doi:10.1002/anie.201703216
5. Kassem, S.; Lee, A. T. L.; Leigh, D. A.; Marcos, V.; Palmer, L. I.; Pisano, S. *Nature* **2017,** *549,* 374–378. doi:10.1038/nature23677
6. Zhao, D.; Neubauer, T. M.; Feringa, B. L. *Nat. Commun.* **2015,** *6,* No. 6652. doi:10.1038/ncomms7652

7. Barat, R.; Legigan, T.; Tranoy-Opalinski, I.; Renoux, B.; Péraudeau, E.; Clarhaut, J.; Poinot, P.; Fernandes, A. E.; Aucagne, V.; Leigh, D. A.; Papot, S. *Chem. Sci.* **2015,** *6,* 2608–2613. doi:10.1039/C5SC00648A
8. Van der Berg, J. P.; Velema, W. A.; Szymanski, W.; Driessen, A. J. M.; Feringa, B. L. *Chem. Sci.* **2015,** *6,* 3593–3598. doi:10.1039/C5SC00215J
9. Lewis, J. E. M.; Galli, M.; Goldup, S. M. *Chem. Commun.* **2017,** *53,* 298–312. doi:10.1039/C6CC07377H
10. Yu, H.; Luo, Y.; Beverly, K.; Stoddart, J. F.; Tseng, H.; Heath, J. R. *Angew. Chem., Int. Ed.* **2003,** *42,* 5706–5711. doi:10.1002/anie.200352352
11. Green, J. E.; Choi, J. W.; Boukai, A.; Bunimovich, Y.; Johnston-Halperin, E.; Delonno, E.; Luo, Y.; Sheriff, B. A.; Xu, K.; Shin, Y. S.; Tseng, H.-R.; Stoddart, J. F.; Heath, J. R. *Nature* **2007,** *445,* 414–417. doi:10.1038/nature05462
12. Li, Z.-Y.; Zhang, Y.; Zhang, C.-W.; Chen, L.-J.; Wang, C.; Tan, H.; Yu, Y.; Li, X.; Yang, H.-B. *J. Am. Chem. Soc.* **2014,** *136,* 8577–8589. doi:10.1021/ja413047r
13. Wang, W.; Chen, L.-J.; Wang, X.-Q.; Sun, B.; Li, X.; Zhang, Y.; Shi, J.; Yu, Y.; Zhang, L.; Liu, M.; Yang, H.-B. *Proc. Natl. Acad. Sci. U. S. A.* **2015,** *112,* 5597–5601. doi:10.1073/pnas.1500489112
14. Shivanyuk, A.; Rebek, J. *J. Am. Chem. Soc.* **2002,** *124,* 12074–12075. doi:10.1021/ja020607a
15. Bordoli, R. J.; Goldup, S. M. *J. Am. Chem. Soc.* **2014,** *136,* 4817–4820. doi:10.1021/ja412715m
16. Neal, E. A.; Goldup, S. M. *Chem. Commun.* **2014,** *50,* 5128–5142. doi:10.1039/C3CC47842D
17. Talotta, C.; De Simone, N. A.; Gaeta, C.; Neri, P. *Org. Lett.* **2015,** *17,* 1006–1009. doi:10.1021/acs.orglett.5b00115
18. Fuller, A.-M. L.; Leigh, D. A.; Lusby, P. J. *J. Am. Chem. Soc.* **2010,** *132,* 4954–4959. doi:10.1021/ja1006838
19. Talotta, C.; Gaeta, C.; Pierro, T.; Neri, P. *Org. Lett.* **2011,** *13,* 2098–2101. doi:10.1021/ol2005159
20. Talotta, C.; Gaeta, C.; Neri, P. *Org. Lett.* **2012,** *14,* 3104–3107. doi:10.1021/ol3011997
21. Talotta, C.; Gaeta, C.; Qi, Z.; Schalley, C. A.; Neri, P. *Angew. Chem., Int. Ed.* **2013,** *52,* 7437–7441. doi:10.1002/anie.201301570
22. Neri, P.; Sessler, J. L.; Wang, M.-X., Eds. *Calixarenes and Beyond;* Springer: Dordrecht, 2016. doi:10.1007/978-3-319-31867-7
23. Tommasone, S.; Talotta, C.; Gaeta, C.; Margarucci, L.; Monti, M. C.; Csapullo, A.; Macchi, B.; Prete, S. P.; De Araujo, A. L.; Neri, P. *Angew. Chem., Int. Ed.* **2015,** *54,* 15405–15409. doi:10.1002/anie.201508651
24. Soriente, A.; De Rosa, M.; Fruilo, M.; Lepore, L.; Gaeta, C.; Neri, P. *Adv. Synth. Catal.* **2005,** *347,* 816–824. doi:10.1002/adsc.200505023
25. Gaeta, C.; Gregoli, L.; Martino, M.; Neri, P. *Tetrahedron Lett.* **2002,** *43,* 8875–8878. doi:10.1016/S0040-4039(02)02204-9
26. Ikeda, A.; Shinkai, S. *Chem. Rev.* **1997,** *97,* 1713–1734. doi:10.1021/cr960385x
27. Bifulco, G.; Gomez-Paloma, L.; Riccio, R.; Gaeta, C.; Troisi, F.; Neri, P. *Org. Lett.* **2005,** *7,* 5757–5760. doi:10.1021/ol052166g
28. Bifulco, G.; Riccio, R.; Gaeta, C.; Neri, P. *Chem. – Eur. J.* **2007,** *13,* 7185–7194. doi:10.1002/chem.200700238
29. Kanamathareddy, S.; Gutsche, C. D. *J. Org. Chem.* **1992,** *57,* 3160–3166. doi:10.1021/jo00037a037
30. Jaime, C.; De Mendoza, J.; Prados, P.; Nieto, P. M.; Sanchez, C. *J. Org. Chem.* **1991,** *56,* 3372–3376. doi:10.1021/jo00010a036
31. Magrans, J. O.; de Mendoza, J.; Pons, M.; Prados, P. *J. Org. Chem.* **1997,** *62,* 4518–4520. doi:10.1021/jo961943a
32. Arduini, A.; Orlandini, G.; Secchi, A.; Credi, A.; Silvi, S.; Venturi, M. Calixarene Threading by Viologen-Based Axles. In *Calixarenes and Beyond;* Neri, P.; Sessler, J. L.; Wang, M.-X., Eds.; Springer: Dordrecht, 2016; pp 761–781. doi:10.1007/978-3-319-31867-7_29
33. Gaeta, C.; Talotta, C.; De Rosa, M.; Soriente, A.; Neri, P. Calixarene Threading via Superweak Anion. In *Calixarenes and Beyond;* Neri, P.; Sessler, J. L.; Wang, M.-X., Eds.; Springer: Dordrecht, 2016; pp 783–809. doi:10.1007/978-3-319-31867-7_30
34. La Manna, P.; Talotta, C.; Gaeta, C.; Soriente, A.; De Rosa, M.; Neri, P. *J. Org. Chem.* **2017,** *82,* 8973–8983. doi:10.1021/acs.joc.7b01388
35. De Rosa, M.; Talotta, C.; Gaeta, C.; Soriente, A.; Neri, P.; Pappalardo, S.; Gattuso, G.; Notti, A.; Parisi, M. F.; Pisagatti, I. *J. Org. Chem.* **2017,** *82,* 5162–5168. doi:10.1021/acs.joc.7b00406
36. Gaeta, C.; Talotta, C.; Margarucci, L.; Casapullo, A.; Neri, P. *J. Org. Chem.* **2013,** *78,* 7627–7638. doi:10.1021/jo401206j
37. Gaeta, C.; Talotta, C.; Mirra, S.; Margarucci, L.; Casapullo, A.; Neri, P. *Org. Lett.* **2013,** *15,* 116–119. doi:10.1021/ol303142c
38. Gaeta, C.; Talotta, C.; Farina, F.; Teixeira, F. A.; Marcos, P. A.; Ascenso, J. R.; Neri, P. *J. Org. Chem.* **2012,** *77,* 10285–10293. doi:10.1021/jo3019945
39. Arduini, A.; Bussolati, R.; Credi, A.; Secchi, A.; Silvi, S.; Semeraro, M.; Venturi, M. *J. Am. Chem. Soc.* **2013,** *135,* 9924–9930. doi:10.1021/ja404270c
40. Gaeta, C.; Troisi, F.; Neri, P. *Org. Lett.* **2010,** *12,* 2092–2095. doi:10.1021/ol100578z
41. van Duynhoven, J. P. M.; Janssen, R. G.; Verboom, W.; Franken, S. M.; Casnati, A.; Pochini, A.; Ungaro, R.; de Mendoza, J.; Nieto, P. M.; Prados, P.; Reinhoudt, D. N. *J. Am. Chem. Soc.* **1994,** *116,* 5814–5822. doi:10.1021/ja00092a036
42. Grimme, S. *J. Comput. Chem.* **2006,** *27,* 1787–1799. doi:10.1002/jcc.20495
43. Suezawa, H.; Ishihara, S.; Umezawa, Y.; Tsuboyama, S.; Nishio, M. *Eur. J. Org. Chem.* **2004,** 4816–4822. doi:10.1002/ejoc.200400373

License and Terms

BEILSTEIN JOURNAL OF ORGANIC CHEMISTRY

Tetrathiafulvalene – a redox-switchable building block to control motion in mechanically interlocked molecules

Hendrik V. Schröder and Christoph A. Schalley*

Review

Open Access

Address:
Institut für Chemie und Biochemie, Organische Chemie, Freie Universität Berlin, Takustraße 3, 14195 Berlin, Germany

Email:
Christoph A. Schalley* - c.schalley@fu-berlin.de

* Corresponding author

Keywords:
artificial molecular machines; mechanically interlocked molecules; molecular switches; supramolecular chemistry; tetrathiafulvalene

Beilstein J. Org. Chem. **2018,** *14,* 2163–2185.
doi:10.3762/bjoc.14.190

Received: 13 April 2018
Accepted: 01 August 2018
Published: 20 August 2018

This article is part of the thematic issue "Macrocyclic and supramolecular chemistry".

Guest Editor: M.-X. Wang

Abstract

With the rise of artificial molecular machines, control of motion on the nanoscale has become a major contemporary research challenge. Tetrathiafulvalenes (TTFs) are one of the most versatile and widely used molecular redox switches to generate and control molecular motion. TTF can easily be implemented as functional unit into molecular and supramolecular structures and can be reversibly oxidized to a stable radical cation or dication. For over 20 years, TTFs have been key building blocks for the construction of redox-switchable mechanically interlocked molecules (MIMs) and their electrochemical operation has been thoroughly investigated. In this review, we provide an introduction into the field of TTF-based MIMs and their applications. A brief historical overview and a selection of important examples from the past until now are given. Furthermore, we will highlight our latest research on TTF-based rotaxanes.

Introduction

Undoubtedly, the exploration of nature's molecular machines in the last century led to a paradigm change of how we think about working and organization processes on the molecular level [1-3]. Inspired by the way how energy and concentration gradients control repetitive motions of these biological nanomachines, researchers have been seeking for synthetic analogues, i.e., artificial molecular machines (AMMs), with the ultimate goal to convert energy into directional mechanical motion on the nanoscale [4-6]. The field of AMMs beautifully coalesces the desire of reproducing the versatile functions of nature's biomachinery and the miniaturization of macroscopic technical devices made by man. Although the field of AMMs is relatively young, the Nobel Prize in 2016 for Jean-Pierre Sauvage [7], Sir J. Fraser Stoddart [8], and Bernard L. Feringa [9] "for the

design and synthesis of molecular machines" is an outstanding appreciation of the public and scientific community.

Mechanically interlocked molecules (MIMs) such as rotaxanes [10] or catenanes [11] are ideally suited for the construction of AMMs. In comparison to covalently linked molecules, the mechanical bond provides cohesive supramolecular assemblies with unique properties and a high flexibility and mobility of the subcomponents in a small molecular space. To control molecular motion, one of the most important construction principles to transform a simple MIM into an AMM is to implement a switching unit into the molecular framework, which is reversibly addressable by external stimuli [12,13]. A variety of different stimuli to control MIMs has been reported ranging, for example, from physical stimuli such as electrons, light, temperature, pressure, or magnetism to chemical stimuli such as acids/bases, ions, additives, or solvent changes [14]. However, the latter class of stimuli bears the disadvantage to produce chemical "waste" which creates the challenging task to constantly add and remove material to and from the system, if a repetitive operation is desired. Therefore, a "clean" stimulus is often preferred.

One of the most frequently used and thoroughly characterized "clean" switches to control molecular motion of MIMs is tetrathiafulvalene (TTF, **1**) and its derivatives (Figure 1). TTF is a redox-switchable organosulfur compound, which exhibits ideal properties for the electrochemical operation of MIMs. Several excellent reviews on the use of TTF in other supramolecular systems such as macrocycles, cages, and receptor molecules are already available [15-21]. In this review, motifs of construction and working principles of TTF-based MIMs in the past and current literature are summarized and milestones of their development are discussed. In the first part, we will briefly describe how TTF evolved into a key building block for switchable supramolecular architectures and which synthetic breakthroughs enabled this development. We also aim for a tutorial introduction to readers new to the field of TTF-switchable MIMs.

Review

1. Tetrathiafulvalene – an (almost) perfect molecular switch

Whereas inorganic chemists are used to commonly handle metal-based compounds in different oxidation states, only a small selection of organic molecules [22] can be reversibly oxidized or reduced without chemical side reactions or decomposition. TTF is perhaps one of the most popular examples and exists as a classical Weitz type redox system [22] in three different stable oxidation states. The stability of TTF, both in solution and in the solid state [23], makes it an ideal molecular switch.

A first one-electron oxidation [23] converts neutral TTF (**1**) into the radical-cationic species $\mathbf{1}^{\bullet+}$ (Figure 1). The TTF radical cation is one of the rare organic radicals that are long-term stable and even isolable. A second oxidation step yields the dication $\mathbf{1}^{2+}$. Both redox-transitions are fully reversible and have surprisingly low oxidation potentials (0.37 and 0.74 V vs Ag/AgCl in CH_3CN) [24], which enable an easily achievable electrochemical switching under ambient conditions. The stability of all oxidation states – even in the presence of air and moisture – is crucial for the efficient operation and characterization of TTF-based MIMs on a suitable laboratory timescale.

The observed stability of the two oxidation states can be explained by the stepwise aromatization of the TTF system. In the neutral state, TTF consists of two pro-aromatic 1,3-dithiolylidene rings which are connected by a C=C double bond. The first oxidation converts one ring into an aromatic 6π-electron system, which is further stabilized by a mixed-valence resonance structure. The second oxidation yields two aromatic 1,3-dithiolium cations (2 × 6π electrons) which are connected by a C–C single bond.

The change of the electronic structure is also accompanied by conformational changes [25,26] of the TTF skeleton. Neutral TTF has a boat-shaped structure with C_{2v} symmetry. In the

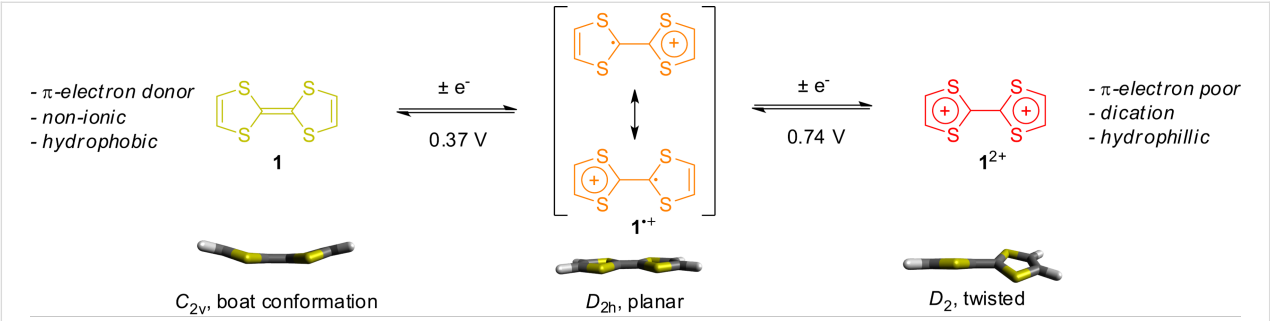

Figure 1: The two one-electron oxidation reactions of tetrathiafulvalene (TTF, **1**) and the corresponding property changes.

radical-cation state, $TTF^{\bullet+}$ planarizes into a D_{2h}-symmetric structure due to its partial aromatization. This property change is widely used to induce cofacial intermolecular stacking interactions. Finally, the TTF^{2+} dication adopts a twisted conformation with D_2 symmetry.

In the neutral state, TTF is a strong π-donor molecule, a property which is used in a plethora of charge-transfer materials and molecules [27]. In supramolecular chemistry [28] and for the construction of MIMs [29], the good π-donor properties of TTF are frequently used to template donor–acceptor complexes with π-electron deficient macrocycles. If TTF undergoes oxidation, the π-donating effect decreases, whereas the TTF^{2+} dication can be considered as a π-electron-poor molecule.

The electrochemical switching of a TTF unit and the change of electronic or conformational properties not necessarily results in a mechanical motion of a MIM. A prerequisite is that at least one of the above-mentioned properties of TTF is interacting with other parts of the MIM. If this property is changed, the previous conformation of the MIM might become unstable and initiates a molecular motion. This simple principle of bistability has been used to create a variety of different switchable TTF-based supramolecular architectures with many versatile applications.

On the macroscopic as well as on the molecular level, even the most efficient switch is useless, if no observable output is generated which helps to detect the switching process [30]. A simple "read out" is provided by the optical properties of TTF in its different switching states. For example, UV–vis spectra of the TTF derivative **2** in the neutral, radical-cation, and dication state are shown in Figure 2. The spectrum of **2** shows only weak absorption above 350 nm which results in a pale yellow solution. The lowest-energy band is the HOMO→LUMO transition of the molecule. The radical-cation $\mathbf{2}^{\bullet+}$ exhibits two strong absorption bands (≈450 and 800 nm), which yield an orange-brown solution. Initially, the low-energy band of $\mathbf{2}^{\bullet+}$ between 600–1000 nm was interpreted as a signature for an unusually stable TTF dimer [31]. However, later investigations showed that this band is an intrinsic SOMO-1→SOMO transition in the $\mathbf{2}^{\bullet+}$ radical cation [32]. The dication $\mathbf{2}^{2+}$ shows a strong band at ≈700 nm which results in a deep-blue solution. These strong color changes differ for differently substituted TTF derivatives and make it very easy to follow the electrochemical switching of TTF, even with the naked eye.

Other optical properties which are very helpful for observing the molecular switching in MIMs are charge-transfer bands. The π-donor TTF can form donor–acceptor complexes with π-electron-poor aromatic compounds often indicated by a green

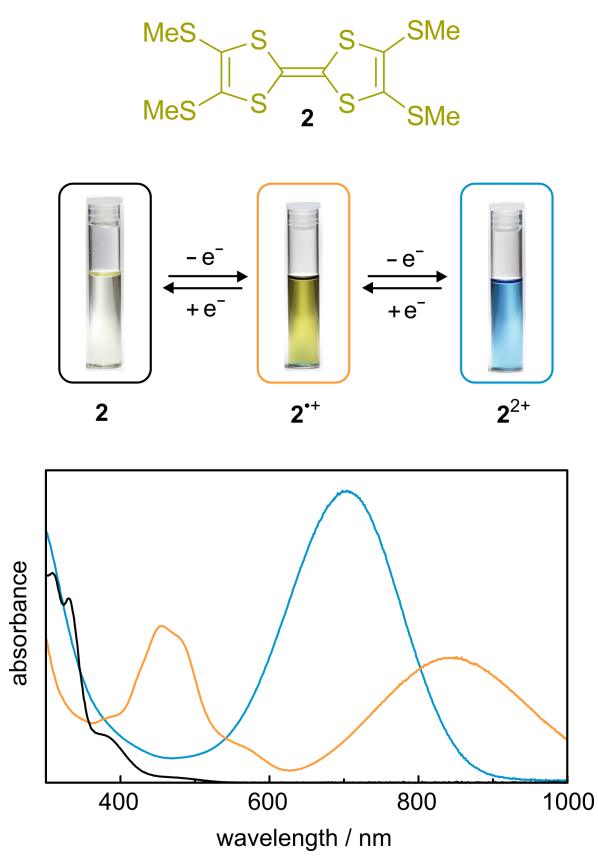

Figure 2: UV–vis spectra and photographs of TTF **2** in its three stable oxidation states (black line = **2**, orange line = $\mathbf{2}^{\bullet+}$, blue line = $\mathbf{2}^{2+}$).

color of the solution [33]. Therefore, the assembly and disassembly of these complexes in solution can be easily traced by the emergence and fading of these characteristic charge-transfer bands.

Another outstanding feature of TTFs is that their radical cations can reversibly form cofacial dimers (Figure 3) [34-36]. The two monomers **1** and $\mathbf{1}^{\bullet+}$ spontaneously self-assemble into a so-called mixed-valence dimer $(\mathbf{1}_2)^{\bullet+}$. A mixed-valence dimer can be identified by splitting of the first TTF oxidation potential into two distinguishable waves. This change in redox behavior can be followed by electrochemical methods such as cyclic voltammetry. Another indication for a mixed-valence dimer interaction can be an emergent low-energy absorption band, usually in the NIR region. Both monomers show usually no absorption in this region.

The radical-cation dimer $(\mathbf{1}^{\bullet+})_2$ instead forms from two $\mathbf{1}^{\bullet+}$ radical cations and exhibits a very unusual binding situation. Whereas both monomers are paramagnetic radicals, the resulting dimer has a diamagnetic character due to radical pairing. Although the distance of ≈3.5 Å between the two $\mathbf{1}^{\bullet+}$ mole-

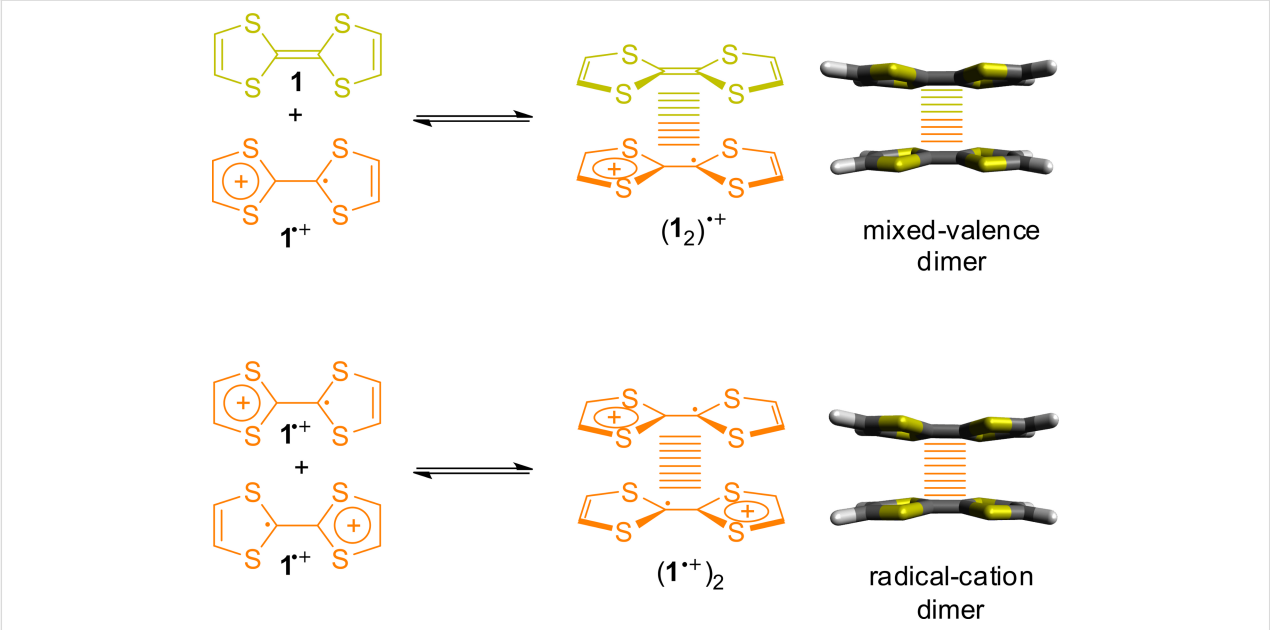

Figure 3: Structure and conformations of two TTF dimers in solution, the mixed-valence and the radical-cation dimer.

cules in the dimer is considerably large in comparison to a C–C bond (≈1.5 Å), the interaction can be considered as a type of multi-centered two-electron bond with covalent character. This type of radical-cation dimer is often called a π-dimer or "pimer" and its formation "pimerization". The radical-cation dimer can be spectroscopically identified by characteristic blue shifts of $TTF^{\bullet+}$ absorption bands. These "Davydov shifts" are a result of the H-aggregate-type arrangement in the dimer [34]. Furthermore, the equilibrium between a paramagnetic monomer and a diamagnetic dimer makes the use of electron paramagnetic resonance (EPR) spectroscopy ideal to follow the dimerization process [36].

Mixed-valence and radical-cation interactions in the solid state are sometimes described as "conductive" and "isolating" form, respectively. However, in solution both dimers display very low stabilities with dimerization energies of only a few kJ mol^{-1} at room temperature [36]. Therefore, these weakly associated dimers are virtually absent at ambient conditions in solution.

A strategy to stabilize the mixed-valence and radical-cation dimer even at room temperature and to overcome the entropic penalty of their formation is to facilitate a spatial proximity of two or more TTF units by a suitable covalent link [37,38]. This pre-organization can also be generated in supramolecular complexes with confined spaces which provide a very high local concentration and shift the equilibrium towards the dimer side. The use of TTF dimerization has been recognized lately as additional possibility to drive motion in MIMs. Recent examples will be discussed in the following section.

2. Evolution of TTF into a key building block in switchable molecular systems

After the first syntheses of native TTF in the early 1970s researches quickly noticed the outstanding electronic properties of this molecule [23,39]. One of the first observations with major impact was the unusual conducting behavior of oxidized TTF salts [40]. The discovery that TTF and the electron-deficient molecule tetracyanoquinodimethane (TCNQ) form charge-transfer salts [41] with the uncommon motif of "segregated stacks" [42] enabled numerous investigations of TTF salts regarding their application in molecular electronics [27,43], organic metals [44], or narrow-band semiconductors [45].

As often in chemical research, major synthetic or analytic breakthroughs are needed to open pathways towards new concepts and applications. Despite the intensive research on TTF during the 70s and 80s, the incorporation of TTF into molecular systems using simple organic chemistry procedures was still challenging at that time.

One of the major synthetic breakthroughs was thus the use of cyanoethyl protective groups for TTF thiolates (Figure 4) [46,47]. Treatment of cyanoethyl-protected 1,3-dithiol-thiolates **A** with one or two equivalents of a strong base such as CsOH yields quantitatively the corresponding cesium thiolates **B** and **D** which are quite stable under standard Schlenk conditions. Addition of an alkyl halide can attach a broad range of different substituents. The cyanoethyl group allows a sequential deprotection and alkylation of 1,3-dithiole-2-thiones **C** and **E** and the corresponding TTF molecules derived from them often in very

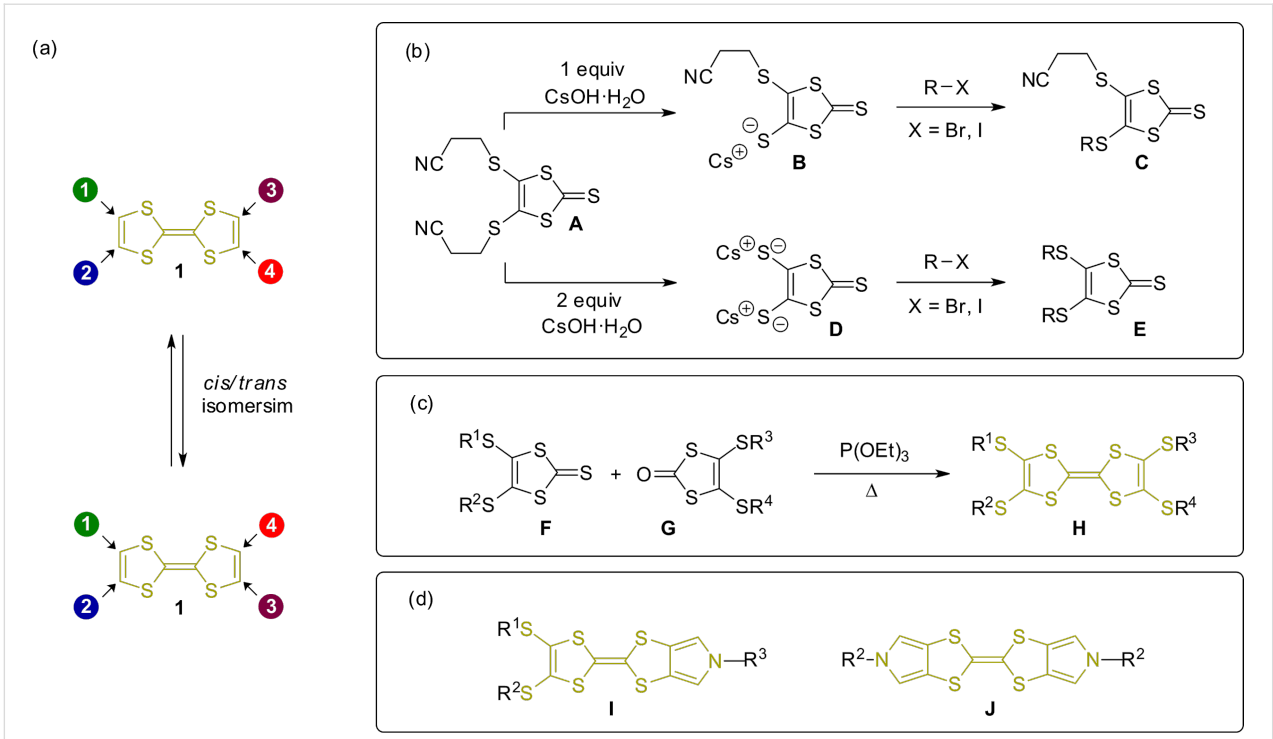

Figure 4: (a) The isomerism problem of TTF. (b)–(d) Major synthetic breakthroughs for the construction of TTF-based supramolecular architectures: (b) Stepwise deprotection/alkylation, (c) phosphite-mediated heterocoupling, and (d) pyrrolo-annulated TTF derivatives **I** and **J**.

good yields. An additional strategy to obtain non-symmetrically substituted TTF derivatives is the stepwise reaction of TTF tetrathiolate with different electrophiles [48].

Another important synthetic advance is the phosphite-mediated heterocoupling of 1,3-dithiol-2-thiones **F** and 1,3-dithiol-2-ones **G** which provides efficient access to TTFs with two differently substituted 1,3-dithiol rings in an efficient way [49]. Simple heating of both monomers (ketone and thioketone) in $P(OMe)_3$ or $P(OEt)_3$ yields the desired hetero dimers **H** often in good yields. In combination with transchalcogenation reactions [50], which allow the transformation of 1,3-dithiol-2-thiones into the corresponding ketones in excellent yields, various types of non-symmetrically substituted TTF moieties can be implemented into organic systems.

However, a synthetic problem which was still intricate is caused by the four substitution sites of the TTF unit, which result in a mixture of *cis* and *trans* isomers, if two different substituents are attached to either one of the two 1,3-dithiolylidene rings. Isomerization can be promoted by trace amounts of acid [51,52] or photochemically [53]. The interconversion usually prevents a sufficient separation of the two isomers on the laboratory timescale. However, substitution of the TTF molecule by electron-withdrawing groups can stabilize the isomers [54] and a separation becomes possible. In particular when it comes to the complex intertwined structure of MIMs, an isolable pure compound is often necessary for a thorough characterization and investigation of their switching properties. One solution to the isomer problem is the introduction of mono- or bipyrrolo-annulated TTF derivatives **I** and **J** [55-57]. The incorporation of these symmetric species into MIMs often circumvents complex isomeric mixtures.

3. Pseudorotaxanes and inclusion complexes: on the way to TTF-based MIMs

Pseudorotaxanes have the general form of a molecular thread encircled by a macrocycle. The difference to rotaxanes is that the axle does not have bulky stopper groups that prevent the deslipping of the wheel. Thus, a pseudorotaxane forms by non-covalent interactions between host and guest without a mechanical bond. Pseudorotaxanes are important precursors of MIMs from which the construction of rotaxanes is achieved by stoppering reactions, while catenanes can be made by macrocyclization of the pseudorotaxane thread. Therefore, we discuss in the following section reports of important pseudorotaxanes and inclusion complexes that contributed to major developments of TTF-based MIMs and AMMs.

The first TTF-based pseudorotaxane was reported by Stoddart and Williams in 1991 (Figure 5) [33]. At this time, they investigated the host–guest properties of the π-electron-poor cyclo-

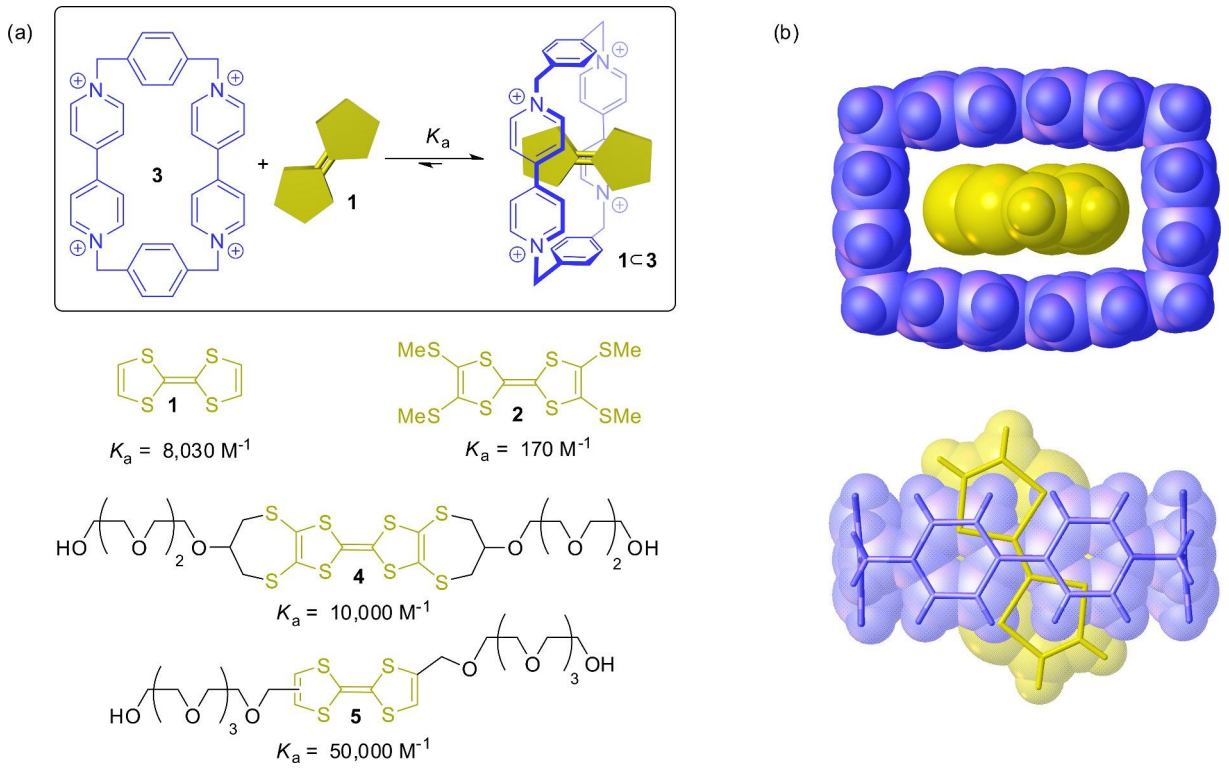

Figure 5: (a) Host–guest equilibrium between π-electron-poor cyclophane **3** and different TTFs with their corresponding association constants in CH_3CN. (b) Crystal structure of host–guest complex **1**⊂**3** [33]. Solvent molecules and counterions are omitted for clarity.

phane cyclobis(paraquat-*p*-phenylene) (**3**) in form of the tetrakis(hexafluorophosphate) salt [58]. The square-shaped host complexes π-electron-rich aromatic compounds such as dihydroxynaphthalenes or dihydroxybenzenes. The π-donor TTF (**1**) also forms a 1:1 complex **1**⊂**3** with this host molecule as shown in solution experiments and by crystallography. The complex formation is immediately visible by an emergent green color of these solutions due to the donor–acceptor interaction.

In later reports, differently substituted TTF derivatives as for example **2**, **4**, and **5** have been investigated towards their binding to host **3** [24,59-63]. π-Electron-rich TTFs form significantly stronger donor–acceptor complexes as π-electron-poor TTFs. However, also the type of substituent on the TTF moiety plays a role in terms of weak secondary binding interactions such as hydrogen bonds [63]. For example TTF **5** which is substituted by ethylene glycol chains displays a high association constant of K_a = 50,000 M^{-1} in acetonitrile. Additionally, extended π-surfaces [64] of TTF derivatives can have a stabilizing effect upon complexation.

TTF (**1**) also forms inclusion complexes with neutral host molecules such as cyclodextrins (Figure 6). This complexation is mainly driven by the hydrophobic effect. α-Cyclodextrin (**6**) molecules encapsulate the hydrophobic TTF (**1**) in aqueous media [65]. Another water-soluble host which can complex TTFs is cucurbit[7]uril (**7**) [66]. However, it is not the neutral form, but the TTF radical cation $\mathbf{1}^{\bullet+}$ which is preferably bound in the cavity of this host. Even the dication $\mathbf{1}^{2+}$ can be hosted by suitable macrocycles. For example, the π-electron-rich wheel **8**, consisting of two doubly-bridged 1,5-dioxynaphthalenes, is able to form a donor–acceptor complex with the π-electron-poor TTF^{2+} dication [26].

An astonishing discovery regarding TTF–cucurbituril complexes was made by Kim and co-workers in 2004 (Figure 7) [67]. The host molecule cucurbit[8]uril (**9**), which is enlarged by an additional glycoluril unit in comparison to **7**, provides sufficient space to accommodate two planar molecules with cofacial orientation [68]. When the water-soluble TTF derivative **10** gets oxidized to its radical cation $\mathbf{10}^{\bullet+}$, a 2:1 complex is formed with a radical-cation dimer $(\mathbf{10}^{\bullet+})_2$ stabilized in the cavity of the host molecule **9**. The presence of the radical-cation dimer complex $(\mathbf{10}^{\bullet+})_2$⊂**9** was demonstrated by NMR, UV–vis and EPR spectroscopy. This was a novelty because stable TTF radical-cation dimers, which are usually only weakly associated species, where not characterized in aqueous medium at room temperature before.

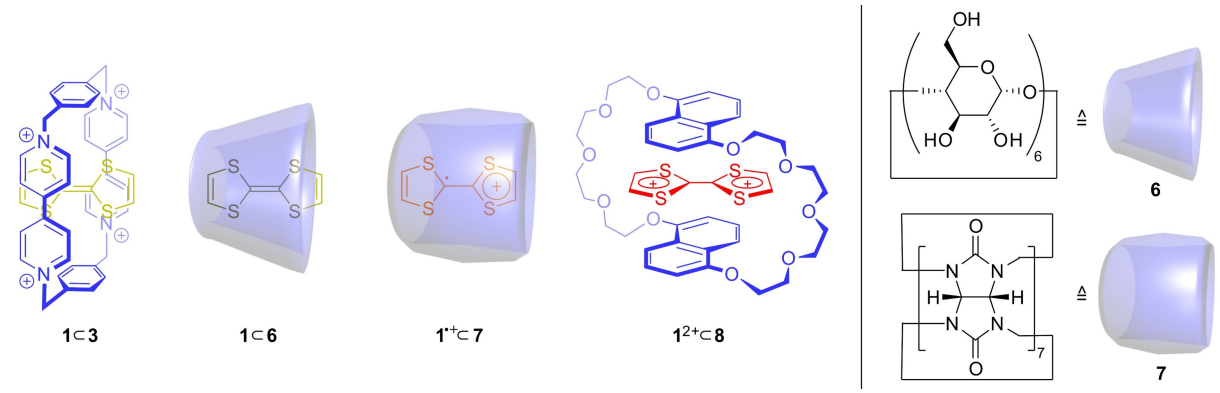

Figure 6: TTF complexes with different host molecules.

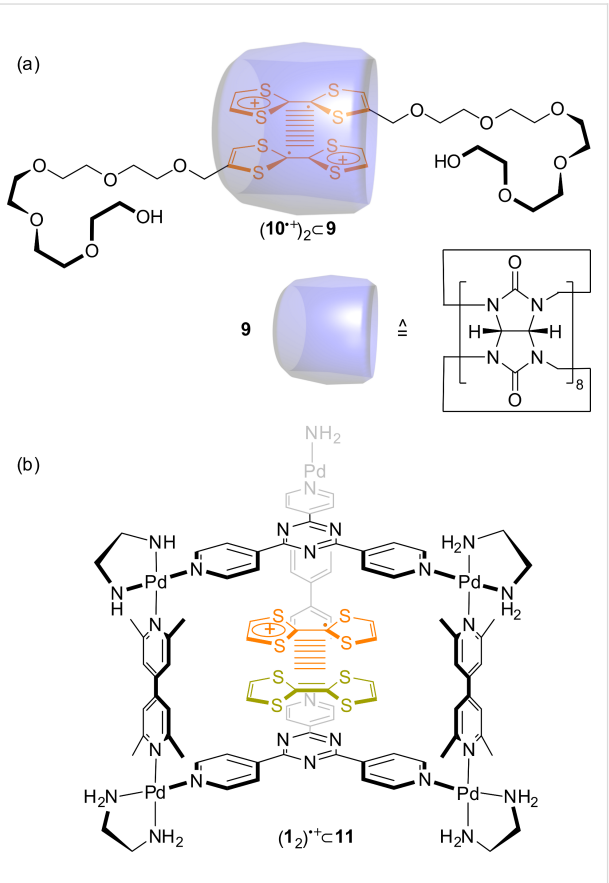

Figure 7: Stable TTF (a) radical-cation and (b) mixed-valence dimers in confined molecular spaces.

A similar observation regarding TTF dimers was made by Fujita and co-workers in 2005 [69]. They used the self-assembled Pd-cage **11** to encapsulate two neutral TTF molecules. Oxidation of the solution yields an ambient-stable TTF mixed-valence dimer $(\mathbf{1}_2)^{\bullet+}$ inside the cage as shown by optical and electrochemical methods.

A further step towards motion control in MIMs was made by investigating the switching of the TTF molecule when different host molecules are available in solution (Figure 8). In a so-called "three-pole supramolecular switch" consisting of a mixture of host **3**, **8**, and TTF (**1**), the TTF molecule can change its position like in a "pea in the shell game" [26]. In its neutral form, TTF (**1**) forms the donor–acceptor complex **1**⊂**3** with host **3**. Higher potentials need to be applied to oxidize TTF (**1**) into its radical-cationic form since the association energy of the donor–acceptor complex must be overcome. After oxidation, the radical-cation $\mathbf{1}^{\bullet+}$ is expelled from host **3** by repulsive Coulombic forces. If $\mathbf{1}^{\bullet+}$ gets further oxidized to the π-electron-poor dication $\mathbf{1}^{2+}$, the π-electron-rich macrocycle **8** can now encapsulate TTF^{2+}. This relatively straightforward concept of electrochemically triggered complexation and expulsion of the TTF molecule from different hosts forms the fundament for motion control in a variety of different MIMs.

To illustrate how this redox-triggered complexation/decomplexation of pseudorotaxanes is transferred into a controlled molecular motion in MIMs, the TTF-based pseudo[1]rotaxane **12** recently reported by us is shown in Figure 9 [70]. In a pseudo[1]rotaxane, the axle molecule is covalently bound to the wheel component. The self-inclusion structure mimics the conformation of a molecular lasso, a structural motif which was also recently found in nature for peptides with high antibacterial efficacy [71]. In **12**, the TTF molecule is not implemented in the thread but in the wheel component. In the neutral state, strong hydrogen bonding between the crown ether wheel and the dialkylammonium station forces a threaded conformation. If the TTF is oxidized, however, charge repulsion between the ammonium station and the TTF moiety weakens the binding. This ultimately leads to an expulsion of the thread from the cavity of the wheel, and thus to an opening of the lasso. This

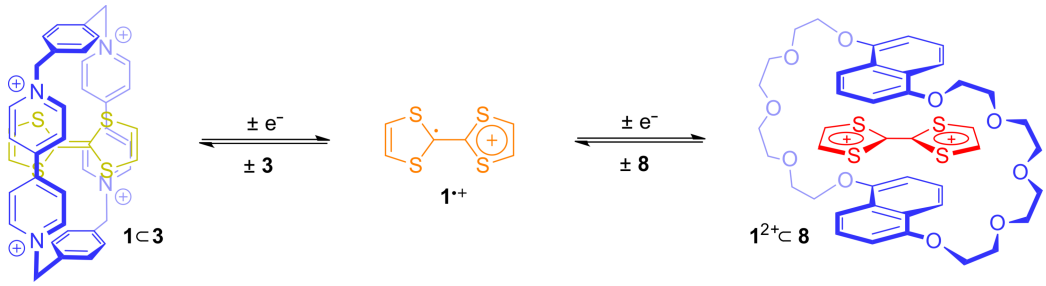

Figure 8: A “three-pole supramolecular switch”: Controlled by its oxidation state, TTF (**1**) jumps back and forth between different host molecules.

example shows how easily a reversible molecular motion can be achieved by redox-switching of the TTF unit.

4. Rotaxanes

Rotaxanes consist of a dumbbell-shaped axle molecule encircled by a macrocycle. Bulky stopper groups at both ends of the axle prevent a deslipping of the wheel. With a development starting from low-yielding statistical synthesis to efficient template-controlled synthesis, rotaxanes have become the workhorse of MIMs in the last three decades. Regarding their use as molecular devices, three types of motions can be potentially controlled in rotaxanes: pirouetting of the wheel around the axle, translation of the wheel along the axle, and a rocking motion of the wheel [72]. However, most reports have focused on the stimuli-controlled translational motion. MIMs in which the wheel position on the axle is controlled by external stimuli are called “switchable molecular shuttles”.

4.1. Switchable molecular shuttles

A schematic illustration of the working principle of non-degenerate TTF-based shuttle rotaxanes is shown in Figure 10. In the ground state co-conformation, the wheel encircles the TTF unit. Upon TTF oxidation, the attractive forces are lowered or even repulsive forces are generated between the TTF unit and

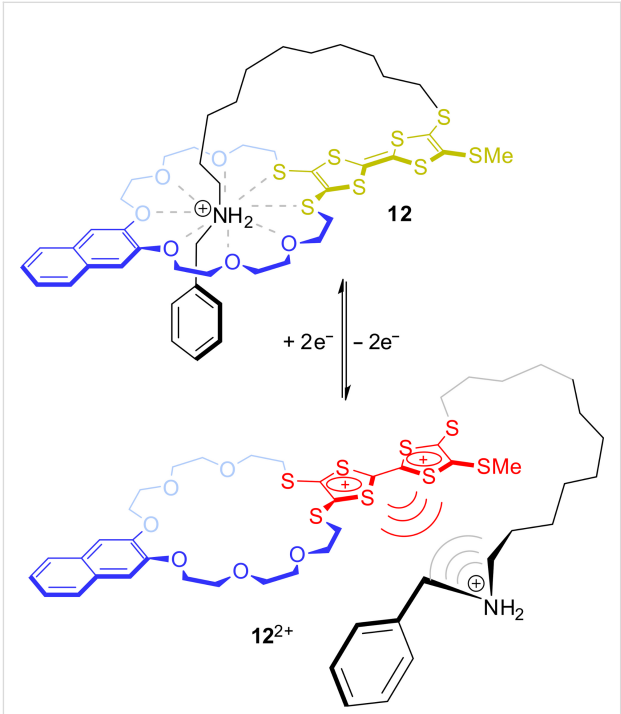

Figure 9: Redox-controlled closing and opening motion of the artificial molecular lasso **12**.

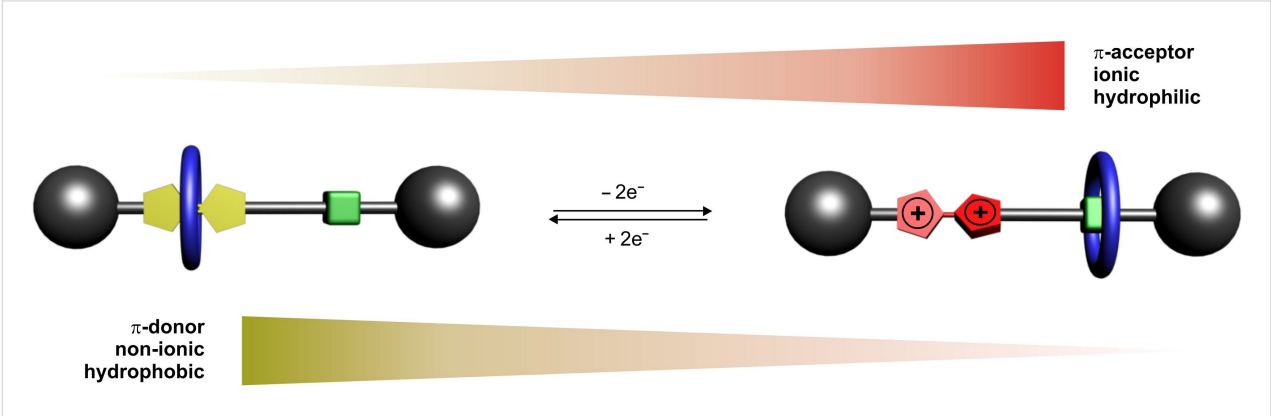

Figure 10: Graphical illustration how a non-degenerate TTF-based shuttle works under electrochemical operation.

the wheel inducing a motion of the wheel towards the now energetically preferred green-colored binding site. Therefore, the most populated and consequently the ground-state co-conformation in the oxidized state is the wheel on the green station. Because of the reversibility of TTF redox reactions, the molecular shuttle can be reversibly switched over many cycles. The work which is generated in the operation of a molecular shuttle is reminiscent of a piston engine used for macroscopic motors. However, one should keep in mind that the transfer of the concepts of macroscopic machines to the molecular level may be limited and may even be misleading. In contrast to macroscopic piston engines, the translation of the wheel in a rotaxane occurs through Brownian motion and the switching processes cause merely a shift of the equilibrium between the two positional isomers of the rotaxane. Thus, a transfer of work on the molecular level that is created by wheel translation into a macroscopic force is quite difficult (but not impossible) to achieve.

Closely after the discovery of the donor–acceptor complex **1**⊂**3**, Stoddart and co-workers reported the synthesis of the first TTF-based rotaxane **13** (Figure 11) [73]. The [2]rotaxane was obtained in 8% yield by a high-pressure clipping procedure in which the wheel **3** was formed around the pre-synthesized axle. In DMSO, the macrocycle is predominantly located on the central TTF moiety. However, in acetone, which has a lower polarity, the wheel moves to one of the dihydroxybenzene residues as indicated by ^{1}H NMR and UV–vis spectroscopy. Since the axle molecule is symmetric, the wheel moves back and forward between the two dihydroxybenzene stations (green) and the rotaxane can be considered as a degenerate shuttle.

Subsequently, the groups of Becher and Stoddart reported on a series of similar, but non-degenerate [2]rotaxanes [74,75]. After several structural optimizations, the bistable rotaxane **14** with a high switching efficiency was reported in 2003 (Figure 12) [76]. In the unswitched state, host **3** is located at the TTF binding site. Chemical oxidation to the dication TTF^{2+} triggers a translational motion of the wheel towards the 1,5-dihydroxynaphthalene station (green) as shown by UV–vis and 2D NMR experiments. Chemical reduction with zinc powder restored the spectroscopic properties of the starting state and back-shuttling of

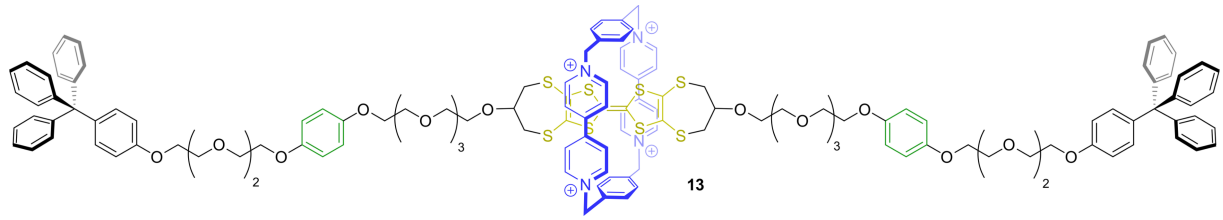

Figure 11: The first TTF-based rotaxane **13**.

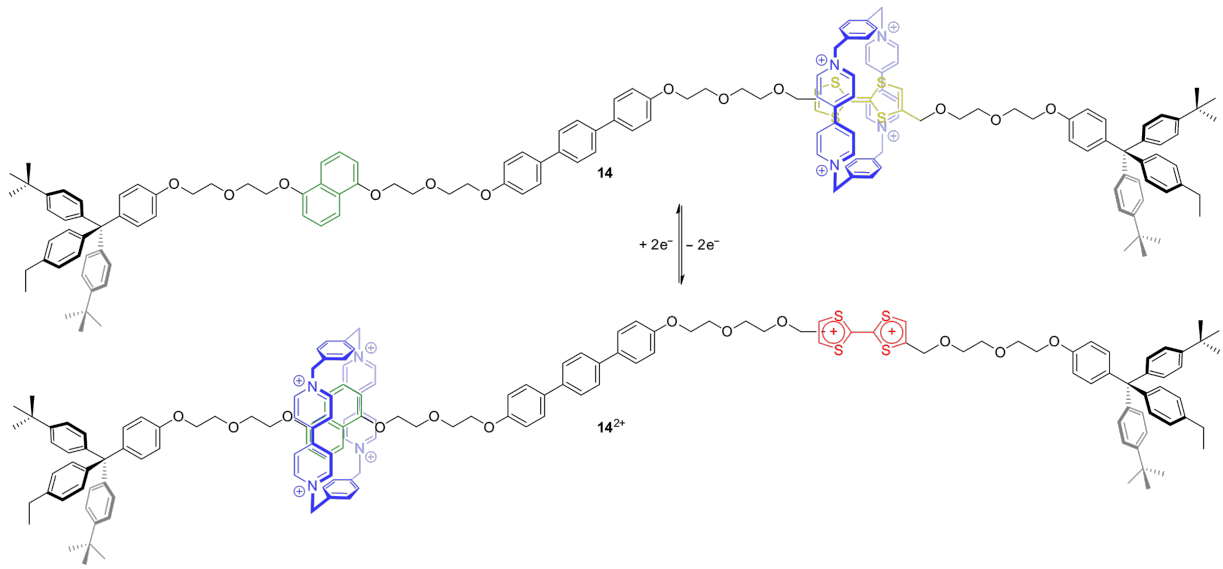

Figure 12: A redox-switchable bistable molecular shuttle **14**.

the wheel to the TTF station occurs. In the TTF^{2+} state, no signals for a free 1,5-dihydroxynaphthalene station were observed which indicates the rotaxane to be completely switched within the detection limit of ^{1}H NMR spectroscopy. The experimental observations and the general switching mechanism of these bistable donor–acceptor rotaxanes were subsequently underpinned by several quantum mechanical studies [77-79].

The concept of TTF-based switchable rotaxanes was also extended to rotaxanes with other macrocycles. In Figure 13, the bistable [2]rotaxane **15** is shown with an α-cyclodextrin (**6**) ring threaded onto a water-soluble axle [80]. The rotaxane was synthesized in 23% yield by a template/capping strategy where one stopper is attached using copper-catalyzed azide–alkyne click chemistry after the formation of the precursor pseudorotaxane. Due to the hydrophobic effect, the neutral TTF is preferred as a station for the wheel over the triazole unit. However, after oxidation, the more hydrophilic dication TTF^{2+} is less favored and the ring moves to the triazole. Both switching states were fully characterized by UV–vis, ^{1}H,^{1}H-NOESY NMR spectroscopy, and cyclic voltammetry. The latter technique revealed an increase of oxidation potential for the first one-electron oxidation, but a second oxidation potential similar to that of the free axle. This indicates that the wheel already moves away from the TTF station upon the first oxidation to the $TTF^{\bullet+}$ radical cation.

Another example for a non-charged TTF-based rotaxane was reported in 2011 (Figure 14) [81]. Very similar to the prior bistable rotaxanes, donor–acceptor interactions dominate the relation of wheel and axle in [2]rotaxane **16**. Here, a π-electron-deficient pyromellitic diimide macrocycle encircles a TTF station (K_a = 6,300 M^{-1}) which is embedded in an axle molecule with two azide residues. The second station, the dihydroxynaphthalene moiety (green), displays a lower association constant of K_a = 5,800 M^{-1}. The pseudorotaxane precursor was end-capped by a double copper-catalyzed azide–alkyne click reaction in CH_2Cl_2 and the rotaxane was isolated in 34% yield. NMR spectroscopy, cyclic voltammetry, and spectroelectrochemistry showed that the wheel translates to the dihydroxynaphthalene station upon TTF oxidation.

The use of TTF in redox-switchable rotaxanes is not limited to the implementation into axle components. Very recently, our group reported on a crown/ammonium rotaxane **17** in which a TTF unit is implemented in the crown-ether wheel (Figure 15) [82]. The rotaxane was synthesized by a catalyst-free nitrile oxide capping strategy in 67% yield. In the neutral state, the wheel is strongly bound to the ammonium station by hydrogen bonds as shown by the high association constant of a structurally similar pseudorotaxane precursor (K_a = 590,000 M^{-1}). The high association constant is a result of the weakly coordinating anion (WCA) used, i.e., tetrakis(3,5-bis(trifluoromethyl)phenyl)borate. Comparison to a structurally similar rotaxane in which the ammonium station is blocked by *N*-acetylation shows that the isoxazole moiety acts as a weak second binding station for the wheel. Oxidation of the TTF unit results in Coulombic repulsion between the wheel and the ammonium station which counteracts the energy of hydrogen bonding. Detailed electrochemical measurements and digital simulations revealed the ring still to be bound to the ammonium station in the $TTF^{\bullet+}$ state. However, after double oxidation a wheel distribution of 1:1 between the ammonium and the isoxazole station was found indicating a dynamic motion between both stations.

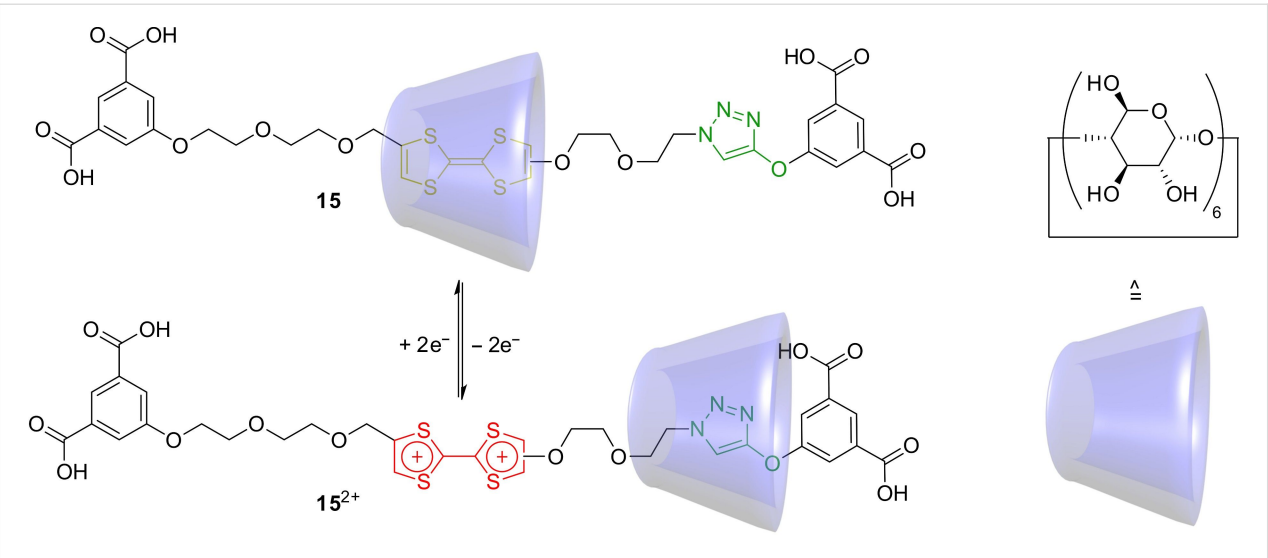

Figure 13: The redox-switchable cyclodextrin-based rotaxane **15**.

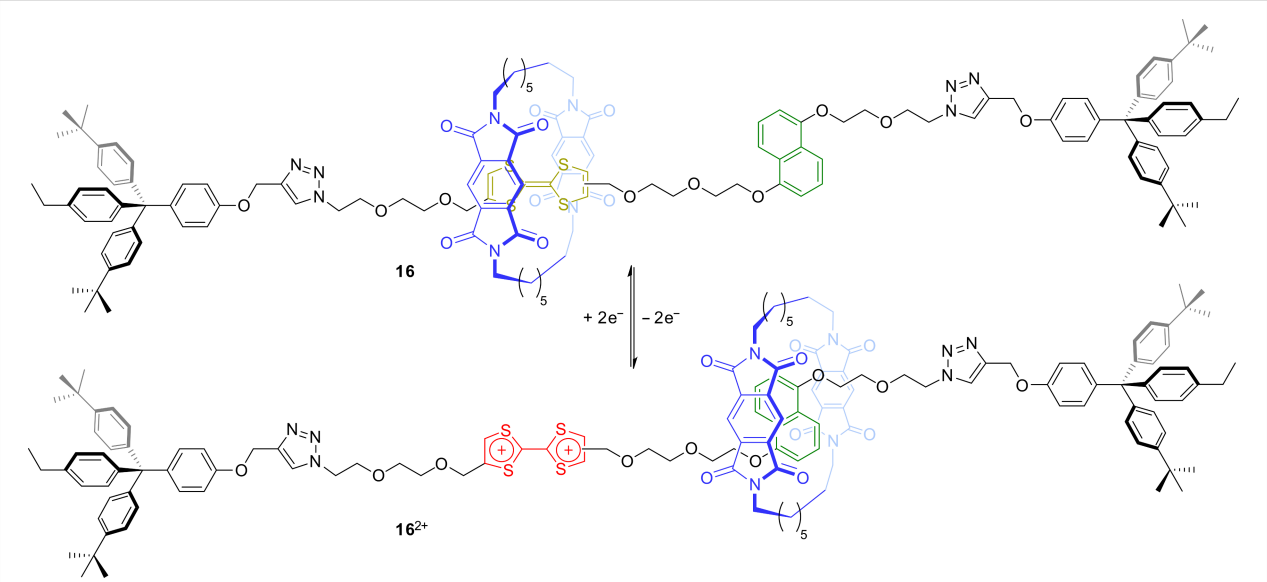

Figure 14: The redox-switchable non-ionic rotaxane **16** with a pyromellitic diimide macrocycle.

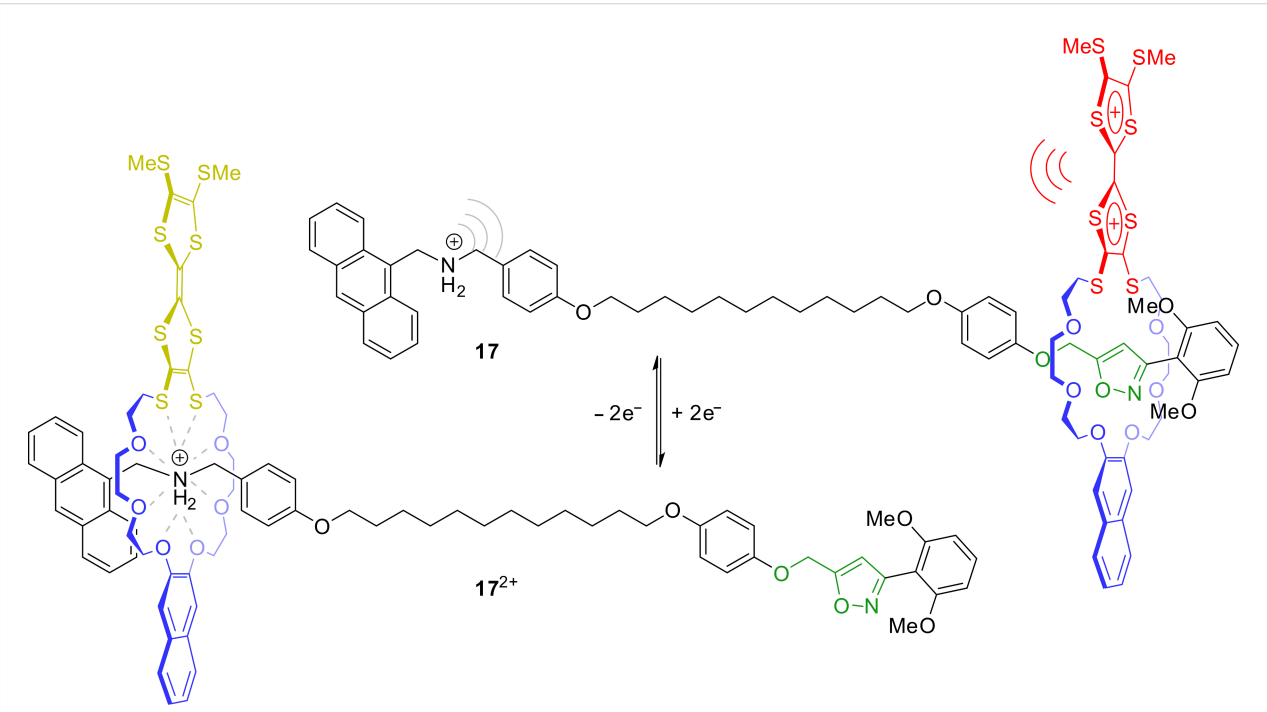

Figure 15: The redox-switchable TTF rotaxane **17** based on a crown/ammonium binding motif.

4.2. Optical devices

The rapid development of redox-switchable MIMs led to considerations to use the unique properties of these molecules for different optoelectronic devices. TTF-based MIMs often display very long-living and stable switching states which are particularly appealing for applications as data storage devices [83] or molecular logic gates [84]. Besides simple molecular electrochromic switches, complex TTF-based MIMs with unique optical properties have been constructed.

In 2012, rotaxane **18** with a structure similar to previously reported donor–acceptor rotaxanes was reported (Figure 16) [85]. However, the axle bears a central azobenzene photoswitch, who's *E*/*Z*-transitions can be controlled by light. The redox-

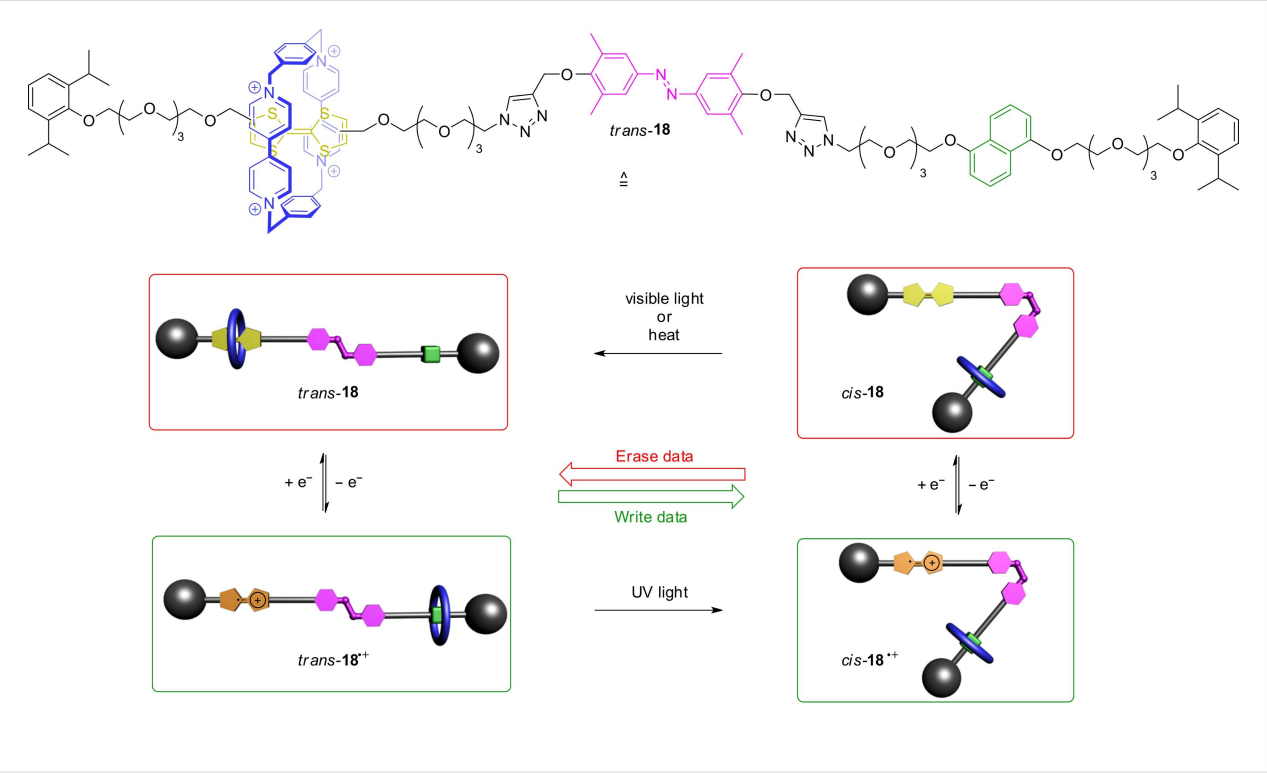

Figure 16: Structure and operation of the electro- and photochemically switchable rotaxane **18** which acts as potential memory device.

switchable shuttle works as previously described and the position of the wheel can be controlled by oxidation or reduction. However, the configuration of the azobenzene strongly influences the life time of each redox-switching state. In the (*E*)-form, the wheel can easily move between the TTF and dihydroxynaphthalene station. In the *Z*-form, this movement is sterically hindered and slowed down. The wheel cannot shuttle to its energetically preferred station. This possibility of orthogonal switching (redox and light) enables an electrochemical "writing" of data which can be subsequently locked by a light stimulus.

The TTF-based doubly interlocked crown/ammonium rotaxane **19** recently reported by us consists of a divalent axle with a π-electron-poor central naphthalene diimide (NDI) unit and a divalent crown-ether wheel with a central TTF unit (Figure 17) [86]. The cofacial donor–acceptor complex whose formation is indicated by a deep green color is forced to stay in a cofacial orientation by mechanical bonding, even when the complex is redox-switched. UV–vis spectroscopy showed the emergent charge-transfer absorption band to display a negative solvochromic effect. Similar to TTF, the NDI unit has three stable oxidation states. However, these are neutral or anionic states and successive reduction of NDI leads to the radical anion and the dianion. Cyclic voltammetry, DFT calculations, and UV–vis spectroscopy confirmed five different redox states (TTF/NDI, $TTF^{\bullet+}$/NDI, TTF^{2+}/NDI, TTF/$NDI^{\bullet-}$, TTF/NDI^{2-}) and shows interesting optical properties in each of these redox states making this type of mechanically constrained donor–acceptor complex very interesting for molecular electronic materials and optoelectronic devices.

4.3. TTF-Based rotaxanes on solid support

If one aims at creating macroscopic effects, the concerted action of many molecular machines is needed. It is then useful to deposit switchable AMMs on interfaces such as a surface of a solid support [87-89]. An ordered array of molecules enables the possibility of concerted switching. The fixed orientation on a surface allows studying molecules with sophisticated techniques such as scanning tunneling microscopy. Furthermore, redox-switchable AMMs, containing for example TTF moieties, can be electrically operated without the need of chemical additives, if conducting solid supports are used. This also opens pathways towards the integration of switchable AMMs into the world of silicon-based chips and electronic circuits.

A landmark in the field of molecular-scale electronic devices is the rotaxane-based 160-kilobit memory which was reported by the groups of Stoddart and Heath in 2007 (Figure 18) [90]. The key idea of this memory is that the switching modes in a bistable rotaxane **20** can be considered as the "1" and "0" states of a binary digit. If the rotaxane shows a hysteretic cur-

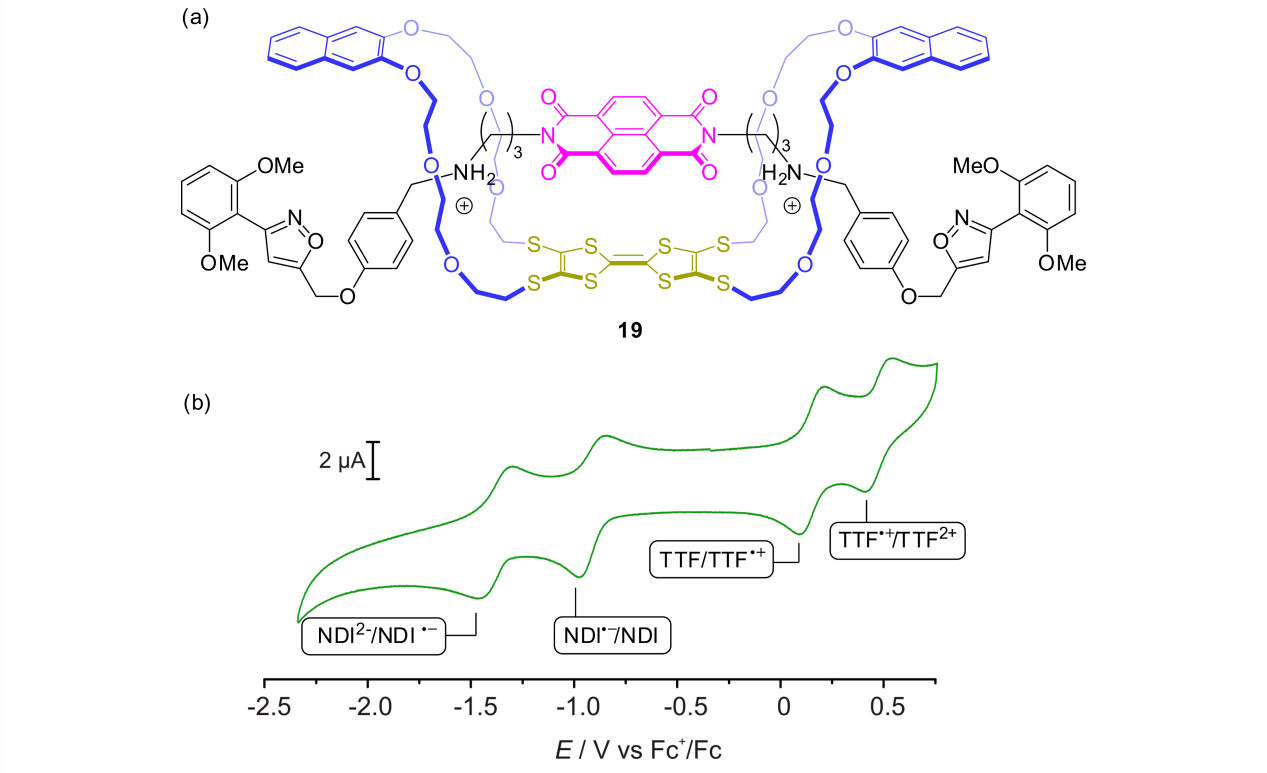

Figure 17: (a) The redox-switchable rotaxane **19** with a donor–acceptor pair which is stable in five different switching states. (b) Cyclic voltammogram showing the transitions between the five oxidation states of **19**.

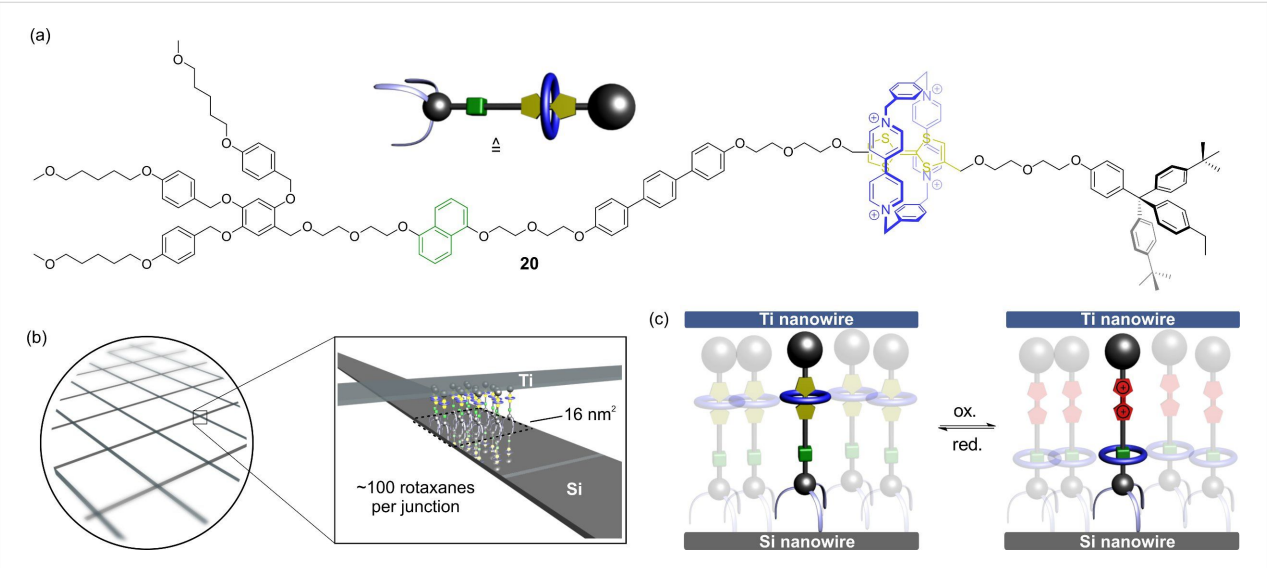

Figure 18: Schematic representation of a molecular electronic memory based on a bistable TTF-based rotaxane. (a) Molecular structure of the amphiphilic [2]rotaxane **20**. (b) Structure of the crossbar device. (c) Switching mechanism of rotaxane **20** in a junction.

rent–voltage curve, a voltage-induced reading and writing of information becomes possible. Although the initial concept of this type of device was developed a few years earlier [91], the optimization of its structure and fabrication was necessary to reach high-level performance [92-94].

The device is based on a crossbar architecture in which a monolayer of amphiphilic rotaxanes is sandwiched by a bottom Si nanowire electrode and a top Ti nanowire electrode. Both layers of nanowires are orthogonal to each other. This produces several crossing points or “junctions” whose areas are defined

by the diameter of the nanowires. In the present example, a very small diameter gives a junction area of only 16 nm^2 which corresponds to approximately 100 rotaxanes per junction. When a high pulse voltage is applied (±1.5 V), the junctions can be switched back and forward between the two switching states of the rotaxane. The written information is then read out by a non-perturbing lower voltage. It turned out that the terphenyl spacer which is implemented into the rotaxane axle is crucial to increase the half-life of the metastable switching state. However, a disadvantage of this particular device was a high fraction of "defect" junctions. Only ≈25% showed a sufficient on/off ratio for a memory device. Furthermore, only a limited number of switching cycles was possible before the junctions were damaged. However, a remarkably high storage density of 10^{11} bits cm^{-1} was reached.

Writing of data with the aid of dendrimer-decorated TTF-rotaxanes was achieved by Gao and co-workers [95]. They deposited a thin-film of bistable donor–acceptor rotaxanes on an indium tin oxide (ITO)-coated substrate. A clean electrochemical switching on the substrate was observed with current–voltage curves showing a clear memory effect. The written data could be read out even after waiting for 12 h.

Besides data storage, a substantial challenge of AMMs is the transfer of molecular motion into a useful macroscopic output. An example of rotaxanes on a solid support which could achieve this is shown in Figure 19 [96]. The [3]rotaxane **21** consists of a symmetric axle molecule in which both axle halves bear a TTF and a hydroxynaphthalene station. In the unswitched state, each TTF station is encircled by a wheel. Oxidation of the TTF units then induces shuttling motions towards the inner hydroxynaphthalene stations, which significantly reduces the wheel–wheel distance. If both wheels are attached to a surface with a suitable anchor, the shuttle motion can be seen as a type of muscle-like contraction generating tensile stress on the sur-

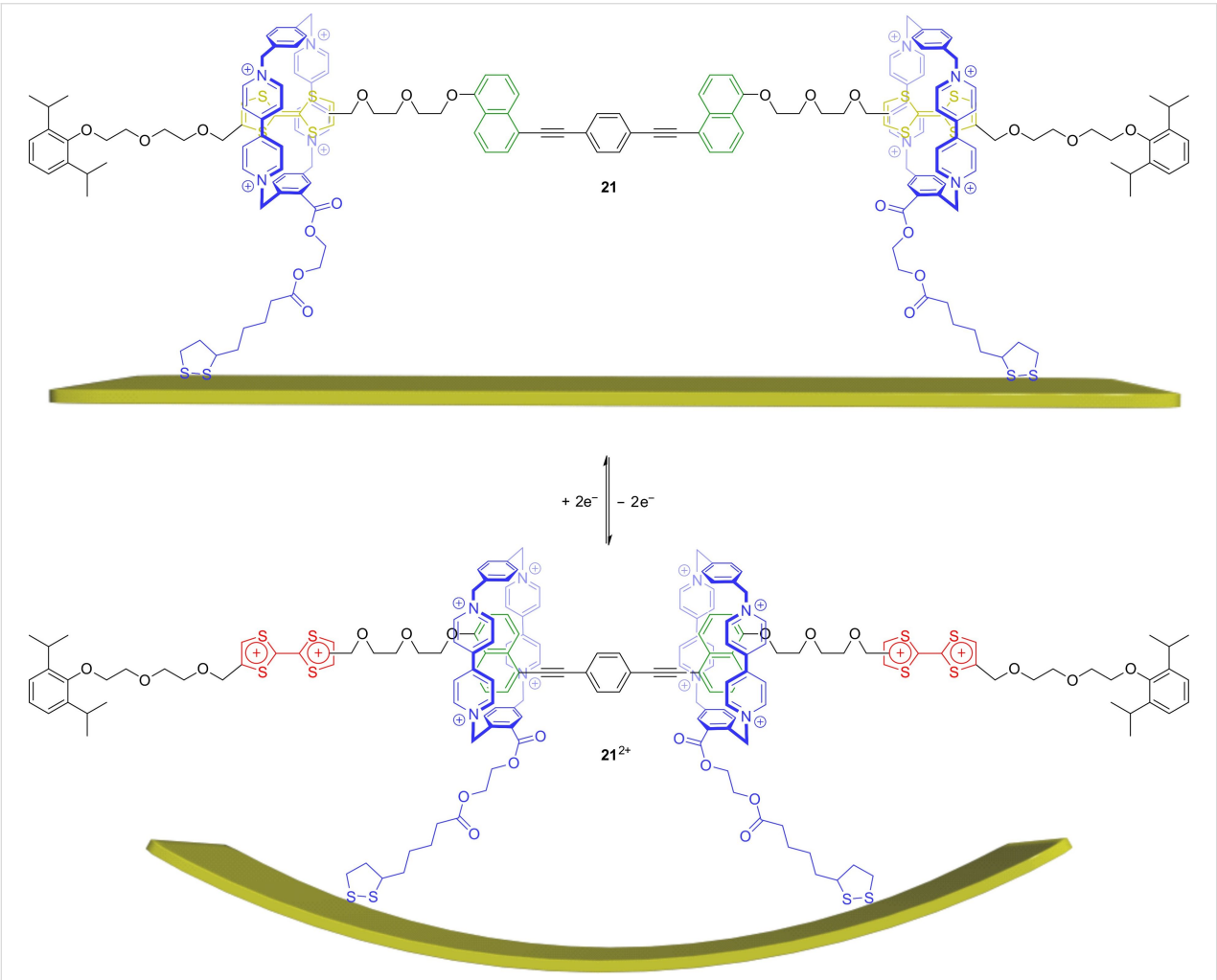

Figure 19: Schematic representation of bending motion of a microcantilever beam with gold surface induced by operation of the redox-switchable [3]rotaxane **21** attached to its surface.

face. Although the force of one contracting rotaxane is quite small, a sufficient number of these "molecular muscles" can accumulate their force and consequently deform a material by concerted switching.

In rotaxane **21**, the two macrocycles are attached by disulfide anchors to the gold surface of microcantilever beams (500 × 100 × 1 µm) and form a self-assembled monolayer. Chemical oxidation leads to a bending and to an upward motion of the beams by ≈35 nm. The addition of ascorbic acid as reductant restores the initial position and the switching cycle can be repeated. To exclude other triggers than the rotaxane contraction, several control experiments were performed. Furthermore, a structurally similar but mechanically inert control compound was synthesized which cannot induce the bending effect.

4.4. TTF Pairing interactions in rotaxanes

Although TTF is widely used in switchable molecular shuttles, rotaxanes with TTF–dimer interactions are rare. One example was published by Stoddart and co-workers in 2008 (Figure 20) [97]. The tripodal [4]rotaxane **22**, consisting of a trivalent axle, in which each arm is encircled by a host molecule **3**, was synthesized by a copper-catalyzed click protocol in 40% yield. A combination of electrochemical and spectroscopic methods was used to investigate a potential TTF-dimer formation. As comparison, they characterized also the trivalent dumbbell precur-

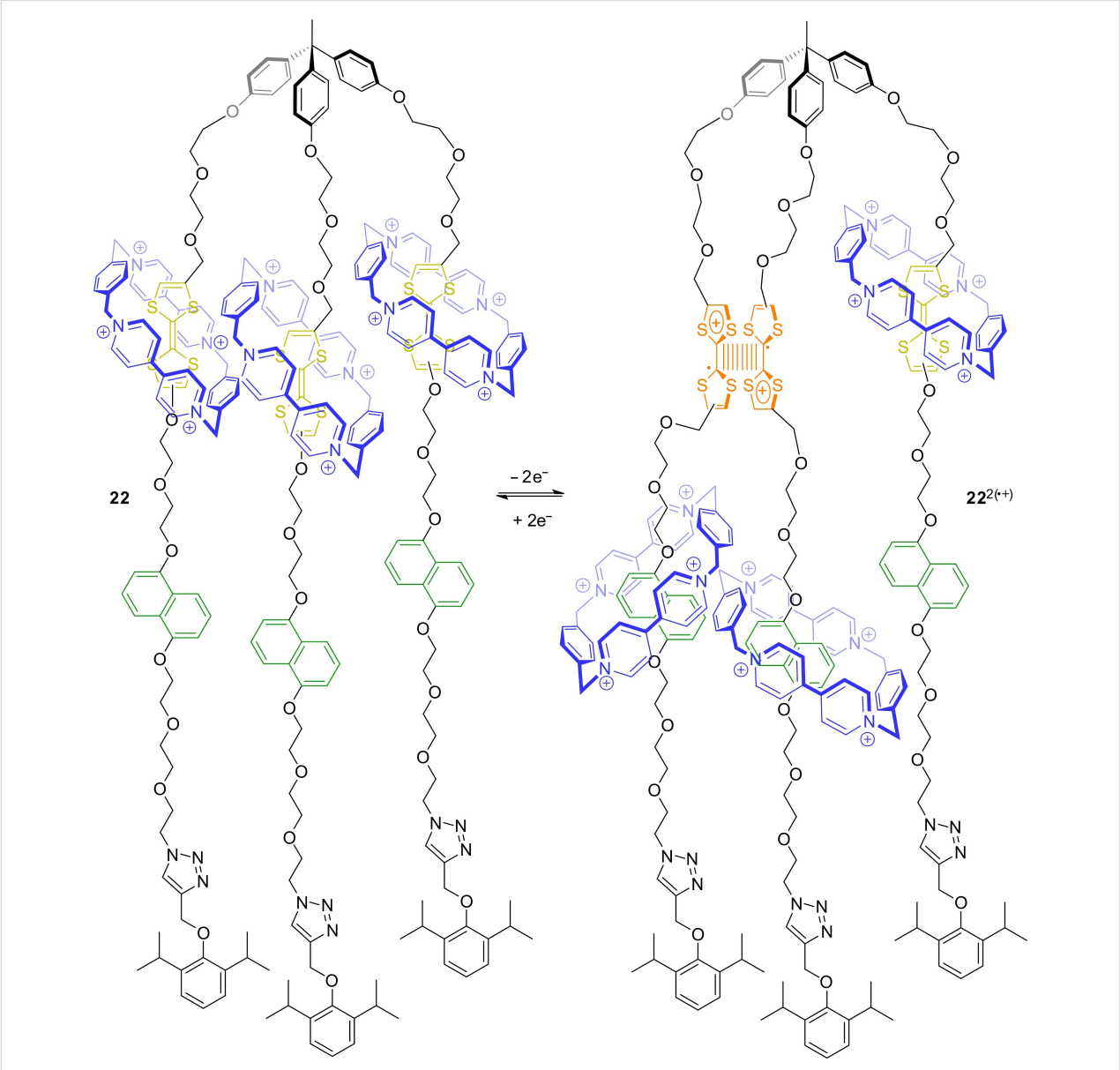

Figure 20: TTF-dimer interactions in a redox-switchable tripodal [4]rotaxane **22**.

sor without wheels. It was shown that mixed-valence interactions $(TTF_2)^{\bullet+}$ and radical-cation interactions $(TTF^{\bullet+})_2$ are present during the successive oxidation of the free axle. However, only the radical-cation dimer interaction was observed in the case of [4]rotaxane **22**. This discrepancy can be explained by a simple energy balance. For a mixed-valence interaction, at least two TTF/$TTF^{\bullet+}$ units need to be free. Thus, after one-electron oxidation which liberates one $TTF^{\bullet+}$ from the cavity of **3**, still the energy of one donor–acceptor complex has to be overcome to enable a mixed-valence interaction. This is not the case for the free trivalent axle. After double oxidation, two $TTF^{\bullet+}$ stations are free and a radical-cation interaction is favored. This example nicely shows that all energy contributions in each switching state of a system as a whole need to be considered for the design and operation of an AMM.

In addition to the variety of TTF-based rotaxane shuttles, we recently reported a [3]rotaxane in which the pirouetting motion of wheels can be controlled by electrochemical switching [98]. Figure 21 shows the [3]rotaxane **23** which bears two cofacially oriented TTF crown ethers on a divalent ammonium axle. The distance between the wheels is convenient for TTF-dimer interactions. In the non-switched neutral state of both TTFs, the wheels adopt a *syn* co-conformation caused by weak non-covalent interactions between the wheels. One-electron oxidation yielding $\mathbf{23}^{\bullet+}$ enables mixed-valence interactions $(TTF_2)^{\bullet+}$ between the cofacial TTF units. This TTF-dimer interaction "clutches" the two wheels and synchronizes their pirouetting motions around the axle. Also the next stable oxidation state ($\mathbf{23}^{2(\bullet+)}$) shows attractive wheel–wheel interactions in form of a TTF radical-cation dimerization $(TTF^{\bullet+})_2$. However, further oxidation leads to the fully oxidized $\mathbf{23}^{4+}$ in which both TTF^{2+} units repeal each other. The Coulombic repulsion "declutches" the two wheels and they adopt an *anti* co-conformation. As shown by experiments and quantum chemical calculations, the wheels cannot be fully disengaged; however, the wheel–wheel interactions strongly differ for the different oxidation states. The controlled clutching and declutching of **23** by electrochemical stimuli is reminiscent of the operation of a macroscopic friction clutch, a common technical device used in motor vehicles. Furthermore, rotaxane **23** can be used as novel supramolecular gearing system for the transmission of rotational motion at the molecular level.

5. Rotacatenanes

In 2011, the group of Stoddart described the fusion of a rotaxane and a catenane, a so-called "rotacatenane" (Figure 22) [99]. The rotacatenane **24** consists of their previously used rotaxane framework except that the enlarged cyclophane cyclobis(paraquat-4,4′-biphenylene) is used as wheel component. The cavity of this macrocycle is large enough to host two planar molecules in a cofacial arrangement. Starting from the pre-assembled catenane, the axle molecule is threaded through the wheel and end-capped by a copper-catalyzed click reaction.

A variety of different spectroscopic and electrochemical methods was applied to reveal the switching behavior of **24** and its stable co-conformations in each switching state. In the

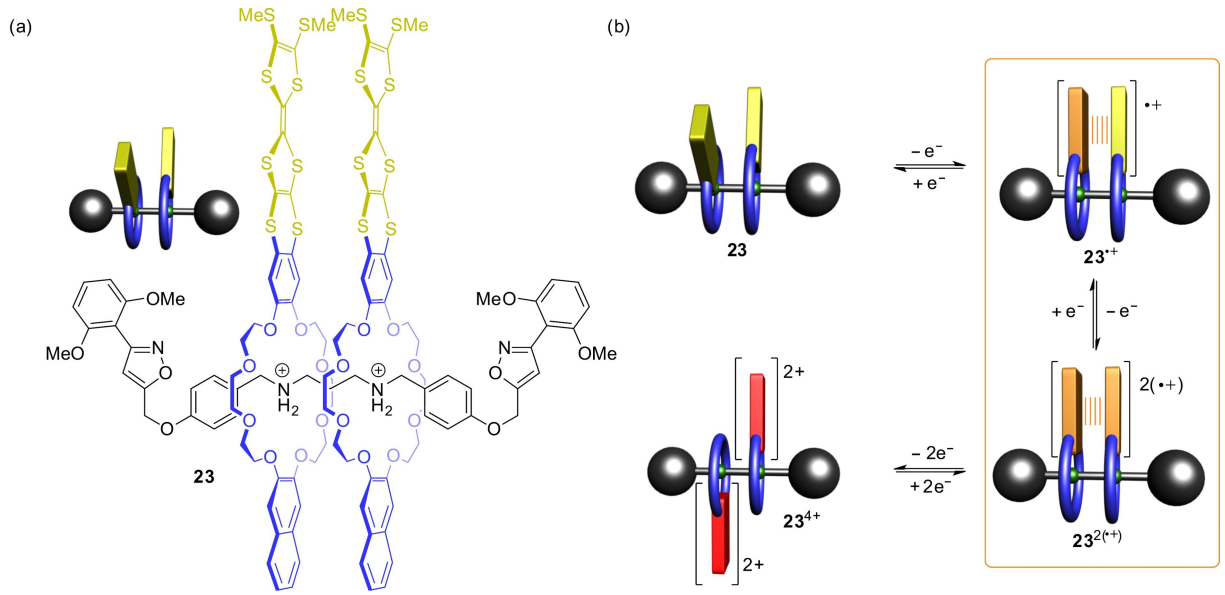

Figure 21: (a) A molecular friction clutch **23** which can be operated by electrochemical stimuli. (b) Schematic representation of **23** in its four stable oxidation states with corresponding wheel co-conformations.

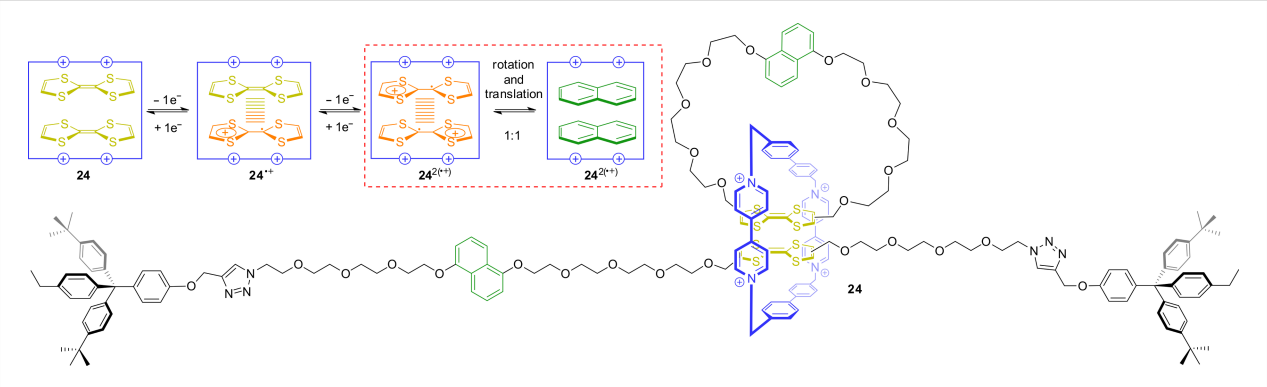

Figure 22: Fusion between rotaxane and catenane: a [3]rotacatenane **24** which can stabilize TTF dimers.

unswitched state, both TTF units are stacked in the cavity of the wheel. One-electron oxidation to $\mathbf{24}^{\bullet+}$ creates a stabilized mixed-valence interaction between these units as evidenced by an emergent NIR band. Further oxidation, converts the two TTF units into a radical-cation dimer $(TTF^{\bullet+})_2$. However, the Coulombic repulsion in this six-fold charged complex destabilizes the radical-cation dimer and the system converts into a second stable co-conformation in which both dihydroxynaphthalene units are inside the cavity of the wheel. To achieve this conformer, two types of motion, a circumrotation and a translational motion, must occur. The equilibrium between these two co-conformations of $\mathbf{24}^{2(\bullet+)}$ was determined to be approximately 1:1. Further oxidation drives the equilibrium completely to the side of the co-conformation in which both dihydroxynaphthalene units are encircled. This TTF-based system is an intriguing example of synergetic molecular motions triggered by redox stimuli.

6. Catenanes

Catenanes consist of at least two intertwined macrocycles which are mechanically interlocked. The structure cannot be opened without breaking a covalent bond. In contrast to rotaxanes in which the wheel is only held on the axle component by steric hindrance of stopper groups, a catenane is a truly topologically interlocked species bearing a mechanical bond. However, the construction, chemical behavior, and operation of structurally related rotaxanes and catenanes are often very similar. The motion which can be controlled by external stimuli is the rotation (or circumrotation) of the wheels relative to each other.

The first TTF-based catenane **25** was described by the groups of Becher and Sauvage in 1994 (Figure 23) [100]. Starting from a phenanthroline macrocycle bearing a TTF unit, a copper(I)-template was used to obtain the TTF-based catenane **25** in 14% yield, which was previously developed by Sauvage [101]. The authors aimed for a further development of this construction motif towards donor–acceptor rotaxanes with efficient charge separation leading to a broad variety of topologically complex TTF catenanes and cage compounds [52,74,102-104].

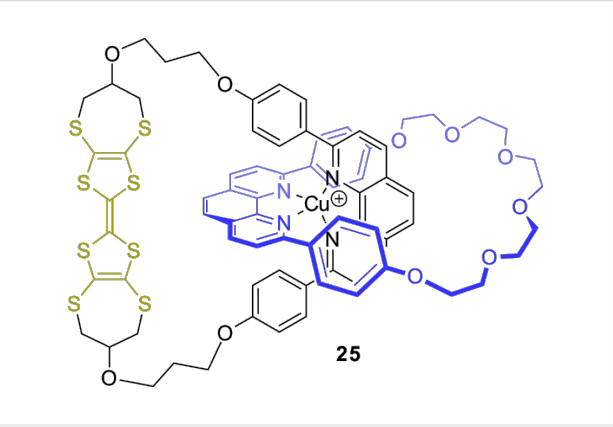

Figure 23: The first TTF-based catenane **25**.

6.1. Stimuli-responsive circumrotation

The TTF-based catenane **26** allows implementing a stimuli-responsive circumrotation motion (Figure 24) [105]. Similar to the corresponding donor–acceptor rotaxanes, the macrocycle preferentially encircles the TTF unit instead of the dihydroxynaphthalene station in the unswitched state. As shown by ^{1}H NMR and UV–vis spectroscopy as well as cyclic voltammetry, chemical oxidation to the TTF^{2+} dication triggers an expulsion of the former station and the wheel moves to the alternative dihydroxynaphthalene station. Chemical reduction with ascorbic acid or $Na_2S_2O_5$ restores the initial spectroscopic properties and the initial co-conformation of the catenane.

A tristable molecular switch based on a [2]catenane with three different stations was created by Wasielewski, Stoddart, and co-workers in 2015 (Figure 25) [106]. The catenane **27** is made of a macrocycle with a TTF, a 4,4′-bipyridinium and a dihydroxynaphthalene recognition site which is encircled by a cyclobis(paraquat-*p*-phenylene) wheel. In the resting state, the

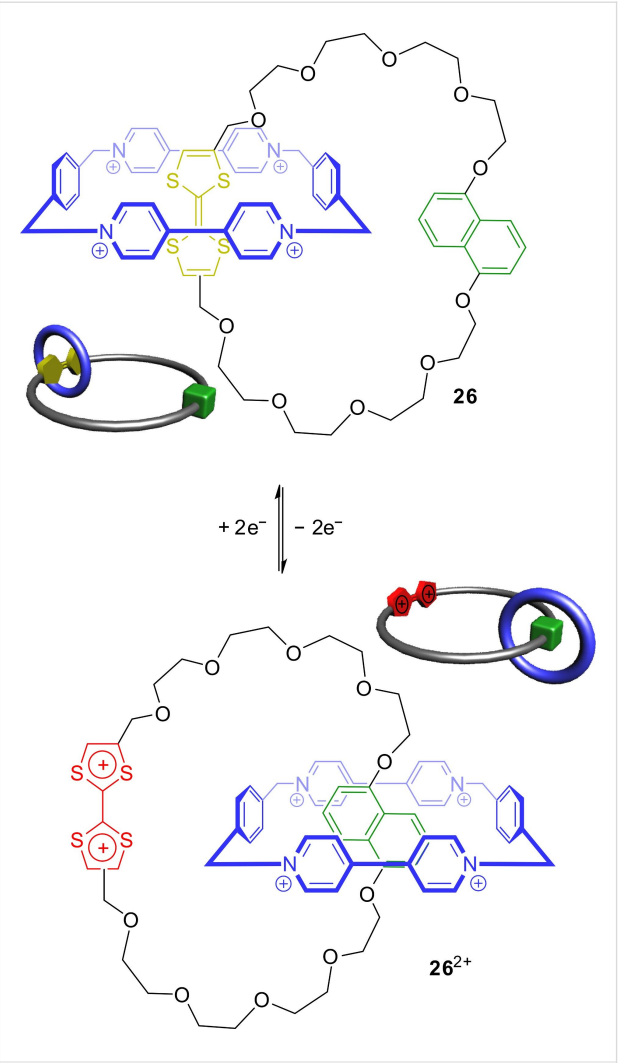

Figure 24: Electrochemically controlled circumrotation of the bistable catenane **26**.

wheel is located at the TTF unit forming a donor–acceptor complex with a green color. Oxidation moves the ring to the second π-electron-rich station, the dihydroxynaphtalene. This donor–acceptor complex has a reddish color. However, in contrast to other bistable catenanes, the third 4,4′-bipyridinium station is also redox-active. Reduction of the system leads to a 4,4′-bipyridinium radical cation which forms a purple trisradical complex with the doubly reduced cyclobis(paraquat-*p*-phenylene). Electrochemical and several spectroscopic techniques showed that, overall, six stable oxidation states – each of them with a unique color – and three co-conformations are accessible in this single compound.

6.2. Switchable catenanes in ordered arrays

Besides ordered arrays on surfaces, on nanoparticles or in Langmuir–Blodgett films, a possibility to arrange bistable catenanes in an ordered fashion is to incorporate them into the rigid scaffold of a metal-organic framework (MOF) [107]. An advantage of this strategy is that the relatively labile organic switches are protected from degradation in this solid material. In 2016, the groups of Hupp, Farha, and Stoddart reported on a bistable donor–acceptor catenane **28** which is inserted in the Zr-based MOF **NU-1000** (Figure 26) [108]. The MOF **NU-1000** consists of Zr_6 nodes which are bridged by 1,3,6,8-tetrakis(*p*-carboxyphenyl)pyrene ligands [109]. Four hydroxy groups of each metal cluster are pointing into the mesoporous channels of the MOF and can be post-functionalized. Similar to a previous report about rotaxanes implemented into a MOF [110], the catenane was attached to the MOF framework by a so-called solvent-assisted ligand incorporation protocol. A degree of incorporation of ≈0.65 catenanes per Zr_6 node could be achieved as shown by ^{1}H NMR and coupled plasma atomic emission spectroscopy. This degree of functionalization results in a density of

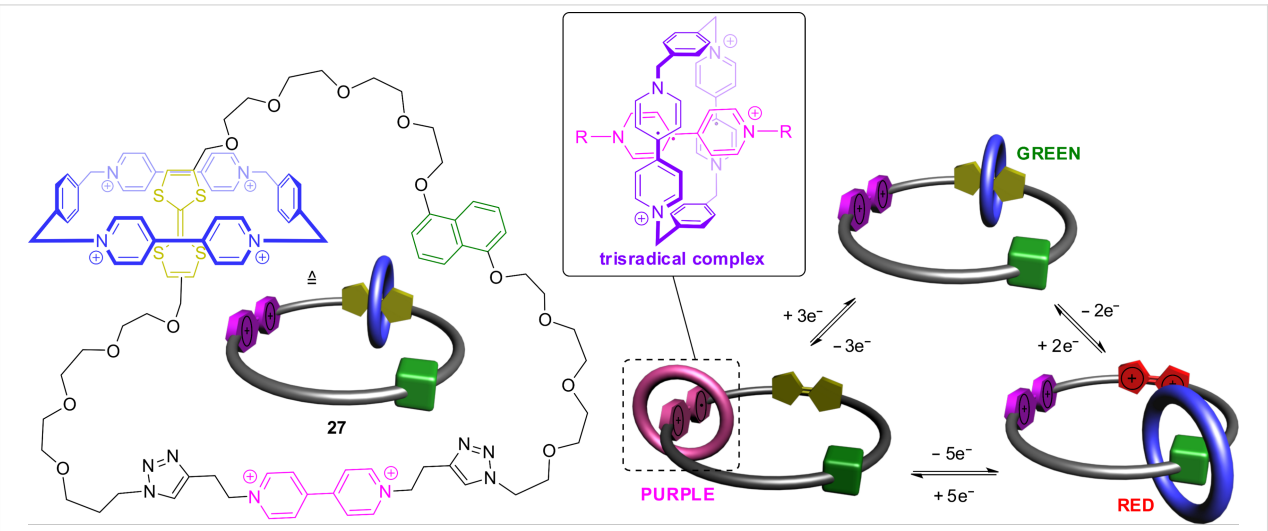

Figure 25: A tristable switch based on the redox-active [2]catenane **27** with three different stations.

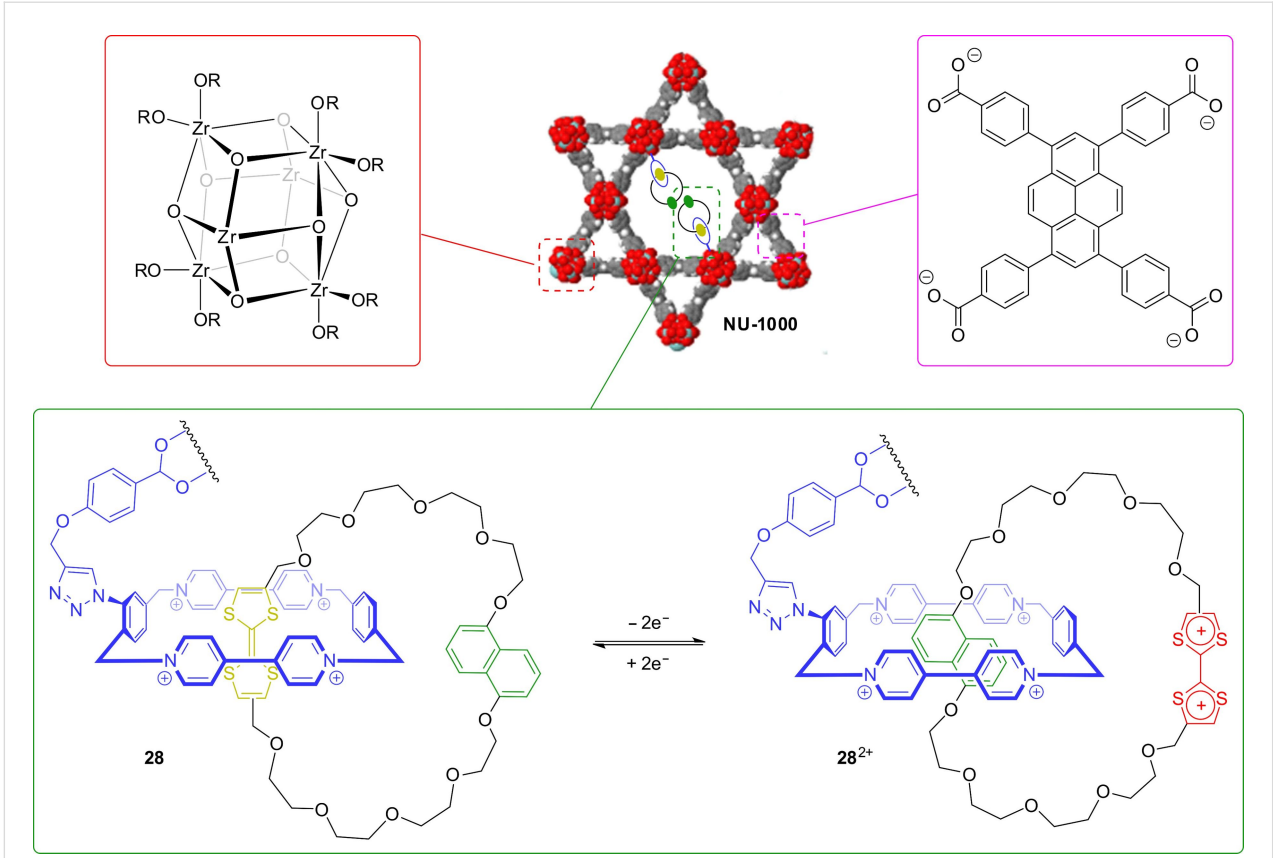

Figure 26: Structure of catenane-functionalized MOF **NU-1000** [108] with structural representation of subcomponents. The TTF-based catenane **28** can be reversibly switched inside the MOF.

ordered catenanes of 8.8×10^{19} units cm^{-3} in the MOF. Cyclic voltammetry in combination with chemical oxidation/reduction and powder-UV–vis–NIR spectroscopy showed the catenane to be reversibly switched inside the MOF.

6.3. TTF Dimer interactions in catenanes

Catenanes are ideally suited structures to enable the formation of TTF dimers, which need a confined molecular space to be stable at room temperature in solution. In 2010, the groups of Cooke and Stoddart described two [3]catenanes consisting of a cyclobis(paraquat-4,4′-biphenylene) and two TTF-based macrocycles (Figure 27a) [111]. Crystal structures of catenanes **29** and **30** showed that both TTF units are in the cavity of the central ring in the unswitched state. During the stepwise oxidation, both catenanes display characteristic spectroscopic features for stable mixed-valence $(TTF_2)^{\bullet+}$ and radical-cation $(TTF^{\bullet+})_2$ dimers. The authors call the stabilizing environment of a [3]catenane a "molecular flask". However, whereas catenane **29** is directly oxidized from its radical-cation-dimer state (**29**$^{2(\bullet+)}$) to the fully oxidized **29**$^{4+}$ state, the alkyne-based catenane shows a metastable disproportionation equilibrium between the **30**$^{3+}$ state and the **30**$^{2(\bullet+)}$/**30**$^{4+}$ states. The authors explain the discrepancy by the additional binding energy of the dihydroxynaphthalene stations in **29**$^{4+}$ to the cyclobis(paraquat-4,4′-biphenylene) wheel. Therefore, the Coulomb repulsion and the subsequent expulsion of the TTF^{2+} units from the cavity of the central ring lead to a circumrotation of both outer wheels to a co-conformation in which the second binding stations are located in the cavity of the inner wheel.

In a series of similar self-assembled catenanes with a central metallo-supramolecular wheel (catenane **31** is shown exemplarily in Figure 27b), donor–acceptor interactions and hydrogen bonding generate a neutral TTF dimer that is surrounded by cofacially oriented bipyridinium units [112]. The intertwined structure is locked by formation of platinum(II)–pyridine coordination bonds. Interestingly, the doubly interlocked catenane features the topologic structure of a so-called Solomon link. It was shown that the oxidation of the Solomon link to the **31**$^{\bullet+}$ state creates a stabilized mixed-valence dimer $(TTF_2)^{\bullet+}$. However, in comparison to the structurally similar catenanes in this report, the radical-cation-dimer state $(TTF^{\bullet+})_2$ was only transiently stable. The authors suggest an effect of the constrained structural environment of the TTF units, which rationalizes the

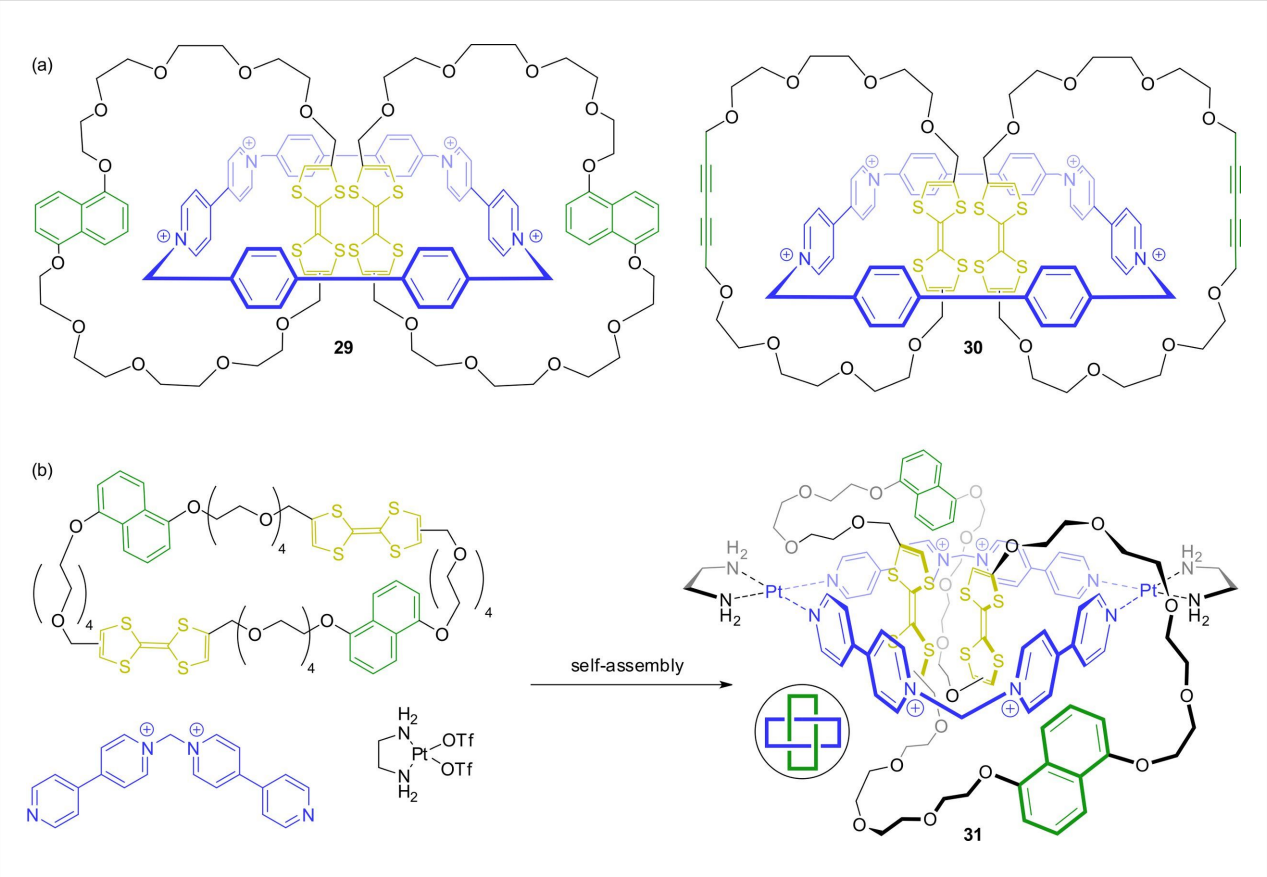

Figure 27: (a) [3]Catenanes **29** and **30** which can stabilize mixed-valence or radical-cation dimers of TTF. (b) Self-assembly synthesis of the molecular Solomon link **31** incorporating two TTF units.

reduced stability of the radical-cation dimer. Thus, also topological effects have to be considered for TTF dimer formation in redox-switchable MIMs.

Conclusion

The organosulfur compound TTF developed from a molecular switch with multiple electronic and material applications to one of the most widely used building blocks for the construction of stimuli-responsive MIMs and functional molecular devices. The development of straightforward organic reactions to implement TTFs in rotaxane or catenane structures lead to a variety of different construction motifs. Its high stability in three different oxidation states and the change of multiple properties during these successive oxidations are ideally suited to drive molecular motions in MIMs. Additionally, the optoelectronic and magnetic properties of TTF make it very easy to follow the stimuli-induced motion and the conformational changes accompanying it. TTF dimer interactions are relatively new yet offer an outstanding additional possibility to control molecular motion. In future, the already somewhat explored pathway to ordered arrays of TTF-based AMMs on surfaces or in (Sur)MOFs will enable macroscopic effects caused by concerted electrochemical switching. Furthermore, the disadvantage of degradation of these organic molecules can be potentially overcome by incorporation into more robust materials. The initial dream that AMMs can be used one day to perform different tasks on the molecular level becomes slowly but steadily true. TTF and its derivatives will continue to contribute to this process.

Acknowledgements

We thank the Deutsche Forschungsgemeinschaft (CRC 765) for funding.

ORCID® iDs

Hendrik V. Schröder - https://orcid.org/0000-0002-6126-0055
Christoph A. Schalley - https://orcid.org/0000-0002-8634-3578

References

1. Boyer, P. D. *Annu. Rev. Biochem.* **1997,** *66,* 717–749. doi:10.1146/annurev.biochem.66.1.717
2. Kinbara, K.; Aida, T. *Chem. Rev.* **2005,** *105,* 1377–1400. doi:10.1021/cr030071r
3. Hirokawa, N.; Noda, Y.; Tanaka, Y.; Niwa, S. *Nat. Rev. Mol. Cell Biol.* **2009,** *10,* 682–696. doi:10.1038/nrm2774

4. Balzani, V.; Credi, A.; Raymo, F. M.; Stoddart, J. F. *Angew. Chem., Int. Ed.* **2000,** *39,* 3348–3391. doi:10.1002/1521-3773(20001002)39:19<3348::AID-ANIE3348>3.0.CO;2-X
5. Coskun, A.; Banaszak, M.; Astumian, R. D.; Stoddart, J. F.; Grzybowski, B. A. *Chem. Soc. Rev.* **2012,** *41,* 19–30. doi:10.1039/C1CS15262A
6. Erbas-Cakmak, S.; Leigh, D. A.; McTernan, C. T.; Nussbaumer, A. L. *Chem. Rev.* **2015,** *115,* 10081–10206. doi:10.1021/acs.chemrev.5b00146
7. Sauvage, J.-P. *Angew. Chem., Int. Ed.* **2017,** *56,* 11080–11093. doi:10.1002/anie.201702992
8. Stoddart, J. F. *Angew. Chem., Int. Ed.* **2017,** *56,* 11094–11125. doi:10.1002/anie.201703216
9. Feringa, B. L. *Angew. Chem., Int. Ed.* **2017,** *56,* 11060–11078. doi:10.1002/anie.201702979
10. Xue, M.; Yang, Y.; Chi, X.; Yan, X.; Huang, F. *Chem. Rev.* **2015,** *115,* 7398–7501. doi:10.1021/cr5005869
11. Gil-Ramírez, G.; Leigh, D. A.; Stephens, A. J. *Angew. Chem., Int. Ed.* **2015,** *54,* 6110–6150. doi:10.1002/anie.201411619
12. Feringa, B. L. *Acc. Chem. Res.* **2001,** *34,* 504–513. doi:10.1021/ar0001721
13. Kassem, S.; van Leeuwen, T.; Lubbe, A. S.; Wilson, M. R.; Feringa, B. L.; Leigh, D. A. *Chem. Soc. Rev.* **2017,** *46,* 2592–2621. doi:10.1039/C7CS00245A
14. Ballardini, R.; Balzani, V.; Credi, A.; Gandolfi, M. T.; Venturi, M. *Acc. Chem. Res.* **2001,** *34,* 445–455. doi:10.1021/ar000170g
15. Jørgensen, T.; Hansen, T. K.; Becher, J. *Chem. Soc. Rev.* **1994,** *23,* 41–51. doi:10.1039/CS9942300041
16. Simonsen, K. B.; Becher, J. *Synlett* **1997,** 1211–1220. doi:10.1055/s-1997-1001
17. Nielsen, M. B.; Becher, J. *Liebigs Ann./Recl.* **1997,** 2177–2187. doi:10.1002/jlac.199719971103
18. Nielsen, M. B.; Lomholt, C.; Becher, J. *Chem. Soc. Rev.* **2000,** *29,* 153–164. doi:10.1039/a803992e
19. Bryce, M. R. *J. Mater. Chem.* **2000,** *10,* 589–598. doi:10.1039/a908385e
20. Canevet, D.; Sallé, M.; Zhang, G.; Zhang, D.; Zhu, D. *Chem. Commun.* **2009,** 2245–2269. doi:10.1039/b818607n
21. Jana, A.; Ishida, M.; Park, J. S.; Bähring, S.; Jeppesen, J. O.; Sessler, J. L. *Chem. Rev.* **2017,** *117,* 2641–2710. doi:10.1021/acs.chemrev.6b00375
22. Deuchert, K.; Hünig, S. *Angew. Chem., Int. Ed. Engl.* **1978,** *17,* 875–886. doi:10.1002/anie.197808753
23. Wudl, F.; Smith, G. M.; Hufnagel, E. J. *J. Chem. Soc. D* **1970,** 1453–1454. doi:10.1039/c29700001453
24. Devonport, W.; Blower, M. A.; Bryce, M. R.; Goldenberg, L. M. *J. Org. Chem.* **1997,** *62,* 885–887. doi:10.1021/jo960951o
25. Scott, B. A.; La Placa, S. J.; Torrance, J. B.; Silverman, B. D.; Welber, B. *J. Am. Chem. Soc.* **1977,** *99,* 6631–6639. doi:10.1021/ja00462a026
26. Ashton, P. R.; Balzani, V.; Becher, J.; Credi, A.; Fyfe, M. C. T.; Mattersteig, G.; Menzer, S.; Nielsen, M. B.; Raymo, F. M.; Stoddart, J. F.; Venturi, M.; Williams, D. J. *J. Am. Chem. Soc.* **1999,** *121,* 3951–3957. doi:10.1021/ja984341c
27. Bryce, M. R. *Adv. Mater.* **1999,** *11,* 11–23. doi:10.1002/(SICI)1521-4095(199901)11:1<11::AID-ADMA11>3.0.CO;2-3
28. Das, A.; Ghosh, S. *Angew. Chem., Int. Ed.* **2014,** *53,* 2038–2054. doi:10.1002/anie.201307756
29. Griffiths, K. E.; Stoddart, J. F. *Pure Appl. Chem.* **2008,** *80,* 485–506. doi:10.1351/pac200880030485
30. Andréasson, J.; Pischel, U. *Chem. Soc. Rev.* **2010,** *39,* 174–188. doi:10.1039/B820280J
31. Spanggaard, H.; Prehn, J.; Nielsen, M. B.; Levillain, E.; Allain, M.; Becher, J. *J. Am. Chem. Soc.* **2000,** *122,* 9486–9494. doi:10.1021/ja000537c
32. Khodorkovsky, V.; Shapiro, L.; Krief, P.; Shames, A.; Mabon, G.; Gorgues, A.; Giffard, M. *Chem. Commun.* **2001,** 2736–2737. doi:10.1039/B104934H
33. Philp, D.; Slawin, A. M. Z.; Spencer, N.; Stoddart, J. F.; Williams, D. J. *J. Chem. Soc., Chem. Commun.* **1991,** 1584–1586. doi:10.1039/c39910001584
34. Torrance, J. B.; Scott, B. A.; Welber, B.; Kaufman, F. B.; Seiden, P. E. *Phys. Rev. B* **1979,** *19,* 730–741. doi:10.1103/PhysRevB.19.730
35. Bozio, R.; Zanon, I.; Girlando, A.; Pecile, C. *J. Chem. Phys.* **1979,** *71,* 2282–2293. doi:10.1063/1.438564
36. Rosokha, S. V.; Kochi, J. K. *J. Am. Chem. Soc.* **2007,** *129,* 828–838. doi:10.1021/ja064166x
37. Christensen, C. A.; Becher, J.; Christensen, C. A.; Goldenberg, L. M.; Bryce, M. R. *Chem. Commun.* **1998,** 509–510. doi:10.1039/a707504i
38. Hasegawa, M.; Nakamura, K.-i.; Tokunaga, S.; Baba, Y.; Shiba, R.; Shirahata, T.; Mazaki, Y.; Misaki, Y. *Chem. – Eur. J.* **2016,** *22,* 10090–10101. doi:10.1002/chem.201601785
39. Coffen, D. L. *Tetrahedron Lett.* **1970,** *11,* 2633–2636. doi:10.1016/S0040-4039(01)98299-1
40. Wudl, F.; Wobschall, D.; Hufnagel, E. J. *J. Am. Chem. Soc.* **1972,** *94,* 670–672. doi:10.1021/ja00757a079
41. Ferraris, J.; Cowan, D. O.; Walatka, V.; Perlstein, J. H. *J. Am. Chem. Soc.* **1973,** *95,* 948–949. doi:10.1021/ja00784a066
42. Kistenmacher, T. J.; Phillips, T. E.; Cowan, D. O. *Acta Crystallogr., Sect. B: Struct. Crystallogr. Cryst. Chem.* **1974,** *30,* 763–768. doi:10.1107/S0567740874003669
43. Bendikov, M.; Wudl, F.; Perepichka, D. F. *Chem. Rev.* **2004,** *104,* 4891–4946. doi:10.1021/cr030666m
44. Wudl, F. *Acc. Chem. Res.* **2002,** *17,* 227–232. doi:10.1021/ar00102a005
45. Jérome, D.; Schulz, H. J. *Adv. Phys.* **2006,** *31,* 299–490. doi:10.1080/00018738200101398
46. Becher, J.; Lau, J.; Leriche, P.; Mørk, P.; Svenstrup, N. *J. Chem. Soc., Chem. Commun.* **1994,** 2715–2716. doi:10.1039/C39940002715
47. Simonsen, K. B.; Svenstrup, N.; Lau, J.; Simonsen, O.; Mørk, P.; Kristensen, G. J.; Becher, J. *Synthesis* **1996,** *1996,* 407–418. doi:10.1055/s-1996-4216
48. Svenstrup, N.; Rasmussen, K. M.; Hansen, T. K.; Becher, J. *Synthesis* **1994,** 809–812. doi:10.1055/s-1994-25580
49. Blanchard, P.; Sallé, M.; Duguay, G.; Jubault, M.; Gorgues, A. *Tetrahedron Lett.* **1992,** *33,* 2685–2688. doi:10.1016/S0040-4039(00)79057-5
50. Challenger, F.; Mason, E. A.; Holdsworth, E. C.; Emmott, R. *J. Chem. Soc.* **1953,** 292–304. doi:10.1039/jr9530000292
51. Giffard, M.; Frère, P.; Gorgues, A.; Riou, A.; Roncali, J.; Toupet, L. *J. Chem. Soc., Chem. Commun.* **1993,** 944–945. doi:10.1039/C39930000944
52. Li, Z.-T.; Stein, P. C.; Svenstrup, N.; Lund, K. H.; Becher, J. *Angew. Chem., Int. Ed. Engl.* **1995,** *34,* 2524–2528. doi:10.1002/anie.199525241

53. Ballardini, R.; Balzani, V.; Becher, J.; Di Fabio, A.; Gandolfi, M. T.; Mattersteig, G.; Nielsen, M. B.; Raymo, F. M.; Rowan, S. J.; Stoddart, J. F.; White, A. J. P.; Williams, D. J. *J. Org. Chem.* **2000,** *65,* 4120–4126. doi:10.1021/jo0001941
54. Sallé, M.; Gorgues, A.; Jubault, M.; Boubekeur, K.; Batail, P. *Tetrahedron* **1992,** *48,* 3081–3090. doi:10.1016/S0040-4020(01)92250-1
55. Chen, W.; Cava, M. P.; Takassi, M. A.; Metzger, R. M. *J. Am. Chem. Soc.* **1988,** *110,* 7903–7904. doi:10.1021/ja00231a066
56. Jeppesen, J. O.; Perkins, J.; Becher, J.; Stoddart, J. F. *Org. Lett.* **2000,** *2,* 3547–3550. doi:10.1021/ol006387s
57. Jeppesen, J. O.; Becher, J. *Eur. J. Org. Chem.* **2003,** 3245–3266. doi:10.1002/ejoc.200300078
58. Odell, B.; Reddington, M. V.; Slawin, A. M. Z.; Spencer, N.; Stoddart, J. F.; Williams, D. J. *Angew. Chem., Int. Ed. Engl.* **1988,** *27,* 1547–1550. doi:10.1002/anie.198815471
59. Anelli, P.-L.; Asakawa, M.; Ashton, P. R.; Bissell, R. A.; Clavier, G.; Górski, R.; Kaifer, A. E.; Langford, S. J.; Mattersteig, G.; Menzer, S.; Philp, D.; Slawin, A. M. Z.; Spencer, N.; Stoddart, J. F.; Tolley, M. S.; Williams, D. J. *Chem. – Eur. J.* **1997,** *3,* 1113–1135. doi:10.1002/chem.19970030719
60. Brøndsted Nielsen, M.; Hansen, J. G.; Becher, J. *Eur. J. Org. Chem.* **1999,** 2807–2815. doi:10.1002/(SICI)1099-0690(199911)1999:11<2807::AID-EJOC2807>3.0.CO;2-N
61. Asakawa, M.; Ashton, P. R.; Balzani, V.; Credi, A.; Mattersteig, G.; Matthews, O. A.; Montalti, M.; Spencer, N.; Stoddart, J. F.; Venturi, M. *Chem. – Eur. J.* **1997,** *3,* 1992–1996. doi:10.1002/chem.19970031214
62. Asakawa, M.; Ashton, P. R.; Balzani, V.; Boyd, S. E.; Credi, A.; Mattersteig, G.; Menzer, S.; Montalti, M.; Raymo, F. M.; Ruffilli, C.; Stoddart, J. F.; Venturi, M.; Williams, D. J. *Eur. J. Org. Chem.* **1999,** 985–994. doi:10.1002/(SICI)1099-0690(199905)1999:5<985::AID-EJOC985>3.0.CO;2-O
63. Kristensen, R.; Andersen, S. S.; Olsen, G.; Jeppesen, J. O. *J. Org. Chem.* **2017,** *82,* 1371–1379. doi:10.1021/acs.joc.6b02466
64. Nielsen, M. B.; Jeppesen, J. O.; Lau, J.; Lomholt, C.; Damgaard, D.; Jacobsen, J. P.; Becher, J.; Stoddart, J. F. *J. Org. Chem.* **2001,** *66,* 3559–3563. doi:10.1021/jo010173m
65. Schmidt, P. M.; Brown, R. S.; Luong, J. H. T. *Chem. Eng. Sci.* **1995,** *50,* 1867–1876. doi:10.1016/0009-2509(95)00046-8
66. Zhang, Y.-M.; Chen, Y.; Zhuang, R.-J.; Liu, Y. *Supramol. Chem.* **2011,** *23,* 372–378. doi:10.1080/10610278.2010.521828
67. Ziganshina, A. Y.; Ko, Y. H.; Jeon, W. S.; Kim, K. *Chem. Commun.* **2004,** 806–807. doi:10.1039/B316651A
68. Jeon, W. S.; Kim, H.-J.; Lee, C.; Kim, K. *Chem. Commun.* **2002,** 1828–1829. doi:10.1039/B202082C
69. Yoshizawa, M.; Kumazawa, K.; Fujita, M. *J. Am. Chem. Soc.* **2005,** *127,* 13456–13457. doi:10.1021/ja053508g
70. Schröder, H. V.; Wollschläger, J. M.; Schalley, C. A. *Chem. Commun.* **2017,** *53,* 9218–9221. doi:10.1039/C7CC05259F
71. Maksimov, M. O.; Pan, S. J.; James Link, A. *Nat. Prod. Rep.* **2012,** *29,* 996–1006. doi:10.1039/c2np20070h
72. Olson, M. A.; Botros, Y. Y.; Stoddart, J. F. *Pure Appl. Chem.* **2010,** *82,* 1569–1574. doi:10.1351/PAC-CON-10-02-09
73. Ashton, P. R.; Bissell, R. A.; Spencer, N.; Stoddart, J. F.; Tolley, M. S. *Synlett* **1992,** *1992,* 923–926. doi:10.1055/s-1992-21542
74. Li, Z.-T.; Stein, P. C.; Becher, J.; Jensen, D.; Mørk, P.; Svenstrup, N. *Chem. – Eur. J.* **1996,** *2,* 624–633. doi:10.1002/chem.19960020605
75. Jeppesen, J. O.; Perkins, J.; Becher, J.; Stoddart, J. F. *Angew. Chem., Int. Ed.* **2001,** *40,* 1216–1221. doi:10.1002/1521-3773(20010401)40:7<1216::AID-ANIE1216>3.0.CO;2-W
76. Tseng, H.-R.; Vignon, S. A.; Stoddart, J. F. *Angew. Chem., Int. Ed.* **2003,** *42,* 1491–1495. doi:10.1002/anie.200250453
77. Deng, W. Q.; Muller, R. P.; Goddard, W. A., III. *J. Am. Chem. Soc.* **2004,** *126,* 13562–13563. doi:10.1021/ja036498x
78. Jang, Y. H.; Hwang, S.; Kim, Y.-H.; Jang, S. S.; Goddard, W. A., III. *J. Am. Chem. Soc.* **2004,** *126,* 12636–12645. doi:10.1021/ja0385437
79. Jang, Y. H.; Goddard, W. A., III. *J. Phys. Chem. B* **2006,** *110,* 7660–7665. doi:10.1021/jp055473c
80. Zhao, Y.-L.; Dichtel, W. R.; Trabolsi, A.; Saha, S.; Aprahamian, I.; Stoddart, J. F. *J. Am. Chem. Soc.* **2008,** *130,* 11294–11296. doi:10.1021/ja8036146
81. Olsen, J.-C.; Fahrenbach, A. C.; Trabolsi, A.; Friedman, D. C.; Dey, S. K.; Gothard, C. M.; Shveyd, A. K.; Gasa, T. B.; Spruell, J. M.; Olson, M. A.; Wang, C.; Jacquot de Rouville, H.-P.; Botros, Y. Y.; Stoddart, J. F. *Org. Biomol. Chem.* **2011,** *9,* 7126–7133. doi:10.1039/c1ob05913k
82. Schröder, H. V.; Sobottka, S.; Nößler, M.; Hupatz, H.; Gaedke, M.; Sarkar, B.; Schalley, C. A. *Chem. Sci.* **2017,** *8,* 6300–6306. doi:10.1039/C7SC02694C
83. Feringa, B. L.; Jager, W. F.; de Lange, B. *Tetrahedron* **1993,** *49,* 8267–8310. doi:10.1016/S0040-4020(01)81913-X
84. de Silva, A. P.; Dixon, I. M.; Gunaratne, H. Q. N.; Gunnlaugsson, T.; Maxwell, P. R. S.; Rice, T. E. *J. Am. Chem. Soc.* **1999,** *121,* 1393–1394. doi:10.1021/ja982909b
85. Avellini, T.; Li, H.; Coskun, A.; Barin, G.; Trabolsi, A.; Basuray, A. N.; Dey, S. K.; Credi, A.; Silvi, S.; Stoddart, J. F.; Venturi, M. *Angew. Chem., Int. Ed.* **2012,** *51,* 1611–1615. doi:10.1002/anie.201107618
86. Schröder, H. V.; Hupatz, H.; Achazi, A. J.; Sobottka, S.; Sarkar, B.; Paulus, B.; Schalley, C. A. *Chem. – Eur. J.* **2017,** *23,* 2960–2967. doi:10.1002/chem.201605710
87. Love, J. C.; Estroff, L. A.; Kriebel, J. K.; Nuzzo, R. G.; Whitesides, G. M. *Chem. Rev.* **2005,** *105,* 1103–1170. doi:10.1021/cr0300789
88. Balzani, V.; Credi, A.; Venturi, M. *ChemPhysChem* **2008,** *9,* 202–220. doi:10.1002/cphc.200700528
89. Ariga, K.; Mori, T.; Nakanishi, W.; Hill, J. P. *Phys. Chem. Chem. Phys.* **2017,** *19,* 23658–23676. doi:10.1039/C7CP02280H
90. Green, J. E.; Choi, J. W.; Boukai, A.; Bunimovich, Y.; Johnston-Halperin, E.; Delonno, E.; Luo, Y.; Sheriff, B. A.; Xu, K.; Shin, Y. S.; Tseng, H.-R.; Stoddart, J. F.; Heath, J. R. *Nature* **2007,** *445,* 414–417. doi:10.1038/nature05462
91. Luo, Y.; Collier, C. P.; Jeppesen, J. O.; Nielsen, K. A.; Delonno, E.; Ho, G.; Perkins, J.; Tseng, H.-R.; Yamamoto, T.; Stoddart, J. F.; Heath, J. R. *ChemPhysChem* **2002,** *3,* 519–525. doi:10.1002/1439-7641(20020617)3:6<519::AID-CPHC519>3.0.CO;2-2
92. Collier, C. P.; Mattersteig, G.; Wong, E. W.; Luo, Y.; Beverly, K.; Sampaio, J.; Raymo, F. M.; Stoddart, J. F.; Heath, J. R. *Science* **2000,** *289,* 1172–1175. doi:10.1126/science.289.5482.1172
93. Yu, H.; Luo, Y.; Beverly, K.; Stoddart, J. F.; Tseng, H.-R.; Heath, J. R. *Angew. Chem., Int. Ed.* **2003,** *42,* 5706–5711. doi:10.1002/anie.200352352
94. Tseng, H.-R.; Wu, D.; Fang, N. X.; Zhang, X.; Stoddart, J. F. *ChemPhysChem* **2004,** *5,* 111–116. doi:10.1002/cphc.200300992

95. Feng, M.; Guo, X.; Lin, X.; He, X.; Ji, W.; Du, S.; Zhang, D.; Zhu, D.; Gao, H. *J. Am. Chem. Soc.* **2005,** *127,* 15338–15339. doi:10.1021/ja054836j
96. Huang, T. J.; Brough, B.; Ho, C.-M.; Liu, Y.; Flood, A. H.; Bonvallet, P. A.; Tseng, H.-R.; Stoddart, J. F.; Baller, M.; Magonov, S. *Appl. Phys. Lett.* **2004,** *85,* 5391–5393. doi:10.1063/1.1826222
97. Aprahamian, I.; Olsen, J.-C.; Trabolsi, A.; Stoddart, J. F. *Chem. – Eur. J.* **2008,** *14,* 3889–3895. doi:10.1002/chem.200800191
98. Schröder, H. V.; Mekic, A.; Hupatz, H.; Sobottka, S.; Witte, F.; Urner, L. H.; Gaedke, M.; Pagel, K.; Sarkar, B.; Paulus, B.; Schalley, C. A. *submitted.*
99. Barin, G.; Coskun, A.; Friedman, D. C.; Olson, M. A.; Colvin, M. T.; Carmielli, R.; Dey, S. K.; Bozdemir, O. A.; Wasielewski, M. R.; Stoddart, J. F. *Chem. – Eur. J.* **2011,** *17,* 213–222. doi:10.1002/chem.201002152
100. Jørgensen, T.; Becher, J.; Chambron, J.-C.; Sauvage, J.-P. *Tetrahedron Lett.* **1994,** *35,* 4339–4342. doi:10.1016/S0040-4039(00)73348-X
101. Dietrich-Buchecker, C. O.; Sauvage, J.-P.; Kintzinger, J. P. *Tetrahedron Lett.* **1983,** *24,* 5095–5098. doi:10.1016/S0040-4039(00)94050-4
102. Nielsen, M. B.; Li, Z.-T.; Becher, J. *J. Mater. Chem.* **1997,** *7,* 1175–1187. doi:10.1039/a700129k
103. Li, Z.-T.; Becher, J. *Chem. Commun.* **1996,** 639–640. doi:10.1039/CC9960000639
104. Nielsen, M. B.; Thorup, N.; Becher, J. *J. Chem. Soc., Perkin Trans. 1* **1998,** 1305–1308. doi:10.1039/a707854d
105. Asakawa, M.; Ashton, P. R.; Balzani, V.; Credi, A.; Hamers, C.; Mattersteig, G.; Montalti, M.; Shipway, A. N.; Spencer, N.; Stoddart, J. F.; Tolley, M. S.; Venturi, M.; White, A. J. P.; Williams, D. J. *Angew. Chem., Int. Ed.* **1998,** *37,* 333–337. doi:10.1002/(SICI)1521-3773(19980216)37:3<333::AID-ANIE333>3.0.CO;2-P
106. Sun, J.; Wu, Y.; Wang, Y.; Liu, Z.; Cheng, C.; Hartlieb, K. J.; Wasielewski, M. R.; Stoddart, J. F. *J. Am. Chem. Soc.* **2015,** *137,* 13484–13487. doi:10.1021/jacs.5b09274
107. Rowsell, J. L. C.; Yaghi, O. M. *Microporous Mesoporous Mater.* **2004,** *73,* 3–14. doi:10.1016/j.micromeso.2004.03.034
108. Chen, Q.; Sun, J.; Li, P.; Hod, I.; Moghadam, P. Z.; Kean, Z. S.; Snurr, R. Q.; Hupp, J. T.; Farha, O. K.; Stoddart, J. F. *J. Am. Chem. Soc.* **2016,** *138,* 14242–14245. doi:10.1021/jacs.6b09880
109. Mondloch, J. E.; Bury, W.; Fairen-Jimenez, D.; Kwon, S.; DeMarco, E. J.; Weston, M. H.; Sarjeant, A. A.; Nguyen, S. T.; Stair, P. C.; Snurr, R. Q.; Farha, O. K.; Hupp, J. T. *J. Am. Chem. Soc.* **2013,** *135,* 10294–10297. doi:10.1021/ja4050828
110. McGonigal, P. R.; Deria, P.; Hod, I.; Moghadam, P. Z.; Avestro, A.-J.; Horwitz, N. E.; Gibbs-Hall, I. C.; Blackburn, A. K.; Chen, D.; Botros, Y. Y.; Wasielewski, M. R.; Snurr, R. Q.; Hupp, J. T.; Farha, O. K.; Stoddart, J. F. *Proc. Natl. Acad. Sci. U. S. A.* **2015,** *112,* 11161–11168. doi:10.1073/pnas.1514485112
111. Spruell, J. M.; Coskun, A.; Friedman, D. C.; Forgan, R. S.; Sarjeant, A. A.; Trabolsi, A.; Fahrenbach, A. C.; Barin, G.; Paxton, W. F.; Dey, S. K.; Olson, M. A.; Benítez, D.; Tkatchouk, E.; Colvin, M. T.; Carmielli, R.; Caldwell, S. T.; Rosair, G. M.; Hewage, S. G.; Duclairoir, F.; Seymour, J. L.; Slawin, A. M. Z.; Goddard, W. A., III; Wasielewski, M. R.; Cooke, G.; Stoddart, J. F. *Nat. Chem.* **2010,** *2,* 870–879. doi:10.1038/nchem.749
112. Frasconi, M.; Kikuchi, T.; Cao, D.; Wu, Y.; Liu, W.-G.; Dyar, S. M.; Barin, G.; Sarjeant, A. A.; Stern, C. L.; Carmieli, R.; Wang, C.; Wasielewski, M. R.; Goddard, W. A., III; Stoddart, J. F. *J. Am. Chem. Soc.* **2014,** *136,* 11011–11026. doi:10.1021/ja504662a

License and Terms

BEILSTEIN JOURNAL OF ORGANIC CHEMISTRY

Dynamic light scattering studies of the effects of salts on the diffusivity of cationic and anionic cavitands

Anthony Wishard and Bruce C. Gibb*

Full Research Paper

Open Access

Address:
Department of Chemistry, Tulane University, New Orleans, LA 70118, USA

Email:
Bruce C. Gibb* - bgibb@tulane.edu

* Corresponding author

Keywords:
cavitand; dynamic light scattering; Hofmeister effect; ion–ion interactions; water

Beilstein J. Org. Chem. **2018,** *14,* 2212–2219.
doi:10.3762/bjoc.14.195

Received: 04 May 2018
Accepted: 15 August 2018
Published: 23 August 2018

This article is part of the thematic issue "Macrocyclic and supramolecular chemistry".

Guest Editor: M.-X. Wang

Abstract

Although alkali halide salts play key roles in all living systems, the physical models used to describe the properties of aqueous solutions of salts do not take into account specific ion–ion interactions. To identify specific ion–ion interactions possibly contributing to the aggregation of proteins, we have used dynamic light scattering (DLS) to probe the aggregation of charged cavitands. DLS measurements of negatively charged **1** in the presence of a range of alkali metal halides reveal no significant aggregation of host **1** as a function of the nature of the cation of the added salt. Only at high concentrations could trace amounts of aggregation be detected by ^{1}H NMR spectroscopy. Contrarily, **1** was readily aggregated and precipitated by $ZnCl_2$. In contrast, although fluoride and chloride did not induce aggregation of positively charged host **2**, this cavitand exhibited marked aggregation as a function of bromide and iodide concentration. Specifically, bromide induced small but significant amounts of dimerization, whilst iodide induced extreme aggregation. Moreover, in these cases aggregation of host **2** also exhibited a cationic dependence, with an observed trend $Na^+ > Li^+ > K^+ \approx Cs^+$. In combination, these results reveal new details of specific ion pairings in aqueous solution and how this can influence the properties of dissolved organics.

Introduction

Although all life on planet Earth depends on aqueous solutions, our understanding of aqueous supramolecular chemistry is limited. As a result, as Smith has eloquently pointed out [1], the effects of buffers and salts on dissolved organics can be quite bewildering. Why is this? The proverbial elephant in the room is that classical theories of electrolytes rest on the assumptions that all ions are point charges that only form non-specific interactions. The ramifications of this are innumerable. For example, pH measurements are based on extended Debye–Hückel theory [2] and Poisson–Boltzmann distribution [3] to describe ionic

profiles near the glass-electrode surface. These classical models may be good approximations for ions such as Li^+ and F^-, but they are poor models for ions that don't behave as hard point charges [4]. Correspondingly, IUPAC advises researchers to avoid pH measurements above 0.1 M to minimize errors [5]. Related problems lie with Derjaguin, Landau, Verwey and Overbeek (DLVO) theory as a model of the aggregation of aqueous dispersions. DLVO often quantitatively succeeds, but it fails to predict ion specific effects [4,6,7]. Similarly, it is becoming increasingly evident that the Hofmeister and reverse Hofmeister effects [8,9] – most commonly discussed in terms of how salts affect biomacromolecules – can only be fully understood in terms of specific ion–ion, ion–water, and/or ion–macromolecule interactions [4,10,11].

Although many attempts have been made to amend these and other classical models [4], success has been limited because of our lack of understanding of the specific supramolecular properties of individual ions. There is therefore an opportunity for supramolecular chemists (who by their very training demand specificity of interactions) to help build a full understanding of ion-specific interactions in water and help usher the troubling elephant out of the room.

Recently we demonstrated how host molecules can engender the Hofmeister [12,13] and the reverse Hofmeister effects [14]. In regards to the former, we have shown how poorly solvated anions such as SCN^- have an affinity for non-polar surfaces. Because of this, they can compete with the interactions between two non-polar surfaces in a host–guest complexation event and can induce an apparent weakening of the hydrophobic effect akin to how these anions can partially unfold proteins. Alternatively, poorly solvated anions can also associate closely with cationic groups, induce charge neutralization, and engender aggregation and/or precipitation. In other words, they can also cause an apparent increase in the hydrophobic effect. This is the reverse Hofmeister effect, and in complex biomacromolecules we surmise that both effects are in operation, and that in very general terms it is the balance between these that dictates the properties of a particular macromolecule under specific conditions. Cations can also induce Hofmeister effects, but these are usually much weaker, and we believe there are two reasons for this. First, simple metal cations are generally more strongly solvated than comparable anions that can induce Hofmeister effects. Second, the anions that predominate in biomacromolecules are carboxylates, phosphates and sulfates, and the strong solvation of these means that it is hard for a cation to form an ion pair and induce Hofmeister effects.

To explore these ideas further we report here the responses of two deep-cavity cavitands, octacarboxylate **1** (counter ion Na^+) [15,16] and positand **2** (counter ion Cl^-) [14] (Figure 1), to different salts using dynamic light scattering (DLS) [17-20]. Respectively functionalized with carboxylates and trimethylammonium groups, these hosts are expected to possess unique ion-pairing properties and hence have very different reverse-Hofmeister responses to added salts. More specifically, both octacarboxylate **1** and positand **2** have a non-polar cavity that can function as an anion (but not to our knowledge a cation) binding site. Anion binding to the cavity of positively charged **2** is stronger than to negatively charged **1** [13,14], but nevertheless anion binding to **1** can be as strong as 4.60 kcal mol^{-1}. Host **2** has a second anion binding site in the form of the crown of trimethylammoniums "under" the primary bowl [14], and correspondingly the four chelating carboxylates of the crown of **1** may be a reasonable cation binding site. Furthermore, in addition to these specific cavity and crown sites, the individual charge groups of **1** and **2** can function as weak (pseudo-specific) binding sites for ions of opposite charge.

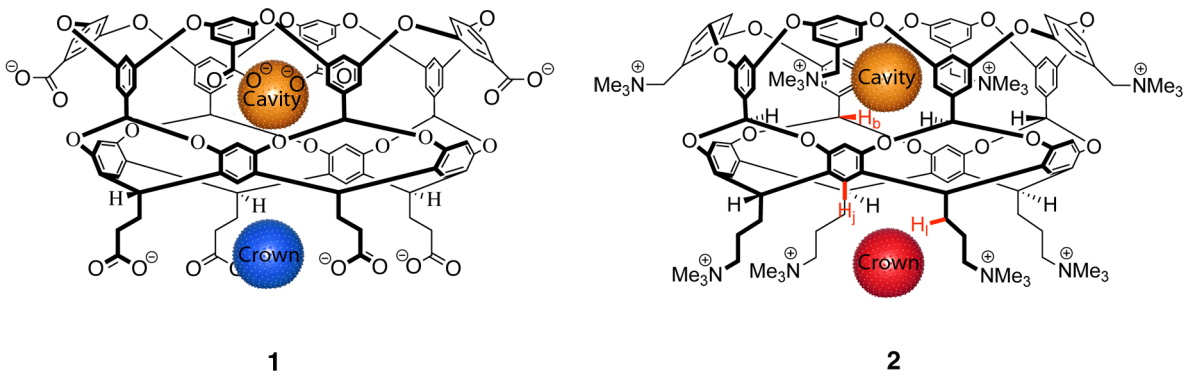

Figure 1: Chemical structures of octaacid **1** and positand **2** showing the anionic binding sites of the two hosts (orange and red) and the potential cationic binding site of **1** (blue).

Results and Discussion

To determine the effects of salts on **1** (counter ion Na^+) DLS was used to monitor its observed hydrodynamic volume during titration with various halide salts. The fifteen salts studied were a matrix of the alkali metal cations Li^+, Na^+, K^+, and Cs^+ in combination with the halides F^- through I^-, the one omission being poorly soluble lithium fluoride (maximum solubility = 0.134 g mL^{-1}). Unsurprisingly, given the pK_a values of carboxylic acids, host **1** has limited solubility in unbuffered water. Thus for solubility reasons, titrations of **1** were performed in 20 mM NaOH solution (see Supporting Information File 1, Figure S2, for more details). In each case titrations were taken to 100 mM salt where it was assumed that the host is fully screened [21-23]. Figure 2 shows the effects of the different salts on the observed size of **1**.

The reported hydrodynamic diameters were calculated using the Stokes–Einstein equation (Equation 1), which assumes host **1** is a spherical particle,

$$D = \frac{k_b T}{6\pi\eta r_H}, \quad (1)$$

where D is the diffusion constant, k_b is the Boltzmann constant, T is the temperature, η is the viscosity of the solution, and r_H is the hydrodynamic radius.

In all cases, at the initial 20 mM concentration of NaOH the light scattering induced by **1** was weak. This resulted in relatively flat autocorrelation functions generated from the measured fluctuations in scattered light. Consequently, the recorded size of the host was both anomalously small and highly variable, covering the range 1.0 to 1.7 nm (Figure 2). This compares to molecular models which show host **1** approximates to an anti-cube (square antiprism) with sides of ≈ 2.0 nm. The weak light scattering of **1** was attributed to the high charge density of the host and the low ionic strength of the solution engendering significant Coulombic interactions between host molecules [24]. Titrating samples with the different salts led to much stronger light scattering and an apparent increase in the hydrodynamic diameter of the host to a more realistic ≈ 2 nm. In all cases, however, the nature of the cation had no perceivable effect; each metal ion resulted in a hydrodynamic diameter for **1** of 2.1 ± 0.2 nm (Table 1). The invariance in these results reveals the power of the carboxylate as a water-solubilizing

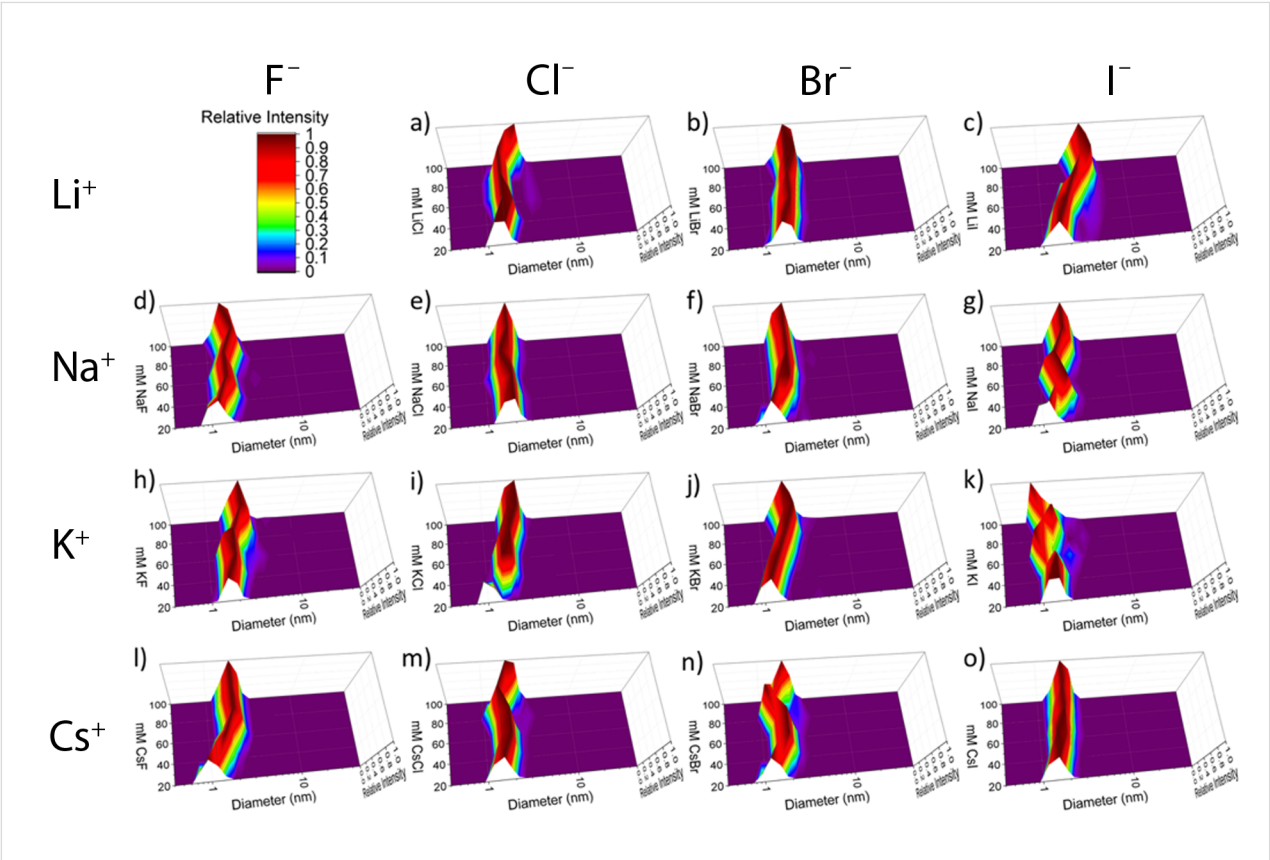

Figure 2: Representative plots of the volume-weighted distribution obtained by DLS for salts titrated into 2.00 mM **1**: a) LiCl, b) LiBr, c) LiI, d) NaF, e) NaCl, f) NaBr, g) NaI, h) KF, i) KCl, j) KBr, k) KI, l) CsF, m) CsCl, n) CsBr, o) CsI. Scale shown in the upper-left corner. The *x*-axis represents hydrodynamic diameter, the *y*-axis the concentration of the respective salt (mM), and the *z*-axis the relative intensity.

Table 1: Summary of titration data from DLS experiments.

cation	anion	host **1**[a,b] max. dia. (nm)	host **2**[a,b] max. dia. (nm)	*n*-mer aggregate[b] # (for host **2**)
Li^+	F^-	_[c]	_[c]	
	Cl^-	2.1 ± 0.0	2.1 ± 0.1	
	Br^-	2.1 ± 0.2	2.5 ± 0.0	1.7 ± 0.0
	I^-	2.0 ± 0.0	14.3 ± 0.5[d]	314 ± 32[d]
Na^+	F^-	1.8 ± 0.1	1.8 ± 0.3	
	Cl^-	2.0 ± 0.2	2.1 ± 0.1	
	Br^-	1.8 ± 0.0	2.6 ± 0.1	1.8 ± 0.1
	I^-	2.0 ± 0.1	18.6 ± 3.1[d]	764 ± 260[d]
K^+	F^-	2.1 ± 0.4	2.0 ± 0.1	
	Cl^-	2.1 ± 0.1	2.0 ± 0.0	
	Br^-	2.1 ± 0.1	2.4 ± 0.1	1.4 ± 0.1
	I^-	2.2 ± 0.3	11.6 ± 0.8	170 ± 37
Cs^+	F^-	1.9 ± 0.0	2.0 ± 0.3	
	Cl^-	2.0 ± 0.1	2.0 ± 0.0	
	Br^-	1.9 ± 0.1	2.4 ± 0.0	1.5 ± 0.0
	I^-	1.9 ± 0.1	11.9 ± 0.2	180 ± 10

[a]Determination of the maximum hydrodynamic diameter (max. dia.) was made regardless of the salt concentration at which the maximum size occurred. In the event of a bimodal distribution, the mode that accounted for >10% of the total distribution and had the largest diameter was used to determine max. dia. [b]Values are the average of two datasets. [c]For solubility reasons titrations with LiF were not performed. [d]Values are the average of three or more datasets.

group. Although its pK_a may not be optimal for deprotonation at neutral or physiological pH, its small size and relatively high free energy of hydration (−373 kJ mol^{-1}) ensure that ion-pairing effects are not strong. This was further confirmed by ^{1}H NMR spectroscopy (Supporting Information File 1, Figure S3), which revealed only trace amounts of host aggregation (≈5%). Furthermore, even at 100 mM salt concentration, ^{1}H NMR spectroscopy failed to show any significant association of Cs^+ to the crown of four carboxylates. Thus, although this crown is the most obvious potential cation binding site, we see no evidence of specific complexation here. More generally, despite the high charge density of **1**, monovalent alkali metal ions cannot associate with it sufficiently to induce significant aggregation and a reverse Hofmeister effect. This was not, however, the case with divalent metal ions, which are well recognized to interact strongly with carboxylates and induce aggregation [25]. Thus, visual inspection upon the addition of $ZnCl_2$ to give a 100 mM salt concentration revealed extensive precipitation of the host. Returning to the point that the majority of anionic groups in biomacromolecules are strongly solvated, it is interesting to contemplate the idea that the prevalence of alkali metal ions in the environment exerted evolutionary pressures on biomacromolecules to select carboxylate, phosphates and sulfates and hence minimize ion pairing, charge neutralization, and deleterious precipitation effects in living systems.

Overall, octacarboxylate **1** is a binder of large, polarizable anions in its non-polar pocket [12], but is not a perceptible binder of alkali metal cations. Building on this, we carried out similar DLS studies with host **2** (counter ion Cl^-) using the same aforementioned salts (Figure 3). In a previous work, our DLS studies of this host involved solutions buffered with 40 mM phosphate (pH 7.3) [14]. Under these conditions, the initially measured sizes in the absence of added salt were consistently 1.9–2.1 nm; values that match the modeling of the host. In stark contrast to this earlier work, but analogously to host **1**, when we examined solutions of **2** in the absence of any added buffer and salt, light scattering was weak. This resulted in flat autocorrelation functions and again an anomalously small and highly variable hydrodynamic volume (0.5–1.4 nm). This issue noted, at the titration point of 80 mM salt the curvature of the autocorrelation function greatly increased, and the observed hydrodynamic diameter approached the expected ≈2.0 nm. Hence although for all of the studies here the starting point for each titration was 20 mM salt, the first data point for each titration was ignored.

An obvious trend in the data for host **2** (Figure 3) is how the nature of the halide affects aggregation. Over all concentrations of F^- salts the hydrodynamic diameter of the host was anomalously small, with maximum diameters measured in the pres-

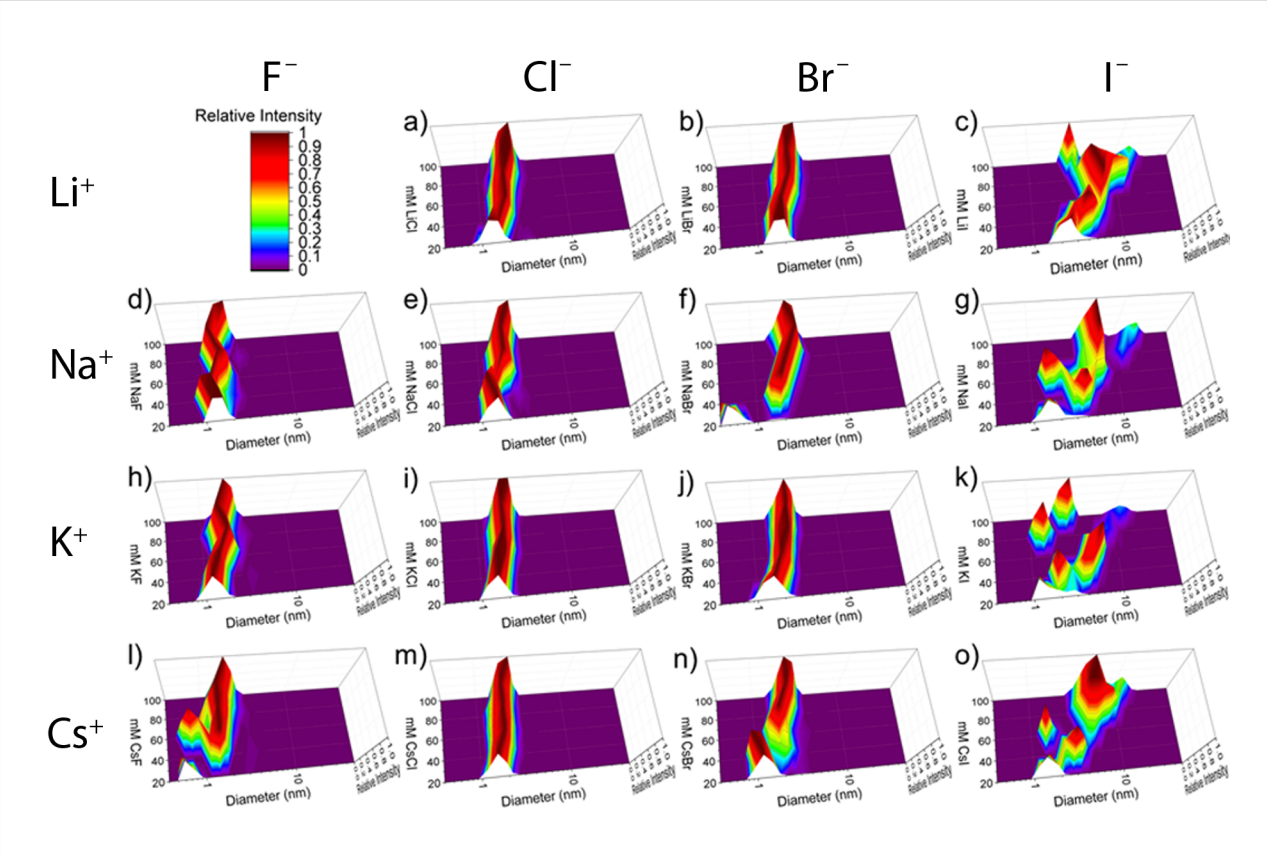

Figure 3: Representative plots of the volume-weighted distribution obtained by DLS for salts titrated into 2.00 mM **2**: a) LiCl, b) LiBr, c) LiI, d) NaF, e) NaCl, f) NaBr, g) NaI, h) KF, i) KCl, j) KBr, k) KI, l) CsF, m) CsCl, n) CsBr, o) CsI. Scale shown in the upper left corner. The *x*-axis represents hydrodynamic diameter, the *y*-axis the concentration of the respective salt (mM), and the *z*-axis the relative intensity.

ence of NaF, KF, and CsF being 1.6, 1.9, and 1.8 nm. The strongly solvated F^- ion [26] has a very weak affinity for host **2** [14], and we therefore interpret these small hydrodynamic diameters to limited binding to host **2** and hence an inability to screen interhost interactions. In contrast, in the presence of at least 80 mM Cl^- salts the hydrodynamic diameter of host **2** was consistently within the expected range of 2.0–2.1 nm. Thus, independent of the metal cation Cl^- is an ideal anion for effectively screening intermolecular charge–charge interactions between the host (Table 1). The case of Br^- was quite different. For all salts, the addition of Br^- leads to an increase in the hydrodynamic diameter, with NaBr giving the largest increase to 2.6 nm. This corresponds to the formation of a dimer aggregate. Aggregation was even more extreme with the I^- salts. All I^- salts caused extensive aggregation of the host, and a determination of the maximum size induced by the four salts ranged from 170 and 180-mers in the presence of KI and CsI, to ≈724-mers for NaI. Evidently the difference in the free energies of solvation of Br^- and I^- (ΔG_{hyd} = −321 and −283 kJ mol^{-1}, respectively) is key to allowing more ion pairing between the trimethylammonium groups of **2** and I^- to induce substantial aggregation.

The data for the I^- salts illustrate a further complexity to the ability of salts to induce precipitation of ammonium ions such as **2**. Thus, although the aggregation induced by KI and CsI are not significantly different, there is a trend for cation-induced aggregation of cationic **2**: namely $Na^+ > Li^+ > K^+ \approx Cs^+$. This cation effect must be indirect. If the counter ions of **2** (Cl^-) are viewed as non-coordinating, this phenomenon can be interpreted as arising from a simple competition between the two "hosts" **2** and M^+ (Scheme 1). In such a system, I^- can only associate with host **2** and induce charge neutralization and aggregation when it is in the free state, but if it itself strongly associates with the counter ion of the salt then it will not be able to bind strongly to **2**.

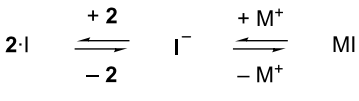

Scheme 1: Visualization of the competitive equilibrium between iodide binding to host **2** or associating with its alkali metal cation M^+. Non-competing Cl^- is omitted for simplicity.

There is a well-established "volcano plot" relationship between the standard heat of solution of crystalline alkali halides and the difference between the absolute free energy (or heat) of hydration of the corresponding anion and cation [27,28]. As a result, in the words of Fajans, "in the case of alkali halides, the solubility in a number of salts with the same cation (anion) and different anions (cations) is at a minimum when the cation and anion are approximately equal and increases with increasing difference of the ionic radii" [29]. This has been built upon by Collins who proposed that the difference in heats of hydration of a cation and anion is a surrogate for the extent of anion pairing in solution; that small (large) anions preferentially bind with small (large) cations, whereas large size differences lead to weak association [30]. Thus, this law of matching water affinities (LMWA) suggests that in aqueous solution CsI is more strongly ion-paired than LiI. The observed trend in the aggregation of **2** (NaI > LiI > KI ≈ CsI) is therefore not in full agreement with the LMWA. The LMWA correlates with our data that K^+ and Cs^+ should pair strongly with I^- and therefore induce weak aggregation. However, it also predicts that Li^+ and I^- should form the weakest ion pair and that therefore LiI should be the greatest aggregator of **2**. As Table 1 reveals, this is not the case; it is NaI that has the strongest influence on the host.

A straightforward answer for this may be that entropy is a part of the aggregation of **2**, whereas the LMWA is purely enthalpically based. Additionally, however, the absolute heats of hydration of anions and cations calculated by Morris make many assumptions, and in part rely on models that assume ideality for their determinations.

Cation effects for the bromide salts are less pronounced than those of the iodide salts, nevertheless there are small but significant differences between the pairs of cations Li^+/Na^+ and K^+/Cs^+. The former pair, as would be expected considering the data for iodide salts, leads to greater aggregation than that observed with the potassium and cesium salts. These results reveal that in contrast to host **1**, the weakly solvated groups of **2** result in significant ion-pairing effects that can, in extreme cases such as I^- salts, lead to a pronounced reverse Hofmeister effect. Importantly, our DLS studies reveal that this effect is also influenced indirectly by the nature of the cation of the salt.

Conclusion

Dynamic light scattering reveals the ion-specific interactions of carboxylate and trimethylammonium groups, and hence the inherent asymmetry between negatively and positively charged molecules. The negatively charged solubilizing groups of host **1** are relatively strongly solvated, so much so that the nature of the alkali metal cation has very little effect on aggregation. Divalent metal ions are required to induce aggregation in this host. In contrast, the more weakly solvated charged groups of **2** allow ion-specific interactions with halide anions. Specifically, weakly solvated I^-, and to a lesser extent Br^-, can associate closely with host **2**, induce charge neutralization, and hence bring about aggregation. Importantly, because of the power of I^- to induce aggregation in **2** it is even possible to observe how ion pairing within a salt can influence its aggregation ability. Considering the ubiquity of alkali metal halide ions in Nature, we are examining other systems to provide greater detailing of how the balance of ion pairing in two-cation/two-anion systems influences Hofmeister effects.

Experimental

Reagents were purchased from the commercial supplier Sigma-Aldrich Corp. and were used without further purification. Deuterated solvents were purchased from Cambridge Isotopes and used without further purification. Hosts **1** and **2** were synthesized by the procedures reported previously [15,16,31]. All ^{1}H NMR spectra were collected on a Bruker 500 MHz spectrometer at 25 °C. Spectral processing was performed using Mnova software (Mestrelab Research, S.L.). All dynamic light scattering measurements were performed on a Nicomp ZLS Z3000 particle size analyzer (Particle Sizing Systems – Port Richey, FL), with a 50 mW laser diode (660 nm wavelength) and an avalanche photodiode (APD) detector. Measurements of scattered light were made at 90°, with data collected at 23 °C and processed using a non-negative least squares Nicomp analysis.

DLS solution preparation and analysis procedures

All solutions of **1** were prepared in 20.0 mM NaOH in 18.2 MΩ·cm Milli-Q H_2O. Solutions of **2** were prepared in unbuffered 18.2 MΩ·cm Milli-Q H_2O. All host solutions were prepared at a concentration of 2.00 mM. Solutions of **1** and **2** were titrated with a 2.00 M salt solution in aliquots of 20 mM until reaching a final concentration of 100 mM (50 equiv) salt. Dilution of the host solution during the titration was maintained at <5% for all titrations.

Samples were centrifuged for 10 min at 10,000 rpm prior to each titration but not centrifuged thereafter. Solutions of host were titrated with salt, then shaken and vortexed to ensure mixing before acquiring DLS measurements. For each data point in a titration, analyses were performed in quadruplicate at a channel width of 5 μs. Particularly, at low salt concentrations, weak light scattering resulted in a flat autocorrelation curve; this data was immediately discarded. Of the remaining data, that with the lowest fit error was kept. At every salt concentration, the data was replicated a minimum of one time using a separate solution of host. Those data were then averaged and presented

herein. Results shown are representative of the volume-weighted distribution. Surface plots of the raw, volume-weighted distribution data were plotted using OriginPro software.

NMR solution sample preparation and analysis procedures

Monodispersity of the host **1** solution was confirmed by Pulsed Gradient Spin Echo (PGSE) NMR (Supporting Information File 1, Figure S1) in H_2O locked with D_2O in a 5 mm coaxial capillary insert (Wilmad-Labglass – Vineland, NJ). The concentration of the stock solid was determined by titration in triplicate with a 25.0 mM sodium ethanesulfonate (SES) solution, and integration of the methyl or methylene peaks of ethanesulfonate and the H_1 peak of the host.

Solutions for NMR titrations were prepared in 13.0 mM NaOH in D_2O (Supporting Information File 1, Figure S2). Titrations of the host were carried out with 2.0 mM host solutions. Stock solutions of NaOH were prepared at 286.0 mM. An aliquot of 0.5 mL of host was titrated in an NMR tube with careful addition of small aliquots of NaOH. Analysis of **1** with CsCl was performed by the addition of a 2.00 M CsCl solution to a 2.0 mM host solution such that the final CsCl concentration was 100 mM (50 equiv) and dilution of the host was 5% (Supporting Information File 1, Figure S3).

Supporting Information

Supporting Information File 1

Additional analytical data and NMR spectra.
[https://www.beilstein-journals.org/bjoc/content/supplementary/1860-5397-14-195-S1.pdf]

Acknowledgements

The authors gratefully acknowledge the support of the National Institutes of Health (GM 098141). A.W. also acknowledges the Louisiana Board of Regents for a graduate student fellowship (LEQSF(2013-18)-GF-13).

ORCID® iDs

Anthony Wishard - https://orcid.org/0000-0003-2265-2053
Bruce C. Gibb - https://orcid.org/0000-0002-4478-4084

References

1. Chan, C. W.; Smith, D. K. *Supramol. Chem.* **2017,** *29,* 688–695. doi:10.1080/10610278.2016.1234711
2. Debye, P.; Hückel, E. *Phys. Z.* **1923,** *24,* 185–206.
3. Honig, B.; Nicholls, A. *Science* **1995,** *268,* 1144–1149. doi:10.1126/science.7761829
4. Salis, A.; Ninham, B. W. *Chem. Soc. Rev.* **2014,** *43,* 7358–7377. doi:10.1039/c4cs00144c
5. Buck, R. P.; Rondinini, S.; Covington, A. K.; Baucke, F. G. K.; Brett, C. M. A.; Camoes, M. F.; Milton, M. J. T.; Mussini, T.; Naumann, R.; Pratt, K. W.; Spitzer, P.; Wilson, G. S. *Pure Appl. Chem.* **2002,** *74,* 2169–2200. doi:10.1351/pac200274112169
6. Liang, Y.; Hilal, N.; Langston, P.; Starov, V. *Adv. Colloid Interface Sci.* **2007,** *134–135,* 151–166. doi:10.1016/j.cis.2007.04.003
7. Bostrom, M.; Lima, E. R. A.; Tavares, F. W.; Ninham, B. W. *J. Chem. Phys.* **2008,** *128,* 135104. doi:10.1063/1.2873307
8. Hofmeister, F. *Arch. Exp. Pathol. Pharmakol.* **1888,** *24,* 247–260. doi:10.1007/bf01918191
9. Kunz, W.; Henle, J.; Ninham, B. W. *Curr. Opin. Colloid Interface Sci.* **2004,** *9,* 19–37. doi:10.1016/j.cocis.2004.05.005
10. Jungwirth, P.; Cremer, P. S. *Nat. Chem.* **2014,** *6,* 261–263. doi:10.1038/nchem.1899
11. Collins, K. D.; Washabaugh, M. W. *Q. Rev. Biophys.* **1985,** *18,* 323–422. doi:10.1017/s0033583500005369
12. Carnegie, R. S.; Gibb, C. L. D.; Gibb, B. C. *Angew. Chem., Int. Ed.* **2014,** *53,* 11498–11500. doi:10.1002/anie.201405796
13. Sokkalingam, P.; Shraberg, J.; Rick, S. W.; Gibb, B. C. *J. Am. Chem. Soc.* **2016,** *138,* 48–51. doi:10.1021/jacs.5b10937
14. Jordan, J. H.; Gibb, C. L. D.; Wishard, A.; Pham, T.; Gibb, B. C. *J. Am. Chem. Soc.* **2018,** *140,* 4092–4099. doi:10.1021/jacs.8b00196
15. Gibb, C. L. D.; Gibb, B. C. *J. Am. Chem. Soc.* **2004,** *126,* 11408–11409. doi:10.1021/ja0475611
16. Liu, S.; Whisenhunt-loup, S. E.; Gibb, C. L. D.; Gibb, B. C. *Supramol. Chem.* **2011,** *23,* 480–485. doi:10.1080/10610278.2010.550290
17. Roland, C. D.; Li, H.; Abboud, K. A.; Wagener, K. B.; Veige, A. S. *Nat. Chem.* **2016,** *8,* 791–796. doi:10.1038/nchem.2516
18. Deshmukh, S. A.; Solomon, L. A.; Kamath, G.; Fry, H. C.; Sankaranarayanan, S. K. R. S. *Nat. Commun.* **2016,** *7,* No. 12367. doi:10.1038/ncomms12367
19. Sato, K.; Ji, W.; Palmer, L. C.; Weber, B.; Barz, M.; Stupp, S. I. *J. Am. Chem. Soc.* **2017,** *139,* 8995–9000. doi:10.1021/jacs.7b03878
20. Chen, S.; Polen, S. M.; Wang, L.; Yamasaki, M.; Hadad, C. M.; Badjić, J. D. *J. Am. Chem. Soc.* **2016,** *138,* 11312–11317. doi:10.1021/jacs.6b06562
21. Boström, M.; Tavares, F. W.; Bratko, D.; Ninham, B. W. Ion Specific Interactions Between Pairs of Nanometer Sized Particles in Aqueous Solutions. In *Smart Colloidal Materials. Progress in Colloid and Polymer Science;* Richtering, W., Ed.; Springer: Berlin, 2006; Vol. 133, pp 74–77. doi:10.1007/2882_060
22. Salis, A.; Pinna, M. C.; Bilaničová, D.; Monduzzi, M.; Lo Nostro, P.; Ninham, B. W. *J. Phys. Chem. B* **2006,** *110,* 2949–2956. doi:10.1021/jp0546296
23. Smith, A. M.; Lee, A. A.; Perkin, S. *J. Phys. Chem. Lett.* **2016,** *7,* 2157–2163. doi:10.1021/acs.jpclett.6b00867
24. Hassan, P. A.; Rana, S.; Verma, G. *Langmuir* **2015,** *31,* 3–12. doi:10.1021/la501789z
25. Kherb, J.; Flores, S. C.; Cremer, P. S. *J. Phys. Chem. B* **2012,** *116,* 7389–7397. doi:10.1021/jp212243c
26. Marcus, Y. *Ion Properties;* Marcel Dekker, Inc.: New York, 1997; p 259.
27. Morris, D. F. C. *Struct. Bonding* **1968,** *4,* 63–82. doi:10.1007/BFb0119185
28. Morris, D. F. C. *Struct. Bonding* **1969,** *6,* 157–159. doi:10.1007/BFb0118857
29. Fajans, K. *Naturwissenschaften* **1921,** *9,* 729–738. doi:10.1007/bf01487182

30. Collins, K. D. *Biophys. J.* **1997,** *72,* 65–76. doi:10.1016/s0006-3495(97)78647-8
31. Hillyer, M. B.; Gibb, C. L. D.; Sokkalingam, P.; Jordan, J. H.; Ioup, S. E.; Gibb, B. C. *Org. Lett.* **2016,** *18,* 4048–4051. doi:10.1021/acs.orglett.6b01903

License and Terms

BEILSTEIN JOURNAL OF ORGANIC CHEMISTRY

Synthesis of a water-soluble 2,2′-biphen[4]arene and its efficient complexation and sensitive fluorescence enhancement towards palmatine and berberine

Xiayang Huang[1,2], Xinghua Zhang[*1], Tianxin Qian[2], Junwei Ma[2], Lei Cui[2] and Chunju Li[*1,2]

Full Research Paper

Open Access

Address:
[1]School of Chemical and Environmental Engineering, Shanghai Institute of Technology, 100 Hai-Quan Road, Shanghai 201418, P. R. China and [2]Department of Chemistry, Center for Supramolecular Chemistry and Catalysis, Shanghai University, Shanghai 200444, P. R. China

Email:
Xinghua Zhang[*] - xhzhang@sit.edu.cn; Chunju Li[*] - cjli@shu.edu.cn

* Corresponding author

Keywords:
berberine; biphenarenes; host–guest complexes; molecular recognition; palmatine

Beilstein J. Org. Chem. **2018,** *14,* 2236–2241.
doi:10.3762/bjoc.14.198

Received: 01 May 2018
Accepted: 15 August 2018
Published: 27 August 2018

This article is part of the thematic issue "Macrocyclic and supramolecular chemistry".

Guest Editor: M.-X. Wang

Abstract

A water-soluble 2,2′-biphen[4]arene (2,2'-CBP4) containing eight carboxylato moieties was synthesized and characterized. Its complexation behavior towards two alkaloids, palmatine (**P**) and berberine (**B**), was investigated by means of fluorescence and ^{1}H NMR spectroscopy in aqueous phosphate buffer solution (pH 7.4). In the presence of 2,2'-CBP4, ^{1}H NMR signals of **P** and **B** displayed very large upfield shifts, indicating the formation of inclusion complexes with strong binding affinities. Fluorescence titration experiments showed that **P** and **B** exhibited dramatic fluorescence enhancement of more than 600 times upon complexation with 2,2'-CBP4. Particularly, the fluorescence intensity is strong enough to be readily distinguished by the naked eye. Although the two guests have similar structures, the association constant of **B** with 2,2'-CBP4 (K_a = (2.29 ± 0.27) × 10^6 M^{-1}) is 3.9 times larger than that of **P** (K_a = (5.87 ± 0.24) × 10^5 M^{-1}).

Introduction

Host–guest chemistry in water is significantly important due to its extensive applications in biology, medicine, and environment. Cyclodextrins [1-4], cucurbiturils [5-11], and calixarenes [12-20] have been widely used in aqueous supramolecular chemistry. In the past ten years, the chemistry of pillar[*n*]arenes has developed very quickly because of their specific structures and interesting host–guest properties [21-32]. Water-soluble pillar[*n*]arene derivatives, especially those containing carboxyl-

ato moieties, showed low cell toxicity and good biocompatibility, and have been applied in biomedical applications such as bioimaging and self-assembled drug delivery systems [33-40]. For example, our group demonstrated a direct host–guest complexation-based drug delivery system for oxaliplatin by carboxylatopillar[6]arene [36]. The encapsulation could not only improve the drug's stability in the blood stream, but also be effectively dis-assembled in the acidic tumor environment, and thus improve the anticancer activity of oxaliplatin in vivo.

In 2015, we introduced a new class of macrocyclic arenes, 4,4'-biphen[*n*]arenes (*n* = 3,4) with 4,4'-biphenol or 4,4'-biphenol ether monomers linked by $-CH_2-$ bridges [41], which have received much attention due to their convenient synthesis and modification method, novel topological structures and excellent cavity host–guest properties [41-46]. In 2017, another type of biphen[*n*]arenes with 2,2'-disubstituted biphenyl units, 2,2'-biphen[*n*]arenes (*n* = 4–8), have been designed and synthesized [47].

To date, the complexation of biological and pharmaceutical molecules by biphen[*n*]arenes in water have not been reported. In this work, we wish to report the synthesis of the first water-soluble 2,2'-biphen[4]arene bearing multiple carboxylato moieties, 2,2'-CBP4 (Scheme 1), and its binding behavior and fluorescent spectrum characteristic towards two alkaoilds, palmatine (**P**) and berberine (**B**), in water solution. In particular, the fluorescence intensities of the two guests have been considerably enhanced after complexation. As a member of isoquinoline alkaloids' family, **P** and **B** can produce singlet oxygen ($^1O_2$) and oxide biological substrates under light, and thereby have applications in photodynamic therapy (PDT) [48-50]. However, their low quantum yields limit such applications, which could be potentially improved or restored by the present encapsulation-induced fluorescence enhancement.

Results and Discussion

Synthesis

Scheme 1 shows the synthetic route of 2,2'-CBP4 [51], which is very similar with the procedure of water-soluble 4,4'-biphenarene [46]. Perhydroxylated 2,2'-biphen[4]arene, (2,2'-OHBP4) with hydroxy reaction sites was quantitatively prepared by the deprotection of 2,2'-OEtBP4 using excess BBr_3. The nucleophilic substitution reaction of 2,2'-OHBP4 and ethyl

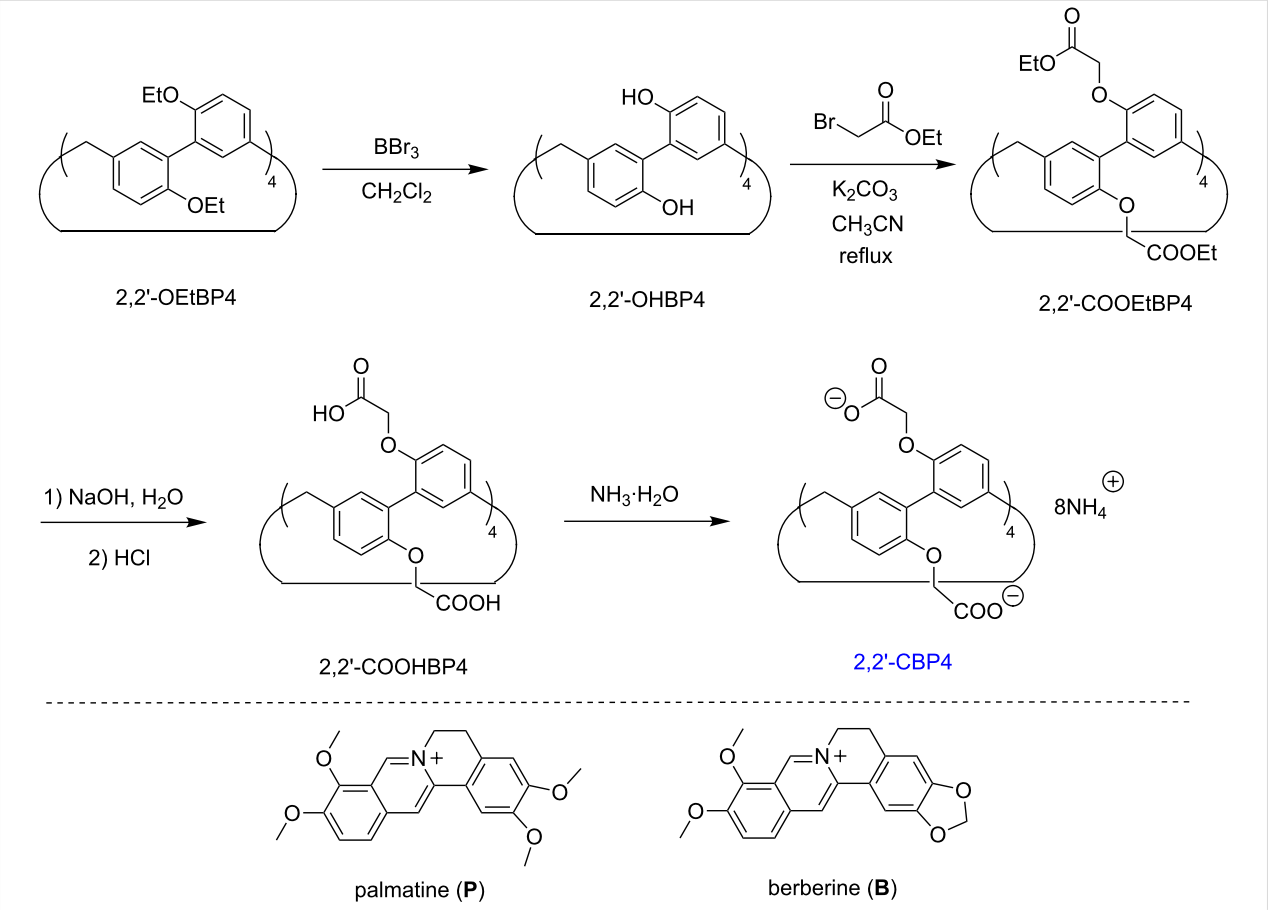

Scheme 1: Synthesis of 2,2'-CBP4 and the chemical structures of **P** and **B**.

bromoacetate, K_2CO_3 as the base, afforded 2,2'-COOEtBP4 in 88% yield. The hydrolysis of 2,2'-COOEtBP4 in NaOH solution and then acidification with HCl yielded 2,2'-COOHBP4 in a high yield of 87%. Water soluble 2,2'-CBP4 was quantitavely prepared by the acid-base reaction of 2,2'-COOHBP4 and aqueous ammonia solution. The total yield is up to 77%. As expected, 2,2'-CBP4 has a very good solubility (≥10 mM) in water.

^{1}H NMR spectra

^{1}H NMR experiments of **P** and **B** with 2,2'-CBP4 in deuterated phosphate buffer (pD 7.4) were carried out to examine the host–guest complexation (Figure 1 and Figure S9 in Supporting Information File 1). From Figure 1, upon addition of the host, all the peaks of alkaloid **B** displayed upfield shifts and broadening compared with the free guest. Especially, the chemical shifts for the middle protons, H1–6, and H10–11, are larger than those for the ending H7–9. These results indicate that berberine was engulfed by the cavity of 2,2'-CBP4 to form a pseudorotaxane-type inclusion complex. Similar complexation-induced NMR changes were observed for the host–guest mixture of **P** and 2,2'-CBP4 (Supporting Information File 1, Figure S9), suggesting a similar binding mode of an inclusion complex.

The host–guest encapsulation was then confirmed by 2D NOESY experiments, as shown in Figures S10 and S11, Supporting Information File 1. For example, in the 2D NOESY spectra of host–guest mixture of 2,2'-CBP4 and **B**, NOE correlations were clearly observed between the middle protons H1 and H10 of **B** with the methylene H_c of 2,2'-CBP4, and between the aromatic protons (H_b) of 2,2'-CBP4 and H2 of **B** (Supporting Information File 1, Figure S11).

To examine the fluorecence behavior and to quantitatively assess the complexation of the two alkaloids and 2,2'-CBP4, spectral titrations of **P**/**B** and 2,2'-CBP4 were performed in the phosphate buffer solution of pH 7.4 at 298 K. As can be seen from Figure 2 and Supporting Information File 1, Figure S10, compounds **P** and **B** alone only displayed fairly feeble fluorescence emission. Upon addition of 2,2'-CBP4, the fluorescence intensity was remarkably improved more than 600 times (Figure 2 and Supporting Information File 1, Figure S10). This was due to the effect of lowering polar microenvironment when **P** or **B** was included by 2,2'-CBP4; the guest emits stronger fluorescence in a more hydrophobic microenvironment [48]. Combined with NMR results, we can unambiguously conclude the alkaloid molecules must insert into the hydrophobic cavity of 2,2'-CBP4 to form inclusion complexes. Interestingly, the emission intensities can be easily identified by the naked eye under UV light of 365 nm. As can be seen from Figure 3, **P**, **B** and 2,2'-CBP4 alone are almost nonfluorescent; the host–guest mixture shows very strong yellow fluorescence.

Through analyzing the sequential changes about fluorescence intensity (ΔF) of guest that occurred with changes in host concentration, the association constants (K_a) could be calculated. The complexation stoichiometry for each binding event was de-

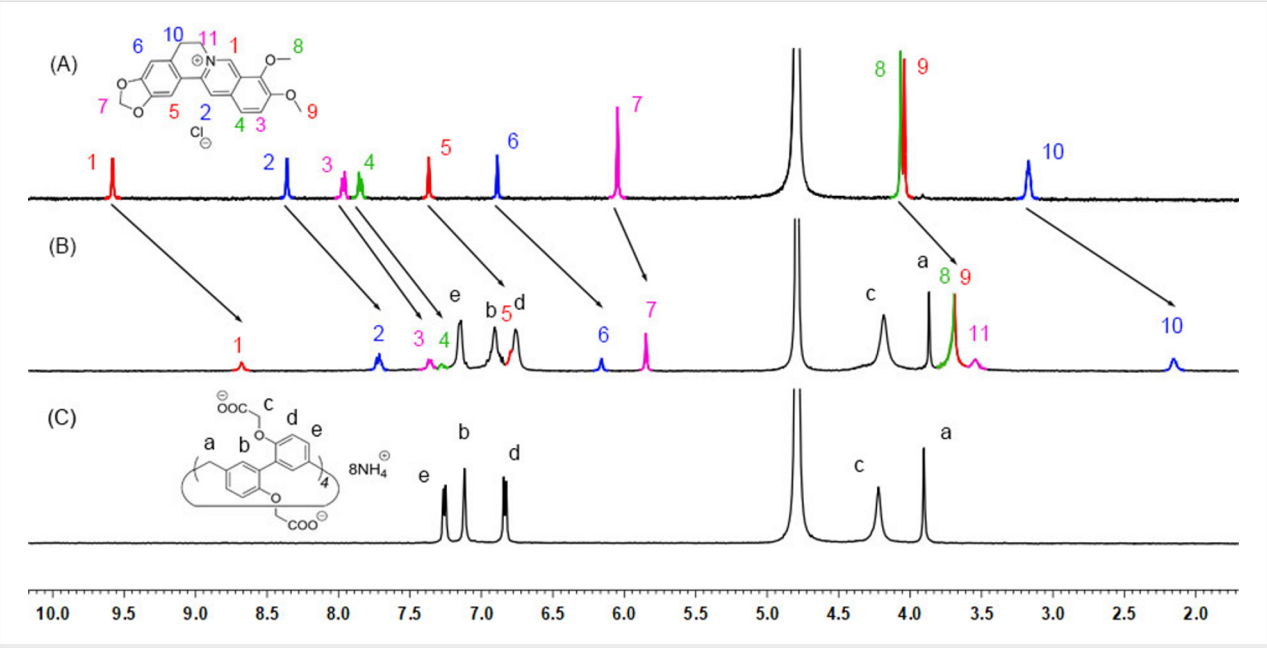

Figure 1: ^{1}H NMR spectra (500 MHz, 293 K) of (A) **B** (2.0 mM), (B) **B** (2.0 mM) + 2,2'-CBP4 (2.0 mM) and (C) 2,2'-CBP4 (2.0 mM) in deuterated phosphate buffer (pD 7.4).

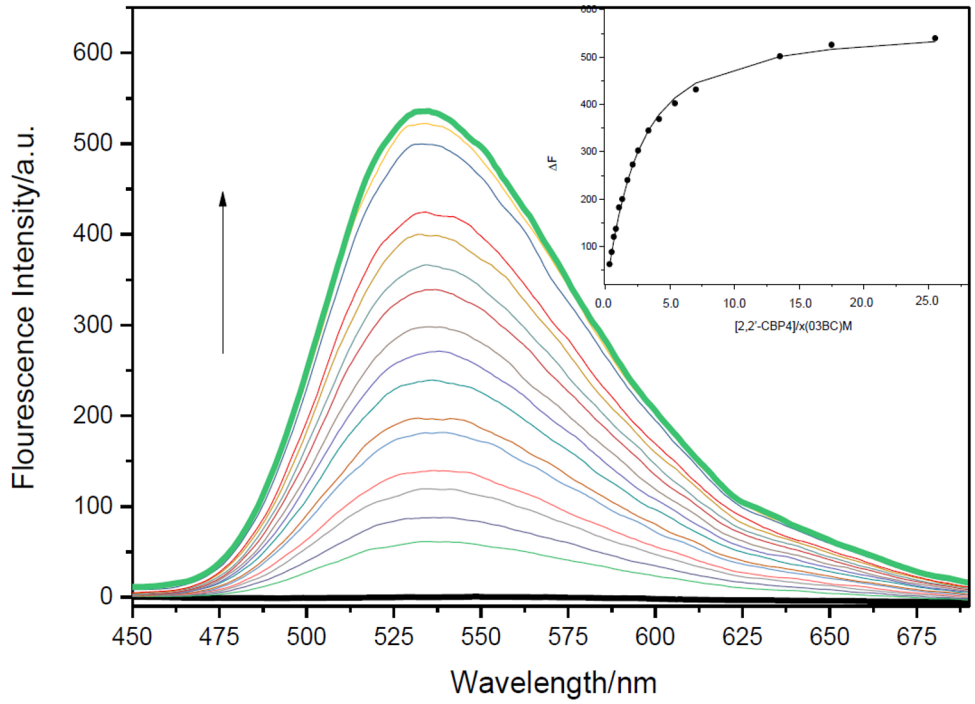

Figure 2: Fluorescence spectra of **P** in the absence and presence of 2,2'-CBP4 in aqueous phosphate buffer solution at pH 7.4 at 298 K. The excitation wavelength is at 352.0 nm. Inset: the nonlinear least-squares analysis to calculate the association constant using the fluorescence emission at 530 nm.

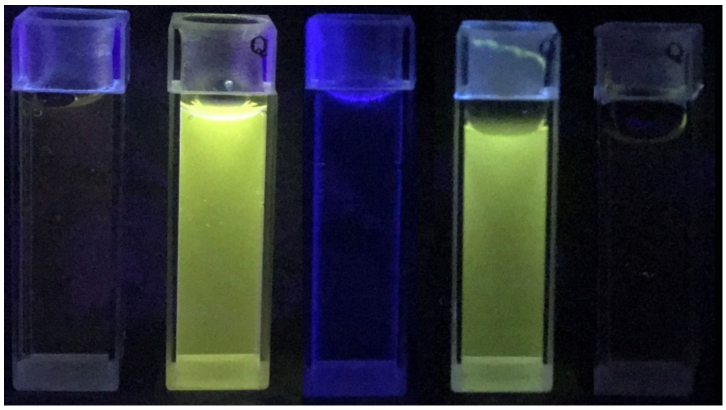

Figure 3: Visible emission observed from samples of **P** and **B** in the absence and presence of 2,2'-CBP4 under a UV lamp (365 nm). Left to right: **P**, **P** + 2,2'-CBP4, 2,2'-CBP4, **B** + 2,2'-CBP4 and **B**.

termined to be 1:1 by Job plot analysis (Supporting Information File 1, Figures S13 and S14). The nonlinear least-squares curve-fitting method was used to analysis. For each host–guest pair, an excellent fit with an R value larger than 0.99 was obtained. It was found that 2,2'-CBP4 formed stable complexes with the two positively charged alkaloids, giving K_a values of $(5.87 \pm 0.24) \times 10^5$ M^{-1} and $(2.29 \pm 0.27) \times 10^6$ M^{-1} for **P** and **B**, respectively. π···π interactions, hydrophobic interactions and electrostatic attractions should play important roles in the association process. Although having similar structures, these two guests gave very different association constants. The substitution of 1,3-dioxole for two methoxy groups in **P**, affording **B**, considerably increases the K_a value of 3.9 times (Table 1). One possible reason is that the size of **B** with 1,3-dioxole, smaller than that for **P** with two methoxy groups, matches better with the cavity of 2,2'-CBP4.

Table 1: Association constants (K_a/M^{-1}) for 1:1 intermolecular complexation of **P** and **B** with 2,2'-CBP4 in phosphate buffer solution (pH 7.4) at 298 K.

host	guest	K_a [M^{-1}]	Ex [nm]	Em [nm]
2,2'-CBP4	**P**	(5.87 ± 0.24) × 10^5	352	533
2,2'-CBP4	**B**	(2.29 ± 0.27) × 10^6	352	530

Conclusion

In summary, we have synthesized a water-soluble 2,2'-biphen[4]arene, 2,2'-CBP4, for the first time and studied its complexation towards two alkaloid guests, **P** and **B**. ^{1}H NMR and fluorescence results indicate the formation of inclusion complexes with strong stability. The association constants are in the magnitude of 10^5–10^6 M^{-1}. Upon complexation with 2,2'-CBP4, both alkaloid guests exhibit a significant fluorescence intensity enhancement and the intensity is strong enough to be distinguished by the naked eye. The easy accessibility, good water-solubility and nice binding properties make 2,2'-CBP4 be applicable in the biomedical field, for example, chemical sensors, drug delivery, supramolecular amphiphiles, etc.

Experimental

2,2'-OEtBP4 was synthesized according to our previously reported method [47]. **P** and **B** were purchased from Shanghai Aladdin Bio-Chem Technology Co.,LTD. ^{1}H NMR and ^{13}C NMR spectra were recorded on a Bruker AV500 instrument. The fluorescence emission spectra were determined with a SHIMADZU RF5301 spectrometer. Deuterated phosphate buffer solutions (20 mM) of pD 7.4 for ^{1}H NMR experiments were prepared by mixing K_2DPO_4 deuterium oxide solution (20 mM) and KD_2PO_4 deuterium oxide solution (20 mM) according to the calculated volume ratios. The pH/pD values of the buffer solutions were verified on a pH-meter calibrated with two standard buffer solutions.

Supporting Information

Supporting Information File 1

Experimental details and the ^{1}H and ^{13}C NMR spectra of 2,2'-biphen[4]arene derivatives, additional ^{1}H NMR spectra of host–guest mixture, job plots, and the determination of the association constants.
[https://www.beilstein-journals.org/bjoc/content/supplementary/1860-5397-14-198-S1.pdf]

Acknowledgements

This work was supported by the National Natural Science Foundation of China (21472122 and 21772118), the Shanghai "Pujiang Program" (16PJD024), and the "Shuguang Program" of the Shanghai Education Development Foundation and Shanghai Municipal Education Commission.

References

1. Harada, A.; Hashidzume, A.; Yamaguchi, H.; Takashima, Y. *Chem. Rev.* **2009,** *109,* 5974–6023. doi:10.1021/cr9000622
2. Chen, Y.; Liu, Y. *Chem. Soc. Rev.* **2010,** *39,* 495–505. doi:10.1039/B816354P
3. Nepogodiev, S. A.; Stoddart, J. F. *Chem. Rev.* **1998,** *98,* 1959–1976. doi:10.1021/cr970049w
4. Liao, X.-J.; Chen, G.-S. *Chin. Chem. Lett.* **2016,** *27,* 583–587. doi:10.1016/j.cclet.2016.02.022
5. Walker, S.; Oun, R.; McInnes, F. J.; Wheate, N. J. *Isr. J. Chem.* **2011,** *51,* 616–624. doi:10.1002/ijch.201100033
6. Ma, D.; Hettiarachchi, G.; Nguyen, D.; Zhang, B.; Wittenberg, J. B.; Zavalij, P. Y.; Briken, V.; Isaacs, L. *Nat. Chem.* **2012,** *4,* 503–510. doi:10.1038/nchem.1326
7. Lazar, A. I.; Biedermann, F.; Mustafina, K. R.; Assaf, K. I.; Hennig, A.; Nau, W. M. *J. Am. Chem. Soc.* **2016,** *138,* 13022–13029. doi:10.1021/jacs.6b07655
8. Li, C.; Li, J.; Jia, X. *Org. Biomol. Chem.* **2009,** *7,* 2699–2703. doi:10.1039/b820852b
9. Chen, Y.; Huang, Z.; Zhao, H.; Xu, J.-F.; Sun, Z.; Zhang, X. *ACS Appl. Mater. Interfaces* **2017,** *9,* 8602–8608. doi:10.1021/acsami.7b01157
10. Murray, J.; Kim, K.; Ogoshi, T.; Yao, W.; Gibb, B. C. *Chem. Soc. Rev.* **2017,** *46,* 2479–2496. doi:10.1039/C7CS00095B
11. Wu, W.; Song, S.; Cui, X.; Sun, T.; Zhang, J.-X.; Ni, X.-L. *Chin. Chem. Lett.* **2018,** *29,* 95–98. doi:10.1016/j.cclet.2017.08.049
12. Gutsche, C. D. *Acc. Chem. Res.* **1983,** *16,* 161–170. doi:10.1021/ar00089a003
13. Guo, D.-S.; Uzunova, V. D.; Su, X.; Liu, Y.; Nau, W. M. *Chem. Sci.* **2011,** *2,* 1722–1734. doi:10.1039/c1sc00231g
14. Zhang, G.-W.; Li, P.-F.; Meng, Z.; Wang, H.-X.; Han, Y.; Chen, C.-F. *Angew. Chem., Int. Ed.* **2016,** *55,* 5304–5308. doi:10.1002/anie.201600911
15. Jia, F.; He, Z.; Yang, L.-P.; Pan, Z.-S.; Yi, M.; Jiang, R.-W.; Jiang, W. *Chem. Sci.* **2015,** *6,* 6731–6738. doi:10.1039/C5SC03251B
16. Guo, Q.-H.; Fu, Z.-D.; Zhao, L.; Wang, M.-X. *Angew. Chem., Int. Ed.* **2014,** *53,* 13548–13552. doi:10.1002/anie.201407670
17. Guo, Q.-H.; Zhao, L.; Wang, M.-X. *Angew. Chem., Int. Ed.* **2015,** *54,* 8386–8389. doi:10.1002/anie.201503179
18. Li, C.; Xu, Q.; Li, J.; Jia, X. *J. Inclusion Phenom. Macrocyclic Chem.* **2009,** *64,* 37–42. doi:10.1007/s10847-009-9533-x
19. Megyesi, M.; Biczók, L. *Chem. Phys. Lett.* **2006,** *424,* 71–76. doi:10.1016/j.cplett.2006.04.016
20. Xiao, T.; Wang, L. *Tetrahedron Lett.* **2018,** *59,* 1172–1182. doi:10.1016/j.tetlet.2018.02.028
21. Ogoshi, T.; Kanai, S.; Fujinami, S.; Yamagishi, T.-a.; Nakamoto, Y. *J. Am. Chem. Soc.* **2008,** *130,* 5022–5023. doi:10.1021/ja711260m
22. Wanderlind, E. H.; Liz, D. G.; Gerola, A. P.; Affeldt, R. F.; Nascimento, V.; Bretanha, L. C.; Montecinos, R.; Garcia-Rio, L.; Fiedler, H. D.; Nome, F. *ACS Catal.* **2018,** *8,* 3343–3347. doi:10.1021/acscatal.8b00901
23. Yang, K.; Pei, Y.; Wen, J.; Pei, Z. *Chem. Commun.* **2016,** *52,* 9316–9326. doi:10.1039/C6CC03641D
24. Ji, X.-F.; Xia, D.-Y.; Yan, X.; Wang, H.; Huang, F.-H. *Acta Polym. Sin.* **2017,** 9–18.

25. Jiang, B.; Wang, W.; Zhang, Y.; Lu, Y.; Zhang, C.-W.; Yin, G.-Q.; Zhao, X.-L.; Xu, L.; Tan, H.; Li, X.; Jin, G.-X.; Yang, H.-B. *Angew. Chem., Int. Ed.* **2017,** *56,* 14438–14442. doi:10.1002/anie.201707209
26. Jie, K.; Liu, M.; Zhou, Y.; Little, M. A.; Bonakala, S.; Chong, S. Y.; Stephenson, A.; Chen, L.; Huang, F.; Cooper, A. I. *J. Am. Chem. Soc.* **2017,** *139,* 2908–2911. doi:10.1021/jacs.6b13300
27. Strutt, N. L.; Zhang, H.; Schneebeli, S. T.; Stoddart, J. F. *Acc. Chem. Res.* **2014,** *47,* 2631–2642. doi:10.1021/ar500177d
28. Wang, Y.; Ping, G.; Li, C. *Chem. Commun.* **2016,** *52,* 9858–9872. doi:10.1039/C6CC03999E
29. Li, C.; Zhao, L.; Li, J.; Ding, X.; Chen, S.; Zhang, Q.; Yu, Y.; Jia, X. *Chem. Commun.* **2010,** *46,* 9016–9018. doi:10.1039/c0cc03575k
30. Nierengarten, I.; Nothisen, M.; Sigwalt, D.; Biellmann, T.; Holler, M.; Remy, J.-S.; Nierengarten, J.-F. *Chem. – Eur. J.* **2013,** *19,* 17552–17558. doi:10.1002/chem.201303029
31. Li, Z.-Y.; Zhang, Y.; Zhang, C.-W.; Chen, L.-J.; Wang, C.; Tan, H.; Yu, Y.; Li, X.; Yang, H.-B. *J. Am. Chem. Soc.* **2014,** *136,* 8577–8589. doi:10.1021/ja413047r
32. Si, W.; Xin, P.; Li, Z.-T.; Hou, J.-L. *Acc. Chem. Res.* **2015,** *48,* 1612–1619. doi:10.1021/acs.accounts.5b00143
33. Zhang, H.; Ma, X.; Nguyen, K. T.; Zhao, Y. *ACS Nano* **2013,** *7,* 7853–7863. doi:10.1021/nn402777x
34. Chi, X.; Ji, X.; Xia, D.; Huang, F. *J. Am. Chem. Soc.* **2015,** *137,* 1440. doi:10.1021/ja512978n
35. Cao, Y.; Li, Y.; Hu, X.-Y.; Zou, X.; Xiong, S.; Lin, C.; Wang, L. *Chem. Mater.* **2015,** *27,* 1110–1119. doi:10.1021/cm504445r
36. Li, B.; Meng, Z.; Li, Q.; Huang, X.; Kang, Z.; Dong, H.; Chen, J.; Sun, J.; Dong, Y.; Li, J.; Jia, X.; Sessler, J. L.; Meng, Q.; Li, C. *Chem. Sci.* **2017,** *8,* 4458–4464. doi:10.1039/C7SC01438D
37. Ping, G.; Wang, Y.; Shen, L.; Wang, Y.; Hu, X.; Chen, J.; Hu, B.; Cui, L.; Meng, Q.; Li, C. *Chem. Commun.* **2017,** *53,* 7381–7384. doi:10.1039/C7CC02799K
38. Yu, G.; Yu, W.; Shao, L.; Zhang, Z.; Chi, X.; Mao, Z.; Gao, C.; Huang, F. *Adv. Funct. Mater.* **2016,** *26,* 8999–9008. doi:10.1002/adfm.201601770
39. Sathiyajith, C.; Shaikh, R. R.; Han, Q.; Zhang, Y.; Meguellati, K.; Yang, Y.-W. *Chem. Commun.* **2017,** *53,* 677–696. doi:10.1039/C6CC08967D
40. Li, C.; Ma, J.; Zhao, L.; Zhang, Y.; Yu, Y.; Shu, X.; Li, J.; Jia, X. *Chem. Commun.* **2013,** *49,* 1924–1926. doi:10.1039/c3cc38622h
41. Chen, H.; Fan, J.; Hu, X.; Ma, J.; Wang, S.; Li, J.; Yu, Y.; Jia, X.; Li, C. *Chem. Sci.* **2015,** *6,* 197–202. doi:10.1039/C4SC02422B
42. Ma, J.; Deng, H.; Ma, S.; Li, J.; Jia, X.; Li, C. *Chem. Commun.* **2015,** *51,* 6621–6624. doi:10.1039/C5CC01470K
43. Zhou, J.; Yu, G.; Shao, L.; Hua, B.; Huang, F. *Chem. Commun.* **2015,** *51,* 4188–4191. doi:10.1039/C5CC00225G
44. Lande, D. N.; Rao, S. S.; Gejji, S. P. *ChemPhysChem* **2016,** *17,* 2197–2209. doi:10.1002/cphc.201600186
45. Zhou, J.; Yang, J.; Hua, B.; Shao, L.; Zhang, Z.; Yu, G. *Chem. Commun.* **2016,** *52,* 1622–1624. doi:10.1039/C5CC09088A
46. Ma, J.; Meng, Q.; Hu, X.; Li, B.; Ma, S.; Hu, B.; Li, J.; Jia, X.; Li, C. *Org. Lett.* **2016,** *18,* 5740–5743. doi:10.1021/acs.orglett.6b03005
47. Dai, L.; Ding, Z.-J.; Cui, L.; Li, J.; Jia, X.; Li, C. *Chem. Commun.* **2017,** *53,* 12096–12099. doi:10.1039/C7CC06767D
48. Flors, C.; Nonell, S. *Acc. Chem. Res.* **2006,** *39,* 293–300. doi:10.1021/ar0402863
49. Hirakawa, K.; Kawanishi, S.; Hirano, T. *Chem. Res. Toxicol.* **2005,** *18,* 1545–1552. doi:10.1021/tx0501740
50. Inbaraj, J. J.; Kukielczak, B. M.; Bilski, P.; Sandvik, S. L.; Chignell, C. F. *Chem. Res. Toxicol.* **2001,** *14,* 1529–1534. doi:10.1021/tx0155247
51. Dai, L.; Li, C.; Jia, X. China Patent CN107245028A, 2017.

License and Terms

BEILSTEIN JOURNAL OF ORGANIC CHEMISTRY

Coordination-driven self-assembly of discrete Ru_6–Pt_6 prismatic cages

Aderonke Ajibola Adeyemo and Partha Sarathi Mukherjee*§

Full Research Paper

Open Access

Address:
Department of Inorganic and Physical Chemistry, Indian Institute of Science, Bangalore 560 012, India

Email:
Partha Sarathi Mukherjee* - psm@iisc.ac.in

* Corresponding author
§ Tel.: +91-80-22933352; Fax: +91-80-23601552

Keywords:
arene–ruthenium(II); heterometallic cages; platinum metalloligand; self-assembly; supramolecular architectures

Beilstein J. Org. Chem. **2018,** *14,* 2242–2249.
doi:10.3762/bjoc.14.199

Received: 27 April 2018
Accepted: 14 August 2018
Published: 27 August 2018

This article is part of the thematic issue "Macrocyclic and supramolecular chemistry".

Guest Editor: M.-X. Wang

Abstract

The coordination-driven self-assembly of two new Ru_6–Pt_6 hexanuclear trigonal prismatic cages comprising arene–ruthenium(II) clips (**1a(NO$_3$)$_2$** and **1b(NO$_3$)$_2$**) and a tritopic platinum(II) metalloligand **2** has been performed in methanol at room temperature. The [3 + 2] hexanuclear cages **3a** and **3b** were isolated in good yields and characterized by well-known spectroscopic techniques including multinuclear NMR, mass spectrometry, UV–vis and infrared studies. Geometry optimization revealed the shapes and sizes of these hexanuclear prismatic cages. The combination of ruthenium and platinum metal center in a one-pot self-assembly reaction showcases the construction of aesthetically elegant heterometallic structures in supramolecular chemistry leading to the formation of a single major product.

Introduction

Coordination-driven self-assembly of discrete architectures has evolved as a unique protocol to construct elegant supramolecular architectures of different shapes, sizes and functionalities over the last two decades [1-23]. These 2D and 3D-supramolecular architectures mostly comprise pure organic ligands as electron-rich donors and transition metals as electron-deficient acceptors. Diverse functionalities embedded in these homometallic architectures have found useful applications in chemical sensing [24-35], catalysis [11,36-46], drug delivery [47-51] and host–guest chemistry [52-56] among others. The cardinal prerequisites to obtain these self-assembled supramolecular architectures include stoichiometry and conformational complementarity on the binding sites of the building blocks [57-61]. However, the use of a single metal and a single organic ligand design may limit the structural diversity as well as the functionality of homometallic supramolecular architectures. In the last few years, enormous efforts have been channeled towards multicomponent self-assembly involving the construc-

tion of sophisticated heterobimetallic supramolecular architectures in a one-pot reaction and their functional properties are currently being explored [55,62-70]. The incorporation of two different metal centers in a supramolecular architecture can impart different functional properties arising from each of the metals and/or the organic components which is quite interesting.

The metalloligand synthetic approach has been efficiently used to achieve the construction of heterobimetallic supramolecular architectures in order to minimize the formation of two independent homometallic architectures or a mixture of products [71-78]. The metalloligand is a kinetically stable coordination complex with a metal center and one or more appended donor site(s) which can further coordinate to another metal center [79-83]. Such metalloligands are predesigned and encrypted with the desired functional properties before they are used in self-assembly reactions so as to induce the desired functional properties into the final supramolecular architecture [84-92]. Hence, the metalloligand becomes the electron-rich building block which offers structural rigidity while the second metal is the electron-acceptor building block. The facile self-assembly of 2D-heterobimetallic supramolecular architectures are well reported in the literature [24,93,94], however, 3D-heterobimetallic systems are still less explored [95-97].

Dinuclear arene–ruthenium(II) acceptor clips/building blocks have been extensively utilized in supramolecular chemistry because of their rigid directionality toward electron-rich donors due to their restricted coordination sites as a result of the fixed position of the *p*-cymene moiety [24,93,98-103]. Our group and others have contributed substantially to the chemistry of self-assembled homometallic ruthenium architectures and their applications [100,102-108]. In broadening this research scope, herein, we describe the coordination-driven self-assembly of two new Ru–Pt heterometallic prismatic cages **3a** and **3b** obtained from the reaction of two arene–ruthenium(II) clips **1a** and **1b** and tritopic platinum(II) metalloligand **2** in methanol/chloroform mixture in 3:2 ratio (Scheme 1). Both cages were fully characterized by ^{1}H, ^{31}P, ^{195}Pt, ^{1}H,^{1}H COSY, DOSY NMR, electrospray ionization mass spectrometry, and UV–vis analysis. Further structural insights were revealed by computational studies.

Results and Discussion

The triplatinum metalloligand **2** was synthesized through a four-step reaction involving a Sonogashira coupling (Scheme 2) and the crude product was purified by column chromatography to obtain **2** as a yellow powder. The three intermediates **A**, **B** and **C** were also characterized by ^{1}H, ^{31}P, ^{195}Pt and ^{13}C NMR analyses (see Supporting Information File 1, Figures S1–S8).

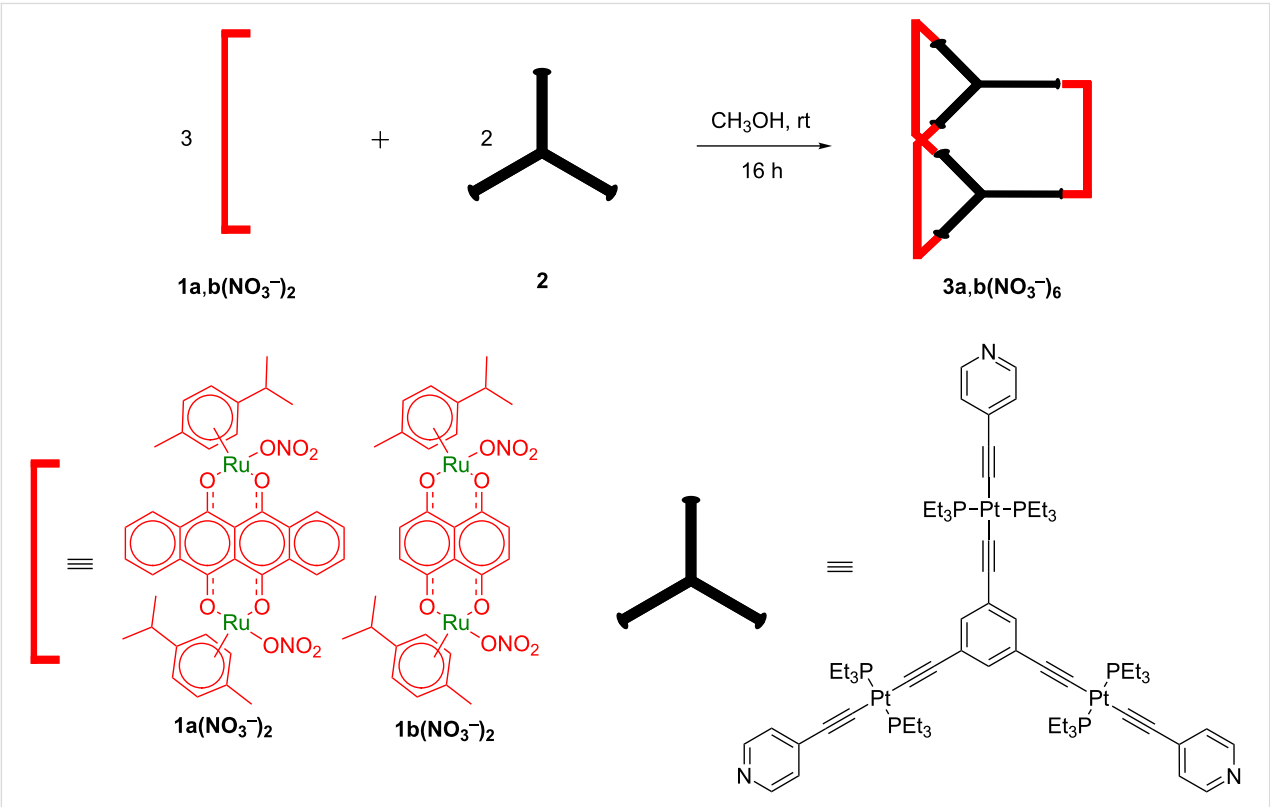

Scheme 1: Self-assembly of the heterometallic prismatic cages.

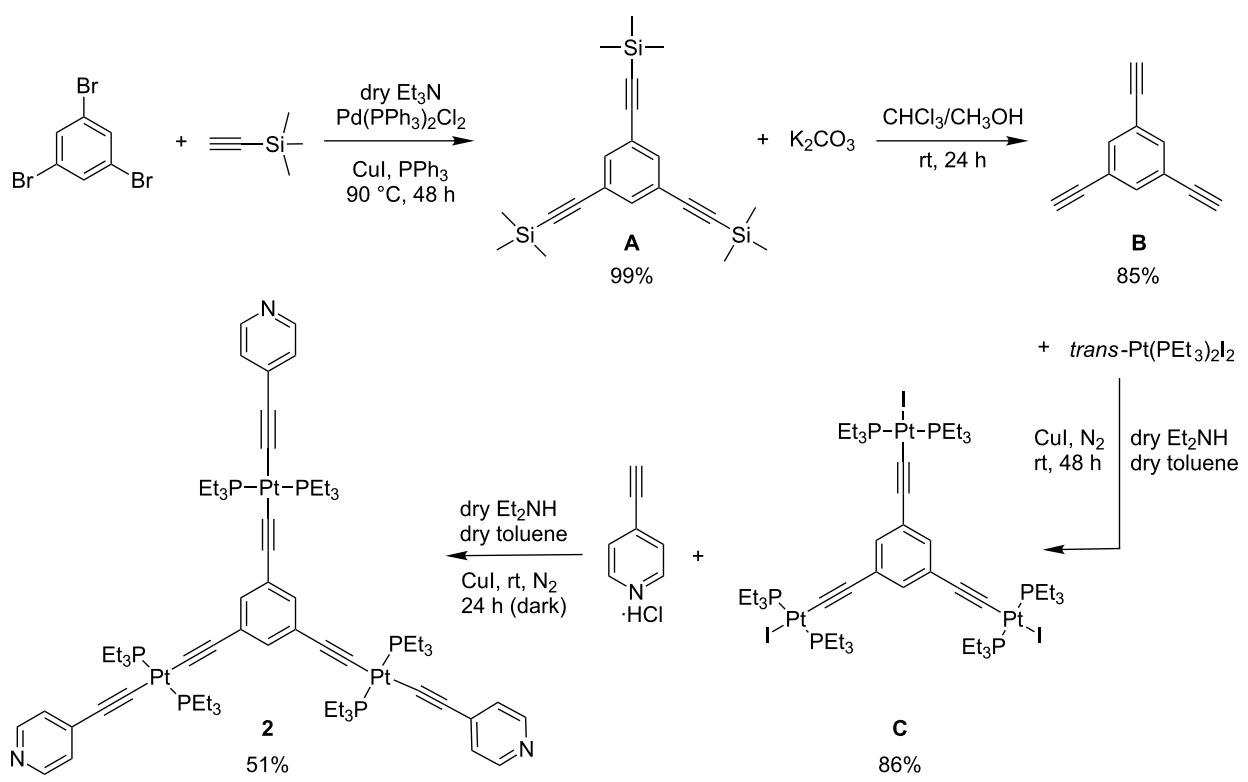

Scheme 2: Synthesis of the platinum metalloligand **2**.

The metalloligand **2** is highly soluble in dichloromethane and chloroform but only partially soluble in methanol and acetonitrile. The ^{1}H, ^{31}P, ^{195}Pt and ^{13}C NMR experiments (Supporting Information File 1, Figures S9–S12) and electrospray ionization mass spectrometry (ESIMS, Supporting Information File 1, Figure S13) of metalloligand **2** evidenced the formation of a pure compound. The ^{1}H NMR spectrum of **2** revealed two doublets and a singlet in the downfield region (8.38–6.99 ppm) corresponding to the pyridyl protons and the central phenyl protons, respectively, while the methylene and methyl protons in the upfield region of the spectrum are observed between 2.16–1.18 ppm (Supporting Information File 1, Figure S9). The ^{31}P NMR spectrum of **2** gave a singlet peak at 11.18 ppm shifting downfield after coordination with the ethynylpyridine moiety, while the singlet ^{195}Pt peak remained almost the same with the precursor compound **C** (Supporting Information File 1, Figure S12). The mass spectrum of **2** shows a $[\mathbf{2} + H]^+$ peak at *m*/*z* 1748.59 (Supporting Information File 1, Figure S13) which is in good agreement with the calculated value of 1748.71 based on the $C_{69}H_{105}N_3P_6Pt_3$ molecular formula.

Self-assembly and characterization of the heterometallic cages

The treatment of the dichloride analogues of **1a** and **1b** with 2.1 equivalents of silver nitrate in methanol at room temperature for 3 hours gave the dinuclear arene–ruthenium(II) clips **1a**,**1b(NO$_3$)$_2$**. As represented in Scheme 1, the self-assembly reactions of methanolic solutions of **1a**,**1b(NO$_3$)$_2$** and methanolic solution of the triplatinum metalloligand **2** at room temperature yielded the trigonal prismatic cages **3a** and **3b**. The heterometallic prismatic cages were isolated as nitrate complexes in good yields. The isolated cages are soluble in methanol, acetonitrile, acetone, nitromethane, dimethyl sulfoxide and partially soluble in chloroform and dichloromethane. The formation of these cages was ascertained by multinuclear NMR experiments and ESIMS analyses.

An upfield shift was observed in the pyridyl protons of cage **3b** as compared to the free triplatinum metalloligand **2** in their ^{1}H NMR spectra while cage **3a** exhibited a downfield shift in the pyridyl protons (Figure 1 and Supporting Information File 1, Figure S14). This chemical shift is due to the coordination of the pyridyl nitrogen atom to the ruthenium metal center while the upfield shift is due to the shielding effect of the methyl/methylene protons of the *p*-cymene moiety. In both cages studied, the aromatic protons of the *p*-cymene moiety in **3a** and **3b** were slightly shifted downfield while the isopropyl and methyl protons of the *p*-cymene moiety in all the cages remained almost unchanged as compared to the arene–ruthenium(II) clips **1a**,**1b(NO$_3$)$_2$**. Additionally, the protons of naph-

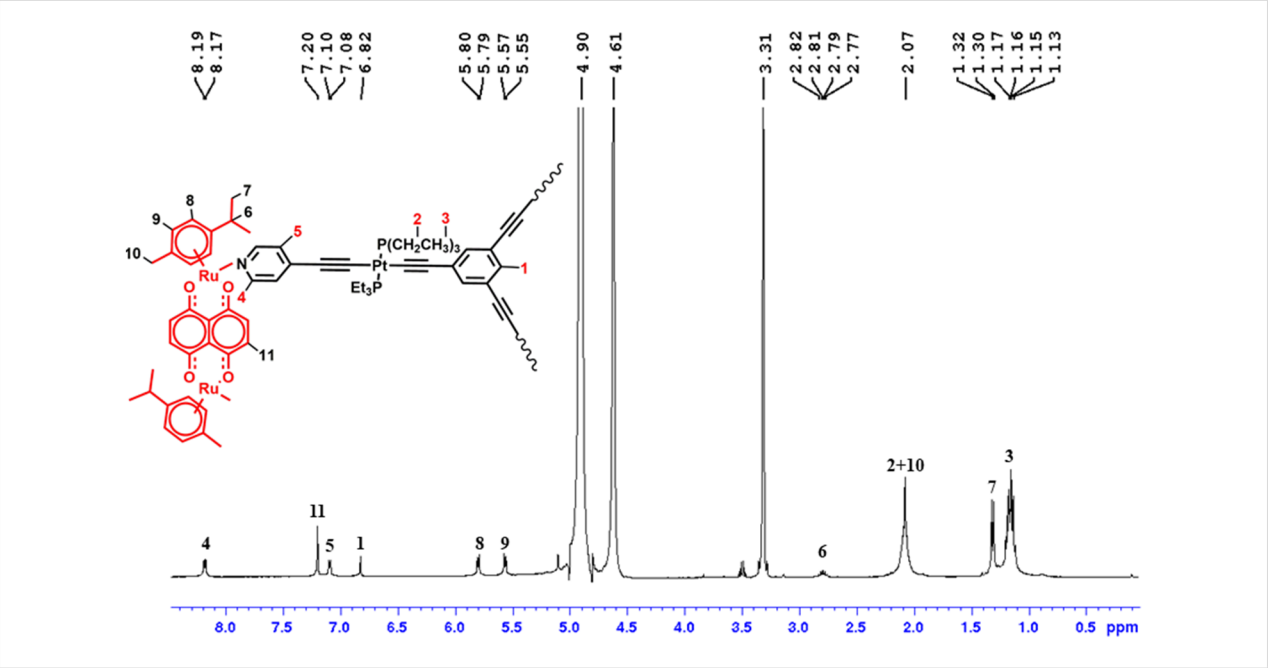

Figure 1: ^{1}H NMR of **3b** in CD_3OD.

thacenedione in **3a** and naphthaquinone in **3b** were not considerably shifted (Figure 1 and Supporting Information File 1, Figure S14). The appearance of a singlet peak in the ^{31}P NMR evidenced the formation of a single product and the fact that the phosphorus moieties are in the same chemical environment (Supporting Information File 1, Figures S15 and S16). The same observation is recorded for the ^{195}Pt NMR analyses of all the heterometallic cages (Supporting Information File 1, Figures S17 and S18).

The DOSY NMR experiments also confirmed the formation of a single product in all the cages with the hydrodynamic radii (r_H) of the heterometallic prismatic cages calculated from the Stokes–Einstein equation using the diffusion coefficients (D) obtained from the DOSY NMR experiments. The obtained values of D from the experiment are −9.631 log (m^2 s^{-1}) for **3a** and −9.567 log (m^2 s^{-1}) for **3b**, respectively. The calculated hydrodynamic radii (r_H) of **3a** and **3b** are 15.57 Å, and 13.43 Å, respectively (Supporting Information File 1, Figures S19 and S20). The ^{1}H,^{1}H COSY NMR spectra also showed the correlation between the protons of the arene–ruthenium(II) clips as well as the correlation between the protons within the metalloligand (Supporting Information File 1, Figures S19 and S20).

The vibrational symmetrical stretching frequency of the coordinated carbonyl groups (ν_{C-O}) in the dinuclear arene–ruthenium(II) clips **1a** and **1b** was found at 1536.16 cm^{-1} for **3a** and 1528.93 cm^{-1} for **3b** in the infrared spectra of the heterometallic cages while the vibrational symmetrical stretching frequency bands of =C–$H_{aromatic}$ showed strong stretching bands at 3074.07 cm^{-1} for **3a** and 3064.78 cm^{-1} for **3b**, respectively. Additionally, the stretching bands at 543.67 cm^{-1} for **3a** and 545.44 cm^{-1} for **3b** correspond to the ν_{Ru-O} symmetrical stretching frequency (Supporting Information File 1, Figure S21).

The UV–vis absorption spectra recorded in methanol at room temperature show intense bands at λ_{max} = 544, 514, 334, 290, 205 nm for **3a** and λ_{max} = 698, 644, 339, 204 nm for **3b**. The intense bands at 335 nm and 291 nm for **2** correspond to charge-transfer transitions, which shift slightly to shorter wavelengths in the spectra of the heterometallic prismatic cages. The peaks in the ranges of 514–698 nm and 204–339 nm can be assigned to intramolecular and intermolecular π–π* transitions and metal-to-ligand charge transfer (MLCT) transitions associated with capped *p*-cymene ruthenium cap, respectively. A hypochromic shift (decrease in absorption intensity) was also observed in the spectra of the heterometallic prismatic cages as compared to the metalloligand probably as a result of coordination of electron-rich metalloligand to the electron-deficient ruthenium center (Figure 2).

Mass spectrometry experiments also established the formation of the heterometallic prismatic cages in which all the cages maintain good stability. The ESIMS analysis of the [3 + 2] self-assembled heterometallic cages showed multiply charged fragmented ions for **3a** at m/z = 1473.83 $[\mathbf{3a}(NO_3^-)_2]^{4+}$, 1166.86 $[\mathbf{3a}(NO_3^-)]^{5+}$, 961.88 $[\mathbf{3a}]^{6+}$; **3b** at m/z = 1398.79

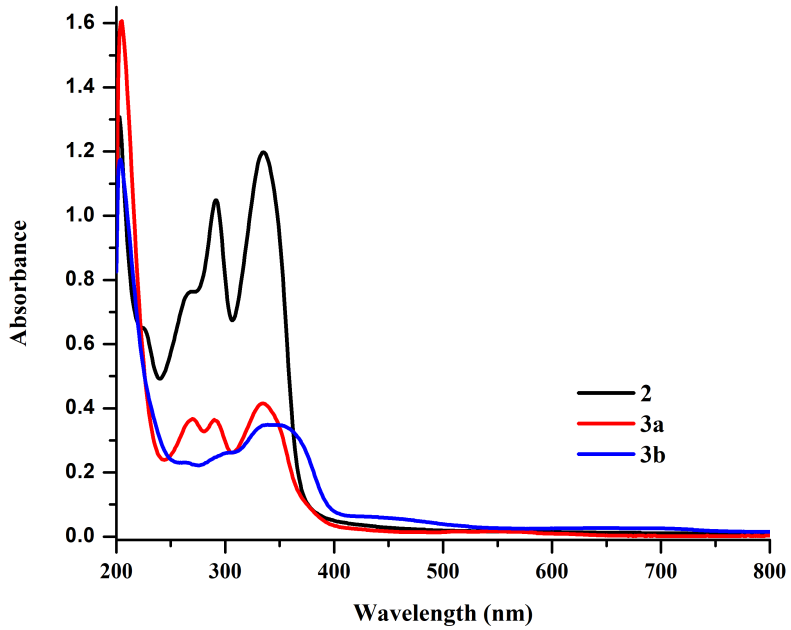

Figure 2: UV–vis spectra of the metalloligand **2** and heterometallic prismatic cages **3a** and **3b** in methanol (1.0×10^{-5} M) at 298 K.

$[\mathbf{3b}(NO_3^-)_2]^{4+}$, 1106.64 $[\mathbf{3b}(NO_3^-)]^{5+}$, 911.87 $[\mathbf{3b}]^{6+}$ and all peaks are well-resolved isotopically and matched with the theoretical isotopic distribution patterns (Figure 3 and Supporting Information File 1, Figure S22).

Geometry optimization of the heterometallic cages

All efforts to obtain single crystals of the prismatic cages were unsuccessful so far. Thus the structures of **3a** and **3b** were optimized to get insights into their structural features. The tritopic platinum(II) metalloligand was optimized using the B3LYP method while the heterometallic cage structures **3a** and **3b** were optimized with the semiempirical method using the PM6 basis set. The energy-minimized structures showed that cage **3a** has a dimension of 8.414 Å × 26.321 Å × 26.755 Å while cage **3b** has a dimension of 8.231 Å × 26.227 Å × 26.598 Å. The phenyl cores of the two triplatinum metalloligands are separated by a distance of 11.376 Å in **3a** and 11.456 Å in **3b**. The phenyl

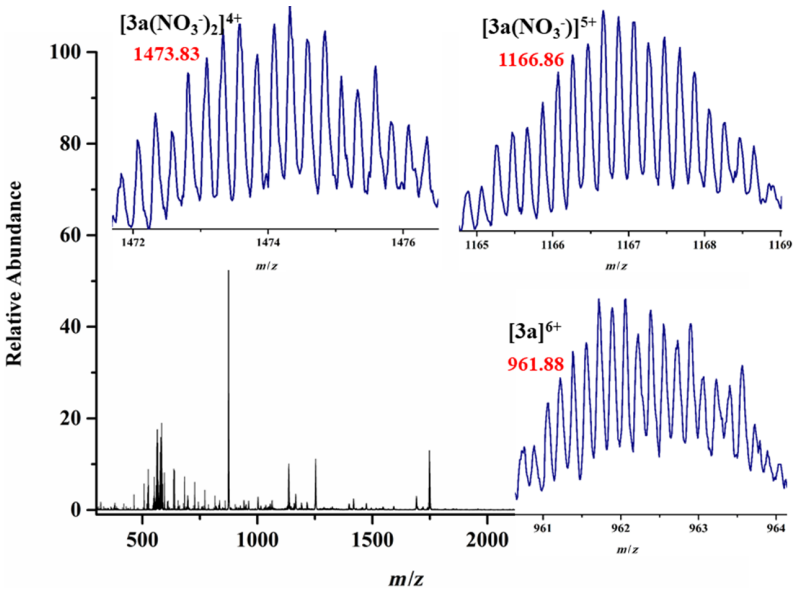

Figure 3: ESIMS spectrum of **3a** in methanol. Inset: experimentally observed isotopic distribution patterns of the charged fragments.

cores are slightly out-of-plane with regards to the pyridyl groups possibly as a result of steric influence upon metal–ligand coordination (Figure 4 and Supporting Information File 1, Figure S23).

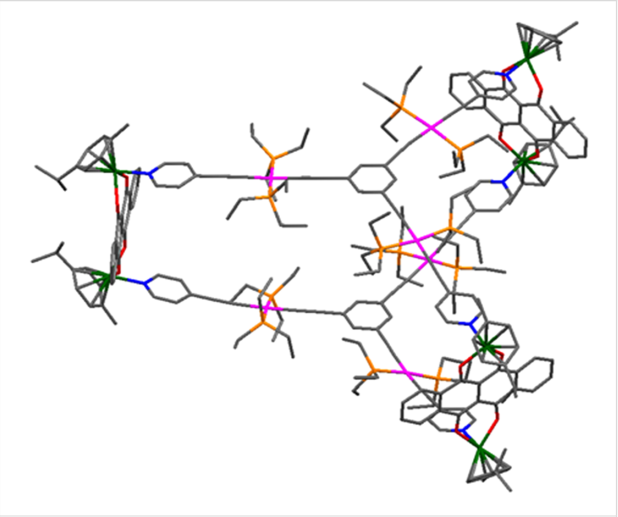

Figure 4: Energy-minimized structure of heterometallic trigonal prismatic cage **3a**. Hydrogen atoms are omitted for the sake of clarity [Ru: green, Pt: pink, O: red, N: blue, P: orange, C: grey].

Conclusion

The metalloligand synthetic approach has been utilized to synthesize heterobimetallic trigonal prismatic coordination cages **3a** and **3b** through the one-pot coordination-driven self-assembly of dinuclear arene–ruthenium(II) clips and a tritopic platinum(II) metalloligand. The formations of the [3 + 2] trigonal prismatic Ru–Pt cages are confirmed by multinuclear NMR and ESIMS studies. The optimized structures of cages **3a** and **3b** showed large prismatic cages composed of twelve metal centers comprising six ruthenium(II) and six platinum(II) metal centers thus showcasing how two different metal components can be incorporated to form a single framework architecture through a one-pot self-assembly strategy.

Supporting Information

Supporting Information File 1

Experimental procedures, multinuclear NMR spectra data, ESIMS data and infrared spectra of the hexanuclear trigonal prismatic cages.
[https://www.beilstein-journals.org/bjoc/content/supplementary/1860-5397-14-199-S1.pdf]

Acknowledgements

A.A.A. is grateful to IISc Bangalore for research fellowship. P.S.M. thanks the Department of Science and Technology (DST), India, for financial support. We acknowledge Mr Prodip Howlader's help for geometry optimization of the cages.

ORCID® iDs

Partha Sarathi Mukherjee - https://orcid.org/0000-0002-7425-7381

References

1. Lehn, J.-M. *Angew. Chem., Int. Ed. Engl.* **1990,** *29,* 1304–1319. doi:10.1002/anie.199013041
2. Lehn, J.-M. *Science* **1993,** *260,* 1762–1763. doi:10.1126/science.8511582
3. Harris, K.; Fujita, D.; Fujita, M. *Chem. Commun.* **2013,** *49,* 6703–6712. doi:10.1039/c3cc43191f
4. Saha, M. L.; Neogi, S.; Schmittel, M. *Dalton Trans.* **2014,** *43,* 3815–3834. doi:10.1039/C3DT53570C
5. Leininger, S.; Olenyuk, B.; Stang, P. J. *Chem. Rev.* **2000,** *100,* 853–908. doi:10.1021/cr9601324
6. Nehete, U. N.; Anantharaman, G.; Chandrasekhar, V.; Murugavel, R.; Walawalkar, M. G.; Roesky, H. W.; Vidovic, D.; Magull, J.; Samwer, K.; Sass, B. *Angew. Chem., Int. Ed.* **2004,** *43,* 3832–3835. doi:10.1002/anie.200453740
7. Lifschitz, A. M.; Rosen, M. S.; McGuirk, C. M.; Mirkin, C. A. *J. Am. Chem. Soc.* **2015,** *137,* 7252–7261. doi:10.1021/jacs.5b01054
8. Smulders, M. M. J.; Riddell, I. A.; Browne, C.; Nitschke, J. R. *Chem. Soc. Rev.* **2013,** *42,* 1728–1754. doi:10.1039/C2CS35254K
9. Newkome, G. R.; Moorefield, C. N. *Chem. Soc. Rev.* **2015,** *44,* 3954–3967. doi:10.1039/C4CS00234B
10. Safont-Sempere, M. M.; Fernández, G.; Würthner, F. *Chem. Rev.* **2011,** *111,* 5784–5814. doi:10.1021/cr100357h
11. Brown, C. J.; Toste, F. D.; Bergman, R. G.; Raymond, K. N. *Chem. Rev.* **2015,** *115,* 3012–3035. doi:10.1021/cr4001226
12. Northrop, B. H.; Chercka, D.; Stang, P. J. *Tetrahedron* **2008,** *64,* 11495–11503. doi:10.1016/j.tet.2008.08.062
13. Guillerm, V.; Kim, D.; Eubank, J. F.; Luebke, R.; Liu, X.; Adil, K.; Lah, M. S.; Eddaoudi, M. *Chem. Soc. Rev.* **2014,** *43,* 6141–6172. doi:10.1039/C4CS00135D
14. Ward, M. D.; Raithby, P. R. *Chem. Soc. Rev.* **2013,** *42,* 1619–1636. doi:10.1039/C2CS35123D
15. Amouri, H.; Desmarets, C.; Moussa, J. *Chem. Rev.* **2012,** *112,* 2015–2041. doi:10.1021/cr200345v
16. Han, Y.-F.; Jin, G.-X. *Acc. Chem. Res.* **2014,** *47,* 3571–3579. doi:10.1021/ar500335a
17. Stock, N.; Biswas, S. *Chem. Rev.* **2012,** *112,* 933–969. doi:10.1021/cr200304e
18. Wang, W.; Wang, Y.-X.; Yang, H.-B. *Chem. Soc. Rev.* **2016,** *45,* 2656–2693. doi:10.1039/C5CS00301F
19. Liu, Y.; Perez, L.; Mettry, M.; Easley, C. J.; Hooley, R. J.; Zhong, W. *J. Am. Chem. Soc.* **2016,** *138,* 10746–10749. doi:10.1021/jacs.6b05897
20. Chen, L.-J.; Chen, S.; Qin, Y.; Xu, L.; Yin, G.-Q.; Zhu, J.-L.; Zhu, F.-F.; Zheng, W.; Li, X.; Yang, H.-B. *J. Am. Chem. Soc.* **2018,** *140,* 5049–5052. doi:10.1021/jacs.8b02386
21. Huang, C.-B.; Xu, L.; Zhu, J.-L.; Wang, Y.-X.; Sun, B.; Li, X.; Yang, H.-B. *J. Am. Chem. Soc.* **2017,** *139,* 9459–9462. doi:10.1021/jacs.7b04659
22. Jiang, B.; Chen, L.-J.; Zhang, Y.; Tan, H.-W.; Xu, L.; Yang, H.-B. *Chin. Chem. Lett.* **2016,** *27,* 607–612. doi:10.1016/j.cclet.2016.03.017
23. Fu, T.-F.; Ao, L.; Gao, Z.-C.; Zhang, X.-L.; Wang, F. *Chin. Chem. Lett.* **2016,** *27,* 1147–1154. doi:10.1016/j.cclet.2016.06.054

24. Vajpayee, V.; Kim, H.; Mishra, A.; Mukherjee, P. S.; Stang, P. J.; Lee, M. H.; Kim, H. K.; Chi, K.-W. *Dalton Trans.* **2011,** *40,* 3112–3115. doi:10.1039/c0dt01481h
25. Mal, P.; Breiner, B.; Rissanen, K.; Nitschke, J. R. *Science* **2009,** *324,* 1697–1699. doi:10.1126/science.1175313
26. Riddell, I. A.; Smulders, M. M. J.; Clegg, J. K.; Nitschke, J. R. *Chem. Commun.* **2011,** *47,* 457–459. doi:10.1039/C0CC02573A
27. Yan, X.; Wang, H.; Hauke, C. E.; Cook, T. R.; Wang, M.; Saha, M. L.; Zhou, Z.; Zhang, M.; Li, X.; Huang, F.; Stang, P. J. *J. Am. Chem. Soc.* **2015,** *137,* 15276–15286. doi:10.1021/jacs.5b10130
28. Kumar, A.; Sun, S.-S.; Lees, A. J. *Coord. Chem. Rev.* **2008,** *252,* 922–939. doi:10.1016/j.ccr.2007.07.023
29. Chen, L.-J.; Ren, Y.-Y.; Wu, N.-W.; Sun, B.; Ma, J.-Q.; Zhang, L.; Tan, H.; Liu, M.; Li, X.; Yang, H.-B. *J. Am. Chem. Soc.* **2015,** *137,* 11725–11735. doi:10.1021/jacs.5b06565
30. Shanmugaraju, S.; Bar, A. K.; Chi, K.-W.; Mukherjee, P. S. *Organometallics* **2010,** *29,* 2971–2980. doi:10.1021/om100202c
31. Kang, S. O.; Llinares, J. M.; Day, V. W.; Bowman-James, K. *Chem. Soc. Rev.* **2010,** *39,* 3980–4003. doi:10.1039/c0cs00083c
32. Han, M.; Michel, R.; He, B.; Chen, Y.-S.; Stalke, D.; John, M.; Clever, G. H. *Angew. Chem., Int. Ed.* **2013,** *52,* 1319–1323. doi:10.1002/anie.201207373
33. Samanta, D.; Mukherjee, P. S. *Chem. Commun.* **2013,** *49,* 4307–4309. doi:10.1039/c2cc37377g
34. Biros, S. M.; Bergman, R. G.; Raymond, K. N. *J. Am. Chem. Soc.* **2007,** *129,* 12094–12095. doi:10.1021/ja075236i
35. Samanta, D.; Mukherjee, S.; Patil, Y. P.; Mukherjee, P. S. *Chem. – Eur. J.* **2012,** *18,* 12322–12329. doi:10.1002/chem.201201679
36. Jans, A. C. H.; Gómez-Suárez, A.; Nolan, S. P.; Reek, J. N. H. *Chem. – Eur. J.* **2016,** *22,* 14836–14839. doi:10.1002/chem.201603162
37. Schneider, M. W.; Oppel, I. M.; Mastalerz, M. *Chem. – Eur. J.* **2012,** *18,* 4156–4160. doi:10.1002/chem.201200032
38. Yoshizawa, M.; Klosterman, J. K.; Fujita, M. *Angew. Chem., Int. Ed.* **2009,** *48,* 3418–3438. doi:10.1002/anie.200805340
39. Howlader, P.; Das, P.; Zangrando, E.; Mukherjee, P. S. *J. Am. Chem. Soc.* **2016,** *138,* 1668–1676. doi:10.1021/jacs.5b12237
40. Murase, T.; Nishijima, Y.; Fujita, M. *J. Am. Chem. Soc.* **2012,** *134,* 162–164. doi:10.1021/ja210068f
41. Salles, A. G., Jr.; Zarra, S.; Turner, R. M.; Nitschke, J. R. *J. Am. Chem. Soc.* **2013,** *135,* 19143–19146. doi:10.1021/ja412235e
42. Zhao, C.; Toste, F. D.; Raymond, K. N.; Bergman, R. G. *J. Am. Chem. Soc.* **2014,** *136,* 14409–14412. doi:10.1021/ja508799p
43. Kaphan, D. M.; Levin, M. D.; Bergman, R. G.; Raymond, K. N.; Toste, F. D. *Science* **2015,** *350,* 1235–1238. doi:10.1126/science.aad3087
44. Neelakandan, P. P.; Jiménez, A.; Thoburn, J. D.; Nitschke, J. R. *Angew. Chem., Int. Ed.* **2015,** *54,* 14378–14382. doi:10.1002/anie.201507045
45. Hasegawa, S.; Horike, S.; Matsuda, R.; Furukawa, S.; Mochizuki, K.; Kinoshita, Y.; Kitagawa, S. *J. Am. Chem. Soc.* **2007,** *129,* 2607–2614. doi:10.1021/ja067374y
46. Shultz, A. M.; Farha, O. K.; Hupp, J. T.; Nguyen, S. T. *J. Am. Chem. Soc.* **2009,** *131,* 4204–4205. doi:10.1021/ja900203f
47. Therrien, B.; Süss-Fink, G.; Govindaswamy, P.; Renfrew, A. K.; Dyson, P. J. *Angew. Chem., Int. Ed.* **2008,** *47,* 3773–3776. doi:10.1002/anie.200800186
48. Lewis, J. E. M.; Gavey, E. L.; Cameron, S. A.; Crowley, J. D. *Chem. Sci.* **2012,** *3,* 778–784. doi:10.1039/C2SC00899H
49. Samanta, S. K.; Moncelet, D.; Briken, V.; Isaacs, L. *J. Am. Chem. Soc.* **2016,** *138,* 14488–14496. doi:10.1021/jacs.6b09504
50. Nguyen, T. D.; Liu, Y.; Saha, S.; Leung, K. C.-F.; Stoddart, J. F.; Zink, J. I. *J. Am. Chem. Soc.* **2007,** *129,* 626–634. doi:10.1021/ja065485r
51. Ma, Z.; Moulton, B. *Coord. Chem. Rev.* **2011,** *255,* 1623–1641. doi:10.1016/j.ccr.2011.01.031
52. Singh, N.; Jo, J.-H.; Song, Y. H.; Kim, H.; Kim, D.; Lah, M. S.; Chi, K.-W. *Chem. Commun.* **2015,** *51,* 4492–4495. doi:10.1039/C4CC09494H
53. Schmitt, F.; Freudenreich, J.; Barry, N. P. E.; Juillerat-Jeanneret, L.; Süss-Fink, G.; Therrien, B. *J. Am. Chem. Soc.* **2012,** *134,* 754–757. doi:10.1021/ja207784t
54. Lewis, J. E. M.; Elliott, A. B. S.; McAdam, C. J.; Gordon, K. C.; Crowley, J. D. *Chem. Sci.* **2014,** *5,* 1833–1843. doi:10.1039/C4SC00434E
55. Li, H.; Han, Y.-F.; Lin, Y.-J.; Guo, Z.-W.; Jin, G.-X. *J. Am. Chem. Soc.* **2014,** *136,* 2982–2985. doi:10.1021/ja412667t
56. Barry, N. P. E.; Therrien, B. *Eur. J. Inorg. Chem.* **2009,** 4695–4700. doi:10.1002/ejic.200900649
57. Rowan, A. E.; Nolte, R. J. M. *Angew. Chem., Int. Ed.* **1998,** *37,* 63–68. doi:10.1002/(SICI)1521-3773(19980202)37:1/2<63::AID-ANIE63>3.0.CO;2-4
58. Saha, M. L.; Pramanik, S.; Schmittel, M. *Chem. Commun.* **2012,** *48,* 9459–9461. doi:10.1039/c2cc35036j
59. Zheng, Y.-R.; Zhao, Z.; Wang, M.; Ghosh, K.; Pollock, J. B.; Cook, T. R.; Stang, P. J. *J. Am. Chem. Soc.* **2010,** *132,* 16873–16882. doi:10.1021/ja106251f
60. Neogi, S.; Lorenz, Y.; Engeser, M.; Samanta, D.; Schmittel, M. *Inorg. Chem.* **2013,** *52,* 6975–6984. doi:10.1021/ic400328d
61. Stephenson, A.; Ward, M. D. *Dalton Trans.* **2011,** *40,* 10360–10369. doi:10.1039/c1dt10263j
62. Park, Y. J.; Ryu, J. Y.; Begum, H.; Lee, M. H.; Stang, P. J.; Lee, J. *J. Am. Chem. Soc.* **2015,** *137,* 5863–5866. doi:10.1021/jacs.5b01253
63. Govender, P.; Lemmerhirt, H.; Hutton, A. T.; Therrien, B.; Bednarski, P. J.; Smith, G. S. *Organometallics* **2014,** *33,* 5535–5545. doi:10.1021/om500809g
64. Shen, X.-Y.; Zhang, Y.-Y.; Zhang, L.; Lin, Y.-J.; Lin, G.-X. *Chem. – Eur. J.* **2015,** *21,* 16975–16981. doi:10.1002/chem.201502387
65. Singh, N.; Jang, S.; Jo, J.-H.; Kim, D. H.; Park, D. W.; Kim, I.; Kim, H.; Kang, S. C.; Chi, K.-W. *Chem. – Eur. J.* **2016,** *22,* 16157–16164. doi:10.1002/chem.201603521
66. Sepehrpour, H.; Saha, M. L.; Stang, P. J. *J. Am. Chem. Soc.* **2017,** *139,* 2553–2556. doi:10.1021/jacs.6b11860
67. Wise, M. D.; Holstein, J. J.; Pattison, P.; Besnard, C.; Solari, E.; Scopelliti, R.; Bricogne, G.; Severin, K. *Chem. Sci.* **2015,** *6,* 1004–1010. doi:10.1039/C4SC03046J
68. Li, K.; Zhang, L.-Y.; Yan, C.; Wei, S.-C.; Pan, M.; Zhang, L.; Su, C.-Y. *J. Am. Chem. Soc.* **2014,** *136,* 4456–4459. doi:10.1021/ja410044r
69. Lu, X.; Li, X.; Guo, K.; Xie, T.-Z.; Moorefield, C. N.; Wesdemiotis, C.; Newkome, G. R. *J. Am. Chem. Soc.* **2014,** *136,* 18149–18155. doi:10.1021/ja511341z
70. Kobayashi, A.; Suzuki, Y.; Ohba, T.; Noro, S.-i.; Chang, H.-C.; Kato, M. *Inorg. Chem.* **2011,** *50,* 2061–2063. doi:10.1021/ic102361d
71. Kent, C. A.; Mehl, B. P.; Ma, L.; Papanikolas, J. M.; Meyer, T. J.; Lin, W. *J. Am. Chem. Soc.* **2010,** *132,* 12767–12769. doi:10.1021/ja102804s

72. Clemente-León, M.; Coronado, E.; Gómez-García, C. J.; Soriano-Portillo, A. *Inorg. Chem.* **2006,** *45,* 5653–5660. doi:10.1021/ic060442x
73. Kumar, G.; Gupta, R. *Chem. Soc. Rev.* **2013,** *42,* 9403–9453. doi:10.1039/c3cs60255a
74. Halper, S. R.; Do, L.; Stork, J. R.; Cohen, S. M. *J. Am. Chem. Soc.* **2006,** *128,* 15255–15268. doi:10.1021/ja0645483
75. Wei, P.; Yan, X.; Huang, F. *Chem. Soc. Rev.* **2015,** *44,* 815–832. doi:10.1039/C4CS00327F
76. Chandler, B. D.; Cramb, D. T.; Shimizu, G. K. H. *J. Am. Chem. Soc.* **2006,** *128,* 10403–10412. doi:10.1021/ja060666e
77. Kitaura, R.; Onoyama, G.; Sakamoto, H.; Matsuda, R.; Noro, S.-i.; Kitagawa, S. *Angew. Chem., Int. Ed.* **2004,** *43,* 2684–2687. doi:10.1002/anie.200352596
78. Kent, C. A.; Liu, D.; Meyer, T. J.; Lin, W. *J. Am. Chem. Soc.* **2012,** *134,* 3991–3994. doi:10.1021/ja211271m
79. Xu, L.; Wang, Y.-X.; Chen, L.-J.; Yang, H.-B. *Chem. Soc. Rev.* **2015,** *44,* 2148–2167. doi:10.1039/C5CS00022J
80. Alvarado, L.; Brewer, G.; Carpenter, E. E.; Viragh, C.; Zavalij, P. Y. *Inorg. Chim. Acta* **2010,** *363,* 817–822. doi:10.1016/j.ica.2009.12.005
81. Li, Q.-J.; Zhao, G.-Z.; Chen, L.-J.; Tan, H.; Wang, C.-H.; Wang, D.-X.; Lehman, D. A.; Muddiman, D. C.; Yang, H.-B. *Organometallics* **2012,** *31,* 7241–7247. doi:10.1021/om3007932
82. Reichel, F.; Clegg, J. K.; Gloe, K.; Gloe, K.; Weigand, J. J.; Reynolds, J. K.; Li, C.-G.; Aldrich-Wright, J. R.; Kepert, C. J.; Lindoy, L. F.; Yao, H.-C.; Li, F. *Inorg. Chem.* **2014,** *53,* 688–690. doi:10.1021/ic402686s
83. Ou-Yang, J.-K.; Chen, L.-J.; Xu, L.; Wang, C.-H.; Yang, H.-B. *Chin. Chem. Lett.* **2013,** *24,* 471–474. doi:10.1016/j.cclet.2013.03.055
84. Chen, B.; Liang, C.; Yang, J.; Contreras, D. S.; Clancy, Y. L.; Lobkovsky, E. B.; Yaghi, O. M.; Dai, S. *Angew. Chem.* **2006,** *118,* 1418–1421. doi:10.1002/ange.200502844
85. Farrusseng, D.; Aguado, S.; Pinel, C. *Angew. Chem., Int. Ed.* **2009,** *48,* 7502–7513. doi:10.1002/anie.200806063
86. Meek, S. T.; Greathouse, J. A.; Allendorf, M. D. *Adv. Mater.* **2011,** *23,* 249–267. doi:10.1002/adma.201002854
87. Farha, O. K.; Hupp, J. T. *Acc. Chem. Res.* **2010,** *43,* 1166–1175. doi:10.1021/ar1000617
88. Wu, C.-D.; Hu, A.; Zhang, L.; Lin, W. *J. Am. Chem. Soc.* **2005,** *127,* 8940–8941. doi:10.1021/ja052431t
89. Corma, A.; García, H.; Llabrés i Xamena, F. X. *Chem. Rev.* **2010,** *110,* 4606–4655. doi:10.1021/cr9003924
90. Dhakshinamoorthy, A.; Alvaro, M.; Corma, A.; Garcia, H. *Dalton Trans.* **2011,** *40,* 6344–6360. doi:10.1039/c1dt10354g
91. Rowsell, J. L. C.; Yaghi, O. M. *Angew. Chem., Int. Ed.* **2005,** *44,* 4670–4679. doi:10.1002/anie.200462786
92. Li, J.-R.; Sculley, J.; Zhou, H.-C. *Chem. Rev.* **2012,** *112,* 869–932. doi:10.1021/cr200190s
93. Vajpayee, V.; Song, Y. H.; Lee, M. H.; Kim, H.; Wang, M.; Stang, P. J.; Chi, K.-W. *Chem. – Eur. J.* **2011,** *17,* 7837–7844. doi:10.1002/chem.201100242
94. Schmittel, M.; Mahata, K. *Inorg. Chem.* **2009,** *48,* 822–824. doi:10.1021/ic8021084
95. Jiang, B.; Zhang, J.; Ma, J.-Q.; Zheng, W.; Chen, L.-J.; Sun, B.; Li, C.; Hu, B.-W.; Tan, H.; Li, X.; Yang, H.-B. *J. Am. Chem. Soc.* **2016,** *138,* 738–741. doi:10.1021/jacs.5b11409
96. Wang, L.; Chen, L.-J.; Ma, J.-Q.; Wang, C.-H.; Tan, H.; Huang, J.; Xiao, F.; Xu, L. *J. Organomet. Chem.* **2016,** *823,* 1–7. doi:10.1016/j.jorganchem.2016.09.001
97. Adeyemo, A. A.; Shettar, A.; Bhat, I. A.; Kondaiah, P.; Mukherjee, P. S. *Dalton Trans.* **2018,** *47,* 8466–8475. doi:10.1039/C8DT00962G
98. Gupta, G.; Das, A.; Ghate, N. B.; Kim, T.; Ryu, J. Y.; Lee, J.; Mandal, N.; Lee, C. Y. *Chem. Commun.* **2016,** *52,* 4274–4277. doi:10.1039/C6CC00046K
99. Shanmugaraju, S.; Bar, A. K.; Mukherjee, P. S. *Inorg. Chem.* **2010,** *49,* 10235–10237. doi:10.1021/ic101823s
100. Shanmugaraju, S.; Samanta, D.; Mukherjee, P. S. *Beilstein J. Org. Chem.* **2012,** *8,* 313–322. doi:10.3762/bjoc.8.34
101. Mirtschin, S.; Slabon-Turski, A.; Scopelliti, R.; Velders, A. H.; Severin, K. *J. Am. Chem. Soc.* **2010,** *132,* 14004–14005. doi:10.1021/ja1063789
102. Vajpayee, V.; Song, Y. H.; Yang, Y. J.; Kang, S. C.; Cook, T. R.; Kim, D. W.; Lah, M. S.; Kim, I. S.; Wang, M.; Stang, P. J.; Chi, K.-W. *Organometallics* **2011,** *30,* 6482–6489. doi:10.1021/om200908c
103. Mishra, A.; Dubey, A.; Min, J. W.; Kim, H.; Stang, P. J.; Chi, K.-W. *Chem. Commun.* **2014,** *50,* 7542–7544. doi:10.1039/C4CC01991A
104. Barry, N. P. E.; Furrer, J.; Therrien, B. *Helv. Chim. Acta* **2010,** *93,* 1313–1328. doi:10.1002/hlca.200900422
105. Yan, H.; Suss-Fink, G.; Neels, A.; Stoeckli-Evans, H. *J. Chem. Soc., Dalton Trans.* **1997,** 4345–4350. doi:10.1039/A704658H
106. Samanta, D.; Shanmugaraju, S.; Adeyemo, A. A.; Mukherjee, P. S. *J. Organomet. Chem.* **2014,** *751,* 703–710. doi:10.1016/j.jorganchem.2013.09.037
107. Adeyemo, A. A.; Shanmugaraju, S.; Samanta, D.; Mukherjee, P. S. *Inorg. Chim. Acta* **2016,** *440,* 62–68. doi:10.1016/j.ica.2015.10.029
108. Adeyemo, A. A.; Shettar, A.; Bhat, I. A.; Kondaiah, P.; Mukherjee, P. S. *Inorg. Chem.* **2017,** *56,* 608–617. doi:10.1021/acs.inorgchem.6b02488

License and Terms

BEILSTEIN JOURNAL OF ORGANIC CHEMISTRY

Calixazulenes: azulene-based calixarene analogues – an overview and recent supramolecular complexation studies

Paris E. Georghiou*[1], Shofiur Rahman[1,2], Abdullah Alodhayb[2,3], Hidetaka Nishimura[4], Jaehyun Lee[4], Atsushi Wakamiya[4] and Lawrence T. Scott[5]

Full Research Paper

Open Access

Address:
[1]Department of Chemistry, Memorial University of Newfoundland, St. John's, Newfoundland and Labrador A1B 3X7, Canada, [2]Aramco Laboratory for Applied Sensing Research, King Abdullah Institute for Nanotechnology, King Saud University, Riyadh, Saudi Arabia, [3]Department of Physics and Astronomy, College of Science, King Saud University, Riyadh 11451, Saudi Arabia, [4]Institute for Chemical Research, Kyoto University, Uji, Japan and [5]Merkert Chemistry Center, Boston College, Chestnut Hill, MA, 02467 USA

Email:
Paris E. Georghiou* - parisg@mun.ca

* Corresponding author

Keywords:
azulene; calixarenes; calixazulenes; supramolecular chemistry; tetraalkylammonium salts

Beilstein J. Org. Chem. **2018,** *14,* 2488–2494.
doi:10.3762/bjoc.14.225

Received: 11 July 2018
Accepted: 10 September 2018
Published: 25 September 2018

This article is part of the thematic issue "Macrocyclic and supramolecular chemistry".

Guest Editor: M.-X. Wang

Abstract

Some of the least studied calixarenes are those that consist of azulene rings bridged by -CH_2- groups. Since Lash and Colby's discovery of a simple and convenient method for producing the parent all-hydrocarbon calix[4]azulene, there have been two other all-hydrocarbon calix[4]azulenes which have been synthesized in good yields by their method. This allowed studying their supramolecular properties. This report is of our latest work on the solution-state supramolecular complexation of one of these calix[4]azulenes, namely tetrakis(5,7-diphenyl)calix[4]azulene or "OPC4A", with several electron-deficient tetraalkyammonium salts. As a result of more recent methods developed by us and others employing Suzuki–Miyaura cross-coupling reactions to produce additional functionalized azulenes, the promise of further greater functionalized calixazulenes lies in store to be investigated.

Introduction

Among the great variety of synthetic macrocyclic molecular receptors which have been reported, those that are referred to by their generic name "calixarene" loom large [1-3]. The relatively facile and reproducible syntheses of the classical calix[*n*]arenes **1** in which *n* = 4, 6 or 8, with phenolic groups linked or bridged via methylene groups to form defined three-dimensional basket-like cavities with "upper" or "lower" rims, were developed by Gutsche and co-workers [4-6]. As a result of

Gutsche's synthetic methodologies many researchers have been able to employ these calix[*n*]arenes and modified derivatives thereof in a great variety of ingenious applications. These applications have included a myriad of synthetic modifications to both, or either, of their upper and lower rims, and also to their bridging methylene groups, all of which have resulted in further synthetic endeavours. Much of the groundwork for these endeavours have resulted from the pioneering works which emanated from the research groups of C. D. Gutsche, R. Ungaro, D. N. Reinhoudt, and V. Böhmer to name only just a few. Reinhoudt has recently presented an overview of the historical evolution of the chemistry of the calixarenes [1]. Supramolecular applications, in particular, of many of the great number of creative derivatives of calixarenes which have been and continue to be synthesized are widely being reported in the literature [7].

Besides the classical calixarene phenolic subunits linked by methylene groups, "calixarenes" incorporating other subunits include, but are not limited to, resorcinol [8], hydroquinone [9], naphthols [10], pyrrole [11], heteroaromatics [12] and triptycene [13] in their cavity-containing structures have gained much recent attention. Among the least-studied to date, however, have been the azulene unit-containing calix[4]arene analogues. In 1988 Asao et al. reported the synthesis of the first azulene analogue of the calixarenes, which they called "azulenophane" **2** [14]. They used a semi-convergent route and reported that **2** had a *1,3-alternate* conformation at room temperature and that it "formed crystals with two molecules of benzene" but they reported no other studies. To the best of our knowledge, this is the only "lower-rim" functionalized calix[4]azulene which has been reported to date. In 2002 Lash and Colby's reported a convenient one-step Florisil®-mediated cyclocondensation of azulene with paraformaldehyde to produce an all-hydrocarbon "calix[4]azulene" **3** [15]. Later, Lash et al. reported their synthesis of a second all-hydrocarbon tetra-6-*tert*-butylcalix[4]azulene (**4**) in a similar way, from the reaction of 6-*tert*-butylazulene with formaldehyde [16]. Compound **4** is the first reported "wide-rim" functionalized calix[4]azulene (Figure 1).

Recently, we reported the synthesis of tetrakis(5,7-diphenyl)-calix[4]azulene (**5**) (or octaphenylcalix[4]azulene, "OPC4A", Figure 1) and on its mechanochemically-generated solid-state complex of C_{60}-fullerene [17]. This all-hydrocarbon, wide-rim octaphenyl-functionalized calix[4]azulene was designed to evaluate its potential for encapsulating C_{60} or C_{70} fullerenes. The lack of sufficient solubility of **5** in common organic solvents prevented a fuller examination of its potential supramolecular properties with fullerenes, a topic of particular interest to us [18]. Therefore, the solid state supramolecular complexation properties of **5** were experimentally studied using solid state NMR and XRD experiments, and also theoretically, using a DFT analysis [17]. We previously used a similar solid-state NMR approach to study the solid-state supramolecular properties of tetra-6-*tert*-butylcalix[4]azulene (**4**) [19]. Unlike these two studies, however, in our first study on calixazulenes which we reported in 2015, we were able to demonstrate a chloroform solution-state complexation binding study with Lash and Colby's calix[4]azulene **3** using a series of tetraalkylammonium halides and tetrafluoroborate salts [20]. This study was also supplemented by DFT studies to support the trends observed in the experimentally-derived binding constants. Since these three calix[4]azulenes **3**–**5** are all-hydrocarbon compounds they differ significantly from the better-studied calix[4]arenes, which usually have some heteroatoms such as oxygen, nitrogen or

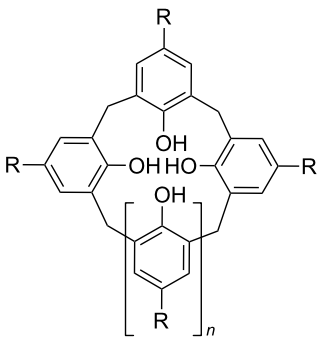

1: R = *t*-Bu and *n* = 1, 3 or 5

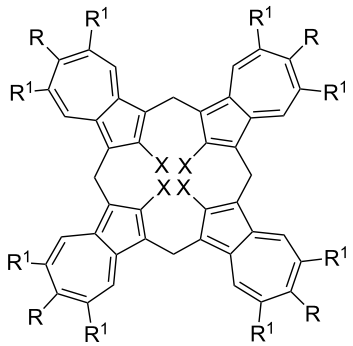

2: R = R^1 = H; X = OMe
3: R = R^1 = X = H
4: R = *t*-Bu; R^1 = X = H
5: R = X = H; R^1 = Ph

Figure 1: Examples of calix[*n*]arenes **1** and calix[4]azulenes **2**–**5**.

sulfur in their structures. As a consequence, compounds **3**–**5** have solubility limitations. Furthermore, the absence of heteroatoms, most commonly hydroxy groups on the "lower" or narrow rim, also limits their "pre-organizational" potential for supramolecular binding, this being of particular interest to us. We now report that we have succeeded in extracting binding constant data from a solution-state UV–vis supramolecular binding study recently concluded with OPC4A. These results and a corresponding DFT study are reported herein.

Results and Discussion

The convenient synthesis of the precursor for OPC4A **5**, namely 5,7-diphenylazulene, which is normally a difficult target molecule, was previously described from a Suzuki–Miyaura coupling reaction of bromobenzene with 5,7-di(Bpin)azulene, which in turn was formed via the exhaustive borylation of azulene with excess bis(pinacolato)diboron (B_2pin_2) [21]. Cyclocondensation of 5,7-diphenylazulene with formaldehyde produced **5** [22] under conditions similar to those used by Lash and Colby in their syntheses of **3** and **4**. Although **5** was not sufficiently soluble in CS_2, benzene, toluene or 1,2-dichlorobenzene to enable ^{1}H NMR solution titration studies to be conducted with fullerene C_{60}, a dilute solution of **5** in dichloromethane-d_2 could be obtained that enabled its NMR characterization. This finding suggested to us that solution complexation studies with other electron-deficient suitable guests could be conducted in dichloromethane (DCM). The concentrations that could be obtained with DCM were too dilute for typical NMR titration studies, but we judged that they could instead be suitable for a UV–vis titration study**.** Indeed, after several preliminary trials, solutions of approximately 1.2 mg of **5** in 100.0 mL of DCM ($\approx 1.1 \times 10^{-5}$ M) could eventually be generated with the help of sonication in a 35 °C water-bath. By way of contrast, initial attempts to create more concentrated solutions in chloroform under similar and higher temperature (60 °C) sonication conditions resulted in the unexpected decomposition of **5**, a finding which was not investigated any further.

With DCM solutions of OPC4A now in hand, titration studies were conducted using 1.0 cm pathlength cells in a thermostated dual beam UV–vis spectrophotometer. Addition of microlitre aliquots of DCM solutions of the respective tetraalkylammonium salts (TRAX; where R = Me, Et; *n*-Bu and X = Cl^-, Br^-, I^- or BF_4^-) resulted in quenching of the absorption spectra in the 300–700 nm range, with visible isosbestic points at ≈460 and 350 nm. Although the changes were small, as was also seen previously in the titration experiments with **3**, they were sufficient to allow for reproducible determinations of the corresponding apparent K_{assoc} values. Each of the full spectra could be subjected to non-linear 1:1 global fit analyses as described by Thordarson [23,24].

Table 1 shows the measured apparent binding or association constants, from which two trends can be discerned: Firstly, the K_{assoc} values with the tetra-*n*-butylammonium halide salts show a trend that is in the order $Cl^- > Br^- > I^-$. This trend is similar to that seen previously with the corresponding tetramethylammonium halides and **3**. Secondly, with respect to the tetraalkylammonium BF_4 salts, the corresponding K_{assoc} trend is in the order *n*-Bu > Et > Me. This trend is in contrast and opposite to that which was seen previously with the unfunctionalized calix[4]azulene **3**.

To shed light on possible explanations for these findings, our attention was again directed to computational results derived from DFT calculations which are increasingly being commonly used in supramolecular chemistry. The ωB97xD functional [25] which combines the long range functional ωB97x with the empirical dispersion correction was used with the standard 6-31G(d) basis set [26]. We had previously described the use of this system in our previous studies in particular, in reference

Table 1: Apparent experimentally-derived binding constants and DFT-computed interaction energies (*IE*) and selected interatomic distances derived from the geometry-optimized structures of the supramolecular complexes and their constituents.[a]

	K_{assoc} ± 15% (M^{-1})	*IE* (kJ mol^{-1})	avg. N···C* dist. in complex (Å)	X···N dist. free guest (Å)	X···N dist. in complex (Å)	Δ X···N dist. (Å)
TBACl	4.4×10^4	−337.805[b]	7.14 ± 0.68	3.79	3.89	0.095
TBABr	3.8×10^4	−315.073[b]	7.13 ± 0.67	4.07	4.14	0.081
TBAI	2.9×10^4	−316.402[b]	7.06 ± 0.66	4.47	4.34	0.13
$TMABF_4$	4.8×10^3	−155.935[c]	4.78 ± 0.18	3.98	4.13	0.15
$TEABF_4$	3.3×10^4	−164.812[c]	5.76 ± 0.45	3.96	4.11	0.15
$TBABF_4$	4.1×10^4	−198.832[c]	7.09 ± 0.68	3.97	4.10	0.13

[a]TBAX: tetra-*n*-butylammonium halide where X = Cl, Br or I; $TRABF_4$: tetraalkylammonium fluoroborate where R = M = methyl; R = E = ethyl or R = B = *n*-butyl. [b]Value derived using ωB97xD/GenECP and [c]Value derived using ωB97xD/6-31G(d).

[20] as being more reliable than the use of B3LYP/6-31G(d) with our systems. Furthermore, for the halide guests and complexes (i.e., for TBACl, TBABr and TBAI) but not with the tetrafluorborate salts, we used relativistic ECPs by Hay and Wadt (LANL) along with the corresponding LANL2DZ basis set augmented with additional *d-, p*-polarizational functions [27-30]. For the $TBABF_4$ salts the ωB97xD/6-31G(d) route was used (see Table 1 and Supporting Information File 1). For each of the individual components, i.e., the tetra-*n*-butylammonium salt, OPC4A and the respective corresponding 1:1 supramolecular complexes, unconstrained geometry optimizations were first conducted in the gas phase. Then, geometries in all cases were optimized within the continuum solvation model (PCM) [31,32] of the DCM solvent, using the default solvent parameters as provided with Gaussian-09 Revision E.01 [33]. The results are summarized in Table 1 and Table 2.

For the free OPC4A host molecule, initial geometry-optimized determinations were made on the possible major conformations, based upon those previously defined in reference [20]. Three distinct conformations (*saddle*, *cone* and *1,2-alternate*) shown in Figure 2, were generated.

Significantly, whereas for **3** which was based upon its X-ray structure, a *partial cone* conformer could be generated and provided a geometry-optimized energy value, the analogous *partial cone* conformation of **5** could not be similarly geometry-optimized. Instead, for **5**, geometry-optimization produced the *1,2-alternate* form shown in Figure 2a. The energies computed with DCM corrections are shown in Table 2 with the *saddle* conformer (Figure 2c) having the lowest energy. Nevertheless, when subjected to geometry optimizations with the individual respective TRAX salt guests, the saddle conformer opened up to generate and accommodate each of the guests in typical "guest-in-*cone*" structures, as can be seen in Figure 3.

The interaction energies (*IE*) were calculated from the corresponding DFT-calculated geometry-optimised components (i.e.,

Table 2: DFT computed energy values for the three different conformations of **5**.

structure	designation	RωB97XD energy (Hartrees)	relative energies (kJ mol^{-1})
5c	*saddle*	−3543.128099	0
5b	*cone*	−3543.11020759[a] and −3543.0596655[b]	46.97[a] and 42.94[b]
5a	*1,2-alternate*	−3543.108789	50.70

[a]Value derived using ωB97xD/6-31G(d) and [b]value derived using ωB97xD/GenECP.

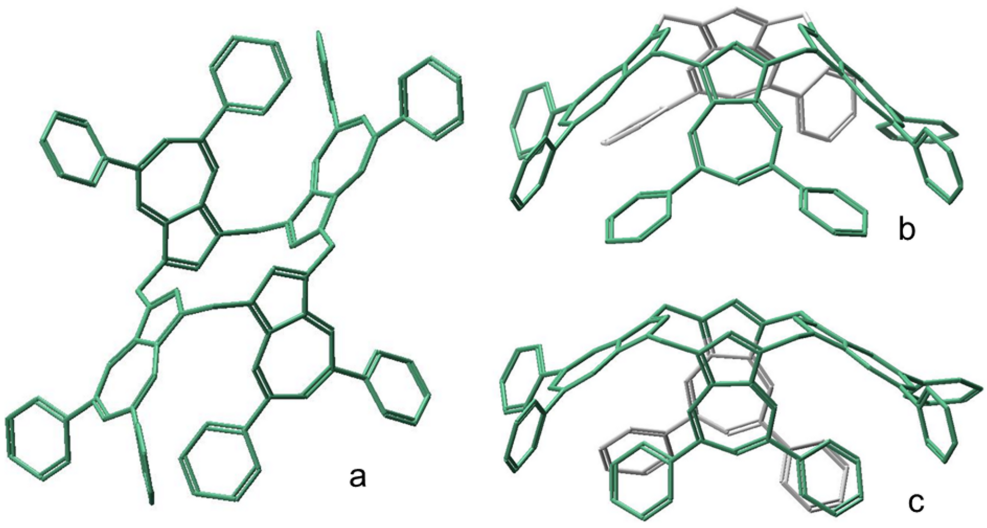

Figure 2: Three major computed conformers of OPC4A; a: *1,2-alternate*; b: *cone* and c: *saddle*.

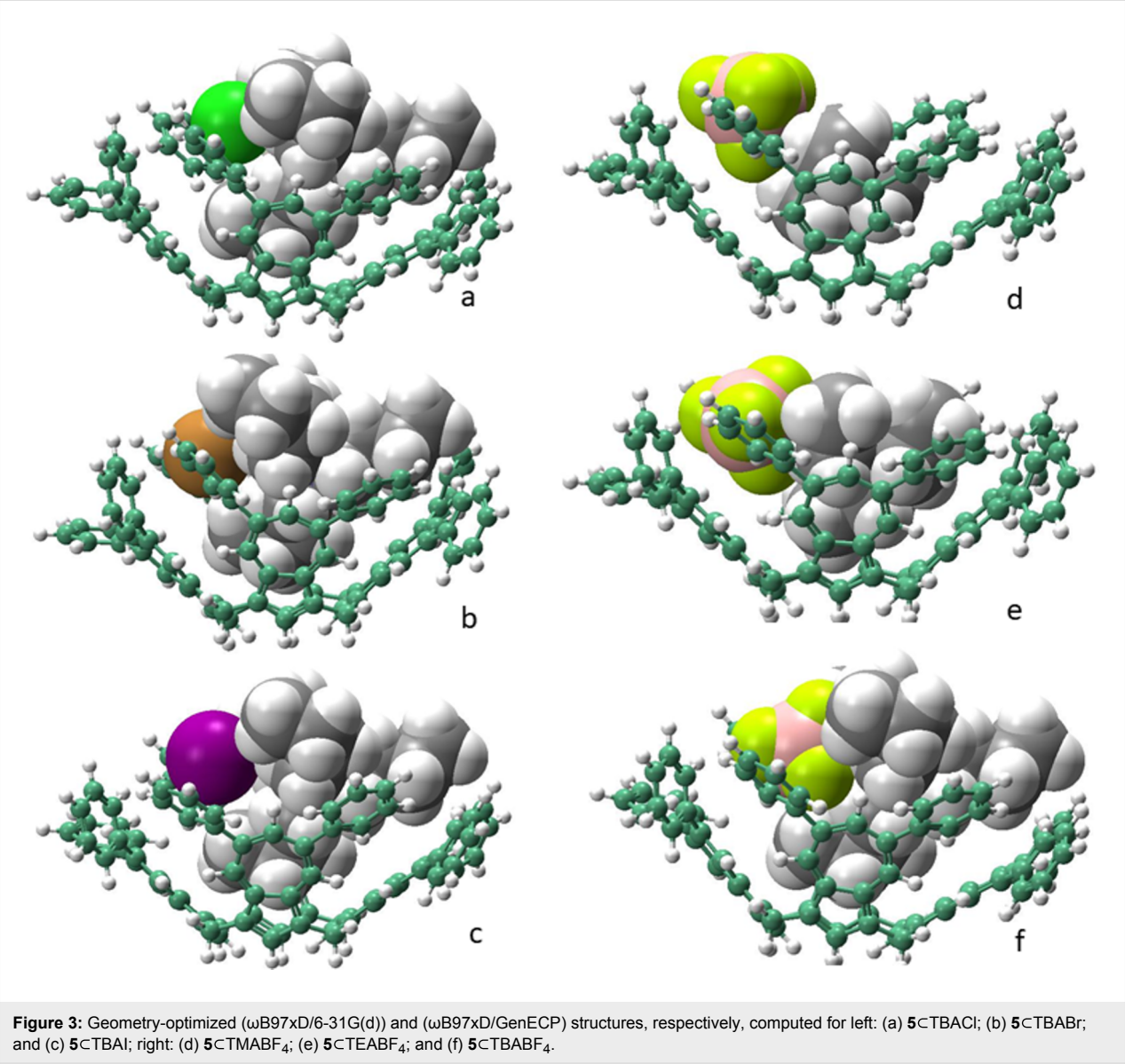

Figure 3: Geometry-optimized (ωB97xD/6-31G(d)) and (ωB97xD/GenECP) structures, respectively, computed for left: (a) **5**⊂TBACl; (b) **5**⊂TBABr; and (c) **5**⊂TBAI; right: (d) **5**⊂$TMABF_4$; (e) **5**⊂$TEABF_4$; and (f) **5**⊂$TBABF_4$.

each of **5** and the respective guest TRAX) as 1:1 complexes according to Equation 1:

$$IE = E_{\text{complex}} - \sum\left(E_{\text{OPC4A}(cone)} + E_{\text{TRAX}}\right), \quad (1)$$

based upon the respective "*cone*" conformation (Figure 2b) energies. These values are shown in Table 1. No easily discernable significant correlation between the interaction energies and the experimentally measured binding constants can be discerned for the three halide salt complexes; the highest *IE* (−337.805 kJ mol^{-1}) was found for the chloride which also had the highest binding constant but the corresponding values for the bromide and iodide salts showed no such correlation. The correlations between the *IE*s and binding constants for the tetrafluoroborate salts, however, are more easily discernable and have the same trends in the order of $TBABF_4$ > $TEABF_4$ > $TMABF_4$. The counterion effects of the halide anions are more significant than those of the fluoroborate anion which is weakly coordinating in the salts employed. This can be seen in Table 1 for the relatively smaller changes in the boron-to-nitrogen distances in the DFT-computed optimized geometry structures of the complexes.

Table 1 also shows the average values of the calculated distances between the quaternary nitrogen atom and the "deepest" carbon atoms (i.e., C-1) in each of the azulenes in the calix[4]azulene bowls. A small trend can be discerned for the halide salt complexes which is opposite to the trend in the measured apparent binding constants. For the tetrafluoroborate

salts, however, the trend of the corresponding average quaternary nitrogen-to-carbon distances are in the opposite direction, which is consistent with the increasing sizes of the alkyl groups *n*-Bu > Et > Me. Clearly, the BF_4 salts show less ambiguous DFT data than those of the halide salts in this study. As can be seen in structures d–f in Figure 3, there are more guest $C–H_{(guest)}–\pi_{(host)}$ interactions possible as the size of the alkyl groups increase from groups Me < Et < *n*-Bu, which could also account for the observed trend in their binding constants.

Conclusion

Based upon the DFT calculations which we previously conducted in the solid-state study of **5** with C_{60}, we postulated that due to the mechanochemical method of combining both components and the spherical nature of C_{60} that a possible interaction mode between host and guest could be as columnar arrays [17]. In this type of array the host molecules which are in *1,3-alternate* conformations align in a "head-to-tail" fashion with the C_{60} molecules able to be accommodated within the opposite clefts. Furthermore, within such an arrangement, in addition to the "face-to-face" π–π interactions between the azulene rings and the C_{60}, "edge-to-face" type interactions with the 2′,6′-protons of the phenyl group substituents of the azulenes are also factors which could stabilize the solid-state supramolecular interactions or complexation. In the present study, however, due to the dilute solution state conditions, only 1:1 complexation modes between **5** and the respective tetraalkylammonium salts was considered. The binding constants were consistent with such an hypothesis. As a result, the DFT-generated complexes considered only such 1:1 "guest in cone" complexes, as shown in Figure 3a–f. Finally, in light of recent developments in the facile syntheses of other functionalzed azulenes as reported by Narita et al. [34] the potential for further syntheses of heterofunctionalized calixazulenes and their supramolecular chemistry may be realized. Further studies by us on these intriguing possibilities are ongoing.

Supporting Information

Supporting Information File 1

Experimental determination of binding constants and DFT calculations.
[https://www.beilstein-journals.org/bjoc/content/supplementary/1860-5397-14-225-S1.pdf]

Supporting Information File 2

MOL files.
[https://www.beilstein-journals.org/bjoc/content/supplementary/1860-5397-14-225-S2.rar]

Acknowledgements

This project was supported by King Saud University, Deanship of Scientific Research, College of Science Research Center, the US National Science Foundation. H. N. and J. L. thank the JSPS for their research fellowship. The computational work has been assisted by the use of computing facilities provided by and with the on-going support of Dr. G. Shamov and Dr. Oliver Stueker of Compute/Calcul Canada via the Westgrid and Acenet facilities. The late Prof. R. Marceau, Vice-President Research, M.U.N. is gratefully acknowledged for research support to PEG.

ORCID® iDs

Paris E. Georghiou - https://orcid.org/0000-0001-9435-6857
Shofiur Rahman - https://orcid.org/0000-0003-4219-4758
Abdullah Alodhayb - https://orcid.org/0000-0003-0202-8712
Atsushi Wakamiya - https://orcid.org/0000-0003-1430-0947
Lawrence T. Scott - https://orcid.org/0000-0003-3496-8506

References

1. Reinhoudt, D. N. Introduction and History. In *Calixarenes and Beyond;* Neri, P.; Sessler, J. L.; Wang, M.-X., Eds.; Springer: Dordrecht, 2016; pp 1–11. doi:10.1007/978-3-319-31867-7_1
2. Asfari, Z.; Bohmer, V.; Harrowfield, J. M.; Vicens, J., Eds. *Calixarenes 2001;* Kluwer Academic: Dordrecht, The Netherlands, 2001.
3. Gutsche, C. D. *Calixarenes Revisited;* RSC Publishing: Cambridge, 1998.
4. Gutsche, C. D.; Iqbal, M. *Org. Synth.* **1990,** *68,* 234. doi:10.15227/orgsyn.068.0234
5. Munch, J. H.; Gutsche, C. D. *Org. Synth.* **1990,** *68,* 243. doi:10.15227/orgsyn.068.0243
6. Gutsche, C. D.; Dhawan, B.; Leonis, M.; Stewart, D. *Org. Synth.* **1990,** *68,* 238. doi:10.15227/orgsyn.068.0238
7. A recent (August, 2018) search on *Web of Science* using the term "calixarenes" returned a total of 5275 publications. Data derived with permission from Clarivate Analytics *Web of Science.* © Copyright Clarivate Analytics 2018. All rights reserved.
8. D'Acquarica, I.; Ghirga, F.; Ingallina, C.; Quaglio, D.; Zappia, G.; Uccello-Barretta, G.; Balzano, F.; Botta, B. Resorc[4]arenes as Preoranized Synthons for Surface Recognition and Host–Guest Chemistry. In *Calixarenes and Beyond;* Neri, P.; Sessler, J. L.; Wang, M.-X., Eds.; Springer: Dordrecht, 2016; pp 175–193. doi:10.1007/978-3-319-31867-7_8
9. Ogoshi, T.; Yamagishi, T.-a.; Nakamoto, Y. *Chem. Rev.* **2016,** *116,* 7937–8002. doi:10.1021/acs.chemrev.5b00765
10. Yang, L.-P.; Liu, W.-E.; Jiang, W. *Tetrahedron Lett.* **2016,** *57,* 3978–3985. doi:10.1016/j.tetlet.2016.07.077
11. Vargas-Zúñinga, G. I.; Sessler, J. L.; Bähring, S. Functionalized Calixpyrroles: Building Blocks for Self-Assembly. In *Calixarenes and Beyond;* Neri, P.; Sessler, J. L.; Wang, M.-X., Eds.; Springer: Dordrecht, 2016; pp 285–333. doi:10.1007/978-3-319-31867-7_12
12. Wang, D.-X.; Wang, M.-X. Azacalixaromatics. In *Calixarenes and Beyond;* Neri, P.; Sessler, J. L.; Wang, M.-X., Eds.; Springer: Dordrecht, 2016; pp 363–397. doi:10.1007/978-3-319-31867-7_14
13. Chen, C.-F.; Han, Y. *Acc. Chem. Res.* **2018,** *51,* 2093–2106. doi:10.1021/acs.accounts.8b00268

14. Asao, T.; Ito, S.; Morita, N. *Tetrahedron Lett.* **1988,** *29,* 2839–2842. doi:10.1016/0040-4039(88)85225-0
15. Colby, D. A.; Lash, T. D. *J. Org. Chem.* **2002,** *67,* 1031–1033. doi:10.1021/jo0110101
16. Lash, T. D.; El-Beck, J. A.; Colby, D. A. *J. Org. Chem.* **2009,** *74,* 8830–8833. doi:10.1021/jo901959k
17. Schneider, C.; Nishimura, H.; Lee, J.; Scott, L. T.; Wakamiya, A.; Forbes, R.; Georghiou, P. E. *Supramol. Chem.* **2018,** *30,* 575–582. doi:10.1080/10610278.2017.1415435
18. Georghiou, P. E. Calixarenes and Fullerenes. In *Calixarenes and Beyond;* Neri, P.; Sessler, J. L.; Wang, M.-X., Eds.; Springer: Dordrecht, 2016; pp 879–919. doi:10.1007/978-3-319-31867-7_33
19. Georghiou, P. E.; Schneider, C.; Shamov, G.; Lash, T. D.; Rahman, S.; Giddings, D. S. *Supramol. Chem.* **2016,** *28,* 396–402. doi:10.1080/10610278.2015.1108416
20. Rahman, S.; Zein, A.; Dawe, L. N.; Shamov, G.; Thordarson, P.; Georghiou, P. E. *RSC Adv.* **2015,** *5,* 54848–54852. doi:10.1039/C5RA07802D
21. Nishimura, H.; Eliseeva, M. N.; Wakamiya, A.; Scott, L. T. *Synlett* **2015,** *26,* 1578–1580. doi:10.1055/s-0034-1380686
22. Eliseeva, M. N.; Scott, L. T. *J. Am. Chem. Soc.* **2012,** *134,* 15169–15172. doi:10.1021/ja307547j
23. Thordarson, P. *Chem. Soc. Rev.* **2011,** *40,* 1305–1323. doi:10.1039/C0CS00062K
24. Thordarson, P. Online tools for supramolecular chemistry research and analysis. OpenDataFit; http://supramolecular.org.
25. Chai, J.-D.; Head-Gordon, M. *Phys. Chem. Chem. Phys.* **2008,** *10,* 6615–6620. doi:10.1039/b810189b
26. Ditchfield, R.; Hehre, W. J.; Pople, J. A. *J. Chem. Phys.* **1971,** *54,* 724–728. doi:10.1063/1.1674902
27. Check, C. E.; Faust, T. O.; Bailey, J. M.; Wright, B. J.; Gilbert, T. M.; Sunderlin, L. S. *J. Phys. Chem. A* **2001,** *105,* 8111–8116. doi:10.1021/jp011945l
28. Hay, P. J.; Wadt, W. R. *J. Chem. Phys.* **1985,** *82,* 270–283. doi:10.1063/1.448799
29. Wadt, W. R.; Hay, P. J. *J. Chem. Phys.* **1985,** *82,* 284–298. doi:10.1063/1.448800
30. Hay, P. J.; Wadt, W. R. *J. Chem. Phys.* **1985,** *82,* 299–310. doi:10.1063/1.448975
31. Tomasi, J.; Persico, M. *Chem. Rev.* **1994,** *94,* 2027–2094. doi:10.1021/cr00031a013
32. Tomasi, J.; Mennucci, B.; Cammi, R. *Chem. Rev.* **2005,** *105,* 2999–3094. doi:10.1021/cr9904009
33. *Gaussian 09,* Revision D.01; Gaussian: Wallingford, CT, 2013.
34. Narita, M.; Murafuji, T.; Yamashita, S.; Fujinaga, M.; Hiyama, K.; Oka, Y.; Tani, F.; Kamijo, S.; Ishiguro, K. *J. Org. Chem.* **2018,** *83,* 1298–1303. doi:10.1021/acs.joc.7b02820

License and Terms